

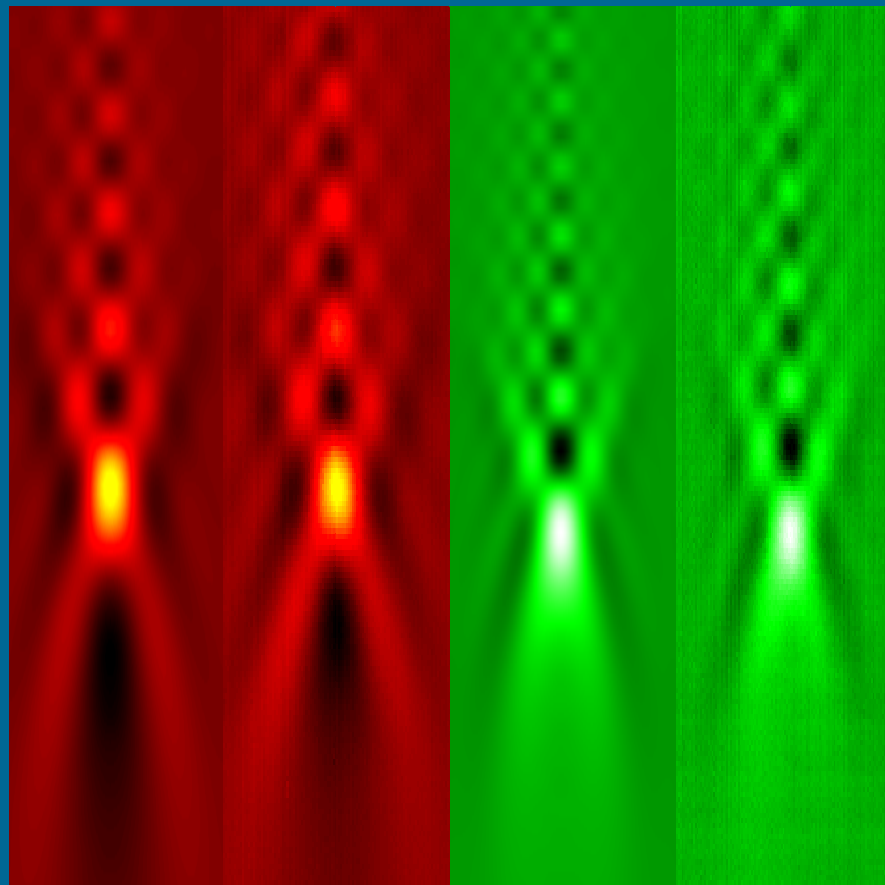
UNIVERSITÄT LEIPZIG

# REPORT

Institute für Physik

The Physics Institutes

2010





The Physics Institutes of Universität Leipzig, Report 2010  
M. Grundmann (Ed.)

Technical Editor: Anja Heck

This work is subject to copyright. All rights are reserved.  
© Universität Leipzig 2011

Printed in Germany by  
MERKUR Druck und Kopierzentrum GmbH, Leipzig

online available at  
[http://www.uni-leipzig.de/~exph2/report\\_2010.pdf](http://www.uni-leipzig.de/~exph2/report_2010.pdf)

### **Front cover**

The frontcover images show the light intensity scattered by a single 60 nm gold nanoparticle in the forward direction at a wavelength of 532 nm (green) and 635 nm (red). The images have been recorded by moving the particle through the focus of a confocal microscopy setup in axial direction and perpendicular to it. The left image of each pair represents the theoretical prediction by a generalized Lorenz-Mie Theory.

### **Back covers**

Recent book publications.



**Institut für Experimentelle Physik I  
Institut für Experimentelle Physik II  
Institut für Theoretische Physik**

**Fakultät für  
Physik und Geowissenschaften**

**Universität Leipzig**

**Institute for Experimental Physics I  
Institute for Experimental Physics II  
Institute for Theoretical Physics**

**Faculty of Physics and Earth Sciences**

**Universität Leipzig**

**Report 2010**



## **Addresses**

### **Institute for Experimental Physics I**

Linnéstraße 5

D-04103 Leipzig, Germany

Phone: +49 341 97-32551

Fax: +49 341 97-32599

WWW: <http://www.uni-leipzig.de/physik/index.php/exp-1.html>

Mailing

address: Postfach 100 920, D-04009 Leipzig, Germany

### **Institute for Experimental Physics II**

Linnéstraße 5

D-04103 Leipzig, Germany

Phone: +49 341 97-32650

Fax: +49 341 97-32668

WWW: <http://www.uni-leipzig.de/physik/index.php/exp-2.html>

Mailing

address: Postfach 100 920, D-04009 Leipzig, Germany

### **Institute for Theoretical Physics**

Vor dem Hospitaltore 1

D-04103 Leipzig, Germany

Phone: +49 341 97-32420

Fax: +49 341 97-32548

WWW: <http://www.uni-leipzig.de/physik/index.php/thph.html>

Mailing

address: Postfach 100 920, D-04009 Leipzig, Germany



# Preface

This 2010 Report of the Physics Institutes of the Universität Leipzig presents to you an overview of our research in numerous projects, enjoyably conducted with colleagues and partners worldwide. We are grateful to our guests for enriching our academic year with their contributions in the colloquium and within the work groups.

We are grateful for many years of fruitful work of our colleagues Profs. Klaus Sibold and Tilman Butz who have now retired. For their new challenges we wish them all the best. As new colleague we welcome Prof. Bernd Rosenow (succession Salmhofer) who fills the chair for Statistical Physics and strengthens theoretical work on solid-state quantum systems. We are also looking forward to fruitful collaboration with Prof. Felix Otto, newly appointed director at the Max Planck Institute for Mathematics in the Sciences.

2010 has seen the BuildMoNa Symposium on the 'Physics of Cancer', bringing together experts on the detection and treatment of cancer using physical methods. The meeting starts a series supported also by NIH, DKFZ and the US Congress. In honor of the 80th birthday of Armin Uhlmann, the workshop 'Mathematics and Quantum Physics' was held in the Institute for Theoretical Physics.

The Sächsische Forschergruppe FOR 877 'From Local Constraints to Macroscopic Transport', a joint initiative with colleagues from Dresden and Chemnitz, has been successfully prolonged for a second three-year funding period. A joint project of Leibniz-Institute of Surface Modification (IOM) and the Institute of Experimental Physics II within the competitive framework of 'Senatsausschuss Wissenschaft' supports further close cooperation on the physics of nanostructures. The new Collaborative Research Center TRR 102 'Polymers under multiple constraints: restricted and controlled molecular order and mobility' together with colleagues in Halle will start its work in July 2011.

Most of our activities are only possible due to the generous support from various funding agencies for which we are very grateful and which is individually acknowledged in the brief reports.

Leipzig,  
May 2011

*M. Grundmann*  
*J. A. Käs*  
*R. Verch*  
Directors



# Contents

<b>1</b>	<b>Structure and Staff of the Institutes</b>	<b>21</b>
1.1	Institute for Experimental Physics I . . . . .	21
1.1.1	Office of the Director . . . . .	21
1.1.2	Molecular Nano-Photonics, Molekulare Nanophotonik [MON] . . . . .	21
1.1.3	Molecular Physics, Molekülphysik [MOP] . . . . .	21
1.1.4	Physics of Interfaces, Grenzflächenphysik [GFP] . . . . .	22
1.1.5	Soft Matter Physics, Physik der weichen Materie [PWM] . . . . .	23
1.2	Institute for Experimental Physics II . . . . .	25
1.2.1	Office of the Director . . . . .	25
1.2.2	Magnetic Resonance of Complex Quantum Solids, Magnetische Resonanz Komplexer Quantenfestkörper [MQF] . . . . .	25
1.2.3	Nuclear Solid State Physics, Nukleare Festkörperphysik [NFP] . . . . .	26
1.2.4	Semiconductor Physics, Halbleiterphysik [HLP] . . . . .	26
1.2.5	Solid State Optics and Acoustics, Festkörperoptik und -akustik [FKO] . . . . .	28
1.2.6	Superconductivity and Magnetism, Supraleitung und Magnetismus [SUM] . . . . .	28
1.3	Institute for Theoretical Physics . . . . .	29
1.3.1	Office of the Director . . . . .	29
1.3.2	Computational Quantum Field Theory, Computerorientierte Quantenfeldtheorie [CQT] . . . . .	29
1.3.3	Molecular Dynamics / Computer Simulation, Moleküldynamik / Computersimulation [MDC] . . . . .	30
1.3.4	Quantum Field Theory and Gravity, Quantenfeldtheorie und Gravitation [QFG] . . . . .	31
1.3.5	Statistical Physics, Statistische Physik [STP] . . . . .	31
1.3.6	Theory of Condensed Matter, Theorie der kondensierten Materie [TKM] . . . . .	32
1.3.7	Theory of Elementary Particles, Theorie der Elementarteilchen [TET] . . . . .	32

<b>I</b>	<b>Institute for Experimental Physics I</b>	<b>33</b>
<b>2</b>	<b>Molecular Nanophotonics</b>	<b>35</b>
2.1	Introduction . . . . .	35
2.2	Photothermal Microscopy: Signal Generation . . . . .	36
2.3	Self-Propelled Thermophoretic Particles . . . . .	37
2.4	Twin-Focus Photothermal Correlation Spectroscopy . . . . .	38
2.5	Angle Resolved Fluorescence Spectroscopy in Photonic Crystals . . . . .	40
2.6	Single Molecule Diffusion in Liquid Crystals . . . . .	41
2.7	Surface Charges on CdSe/ZnS Semiconductor Quantum Dots in Apolar Solvents . . . . .	42
2.8	Funding . . . . .	43
2.9	Organizational Duties . . . . .	44
2.10	External Cooperations . . . . .	44
2.11	Publications . . . . .	44
2.12	Graduations . . . . .	46
2.13	Guests . . . . .	46
<b>3</b>	<b>Molecular Physics</b>	<b>49</b>
3.1	Introduction . . . . .	49
3.2	Glassy dynamics of mono-molecular layers of poly(2-vinyl pyridine) . . . . .	50
3.3	Glassy dynamics and glass transition in nanometric thin layers of polystyrene . . . . .	51
3.4	Glassy dynamics in thin layers of cis-polyisoprene . . . . .	51
3.5	Molecular dynamics of cis-polyisoprene under geometrical confinement . . . . .	53
3.6	Rotational and translational diffusion in hyper-branched polyglycerols . . . . .	55
3.7	Dielectric properties of ionic liquids: the effect of temperature and pressure . . . . .	56
3.8	Diffusion in ionic liquids: the interplay between molecular structure and dynamics . . . . .	57
3.9	Charge transport and dipolar relaxations in alkali metal-based ionic liquids . . . . .	58
3.10	Charge transport in confined ionic liquids . . . . .	59
3.11	Liquid crystals in confining geometry . . . . .	60
3.12	Infrared transition moment orientational analysis (IR-TMOA) . . . . .	61
3.13	Hierarchies in the structural organization of spider silk- A quantitative combined model . . . . .	62
3.14	Receptor/ligand-interaction as studied on a single molecule level . . . . .	63
3.15	Forces within single pairs of charged colloids in aqueous Solutions of ionic liquids as studied by optical tweezers . . . . .	63
3.16	Forces of interaction between grafted, blank and grafted-blank colloids by using optical tweezers . . . . .	64
3.17	Interaction forces between a single pair of charged colloids as measured by Optical Tweezers . . . . .	67
3.18	The effective hydrodynamic radius of single DNA-grafted colloids as measured by fast brownian motion analysis . . . . .	67

3.19	Single colloid electrophoresis on DNA-grafted colloids . . . . .	69
3.20	Funding . . . . .	70
3.21	External Cooperations . . . . .	71
3.22	Publications . . . . .	72
3.23	Graduations . . . . .	73
3.24	Guests . . . . .	74
<b>4</b>	<b>Physics of Interfaces</b>	<b>75</b>
4.1	Introduction . . . . .	75
4.2	Freezing-Melting Hysteresis of Fluids in Disordered Pores . . . . .	76
4.3	Diffusion and Phase Equilibria of Binary Fluids in Mesopores . . . . .	77
4.4	Self-Diffusion of Polystyrene Solutions in Porous Acrylate-Based Monoliths Studied by $^1\text{H}$ PFG NMR . . . . .	78
4.5	Self-Diffusion Studies in CuBTC by PFG NMR and MD Simulations . . . . .	79
4.6	$^{13}\text{C}$ NMR Diffusion Studies with $\text{CO}_2$ Adsorbed in MOF CuBTC . . . . .	80
4.7	NMR Studies of Benzene Mobility in Metal-Organic Framework MOF-5 . . . . .	81
4.8	Combining MAS and PFG NMR for the Investigation of Mixtures in Porous Materials . . . . .	82
4.9	Low-Field High-Pressure NMR Porosimetry . . . . .	82
4.10	Anomalies in the Diffusion of Small Molecules in MOF ZIF-8 . . . . .	84
4.11	Zeolitic Imidazolate Framework-8 Molecular Sieve Membrane: From Molecular Diffusion to Membrane Permeation . . . . .	85
4.12	Diffusion Studies on Large-Crystal Ferrierite Zeolites . . . . .	86
4.13	Configurational entropy and intersection blocking effects in multi-component systems in MFI-type zeolites studied by IR microscopy . . . . .	87
4.14	Studies on Adsorption Energy Distributions Computation from Ad- sorption Isotherms by the Ansatz Method . . . . .	88
4.15	Further Advancements in Predicting Adsorption Equilibria using Ex- cess Formalism: Calculation of Adsorption Excesses at the Liquid/Solid Interface . . . . .	89
4.16	Unusual Adsorption Behavior of a Highly Flexible Copper-Based MOF . . . . .	90
4.17	Funding . . . . .	91
4.18	Organizational Duties . . . . .	93
4.19	External Cooperations . . . . .	93
4.20	Publications . . . . .	96
4.21	Graduations . . . . .	102
<b>5</b>	<b>Soft Matter Physics</b>	<b>105</b>
5.1	Introduction . . . . .	105
5.2	Are biomechanical changes necessary for tumor progression? . . . . .	106
5.3	Pattern Formation of actin networks within cell-sized droplets and bulk experiments . . . . .	109
5.4	Origin and Spatial Distribution of Forces in Motile Cells – From fish keratocytes to neuronal growth cones . . . . .	110
5.5	Optical properties of retinal glial cells . . . . .	112

5.6	Oscillations in the lateral pressure in lipid monolayers induced by non-linear chemical dynamics . . . . .	114
5.7	Funding . . . . .	116
5.8	Organizational Duties . . . . .	117
5.9	External Cooperations . . . . .	118
5.10	Publications . . . . .	119
5.11	Graduations . . . . .	121
5.12	Guests . . . . .	123
5.13	Awards . . . . .	123
<b>II</b>	<b>Institute for Experimental Physics II</b>	<b>125</b>
<b>6</b>	<b>Magnetic Resonance of Complex Quantum Solids</b>	<b>127</b>
6.1	Introduction . . . . .	127
6.2	High sensitivity nuclear magnetic resonance probe for anvil cell pressure experiments . . . . .	127
6.3	Cw and Pulsed ESR Spectroscopy of Paramagnetic Framework Cupric Ions in the Zn(II) Doped Porous Coordination Polymer $\text{Cu}_{3-x}\text{Zn}_x(\text{btc})_2$ .	128
6.4	Photodimerization kinetics of co-crystals of <i>trans</i> cinnamamide and phthalic or oxalic acid . . . . .	129
6.5	Optimized NMR Spectroscopic Strategy to Characterize Water Dynamics in Soil Samples . . . . .	129
6.6	Effects of Varying Water Adsorption on $\text{Cu}_3(\text{BTC})_2$ Metal-Organic Framework (MOF) as Studied by $^1\text{H}$ and $^{13}\text{C}$ Solid-State NMR Spectroscopy .	129
6.7	The Jahn-Teller effect in $\text{Cr}^{5+}$ -doped $\text{PbTiO}_3$ : a multi-frequency electron paramagnetic resonance study . . . . .	130
6.8	Size Effects in Fine Barium Titanate Particles . . . . .	130
6.9	Funding . . . . .	131
6.10	Organizational Duties . . . . .	132
6.11	External Cooperations . . . . .	132
6.12	Publications . . . . .	133
6.13	Graduations . . . . .	138
6.14	Guests . . . . .	138
<b>7</b>	<b>Nuclear Solid State Physics</b>	<b>141</b>
7.1	Introduction . . . . .	141
7.2	Spatially resolved quantification of elements in sense associated organs of <i>Drosophila melanogaster</i> . . . . .	142
7.3	Ion beam analysis of atherosclerotic lesions . . . . .	142
7.4	Microcarrier processing in cells using magnetite nanoparticles as reporters . . . . .	144
7.5	Quantification of nanoparticles uptake and distribution in culture cells (A549) at the single cell level . . . . .	146
7.6	Trace element analysis of meteorites using particle induced X-ray emission	147
7.7	High resolution STIM- and PIXE-Tomography . . . . .	148

7.8	In-situ measurement of the resistivity of multi graphene under ion irradiation . . . . .	150
7.9	Creation of 3D microsculptures in PMMA by proton irradiation from multiple angles . . . . .	151
7.10	Structured Agar surfaces produced with PBW for developing neuronal networks with defined topology . . . . .	152
7.11	Creation of multilevel Ni-microstructures and submicrometer structures in InP by PBW . . . . .	153
7.12	Improvement of the energy resolution of the STIM and RBS setup at the LIPSION nanoprobe . . . . .	154
7.13	Investigation of TiO <sub>2</sub> nanomaterials by TDPAC . . . . .	154
7.14	Funding . . . . .	155
7.15	Organizational Duties . . . . .	156
7.16	External Cooperations . . . . .	157
7.17	Publications . . . . .	158
7.18	Graduations . . . . .	163
7.19	Guests . . . . .	164
<b>8</b>	<b>Semiconductor Physics</b>	<b>165</b>
8.1	Introduction . . . . .	165
8.2	Epitaxial Domains . . . . .	166
8.3	Low-temperature processed Schottky-gated field-effect transistors based on amorphous gallium-indium-zinc-oxide thin films . . . . .	168
8.4	Light and temperature stability of fully transparent ZnO-based inverter circuits . . . . .	170
8.5	Gate- and drain-Lag effects in (Mg,Zn)O-based metal-semiconductor field-effect Transistors . . . . .	172
8.6	Transparent rectifying contacts for visible-blind ultraviolet photo-diodes based on ZnO . . . . .	174
8.7	Wavelength-selective metal-semiconductor-metal photodetectors based on (MgZn)O-heterostructures . . . . .	176
8.8	Multi-barrier ZnO-Schottky contacts . . . . .	178
8.9	ZnO-based microresonators – design, photonic mode structure, and mode occupation . . . . .	179
8.9.1	Cavity-photon dispersion in anisotropic planar microresonators	180
8.9.2	Non-linear occupation of the lower polariton branch in a ZnO-based microresonator . . . . .	181
8.9.3	ZnO mesa-structures in planar microcavities . . . . .	182
8.9.4	Planar microresonators with a MgZnO/ZnO-quantum well . . .	183
8.10	Index matching in BaTiO <sub>3</sub> / SrTiO <sub>3</sub> heterostructures . . . . .	185
8.11	Investigation of the temperature-dependent exciton localization in MgZnO	187
8.12	Photoluminescence and transmission spectroscopy on ZnO/MgZnO quantum well structures . . . . .	188
8.13	Thermal stability of ZnO/ZnCdO/ZnO double heterostructures . . . . .	190
8.14	MgZnO/ZnO quantum well nanowire heterostructures with large confinement energies . . . . .	191
8.15	Strain distribution in bent ZnO microwires . . . . .	192

8.16	Characteristics of excitons in a 1D model alloy . . . . .	194
8.17	Hexagonal phase of BaTiO <sub>3</sub> occurring in BaTiO <sub>3</sub> -ZnO-heterostructures at room temperature . . . . .	195
8.18	Strain in Mg <sub>x</sub> Zn <sub>1-x</sub> O ( $x \leq 0.04$ ) thin films on ZnO:Al buffer . . . . .	197
8.19	Magnetic properties of manganese doped Zirconia thin films . . . . .	198
8.20	Structural and electrical properties of zinc ferrite thin films grown by pulsed-laser deposition . . . . .	199
8.21	Structural and magnetic properties of Zn <sub>1-x</sub> Fe <sub>x</sub> O <sub>z</sub> thin films grown on a-sapphire for $0.1 \leq x \leq 0.67$ . . . . .	201
8.22	Electrical and structural properties of Zn-Co-O thin films . . . . .	203
8.23	Electrical conductivity of Mn-doped Zirconia thin films. . . . .	205
8.24	Electrical and optical properties of H plasma-doped ZnO single crystals	206
8.25	Thermal admittance spectroscopy on non-polar a-plane homoepitaxial ZnO thin films . . . . .	208
8.26	Strain induced deep states in MgZnO . . . . .	210
8.27	Nickel-related defects in ZnO thin films . . . . .	211
8.28	Luminescence properties of fresnoite Ba <sub>2</sub> TiSi <sub>2</sub> O <sub>8</sub> thin films and bulk materials . . . . .	213
8.29	Identification of pre-breakdown mechanism of silicon solar cells at low reverse voltages . . . . .	214
8.30	Funding . . . . .	216
8.31	Organizational Duties . . . . .	218
8.32	External Cooperations . . . . .	219
8.33	Publications . . . . .	220
8.34	Graduations . . . . .	228
8.35	Guests . . . . .	230
<b>9</b>	<b>Solid State Optics and Acoustics</b>	<b>231</b>
9.1	Introduction . . . . .	231
9.2	Characterization of acoustic lenses with the Foucault test by confocal laser scanning microscopy . . . . .	232
9.3	Determination of longitudinal sound velocity and acoustic impedance of thin chitosan films by phase-sensitive acoustic microscopy . . . . .	235
	9.3.1 V(z) technique for materials characterization . . . . .	236
	9.3.2 PSAM acoustic reflectivity analysis . . . . .	237
9.4	Advances in phase-sensitive acoustic microscopy studies of thin poly- mer blend films: annealing effects and micro-elastic characterization of PS/PMMA blends . . . . .	238
	9.4.1 Structural Characterization . . . . .	238
	9.4.2 Quantitative Characterization . . . . .	240
9.5	Synchronous monitoring of muscle dynamics and muscle force for max- imum isometric tetanus . . . . .	242
	9.5.1 Method . . . . .	243
	9.5.2 Discussion . . . . .	244
	9.5.3 Conclusion . . . . .	245
	9.5.4 Acknowledgement . . . . .	245

9.6	Focused GHz ultrasound as a tool for micro-displacement and cell manipulation . . . . .	246
9.6.1	Conclusion . . . . .	247
9.7	Lumped circuit mechanical models and lattice dynamics approach to the dependence of the time-of-flight of bulk and guided acoustical modes on elongation . . . . .	248
9.7.1	Harmonic vibrations . . . . .	248
9.7.2	Generalized vibrations including harmonic and anharmonic effects	249
9.7.3	Conclusion . . . . .	251
9.7.4	Acknowledgement . . . . .	252
9.8	Funding . . . . .	252
9.9	Organizational Duties . . . . .	252
9.10	External Cooperations . . . . .	253
9.11	Publications . . . . .	253
9.12	Graduations . . . . .	255
9.13	Guests . . . . .	255
<b>10</b>	<b>Superconductivity and Magnetism</b>	<b>257</b>
10.1	Introduction . . . . .	257
10.2	Tailoring Magnetic Interlayer Coupling in $\text{La}_{0.7}\text{Sr}_{0.3}\text{MnO}_3/\text{SrRuO}_3$ Superlattices . . . . .	257
10.3	Inverted hysteresis and giant exchange bias in $\text{La}_{0.7}\text{Sr}_{0.3}\text{MnO}_3/\text{SrRuO}_3$ superlattices . . . . .	258
10.4	Structural symmetry and magnetocrystalline anisotropy of $\text{SrRuO}_3$ films on $\text{SrTiO}_3$ (001) . . . . .	259
10.5	Detection of ferromagnetic signals in common diamagnetic oxide crystals	260
10.6	Disordered electrical potential observed on the surface of $\text{SiO}_2$ by electric field microscopy . . . . .	261
10.7	The influence of $\text{Ga}^+$ irradiation on the transport properties of mesoscopic conducting thin films . . . . .	262
10.8	Giant negative photoresistance of $\text{ZnO}$ single crystals . . . . .	263
10.9	Funding . . . . .	264
10.10	Organizational Duties . . . . .	264
10.11	External Cooperations . . . . .	265
10.12	Publications . . . . .	266
10.13	Graduations . . . . .	268
10.14	Guests . . . . .	268
<b>III</b>	<b>Institute for Theoretical Physics</b>	<b>271</b>
<b>11</b>	<b>Computational Quantum Field Theory</b>	<b>273</b>
11.1	Introduction . . . . .	273
11.2	Large-Scale Computer Simulations of Spin Glasses . . . . .	274
11.3	Shape Anisotropy of Polymers in Disordered Environment . . . . .	276
11.4	Scaling Behaviour of Self-Avoiding Walks on Critical Ising Clusters . .	278

11.5	Mass Transport by Thermal Ratchets . . . . .	279
11.6	Stochastic Transport Models . . . . .	281
11.7	Birth of the First Large Condensation Droplet . . . . .	282
11.8	Hierarchies in Peptide Nucleation Transitions . . . . .	284
11.9	Polymer Crystallization with Advanced Multicanonical Monte Carlo Methods . . . . .	286
11.10	The Influence of Grafting onto Freezing, Collapse and Adsorption of a Single Polymer in Solution . . . . .	287
11.11	Thermodynamics of Polymer Adsorption to a Flexible Membrane . . .	289
11.12	Microscopic Mechanism of Peptide Adhesion to Semiconductor Sub- strates: Simulations and Experiments . . . . .	290
11.13	Replica-Exchange Simulations of Polymers on GPUs . . . . .	292
11.14	Ground-State Analysis of Tip4p Water Parameterizations in the Ice $I_h$ Phase . . . . .	294
11.15	Quantum Critical Phenomena in Uniform and Mixed Heisenberg Spin Chains . . . . .	295
11.16	Re-Examining the Quantum Compass Model with Screw-Periodic Bound- ary Conditions . . . . .	296
11.17	Monte Carlo Simulations with the Worm Algorithm . . . . .	298
11.18	Self-Adaptive Simulations of Critical Phenomena . . . . .	300
11.19	Critical Amplitude Ratios of the Baxter-Wu Model . . . . .	301
11.20	Geometrothermodynamics Applied to Black Holes . . . . .	302
11.21	Cross Correlations in Statistical Error Estimation . . . . .	303
11.22	Funding . . . . .	304
11.23	Organizational Duties . . . . .	306
11.24	External Cooperations . . . . .	307
11.25	Publications . . . . .	310
11.26	Graduations . . . . .	315
11.27	Guests . . . . .	315
<b>12</b>	<b>Molecular Dynamics / Computer Simulation</b>	<b>319</b>
12.1	Introduction . . . . .	319
12.2	Analytical Treatment and Computer Simulations of the influence of the crystal surface on the exchange of guest molecules between zeolite nanocrystals and the surrounding gas phase . . . . .	320
12.3	Diffusion and Rotation of Water in the Zeolite Chabazite . . . . .	320
12.4	Investigation of the rotation and diffusion of pentane in the zeolite ZK5	321
12.5	Diffusion of Guest Molecules in Metal Organic Frameworks . . . . .	322
12.6	Funding . . . . .	322
12.7	Organizational Duties . . . . .	323
12.8	External Cooperations . . . . .	323
12.9	Publications . . . . .	324
12.10	Graduations . . . . .	325
12.11	Guests . . . . .	325

<b>13 Quantum Field Theory and Gravity</b>	<b>327</b>
13.1 Temperature Dependence of the Casimir Force . . . . .	327
13.2 Higher order correlation corrections to color ferromagnetic vacuum state at finite temperature . . . . .	327
13.3 Structure of the gauge orbit space and study of gauge theoretical models	328
13.4 Quantum field theory on non-commutative geometries, quantum field theory and cosmology, generally covariant quantum field theory . . . .	329
13.5 Funding . . . . .	329
13.6 Organizational Duties . . . . .	330
13.7 External Cooperations . . . . .	331
13.8 Publications . . . . .	332
13.9 Graduations . . . . .	333
13.10 Guests . . . . .	334
<b>14 Statistical Physics</b>	<b>335</b>
14.1 Introduction . . . . .	335
14.2 Dynamical Conductivity at the Dirty Superconductor-Metal Quantum Phase Transition . . . . .	336
14.3 Quantitative description of Josephson-like tunneling in quantum Hall exciton condensates . . . . .	338
14.4 Funding . . . . .	339
14.5 Organizational Duties . . . . .	339
14.6 External Cooperations . . . . .	339
14.7 Publications . . . . .	340
14.8 Guests . . . . .	341
<b>15 Theory of Condensed Matter</b>	<b>343</b>
15.1 Introduction . . . . .	343
15.2 First-passage and First-exit Times of a Bessel-like Stochastic Process . . . . .	344
15.3 Stochastic Phenomena in Systems with Many Degrees of Freedom . . . . .	344
15.4 Randomly Evolving Idiotypic Networks . . . . .	345
15.5 T Cell Regulation and Allergy . . . . .	346
15.6 Tube width Fluctuations in F-Actin Solutions . . . . .	347
15.7 Dynamical stretching and relaxation response of a biopolymer held by an optical trap . . . . .	348
15.8 Inelastic mechanics of biopolymer networks . . . . .	349
15.9 Hot Brownian Motion—Effective Theory and Molecular Simulation . .	349
15.10 Aeolian sand transport . . . . .	350
15.11 Funding . . . . .	351
15.12 Organizational Duties . . . . .	352
15.13 External Cooperations . . . . .	353
15.14 Publications . . . . .	354
15.15 Graduations . . . . .	356
15.16 Awards . . . . .	357

**Author Index**

**359**

# 1

## Structure and Staff of the Institutes

### 1.1 Institute for Experimental Physics I

#### 1.1.1 Office of the Director

Prof. Dr. Josef A. Käs (director)

Prof. Dr. Frank Cichos (vice director)

#### 1.1.2 Molecular Nano-Photonics, Molekulare Nanophotonik [MON]

Prof. Dr. Frank Cichos

##### Secretary

Christine Adolph

##### Technical staff

Dipl.-Phys. Uwe Weber

##### PhD candidates

Subhasis Adhikari, M.Sc.

Dipl.-Phys. Nicole Amecke

Dipl.-Phys. Nils Neubauer

Dipl.-Phys. Martin Pumpa

Dipl.-Phys. Romy Radünz

Markus Selmke

Dipl.-Phys. Rebecca Wagner

##### Students

Marco Braun

Leander Fiedler

Georg Kropat

#### 1.1.3 Molecular Physics, Molekülphysik [MOP]

Prof. Dr. F. Kremer

**Secretary**

Karin Girke

**Technical staff**

Hartmut Domröse

Ines Grünwald

Dipl.-Phys. Cordula Bärbel Krause

Dipl.-Ing. Jörg Reinmuth

Dipl.-Phys. Wiktor Skokow

**Academic staff**

Dr. Mahdy El Mahdy

Dr. Christof Gutsche

Dr. Malgozarta Jasiurkowska

Dr. Periklis Papadopoulos

Dr. Joshua Rume Sangoro

**PhD candidates**

Roxana Ene, M. Sc.

Ciprian Ghiorghita Iacob, M. Sc.

Dipl. -Phys. Kati Kegler

Wycliffe Kiprop Kipnusu, M. Sc.

Dipl. -Phys. Wilhelm Kossack

Dipl. -Phys. Christina Krause

Emmanuel Urandu Mapesa, M. Sc.

Ilya Semenov, M. Sc.

Dipl. -Phys. Gunter Stober

Dipl. -Phys. Martin Treß

Dipl. -Phys. Olaf Überschär

Dipl. -Phys. Carolin Wagner

**Students**

Tilman Schubert

Tim Stangner

Immanuel Weidner

**1.1.4 Physics of Interfaces,  
Grenzflächenphysik [GFP]**

Dr. habil. Frank Stallmach

**Technical staff**

Dipl.-Phys. Cordula Bärbel Krause

Lutz Moschkowitz

Stefan Schlayer

**Academic staff**

Dr. Christian Chmelik  
Dr. Muslim Dvoyashkin  
Prof. Dr. Dieter Freude  
Dr. Karen Friedemann  
Dr. habil. Grit Kalies  
Prof. Dr. Jörg Kärger  
Dr. Sergej Naumov  
Dr. habil. Frank Stallmach  
Dr. Rustem Valiullin

**PhD candidates**

Dipl.-Phys. Steffen Beckert  
Dipl.-Phys. Tomas Binder  
Dipl.-Chem. Filipe Furtado  
Dipl.-Phys. Marcel Gratz  
Dipl.-Phys. Florian Hibbe  
Dipl.-Phys. Carsten Horch  
Dipl.-Math. Daria Kondrashova  
Dipl.-Phys. Dirk Mehlhorn  
Dipl.-Geol. Ivonne Mitreiter  
Dipl.-Phys. Anne-Kristin Pusch  
Dipl.-Phys. Tobias Titze  
Dipl.-Phys. Markus Wehring  
Dipl.-Phys. Philipp Zeigermann

**Students**

Ramona Y.G. Baum  
Maria Fuchs  
Markus Fuchs  
Stefan Hertel  
Kathleen Kirchner  
Tom Kirchner  
Alexander Lauerer  
André Müller  
Friederike Pielenz  
Tino Viertel  
Erik Zabel

**1.1.5 Soft Matter Physics,  
Physik der weichen Materie [PWM]**

Prof. Dr. Josef A. Käs

**Secretary**

Claudia Brück

**Technical Staff**

Dipl.-Ing. Undine Dietrich  
Dipl.-Phys. Bernd Kohlstrunk  
Ing. Elke Westphal

**Academic Staff**

Dr. Mareike Zink  
Dr. Claus Fütterer

**PhD candidates**

Silke Agte, M. Sc.  
Dipl.-Phys. Claudia Brunner  
Valentina Dallacasagrande, M. Sc.  
Susanne Ebert, M. Sc.  
Anatol Fritsch, M. Sc.  
Thomas Fuhs, M. Sc.  
Markus Gyger, M. Sc.  
Dipl.-Phys. Florian Huber  
Dipl.-Phys. Tobias Kießling  
Dipl.-Phys. Melanie Knorr  
Dipl.-Phys. Karla Müller  
Kenechukwu David Nnetu, M. Sc.  
Dipl. Phys. Steve Pawlizak  
Dipl.-Phys. Philipp Rauch  
Dipl.-Phys. Florian Ruckerl  
Dipl. Phys. Sebastian Schmidt  
Dipl. Phys. Jörg Schnauß  
Dipl. Phys. Carsten Schuldt  
David Smith, M. Sc.  
Dipl.-Phys. Roland Stange  
Dipl.-Phys. Dan Strehle  
Dipl.-Phys. Franziska Wetzell  
Dipl.-Phys. Lydia Woiterski

**Students**

Uta Allenstein  
Katharina Ander  
Sebastian Ehrig  
Thomas Els  
Martin Glaser  
Tom Golde  
Steffen Grosser  
Chris Händel  
Tina Händler  
Paul Heine  
Christian Heinrichs  
Lukas Hild  
Tim Hohmann

Michael Krahe  
Sebastian Koth  
Hans Kubitschke  
Sascha Loebel  
Christoph Matern  
Erik Morawetz  
Marcus Purfürst  
Wolfram Pönisch  
Christian Rast  
Angelika Rauch  
Maren Romeyke  
Daniel Rose  
Eva Rose  
Lydia Reuter  
Johannes Stelzer  
Carsten Vogt  
Iris Vonderhaid  
Enrico Warmt  
Luisa Zobelt

## **1.2 Institute for Experimental Physics II**

### **1.2.1 Office of the Director**

Prof. Dr. Marius Grundmann (director)  
Prof. Dr. Tilman Butz (vice director)

since December 2010:

Prof. Dr. Marius Grundmann (director)  
Prof. Dr. Pablo Esquinazi (vice director)

### **1.2.2 Magnetic Resonance of Complex Quantum Solids, Magnetische Resonanz Komplexer Quantenfestkörper [MQF]**

Prof. Dr. Jürgen Haase

#### **Secretary**

Sophie Jung

#### **Technical staff**

Dipl.-Phys. Gert Klotzsche  
Dipl.-Ing. Kathrin Koch

#### **Academic staff**

PD Dr. Marko Bertmer  
Prof. Dr. Andreas Pöppel  
Dr. Damian Rybicki

**PhD candidates**

Farhana Gul-E-Noor, M.Sc.  
Dipl.-Phys. Ingo Hilschenz  
Anusree Viswanath Kuttatheily, M.Sc.  
Dipl.-Phys. Benno Meier  
Dipl.-Phys. Thomas Meinßner  
Dipl.-Phys. Gregor Thörmer  
Dipl.-Phys. Alexander Jäger  
Dipl.-Chem. Bettina Jee  
Michael Jurkutat, M.Sc.  
Dimo Ivanov, M. Sc.

**1.2.3 Nuclear Solid State Physics,  
Nukleare Festkörperphysik [NFP]**

Prof. Dr. Tilman Butz

**Technical staff**

Carsten Pahnke  
Dipl.-Ing. Joachim Starke

**Academic staff**

Dr. Frank Menzel  
Dr. Daniel Spemann  
Dr. Jürgen Vogt

**PhD candidates**

Dipl.-Phys. Tobias Andrea  
Nirva Barapatre, M.Sc.  
Dipl.-Phys. René Feder  
Dipl.-Phys. Steffen Jankuhn  
Dipl.-Phys. (Med.-Phys.)Torsten Koal  
Dipl.-Phys. Christoph Meinecke  
Dipl.-Phys. Martin Rothermel

**1.2.4 Semiconductor Physics,  
Halbleiterphysik [HLP]**

Prof. Dr. Marius Grundmann

**Secretary**

Anja Heck

**SANDiE Network Office/BuildMoNa Office**

Dr. Alexander Weber (Officer)  
Birgit Wendisch (Secretary)

**Technical staff**

Dipl.-Phys. Gabriele Benndorf  
Monika Hahn  
Dipl.-Ing. Holger Hochmuth  
Dipl.-Phys. Jörg Lenzner  
Gabriele Ramm  
Roswitha Riedel

**Academic staff**

Dr. Heiko Frenzel  
Dr. Karsten Goede  
PD Dr. Michael Lorenz  
PD Dr. Rainer Pickenhain  
Prof. Dr. Bernd Rheinländer (retired)  
Dr. Rüdiger Schmidt-Grund  
Dr. Alexander Weber  
Dr. Holger von Wenckstern

**PhD candidates**

Dipl.-Phys. Tammo Böntgen  
Dipl.-Phys. Kerstin Brachwitz  
Dipl.-Phys. Matthias Brandt  
Dipl.-Phys. Christof Peter Dietrich  
Dipl.-Phys. Helena Hilmer  
Dipl.-Phys. Fabian Klüpfel  
Dipl.-Phys. Christian Kranert  
Dipl.-Phys. Alexander Lajn  
Dipl.-Phys. Martin Lange  
Dipl.-Phys. Michael Lorenz  
Dipl.-Phys. Alexander Müller  
Dipl.-Phys. Stefan Müller  
Dipl.-Phys. Friedrich Leonhard Schein  
Dipl.-Phys. Florian Schmidt  
Dipl.-Phys. Matthias Schmidt  
Dipl.-Phys. David Schumacher  
Dipl.-Phys. Marko Stölzel  
Dipl.-Phys. Chris Sturm  
Dipl.-Phys. Gregor Zimmermann  
Dipl.-Phys. Jan Zippel  
Dipl.-Phys. Zhang Zhipeng

**Students**

Michael Bonholzer  
Tobias Diez  
Lars Heerklotz  
Tobias Herzig  
Robert Karsthof  
Johannes Kupper

Annekatriin Meißner  
Katja Mexner  
Tom Michalsky  
Anna Reinhardt  
Peter Schwinkendorf  
Julia Tesch

### **1.2.5 Solid State Optics and Acoustics, Festkörperoptik und -akustik [FKO]**

Prof. Dr. Wolfgang Grill

#### **Secretary**

Annette Käthner

#### **Technical staff**

PTA Hans-Joachim vom Hofe  
Dipl.-Ing. (FH) Ulrike Teschner

#### **Academic staff**

Dr. Gerhard Birkelbach  
Dr. Albert Kamanyi  
Dr. Mieczyslaw Pluta

#### **PhD candidates**

Amro Abdelrahman, M.Sc.  
Esam Eldin Ahmed Mohamed, M.Sc.  
Umar Amjad, M.Sc.  
Dipl.-Phys. Erik von der Burg  
Dipl.-Phys. Moritz von Buttlar  
Albert Kamanyi, M.Sc.  
Zakir Hossain Muhammad, M.Sc.  
Khurram Shahzad Tarar, M.Sc.

#### **Students**

Stefan Friedländer  
Diwaker Jha  
Hermann Klinghammer  
David Schüle  
Markus Sommerfeld

### **1.2.6 Superconductivity and Magnetism, Supraleitung und Magnetismus [SUM]**

Prof. Dr. Pablo Esquinazi

#### **Secretary**

Sandy Ehlers

**Technical staff**

Dr. Winfried Böhlmann  
Klaus Grünwald  
Dipl.-Krist. Annette Setzer

**Academic staff**

Dr. José Barzola-Quiquia  
Dr. Prasanta Kumar Muduli  
PD Dr. Michael Ziese

**PhD candidates**

Ana Ballestar  
Francis Bern (since 11/2010)  
Srujana Dusari  
Muhammad Khalid  
Tuhin Maity  
Humberto Peredo

**Students**

Rosa Bagul  
Francis Bern  
Justus Krüger  
Alexander Lessig  
Thomas Megel  
Axel Molle  
Andreas Schadewitz

## **1.3 Institute for Theoretical Physics**

### **1.3.1 Office of the Director**

Prof. Dr. Rainer Verch (director)  
Prof. Dr. Klaus Kroy (vice director)

**Secretary**

Susan Hussack  
Gabriele Menge  
Lea Voigt

### **1.3.2 Computational Quantum Field Theory, Computerorientierte Quantenfeldtheorie [CQT]**

Prof. Dr. Wolfhard Janke

**Academic staff**

Dr. Elmar Bittner

**PhD candidates**

Dipl.-Phys. Mathias Aust  
Dipl.-Phys. Rainer Bischof  
Dipl.-Phys. Mario Collura (jointly with Nancy Université)  
Dipl.-Phys. Niklas Fricke  
Dipl.-Phys. Monika Möddel  
Dipl.-Phys. Hannes Nagel  
Dipl.-Phys. Andreas Nußbaumer  
Dipl.-Phys. Jeremi Ochab (jointly with Jagiellonian University Krakow)  
Dipl.-Phys. Sebastian Schöbl  
Dipl.-Phys. Micha Wiedenmann

**Students**

Kieran Austin  
Eugen Ehrenpreis  
Max Gerlach  
Jonathan Groß  
Momchil Ivanov  
Steffen Karalus  
Martin Marenz  
Marco Müller  
Andreas Wagner  
Benjamin Winkler  
Johannes Zierenberg

**1.3.3 Molecular Dynamics / Computer Simulation,  
Moleküldynamik / Computersimulation [MDC]**

PD Dr. H. L. Vörtler (Speaker)  
PD Dr. S. Fritzsche

**Academic staff**

PD Dr. H. L. Vörtler  
PD Dr. S. Fritzsche  
Dr. O. Saengsawang

**PhD candidates**

Dipl.-Phys. M. Knauth  
MSc. K. Seehamart  
MSc. R. Channajaree  
Msc. U. Arsawang

**Students**

K. Kirchner  
L. Hertäg  
S. Reimann  
M. Stiller  
P. Schierz

### 1.3.4 Quantum Field Theory and Gravity, Quantenfeldtheorie und Gravitation [QFG]

Prof. Dr. Gerd Rudolph (Speaker)  
Prof. Dr. Rainer Verch

Prof. em. Bodo Geyer (retired)  
Prof. em. Armin Uhlmann (retired)

#### Academic staff

Priv.-Doz. Dr. Michael Bordag  
Dr. José M. Muñoz-Castañeda  
Dr. Matthias Schmidt

#### PhD candidates

MSc Zhirayr Avetisyan  
Dipl.-Phys. Marcus Borris  
Dipl.-Phys. Benjamin Eltzner  
Dipl.-Phys. Alexander Hertsch  
Dipl.-Phys. Thomas Ludwig  
Dipl.-Phys. Jan Zschoche

#### Students

Erik Fuchs  
Florian Fürstenberg  
Leander Fiedler  
Michael Gransee  
Mathias Hänsel  
Martin Hofmann  
André Jäschke  
Alexander Knospe  
Falk Lindner  
Adam Reichold  
Michael Schellenberger Costa  
Martin Teuchler

### 1.3.5 Statistical Physics, Statistische Physik [STP]

Prof. Dr. Bernd Rosenow

#### Academic staff

Dr. Mats Horsdal  
Dr. Timo Hyart  
Dr. Tony Wright

#### PhD candidates

Mirco Milletari, M. Sc.  
Martin Treffkorn, M. Sc.  
Dipl. Phys. Björn Zocher

### **1.3.6 Theory of Condensed Matter, Theorie der kondensierten Materie [TKM]**

Prof. Dr. Ulrich Behn (Speaker)

Prof. Dr. Klaus Kroy

Prof. Dr. Dieter Ihle (retired)

Prof. Dr. Adolf Kühnel (retired)

#### **Academic staff**

Dr. Dipanjan Chakraborty

#### **PhD candidates**

Dipl.-Phys. Jens Glaser

Dipl.-Phys. Marcel Hennes

Dipl.-Phys. Holger Schmidtchen

Dipl.-Phys. Daniel Rings

Dipl.-Phys. Sebastian Sturm

Dipl.-Phys. Lars Wolff

#### **Students**

Frank Anselmi

Jakob Bullerjahn

Matti Gralka

Michael Handrek

Marc Höll

Lukas Kimme

Andreas Kühn

Norma Kühn

Andrea Kramer

Damaris Kröber

Rüdiger Kürsten

Marc Lämmel

Heinz Sachsenweger

Benjamin Werner

Sven Willner

### **1.3.7 Theory of Elementary Particles, Theorie der Elementarteilchen [TET]**

Prof. Dr. Klaus Sibold

#### **Academic staff**

PD Dr. Roland Kirschner

PD Dr. Arwed Schiller

Dr. Meinulf Göckeler

Dr. Yi Liao

#### **PhD candidates**

Dipl.-Phys. Christoph Dehne

Dipl.-Phys. Alexander Ivanov

**I**

**Institute for Experimental Physics I**



# 2

## Molecular Nanophotonics

### 2.1 Introduction

The challenge of experimental physics on the nanoscale is to access local phenomena, that occur for example at interfaces, at specific molecular sites or at certain places within nano-structured materials. These local phenomena may control molecular dynamics, drive self-organization, cause charge separation or alter light propagation. Their importance extends to almost every field involved in future nanotechnology. The research of the molecular nano-photonics group thus aims at the development and application of optical techniques to access nanoscale (dynamical) processes in various fields such as chemical physics, biology or semiconductor physics. The understanding of these dynamical processes shall ultimately lead to a control over single molecules and other nano-objects by applying heat, flow, shear forces, electric fields or current.

The main experimental tool within our research is optical single molecule detection by ultra-sensitive microscopic techniques including time-resolved confocal microscopy, wide-field fluorescence or photothermal microscopy. Single molecules or semiconductor quantum dots provide the ideal local probes to access nanoscale physical properties inside materials while keeping the information on the heterogeneity of the system. Using these techniques recent projects focused on the

- Photothermal detection of single gold nanoparticles and nanorods
- Thermally propelled particles and micromachines
- Nanometric distance measurements with single gold nanoparticle pairs
- Electrochemical manipulation of the emission of colloidal semiconductor nanocrystals
- Defocused imaging of single emitters in photonic crystals
- Single molecule diffusion in ultrathin confined liquid films, polymers and liquid crystals

During the year 2010 the Molecular Nanophotonics Group has achieved the following important scientific goals

- The group has developed a quantitative theoretical framework for single particle light scattering in microscopy.
- The group has developed the foundation for absorption-cross section measurements on single molecules and nanoparticles.
- The group has developed and realized concepts for the thermally induced propulsion of particles at the micro and nanoscale.

In the year 2010, the group has contributed significantly to the extension application of the DFG research unit 877 "From Local Constraints to Macroscopic Transport". We have organized several scientific symposia. Collaborations with the group of Prof. Dr. Klaus Kroy (University Leipzig), Prof. Dr. Michael Mertig (TU Dresden) and Prof. Dr. Haw Yang (Princeton University) have been very fruitful. Collaborative measurements with the groups of Prof. Friedrich Kremer and Prof. Markus Grundmann have been carried out.

*Frank Cichos*

## 2.2 Photothermal Microscopy: Signal Generation

M. Selmke, M. Braun, F. Cichos,

While Photothermal (PT) spectroscopy techniques have been used for many decades as a quantitative tool to study absorption by solutes and solvents, its microscopic counterpart has been introduced very recently only and is not yet understood theoretically. This lack of understanding of the signal origin and even qualitative signal shape did not, however, prevent the ever-increasing interest in and sensitivity of PT microscopy. Nowadays, even single molecules [1] or quantum dots may be detected through their absorption. To further push the detection-limits of PT spectroscopy and imaging techniques we have thus investigated the signal in excruciating detail and finally obtained an equally valid and tested as well as intuitive and neat picture of the signal generation by absorbing finite-sized nano-objects. Three models of varying degree of accuracy have been devised, one of which is an ab-initio description of the electrodynamic scattering problem within the framework of a generalized LORENTZ-MIE theory (GLMT, [2]), the second being a diffraction model based on the Fraunhofer Integral formulation and the third one being an intuitive ray-optics treatment. While the exact model captures the wealth of phenomena observed identically, its mathematical complexity encrypts the physical picture in a non-trivial manner. Nonetheless, it allowed the certain identification of the refractive-index gradient as the source of the signal and unveiled the signature of the action of a nano-lens. The understanding of a single absorber as an effective divergent nano-lens led to a ray-optics approach. The establishment of an effective focal length and Gaussian beam propagation rules have been applied in order to obtain the PT signal: The nano-lens modifies the divergence, depending on the state of divergence of the probing beam at the position of the lens (the heated absorbing particle). The dispersive signature of the PT signal in axial scans is captured qualitatively and semi-quantitatively (up to a factor of order unity) by this simple model.

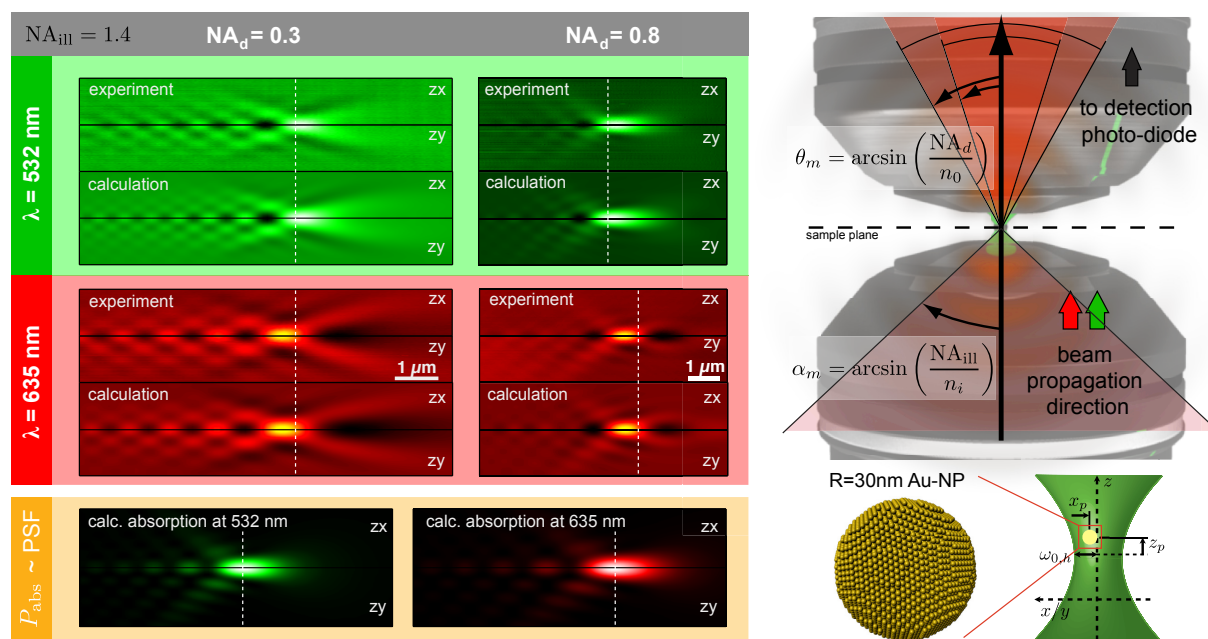


**Figure 2.1:** Confocal scattering signal scans from an 30 nm gold nanoparticle. Comparison of Experiment and Calculation.

Fig. 2.1 displays the results of a full ab-initio treatment of the electromagnetic scattering problem of a cold gold nanoparticle of 30 nm radius. The determined fields were used to calculate the total field Poynting-vector which was integrated over the forward detection angular domain. This detection cone is determined by the numerical aperture of the detection microscope objective. The polarization-resolved details agree with the experimental scans and show an enhanced interference checker-board pattern for low numerical aperture (small detection angle).

- [1] A. Gaiduk, M. Yorulmaz, P. V. Ruijgrok et al., *Science*, 330, 353-356,(2010)
- [2] G. Gouesbet, G. Grehan, B. Maheu, *Journal of Optics-Nouvelle Revue D Optique*, 16, 83-93, (1985).

## 2.3 Self-Propelled Thermophoretic Particles

A. Brugella, F. Cichos,

Using real-time single-particle tracking, we have been able study the dynamics of an asymmetric particle remotely actuated by a thermophoretic heating laser under the condition free of any boundary confinements. We observe strong directionality in the motion of an actuated Janus particle. The directed movement is attributed to the interfacial force caused by the temperature gradient built along the particle surface, where the directionality is a representation of the fidelity of the movement to the particle orientation. From the analysis of movement-orientation correlation, it is deduced that particles obey a directional motion corresponding to the polarity of the particle moving in the direction of the colder side of the particle. The velocity of the particle is found

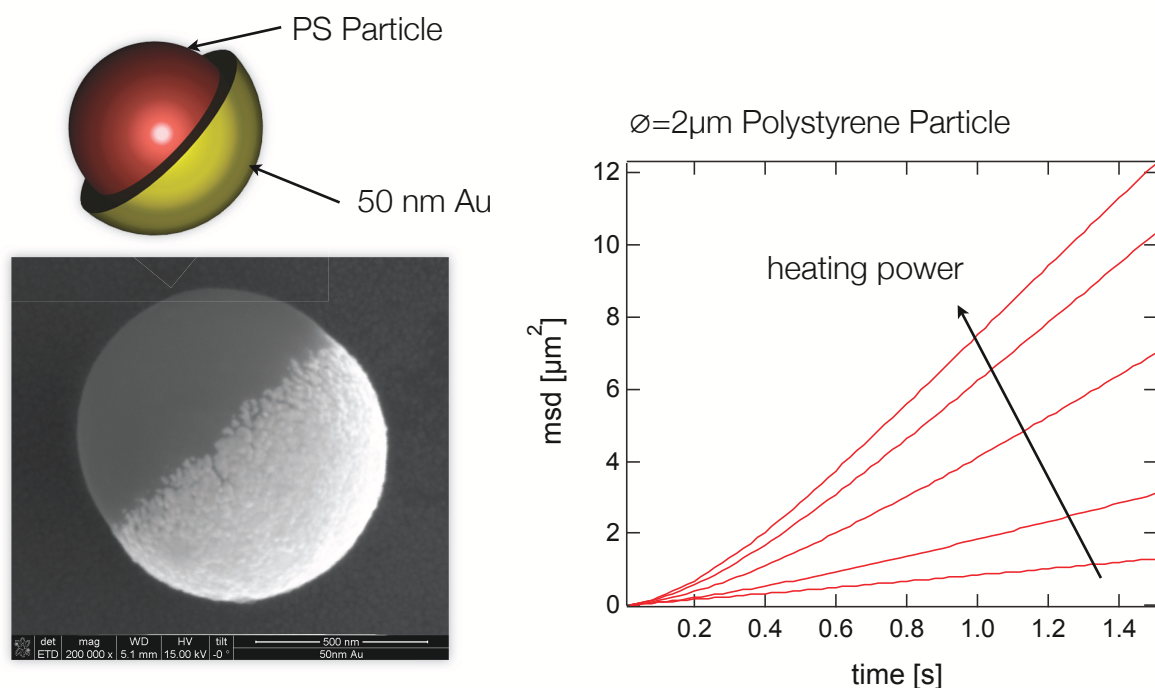


**Figure 2.2:** (left) Electron microscopy image of a single polystyrene particle capped with a 50 nm gold layer. The gold cap is selectively heated by a laser causing a driven Brownian motion in the direction of . The driven Brownian motion is visible in the heating power dependent mean square displacement of the particle (right).

to be proportional to the temperature rise of the gold coated particle side. The directed motion is randomized by the rotational diffusion of the particles. Thus at long times the mean square displacement is found to be purely diffusive again (see Figure 2.2). However, the diffusive motion is strongly enhanced by the thermophoretic driving mechanism. In summary, this type of self-propelled particle delivers the first switchable swimmer employing thermal gradients. More complex structures, which provide stable orientational motion will enhance directional motion and allow for a creation of thermal micromachines.

## 2.4 Twin-Focus Photothermal Correlation Spectroscopy

M. Braun, M. Selmke, D. Rings\*, K. Kroy†, F. Cichos

\*Institute of Theoretical Physics

†Institute of Theoretical Physics

Today, single molecule detection is an indispensable tool to study dynamical processes in complex materials locally by focusing on just one single molecule. It is, however, always restricted to fluorescent probes such as organic dye molecules or quantum dots. Within this project, we develop the technique of photothermal correlation spectroscopy (PhoCS) [1] to trace the dynamics of single non-fluorescent nano-objects such as gold nanoparticles in liquids. Using this technique, the non-equilibrium Brownian motion of

hot gold nanoparticles called Hot Brownian Motion was investigated in collaboration with the group of Prof. Klaus Kroy [2]. Photothermal detection is based on the absorption of light and therefore does not suffer from photo-blinking or photo-bleaching. The role of the absorbed optical energy creates a local temperature field around the absorbing nano-object resulting in a thermal lens, that can be easily detected even though the extinction cross section of the particle itself is far below the single particle detection limit. As the signal generation in photothermal microscopy is now fully understood (XXSelmke2011XX), PhoCS can now be extended to a two focus version, the so-called Twin-PhoCS technique. Here, the phase-relation of the photothermal signal induced by a diffusion particle is used to extract an information on the axial position of the absorbing particle. In particular, the photothermal signal can either be positive or negative for a particle located in the upper or lower part of the detection volume (see Fig. 2.3, *Left*), respectively. The dynamic processes of the diffusion particles may be explored performing a cross-correlation of the positive and negative photothermal signal timetrace (Fig. 2.3, *inset*). In addition, an axial flow can be analyzed by comparing the cross-correlation for positive and negative lagtimes (Fig. 2.3, *Right*). Such an axial flow can be induced by radiation pressure of the involved heating and detection lasers. Using this tool, the radiation pressure can be quantified.

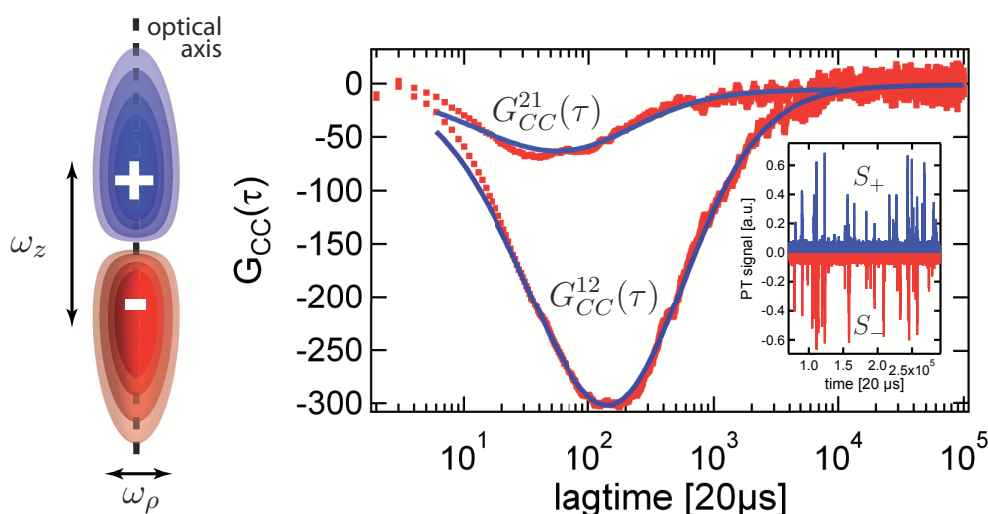


**Figure 2.3:** *Left:* Phase-sensitive photothermal detection volume *Right:* typical cross-correlation for positive ( $G_{CC}^{12}(\tau)$ ) and negative ( $G_{CC}^{21}(\tau)$ ) lagtimes *Inset:* measured timetrace containing positive and negative photothermal signal bursts.

The twin-focus detection volume can be created by adjusting the axial offset of the heating and detection laser focus, i.e. is already intrinsically present. A technical extension of the setup like in conventional dual-focus fluorescence correlation spectroscopy (2fFCS) is not necessary. An implementation of Twin-PhoCS is thus easy and opens up new opportunities to probe the local dynamics of hot nanoparticles, since the advantages of 2fFCS may be adapted to absorbing nano-objects.

- [1] R. Radünz, D. Rings, K. Kroy, F. Cichos, *J. Phys. Chemistry A*, 113, 1674-1677, (2009).
- [2] D. Rings, R. Schachoff, M. Selmke, F. Cichos, K. Kroy, *Phys. Rev. Lett.*, 105, 090604, (2010).

## 2.5 Angle Resolved Fluorescence Spectroscopy in Photonic Crystals

R. Wagner, A. Feist, F. Cichos

Photonic Crystals (PCs) are materials, where the dielectric constant varies periodically on a length scale of the wavelength of visible light. We produce them by vertical deposition of colloidal polystyrene beads, which form a 3D fcc (face centered cubic) lattice. Scattering of light on this structure leads to the development of an optical band structure, which contains so called stop bands, i.e. directions where propagation of light is not possible for a certain wavelength. While the optical density of states is reduced in a stop band, it can be enhanced at the band edges. Since it is direction dependent, the fractional density of optical states (FDoS) has been introduced. It can be measured using internal emitters. An enhanced FDoS amplifies the emission into the corresponding direction, while a reduced FDoS decreases it. Emission spectra are therefore modified as compared to emission in a homogeneous medium.

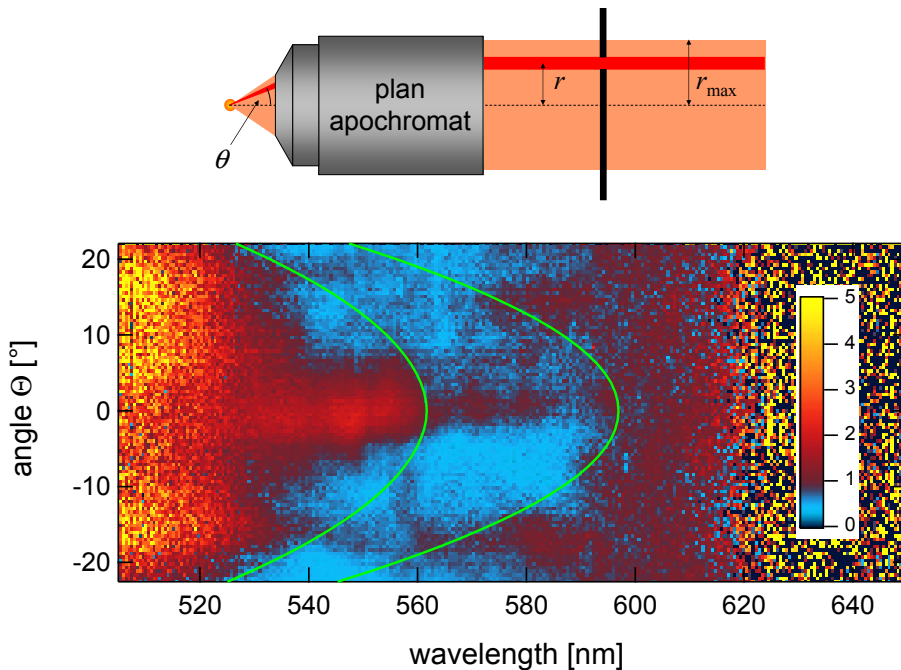


**Figure 2.4:** Top: Definition of quantities for Abbe sine condition. Bottom: FDoS relative to density of states in homogeneous medium. The stop band position clearly follows theoretical predictions. Enhancement is visible for small wavelengths.

We improved a technique we introduced in [1], making it faster and turning it into a method for local measurements. Single fluorescent beads are introduced into the PC to use them as probes for the optical properties of the PC around them. Their emission is detected using an objective with high numerical aperture  $NA$ . Since the objective follows Abbe's sine condition there is a unique relation between the angle of light emission  $\theta$  and the distance  $r$  from the optical axis when the light leaves the objective:

$$\sin \theta = \frac{r NA}{r_{\max} n}$$

Here  $r_{max}$  is the radius of the beam and  $n$  is the effective refractive index of the PC (fig. 2.4, top). By inserting a slit into the parallel beam, that leaves the objective, light from different emission angles is selected. Sending the light through a spectrometer and detecting it using a CCD, up to 100 spectra for different directions can be measured simultaneously. The ratio of the thus measured spectra and spectra of the same beads in a homogeneous medium is the relative FLDoS. It is equal to the ratio of the FDoS in a PC and in a homogeneous medium and is shown in fig. 2.4. The position of the stop band is in agreement to theoretical predictions from band structure simulations performed with a free software package.[2] An enhancement is also visible at the small wavelength edge of the stop band.

[1] M. Barth, A. Gruber, F. Cichos, *Phys. Rev. B*, 72, 085129, (2005).

[2] S. G. Johnson, Steven, J. D. Joannopoulos, *Opt. Express*, 8, 173-190, (2001).

## 2.6 Single Molecule Diffusion in Liquid Crystals

M. Pampa, F. Cichos

In addition to the importance in display technology, liquid crystals (LC) appear in many applications in industry and research. From simple temperature sensors to their use in tuneable photonic crystals and a variety of optical components, wherever they are in use, their unique correlation between structure and dynamics is of importance. To obtain information about this behavior on the  $\mu$  m-scale, we dope the liquid crys-

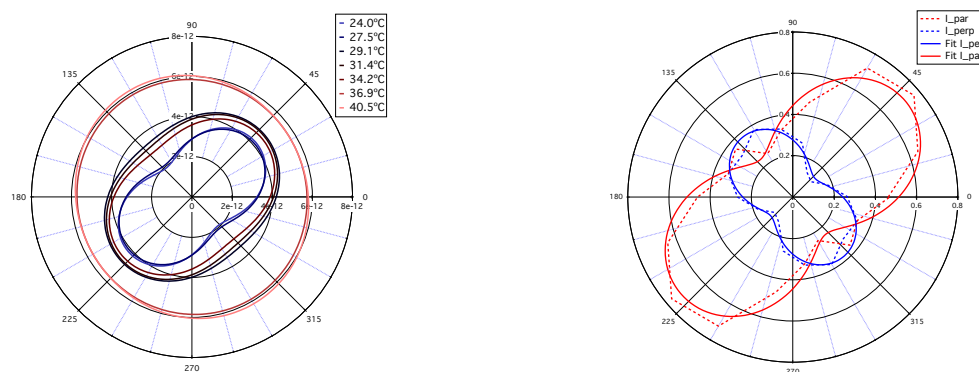


**Figure 2.5:** **left:**Temperature dependent measurement of anisotropic diffusion coefficients in the liquid crystal 8CB. **right:**Angle dependent emission due to polarized excitation, split in two polarization channels, parallel and perpendicular to the polarization of the excitation laser. The symmetry indicates a strong alignment of the fluorophore in the LC matrix.

tal with single fluorescent molecules. The dye reports the dynamical properties of the surrounding LC-Matrix and therefore serve as probes for structure and dynamics. Single molecule tracking experiments at different temperatures reveal a slower motion of the dye molecules in comparison to the LC molecules as studied i.e. in NMR experiments(Fig. 2.5, left graph). Fluorescence depolarization experiments conducted in the group suggest, that the fluorophore is well aligned (Fig. 2.5, right graph) and strongly

interacting with the LC-molecules. This considerably increases the hydrodynamic radius of the dye molecules leading to the slowed down but still anisotropic dynamics of single molecules.

## 2.7 Surface Charges on CdSe/ZnS Semiconductor Quantum Dots in Apolar Solvents

N. Amecke, F. Cichos

CdSe/ZnS semiconductor quantum dots (QDs) are very efficient, photostable, wavelength tunable sources of light in the visible range. They show interrupted emission (blinking) with spectral diffusion and fluctuating lifetime. Those interruptions and shifts are generally assumed to originate from charges tunneling in and out of the crystal core or simply residing and diffusing in its close vicinity. They can lead to non-radiative exciton decay channels (Auger processes) and transition energy shifts (Stark effect). Those effects are distance dependent and strongest for charges directly in the core, being able to quench the fluorescence close to [1] or below the detection limit. However, direct correlation of charged QDs and their emission still needs to be demonstrated. This research project is devoted to the study of quantum dots in electric fields in non-

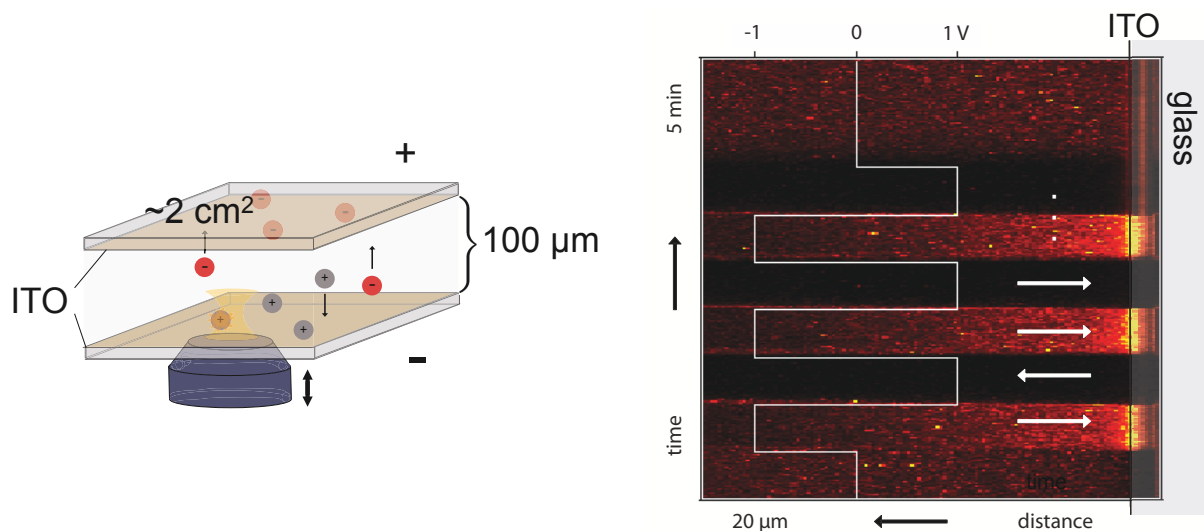


**Figure 2.6:** Left: Measurement cell. Right: Continuous scan of 20 μm per second around the electrode while applying voltage steps of ±1 V

polar solvents to monitor and influence their charge state. This shall help to uncover the details of quantum dot intermittency. For this purpose we have constructed an electrochemical cell for the manipulation of quantum dots in solution and simultaneous fluorescence microscopy. With intensity profiles, velocities and electrical current we can follow the QD motion, charge concentrations and screening in solution. We have thus developed a new method to optically determine charge distribution and motion in a non-polar medium. We find that the majority of fluorescent QDs in toluene (one of the most common solvents) move in the direction of negative potential when a homogeneous electric field is applied. Their remaining high fluorescence intensity and

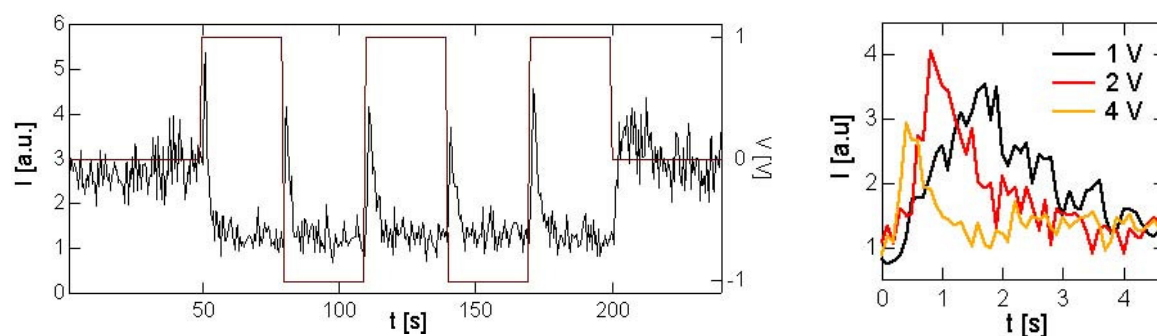


**Figure 2.7:** Fluorescence intensity at equal distance ( $50 \mu\text{m}$ ) from both plates. Left: Passing QDs at  $\pm 1$  V steps. Right: Average of passing QD peak for different voltage steps

lifetime suggest a positive charge on the surface. In contrast, in dodecane, the same QDs show no charge except for a low percentage that can be explained by thermal charging. Comparison of lifetime and intensity in dodecane and toluene show that a positive surface charge itself does not considerably alter a QDs fluorescence. These findings are unexpected and pose new questions on the importance of surface charges in the blinking process.

[1] Nicole Amecke, Frank Cichos, *J. Lum.* 131, 375 - 378, (2011).

## 2.8 Funding

*Light Emission of Single Emitters in 3-dimensional Photonic Crystals*

Frank Cichos

CI 33/5-2

*Ortsaufgelöste Detektion von Struktur und Dynamik in nematischen Phasen biaxialer Moleküle*

Frank Cichos

CI 33/6-1

*FG 877: Constrained Single Molecule Dynamics in Glassy Polymer Systems*

Frank Cichos

CI 33/7-1

*FG 877: Hot Brownian Motion*

Frank Cichos

CI 33/7-2

*FG 877: Static and dynamic properties of DNA-based polymer structures under constraints and confinement*

Frank Cichos

CI 33/11-2

*FG 877: From Local Constraints to Macroscopic Transport*

Frank Cichos

CI 33/12 -1

*BuildMONA, ESF-NFG: Funktionale multiskalige Strukturen*

## 2.9 Organizational Duties

Frank Cichos

- Speaker of the DFG Research Unit 877 "From Local Constraint to Macroscopic Transport"
- Head of the Eignungsfeststellungskommission Fakultät für Physik und Geowissenschaften
- Vice head Promotionsausschuss
- Member of the Prüfungsausschuss
- Member of the Studienkommission
- Organizer of the Physik-Kolloquium der Fakultät für Physik und Geowissenschaften
- Referee: Phys. Rev. B, Phys. Rev. Lett., Nature, Chem. Phys. Lett., Appl. Phys. Lett., ACS Petroleum Research Fund

## 2.10 External Cooperations

**Academic**

- TU Dresden  
Prof. Dr. Michael Mertig
- TU Dresden  
Dr. Ralf Seidel
- TU Chemnitz  
Prof. Dr. Christian von Borczyskowski
- TU Chemnitz  
Dr. Harald Graaf
- Universität Mainz  
Prof. Dr. T. Basché
- Princeton University  
Prof. Dr. H. Yang

## 2.11 Publications

**Journals**

N. Amecke, F. Cichos: Intermediate Intensity Levels During the Emission Intermittency of Single CdSe/ZnS Quantum Dots, J. Lumin. 2010, DOI: 10.1016/j.jlumin.2010.10.026.

S. Adhikari, M. Selmke and F. Cichos: Temperature Dependent Single Molecule Rotational Dynamics in PMA, Physical Chemistry Chemical Physics, 2011, 13, 1849-1856

D. Rings, R. Schachoff, M. Selmke, F. Cichos, K. Kroy, *Phys. Rev. Lett.* 105, 090604, 2010, Hot Brownian Motion

D. Rings, M. Selmke, F. Cichos, K. Kroy: Theory of Hot Brownian Motion, 2010, *Soft Matter*, 2011, 7, 3441-3452

A. Schob, M. Pumpa, M. Selmke, F. Cichos, Measuring Flow Profiles and Slip by Single Molecule Experiments in Thin Liquid Films, *J. Phys. Chem. C*, 2010 (114) 10, p. 4479-4485

D. Kowerko, J. Schuster, N. Amecke, M. Abdel-Mottaleb, R. Dobra, F. Würthner and C. von Borczyskowski: FRET and ligand related NON-FRET processes in single quantum dot-perylene bisimide assemblies, *Phys. Chem. Chem. Phys.*, 2010, 12, 4112-4123

(D. Kowerko, S. Krause, N. Amecke, M. Abdel-Mottaleb, J. Schuster and C. von Borczyskowski: Identification of Different Donor-Acceptor Structures via Förster Resonance Energy Transfer (FRET) in Quantum-Dot-Perylene Bisimide Assemblies, *Int. J. Mol. Sci.* 2009, 10, 5239-5256)

### Talks

R. Wagner: Angle-resolved fluorescence detection by defocused wide-field imaging, 74. DPG Spring Meeting, Regensburg, Germany, 21.-26. March 2010

N. Amecke: Net Charge on Colloidal CdSe/ZnS Evidots in Nonpolar Solvents, 74. DPG Spring Meeting, Regensburg, Germany, 21.-26. March 2010

M. Pumpa: Single Molecule Diffusion in Nematic Liquid Crystals, 74. DPG Spring Meeting, Regensburg, Germany, 21.-26. March 2010

N. Amecke: Fluorescence and Migration of Charged Quantum Dots Dispersed in Toluene, Group Seminar OSMP, TU Chemnitz, Chemnitz, Germany, 22. June 2010

F. Cichos: Photothermal Correlation Spectroscopy, DPC 2010, Argonne National Lab, USA, 20.-25. June 2010

F. Cichos: Photothermal Microscopy Detects a Nanolens, FINW 2010, Biarritz, Frankreich, 21.-24. October 2010

F. Cichos: Molecular Nanophotonics for Biosensor Applications, Workshop des Dresdner Graduiertenkolleg Nano- und Biotechniken für das Packaging elektronischer Systeme, Leipzig, Germany, 29.-30. November 2010

### Posters

G. Kropat, R. Wagner, F. Cichos: Multiple Bragg diffraction in photonic crystals, 74. DPG Spring Meeting, Regensburg, Germany, 21.-26. March 2010

N. Amecke, F. Cichos: Optical Detection of Charged Quantum Dots in Solution, 74. DPG Spring Meeting, Regensburg, Germany, 21.-26. March 2010

N. Amecke, F. Cichos: Positively Charged CdSe/ZnS Quantum Dots in Nonpolar Solvents, NaNaX4, Munich/Tutzing, Germany, 11.-15. April 2010

Marco Braun, Romy Radünz, and Frank Cichos: Temperature mapping of gold nanostructures, 74. DPG Spring Meeting, Regensburg, Germany, 21.-26. March 2010

S. Adhikari, M. Selmke, Frank Cichos, single molecule study on heterogeneous dynamics of polymer PMA close to glass transition temperature, 74. DPG Spring Meeting, Regensburg, Germany, 21.-26. March 2010

M. Selmke, S. Adhikari, F. Cichos: Probing macroscopic viscosity on a sub-nm scale in polymers, CPP 31.4, 74. DPG Spring Meeting, Regensburg, Germany, 21.-26. March 2010

M. Selmke, M. Braun, R. Schachoff, D. Rings, K. Kroy, F. Cichos, Photothermal Correlation Spectroscopy, INTERNATIONAL SOFT MATTER CONFERENCE 2010, Granada, Spain

## 2.12 Graduations

### Diploma

- Georg Kropat  
*Mehrfach-Bragg-Beugung in photonischen Kristallen*  
February 2010
- Marco Braun  
*Optical Temperature Control by Single Gold Nanoparticles*  
December 2010
- Andreas Bregulla  
*Self propelled thermophoretic motion of a gold capped*  
December 2010

### Bachelor

- Armin Feist  
*Angle Resolved Fluorescence Spectroscopy in Photonic Crystals*  
August 2010
- Andre Heber  
*Intensitätsfluktuationen einzelner kolloidaler Halbleiterquantenpunkte*  
November 2010

## 2.13 Guests

- Prof. Dr. Haw Yang  
Princeton University, USA  
05/2010

- Prof. Dr. Markus Arndt  
University Vienna, Austria  
11/2010



# 3

## Molecular Physics

### 3.1 Introduction

*Tempora mutantur nos et mutamur in illis* - times are changing and we are changing in it. While 5 - 10 years ago our group was the first to measure the molecular dynamics in polymer layers as thin as 10 - 20 nm, the focus has changed in the meantime to study molecular assemblies as thin as 2-3 nm and even isolated polymer coils. This could be achieved only due to the development of novel nano-structured electrode arrangements which are now routinely used to determine by Broadband Dielectric Spectroscopy the molecular dynamics in extraordinary wide frequency and temperature ranges. As first result it was shown that the molecular mobility in the 1-dimensional confinement of thin polymer layers is bulk-like down to thicknesses smaller than 5 nm - a finding confirmed as well by Ellipsometry and Calorimetry. Many further highly promising experiments are on course, for instance to unravel the impact of the dimensionality of the geometrical constraints on the dynamics of glass-forming systems. - In our other main fields of activity, polarized time-resolved Fourier-Transform Infrared Spectroscopy and experiments with Optical Tweezers substantial progress was made. The structural levels of organization of spider silk are in the mean time quantitatively understood and the phenomenon of super-contraction in spider silk is well analyzed by deuteration experiments. Furthermore the novel technique of IR Transition Moment Orientational Analysis was developed and proven to be very versatile to analyze the mean orientation and the molecular order parameter of the different moieties in liquid crystalline polymers. In the experiments with Optical Tweezers great progress was made in various fields for instance in determination of the interaction potential between polymer brushes, in measurements on the electrophoretic mobility of single (polymer-grafted) colloids and refined studies on single receptor/ligand contacts. Recently an (HBMG)-application for the first commercially available Optical Tweezers set-up was positively approved - a strong encouragement.

## 3.2 Glassy dynamics of mono-molecular layers of poly(2-vinyl pyridine)

M. Treß, E.U. Mapesa, A. Serghei and F. Kremer

Recently, a preparation method using ultra-flat, highly doped silicon wafers as electrodes which are covered with strongly insulating silica nano-structures as spacers was developed in our group. This enables us to apply Broadband Dielectric Spectroscopy (BDS) to samples which do not exhibit a full surface coverage; in particular, the investigation of the glassy dynamics of ultra-thin layers of polymers down to and below the mono-molecular limit (where the polymer chains form sub-layers) is feasible [1]. In the case of poly(2-vinyl pyridine) (P2VP), it will be possible to study the dynamics of isolated coils which do not interact with each other and hence, can be treated as a statistical average over a single polymer chain in different conformations. First results reveal that in sub-layers with an average thickness of 3 nm neither the mean relaxation rate nor the shape of the relaxation time distribution function is changed compared to the bulk (Fig. 3.1).

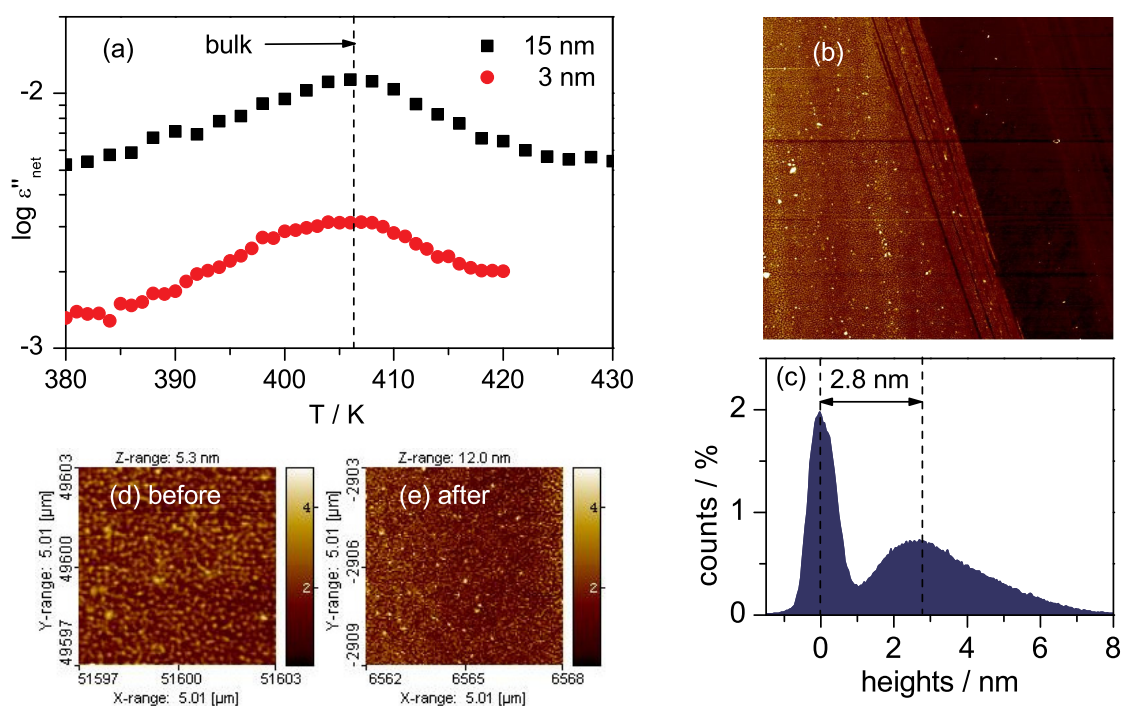


**Figure 3.1:** a) Dielectric loss  $\epsilon''$  versus Temperature of two P2VP samples with thicknesses as indicated recorded at a frequency of 1.2 kHz. The  $\alpha$ -relaxation peak coincides with the corresponding bulk value. b) and c) AFM picture ( $20 \times 20 \mu\text{m}$ ) and histogram of a scratch on the 3-nm-thick sample; the broad distribution of the heights of the polymeric surface indicates the characteristic of a sub-layer. d) and e) AFM pictures ( $5 \times 5 \mu\text{m}^2$ ) of the surface topology of the same sample taken before and after the measurement show the stability of the sample and especially the absence of dewetting; the corresponding values of the root mean square (RMS) roughness are 0.64 nm and 0.96 nm, respectively.

- [1] Tress, M., E. Erber, E. U. Mapesa, H. Huth, J. Müller, A. Serghei, C. Schick, K.-J. Eichhorn, B. Voit and F. Kremer, *Macromolecules*, 43 (2010) 9937-9944

### 3.3 Glassy dynamics and glass transition in nanometric thin layers of polystyrene

E.U. Mapesa, M. Treß, A. Serghei and F. Kremer

In 2009, our group initiated an investigation on the glassy dynamics of ultra-thin ( $\leq 5$  nm) layers of polystyrene (PS) by means of Broadband Dielectric Spectroscopy (BDS) and vis-Ellipsometry under identical and well controlled conditions for a wide range of molecular weights (58.9 kg/mol - 8090 kg/mol). First results examined no shift of  $T_g$  and no broadening in the glassy dynamics for PS layers as thin as 5 nm [1]. Recently, we extended this study by applying AC-calorimetry and X-ray reflectometry and confirmed our previous findings [2]. The characteristic temperature of the  $\alpha$ -relaxation  $T_\alpha$  as well as  $T_g$  of all molecular weights under study lies within a range of 4 K while the experimental error is as big as  $\pm 2$  K. Knowing about the strong impact of the sample preparation the present investigation emphasizes the identical preparation procedures in all applied methods and the resulting coincidence of the findings (Fig. 3.2).

- [1] Mapesa, E. U., M. Erber, M. Treß, A. Serghei, K.-J. Eichhorn, B. Voit and F. Kremer, *EPJ - ST*, 189 (2010) 173-180  
[2] Treß, M., E. Erber, E. U. Mapesa, H. Huth, J. Müller, A. Serghei, C. Schick, K.-J. Eichhorn, B. Voit and F. Kremer, *Macromolecules*, 43 (2010) 9937-9944

### 3.4 Glassy dynamics in thin layers of cis-polyisoprene

E.U. Mapesa, M. Treß and F. Kremer

Broadband Dielectric Spectroscopy (BDS) - in combination with a nanostructured electrode arrangement - is used to study thin layers of cis-1,4-polyisoprene. From the viewpoint of BDS, polyisoprene belongs to a special type of polymers because a part of its molecular dipole moment attached to each monomer unit is aligned along the main chain. This fraction adds up to one dipole moment of the whole polymer chain corresponding to the end-to-end vector of the molecule. This enables the investigation of two distinct relaxation modes taking place at two different length scales: the segmental motion which involves structures of about one nanometer in size (2 to 3 monomer units) and the normal mode which represents the dynamics of the whole macromolecule. Previous studies [1-3] involved the evaporation of a metal counter-electrode onto the spin-cast layer. As a result of this (sandwich) geometry, a confinement-induced mode shows up between the normal and segmental modes, and gains dielectric strength with reducing film thickness at the expense of that of the normal mode. In the current study - where highly insulating silica nanostructures are used as spacers - one interface is free. The spin-cast samples are checked before and after dielectric measurement so that any

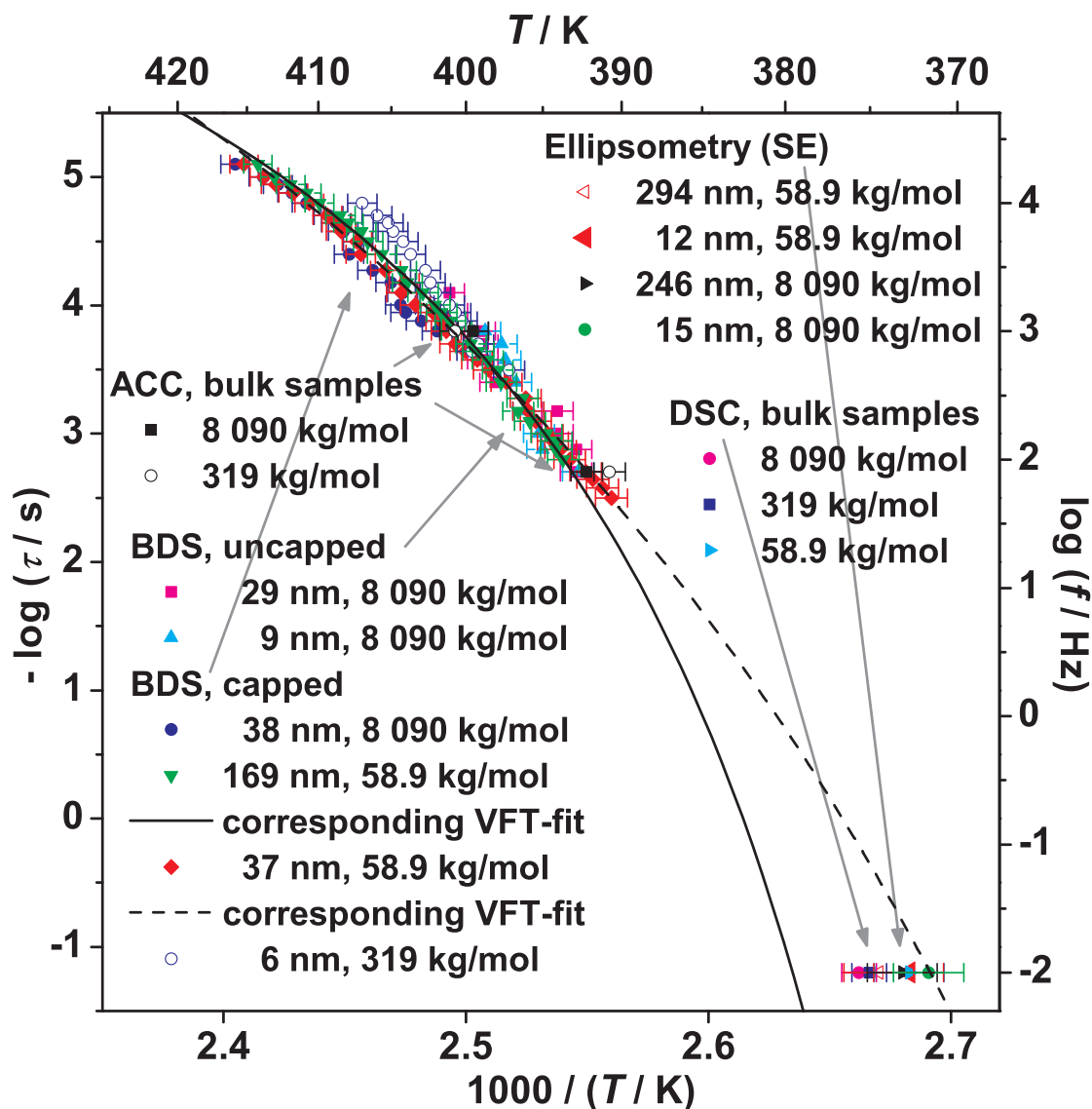


**Figure 3.2:** Logarithm of the inverse relaxation time plotted versus inverse temperature for several PS samples (of diverse thicknesses and molecular weights) measured by different experimental methods as indicated. The dashed and solid line are fits of the Vogel-Fulcher-Tammann equation to the BDS data of the 37 nm and 169 nm sample (58.9 kg/mol). The inset shows the molecular weight dependence of  $T_g$  and  $T_\alpha$  (recorded at a frequency of 1 kHz) for bulk samples measured with different techniques.

dewetted layers are excluded from this study Fig. 3.3). Down to 7 nm, it is observed (figure 2) that: (i) the segmental mode as a local relaxation process is unaffected by the 1-D confinement; (ii) the normal mode becomes faster with decreasing layer thickness; (iii) the normal mode gains dielectric strength with reducing layer thickness; and (iv) the so-called confinement-induced mode does not show up. For a quantitative analysis of these intriguing observations, simulations are planned to be carried out where the chain is treated as an ideal random walk in 3-D taking place between one penetrable and one impenetrable wall. Furthermore, a variation of the molecular weight is envisioned.

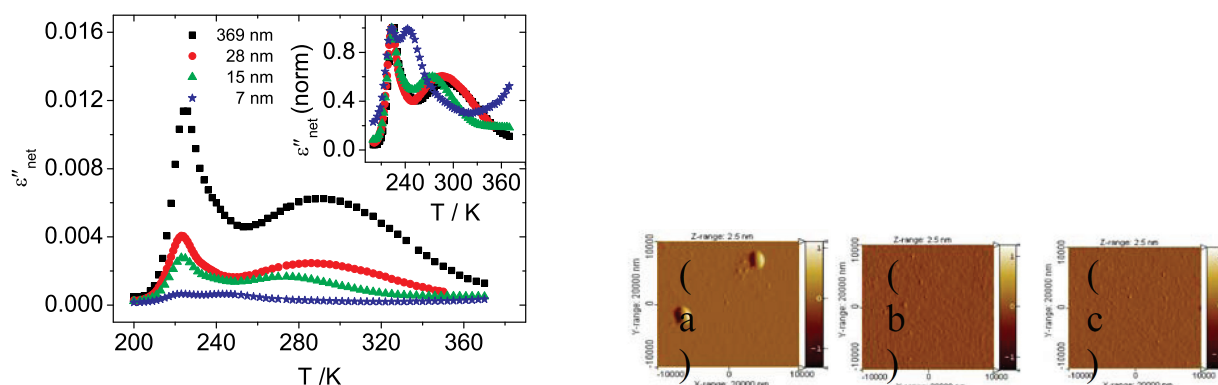


**Figure 3.3:** (a) AFM pictures of the layer surface of a 7-nm PI sample taken (a) immediately after spin-casting, (b) after annealing in high oil-free vacuum before dielectric measurement and (c) after dielectric measurement. The root mean square roughness values are 2.4, 1.9 and 1.8 nm, respectively, showing that the surface remains unchanged during measurement. (b) Net dielectric loss  $\epsilon''_{net}$  versus temperature at a frequency of 80 Hz for polyisoprene (molecular weight  $M_w = 53 \text{ kg/mol}$ ) in thin layers with thicknesses as indicated. Inset: same data normalized with respect to the maximum value of dielectric loss of the segmental mode.

- [1] A. Serghei and F. Kremer, Phys. Rev. Lett. 91, 165702-1 (2003)
- [2] A. Serghei, F. Kremer and W. Kob, Eur. Phys. J. E. 12, 143 (2003)
- [3] E.U. Mapesa, M. Erber, M. Tress, K.J. Eichhorn, A. Serghei, B. Voit and F. Kremer, Eur. Phys. J.-ST. 189, 173 (2010)

### 3.5 Molecular dynamics of cis-polyisoprene under geometrical confinement

W.K. Kipnusu, E.U. Mapesa, C. Iacob, J.R. Sangoro and F. Kremer

Broadband dielectric spectroscopy is employed to study cis 1,4 polyisoprene. In the bulk state two distinct molecular processes are observed. The normal mode process due to dipole component parallel to the chain contour appears at higher temperatures (lower frequencies) and is proportional to the correlation function of the fluctuations of the end-to-end vector of the whole polymer chain. Segmental mode which appears at lower temperatures (higher frequencies) as shown in Fig. 3.4, is associated to the dynamic glass transition. Both of the two processes are proportional to the monometric friction coefficients [1] and hence have the same temperature dependence as seen on the inset of Fig. 3.4). A counterbalance between finite-size effects and surface effects are expected to influence molecular dynamics of these processes when the polymer melt is confined in cylindrical nanopores especially when the pore diameter is less than the radius of gyration of the polymer. From previous studies it is noted that the confinement effects is strongly dependent on the topology and dimensionality of the confining matrices [2,3,4]. In the current study, 2-D confinement of cis-1,4 polyisoprene in unidirectional nanoporous silica matrices will be compared with 1-D confinement in

spin cast thin films where silica nanostructures are used as spacers leaving one interface free. Nanoporous silica matrices are obtained after oxidation of porous silicon prepared by anodization of highly p- doped (100) oriented silicon substrates in HF electrolyte solution. This process leads to highly anisotropic pores running perpendicular to the surface of the wafer (Fig. 3.4) (a)). Self- diffusion coefficients of cis 1,4 polyisoprene in bulk state and when confined in the nanoporous host systems will also be probed using both dielectric spectroscopy and pulse field gradient NMR spectroscopy.

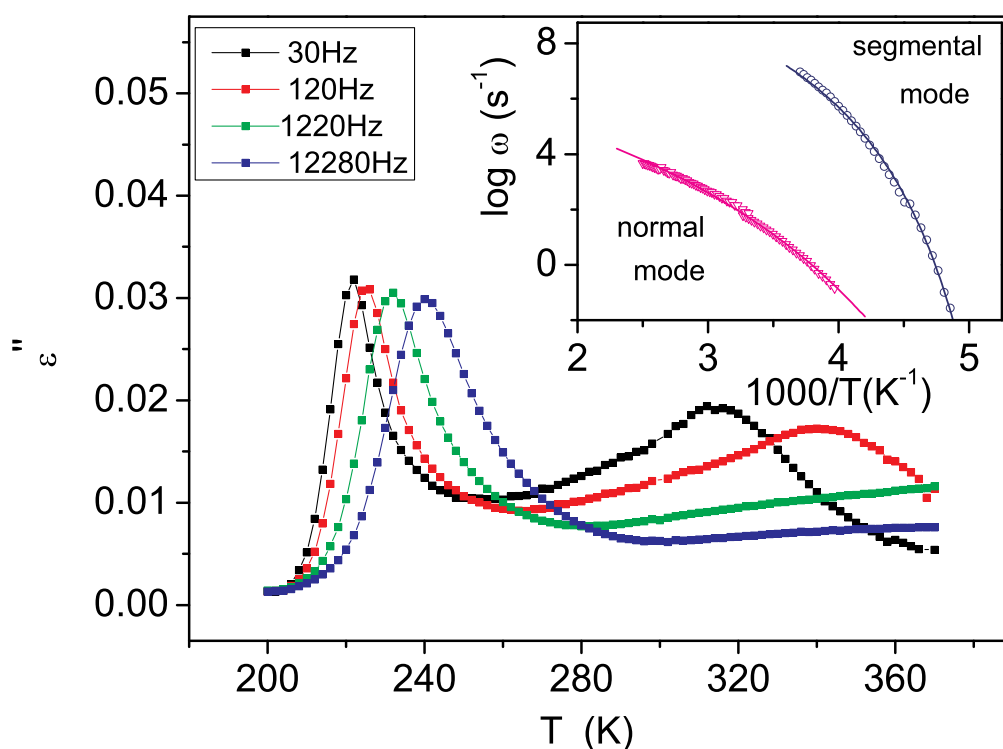


**Figure 3.4:** dielectric loss vs temperature at the indicated frequencies for bulk cis 1,4 polyisoprene ( $M_w=53\text{kg/mole}$ ). The inset shows temperature dependence of the segmental and the normal modes- lines represents the VFT fits.

- [1] K. Kojio, S. Jeon and S. Granik, *Eur.Phys.J.E.* 8 167 (2003)
- [2] A. Serghei and F. Kremer, *Phy.Rev. Lett.* 91, 165702-1 (2003)
- [1] R. Kimmich and N. Fatkullin, *Macromolecules*, in press (2011)
- [1] P. Floudas and G. Fleischer, *Europhys.Lett.*, 40 (6) 685(1997)

### 3.6 Rotational and translational diffusion in hyper-branched polyglycerols

T. Schubert, J.R. Sangoro, C. Iacob and F. Kremer

Dendritic polyglycerols are under intense investigation due to the wide range of applications envisaged in biomedical sciences and especially drug delivery. In the current study, rotational and translational diffusion in a series of hyperbranched polyglycerols (HPGs) are investigated by a combination of broadband dielectric spectroscopy (BDS), pulsed field gradient nuclear magnetic resonance (PFG NMR), rheology, frequency-dependent (ACC) as well as differential scanning calorimetry (DSC). The dielectric spectra are dominated by conductivity contribution at higher temperatures (and lower frequencies) whereas two closely adjacent secondary dipolar relaxation processes are observed at lower temperatures for all the samples investigated. Analysis of the real part of the complex dielectric function based on the Kramers-Kronig relations enables the separation of the latter. The slower dipolar relaxation is attributed to rotational diffusion - an assignment supported by rheological and calorimetric results. The Stokes-Einstein relation linking rotational and translational diffusion is shown to hold for the (low molecular weight) polymers investigated Fig. 3.5).

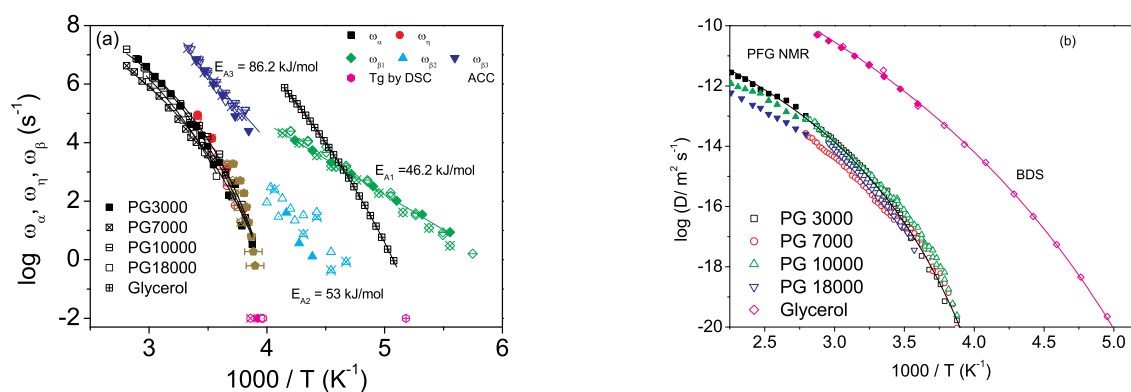


**Figure 3.5:** (a) Thermal activation plot of the structural  $\alpha$ -relaxation rates (squares) of polyglycerols with indicated molecular weights in g/mol (filled: 3000; crossed: 7000; dashed: 10000; open: 18000) in comparison to glycerol (crossed). The mechanical relaxation rates (circles) determined from rheology data are also shown. The secondary ( $\beta$ -) relaxation rates (triangles and diamonds) for the indicated molecular weights are also shown. Solid lines are fits by the Vogel-Fulcher-Tammann equation. (b) Temperature dependence of the diffusion coefficient as obtained from the structural  $\alpha$ -relaxation (open) and PFG-NMR (filled) measurements for the given molecular weight. Logarithm is to base 10.

- [1] M. Calderón, M. A. Quadir, S. K. Sharma, and R. Haag, Dendritic polyglycerols for biomedical applications. *Adv. Mater.* 22, 190-218 (2010)
- [2] J. R. Sangoro et al., Rotational and translational diffusion in hyperbranched polyglycerols, Under preparation.

### 3.7 Dielectric properties of ionic liquids: the effect of temperature and pressure

J.R. Sangoro and F. Kremer

Broadband dielectric spectroscopy is employed to investigate the influence of temperature and pressure on charge transport in ionic liquids. The dielectric spectra are dominated - on the low-frequency side - by electrode polarization effects while, for higher frequencies, charge transport in a disordered matrix is the underlying physical mechanism. Identical Vogel-Fulcher-Tammann-type dependence of the main quantities characterizing charge transport with respect to temperature and pressure is obtained (Fig. 3.5a). While the absolute values of dc conductivity and the characteristic charge transport rate vary over more than 10 decades with temperature, pressure and upon systematic structural variation of the ILs, a coinciding plot of the transport parameters is obtained (Fig. 3.5b). This is discussed within the framework of the concept of glassy dynamics assisted charge transport traced back to Einstein, Einstein-Smoluchowski, and Maxwell relations [1].

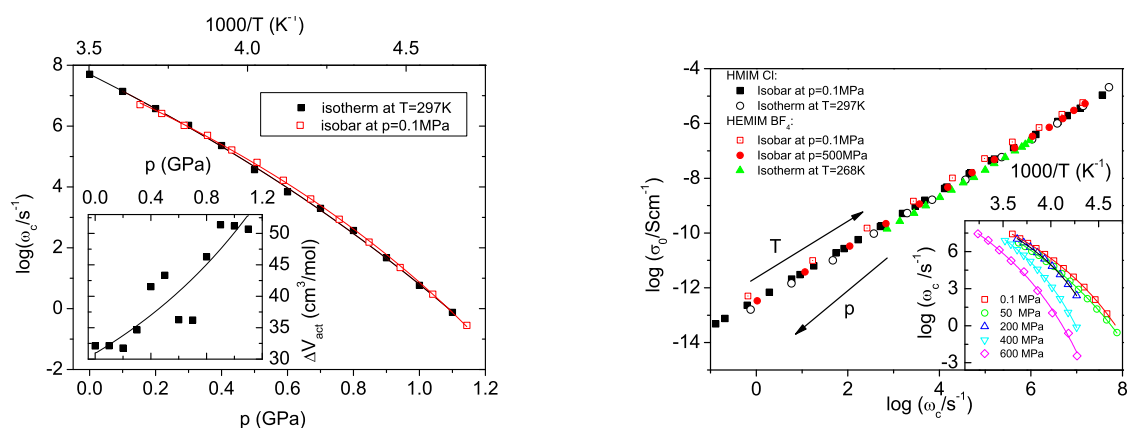


**Figure 3.6:** (a) The characteristic rate of charge transport,  $\omega_c$ , for the HMIM Cl ionic liquid at different pressure (isotherm) and as a function of inverse temperature (isobar). Inset: The apparent activation volume at different pressure as indicated. (b) The dc conductivity,  $\sigma_0$ , versus  $\omega_c$ , for two ionic liquids as indicated. The data for all ionic liquids are obtained from dielectric measurements at ambient pressure except for the HMIM Cl for which the transport quantities are also measured at different pressures as indicated. This plot experimentally demonstrates the universality of charge transport in ionic liquids. The error bars are comparable to the size of the symbols, if not specified otherwise. Log is used to refer to logarithm to base 10.

- [1] Broadband Dielectric Spectroscopy, edited by F. Kremer and A. Schönhal, Springer (2003).
- [2] J. R. Sangoro, A. Serghei, S. Naumov, P. Galvosas, J. Kärger, C. Wespe, F. Bordusa, and F. Kremer, Phys. Rev. E 77, 051202 (2008).
- [3] J. R. Sangoro et al, J. Chem. Phys. 128, 214509 (2008)
- [4] J. R. Sangoro, C. Iacob, A. Serghei, C. Friedrich, F. Kremer, Phys. Chem. Chem. Phys. 11, 913 (2009)
- [5] J. R. Sangoro et al. (2011), under preparation

### 3.8 Diffusion in ionic liquids: the interplay between molecular structure and dynamics

J.R. Sangoro, C. Iacob and F. Kremer

Diffusion in a series of bis(trifluorosulfonyl)imide-based ionic liquids is investigated by a combination of Broadband Dielectric Spectroscopy (BDS) and Pulsed Field Gradient Nuclear Magnetic Resonance (PFG NMR). It is demonstrated that the mean jump lengths increase with the molecular volumes determined from quantum-chemical calculations. This provides a direct means - via Einstein-Smoluchowski relation - to determine the diffusion coefficient by BDS over more than 8 decades unambiguously and in quantitative agreement with PFG NMR measurements (see Fig. 3.7). Unprecedented possibilities in the study of charge transport and dynamic glass transition in ionic liquids are thus opened [1].

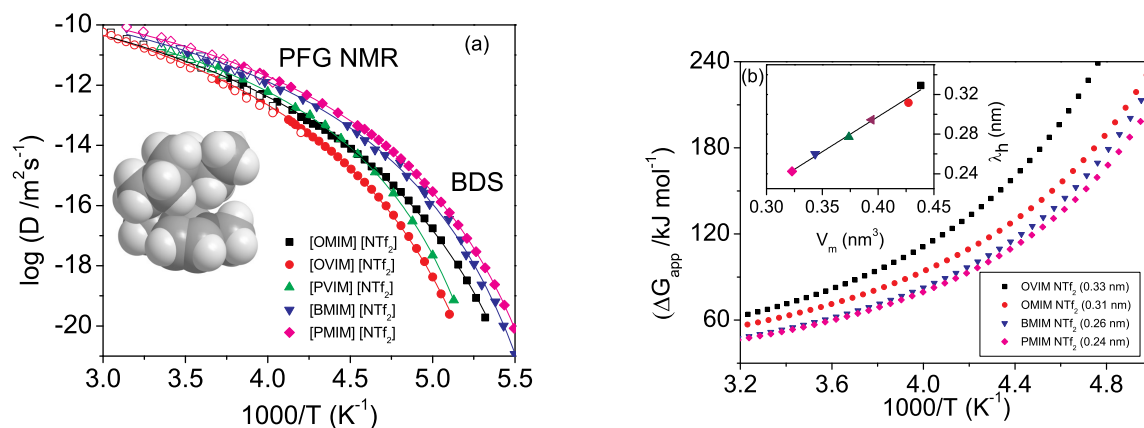


**Figure 3.7:** (a) Diffusion coefficients determined from broadband dielectric spectra by employing the Einstein-Smoluchowski equation (using  $\omega_c$  as the characteristic hopping rate) and independently measured by PFG NMR (open symbols). The lines denote fits by the Vogel-Fulcher-Tammann equation. Inset: One of the possible conformations of the [OMIM] cation. (b) The apparent activation energy,  $\Delta G$ , of diffusivity in a series of bis(trifluoromethylsulfonyl)imide-based ionic liquids at different temperatures (determined from the VFT fits presented in Fig. 3.7a).  $\Delta G$  increases with the mean ion jump lengths (indicated in brackets). Inset: The mean jump lengths (from a combination of broadband dielectric spectroscopy and PFG NMR measurements) as a function of the molecular volume (from quantum chemical calculations) of the ionic liquids investigated.

[1] J. R. Sangoro et al., *Soft Matter* 7 1678 (2011).

### 3.9 Charge transport and dipolar relaxations in alkali metal-based ionic liquids

J.R. Sangoro, C. Iacob and F. Kremer

Charge transport and dipolar relaxations in novel alkali metal-based carboxylate ionic liquids are investigated in a wide frequency and temperature range by means of Broadband Dielectric Spectroscopy (BDS) [1-2]. The dielectric spectra are described at lower temperatures in terms of dipolar relaxations whereas hopping conduction in a random spatially varying energy landscape is quantitatively shown to dominate the spectra at higher temperatures (see Fig. 3.8) (a). Based on detailed analysis of the dielectric relaxation strength in its temperature dependence, the slower secondary relaxation process is attributed to molecular fluctuation of ion-pairs (sodium and carboxylate ions) while the localized motion of the carboxylate anion gives rise to the faster process observed (see Fig. 3.8) (b)). Experimental evidence for the existence of long-lived ion pairs in an ionic liquid is thus provided [2].

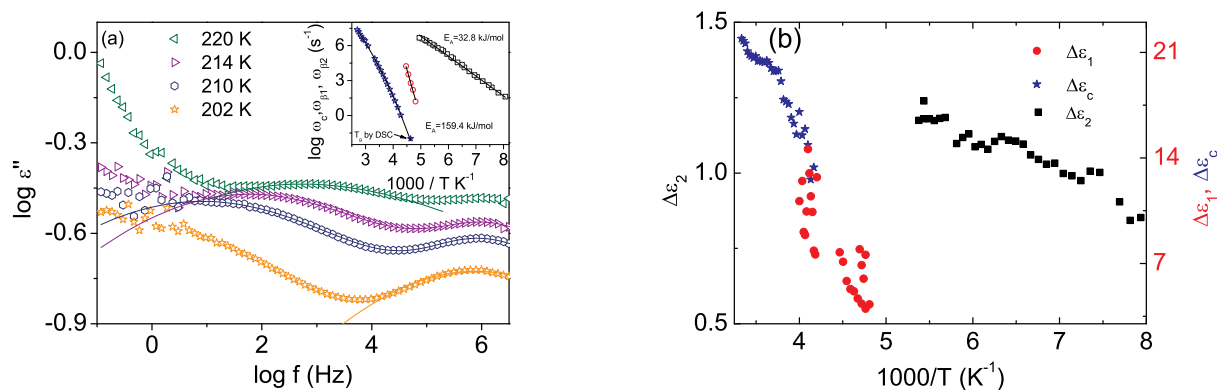


**Figure 3.8:** (a) Imaginary part of the complex dielectric function versus frequency at different temperatures illustrating the secondary relaxation processes in the sodium 2,5,8,11-tetraoxatridecan-13-oate ([Na][TOTO]) ionic liquid. Inset: Arrhenius-type temperature dependence of the secondary relaxation rates ( $\omega_{\beta}$ ) of [Na] [TOTO] at lower temperatures (114 K to 225 K). The activation energies are indicated. (b) The temperature dependence of the dielectric relaxation strength corresponding to charge transport  $\Delta \epsilon_c$  as well as the two secondary dipolar relaxations  $\Delta \epsilon_{\beta_1}$  and  $\Delta \epsilon_{\beta_2}$ .

- [1] O. Zech, J. Hunger, J. R. Sangoro, C. Iacob, F. Kremer, W. Kunz, and R. Buchner Phys. Chem. Chem. Phys., 12, 14341-14350 (2010).  
 [2] J. R. Sangoro et al., Charge transport and dipolar relaxations in metal-based ionic liquids, Under preparation.

### 3.10 Charge transport in confined ionic liquids

C. Iacob, J.R. Sangoro and F. Kremer

Charge transport in tetrafluoroborate ( $\text{BF}_4$ ) and bis[trifluoromethylsulfonyl]imide (NTf<sub>2</sub>) based ionic liquids (ILs) in nanoporous silica membranes (average diameters :7.5, 9.5 and 10.4 nm ) - prepared by electrochemical etching of (100) p-type silicon - is investigated in a wide frequency and temperature range by a combination of Broadband Dielectric Spectroscopy (BDS) and Pulsed Field Gradient Nuclear Magnetic Resonance (PFG NMR) [1,2]. By applying the Einstein-Smoluchowski relation to the dielectric spectra, diffusion coefficient is obtained in quantitative agreement with independent PFG NMR measurements (Fig. 3.9)A (our PFG-NMR data are in agreement with the results reported by Bogno et al.). We experimentally show for the first time that the ionic mobility of the studied ILs at lower temperatures is enhanced by more than two decades under nano-confinement geometry in comparison with the bulk value. The results are interpreted in terms of changes in the ion packing under condition of geometrical confinement.

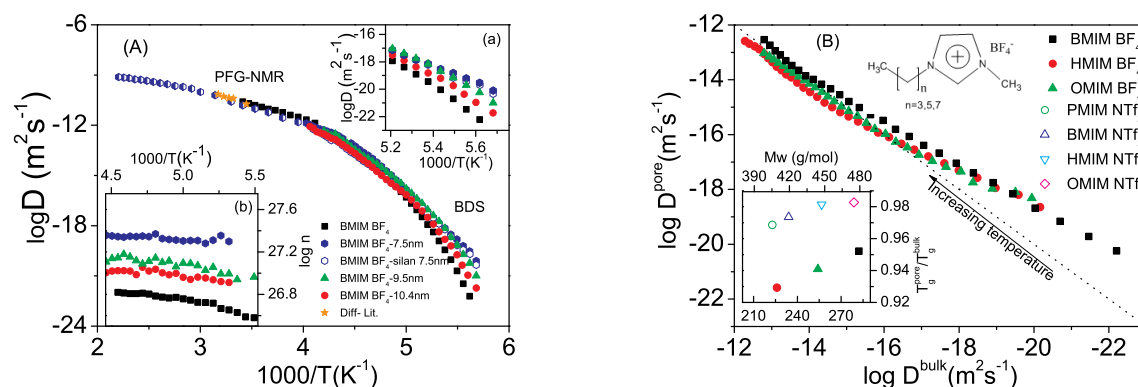


**Figure 3.9:** (A) Diffusion coefficients determined by applying the Einstein-Smoluchowski equation to the dielectric spectra of BMIM  $\text{BF}_4$  (in bulk and nanopores denoted by filled symbols) and measured by PFG NMR (represented by half filled symbols). The star symbols represent the experimental diffusion coefficients using DOSY NMR from Bogno et al., which are in a good agreement with our PFG NMR and BDS measurements [3]. Inset: (a) enlargement of the spectra at lower temperatures and (b) effective number density of charge carriers of BMIM  $\text{BF}_4$  in silica membranes with different pore sizes as a function of inverse temperature. (B) Diffusion coefficients of  $\text{BF}_4$ -based ionic liquids in 7.5nm silica nanopores versus bulk diffusion coefficients. Arbitrary dotted line represents 1:1 ratio between diffusion coefficients in pores and in bulk. Insets: Molecular weight for the  $\text{BF}_4$ - and NTf<sub>2</sub>- based ionic liquids as a function of the ratio of the glass transition temperatures in pores, and bulk respectively. The structure of  $\text{BF}_4$ -based ionic liquids is indicated.

- [1] C. Iacob, J. R. Sangoro, P. Papadopoulos, T. Schubert, S. Naumov, R. Valluilin, J. Kärger, and F. Kremer Phys. Chem. Chem. Phys., 12, 13798-13803 (2010) .  
 [2] C. Iacob, J. R. Sangoro, J. Kärger and F. Kremer, under preparation.  
 [1] A. Bogno, F. D'Amico and G. Saielli, J.Mol.Liq.131-132, 17-23 (2007)

### 3.11 Liquid crystals in confining geometry

M. Jasiurkowska, C. Iacob, P. Papadopoulos, F. Kremer, M. Massalska-Arodz

The molecular dynamics of 4-heptan-4'-isothiocyanatobiphenyl (abbreviated as 7BT) in confinement of cylindrical nanopores is studied by means of Broadband Dielectric Spectroscopy (BDS). In bulk, the investigated compound shows only one liquid crystalline phase [1,2], the highly ordered smectic E (SmE) phase, characterised by the orthorhombic arrangement of molecules within the layers. The confinement leads to modification of the dynamics of the molecular motion. The relaxation process around short axis ( $\delta$ -relaxation) is faster in the pore than in the bulk and its temperature dependence is described by Arrhenius formula. The value of activation energy of the  $\delta$ -relaxation is slightly higher for sample into pores than this obtained for a bulk of the SmE phase. The second process attributed to a librational motion of the molecules appears in the relaxation rates two decades faster than  $\delta$ -relaxation. With decreasing temperature both processes merge and their sum follows the temperature curve of the II process. The crystallization temperature is significantly reduced in comparison to the value for bulk and its dependence on pore sizes (Fig. 3.10).

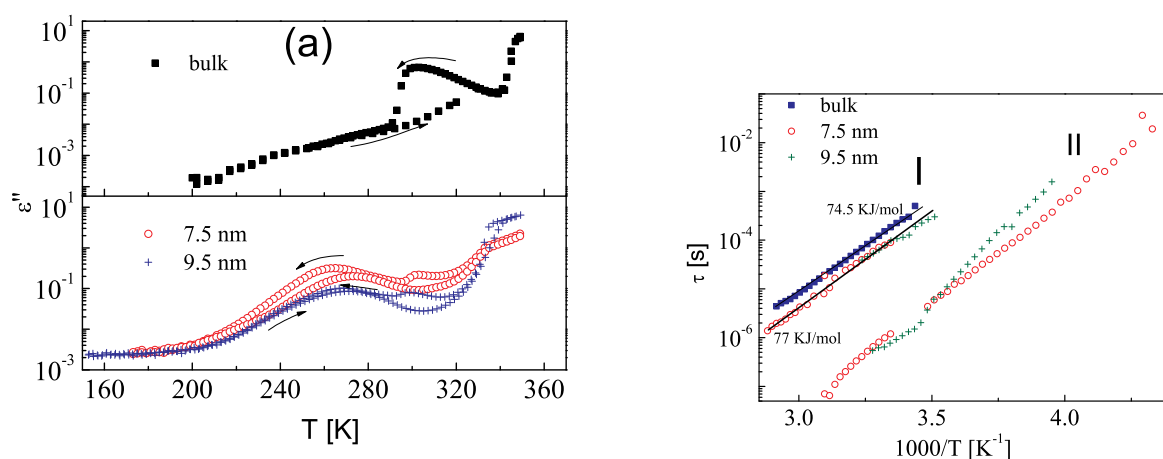


**Figure 3.10:** (a) Dielectric loss  $\epsilon''$  for 7BT measured at 3.21 kHz as a function of temperature on cooling and subsequent heating of the bulk sample and in pores of 7.5 nm and 9.5 nm. b) the activation pot, relaxation process I corresponds to  $\delta$ -relaxation, process II is assigned to the librational motion of the molecules close to walls.

- [1] M. Jasiurkowska, A. Budziak, J. Czub, M. Massalska-Arodz, S. Urban, *Liq. Cryst.* 2008, 35, 513.
- [2] M. Jasiurkowska, J. Ściesiński, M. Massalska-Arodz, J. Czub, R. Pelka, E. Juszyńska, Y. Yamamura, K. Saito, *J. Phys. Chem. B* 2009, 113, 7435.

### 3.12 Infrared transition moment orientational analysis (IR-TMOA)

W. Kossack, P. Papadopoulos and F. Kremer

A novel spectroscopic approach has been developed, that reveals a complete characterization of the quadratic averaged orientation of the different infrared transition dipole moments in any IR-translucent material. Using a rotary measurement setup, the electric field in the sample can be varied in all three dimensions (see inset). Since, the absorption coefficient is explicitly dependent on the relative orientation of the transition dipoles and the electric polarization (see Fig. 3.11), one is enabled to quantify the fraction of ordered molecular moieties and their orientation [1]. Based on this technique thin, substrate supported, polymer films are studied in order to investigate their interaction with solid-state interfaces according to their specificity and range for different combinations of polymers and substrates, addressing the recent question of confinement and its extension.

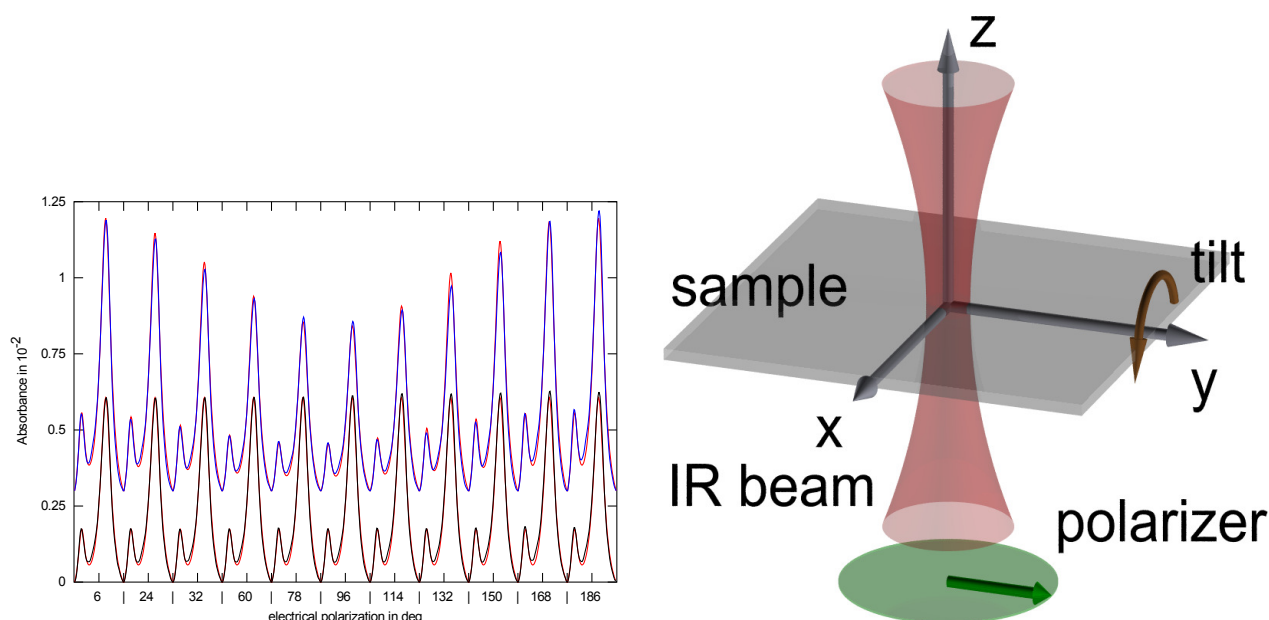


**Figure 3.11:** Polarization (with respect to the  $y$  axis) and inclination (tilt) dependence of baseline corrected  $\text{CH}_2$  stretching vibrations of polystyrene ( $\sim 40$  nm) on  $\text{BaF}_2$ . For comparison the bands for different electrical polarizations are put next to each other: The  $x$  axis shows wavenumbers from  $2833$  to  $2981\text{cm}^{-1}$  for each polarization (between each two upright lines). The small peaks correspond to symm.  $\text{CH}_2$  stretching ( $2850\text{ cm}^{-1}$ ), the big peaks to asymm.  $\text{CH}_2$  stretching ( $2920\text{ cm}^{-1}$ ). The black and blue lines show the spectra for  $0^\circ$  and  $60^\circ$  inclination, where the latter is shifted by  $0.3 \times 10^{-2}$  units upwards. The red lines are the corresponding fits. As expected absorption shows no polarization dependence for normal incidence, where the  $60^\circ$  incidence spectra vary symmetrically around  $90^\circ$  polarization direction. The inset shows the measurement geometry.

[1] W. Kossack, P. Papadopoulos, P. Heinze, H. Finkelmann, F. Kremer, *Macromolecules*, 43, 7532-7539 (2010).

### 3.13 Hierarchies in the structural organization of spider silk- A quantitative combined model

R. Ene, P. Papadopoulos and F. Kremer

Polarized IR-spectroscopic and mechanical measurements are combined to analyse the conformational changes in hydrogenated and partially deuterated major ampullate spider silk of *Nephila edulis* Fig. 3.12)a) [1]. Special attention is given to supercontraction and to the case where the latter is hindered by mechanical constraints. Crystal stress can be measured from the frequency shift of main-chain vibrations. The results show that in both states of silk a serial arrangement between the crystalline and amorphous phase dominates the nanostructure. The determination of the molecular order parameters of the different moieties proves that the amide hydrogen exchange is a selective process, taking place at the surface of  $\beta$ -sheet nanocrystals, implying that these regions are accessible by water[2]. The mechanical properties are changing dramatically when the fiber is wet ("supercontraction") due to the fact that the pre-stress of the chains interconnecting the nanocrystals is irreversibly released. In course of this a novel network of H-bonds is formed, a process which can be suppressed if supercontraction is hindered. A three-component combined model of crystals in serial arrangement with amorphous chains and a fraction of chains bypassing them can describe all states of spider silk, assuming hydrogen bonding of worm-like chains at low pre-strain Fig. 3.12)b) [3].

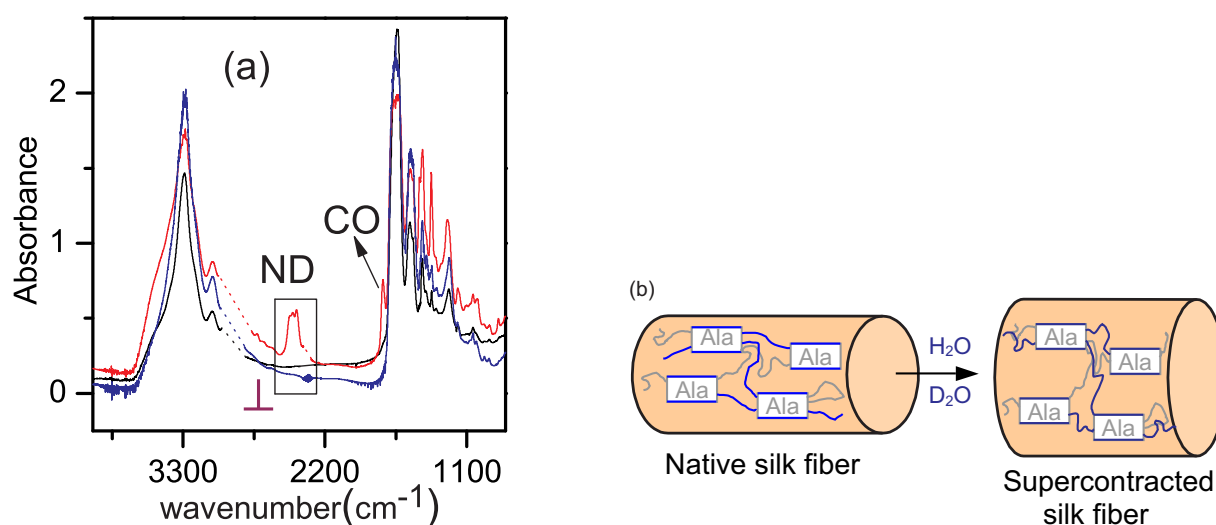


**Figure 3.12:** (a) IR absorption spectrum of major ampullate silk from *Nephila edulis* in native state (black curve) and supercontracted state (H<sub>2</sub>O-blue curve and D<sub>2</sub>O-red curve). The spectral region highlighted in the rectangle contains the ND bands resulted from the exchange of hydrogen with deuterium, (b) Accessibility of silk proteins to water. The exchange of amide hydrogens takes place primarily at highly ordered moieties, including amorphous chains with high pre-strain and possibly parts of the alanine nanocrystal surface (marked with blue).

- [1] P. Papadopoulos, R. Ene, I. Weidner, F. Kremer *Macromol. Rapid Commun* 30, 851-857 (2009).  
 [2] R.Ene, P. Papadopoulos, F. Kremer *Polymer* 51, 4784-4789 (2010).

[3] R. Ene, P. Papadopoulos, F. Kremer, *Soft Matter* 5, 4568-4574 (2009)

### 3.14 Receptor/ligand-interaction as studied on a single molecule level

C. Wagner, D. Singer, R. Hoffmann and F. Kremer

Optical tweezers-assisted dynamic force spectroscopy is employed to investigate specific receptor/ligand-bonds on a single contact level. The specific binding of two monoclonal antibodies, HPT-110 and HPT-104, to synthetic tau-peptides with different phosphorylation pattern is analyzed. The specificity of HPT-110 to the tau-peptide containing a phosphorylation at Ser235 and of HPT-104 to the tau-peptide containing a phosphorylation at Thr231 is confirmed (Fig. 3.13 a). Additionally, our approach allows for a detailed characterization of the unspecific interactions that are observed between HPT-104 and the peptide phosphorylated only at Ser235 and between HPT-110 and the peptide phosphorylated only at Thr231. By analyzing the measured rupture-force distributions it is possible to separate unspecific from specific interactions. Thereby for the latter characteristic parameters like the lifetime of the bond without force  $\tau_0$ , the characteristic length  $x_{fs}$  and the free energy of activation  $\Delta G$  are determined (Fig. 3.13 b). The results are in accordance with conventional ELISA tests but offer a much more refined insight.

[1] M. Salomo et al., *Eur. Biophys. J.* 37 927-934 (2008).

[2] C. Wagner et al., The interaction of tau-peptides and monoclonal antibodies as studied by optical tweezers assisted dynamic force spectroscopy, *Soft Matter*, in press.

### 3.15 Forces within single pairs of charged colloids in aqueous Solutions of ionic liquids as studied by optical tweezers

M.M. Elmahdy, C. Gutsche and F. Kremer

Forces of interaction within single pairs of negatively charged microsized colloids in aqueous solutions of water miscible room temperature ionic liquids (RTILs) have been measured at varying concentrations and pH by using optical tweezers (OT) [1]. Three different water miscible RTILs (1-Butyl-3-methylimidazolium tetrafluoroborate [BMIM-BF<sub>4</sub>], 1-Butyl-3-methylimidazolium trifluoromethanesulfonate [BMIM-TfO] and 1-Butyl-3-methylimidazolium chloride [BMIM-Cl]) having the same organic cation [BMIM]<sup>+</sup> and different inorganic anions ([BF<sub>4</sub>]<sup>-</sup>, [TfO]<sup>-</sup> and Cl<sup>-</sup>) are used and compared with the high temperature molten salt (KCl). The experimental data are well described by a size-corrected screened Coulomb interaction approach which originates from the linearized Poisson-Boltzmann (PB) equation [2]. The effective surface charge

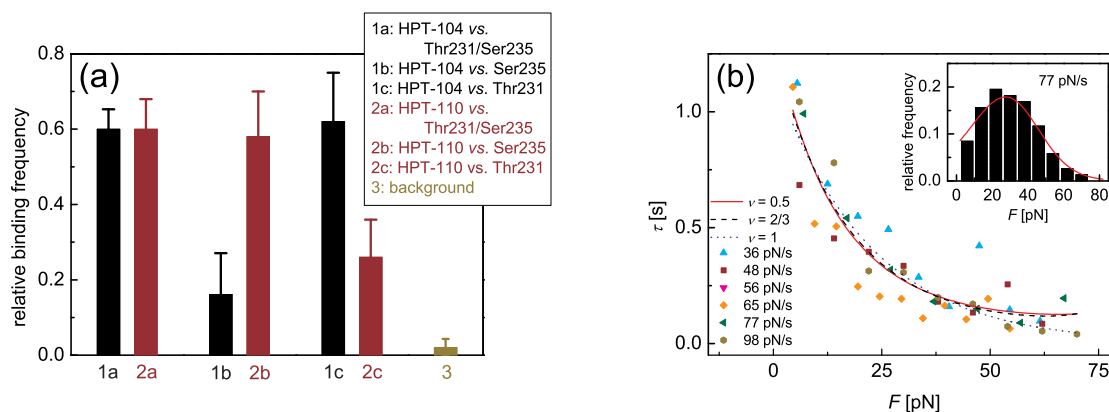


**Figure 3.13:** (a) The median relative binding frequency of each of the mAbs HPT-104 and HPT-110 to double-phosphorylated peptides and to peptides mono-phosphorylated at Thr231 and Ser235 is shown. The median frequency of both, HPT-104 and HPT-110 to the double-phosphorylated peptide is  $\sim 0.6$ . The binding frequency of HPT-104 to the peptide only phosphorylated at Thr231 is similar, whereas its binding frequency to the peptide phosphorylated at Ser235 is with  $\sim 0.25$  significantly lower. For the mAb HPT-110 the result is vice versa: its binding frequency to the peptide mono-phosphorylated at Ser235 is significantly higher than to the peptide mono-phosphorylated at Thr231. The last column indicates the level of the "background", which consists of interactions that are not caused by an interaction between receptor and ligand molecules. This "background" is with a binding frequency of  $<2\%$  found to be negligible. b) The lifetime  $\tau$  of the interaction between HPT-110 and the double-phosphorylated peptide is shown in dependence on the force for 6 different loading rates as indicated by the different symbols. The data is fitted globally to a well-known theoretical model. Inset: Histogram of the measured rupture forces at a loading rate of 77 pN. The red line indicates the theoretical distribution of rupture forces according to the theoretical model after inserting the parameters obtained by fitting  $\tau(F)$ .

density  $\sigma$  derived from the fitted force-separation data is found to be concentration and pH dependent (Fig. 3.14)).

[1] M.M. Elmahdy, C. Gutsche, F. Kremer J. Phys. Chem. C 114, 19452 (2010).

[2] C. Gutsche, U.F. Keyser, K. Kegler, F. Kremer Physical Review E 76, 031403 (2007)

### 3.16 Forces of interaction between grafted, blank and grafted-blank colloids by using optical tweezers

T. Stangner, M.M. Elmahdy, C. Gutsche and F. Kremer

The forces of interaction between blank SiO<sub>2</sub> colloids (diameter:  $\sim 4.85 \pm 0.05 \mu\text{m}$ ), poly (acrylic-acid) (PAA) grafted colloids and the asymmetric blank-grafted colloids are measured with high precision ( $\pm 50 \text{ fN}$ ) by means of Optical Tweezers. Parameters to be varied beside the surface modification are the concentration and the valency of the added salt. The Derjaguin-Landau-Verwey-Overbeek (DLVO) theory [1] is used for the characterization of the blank colloids. Good agreement was found (Fig. 3.15)a). Therefore electrostatic contributions dominate the interaction [1]. The interaction between

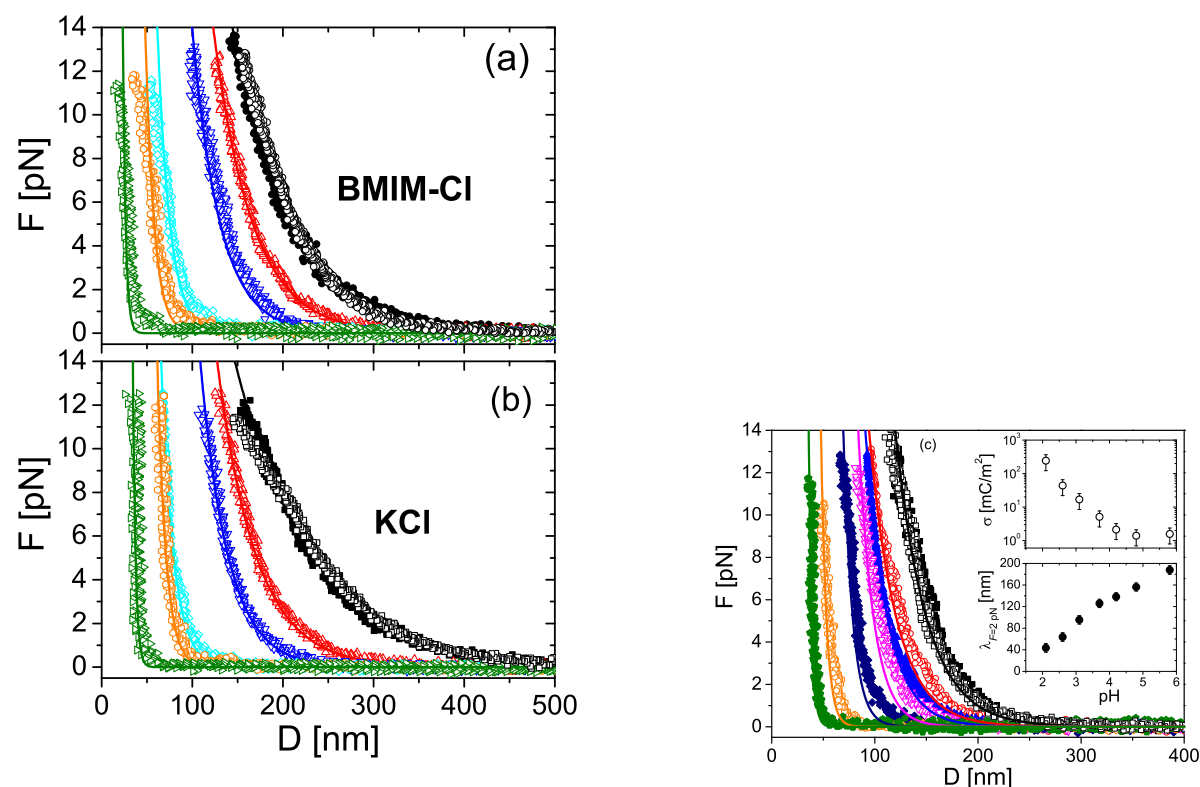


**Figure 3.14:** Forces vs. separation  $D$  as measured for a single pair of blank PS colloids in aqueous solution of two different types of salts (BMIM-Cl and KCl). Symbols represent the experimental data while the solid lines represent the fits with the size-corrected screened Coulomb interaction approach. (a) BMIM-Cl at fixed pH 5.8 and different concentrations:  $2.2 \times 10^{-5}$  M (black full circles),  $5 \times 10^{-5}$  M (red open up-triangles),  $1 \times 10^{-4}$  M (blue open down-triangles),  $5 \times 10^{-4}$  M (cyan open diamond),  $1 \times 10^{-3}$  M (orange open hexagon), 0.01 M (olive open right-triangles) and the reproducibility at  $2.2 \times 10^{-5}$  M (black open circles). (b) KCl at fixed pH 5.8 and different concentrations:  $1.2 \times 10^{-5}$  M (black full squares),  $5 \times 10^{-5}$  M (red open up-triangles),  $1 \times 10^{-4}$  M (blue open down-triangles),  $5 \times 10^{-4}$  M (cyan open diamond),  $1 \times 10^{-4}$  M (orange open hexagon), 0.01 M (olive open right-triangles), and the reproducibility check at  $1.2 \times 10^{-5}$  M (black open squares). (c) BMIM-Cl at fixed concentration of  $1 \times 10^{-4}$  M and different pH values of 2.1 (olive full pentagon), 2.6 (orange open hexagon), 3.1 (navy full diamond), 3.7 (magenta open down-triangles), 4.2 (blue full up-triangles), 4.8 (red open circles), 5.8 (black full squares) and the reproducibility at pH 2.1 (black open squares). Inset of (c): interaction length at force of 2 pN ( $\lambda_{F=2 \text{ pN}}$ ) versus pH at fixed BMIM-Cl concentration of  $1 \times 10^{-4}$  M (black full circles). The pH-dependence of the effective surface charge density  $\sigma$  obtained from the fitting of the force separation curves.

PAA-grafted colloids is characterized by a model published by Jusufi et al. including entropic parts to the overall interaction force [1] (Fig. 3.15b). The asymmetric case, blank vs. grafted, was fitted by using the Alexander-De Gennes-Model (AdG model), which only take into account the steric force and non-charged colloids (Fig. 3.15c). Using the model-independent interaction length at a force of  $F=2 \text{ pN}$ , the experimental results suggest that the interaction between the asymmetric case can be described as

a superposition of half the interaction length of the blank and half of the interaction length of the grafted colloids (Fig. 3.15 d).

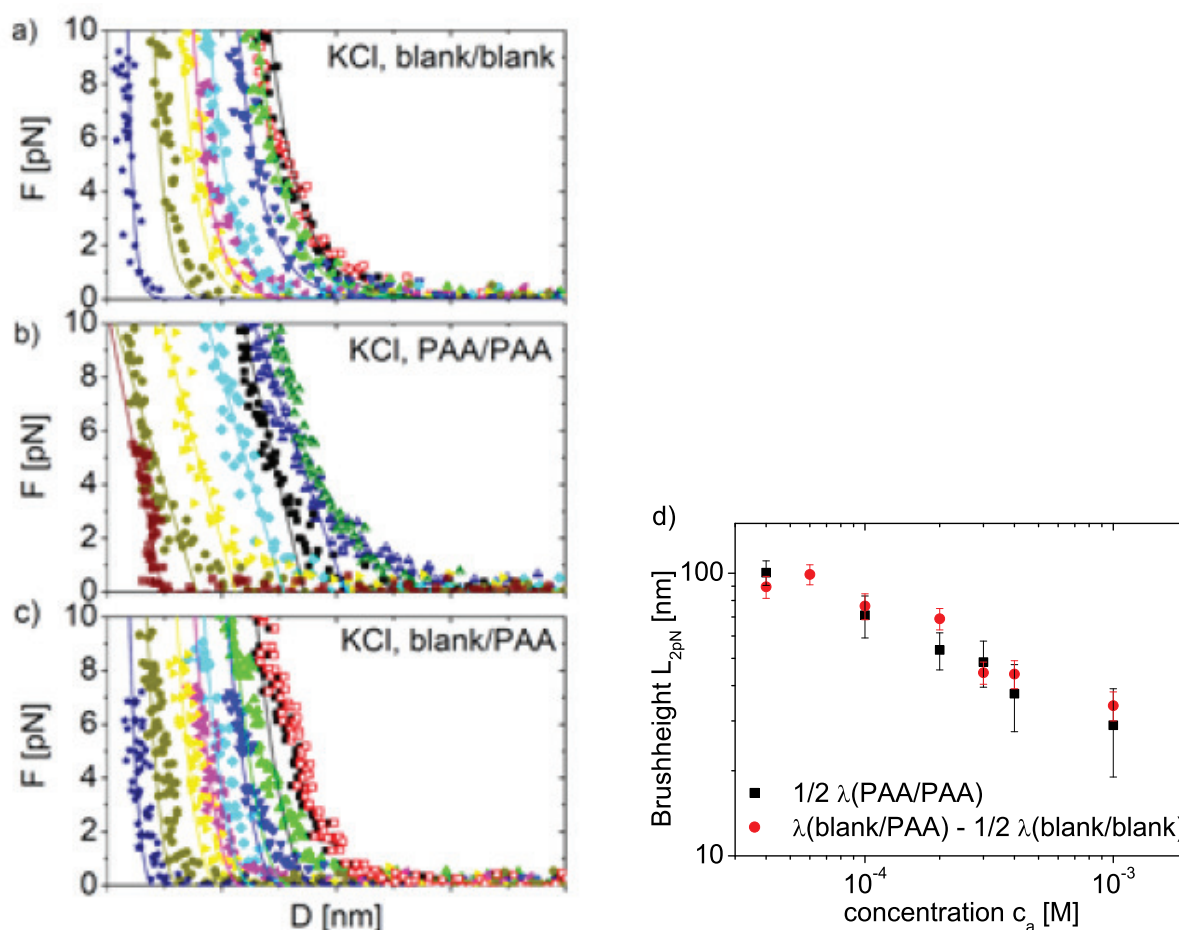


**Figure 3.15:** a-c) Force  $F$  vs. separation  $D$  for three different pairs of  $\text{SiO}_2$  colloids (diameter  $\sim 4.85 \pm 0.05 \mu\text{m}$ ) in aqueous solution (pH 7.3) of varying KCl concentration and surface modification from experiments (symbols). a) Concentration dependence for blank/blank: 0.04 mM (black squares), 0.06 mM (green up-triangles), 0.1 mM (blue down-triangles), 0.2 mM (cyan diamonds), 0.3 mM (magenta left-triangles), 0.4 mM (yellow right-triangles), 1 mM (dark yellow diamonds), 4 mM (navy blue stars). To ensure the full reproducibility of the medium exchange, the cell was flushed again with 0.04 mM (open red squares). The solid lines correspond to the fits using DLVO theory. b) Concentration dependence for PAA/PAA: 0 mM (half-open royal triangles and half-open olive triangles for reproducibility), 0.04 mM (black squares), 0.2 mM (cyan diamonds), 0.4 mM (yellow right-triangles), 1 mM (dark yellow diamonds), 3 mM (open crossed wine red squares). The solid lines correspond to the fits using Jusufi theory. c) Concentration dependence for blank/PAA: 0.04 mM (black squares and open red squares for reproducibility), 0.06 mM (green up-triangles), 0.1 mM (blue down-triangles), 0.2 mM (cyan diamonds), 0.3 mM (magenta left-triangles), 0.4 mM (yellow right-triangles), 1 mM (dark yellow diamonds), 4 mM (navy blue stars). The solid lines correspond to the fits using AdG theory. d) Comparison between the model-independent brush height (half the interaction length) for PAA/PAA (black squares) and blank/PAA (red circles) in dependence of salt concentration. Both datasets coincide what suggests that the interaction between blank/PAA is dominated by electrostatic and entropic contributions.

- [1] C. Gutsche et al., *Physical Review E* 76, 031403 (2007)
- [2] C. Gutsche et al. *JPCM* accepted 2010
- [3] A. Jusufi et al., *Colloid Polym Sci.* 282, 910 (2004)
- [4] G. Dominguez-Espinosa et al., *Polymer*, 49(22):4802-4807, 2008.

### 3.17 Interaction forces between a single pair of charged colloids as measured by Optical Tweezers

C. Gutsche, T. Stangner, M.M. Elmahdy and F. Kremer

Optical Tweezers are an excellent tool to investigate the interaction force between a single pair of spherical charged colloids (diameters: polystyrene  $2.24 \pm 0.02 \mu\text{m}$  silica  $\sim 4.85 \pm 0.05 \mu\text{m}$ ) [1,2,4]. The concentration dependence was recorded under different conditions e.g. varying salt concentration and valency (see Fig. 3.16) a-f). The data are well described by Derjaguin-Landau-Verwey-Overbeek (DLVO) theory [2,3]. A comparison of the fitted  $Z$  and  $R$  among different colloidal pairs of PS with monovalent counterions reveals that the radii are virtually the same whereas the obtained charges range from  $Z \approx 200\,000$  to  $450\,000$ . For a given pair of colloids, at an increasing counterion valence, the fitted radius  $R$  remains essentially constant whereas the fitted charge  $Z$  decreases [2,4]. For reasons of comparison, data for silica colloids (diameter  $4.85 \pm 0.05 \mu\text{m}$ ) are plotted in Figure 1 d-f and show a similar valence dependence. We attribute the latter effect to the neglect of the small-ion correlations in the DLVO theory, which gain importance at increasing counterion valence. The neglect of those leads to an underestimation of screening of the colloids while the functional force-separation dependence is essentially preserved.

- [1] M.M. Elmahdy, A. Drechsler, C. Gutsche, A. Synytska, P. Uhlmann, F. Kremer, M. Stamm, *Langmuir* 25, 12894 (2009)
- [2] C. Gutsche, U.F. Keyser, K. Kegler, F. Kremer, *Physical Review E* 76, 031403 (2007)
- [3] B.V. Derjaguin, L. Landau, *Acta Physicochim. URSS* 14, 633 (1941)
- [4] C. Gutsche et al. *JPCM* accepted 2010

### 3.18 The effective hydrodynamic radius of single DNA-grafted colloids as measured by fast brownian motion analysis

O. Ueberschär, C. Wagner, T. Stangner, C. Gutsche and F. Kremer

Optical tweezers accomplished with fast position detection enable one to carry out Brownian motion analysis of single DNA-grafted colloids (grafting density:  $\sim 1000$  molecules per particle, molecular weight: 4000 bp) in media of varying NaCl concentration. By that the effective hydrodynamic radius of the colloid under study is determined and found to be strongly dependent on the conformation of the grafted

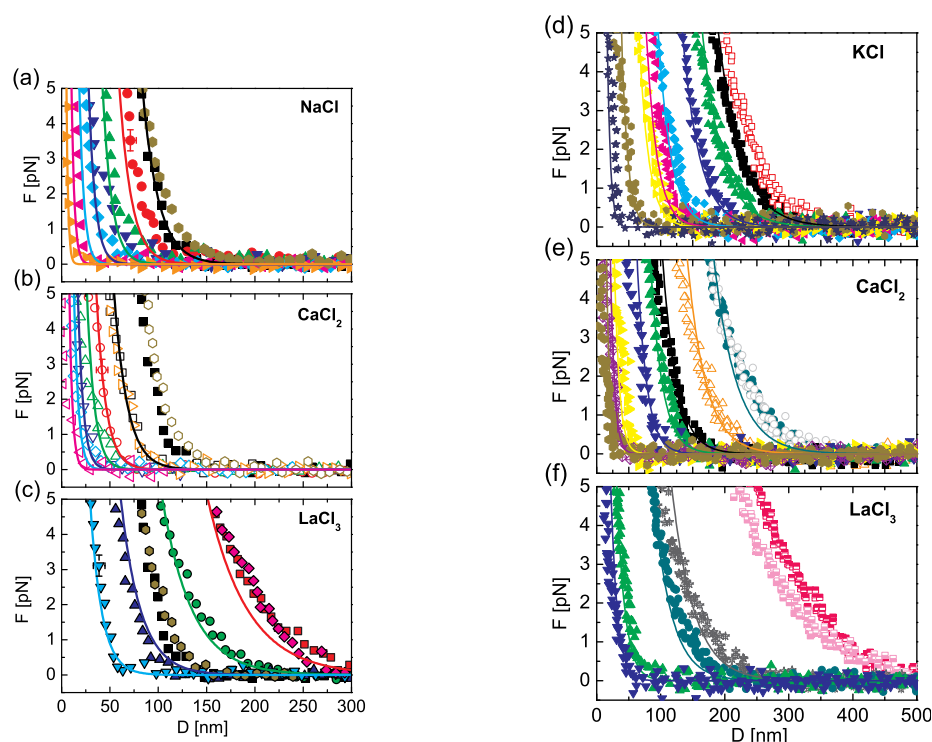


**Figure 3.16:** (a-c) Force  $F$  vs. separation  $D$  for one single pair of Polystyrene (PS) colloids (diameter  $\sim 2.24 \pm 0.02 \mu\text{m}$ ) in aqueous solution of varying salt and salt concentrations from experiments (symbols) and the DLVO theory with fitted values of the parameters  $Z$  and  $R$  (curves). (a) NaCl at 0.3 mM (black squares), 0.55 mM (red circles), 1 mM (green triangles), 2 mM (blue nablas), 4 mM (cyan diamonds), 10 mM (magenta left triangles), and 30 mM (orange right triangles). To ensure a full reproducibility of the exchange of the medium and to exclude hysteresis effects due to possible adsorption effects on the colloids the sample cell was flushed again with 0.3 mM NaCl (gold diamonds). (b) CaCl<sub>2</sub> at 0.15 mM (black open squares), 0.3 mM (red open circles); 0.5 mM (green open triangles), 1 mM (blue open nablas), 1.5 mM (cyan open diamonds), 3 mM (magenta open left triangles), 0.15 mM (orange open right triangles), and finally 0.3 mM NaCl (gold open diamonds). (c) LaCl<sub>3</sub> at 3 μM (black red filled square), 10 μM (black green filled circle), 30 μM (black blue filled triangle), 100 μM (black cyan filled nablas), 3 μM (black magenta filled diamonds), and 0.3 mM NaCl solution (black gold filled diamonds). Some indicative error crosses are given. (d-f) Force  $F$  vs. separation  $D$  for a single pair of blank SiO<sub>2</sub> colloids (diameter  $\sim 4.85 \pm 0.05 \mu\text{m}$ ) in aqueous solution of varying salt and salt concentration from experiments (symbols) and the DLVO theory with fitted values of the parameters  $Z$  and  $R$  (curves). (d) Concentration dependence of KCl: 0.04 mM (black squares), 0.06 mM (green up-triangles), 0.1 mM (blue down-triangles), 0.2 mM (cyan diamonds), 0.3 mM (magenta left-triangles), 0.4 mM (yellow right-triangles), 1 mM (dark yellow diamonds), 4 mM (navy blue stars). To ensure the full reproducibility of the medium exchange, the cell was flushed again with 0.04 mM (open red squares). (e) Concentration dependence of CaCl<sub>2</sub>: 0.01 mM (dark cyan circles and open grey circles for reproducibility), 0.02 mM (orange open up-triangles), 0.04 mM (black squares), 0.06 mM (green up-triangles), 0.1 mM (blue down-triangles), 0.4 mM (yellow right-triangles), 0.6 mM (violet crossed open squares) and 1 mM (dark yellow diamonds). (f) Concentration dependence of LaCl<sub>3</sub>: 1 μM (pink half open up squares and light magenta half open down squares for reproducibility), 5 μM (grey open stars), 0.01 mM (dark cyan circles), 0.06 mM (green up-triangles) and 0.1 mM (blue down-triangles).

DNA chains. Our results compare well both with recent measurements of the pair interaction potential between DNA-grafted colloids (Kegler et al. [2]) and with microfluidic studies (Gutsche et al. [3]). The observed scaling of the brush height with the ion concentration is in full accord with the pertinent theoretical predictions by Pincus, Birshtein and Borisov (Fig. 3.17)).

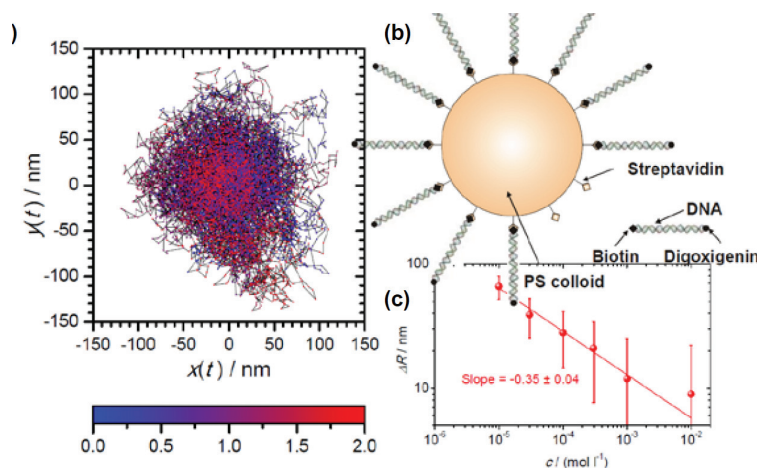


**Figure 3.17:** (a) The centre of the colloid as determined by our two-dimensional intensity profile fit is subject to Brownian motion, which becomes apparent from the depicted trajectory. (b) Schematic of a streptavidin-coated microsphere to which DNA molecules are grafted. (c) The increase  $\Delta R$  of the hydrodynamic radius with respect to different NaCl concentrations as measured for a single DNA-grafted colloid in the salted regime (to logarithmic scale). The linear fit of  $\Delta R$  vs. the NaCl concentration  $c$  yields a power law scaling  $\Delta R \propto c^{-\gamma}$  with an exponent of  $\gamma = 0.35 \pm 0.04$ . The molecular weight of the DNA molecules is 4000 base pairs. The reversibility of the salt-induced conformational change of the DNA brush as reflected in has successfully been verified.

- [1] O. Ueberschär, C. Wagner, T. Stangner, C. Gutsche, F. Kremer, *Polymer*, in press (2010).
- [2] K. Kegler, M. Konieczny, G. Dominguez-Espinosa, C. Gutsche, M. Salomo, F. Kremer, C. N. Likos, *Phys Rev Lett* 100, 118302 (2008).
- [3] C. Gutsche, M. Salomo, Y. W. Kim, R. R. Netz, F. Kremer, *Microfluid Nanofluid* 2, 381-386 (2006).

### 3.19 Single colloid electrophoresis on DNA-grafted colloids

I. Semenov, P. Papadopoulos and F. Kremer

The novel method of Single Colloid Electrophoresis (SCE) [1,2] is applied to determine the electrophoretic mobility of single blank and DNA-grafted colloids. For that Optical tweezers are employed to measure separately the complex electrophoretic mobility of a single colloid and the complex electroosmotic response of the surrounding medium.

For the bare particles pronounced effects are observed in dependence on concentration and valency of the ions in the surrounding medium and on its pH. For monovalent KCl solutions for instance a peak of the electrophoretic mobility at low concentrations is found (Fig. 3.18)) which agrees well with the predictions of the standard electrokinetic model [3]. For trivalent  $\text{LaCl}_3$  solutions at high concentrations charge inversion of the colloid as a whole takes place. SCE is extended to polyelectrolyte-grafted colloids. This enables one to determine (Fig. 3.18)) for the first time the electrophoretic mobility of soft (DNA-grafted) particles under conditions of varying concentration and valency of the ions in the surrounding medium and to compare with the predictions of an approach suggested by Hill and Saville [4].

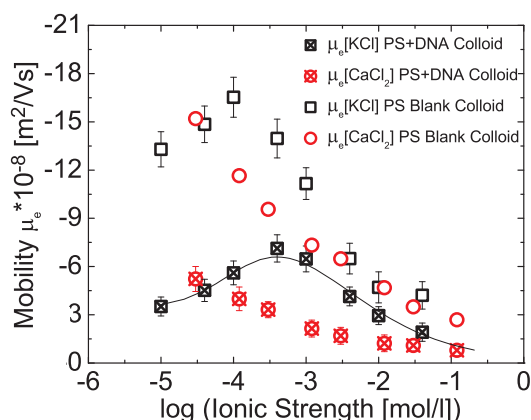


**Figure 3.18:** Electrophoretic mobility vs. ionic strength of KCl and  $\text{CaCl}_2$  aqueous solutions for a single DNA grafted (4000 bps, 1250 molecules per colloid) and similar blank negatively charged PS colloid (diameter:  $2.0 \mu\text{m}$ ). Laser power 0.2 W. Electric AC field frequency 12.5 Hz For comparison the electrophoretic mobility in KCl solutions predicted by the Hill and Saville approach is displayed (solid line).

- [1] I. Semenov et al., *Journal of Colloid and Interface Science* 337, 260 (2009)
- [2] O. Otto et al., *Review of Scientific Instruments* 79, 023710 (2008).
- [3] I. Semenov et al., *Journal of Physics: Condensed Matter* 22, 494109 (2010).
- [4] R. J. Hill, and D. A. Saville, *Colloid Surf. A-Physicochem. Eng. Asp.* 267, 31 (2005).

## 3.20 Funding

*DFG-Teilprojekt im Rahmen des Schwerpunktprogramms "Nano- und Mikrofluidik: Von der molekularen Bewegung zur kontinuierlichen Strömung"*

*SPP 1164 DFG-Schwerpunktprogramm 1164*

Prof. Dr. F. Kremer

KR 1138/14-3 (2006-2010)

*DFG-Projekt "Charge transport and glassy dynamics in ionic liquids" SPP 1191*

Prof. Dr. F. Kremer

KR 1138/20-3 (2010-2012)

*DFG-Projekt "Physicochemical characterisation of ionic liquids-mediated peptide acylation reactions" SPP 1191*

Prof. Dr. F. Kremer

KR 1138/18-2 (2008-2010)

*DFG-Projekt "In-Situ Untersuchung der Wechselwirkungskräfte an Polyelektrolytbürsten"*

Prof. Dr. F. Kremer

KR 1138/20-2 (2009-2011)

*FOR877, DFG-Projekt: "From local constraints to macroscopic transport: Dynamics of DNA under tension and confinement"*

Prof. Dr. F. Kremer and Prof. Dr. K. Kroy

KR 1138/21-1 (2007-2010)

*SPP "Polymer-Festkörper-Kontakte: Grenzflächen und Interphasen" DFG-Teilprojekt "Interfacial dynamic of polymers in interaction with solid substrates"*

*DFG-Projekt "In-situ Untersuchung der Wechselwirkungskräfte an Polyelektrolytbürsten"*

Prof. Dr. F. Kremer

KR 1138/23-1 (2008-2011)

*Prof. Dr. F. Kremer is Principal Investigator and Lecturer in the International Research Training Group "Diffusion in Porous Materials" headed by Prof. Dr. R. Gläser and Prof. Dr. F. Kapteijn.*

*Prof. Dr. F. Kremer is Principal Investigator in the "Leipzig School of Natural Sciences - Building with Molecules and Nano-Objects" in the framework of a Graduate School funded by the "Federal Excellence Initiative". This supports several Ph.D. projects.*

## 3.21 External Cooperations

### Academic

- Université Lyon 1, CNRS, Ingénierie des Matériaux Polymères, France  
Dr. Anatoli Serghei
- Universität Rostock  
Prof. Dr. Christoph Schick and Dr. Heiko Huth
- University of Silesia, Poland  
Prof. Marian Paluch and Dr. Michael Mierzwa
- University of Regensburg  
Prof. Dr. Richard Buchner
- Niederrhein University of Applied Sciences  
Prof. Dr. Veronika Strehmel
- University of Leipzig  
Prof. Dr. Jörg Kärger, Dr. Rustem Valliulin
- MPIP, Mainz)  
Dr. Periklis Papadopolous

- MPI, Halle  
Dr. M. Alexe
- IOM, Leipzig  
Dr. D. Hirsch
- The Henryk Niewodniczanski Institute of Nuclear Physics, Polish Academy of Sciences, Kraków)  
Prof. Maria Massalska Arodź

### Industry

- Novocontrol GmbH, Hundsangen, Germany
- Clariant Produkte (Deutschland) GmbH, Frankfurt am Main, Germany
- Comtech GmbH, München, Germany
- inotec FEG mbH, Markkleeberg, Germany

## 3.22 Publications

### Journals

Krause, C., J.R. Sangoro, C. Iacob and F. Kremer "Charge transport and dipolar relaxations in imidazolium-based ionic liquids" *J. Phys. Chem. B*, 114(1), 382-386 (2010)

Papadopoulos, P., P. Heinze, H. Finkelmann, F. Kremer "Electromechanical properties of smectic C\* liquid crystal elastomers under shear" *Macromolecules* 43 (16) 6666-6670 (2010) DOI:10.1021/ma1005028

Serghei, A., J. Lutkenhaus, D. Miranda, K. McEnnis, F. Kremer, T.P. Russel "Density fluctuations and phase transitions of ferroelectric polymer nanowires" *Small* Vol. 6,16 1822-1826 (2010) DOI: 10.1002/sml.201000562

C. Iacob, J. R. Sangoro, P. Papadopoulos, T. Schubert, S. Naumov, R. Valiullin, J. Kärger and F. Kremer "Charge transport and diffusion of ionic liquids in nanoporous silica membranes" *Phys. Chem. Chem. Phys.* 12, p.13798-13803 (2010), DOI:10.1039/c004546b

Mapesa, E.U., M. Erber, M. Treß, K.-J. Eichhorn, A. Serghei, B. Voit and F. Kremer "Glassy dynamics in nanometer thin layers of polystyrene" *Europ. Phys. J. - Special Topics* 189, 173-180 (2010), DOI: 10.1140/epjst/e2010-01320-2

Erber, M., M. Treß, E.U. Mapesa, A. Serghei, K.-J. Eichhorn, B. Voit and F. Kremer "Glassy dynamics and glass transition in thin polymer layers of PMMA deposited on different substrates" *Macromolecules* 43, 7729 (2010), DOI: 10.1021/ma100912r

Ene, R., P. Papadopoulos, F. Kremer "Partial deuteration probing structural changes in supercontracted spider silk" *Polymer* 51, 21, 4784-4789 (2010)

Drechsler, A., A. Synytska, P. Uhlmann, M. M. Elmahdy, M. Stamm, F. Kremer "Interaction forces between micro-sized silica particles and weak polyelectrolyte brushes at varying pH and salt concentration" *Langmuir* 26 (9) 6400-6410 (2010) DOI:10.1021/la904103z

Treß, M., M. Erber, E.U. Mapesa, H. Huth, J. Müller, A. Serghei, C. Schick, K.-J. Eichhorn, B. Voit and F. Kremer "Glassy Dynamics and Glass Transition in Nanometric Thin Layers of Polystyrene" *Macromolecules* 43, 9937-9944 (2010) DOI: 10.1021/ma102031k

Elmahdy, M., C. Gutsche, F. Kremer "Forces within single pairs of charged colloids in aqueous solutions of ionic liquids as studied by optical tweezers" *J Phys Chem. C* 114, 19452-19458 (2010)

W. Kossack, P. Papadopoulos, P. Heinze, H. Finkelmann, F. Kremer "Transition Moment Orientation Analysis on a Smectic C Liquid Crystalline Elastomer film" *Macromolecules* 43, 18, 7532-7539 (2010), DOI:10.1021/ma101121f

Semenov, P. Papadopoulos, G. Stober, and F. Kremer "Ionic concentration- and pH-dependent electrophoretic mobility as studied by Single Colloid Electrophoresis" *J. Phys.: Condens. Matter* 22, 494109 (2010)

Zech, O., J. Hunger, J.R. Sangoro, C. Iacob, F. Kremer, W. Kunz, R. Buchner "Correlation between polarity parameters and dielectric properties of [Na][TOTO] - a sodium ionic liquid" *Phys. Chem. Chem. Phys.* 12, 14341-14350 (2010) DOI:10.1039/c0cp00840k

Turky, G., J.R. Sangoro, M. Abdel-Rehim, F. Kremer "Secondary Relaxations and Electrical Conductivity in Hyperbranched Polyester Amides" *J. Polym. Sci. B: Polym. Phys.* 48,14, 1651-1657 (2010)

Gutsche, C., M.M. Elmahdy, K. Kegler, I. Semenov, T. Stangner, O. Otto, O. Ueberschaer, U.F. Keyser, M. Krueger, M. Rauscher, R. Weeber, J. Harting, Y.W. Kim, V. Lobaskin, R.R. Netz, F. Kremer "Micro-Rheology on (Polymer-Grafted) Colloids Using Optical Tweezers" *Journal of Physics: Condensed Matter*, in press (2010)

## 3.23 Graduations

### Doctorate

- M. Sc. Joshua Rume Sangoro  
*Rotational and Translational Diffusion in Ionic Liquids*  
May 2010
- Dipl.-phys. Christof Gutsche  
*Rheologische Untersuchungen an einzelnen Kolloiden mit Optischen Pinzetten*  
2010
- Dipl.-phys. Kati Kegler  
*Kraftmessungen zwischen DNS-beschichteten Kolloiden mittels Optischer Pinzette*  
2010

### Diploma

- Christina Krause  
*Charge transport and dipolar relaxations in imidazolium-based ionic liquids*  
February 2010

- Tim Stanger  
*Wechselwirkungskräfte zwischen Polymergepfropften Kolloiden*  
October 2010

### **Bachelor**

- Emmanouil Veroutis  
*Effects of mechanical fields on the nanocrystals of biaxially oriented Nylon6, as studied by IR spectroscopy*  
November 2010
- Christian Rudolf  
*Radius- und Temperaturmessung von mikrometergroßen Kolloiden mit Hilfe einer optischen Falle*  
September 2010
- Peter Schlupp  
*Thermoelektrische Untersuchungen an den ionischen Flüssigkeiten 1-Hexyl 3 Methylimidazolium Triflat und 1-Hexyl 3 Methylimidazolium Hexafluorophosphat*  
April 2010

## **3.24 Guests**

- Prof. Dr. Gamal Turkey  
National Research Center, Cairo, Egypt  
2010

# 4

## Physics of Interfaces

### 4.1 Introduction

The department of Physics of Interfaces (Grenzflächenphysik, GFP) is in a transition state since April 2009. From the 17 scientists employed in the Group at the end of 2010, 14 were financed as PhD students or post-docs via third party funding and two received a grand as Heisenberg fellow of the DFG. Especially, the good situation in the third party funding allowed us to successfully contribute to research and teaching within the Institute of Experimental Physics I. Teaching obligations in several main courses of Experimental Physics were taken over by scientists and PhD students of the group. A total of three Master/Diploma thesis and seven Bachelor projects was successfully completed in 2010.

Research highlights in 2010 were our contributions to national and international collaborative research projects like the the Priority Research Programme "Porous Metal-Organic Frameworks" (DFG SPP 1362), the Research Group "From Local Constraints to Macroscopic Transport" (DFG SFG 807), the International Research Training Group "Diffusion in Porous Materials" (DFG IRTG 1056/2) and the Collaborative EU-India research project "Advanced Materials as CO<sub>2</sub> removers" (AMCOS, CP-FP 233502).

Jointly with the SPP "Porous Metal-Organic Frameworks", members of our group organized and contributed to the 11th IRTG workshop on "Experimental Methods of Adsorption and Diffusion Studies" (Leipzig/Eibenstock, 22nd - 25th März 2010). In September 2010 about 200 scientists came to Leipzig to attend the 10th Bologna Conference on Magnetic Resonance in Porous Media (MRPM 10, Leipzig, 12th - 16th September 2010), which was also organized by our group.

Please find below detailed descriptions of our research activities and project achievements in the field of molecules interacting with internal surfaces of micro- and mesoporous materials for 2010. If you are interested in our research, please do not hesitate to contact us.

## 4.2 Freezing-Melting Hysteresis of Fluids in Disordered Pores

D. Kondrashova, C. Reichenbach, R. Valiullin

Fluids confined to mesopores often exhibit a rich variety of phenomena not typical for bulk substances. Among them, hysteretic melting-freezing phase transitions have attracted particular attention and have been thoroughly studied. However, some aspects of these phenomena are still subject of experimental and theoretical studies [1]. In this contribution, we report on freezing and melting behavior of nitrobenzene confined to pores of Vycor porous glass as revealed by nuclear magnetic resonance cryoporometry [2]. The two transitions are found to exhibit a broad hysteresis loop, typical for liquids in mesoporous solids with random pore structure. To get deeper insight into the particular mechanisms leading to the hysteresis observed, scanning experiments (see Fig. 4.1) exploiting temperature reversal upon incomplete freezing or melting have been performed. Notably, such scanning experiments have frequently been used in the context of sorption hysteresis, but rarely addressed for freezing/melting phenomena [3].

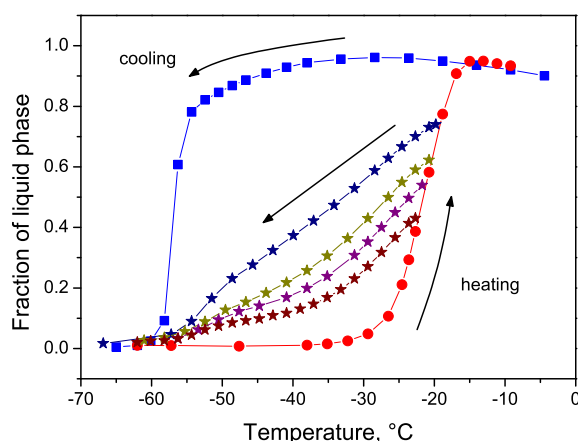


**Figure 4.1:** Freezing cryoporometry experiments extended to record the scanning behavior.

The experiments performed in this way clearly show that different cooling and warming histories result in different solid-liquid configurations within the random pore system. Further evolution of the thus attained configurations with changing temperature unveiled important information about the transition pathways. In particular, these experiments indicated the occurrence of a pronounced pore-blocking for freezing, resulting in a temperature-delayed freezing transition via invasion-percolation [4]. The melting, on the other hand, is found to occur homogeneously over the whole pore network and to resemble properties typical of the equilibrium transition.

[1] G. H. Findenegg et al.: *ChemPhysChem* **9**, 2651 (2008)

[2] D. Kondrashova et al.: *Langmuir* **26**, 6380 (2010)

[3] E. Molz et al.: *Phys. Rev. B* **48**, 5741 (1993)

[4] A. Khokhlov et al.: *New J. Phys.* **9**, 272 (2007)

### 4.3 Diffusion and Phase Equilibria of Binary Fluids in Mesopores

P. Zeigermann, M. Dvoyashkin, R. Valiullin

The formation of adsorption hysteresis in mesoporous material with random pore structure (e.g. Vycor) may be interrelated with different distributions of the fluid density attained along different paths of the system preparation. To gain insight into the microscopic details of these distributions, in addition to the main sorptive liquid (cyclohexane) a small amount of a probe liquid with a substantially lower vapor pressure has been added (10%vol tetrakis(2-ethylhexoxy)silane, TEHOS). The molecular self-diffusivities of both liquids have been traced using pulsed field gradient NMR. The analysis of the results obtained yielded diffusivities of both cyclohexane and TEHOS [1]. Because of their different vapor pressures, the two molecular species explore different spaces occupied by the capillary-condensed (accessible for both species) and gaseous (accessible only for the molecules of the main sorptive) phases. Figures 4.2a and b show the cyclohexane and the TEHOS self-diffusivities, obtained at different states of the desorption isotherm. The self-diffusivities of the two liquid components exhibit opposite dependencies on pore loading. At partial pore loadings cyclohexane, as a liquid with sufficiently high vapor pressure, can explore the pore interiors containing the gaseous phase via Knudsen diffusion. Thus, by increasing the volume available for the gaseous phase and by increasing density of cyclohexane molecules there, the transport of cyclohexane can be enhanced. In contrast, because TEHOS molecules cannot escape into the gaseous phase, domains filled with the gaseous cyclohexane do form additional transport resistances for TEHOS. Therefore, the diffusivity of TEHOS decreases with decreasing pore loading.

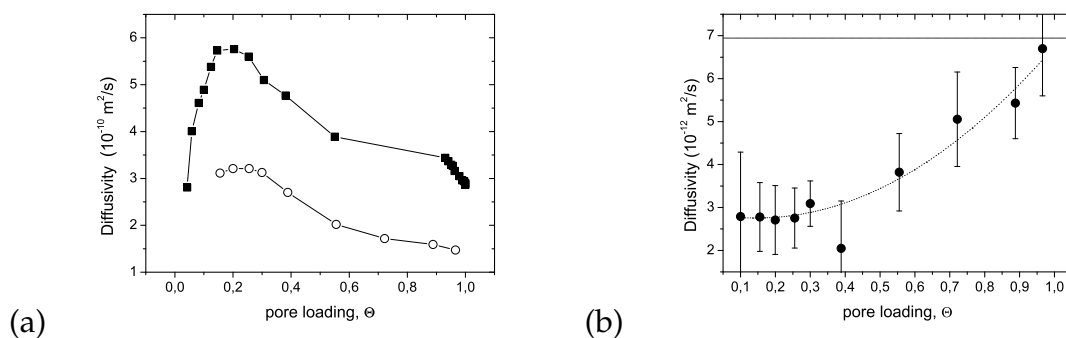


**Figure 4.2:** Self-diffusivities of pure cyclohexane (a, filled symbols), the cyclohexane in the cyclohexane-TEHOS mixture (a, open symbols) and TEHOS in the cyclohexane-TEHOS mixture (b) as a function of the overall pore loading as observed by PFG NMR upon desorption.

[1] P. Zeigermann et al.: *Adsorption* **17**, 69 (2011)

## 4.4 Self-Diffusion of Polystyrene Solutions in Porous Acrylate-Based Monoliths Studied by $^1\text{H}$ PFG NMR

S. Beckert, F. Stallmach, R. Bandari\*, M.R. Buchmeiser\*

\*Institut für Polymerchemie, Universität Stuttgart

The pulsed field gradient (PFG) nuclear magnetic resonance (NMR) method has been used to study the molecular self-diffusion of polystyrene (PS) solutions in porous acrylate-based monoliths [1, 2] (see Fig. 4.3a). It was found that the characteristic concentration and molar mass dependencies of the PS self-diffusion in the solution (describable by the Zimm- and Doi-Edwards models [3, 4]) remain unchanged in case that the self-diffusion occurred in this porous material (see Fig. 4.3b). However, the self-diffusion coefficients of the PS were reduced in the monoliths by a constant factor, which is independent of molar mass and concentration. This constant factor represents the tortuosity of the porous monoliths and agrees with the reduction of the initial turnover frequency found in the ring-closing metathesis reaction of diethyl diallyl malonate catalyzed in these monoliths [5].

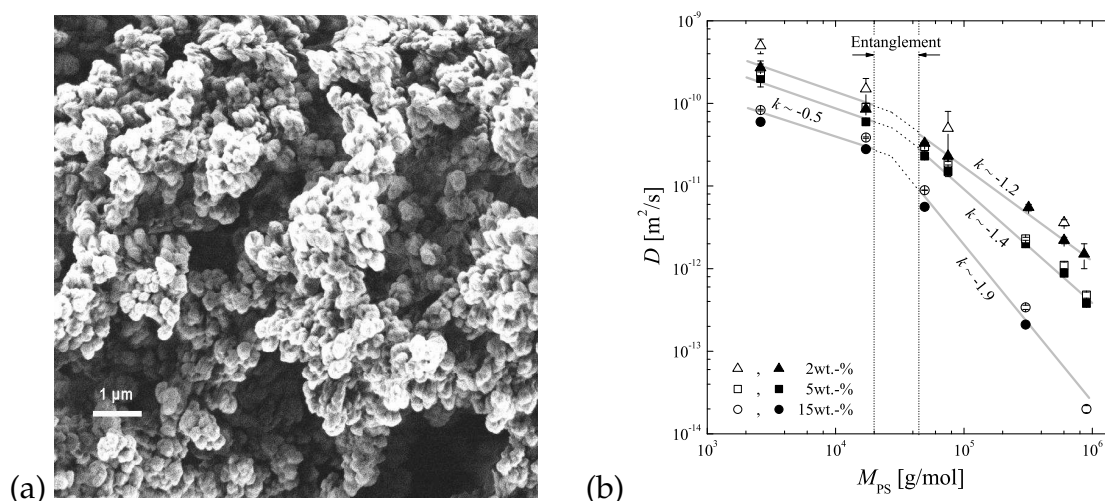


**Figure 4.3:** (a) REM picture of the porous acrylate-based monoliths. (b) Double logarithmic representation of the self-diffusion coefficients  $D$  in dependence of the molar mass  $M_{\text{PS}}$  for the different concentrations of PS dissolved in deuterated benzene (*open symbols*) and of PS dissolved in deuterated benzene soaked into the porous monoliths (*full symbols*) [6].

- [1] F. Sinner, M.R. Buchmeiser: *Angew. Chem.* **112**, 1491 (2000)
- [2] F. Sinner, M.R. Buchmeiser: *Macromolecules* **33**, 5777 (2000)
- [3] B.H. Zimm: *J. Chem. Phys.* **24**, 269 (1956)
- [4] M. Doi, S.F. Edwards: *J. Chem. Soc., Faraday Trans. 2* **74**, 1789 (1978)
- [5] J.O. Krause et al.: *Macromol. Rapid Commun.* **24**, 875 (2003)
- [6] S. Beckert et al.: *Macromolecules* **43**, 9441 (2010)

## 4.5 Self-Diffusion Studies in CuBTC by PFG NMR and MD Simulations

M. Wehring, J. Gascon\*, D. Dubbeldam<sup>†</sup>, F. Kapteijn\*, R.Q. Snurr<sup>‡</sup>, F. Stallmach

\*Catalysis Engineering, DelftChemTech, Delft University of Technology, Delft, The Netherlands

<sup>†</sup>Faculty of Science, University of Amsterdam, Amsterdam, The Netherlands

<sup>‡</sup>Chemical and Biological Engineering Department, Northwestern University, Evanston, USA

Self-diffusion and relaxation time studies of C<sub>3</sub> to C<sub>6</sub> hydrocarbons adsorbed in the microporous metal-organic framework CuBTC [1] were performed by nuclear magnetic resonance (NMR) in the temperature range of 193 K to 373 K [2]. The presence of paramagnetic copper species in the solid CuBTC framework leads to short longitudinal ( $T_1$ ) and transverse ( $T_2$ ) relaxation times of the hydrocarbons with typical values of  $T_1 \lesssim 10$  ms and  $T_2 \lesssim 3$  ms. Under these conditions, pulsed field gradient NMR self-diffusion studies [3] could only be performed at short observation times using the primary spin echo sequence with high-intensity pulsed magnetic field gradients. The obtained temperature dependent self-diffusion coefficients were analysed using an Arrhenius approach (see Fig. 4.4). The activation energies of the alkanes are in the range of 6.5 kJ/mol to 8.5 kJ/mol increasing slightly with increasing number of carbon atoms. Significantly higher values were found for propene (13.2 kJ/mol) and 1-butene (15.0 kJ/mol). These tendencies are consistent with corresponding measurements of heats of adsorption [2, 4] and with data obtained in MD simulations [2, 5]. The MD simulation show a strong dependence of the heat of adsorption and diffusion on loading and temperature. This is caused by the preferential adsorption of small alkanes like propane and butane in the side pockets of the CuBTC structure at low loading and temperature.

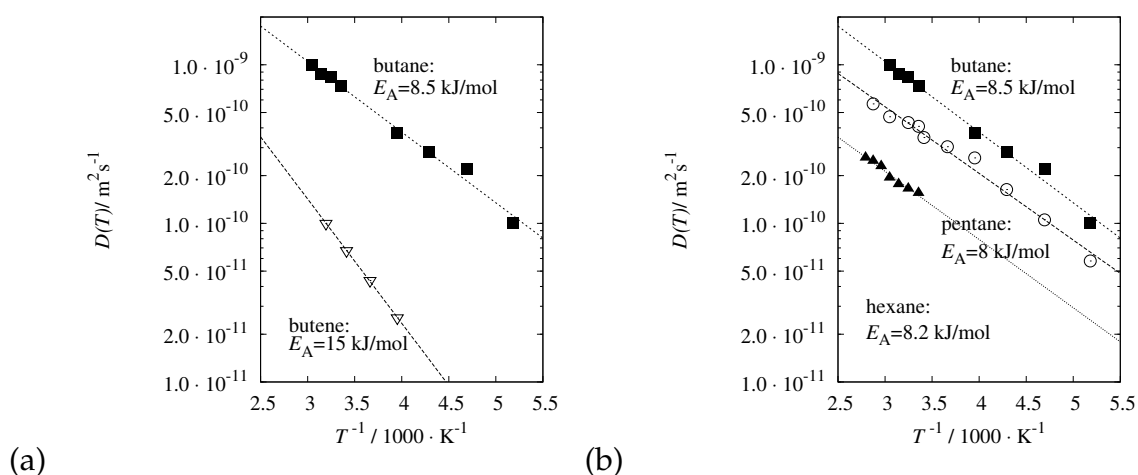


**Figure 4.4:** Intracrystalline self-diffusion coefficients of *n*-butane (black squares), 1-butene (empty triangles) (a) and *n*-butane (black squares), *n*-pentane (circles), *n*-hexane (full triangles) (b), with the corresponding activation energies of self-diffusion.

[1] S. S.-Y. Chui et al.: Science **283**, 1148 (1999)

- [2] M. Wehring et al.: J. Phys. Chem. C **114**, 10527 (2010)  
 [3] F. Stallmach, P. Galvosas: Ann. R. NMR S. **61**, 51 (2007)  
 [4] D. Farrusseng et al.: Langmuir **25**, 7383 (2009)  
 [5] C. Chmelik et al.: Micropor Mesopor. Mat. **117**, 22 (2009)

## 4.6 $^{13}\text{C}$ NMR Diffusion Studies with $\text{CO}_2$ Adsorbed in MOF CuBTC

A.-K. Pusch, S. Schlayer, F. Stallmach

Metal organic frameworks (MOF) are currently explored for their suitability for gas separations. Computer simulations for separation of mixtures of  $\text{CH}_4/\text{H}_2$ ,  $\text{CO}_2/\text{CH}_4$ , and  $\text{CO}_2/\text{H}_2$  permeating through IRMOF-1 and CuBTC membranes already exist in literature [1]. In this work experimental studies of  $\text{CO}_2$  in CuBTC [2] were performed by means of pulsed field gradient (PFG) NMR [3]. As experimental setup for  $^{13}\text{C}$  NMR necessary for the  $\text{CO}_2$  measurements a commercial double resonance  $^1\text{H}/\text{X}$ -band NMR probe was equipped with a Maxwell-type gradient coil. Using the available gradient current facilities on the homebuild NMR spectrometer FEGRIS FT [3], the current design is able to provide bipolar pulsed field gradients of up to 15 T/m.

NMR diffusion studies were carried out at 101 MHz  $^{13}\text{C}$  resonance frequency in a temperature range from 198 K to 348 K and for different loadings (94 mg/g to 284 mg/g). For all loadings the transverse relaxation times are long enough to allow the application of the 13-interval pulse sequence [3]. The spin echo attenuations fit a bi-exponential model yielding the long-range self-diffusion coefficient ( $\sim 10^{-8}\text{m}^2/\text{s}$ ) through the bed of the MOF, the intracrystalline self-diffusion coefficient ( $\sim 10^{-9}\text{m}^2/\text{s}$ ) within the MOF and their respective relative amounts (Fig. 4.5). The obtained temperature dependent self-diffusion coefficients were analyzed using an Arrhenius approach. The activation energy of the carbon dioxide in CuBTC is approximately 7 kJ/mol. Our results show that carbon dioxide is very mobile in the MOF CuBTC and may easily diffuse through the external crystall boundary.

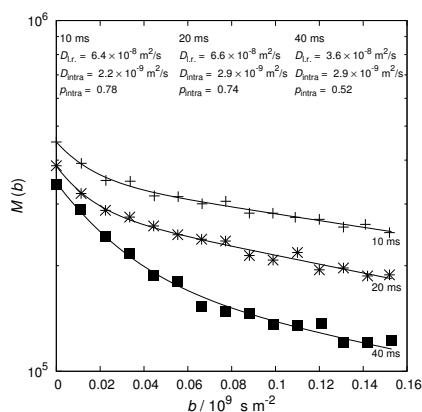


Figure 4.5: Spin-echo attenuation curves at 298 K for different diffusion times.

- [1] D.S. Sholl et al.: Langmuir **19**, 11786 (2009)  
 [2] S.S.-Y. Chui et al.: Science **283**, 1148 (1999)  
 [3] F. Stallmach, P. Galvosas: Ann. R. NMR S. **69**, 51 (2007)

## 4.7 NMR Studies of Benzene Mobility in Metal-Organic Framework MOF-5

S. Hertel, S. Amirjalayer\*, M. Gratz, J. Lincke<sup>†</sup>, H. Krautscheid<sup>†</sup>, R. Schmid\*, F. Stallmach

\*Lehrstuhl für Anorganische Chemie II, Ruhr-Universität Bochum, Bochum

<sup>†</sup>Fakultät für Chemie und Mineralogie, Universität Leipzig

In this contribution NMR experiments for the investigations of the mobility of benzene molecules adsorbed in MOF-5 are presented and compared to current data available from MD simulations, see Fig. 4.6. For small loadings NMR and MD data agree within the experimental uncertainty. For loadings exceeding 10 molecules per unit cell the NMR data exhibit a pronounced drop and are found to be a factor of three lower than the data obtained by MD simulations. The experimentally observed steep decrease of mobility from low loadings (10 molecules per unit cell) to higher loadings (20 molecules per unit cell) is not reproduced in the MD simulations. It is probably caused by intermolecular forces between benzene molecules, which lead to clustering. Such information about self-diffusion in the high loading regime was not available before and might help to improve future MD simulations.

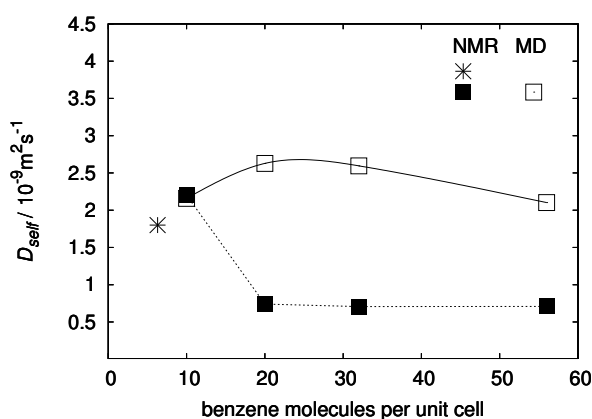


**Figure 4.6:** Loading dependence of the self-diffusion coefficients obtained by PFG NMR (*full symbols* this work; *star* taken from [1]) inside MOF-5 and comparison to the data obtained by MD simulations at  $T = 298\text{K}$  (*open squares* [2]).

- [1] F. Stallmach et. al: Angew. Chem. Int. Edit. **47**, 2123 (2006)  
 [2] S. Amirjalayer et. al: Micropor. Mesopor. Mat. **125**, 90 (2009)

## 4.8 Combining MAS and PFG NMR for the Investigation of Mixtures in Porous Materials

M. Gratz, S. Hertel, M. Wehring, S. Schlayer, F. Stallmach, P. Galvosas\*

\*MacDiarmid Institute, Victoria University, Wellington, New Zealand

The investigation of the individual motional properties of molecular species in a mixture has always been a challenging task. Especially non-invasive methods are rare and often require specialized equipment. By combining two standard NMR techniques we have been able to improve the NMR toolbox and to study mixture diffusion in porous materials.

By application of magic-angle spinning (MAS) using a commercial MAS probe, line broadening in the NMR spectrum may be reduced, enabling the separation of individual species even when they are adsorbed. Furthermore, pulsed field gradients (PFG) of up to  $\pm 2.6$  T/m are incorporated in the NMR experiment and applied by a conventional micro-imaging probe along the axis of rotation. As a result, the high-resolution NMR spectrum is extended by a second dimension, which enables one to derive the motional behaviour for individual lines in the spectra.

To avoid impact of the sample rotation on the diffusion measurements, both components have to be aligned such, that the direction of the applied gradient and the rotational axis coincide. A two-step alignment procedure based on an adapted one-dimensional NMR imaging experiment was developed to match this condition (see [1] for details).

First experiments using a binary mixture of benzene and *n*-hexane adsorbed in the metal-organic framework MOF-5 were already successful. Both components could be identified and extracted from the two-dimensional NMR spectrum (Fig. 4.7). The results for the diffusion constants are consistent with the values given in the literature [2, 3], which were obtained in PFG NMR experiments using similar samples with one single component only.

- [1] M. Gratz, S. Hertel, M. Wehring, F. Stallmach, P. and Galvosas: *Mixture diffusion of adsorbed organic compounds in Metal-Organic Frameworks as studied by MAS PFG NMR*, New J. of Phys., accepted
- [2] F. Stallmach et al.: *Angew. Chem. Int. Edit.* **45**, 2123 (2006)
- [3] S. Hertel, M. Wehring, S. Amirjalayer, M. Gratz, J. Lincke, H. Krautscheid, R. Schmid, F. Stallmach: *NMR studies of benzene mobility in metal-organic framework MOF-5*, submitted to *Eur. Phys. J.*, 2011

## 4.9 Low-Field High-Pressure NMR Porosimetry

C. Horch, A.-K. Pusch, F. Stallmach

Adsorption, storage and transport of gases at high pressures is of particular interest in many fields of chemical, environmental and reservoir engineering. We designed and

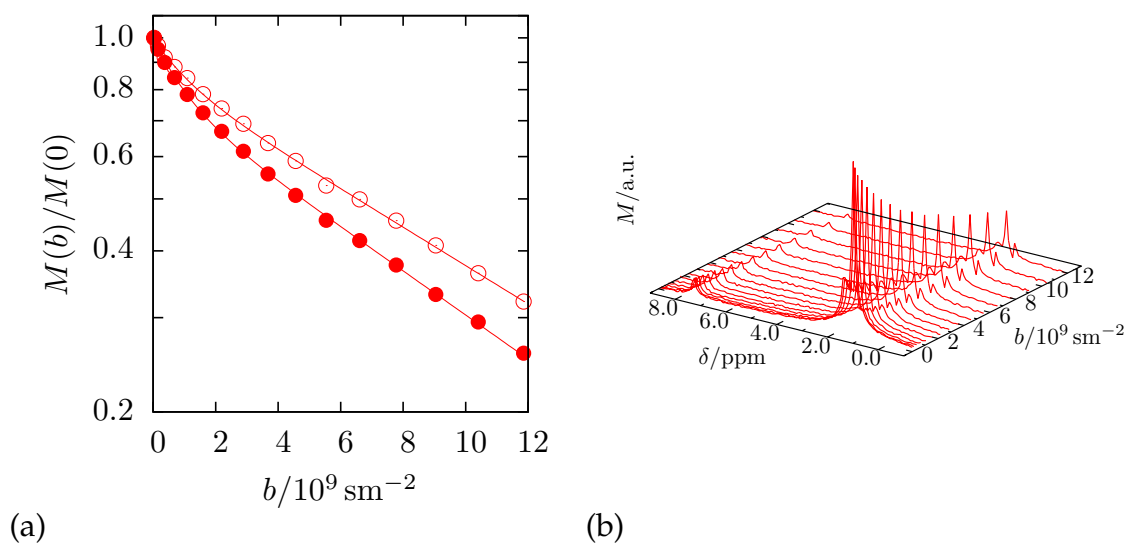


**Figure 4.7:** (a) Attenuated NMR spectrum of benzene and *n*-hexane adsorbed in MOF-5. (b) Extracted spin echo attenuations for the single components ( $\circ$  – benzene,  $\bullet$  – *n*-hexane).

constructed the experimental set-up for low-field NMR relaxation studies at static pressures of up to 30 MPa for in-situ characterization of pore space properties of porous materials. In our high-pressure NMR porosimetry approach, the respective samples are exposed to the elevated gas pressures by a home-built apparatus constructed of stainless steel HiP Taper Seal parts and of a non-metallic NMR compatible pressure-resistant sample vessel made of the high-tensile plastic PEEK. The sensitive sample volume inside the pressure-resistant vessel is a cylinder of about 10 cm<sup>3</sup>. The low-field NMR spectrometer for the relaxation time studies consists of a MARAN DRX console equipped with a home-built shimmed NdFeB permanent magnet arrangement generating a magnetic flux density of 0.119 T (<sup>1</sup>H resonance frequency of 5 MHz) [1].

In the experiments with the nanoporous MOF CuBTC [2], the  $T_2$  relaxation time distributions show well distinct peaks for the high pressure methane gas phase surrounding the porous particles and those adsorbed in the pore space. These NMR signals change characteristically in intensity and  $T_2$  when changing the methane pressure. Co-adsorption of CO<sub>2</sub> leads to replacement of methane by the stronger adsorbed CO<sub>2</sub>, which could be followed by <sup>1</sup>H NMR. The  $T_2$  relaxation time distributions of the co-adsorption show a decreasing intensity and shift of peaks. These observations allow the measurement of adsorption isotherms at elevated pressures and the assignment of preferred adsorption sites in the porous host material. Furthermore, the gas adsorption selectivity is obtained from experimental data. The value agrees well with results of GCMC computer simulations [3, 4].

- [1] C. Horch et al.: Proceedings COMSOL Conference 2009, Milan, Italy. see: <http://cds.comsol.com/access/dl/papers/6717/Horch.pdf>  
 [2] S. Chui et al.: Science **283**, 1148 (1999)  
 [3] S. Keskin et al.: Micropor. Mesopor. Mat. **125** 101 (2009)  
 [4] S. Keskin et al.: Langmuir **25**(19), 11786 (2009)

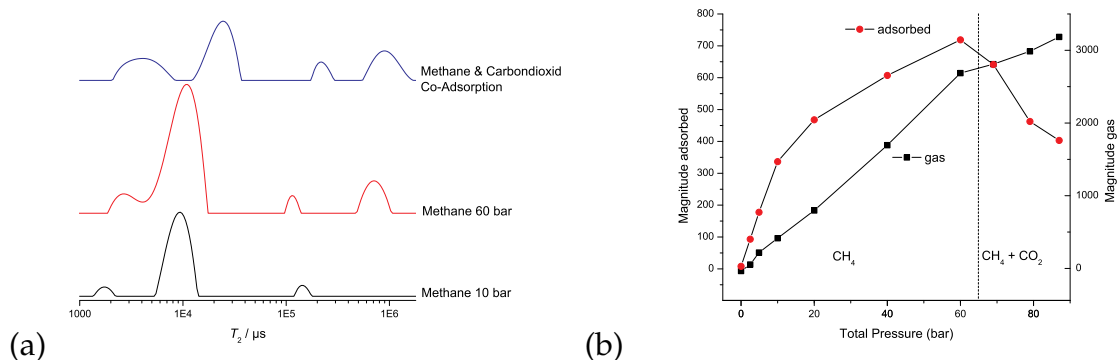


**Figure 4.8:**  $T_2$  relaxation time distributions of adsorption and desorption of  $\text{CH}_4$  (a) and intensities of these peaks plotted over total pressure (b).

## 4.10 Anomalies in the Diffusion of Small Molecules in MOF ZIF-8

T. Binder, H. Bux\*, J. Caro\*, F. Hibbe, T. Titze, C. Chmelik

\*Institut für Physikalische Chemie und Elektrochemie, Leibniz Universität Hannover

In recent years there has been a remarkable upsurge in research activity on metal-organic frameworks (MOFs), in view of several potential applications in storage, separations, and catalysis. A wide variety of MOFs have been synthesized, and investigated. Mass transfer of guest molecules through the outer surface and inside the nanopores is essential for the applicability of the particular system. Direct access to these key quantities is provided by our microscopic techniques of diffusion measurement, viz. IR and interference microscopy. Adsorption and diffusion of a variety of small guest molecules in MOF ZIF-8 was investigated. An unusually strong increase in the methane diffusivity (Fig. 4.9) with loading was found, which may be rationalized by changes in the lattice structure exclusively triggered by methane [1]. This effect is currently investigated in detail using molecular simulations. A second remarkable finding is the experimental evidence for the influence of molecular clustering on mass transfer [2]. Clustering by H-bonding occurs in ZIF-8 for polar molecules like methanol and ethanol. Both effects may provide options to significantly enhance the performance in separations of such molecules.

[1] C. Chmelik and J. Kärger: Chem. Soc. Rev. **39**, 4864 (2010)

[2] C. Chmelik et al.: Phys. Rev. Lett. **104**, 085902 (2010)

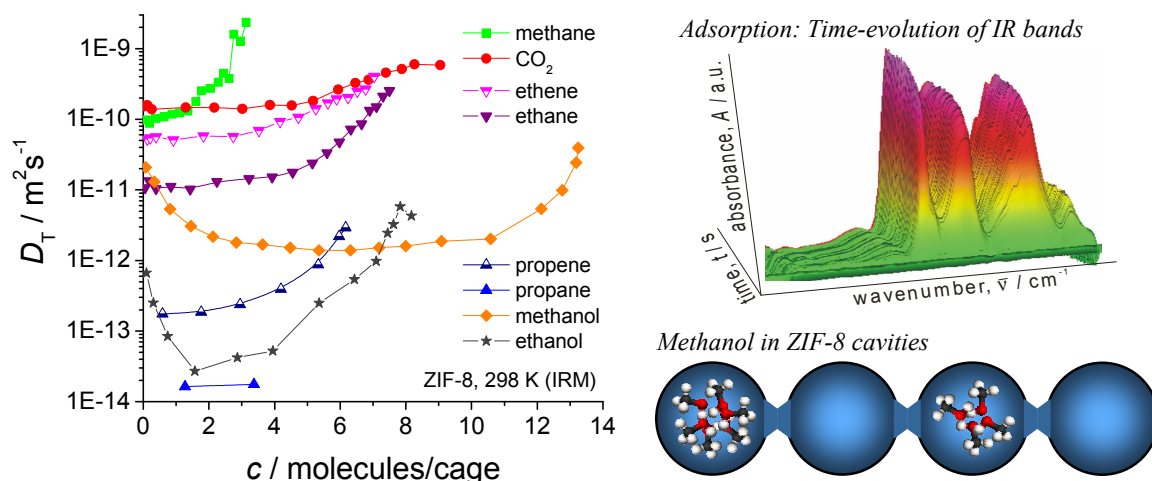


**Figure 4.9:** Loading dependencies of the transport diffusivity for a variety of guest molecules in MOF ZIF-8 at 298 K measured by IR microscopy by recording the time-evolution of IR bands. The flexibility of the framework and clustering of the guest lead to opposite trends in the loading-dependence of the diffusivities [2].

## 4.11 Zeolitic Imidazolate Framework-8 Molecular Sieve Membrane: From Molecular Diffusion to Membrane Permeation

C. Chmelik, H. Bux\*, J. Caro\*, L. Hertäg, M. Knauth, S. Fritzsche, J.M. van Baten<sup>†</sup>, R. Krishna<sup>†</sup>, J. Kärger

\*Institut für Physikalische Chemie und Elektrochemie, Leibniz Universität Hannover

<sup>†</sup>Van't Hoff Institute for Molecular Sciences, University of Amsterdam, The Netherlands

Metal-organic frameworks (MOFs) are new microporous 3D coordination compounds with unique properties. One of the primary features which make MOFs highly interesting as molecular sieve is the so called isorecticular design. Linker molecules can be modified with functional groups or even completely substituted, retaining the framework structure while altering gas adsorption and diffusion properties. The MOF subclass of zeolitic imidazolate frameworks (ZIFs) exhibit exceptionally high thermal and chemical stability. For the first time, membranes as well as large single-crystals of MOF ZIF-8 could be synthesized. By combining IR microscopy (IRM) measurements with molecular simulations, adsorption and diffusion data on large ZIF-8 single crystals were determined (Fig. 4.10a). From the product of adsorption selectivity and diffusion selectivity, the permeation selectivity of a membrane can be estimated (Fig. 4.10b) [1]. The measurements showed  $\text{H}_2/\text{CH}_4$ ,  $\text{CO}_2/\text{CH}_4$  and  $\text{C}_2\text{H}_4/\text{C}_2\text{H}_6$  selectivities above the so called Knudsen separation factor. Moreover the selectivities are in good agreement with the estimated ones, showing it is generally possible to predict the membrane selectivity by a simple estimation based on mixture adsorption and diffusion data [1].

[1] H. Bux et al.: J. Membr. Sci. **369**, 284 (2011).

[2] H. Bux et al.: Adv. Mater. **22**, 4741 (2010).

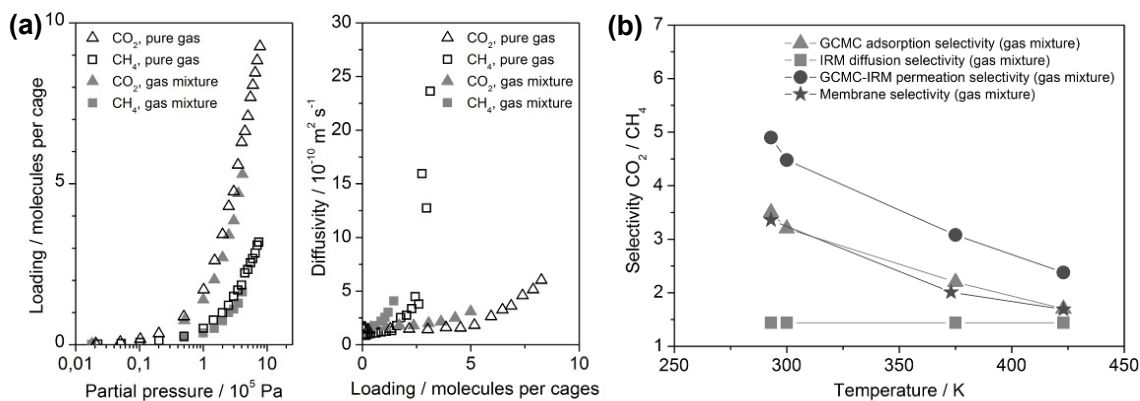


**Figure 4.10:** ZIF-8 adsorption isotherms and diffusion coefficients of CO<sub>2</sub> and CH<sub>4</sub> as pure gases and in binary, equimolar mixture (a) and diffusion selectivity, adsorption selectivity and estimated permeation selectivity of CO<sub>2</sub>/CH<sub>4</sub> in equimolar mixture as function of temperature (b) [2].

## 4.12 Diffusion Studies on Large-Crystal Ferrierite Zeolites

F. Hibbe, C. Chmelik, V.R.R. Marthala\*, J. Kärger, J. Weitkamp\*

\*Institute of Chemical Technology, University of Stuttgart

The potential to record the evolution of intra-particle concentration profiles in transparent nanoporous materials with interference (IFM) and IR microscopy (IRM) has opened a new field of diffusion research [1]. The high spatial and temporal resolution of both techniques does not only enable the determination of accurate (transport-) diffusivity values, but also the observation of transport barriers inside the studied material and on the material surface, directly from the measured concentration profiles (Fig. 4.11a).

In uptake and release experiments of methanol in all-silica and aluminum containing ferrierite crystals, the impact of the chemical composition and different post-synthesis treatments on molecular uptake could be observed: NaOH washing could be identified to open blocked pores for guest uptake, leading to remarkably enhanced uptake rates. Furthermore the diffusion of methanol was found to be anisotropic. The molecules diffuse faster in the 10-ring channels than in the 8-ring channels (Fig. 4.11b). The extent of the observed anisotropy depends on the chemical composition of the crystal and is higher in all-silica crystals than in aluminium-containing crystals (Fig. 4.11c).

[1] L. Heinke et al.: Chem. Eng. Technol. **30**, 995 (2007)

[2] P. Kortunov et al.: J. Phys. Chem. B **110**, 23821 (2006)

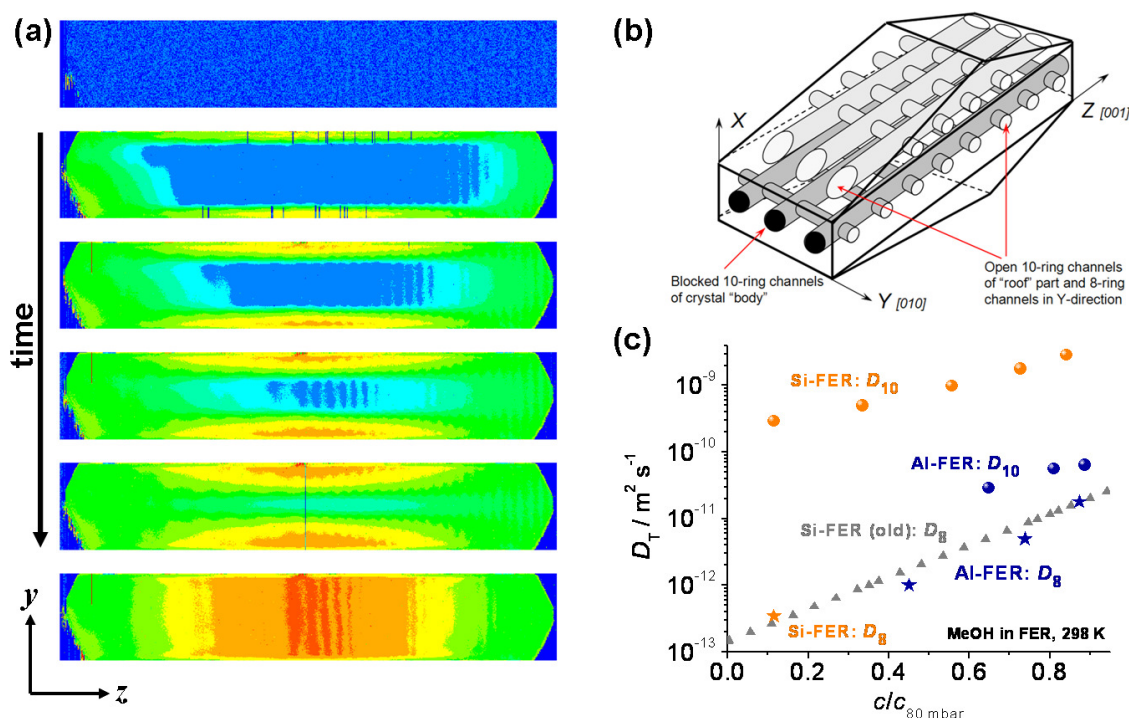


**Figure 4.11:** (a) Uptake of methanol in a NaOH-washed all-silica ferrierite crystal. The profiles clearly indicate fast transport along the 10-ring channels which were opened by the NaOH-washing. (b) Schematic illustration of the pore structure in Ferrierite crystals. (c) Transport diffusivities for methanol in 8- and 10-ring channels of all-silica and aluminium containing Ferrierite (reference data Si-FER (old) taken from [2]).

### 4.13 Configurational entropy and intersection blocking effects in multi-component systems in MFI-type zeolites studied by IR microscopy

T. Titze, C. Chmelik

Diffusion is important in many technological processes, particularly those that utilize nanoporous materials like zeolites for adsorptive separations and catalysis, where mass transfer is often the rate-limiting step. For understanding and predicting such processes knowledge of the adsorption and diffusion behaviour of molecular mixtures is essential. It is known, that branched hydrocarbons like 2-methylpentane favor the intersections of the channels in MFI-type zeolites as adsorption sites and therefore may impede separation processes by “intersection blocking” [1–3]. On the other hand, in molecular simulations “configurational entropy effects” are found predicting that at higher loadings the sorption of linear alkanes is favored above branched alkanes, if molecules with the same C-number are compared. In this study we present a direct experimental evidence of the “configurational entropy effect” in MFI-type zeolites.

IR Microscopy (IRM) is a suitable technique to investigate molecular mixtures, since it is possible to observe different components simultaneously by their characteristic IR bands. In our experiment we chose an MFI type zeolite (silicalite-1), which is one of

the most important frameworks in separation processes. As adsorbate we applied a 1:1 mixture of 2-methylpentane and (fully deuterated) n-hexane, in order to investigate the entropy effects predicted in simulations [1].

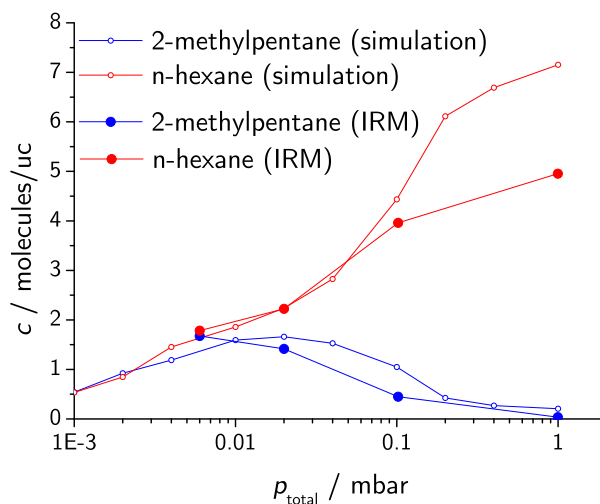


**Figure 4.12:** Isotherms of a 1:1 gas phase mixture of n-hexane and 2-methylpentane at 298 K measured with IRM and compared to CMBC simulation data (replotted from [1]). The decreasing loading of 2-methylpentane for  $c_{\text{total}} > 4$  molecules/uc is a direct experimental evidence of the “configurational entropy effect”.

- [1] R. Krishna, J.M. van Baten: Chem. Eng. J. **140**, 614 (2008)
- [2] C. Chmelik et al.: Micropor. Mesopor. Mat. **125**, 11 (2009)
- [3] J. Caro: Micropor. Mesopor. Mat. **125**, 79 (2009)

## 4.14 Studies on Adsorption Energy Distributions Computation from Adsorption Isotherms by the Ansatz Method

S. Arnrich\*, G. Kalies, P. Bräuer,

\*MATHCCES, Department of Mathematics, RWTH Aachen University

The well-known adsorption integral equation (AIE) for calculating pore size and adsorption energy distributions from adsorption isotherms on porous solids is, from the mathematical point of view, a linear Fredholm integral equation of the first kind and therefore an ill-posed problem [1]:

$$f(s) = \int_J K(s, t) \cdot F(t) dt, \quad s \in I \quad (4.1)$$

where  $I$  and  $J$  are intervals of the real axis  $\mathbb{R}$ .

In the case of adsorption,  $f$  denotes the measured adsorption isotherm and is called *total isotherm*, whereas the kernel  $K$  of the AIS is called *local isotherm*.  $F$  is the pore

size or adsorption energy distribution function either related to measured gas or liquid adsorption isotherms.

There are two approaches for solving the AIE:

- 1) the numerical regularization method
- 2) the fitting of the experimental adsorption data by functions possessing an analytical solution.

Up to now, the second approach was treated without consideration of the ill-posedness.

In our work, we included ill-posedness in the approach, which leads to its specification which we called the ansatz method [2]. By showing that a certain class of ansatz functions cannot be used for describing the total isotherms, we were urged to consider more general solutions being connected with Stieltjes integrals. After applying a general inversion formula we restricted the theoretically possible total isotherms and outlined a feasible general ansatz.

- [1] W. Rudzinski, D.H. Everett, *Adsorption of Gases on Heterogeneous Surfaces*, (Academic Press, London 1992) p 77  
[2] S. Arnrich et al.: *Appl. Surf. Sci.* **256**, 5198 (2010)

## 4.15 Further Advancements in Predicting Adsorption Equilibria using Excess Formalism: Calculation of Adsorption Excesses at the Liquid/Solid Interface

G. Kalies, C. Reichenbach, R. Rockmann\*, D. Enke<sup>†</sup>, P. Bräuer, M. Jaroniec<sup>‡</sup>

\*DBI Gas- und Umwelttechnik GmbH, Leipzig

<sup>†</sup>Institute of Technical Chemistry, University of Leipzig

<sup>‡</sup>Department of Chemistry, Kent State University, Kent, Ohio, USA

Prediction of adsorption equilibria for ternary liquid mixtures on solid surfaces by means of adsorption data for the corresponding three binary liquid mixtures can be improved by combining the thermodynamic excess formalism with geometrical models.

In our work, we examined this new strategy for the prediction of excess adsorption isotherms for four ternary adsorption systems ranging from ideal to highly non-ideal ternary mixtures. The predicted isotherms are discussed and compared with experimental ones as well as with those obtained for a model based on the absolute quantities (see Fig. 4.13)). The results confirm: (i) superiority of predicting adsorption in terms of excess quantities, and (ii) utility of geometrical models for constructing ternary molar compositions on the basis of binary ones to predict equilibria not only for liquid mixtures alone but also for adsorption of liquid mixtures on solid surfaces.

- [1] G. Kalies et al.: *J. Colloid Interf. Sci.* **275**, 410 (2004)  
[2] G. Kalies et al.: *J. Colloid Interf. Sci.* **352**, 504 (2010)

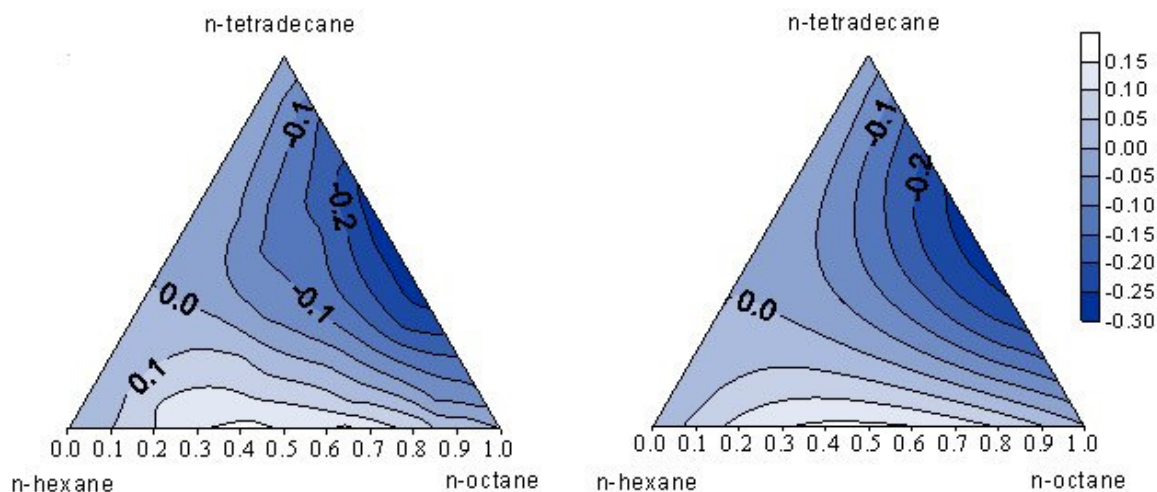


**Figure 4.13:** Adsorption of n-octane from n-hexane(1) / n-octane(2) / n-hexadecane(3) ternary mixture on Carboxen 563 at 298 K. Experimental ternary adsorption excesses (*left*) [1] and predicted ternary adsorption excesses by means of excess quantities (*right*) [2].

## 4.16 Unusual Adsorption Behavior of a Highly Flexible Copper-Based MOF

C. Reichenbach, G. Kalies, J. Lincke\*, D. Lässig\*, H. Krautscheid\*, J. Moellmer†, M. Thommes‡

\*Institute of Inorganic Chemistry, University of Leipzig

†Institut für Nichtklassische Chemie e.V. (INC), Leipzig

‡Quantachrome Instruments, Florida, USA

Due to their network flexibility, metal-organic frameworks (MOFs) may respond to external stimuli such as guest molecules, heat, pressure, humidity and so on by a dynamical transformation of their structure.

In this work we present experimental studies by means of nitrogen and argon physisorption at cryogenic temperature concerning the influence of handling and storage on the recently synthesized highly flexible copper-based MOF  ${}^3_{\infty}[(\text{Cu}_4(\mu_4 - \text{O})(\mu_2 - \text{OH})_2(\text{Me}_2\text{trz}p\text{ba})_4)]$ . Unusual adsorption isotherms (Fig. 4.14) with up to three distinct steps in the adsorbed volume have been found substantiating once more: (i) the high sensitivity of flexible network structures for environmental influences, (ii) the high diversity of physisorption isotherm types for flexible materials including isotherms with several steps and large hysteresis loops, and last not least, (iii) that theoretical methods assuming inert solids cannot be applied to highly flexible materials for calculating pore sizes and other solid state parameters.

[1] J. Lincke et al.: *A Novel Copper-Based MOF Material: Synthesis, Characterization and Adsorption Studies*, *Micropor. Mesopor. Mat.*, in press

[2] C. Reichenbach et al.: *Unusual Adsorption Behavior of a Highly Flexible Copper-Based MOF*, *Micropor. Mesopor. Mat.*, in press

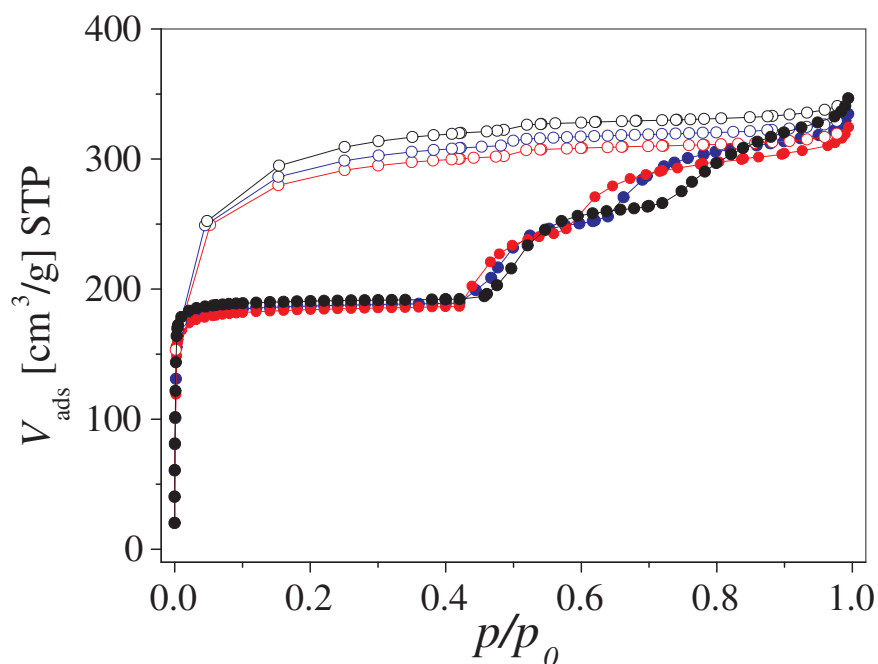


**Figure 4.14:** Nitrogen ad- (*filled symbols*) and desorption (*open symbols*) at 77 K on the same MOF material after repeated adsorption measurements [1, 2].

## 4.17 Funding

*Studying Zeolitic Diffusion by Interference and IR Microscopy.*

Prof. Dr. J. Kärger, Dr. C. Chmelik

DFG-Projekt KA 953/18-3, International Research Group "Diffusion in Zeolites"

*Bestimmung mikroskopischer Kenngrößen der Molekültranslation in Schüttungen nanoporöser Partikel mittels PFG NMR und Monte-Carlo-Simulation.*

Prof. Dr. J. Kärger, Dr. R. Valiullin

DFG-Projekt KA 953/19-2

*Confinement Effects on Diffusion and Reaction in Zeolites, Studied by Dynamic MC Simulations, PFG NMR and Interference/IR Microscopy.*

Prof. Dr. J. Kärger

im DFG-Projekt GRK 1056/1, International Research Training Group "Diffusion in Porous Materials"

*PFG NMR studies of zeolitic diffusion.*

Prof. Dr. P. Galvosas, Prof. Dr. J. Kärger

DGF-Projekt GA 1291/1-2

*PFG NMR investigations on formulated catalysts; Bestimmung von Diffusionskoeffizienten an Katalysatoren.*

Dr. F. Stallmach

BASF AG

*Fourier-Transform-PFG-NMR mit starken Feldgradientenimpulsen zur selektiven Selbstdiffusionsmessung.*

Prof. Dr. J. Kärger, Dr. F. Stallmach  
DFG-Projekt KA 953/16-1

*Innovative Zugabestoffe für die Innere Nachbehandlung von Hochleistungsbeton unter Berücksichtigung der räumlichen und zeitlichen Wasserbilanz.*

Prof. Dr. J. Kärger, Dr. F. Stallmach  
DFG-Projekt KA 953/22-2

*Messung intrakristalliner Diffusions-Reaktions-Profile in Zeolithen mittels IR-Imaging.*

Dr. C. Chmelik, Prof. Dr. J. Kärger  
DFG-Projekt KA 953/20-1

*Messung von Phasenübergängen in mesoskopisch beschränkten Systemen: kombinierter Einsatz von NMR und Molekulardynamik.*

Prof. Dr. J. Kärger, Dr. R. Valiullin  
DFG-Projekt KA 953/21-1

*PFG NMR Untersuchung der Transporteigenschaften von Fluiden in Mesoporen in der Nähe des kritischen Punktes*

Prof. Dr. J. Kärger, Dr. R. Valiullin  
DFG-Projekt KA 953/25-1

*Particle Dynamics in Nano-Structured Channels*

Prof. J. Kärger, Dr. R. Valiullin, Prof. W. Janke  
DFG-Projekt KA 953/27-1

*Transport in microporous MOFs: From molecular diffusion to membrane permeation*

Dr. C. Chmelik, Prof. Dr. J. Kärger  
DFG-Projekt KA 953/29-1, SPP 1362 MOFs

*NMR-Untersuchungen und theoretische Ansätze zur Korrelation des Diffusionsverhaltens in komplementären Porenräumen*

Prof. Dr. J. Kärger, Dr. R. Valiullin, Prof. Dr. A. Bunde  
DFG-Projekt KA 953/30-1

*Thermodynamik und Vorausberechnung der Adsorption von Mischungen*

Dr. G. Kalies  
DFG KA 1560/3-2 und KA 1560/4-2

*Texturelle Charakterisierung von Sandsteinen (Bohrkernen) und kontaminierten Aktivkohlen*

Dr. G. Kalies  
Gaz de France

*Advanced Materials as CO<sub>2</sub> Removers: A Computational Study of CO<sub>2</sub> Sorption Thermodynamics and Kinetics*

Dr. F. Stallmach  
EU project CP-FP 233502 AMCOS

*Fundamental Host-Guest Interactions in Porous Metal Organic Frameworks. A Combined Experimental and Theoretical Approach.*

Dr. F. Stallmach

DFG-Projekt STA 648/1-1, SPP 1362 MOFs

## 4.18 Organizational Duties

Jörg Kärger

- Membership in the Programme Committee "Magnetic Resonance in Porous Media" (Leipzig 2010), "Fundamentals of Adsorption" (Kyoto, Japan 2010), "International Zeolite Conference" (Sorento, Italy 2010), "Diffusion Fundamentals IV" (Troy, USA 2011), in the permanent DECHEMA committees Zeolites and Adsorption and in the Board of Directors of the Magnetic Resonance Centre (MRZ) of Leipzig University
- Membership in Editorial Boards: Diffusion Fundamentals (Online Journal, Editor), Micropor. Mesopor. Mat., Adsorption
- Referee: Nature, Phys. Rev., Phys. Rev. Lett., Angew. Chem., Europhys. Lett., J. Chem. Phys., J. Phys. Chem., Langmuir, Micropor. Mesopor. Mat., Phys. Chem. Chem. Phys., J. Magn. Res.
- Project Reviewer: Deutsche Forschungsgemeinschaft, National Science Foundation (USA)

Rustem Valiullin

- Membership in Scientific Advisory Committee "Bologna MRPM Conference (Ampere Event)"
- Referee: J. Phys. Chem., J. Am. Chem. Soc., Adsorption, Micropor. Mesopor. Mat., Phys. Rev. B, Phys. Rev. Lett., Langmuir

Christian Chmelik

- Membership in Editorial Board: Diffusion Fundamentals
- Referee: J. Phys. Chem., Micropor. Mesopor. Mat.

Grit Kalies

- Referee: J. Phys. Chem., Micropor. Mesopor. Mat., Appl. Surface Sci., Adsorption, J. Coll. Interface Sci.

Frank Stallmach

- Faculty board member
- Referee: Micropor. Mesopor. Mat., Angewandte Chemie, J. Am. Chem. Soc., J. Magn. Res., J. Phys. Chem.
- Project Reviewer: Deutsche Forschungsgemeinschaft

## 4.19 External Cooperations

Academic

- Delft University, Inst.Chem. Tech., Delft, The Netherlands  
Prof. Kapteijn

- Institut de Recherches sur la Catalyse, CNRS, Villeurbanne, France  
Dr. Jobic
- GeoForschungsZentrum Potsdam (GFZ), Potsdam  
H.-M. Schulz
- Helmholtz Zentrum für Umweltforschung UFZ Halle-Leipzig GmbH, Leipzig  
S. Oswald
- Max Planck Institut für Kohlenforschung, Mülheim  
Dr. Schmidt, Prof. Schüth
- Russian Acad. Sci., Boreskov Inst. Catalysis, Siberian Branch, Novosibirsk, Russia  
Dr. Stepanov
- TU München, Lehrstuhl Technische Chemie 2  
Prof. Lercher, Dr. Jentys
- University Medical Center Hamburg-Eppendorf, Hamburg, Germany  
Dr. M. Koch
- Universität Erlangen Nürnberg, Dept. Chem. Engn., Erlangen  
Prof. Schwieger
- Universität Hannover, Dept. Phys. Chem., Hannover  
Prof. Caro, Prof. Heitjans
- Universität Leipzig, Institut für Analytische Chemie, Leipzig  
Prof. Berger
- Universität Leipzig, Institut für Technische Chemie, Leipzig  
Prof. Einicke, Prof. Gläser, Prof. Enke
- Universität Leipzig, Institut für Anorganische Chemie, Leipzig  
Prof. Krautscheid
- Universität Leipzig, Institut für Medizinische Physik und Biophysik, Leipzig  
Prof. Huster
- TU Dresden, Inst. Biophysik, Dresden  
Prof. Brunner
- Universität Stuttgart, Institut für Technische Chemie, Stuttgart  
Prof. Klemm, Prof. Hunger, Prof. Weitkamp
- University Athens, Dept Chem. Engn., Athens, Greece  
Prof. Theodorou
- University of Amsterdam, Faculty of Science, The Netherlands  
Prof. Krishna
- University of Maine, Dept. Chem. Eng., USA  
Prof. Ruthven
- Cleveland University, Chem. and Biomed. Eng., USA  
Prof. Shah
- University of Edinburgh, UK  
Prof. Brandani

- Victoria University of Wellington, MacDiarmid Institute for Advanced Materials and Nanotechnology, School of Chemical and Physical Sciences, New Zealand  
Prof. Galvosas, Prof. Callaghan
- LMU München, Dept. Chemistry and Biochemistry  
Prof. Bräuchle, Dr. C. Jung
- University of Massachusetts, Dept. of Chemical Engineering, Amherst, USA  
Prof. P.A. Monson
- Northwestern University, Dept. of Chem. Eng., Evanston, USA  
Prof. Snurr
- Rutgers University, Dept. of Chem. & Chem. Biol., Piscataway, USA  
Prof. Li, Prof. Olson
- University of Queensland, Division of Chem. Eng., Brisbane, Australia  
Prof. Bhatia
- University of Alicante, Dept. of Inorg. Chem., Alicante, Spain  
Prof. Rodríguez-Reinoso
- University of Anwerpen, Dept. of Chem., Wilrijk, Belgium  
Prof. Cool, Prof. Vansant
- University of Florida, Dept. of Chem. Eng., Gainesville (FL), USA  
Prof. Vasenkov
- Rensselaer Polytechnic Institute, Chem. & Biol. Eng., Troy, USA  
Prof. Coppens
- Kent State University Ohio, Department of Chemistry, USA  
Prof. Jaroniec
- Marie-Curie-Sklodowska-Universität Lublin, Poland  
Prof. Goworek
- DBI Gas- und Umwelttechnik GmbH Leipzig, Germany  
Dr. Rockmann
- Institut Madirel Marseille / Université de Provence, France  
Dr. Denoyel

### Industry

- BASF SE, Ludwigshafen, Germany  
Dr. Müller, Dr. Nestle, G. Herth
- DBI Gas- und Umwelttechnik GmbH, Leipzig, Germany  
Dr. R. Rockmann
- Grace, Worms, Germany  
Dr. McElhiney
- SINTEF, Oslo, Norway  
Prof. Stöcker
- Südchemie, Berlin, Germany  
Dr. Tissler, Dr. Tufar, Dr. Lutz

- Gaz de France, Production and Exploration GmbH Lingen, Germany  
Dr.-Ing. W. Kleinitz

## 4.20 Publications

### Journals

- H. Bux, C. Chmelik, J. M. van Baten, R. Krishna, J. Caro: *Novel MOF-Membrane for Molecular Sieving Predicted by IR-Diffusion Studies and Molecular Modeling*, *Adv. Mater.* **22**, 4741 (2010)
- C. Chmelik and J. Kärger: *In Situ Study on Molecular Diffusion Phenomena in Nanoporous Catalytic Solids*, *Chem. Soc. Rev.* **39**, 4864 (2010)
- C. Chmelik, L. Heinke, R. Valiullin, J. Kärger: *A New View of Diffusion in Nanoporous Materials*, *Chem. Ingen. Tech.* **82**, 779 (2010)
- C. Chmelik and J. Kärger: *Imaging of Transient Guest Profiles in Nanoporous Host Materials: a New Experimental Technique to Study Intra-Crystalline Diffusion*, *Adsorption* **16**, 515 (2010)
- C. Chmelik, H. Bux, J. Caro, L. Heinke, F. Hibbe, T. Titze, J. Kärger: *Mass Transfer in a Nanoscale Material Enhanced by an Opposing Flux*, *Phys. Rev. Lett.* **104**, 085902 (2010)
- C. Chmelik, F. Hibbe, D. Tzoulaki, L. Heinke, J. Caro, J. Li, J. Kärger: *Exploring the Nature of Surface Barriers on MOF Zn(tbip) by Applying IR Microscopy in High Temporal and Spatial Resolution*, *Micropor. Mesopor. Mat.* **129**, 340 (2010)
- D. M. Ruthven, L. Heinke, J. Kärger: *Sorption Kinetics for Surface Resistance Controlled Systems*, *Micropor. Mesopor. Mat.* **132**, 94 (2010)
- G. Kalies, R. Rockmann, D. Tuma, J. Gapke: *Ordered Mesoporous Solids as Model Substances for Liquid Adsorption*, *Appl. Surface Sci.* **256**, 5395 (2010)
- S. Arnrich, G. Kalies, P. Bräuer: *Studies on Adsorption Energy Distributions Computation from Adsorption Isotherms by the Ansatz Method*, *Appl. Surface Sci.* **256**, 5198 (2010)
- R. Chitta, T. Macko, R. Brüll, G. Kalies: *Elution Behaviour of Polyethylene and Polypropylene Standards on Carbon Sorbents*, *J. Chromatography A* **1217**, 7717 (2010)
- G. Kalies, C. Reichenbach, R. Rockmann, D. Enke, P. Bräuer, M. Jaroniec: *Further Advancements in Predicting Adsorption Equilibria Using Excess Formalism: Calculation of Adsorption Excesses at the Liquid/Solid Interface*, *J. Colloid Interface Sci.* **352**, 504 (2010)
- D. Kondrashova, C. Reichenbach, R. Valiullin: *Probing Pore Connectivity in Random Porous Materials by Scanning Freezing and Melting Experiments*, *Langmuir* **26**, 6380 (2010)

M. G. Mazza, M. Greschek, R. Valiullin, J. Kärger, M. Schoen: *Entropy-Driven Enhanced Self-Diffusion in Confined Reentrant Supernematics*, *Phys. Rev. Lett.* **105**, 227802 (2010)

R. Valiullin, J. Kärger: *Comment on "Single-File Diffusion of Confined Water Inside SWNTs: An NMR Study"*, *ACS Nano* **4**, 3537 (2010)

R. Valiullin, S. Naumov, P. Galvosas, J. Kärger, H. J. Woo, F. Porcheron, P. A. Monson: *Comment on "Computer Simulation of Static and Dynamic Properties During Transient Sorption of Fluids in Mesoporous Materials"*, *J. Phys. Chem. C* **114**, 9187 (2010)

S. Beckert, F. Stallmach, R. Bandari, M. R. Buchmeiser: *Self-Diffusion of Polystyrene Solutions in Porous Acrylate-Based Monoliths Studied by  $^1\text{H}$  PFG NMR*, *Macromolecules* **43**, 9441 (2010)

M. Wehring, J. Gascon, D. Dubbeldam, F. Kapteijn, R. Q. Snurr, F. Stallmach: *Self-Diffusion Studies in CuBTC by PFG NMR and MD Simulations*, *J. Phys. Chem. C* **114**, 10527 (2010)

I. Mittreiter, S. Oswald, F. Stallmach: *Investigation of Iron(III)-Release in the Pore Water of Natural Sands by NMR Relaxometry*, *The Open Magnetic Resonance Journal* **3**, 46 (2010)

K. Seehamart, T. Nanok, J. Kärger, C. Chmelik, R. Krishna, S. Fritzsche: *Investigating the Reasons for the Significant Influence of Lattice Flexibility on Self-diffusivity of Ethane in Zn(tbip)*, *Micropor. Mesopor. Mat.* **130**, 92 (2010)

K. Ulrich, P. Galvosas, J. Kärger, F. Grinberg, J. Vernimmen, V. Meynen, P. Cool: *Self-assembly and Diffusion of Block Copolymer Templates in SBA-15 Nanochannels*, *J. Phys. Chem. B* **114**, 4223 (2010)

D. Tzoulaki, L. Heinke, M. Castro, P. Cubillas, M. W. Anderson, W. Zhou, P. A. Wright, J. Kärger: *Assessing Molecular Transport Properties of Nanoporous Materials by Interference Microscopy: Remarkable Effects of Composition and Microstructure on Diffusion in the Silicoaluminophosphate Zeotype STA-7*, *J. Amer. Chem. Soc.* **132**, 11665 (2010)

A. Schönhals, F. Rittig, J. Kärger: *Self-diffusion of Poly(propylene glycol) in Nanoporous Glasses Studied by Pulsed Field Gradient NMR: A Study of Molecular Dynamics and Surface Interaction*, *J. Chem. Phys.* **133**, 0094903 (2010)

### **in press**

J. Lincke, D. Lässig, J. Moellmer, C. Reichenbach, A. Puls, A. Moeller, R. Gläser, G. Kalies, R. Staudt, H. Krautscheid: *A Novel Copper-Based MOF Material: Synthesis, Characterization and Adsorption Studies*, *Micropor. Mesopor. Mat.*  
[doi:10.1016/j.micromeso.2010.11.017](https://doi.org/10.1016/j.micromeso.2010.11.017)

C. Reichenbach, G. Kalies, J. Lincke, D. Lässig, J. Moellmer, H. Krautscheid, M. Thommes: *Unusual Adsorption Behavior of a Highly Flexible Copper-Based MOF*, *Micropor. Mesopor. Mat.* [doi:10.1016/j.micromeso.2011.01.005](https://doi.org/10.1016/j.micromeso.2011.01.005)

M. Gratz, S. Hertel, M. Wehring, S. Schlayer, F. Stallmach and P. Galvosas *MAS PFG NMR Studies of Mixtures in Porous Materials*, *AIP Conf. Proc.*, **1330**

## Talks

V.R.R. Marthala, F. Hibbe, C. Chmelik, J. Kärger, J. Weitkamp: *Synthesis and Diffusion Studies on Large-Crystal Ferrierite Zeolites*, 1st International Workshop ENMIX - Nanostructured materials for sorption, separation and catalysis, Antwerp, Belgium, 04. – 05. October 2010

H. Bux, F.-Y. Liang, Y.-S. Li, J. Cravillon, M. Wiebcke, C. Chmelik, J. Kärger, S. Fritzsche, L. Hertäg, J. Caro: *Transport through Zeolitic Imidazolate Frameworks: From Molecular Diffusion to Membrane Permeation*, MOF 2010 - Metal Organic Frameworks, Marseille, France, 05. – 08. September 2010

C. Chmelik, H. Bux, J. Caro, L. Heinke, F. Hibbe, T. Titze, J. Kärger: *Faster by Opposing the Stream*, 16th International Zeolite Conference, Sorrento, Italy, 04. – 09. July 2010

C. Chmelik and J. Kärger: *Revolution in Diffusion Measurements by IR Micro-Imaging and Interference Microscopy*, 16th International Zeolite Conference, Sorrento, Italy, 04. – 09. July 2010

J. Kärger: *Unprecedented Wealth of Information on Guest Dynamics from Transient Concentration Profiles in Nanoporous Materials*, 10th International Conference on Fundamentals of Adsorption, Awaji, Japan, 23. – 28. May 2010,

C. Chmelik: *Introduction to Diffusion Studies in MOFs by IR and Interference Microscopy*, 2nd Topical Workshop of the SPP 1362 on "Adsorption and Diffusion in MOFs", Leipzig, Germany, 22. – 23. March 2010

F. Hibbe, T. Binder, C. Chmelik, L. Heinke, J. Kärger, W. Schmidt, T. Titze, D. Tzoulaki, U. Wilczok: *Surface Barriers Monitored and Systematically Studied Based on Data from Transient Concentration Profiles*, 22nd German Zeolite Conference, München, Germany, 03. – 05. March 2010

H. Bux, F.-Y. Liang, Y.-S. Li, J. Cravillon, M. Wiebcke, C. Chmelik, J. Kärger, S. Fritzsche, L. Hertäg, J. Caro: *Transport through Zeolitic Imidazolate Frameworks: From Molecular Diffusion to Membrane Permeation*, George-Kokotailo-Award Lecture 2010 at the 22nd German Zeolite Conference, München, Germany, 03. – 05. March 2010

T. Binder, C. Chmelik, W. Schmidt, J. Kärger: *Investigating Surface Barriers of Silicalite-1 Crystals by Means of Interference Microscopy*, Dechema Seminar: Adsorption, Duisburg, Germany, 09. – 10. February 2010

G. Kalies: *Structural and Energetic Characterization of Porous Materials by Adsorption Measurements*, Workshop "Structural Analysis, Spectroscopy and Reactivity of Porous Materials", International Research Training Group "Diffusion in Porous Materials", Utrecht, 8. – 10. November 2010

D. Kondrashova: *Freezing Kinetics in Linear Pores with Disorder*, DPG Spring Meeting, Regensburg, Germany, 21. – 26. March 2010

R. Valiullin: *Anomalous Transport in a Medium Subjected to Phase Transition*, DPG Spring Meeting, Regensburg, Germany, 21. – 26. March 2010

S. Naumov: *Memory Effects in Confined Fluids via Diffusion Measurements*, DPG Spring Meeting, Regensburg, Germany, 21. – 26. March 2010

R. Baum: *Fluid Transport in One-Dimensional Channel Systems*, DPG Spring Meeting, Regensburg, Germany, 21. – 26. March 2010

D. Kondrashova: *Disorder Effects During Freezing in Linear Pores*, The 10th International Conference on Fundamentals of Adsorption, Awaji, Japan, 23. – 28. May, 2010

R. Valiullin: *Fluid Behavior in Macroscopically Long Hierarchical Porous Materials*, The 10th International Conference on Fundamentals of Adsorption, Awaji, Japan, 23. – 28. May, 2010

M. Dvoyashkin: *Adsorption and Dynamics of Fluids in Native and Surface Modified Mesoporous Glasses*, The 10th International Conference on Fundamentals of Adsorption, Awaji, Japan, 23. – 28. May, 2010

R. Valiullin: *Phase State and Dynamics of Fluids in Mesoporous Solids*, The 10th Bologna Conference on Magnetic Resonance in Porous Media, Leipzig, Germany, 12. – 16. September, 2010

S. Naumov: *Memory Effects in Confined Fluids*, The 10th Bologna Conference on Magnetic Resonance in Porous Media, Leipzig, Germany, 12. – 16. September, 2010

P. Zeigermann, M. Dvoyashkin, J. Kärger, R. Gläser, R. Valiullin: *Transport and High Pressure Phase Equilibria in Mesopores*, Magnetic Resonance in Porous Media 2010, Leipzig, Germany, 12. – 16. September 2010

F. Stallmach: *NMR Studies of Host-Guest Interaction in Porous Materials*, EU-India Workshop on Environmental Materials and Modelling, Nagpur, India, 23. November 2010

M. Gratz: *MAS PFG NMR Studies of Mixtures in Porous Materials*, Magnetic Resonance in Porous Media 10, Leipzig, Germany, 13. September 2010

S. Hertel: *NMR Studies of Benzene Mobility in the Metal-Organic Framework MOF-5*, DPG Spring Meeting, Regensburg, Germany, 23. March 2010

J. Kärger: *Unprecedented Wealth of Information from Transient Concentration Profiles*, Leuven University, Belgium, 17. May 2010

J. Kärger: *Diffusion Studies of Guest Molecules in Nanoporous Solids*, Conference on Diffusion in Solids and Liquids (DSL 2010), Moscow, Russia, 1.–4. June 2010

J. Kärger: *Unprecedented Options of Diffusion Research by Monitoring the Evolution of Guest Profiles*, 48th Tutzing Symposium: Adsorption - Delving into the Molecular Scale, Evangelische Akademie Schloss Tutzing, Lake Starnberg, 13.–16. June 2010

J. Kärger: *"Leipzig, Einstein, Diffusion"*, ein englisch-deutscher Stadt- und Wissenschafts(ein)-führer für Fußgänger, Lange Nacht der Wissenschaften, Leipzig, 24. September 2010

**Posters**

C. Chmelik, J. Kärger, H. Bux, J. Caro, L. Hertäg, S. Fritzsche, J. M. van Baten, R. Krishna: *Characterizing Molecular Transport in MOF ZIF-8*, MOF 2010 - Metal Organic Frameworks, Marseille, France, 05. – 08. September 2010

H. Bux, C. Chmelik, J. Kärger, J. Cravillon, M. Wiebcke, S. Fritzsche, J. Caro: *Adsorption, Diffusion and Membrane Permeation of the CO<sub>2</sub>/CH<sub>4</sub> Mixture on the MOF Membrane ZIF-8*, 16th International Zeolite Conference, Sorrento, Italy, 04. – 09. July 2010

C. Chmelik, D. Enke, O. Gobin, P. Galvosas, A. Jentys, H. Jobic, J. Kärger, C. B. Krause, J. Kullmann, J. Lercher, S. Naumov, T. Titze: *Nanoporous Glass as a Model System for a Consistency Check of the Different Techniques of Diffusion Measurement*, 16th International Zeolite Conference, Sorrento, Italy, 04. – 09. July 2010

F. Hibbe, T. Binder, C. Chmelik, L. Heinke, J. Kärger, W. Schmidt, T. Titze, D. Tzoulaki, U. Wilczok: *Monitoring Transient Concentration Profiles as a Novel Route to Identifying and Quantifying Surface Barriers*, 16th International Zeolite Conference, Sorrento, Italy, 04. – 09. July 2010

C. Chmelik, H. Bux, J. Caro, L. Heinke, F. Hibbe, T. Titze, J. Kärger: *May Transport Diffusion in Nanopores be Surpassed by Self-Diffusion?*, 10th International Conference on Fundamentals of Adsorption, Awaji, Japan, 23. – 28. May 2010,

T. Titze, S. Naumov, C. Chmelik, P. Galvosas, C.B. Krause, J. Kullmann, D. Enke, J. Kärger: *Nanoporous Glasses as Novel Model System for Diffusion Studies on the Micrometer Scale*, 10th International Conference on Fundamentals of Adsorption, Awaji, Japan, 23. – 28. May 2010,

T. Binder, F. Hibbe, A. Pietruszka, L. Heinke, D. Tzoulaki, C. Chmelik, U. Wilczok, W. Schmidt, J. Caro, J. Kärger: *The Impact of Non-Ideal and Modified Surfaces of Nanoporous Crystals on Molecular Transport*, 10th International Conference on Fundamentals of Adsorption, Awaji, Japan, 23. – 28. May 2010,

C. Chmelik, H. Bux, J. Caro, J. M. van Baten, R. Krishna, J. Kärger: *Characterizing Molecular Transport of CO<sub>2</sub> and CH<sub>4</sub> in MOF ZIF-8*, 22nd German Zeolite Conference, München, Germany, 03. – 05. March 2010

T. Kirchner, C. Chmelik, H. Bux, J. Caro, L. Heinke, F. Hibbe, T. Titze, J. Kärger: *Measuring Hindered Transport and Self-Diffusion by Means of Optical and NMR Methods*, 22nd German Zeolite Conference, München, Germany, 03. – 05. March 2010

T. Titze, S. Naumov, C. Chmelik, P. Galvosas, C. B. Krause, J. Kullmann, D. Enke, J. Kärger: *Correlating the Results of Different Techniques of Diffusion Measurement in Nanoporous Glasses*, 22nd German Zeolite Conference, München, Germany, 03. – 05. March 2010

T. Titze, S. Naumov, C. Chmelik, P. Galvosas, C. B. Krause, J. Kullmann, D. Enke, J. Kärger: *Correlating the Results of Different Techniques of Diffusion Measurement in Nanoporous Glasses*, 1st International Workshop ENMIX - Nanostructured materials for sorption, separation and catalysis, Antwerp, Belgium, 04. – 05. October 2010

T. Binder, F. Hibbe, A. Pietruszka, L. Heinke, D. Tzoulaki, C. Chmelik, U. Wilczok, W. Schmidt, J. Caro, J. Kärger: *The Impact of Non-Ideal and Modified Surfaces of Nanoporous Crystals on Molecular Transport*, 1st International Workshop ENMIX - Nanostructured materials for sorption, separation and catalysis, Antwerp, Belgium, 04. – 05. October 2010

G. Kalies, R. Rockmann, D. Tuma, S. Arnrich: *Reliable Information on Solids from Liquid-Phase Adsorption*, 9th Conf. Fundamentals of Adsorption, Hyogo, Japan, 23. – 28. Mai 2010

S. Arnrich, G. Kalies, P. Bräuer: *Approximate Solutions to the Adsorption Integral Equation by the Ansatz Method*, 9th Conf. Fundamentals of Adsorption, Hyogo, Japan, 23. – 28. Mai 2010

D. Kondrashova, R. Valiullin: *Freezing and Melting Behavior of Fluids in Random Mesopores*, Magnetic Resonance in Porous Media 10, Leipzig, Germany, 12. – 16. September, 2010

P. Zeigermann, M. Dvoyashkin, R. Valiullin, J. Kärger, R. Gläser: *Transport and High-Pressure Phase Equilibria in Mesopores*, Fundamentals of Adsorption 10, Awaji Island, Japan, 23. – 28. May 2010

P. Zeigermann, M. Dvoyashkin, R. Valiullin, J. Kärger: *Adsorption and Transport Behavior of a Binary Liquid in Mesopores*, Fundamentals of Adsorption 10, Awaji Island, Japan, 23. – 28. May 2010

P. Zeigermann, M. Dvoyashkin, R. Valiullin, J. Kärger: *Transport and High-Pressure Phase Equilibria in Mesopores*, DPG Spring Meeting, Regensburg, Germany, 21. – 26. March 2010

P. Zeigermann, S. Naumov, M. Dvoyashkin, J. Kärger, R. Gläser, R. Valiullin: *Diffusion in Mesoporous Systems*, DZA workshop 2010, Eindhoven, Netherlands, 11. November 2010

A.-K. Pusch, C. Horch, F. Stallmach: *NMR Studies of Diffusion and Adsorption in the Metal Organic Framework CuBTC*, AMCOS Midterm Meeting, Nagpur, India, 22th November 2010

C. Horch, A.-K. Pusch, P. Donkers, F. Stallmach: *Low-Field High-Pressure NMR Porosimetry*, Magnetic Resonance in Porous Media 10, Leipzig, Germany, 13. September 2010

M. Wehring, T. Viertel, F. Debatin, F. Stallmach: *Anisotropic Self-Diffusion of CO<sub>2</sub> and CH<sub>4</sub> in the Microporous Imidazolate MOF IMOF-1*, Magnetic Resonance in Porous Media 10, Leipzig, Germany, 13. September 2010

F. Stallmach, S. Beckert, S. Hertel, C. Horch, A.-K. Pusch, M. Wehring: *NMR Studies of the Diffusional Mobility of Adsorbates in Nanoporous Coordination Polymers*, Magnetic Resonance in Porous Media 10, Leipzig, Germany, 13. September 2010

## 4.21 Graduations

### Diploma

- Tom Kirchner  
*Diffusion as a Probe of Structural Properties of Porous Solids*  
August 2010

### Master

- Ramona Baum  
*Fluid Transport in One-Dimensional Channel Systems*  
April 2010
- Stefan Hertel  
*MAS PFG NMR and ATR-FTIR diffusion measurements in porous coordination polymers*  
September 2010

### Bachelor

- Maria Fuchs  
*Pyknometrische Dichtebestimmungen an porösen Festkörpern*  
November 2010
- Alexander Lauerer  
*Sorptionsuntersuchungen an Ferrieriten mittels IR-Mikroskopie*  
July 2010
- Erik Zabel  
*Sorptions- und Diffusionsuntersuchungen an Cobaltformiat mittels IR-Mikroskopie*  
July 2010
- André Müller  
*Aufbau einer temperierbaren Vakuumapparatur für Diffusionsmessungen mittels IR-Microimaging*  
October 2010
- Friederike Pielenz  
*NMR-Untersuchungen zur Wechselwirkung von CO<sub>2</sub> mit wassergesättigten Gesteinen*  
October 2010
- Tino Viertel  
*NMR-Untersuchungen zur Diffusion von Methan in der metallorganischen Gerüstverbindung IMOF-1*  
September 2010
- Markus Fuchs  
*NMR-Untersuchungen der Selbstdiffusion in wässriger Natriumchlorid- und Harnstofflösung*  
September 2010

- Annemarie Sickert  
*Festkörper-NMR Untersuchungen zur Struktur und Dynamik eines lipidmodifizierten Dipeptids in Membranumgebung*  
July 2010



# 5

## Soft Matter Physics

### 5.1 Introduction

In his book "What is Life?", Schrödinger recognized the immense challenge to explain biological processes by basic physics and chemistry. Consequentially, traditional medical physics had predominately the role to develop devices for medicine such as sophisticated imaging solutions (X-ray, NMR, multiphoton) or laser scalpels. Commencing with Watson and Crick, science has gained tremendous insight into the molecular basis of biological cells. Over 25 000 genes encode the information of human life, and their subsequent transcription and translation add to the complexity of molecular interactions resulting in an insurmountable combinatorial number of relations. Recent progress in biosciences towards a more quantitative description opens a challenging and new pathway for medical physics to use physics underlying biological processes to directly impact diagnosis and therapy. Despite that this approach is still in its infancy, it may redefine medical physics. This kind of research is based on fundamental biological physics and has in its ideal case applied aspects in medical physics. By identifying cellular subunits acting as independent functional modules this complexity becomes tractable and the fundamental physical principles of these modules can be studied.

A prototypical example for such a module is the intracellular scaffold known as the cytoskeleton. The cytoskeleton is the key structural element in cellular organization and is an indicator of pathological changes in cell function. It is a compound of highly dynamic polymers and molecular motors as active nano-elements inside cells. The cytoskeleton mechanically and chemically senses a cell's environment achieving a high sensitivity by using processes such as stochastic resonance. This active polymeric scaffold generates cellular motion and forces in the tens of nanoNewton sufficiently strong to push rigid AFM cantilevers out of the way. These forces are generated by molecular motor-based nano-muscles and by polymerization through mechanisms similar to Feynman's hypothetical thermal ratchet. A new type of polymer physics describes these active polymer networks since the nano-sized motors overcome the inherently slow, often glass-like Brownian polymer dynamics. This results in novel self-organization of the polymer scaffolds and rapid switching between different ordered states. This organization of the cytoskeleton is tightly controlled in cells. Thus, suspended cells' biomechanical properties are well-defined and distinguish different cellular states and cell types with confidence levels of more than 95% (metastatic from non-metastatic cancer cells, stem cells from differentiated cells in adult tissues, etc.). Since cell elasticity

depends highly nonlinear on cytoskeletal composition already small changes in a cell's state are measurable by biomechanical changes and recent polymer theories can be used to deduce the cytoskeletal part of a cell's proteomic condition. Recently, the optical stretcher, a photonic device developed in our laboratory, was demonstrated within a clinical study as a highly sensitive non-invasive tool for mechanical classification of cancer cells [1, 2]. The device's versatility was drastically improved by integration of the capability to rotate cells under observation [3]. The cytoskeleton uses up to 30% of cellular ATP, which is a cell's fuel. Optical gradient forces due to cells' dielectric nature can manipulate the cytoskeleton's consequential active and dynamical state. Opto-molecular coupling between laser light and cytoskeletal processes permits optical control of neuronal growth. The specific opto-molecular influence on membrane and cytoskeletal transport is complex. Cells cannot modulate diffusion by the parameters found in the Einstein equation (temperature, viscosity, molecular size).

Consequentially, cells exhibit rich multifaceted intracellular transport including motor-driven motion and anomalous subdiffusion, which can be probed by the use of nanoparticles as tracers. The cytoskeleton as active, soft condensed matter, with structures on nanometer and micron scales representative of individual proteins and cells, calls forth new biological and polymer physics. Our research group's goals center on unraveling this new physics of the cytoskeleton. The current and future research goals are summarized in the following sections.

*Josef A. Käs*

[1] A. Fritsch et al.: Nat. Phys. (invited article) **6**, 730-732 (2010)

[2] T. Remmerbach et al.: Cancer Res. **69**, 1728 (2009)

[3] M. Kreysing et al.: Opt. Express **16**, 16984 (2008)

## **5.2 Are biomechanical changes necessary for tumor progression?**

M. Zink, A. Fritsch, T. Kiessling, D. Nnetu, F. Wetzel S. Pawlizak, S. Ebert, M. Gyger, J.A. Käs

Almost 50 years ago Steinberg made the observation that two different populations of cells mixed together in a little droplet immediately separate. To understand such behavior he considered cells as liquid-like and determined the surface tension of cell droplets with a self-made plate tensiometer. Steinberg proposed that only cohesion forces between cells are the driving force of cell separation. Following his differential adhesion hypothesis, a mixture of two different cell types in a droplet culture form a spheroid in which cells with lower surface tension embed cells with higher surface tensions to decrease the surface energy of the entire system. Thus, epithelial tumor cells in droplet cultures with normal epithelial cells must surround the normal cells due to their loss in E-cadherin expression and the corresponding decrease in cohesion forces. Nevertheless, such behavior could never been observed and just recently Schötz et al. together with Steinberg showed that the mechanical properties of the cells must be

taken in account together with surface tension differences. Thus, soft cells can develop more contact sides to adjacent cells compared to stiff cells even when the number of adhesion proteins on the cell surface is reduced.

How cells can squeeze along other cells and through the extracellular matrix, change their shape and contact sides to adjacent cells is a major determinant for cell demixing and the formation of compartments in the human body. Thus, the question arises: Is the formation of compartments during embryogenesis which build up the human body only driven by biochemical processes or can we describe such behavior also by considering cell mechanics and cell-cell / cell-matrix interactions? Additionally, can we understand the progression of a tumor in a similar way because a tumor is also a developing tissue?

Considering ontogenetically different tissue compartments as units with different surface tensions, the question what keeps the tumor cells inside their host compartments might similarly be answered as the question why cells separate and form compartments during embryogenesis. Additionally, can the underlying mechanism be employed to understand cell demixing *in vitro*? To investigate such mechanisms from a materials science perspective, the mechanical properties of single cells must be taken into account because stiff cells exhibit less contact sides to other cells which would increase motility. On the other hand, lamellipodial motion and therefore individual cell motility is enhanced for soft cells which can also "squeeze" through the extracellular matrix.

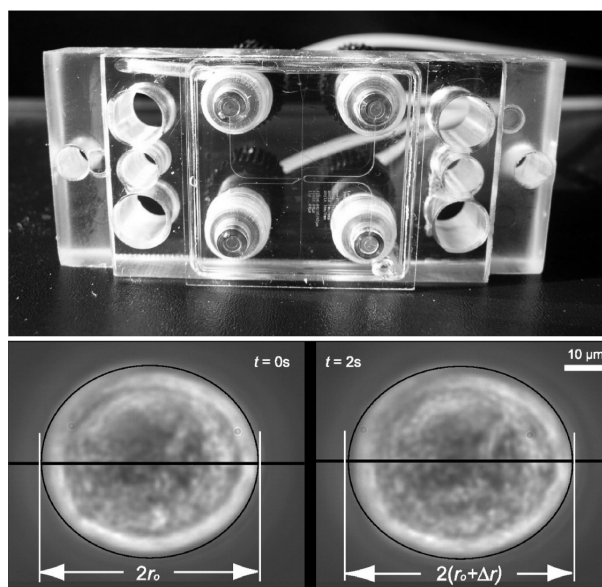


**Figure 5.1:** The Optical Stretcher is a tool to probe viscoelastic properties of individual cells utilizing the pressure refracted light exerts on a surface. Core piece of the Optical Stretcher is a microfluidic chip (top). The cells are in suspension in a flow channel. Individual cells are trapped between two counter-propagating divergent laser beams emitted from opposing optical fibers. By increasing the laser power, the surface stress (due to the light pressure) increases and deforms the cell along the laser axis (bottom).

To this end, we investigated the mechanical properties of primary breast epithelial tumor cells with the Optical Stretcher (Fig. 5.1) and compared their viscoelastic properties with primary epithelial cells from breast reduction surgery (HMEC). The Optical

Stretcher deforms suspended cells between two counter propagation laser beams by momentum transfer from the laser light to the cell. Notably, when these cells isolated from normal and cancerous tissues were investigated, a very interesting difference in the deformability of both cell types was noted: Figure 5.2 shows the distribution of optical deformability of both cell types, stretched with a laser power of 1.2 W. Besides the increased softness of tumor cells compared to normal cell, it is remarkable that very stiff but also very soft cells are present within the tumor sample. When the laser power during stretching is reduced to 0.8 W the distributions change: Both cell types exhibit similar mean deformabilities when stretched with smaller optical forces, whereas the tumor cells have a much broader non-Gaussian distribution. Here, very soft tumor cells can be found which proliferate very fast and were are not present in the healthy sample. Additionally, the tumor sample contains very few cells that actively contract when they are treated with the laser beams of smaller power. Thus, for low deformation forces these cells have the ability to withstand external mechanical excitations and instead of being stretched they actively contract. Such behavior has never been observed before for cell lines.

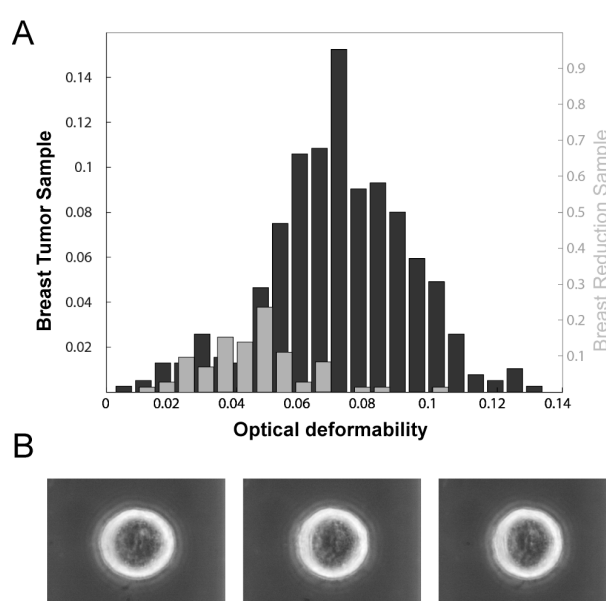


**Figure 5.2:** (A) Optical deformability distribution of parenchymal cells from a malignant human breast tumor (dark grey) and normal breast tissue (bright grey), measured with an Optical Stretcher and a laser power of 1.2 W. For small deformations, where a linear response is observed, the tumor shows a significantly higher fraction of softer cells than the normal cells from breast tissue. (B) When breast tumor cells are weakly stretched with the Optical Stretcher (here: 0.8 W laser power), a small fraction of tumor cells actively resists the pulling force and contracts. This can be seen by the change in cell diameter in the stretching direction.

Why tumor cells soften in parallel with the increase in aggressiveness remains elusive. However, cell softening during malignant transformation offers several advantages for the progression of cancer: Our results indicate that soft cell exhibit enhanced proliferation because mitosis is accelerated. Furthermore, lamellipodial motion and therefore individual cell motility is improved which corresponds to the ability of the cell to invade into the surrounding tissue and metastasize. However, softening alone

cannot be a prerequisite for tumor cells to overcome compartment boundaries. From the materials science perspective two cellular properties are mandatory for metastatic behavior: Individual cell motion and the possibility to adapt the mechanical properties and surface tensions to the local environment. Individual cell motion is usually triggered by a loss of E-cadherin expression - a reduction of cell-cell interaction - a feature characteristic for epithelial-mesenchymal transition of the cell. Such mutations additionally result in a reduction of surface tensions which enhances individual migration through the ECM. The observed active contraction of primary tumor cells due to external forces can be considered as the ability of cells to pre-strain and stiffen the cytoskeleton to (a) reduce the number of contacts to adjacent cells and the ECM and (b) reduce the surface tension even further to overcome compartment boundaries and enter the blood stream. Thus, tumors that already contain contractile cells have the ability to metastasize and must be considered as extremely aggressive even when no secondary tumors have been detected yet.

- [1] A. Fritsch et al.: Nat. Phys. (invited article) **6**, 730-732 (2010)
- [2] C. Brunner et al.: Soft Matter **5**, 2171-2178 (2009)
- [3] T. Remmerbach et al.: Cancer Res. **69**, 1728 (2009)

### 5.3 Pattern Formation of actin networks within cell-sized droplets and bulk experiments

F. Huber, D. Strehle, J. Schnauß, J.A. Käs

Cells appear in an amazing variety, but despite their fundamental differences they all rely on a small amount of proteins to form a shaping scaffold called the cytoskeleton. One major component of this morphological structure is actin, a highly conserved cellular protein. Under physiological conditions actin forms filamentous polymers organizing *in vivo* into networks and/or bundled structures typically associated to linking proteins. In cells these formations can be arranged in higher ordered structures to fulfill various tasks and to mechanically stabilize the cell body itself (Fig. 5.3 A). To investigate origins of effects caused by structural arrangements it is of interest to establish *in vitro* setups to examine actin under controlled conditions.

We have developed a new experimental setup to study the formation of actin networks upon cross-linker activation within cell-sized geometries at physiological actin concentrations and appearing higher ordered structures (Fig. 5.3 B). Instead of molecular motors or cross-linking proteins, which are known to produce higher ordered structures through self-organization or self-assembly, multivalent ions as switchable model-linkers were used.

By employing multivalent ions as linkers we obtained regularly spaced networks of star-like clusters usually attributed to molecular motors. Various parameters were found to affect the formation of different actin network topologies. At higher filament densities surprisingly regular ladder-like stripes and nematic bundle patterns appear. We have shown that the arising actin networks are directly representing the underlying

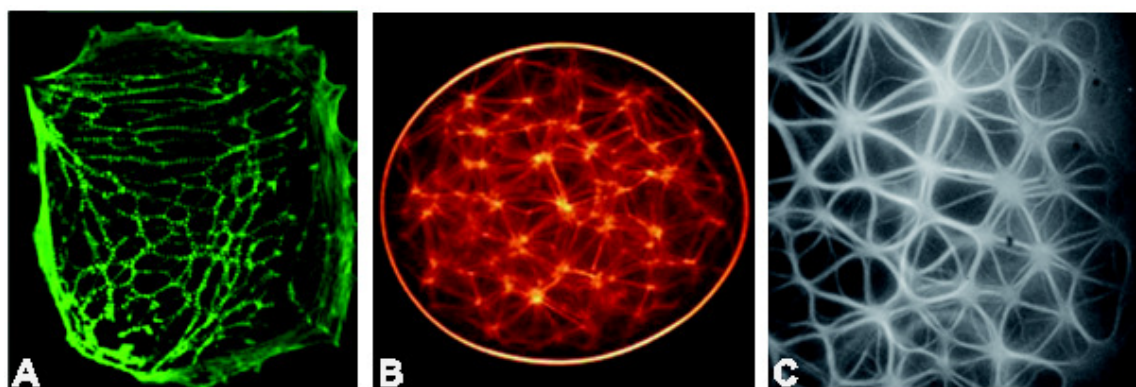


**Figure 5.3:** Higher ordered structures of actin in: (A) a living cell (taken from [1]), (B) a cell-size droplet with multivalent ions as linking molecules, (C) bulk experiments with methylcellulose (MC) as crowding agent.

order of the F-actin solutions. Moreover, the obtained networks display features of cellular networks in the actin cortex and may serve as a simple model system for the cortical actin layer. Observed transitions are fast (seconds to few minutes) and reversible which is of high interest concerning the known ability of living cells to quickly modify their morphology.

Beside effects originating from linking molecules we observed structure formations caused by depletion forces induced by molecular crowding. Since up to 30% of the cellular interior is occupied by macromolecules strong excluded volume effects can be observed within cells. Induced depletion forces can bundle actin filaments as well as form higher ordered topologies (Fig. 5.3 C). *In vitro* bulk experiments as well as experiments in cell-sized droplets with methylcellulose (MC) and polyethylene glycol (PEG) have shown a strong dependency of structure formations and crowding agent. The origin of this effect and pronounced variation between differing crowding agents remain unclear and are subject to further investigations.

[1] A. M. Malek et al.: American Journal of Physiology – Cell Physiology **292**, C1645-C1659 (2007)

## 5.4 Origin and Spatial Distribution of Forces in Motile Cells – From fish keratocytes to neuronal growth cones

C. Brunner, T. Fuhs, P. Rauch, M. Gögler, D. Koch, A. Ehrlicher, J.A. Käs

A fundamental step in cell migration is the advancement of the cell's leading edge. It is generally accepted that this motion is driven by actin polymerization against the plasma membrane but this has not been directly measured. Here we present precise force measurements using a newly established scanning force microscopy (SFM)-technique combined with high resolution imaging and lamellipodium feature tracking analysis. Our SFM-based technique uses the vertical and lateral deflection of a modified cantilever and allows direct measurements of the forces exerted by the cell [1].

A polystyrene bead (blue) glued to a cantilever-tip of an SFM is positioned on the substrate in front of a migrating cell. The cell moves, perpendicular to the cantilever's long axis, towards the bead, and pushes against the bead which leads to a twist of the cantilever and is detected as lateral deflection.

For fast migrating fish keratocytes direct measurements of the maximum forces which are generated at the leading edge of the lamellipodium, retrograde forces within the lamellipodium, and the cell body forces are possible. Through selective manipulation of molecular components by addition of different drugs, such as Jasplakinolide, Cytochalasin D, and ML-7 the measured forces and velocity changes can be compared. This leads to new insights concerning the importance of different force generating processes and reveals actin polymerization as the dominant force generating process at the leading edge. On the other hand myosin does not seem to be responsible for the retrograde flow in the central lamellipodium. We directly measured a force attributed to the retrograde flow within the lamella, which critically demonstrates that the protrusion forces are decoupled from the cell body and are generated exclusively at the leading edge [2].

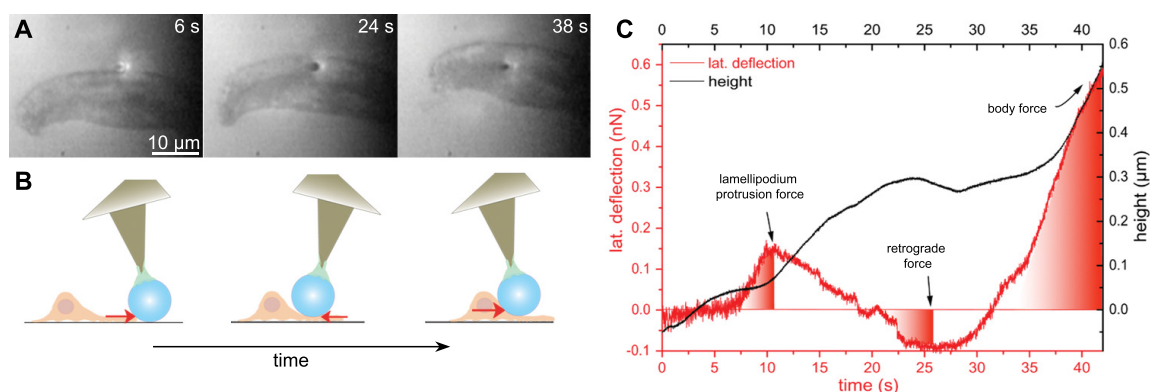


**Figure 5.4:** SFM-Force measurement of a migrating keratocyte. (A) Interference reflection microscopy images: the cell pushes against the cantilevered bead (bright spot) and finally lifts it up. (B) Sketch of the experiment, the cell pushes against the cantilever; the lateral deflection corresponds directly to the force. (C) Lateral deflection signal (red) reflects the forces the cell exerts in different regions of the cell during the measurement.

For slow moving cells such as neurons thermally induced artifacts and longer observation times showed the need for further stabilization of the setup. Thus, we incorporated an optical trap into our SFM-setup to measure, and correct for, substrate's drift. Yet the scan head of the SFM does not allow using the forward scattered signal of the optical trap. To get position information nonetheless we use the backscattered light of our marker bead. With this we can still reduce the drift of the SFM scan head with respect to the substrate to less than 50 nm/h in all 3 dimensions. Using this stabilization it is possible to realize the necessary observation times of 1h and even longer, while still being sensitive in the pN force range.

Measuring these forces for neuronal growth cones will give new insights into neuronal path finding during embryogenesis and nerve regeneration, as these occur in a crowded environment and not in wide open space. During the development of the central nervous system or after injury neurons have to (re-)establish connections over distances of

up to several millimeters. This task is not trivial and the growth cone, a motile sensory structure at the tip of outgrowing axons has to overcome mechanical resistance of the tissue in order to follow various guidance cues on its way to individual target areas. In contrast to other motile cellular structures the activity of growth cones seems to be increased on relatively soft substrates. This is probably due to the rather soft mechanical environment these cells face during initial network development. However, the question arises how the molecular mechanics of growth cones differ from that of other cells and allow them to perfectly move on very compliant materials with the same molecular equipment like other cells that prefer stiffer environments. A combination of fluctuating actin bundles at the leading edge termed filopodia and densely packed microtubules pushing from the back might contribute to the unique abilities of neuronal growth cones. Many of the underlying processes remain unclear and the aforementioned force measurements will be able to reveal important details about the generation and distribution of forces within the growth cone. Insights in this field will contribute to a better understanding of the internal mechanics of these structures and eventually improve the prognosis after injuries of the nervous system.

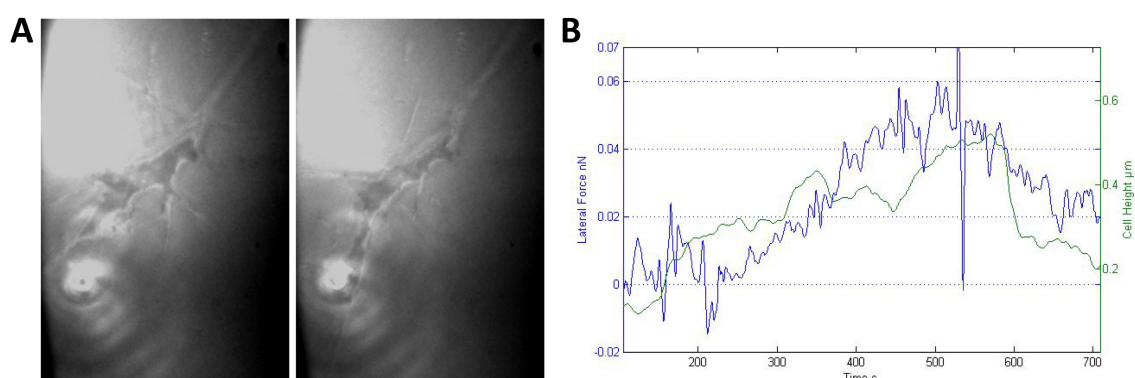


**Figure 5.5:** SFM-Force measurement of a growth cone of a NG-108 neuronal cell. (A) Interference reflection microscopy images, (B) Lateral deflection signal (blue).

- [1] C. A. Brunner et al.: *European Biophys. J.* **35**, 713-719 (2006)
- [2] M. Goegler et. al: *Biophys. J.* (under Review)

## 5.5 Optical properties of retinal glial cells

S. Agte, A. Reichenbach\*, J.A. Käs

\*Paul Flechsig Institute for Brain Research, Universität Leipzig

Vision is one of the most important senses of vertebrates. The basic functions of the retina, a thin cell layer that mediates vision, are well understood. However, it is still unclear how light reaches the light-sensitive cells. In the vertebrate eye the photoreceptor cells are on the back side of the retina. Therefore, light has to pass all retinal layers on its way to the photoreceptors before it is converted into an electro-chemical

signal. From a physical perspective scattering of light is expected which contradicts the excellent visual abilities of vertebrates.

Research into the design of specific retinal cells has revealed that certain cells are able to overcome the visual obstacles along the retinal light path. Already in 1981 Enoch *et al.* discovered wave guide properties of photoreceptor segments, which conduct signal transduction inside the receptor cell (Fig. 5.6a: 3). Analysis of the nuclear chromatin structure combined with theoretical modelling has shown that the nuclei of rod cells in nocturnal animals form natural lens systems to focus the light to the photoreceptor segments [1, 2] (Fig. 5.6a: 2). Recently our group has demonstrated that Müller radial glial cells display a suitable refractive index to allow light guidance. Indeed further experiments have shown that Müller cells can bridge the laser light path between two glass fibers [3] (Fig. 5.6a: 1). However, these observations were made on isolated cells surrounded by homogenous fluids with refractive indices that differ from the complex optical landscape a glial cell experiences *in vivo* in the retina. Therefore it remains unproven if Müller cells *in vivo* act like light-guiding elements.

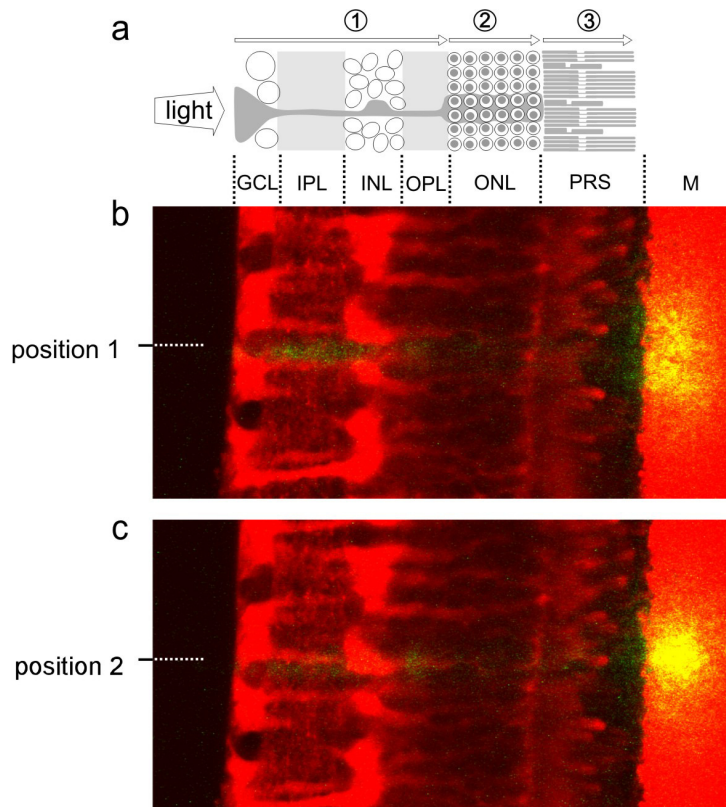


**Figure 5.6:** (a) Light path through the inverted vertebrate retina. (1) The Müller cell (dark grey) act as light fiber to channel the light to photoreceptor nuclei [3]. (2) The rod nuclei of nocturnal mammals form stacks of lenses [2]. (3) The light-sensitive photoreceptor segments are light fibers by themselves. (b, c) Pathway of light through the vital retina. The light source (green laser light of a single mode fiber) is either placed between two Müller cells (position 1) or in front of a Müller cell (position 2). green: laser light scattering, red: fluorescence of mitotracker orange, which pre-dominantly stains the Müller cells, GCL: ganglion cell layer, IPL/OPL: inner and outer plexiform layer, INL/ONL: inner and outer plexiform layer, PRS: photoreceptor segments, M: artificial membrane to visualize the transmitted light scattering.

For the first time this project investigated the Müller cell light guidance in the intact retinal tissue. Therefore we scanned a single-mode fiber delivering a thin, green laser beam onto the vitread surface of a retinal slice preparation (Fig. 5.6b, c). This small radiation source enables to illuminate individual Müller cell endfeet. For light that hits a Müller cell endfoot (Fig. 5.6c), intraretinal light scattering is minimized especially in the plexiform layers. These layers consist of synapses which sizes are of the order of the visible wavelength, the right range to deteriorate light signals by scattering. In addition to the intraretinal scattering, a membrane behind the retina served as artificial screen for the transmitted light. When the light enters a Müller cell, the projected light on the membrane is confined to a small area so that the light intensity arriving at the photoreceptors is high. Therefore, this mechanism increases the signal-to-noise ratio which contributes to a high sensitivity of rods during night vision and the contrast sensitivity of cones. We have further shown that the ratio between the numbers of Müller cells and cone cells - responsible for sharp vision - is roughly one. This results let us suggest that Müller cells play a significant role in cone vision.

- [1] M. Kreysing et al.: Opt. Lett. **35**, 2639-2641 (2010)
- [2] I. Solovei et al.: Cell **137**, 356-368 (2009)
- [3] K. Franze et al.: Proc. Natl. Acad. Sci. **104**, 8287-8292 (2007)

## 5.6 Oscillations in the lateral pressure in lipid monolayers induced by nonlinear chemical dynamics

U. Dietrich, S. Alonso\*, C. Händel, M. Bär\*, J.A. Käs

\*Physikalisch-Technische Bundesanstalt, Berlin

At physiological temperature - the cell membrane is in a liquid-crystalline state. This fluid state enables the diffusion of membrane molecules or compartments within the membrane interface. Hence, the chemical reactions at the cell membrane and the ability of membrane molecules or compartments to diffuse should result in reaction-diffusion-processes. Based on specific molecular interactions, spatial and temporal pattern formation could be observed. Hereby, one of the prominent example processes is the myristoyl-electrostatic switch (ME-switch). It constitutes the specific interaction between the myristoylated alanin-rich C kinase substrate (MARCKS protein), present in the cell interior, and the acidic membrane lipid phosphatidylinositol 4,5-bisphosphate (PIP(2)). Induced by specific enzymes, MARCKS protein can attach to and detach from the membrane and carry out so a regulating function, involved in the signal transduction of the cell.

To study the pattern formation within the membrane interface we used the Langmuir monolayer technique. In this reduced scheme, the monolayer represents the inner layer of the membrane and the Langmuir subphase the cell interior. First, we studied the interaction of MARCKS peptides (consisting on the effector domain of MARCKS proteins) with a mixed DPPC/PIP(2) monolayer, whereby the zwitterionic membrane lipid DPPC only builds the matrix for the twofold negatively charged PIP(2). The highly positively charged MARCKS peptide interacts selectively with PIP(2). Hereby, one

peptide can bind three to four PIP(2) molecules, which results in a phase separation into MARCKS/PIP(2) microdomains. Due to the enrichment of PIP(2) in the disordered phase of the mixed monolayer - these microdomains are also enriched in the disordered phase which relates to an increase of the distances between the ordered DPPC domains. Moreover, the integration of MARCKS peptide into the mixed monolayer leads to a higher area requirement of the system. Consequently, the adsorption of MARCKS peptide at the monolayer at constant area yields an increase of the lateral pressure (Fig. 5.7).

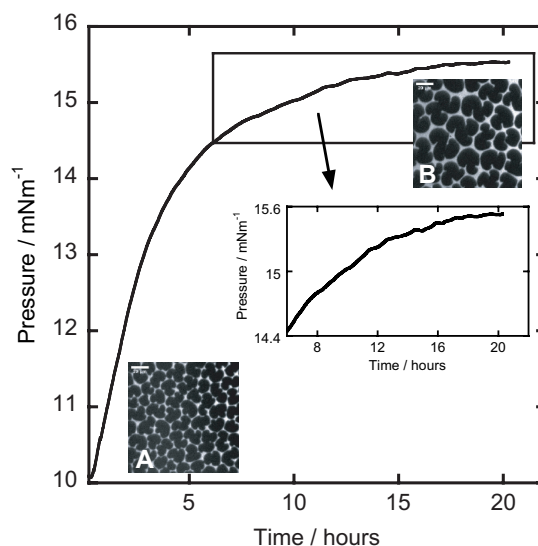


**Figure 5.7:** Increase of lateral pressure in the compressed monolayer due to attachment of MARCKS peptide, the fluorescence micrographs illustrate the initial state (A) and the state after attachment (B).

Vice versa, the lateral pressure of the monolayer should decrease in case of detachment of MARCKS peptide from the monolayer, which will be induced by its interaction with protein kinase C (PKC). The attachment of negatively charged phosphate groups to the effector domain of MARCKS peptide, caused by the enzyme PKC, yields a neutralization of the positive charges of the basic residues and abolishes the electrostatic contribution of the effector domain to the membrane binding. In the cell - the dephosphorylation of MARCKS by phospholipases enables an anew attachment of MARCKS at the membrane.

In the monolayer experiment, we introduce PKC in the subphase after the saturation of the monolayer with peptide. The injection of PKC immediately generates a decrease in lateral pressure up to the initial pressure. The lateral pressure increases again and oscillations have been observed over a period of hours, whereby an excess of unphosphorylated MARCKS peptide in the subphase simulate its dephosphorylation. Thus, we were able to induce a cyclic translocation of the peptide in the monolayer (Fig. 5.8A).

With the help of this experimental result - a mathematical formulation of a reaction-diffusion model could be developed in cooperation with the working group "Modelling and Simulation" of the Physikalisch-Technische Bundesanstalt" Berlin. This model predicts oscillations with large temporal periods (Fig. 5.8B,C). The period of the oscillations

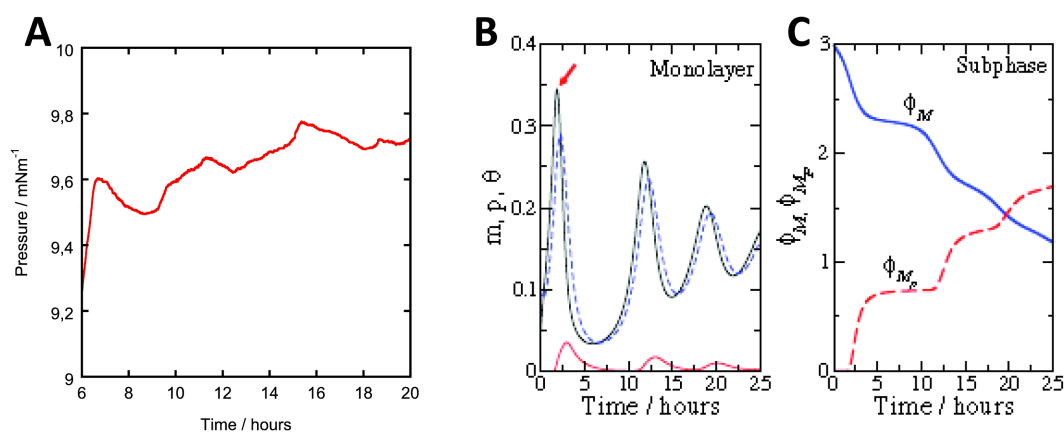


**Figure 5.8:** (A) Oscillations in the lateral pressure in the monolayer after injection of PKC (and after the immediate decrease up to the initial pressure of the monolayer). (B, C) Temporal evolution of  $m$  (concentration of peptide, black line),  $p$  (concentration of PKC, red line) and  $\theta$  (accessible quantity of free PIP(2), dashed blue line) at the monolayer (B), and of the fractions free peptide  $\Phi_M$  (solid blue line) and phosphorylated peptide  $\Phi_{M_p}$  (dashed red line) in the subphase (C) during a numerical simulation. The red arrow shows the moment of the introduction of PKC.

mainly depends on the dynamics of the domains and fluid channels.

The slow increase of the lateral pressure due to the attachment of MARCKS peptide at the monolayer (Fig. 5.7) can be reproduced considering the diffusion of the peptide through the subphase and a simple binding dynamics to the monolayer. This process has been employed for the estimation of the parameters in the model. The introduction of PKC produces a cyclic change in the monolayer. This type of interactions combined with transport processes (diffusion) may help to understand temporal and spatial aspects on cell signaling. The damped pressure oscillations following the initial detachment of MARCKS peptide is an evidence of non-linear interactions because kinetic oscillations are a typical signature of non-linear processes. The developed model shows that the feedback provided by the non-linear binding rates of peptides and enzymes to the monolayer and the coupling of the monolayer's structure with the peptide concentration are the most important ingredients for the obtained oscillations.

[1] S. Alonso et al.: Biophys. J. (in press), doi:10.1016/j.bpj.2010.12.3702

## 5.7 Funding

*Leipziger Schule der Naturwissenschaften - Bauen mit Molekülen und Nano-Objekten*  
 Prof. Dr. E. Hey-Hawkins, Prof. Dr. M. Grundmann and Prof. Dr. J. A. Käs  
 BuildMoNa - Graduiertenschule

*InterNeuro*

Prof. Dr. J. A. Käs and Dr. J. Guck  
 DFG Graduiertenkolleg (GRK 1097) in Leipzig

*Von lokaler Beschränkung bis zu makroskopischem Transport*

Prof. Dr. F. Cichos, Prof. Dr. J. Käs et al.  
DFG-Forschergruppe ("Sächs. Forschergruppe")

*Optical Stretcher Methode zur Krebsdiagnose an Biopsien*  
Prof. Dr. J. Käs  
EXPRIMAGE-Forschungsverbund

*Inhärente zelluläre, physikalische und Materialeigenschaften zur molekular Marker-freien Isolierung und Charakterisierung seltener Zelltypen*  
Prof. Dr. J. Käs, Prof. Dr. A. Robitzki et al.  
-Theranostik- / SAB-Projekt

*Zuverlässige Untersuchung und gezielte Modifikation der mechanischen Eigenschaften retinaler Zellen bei Netzhauterkrankungen und in Glianarben*  
Prof. Dr. J. Käs, Prof. Dr. A. Reichenbach et al.  
Teilprojekt 2 / SAB-Projekt

*Optische Messung zellulärer Materialeigenschaften für pharmakologische Hochdurchsatzverfahren (Agescreen)*  
Prof. Dr. J. Käs  
BMBF Verbundprojekt

## 5.8 Organizational Duties

J. A. Käs

- 464<sup>th</sup> Wilhelm und Else Heraeus-Seminar, Organization: Prof. Dr. J. Käs and Dr. C. Fütterer, Physikzentrum Bad Honnef, August 28 – September 3, 2010
- BuildMoNa-Minisymposium "Physics of Cancer", Organization: Prof. Dr. J. Käs and Dr. M. Zink, October 25 – 26, 2010
- PWM Winterschool Spindlermühle, CZ, March 6 – 13, 2010
- PWM Summerschool Zingst, August 8 – 15, 2010
- Advisory committee for soft matter physics, NASA, USA
- Chair, scientific advisory board, Evacyte Inc., USA
- CNRS review committee, Institute Curie, Paris
- Journal review: Nature, Physical Review Letters, Physical Review E, Biophysical Journal, Biophysica and Biochemica Acta, Biochemistry, Proceedings of the National Academy of Science, European Biophysical Journal, Langmuir
- Grant review: National Science Foundation, Div. of Materials Research; National Science Foundation, Div. of Cellular Organization; National Science Foundation, Div. of Computational Biology; National Science Foundation, Div. of Physics, Special Programs; Deutsche Forschungsgemeinschaft, Alexander von Humboldt Foundation, Deutsche Studienstiftung, Centre National de Reserche

## 5.9 External Cooperations

### Academic

- MD Anderson Cancer Center, Houston, Texas  
Prof. Dr. Michel Follen
- Center for Nonlinear Dynamics, Austin, Texas  
Prof. Dr. Harry Swinney
- University of Texas at Austin  
Prof. Dr. Ken Shih
- University of Texas at Austin  
Prof. Dr. Mark Raizen
- Institute Curie, Paris  
Prof. Dr. Jean-Francois Joanny
- ESPCI, Paris  
Prof. Dr. Jacques Prost
- Cea Saclay, France  
Prof. Dr. Marie-France Carlier
- Princeton  
Prof. Dr. Robert Austin
- University of Saarbruecken  
Prof. Dr. Walter Zimmermann
- MPI for Colloids and Interfaces, Potsdam-Golm  
Prof. Dr. Reinhardt Lipowsky
- MPI for Complex Systems, Dresden  
Prof. Dr. Frank Jülicher
- Indiana Purdue University, Indianapolis, USA  
Prof. Dr. Christoph Naumann
- Universität Münster  
Dr. Jürgen Schnekenburger
- University of Maryland, USA  
Prof. Dr. Wolfgang Losert
- University of Maryland School of Medicine, USA  
Prof. Dr. Stuart Martin
- Deutsches Krebsforschungszentrum (DKFZ), Heidelberg  
Dr. Evgeny Gladilin

### Industry

- Carl Zeiss MicroImaging GmbH, Jena  
Dr. Christian Dietrich

- Beiersdorf AG, Hamburg  
Dr. Th. Blatt
- Euroderm GmbH, Leipzig  
Dr. A. Emmendorffer
- Evotec GmbH, Dresden  
Dr. Th. Bauer
- FAUN GmbH, Leipzig  
F. Fischer
- GeSim mbH, Dresden  
Dr. S. Howitz
- JPK Instruments, Berlin  
Dr. Th. Jähnke
- Niendorf & Hamper, Hamburg  
Prof. A. Niendorf
- Qiagen GmbH, Hilden  
Dr. Th. Singer
- ibidi GmbH  
Dr. V. Kahl, Dr. R. Zantle

## 5.10 Publications

### Journals

M. Zink, A. Fritsch, F. Wetzel, K. D. Nnetu, T. Kießling, J. A. Käs: *Probing the physics of tumor cells from mechanical perspectives*, Cell News **36**, Issue 4, 17-21 (2010)

J. Galle, A. Bader, P. Hepp, W. Grill, B. Fuchs, J.A. Käs, A. Krinner, B. MarquaB, K. Muller, J. Schiller, R.M. Schulz, M. von Buttlar, E. von der Burg, M. Zscharnack, M. Loffler: *Mesenchymal Stem Cells in Cartilage Repair: State of the Art and Methods to monitor Cell Growth, Differentiation and Cartilage Regeneration*, Current Medicinal Chemistry **17**, Issue 21, 2274-2291 (2010)

C. Schulze, F. Wetzel, Th. Kueper, A. Malsen, G. Muhr, S. Jaspers, Th. Blatt, K.-P. Wittern, H. Wenck, J. A. Käs: *Stiffening of Human Skin Fibroblasts with Age*, Biophysical Journal **99**, Issue 8, 2434-2442 (2010)

A. Fritsch, M. Höckel, T. Kiessling, K. D. Nnetu, F. Wetzel, M. Zink, J. A. Käs: *Are biomechanical changes necessary for tumour progression?*, Nature Physics **6**, Issue 10, 730-732 (2010)

B. Kemper, P. Langehanenberg, A. Höink, G. von Bally, F. Wottowah, S. Schinkinger, J. Guck, J. A. Käs, I. Bredebusch, J. Schnekenburger, K. Schütze: *Monitoring of Laser Micromanipulated Optically Trapped Cells by Digital Holographic Microscopy*, Journal of Biophotonics **3**, Issue 7, 425-431 (2010)

Y. Ma, M. Zink, S. G. Mayr: *Biocompatibility of single crystalline Fe<sub>70</sub>Pd<sub>30</sub> ferromagnetic shape memory films*, Applied Physics Letters **96**, Issue 21, 213703 (2010)

**in press**

B. Stuhmann, F. Huber, J. A. Käs: *Robust organization principles of protrusive biopolymer networks in migrating living cells*, PLoS One (2010)

S. Alonso, U. Dietrich, C. Händel, J. A. Käs, M. Bär: *Oscillations in the lateral pressure of lipid monolayers induced by nonlinear chemical dynamics of the second messengers MARCKS and protein kinase C*, Biophysical Journal (2010)

Y.-B. Lu, I. Iandiev, M. Hollborn, N. Körber, E. Ulbricht, P. G. Hirrlinger, Th. Pannicke, E.-Q. Wei, A. Bringmann, H. Wolburg, U. Wilhelmsson, M. Pekny, P. Wiedemann, A. Reichenbach, J. A. Käs: *Reactive glial cells: increased stiffness correlates with increased intermediate filament expression*, The FASEB Journal (2010)

D. Strehle, J. Schnauß, C. Heussinger, J. Alvarado, M. Bathe, J. Käs, B. Gentry: *Transiently crosslinked F-actin bundles*, European Biophysical Journal (2010)

**Talks**

PWM Winter School, Spindler-Mühle, Tschechische Republik, Organizer, February, 2009

Institutskolloquium ILM Leipzig, Professor Thiery, "Feeling for Cells with light", Feb. 17, 2010 (invited talk)

Americal Physical Society Meeting 2010, Portland, USA, "Soft Brains, Signal Amplification through Noise, and Taking the Bull by its horns", March 15 – 21, 2010 (invited talk)

DPG Frühjahrstagung, Regensburg, "Feeling for Cells with light", March 21 – 26, 2010 (invited talk)

Materials Research Society Spring Meeting 2010, San Francisco, USA, "Feeling for Cells with light", April 5 – 9, 2010 (invited talk)

Conference "Trends in Optical Micromanipulation II", Obergurgel, Austria, "Feeling for Cells with light", April 11 – 16, 2010

ADeutsches Krebsforschungszentrum (DKFZ), Heidelberg: Pankreas Meeting, "Soft Brains, Signal Amplification through Noise, and Taking the Bull by its horns", April 21, 2010 (invited talk)

International Conference on Laser Application in Life Sciences, Oulu, Finland, "Feeling for Cells with light: Illuminating the role of biomechanics for tumor progression", June 9 – 11, 2010 (invited talk)

Fraunhofer Institut für Kurzzeitdynamik, Ernst-Mach-Institut (EMI), Freiburg i. Br., "Feeling for Cells with light: Illuminating the role of biomechanics for tumor progression", June 29, 2010 (invited talk)

6. Symposium des BMBF-Forschungsschwerpunktes Biophotonik, Ulm, "Der Optical Stretcher, die Biomechanik des Tumorwachstums", September 22 – 24, 2010 (invited talk)

3<sup>rd</sup> BuildMoNa Workshop for Doctoral Candidates, Wittenberg, October 4 – 5, 2010

JPK Workshop: 9<sup>th</sup> International Symposium, Berlin, Scanning Probe Microscopy and Optical Tweezers in Life sciences, "Der Optical Stretcher, die Biomechanik des Tumorwachstums", October 6 – 7, 2010 (invited talk)

Cancer Colloquium VII, Bute Medical School, St. Andrews, UK, "Are biomechanical chances necessary for tumor progression?", November 9 – 12, 2010 (invited talk)

### Patents

Josef Käs, Mark Raizen, Valery Milner, Timo Betz and Allen Ehrlicher: U.S. Patent # 7435568 "Optical Cell Guidance", European and Asian patents are pending

Josef Käs and Jochen Guck: U.S. Patent # 6067859 "Optical Stretcher"

Josef Käs and Jochen Guck: European Patent # 1059871 "Optical Stretcher" for Germany, Great Britain, France, Switzerland, Italy and Spain

Jochen Guck, Josef Käs, Moritz Kreysing: European Patent # 193549811 "Anordnung und Verfahren zur berührunglosen Ausrichtung und Drehung von Partikeln durch anisotrope, elektromagnetische Strahlungsfelder"

Josef Käs und Jochen Guck: German Patent Application # 10 2010 041 912.5 "Verfahren zur Diagnose und/oder Prognose von Krebserkrankungen durch Analyse der mechanischen Eigenschaften von Tumorzellen", submitted October 2010.

## 5.11 Graduations

### Doctorate

- David Smith M. Sc.  
*Control of mechanical and organizational parameters in the cytoskeleton through dissipation and relaxation*  
March 2009
- Florian Ruckerl, M. Sc.  
*Diffusion and interaction of colloids within lipid membranes*  
August 2010

### Diploma

- Jörg Schnauß  
*Filamentous actin bundles – between elasticity and plasticity*  
January 2010

- Sebastian Schmidt  
*The neuron-silicon-junction based on ZnO devices*  
January 2010
- Sebastian Ehrig  
*Active polymer networks on microstructure environments*  
May 2010
- Carsten Vogt  
*Active polymer films in emulsion – in vitro experiments on actin polymerization networks*  
May 2010
- Christoph Schneider  
*Measurement of the angle of the transition dipole moment of a fluorophore and of a DNA nanotube to which the fluorophore is bound*  
September 2010
- Tina Händler  
*Passive and active stress-strain response of biological cells*  
October 2010
- Chris Händel  
*Pattern formation in phospholipid membranes*  
November 2010

## **Bachelor**

- Tom Golde  
*Control of optomechanical wiggling experiments on semiflexible polymer bundles*  
April 2010
- Christian Heinrichs  
*Evaluation of optical micromanipulation experiments on semiflexible polymer bundles*  
May 2010
- Wolfram Pönisch  
*Fluktuationsanalyse von neuronalem Wachstumskegeln*  
June 2010  
Maren Romeyke  
*Strukturelle Eigenschaften des Zytoskeletts*  
September 2010
- Hans Kubitschke  
*Untersuchung von oralen krebsartigen und nicht-krebsartigen Keratinozyten im Hinblick auf mechanisches Verhalten*  
October 2010
- Jürgen Lippoldt  
*Change of lateral organisation in model membranes*  
December 2010

- Erik W. Morawetz  
*Introducing a device for the observation of lateral microstructures in liquid crystalline lipid phases*  
December 2010

## 5.12 Guests

- M. Sc. Valentina dallacasagrande  
EU-research assistant at the Paul-Flechsig-Institut for brain research and the Dept. Softmatter Physics, Universität Leipzig, March 2010 – approx. 2012
- Iris Vonderhaid  
Technische Universität Wien, September 21, 2010 – approx. August 2011
- Dr. Evgeny Gladilin  
DKFZ Heidelberg, November 29 – December 3, 2010

## 5.13 Awards

- Prof. Dr. J. Käs  
Wolfgang-Paul Prize awarded by the Alexander von Humboldt Foundation
- Prof. Dr. J. Käs  
Distinguished Lecturer, SigmaXi Academic Honor Society, USA
- Prof. Dr. J. Käs  
Adjunct Professor, Department of Biomedical Engineering, University of Texas at Austin



**II**

**Institute for Experimental Physics II**



# 6

## Magnetic Resonance of Complex Quantum Solids

### 6.1 Introduction

The electronic properties of quantum-solids in which the electrons exhibit strong correlations with each other or with the lattice are particularly rich and will be of special importance in future functional materials. In addition, such solids are challenging for experiment, as well as theory, as the more than twenty-year history of high-temperature superconductivity shows: we still do not understand the electronic structure of these systems. One particular aspect of strongly correlated electronic materials is their tendency towards nano-scale electronic phase separation. Even in perfect lattices, electronic nano-structures can form. The investigation of such materials requires the use of methods that can give detailed information. Here, magnetic resonance, on nuclei and electrons, is of particular interest as they not only have atomic scale resolution, but also yield bulk information in contrast to surface techniques. We explore the properties of these materials with tailored new techniques of magnetic resonance.

*Jürgen Haase*

### 6.2 High sensitivity nuclear magnetic resonance probe for anvil cell pressure experiments

J. Haase, Th. Meissner, B. Meier, D. Rybicki, P.L. Alireza<sup>\*</sup>, S.K. Goh<sup>†</sup>

<sup>\*</sup>Department of Physics and Astronomy, University College London, United Kingdom

<sup>†</sup>Cavendish Laboratory, University of Cambridge, United Kingdom

A novel approach that uses radio-frequency microcoils in the high-pressure region of anvil cells with Nuclear Magnetic Resonance (NMR) experiments is described. High-sensitivity Al NMR data at 70 kbar for Al metal are presented for the first time. An expected decrease in the Al Knight shift at 70 kbar is observed, as well as an unexpected change in the local charge symmetry at the Al nucleus. The latter is not predicted by chemical structure analysis under high pressure

### 6.3 Cw and Pulsed ESR Spectroscopy of Paramagnetic Framework Cupric Ions in the Zn(II) Doped Porous Coordination Polymer $\text{Cu}_{3-x}\text{Zn}_x(\text{btc})_2$

B. Jee, A. Pöpl

In the parent metal-organic framework  $\text{Cu}_3(\text{btc})_2$  material the Cu(II) pairs in the paddle-wheel building blocks of the framework give rise to an antiferromagnetic spin state with an electron spin resonance (ESR) silent  $S = 0$  ground state. The thermally excited  $S = 1$  state of the Cu(II) pairs can be observed for temperature above 80 K by ESR spectroscopy but gives just rise to an exchanged narrowed resonance line preventing the exploration of any structural details in the environment of the paddle-wheel units. However, magnetically diluted paramagnetic binuclear Cu-Zn clusters can be formed by substitution of Cu(II) ions by Zn(II) at low doping levels as already known for zinc-doped copper acetate monohydrate. Indeed, ESR, hyperfine sublevel correlation spectroscopy (HYSCORE) and pulsed electron nuclear double resonance (ENDOR) verify the successful incorporation of zinc ions at cupric ion sites into the framework of the resulting  $\text{Cu}_{3-x}\text{Zn}_x(\text{btc})_2$  coordination polymer (Fig. 6.1). The formation of such paramagnetic binuclear Cu-Zn paddle wheel building blocks allows the investigation of the interaction between the Cu(II) ions and various adsorbates by advanced pulsed ESR methods with high accuracy now. As a first example we have presented the adsorption of methanol over  $\text{Cu}_{3-x}\text{Zn}_x(\text{btc})_2$ , which was found to coordinate directly to the Cu(II) ions via their open axial binding site [1].

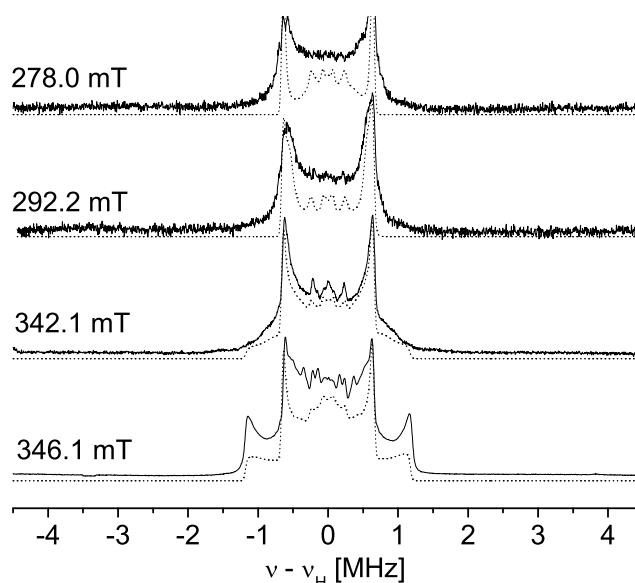


**Figure 6.1:** Experimental (solid lines) and simulated (dashed lines) orientation-selective X-band  $^1\text{H}$  Davies ENDOR spectra of Cu(II) species in the dehydrated  $\text{Cu}_{3-x}\text{Zn}_x(\text{btc})_2$  at 6 K.

- [1] B. Jee, K. Eisinger, F. Gul-E-Noor, M. Bertmer, M. Hartmann, D. Himsl, A. Pöpl: *J. Phys. Chem. C* **114**, 16630 (2010)

## 6.4 Photodimerization kinetics of co-crystals of *trans* cinnamamide and phthalic or oxalic acid

D. Blaschke, M. Bertmer

Two molecules of cinnamamide can be photodimerized to a cyclobutane-ring containing moiety. By co-crystallization with a diacid, because of hydrogen-bonding a different orientation of the two cinnamamide molecules in the crystal structure can be obtained that lead to a different molecule after photodimerization. The topic of this study is to use solid-state NMR techniques to evaluate the effects of co-crystallization on photodimerization rate and to document the spectroscopic signal assignment. For this,  $^1\text{H}$  and  $^{13}\text{C}$  NMR spectra are obtained and together with  $^1\text{H}$  spin-lattice relaxation times analyzed to follow the photodimerization process. The ultimate application of these materials could be as reversible cross-linking agents in polymers and for optical memory applications. For further investigations, effects of different cations for complexation will be tested with respect to crystal structures and different photodimerization products.

## 6.5 Optimized NMR Spectroscopic Strategy to Characterize Water Dynamics in Soil Samples

A. Jäger, M. Bertmer

$^1\text{H}$  Wideline-NMR spectra of soil samples offer the possibility to analyze proton containing soil material based on their mobility. Care has to be taken to remove unwanted signal contributions from the probe background. We demonstrate that unstructured wideline spectra can be analyzed straightforwardly by a combination of a Gaussian line for rigid and a Lorentzian line for mobile protons. This is used to study effects of hydrogen-bonded water networks upon heat treatment for a series of different soil samples with varying water content as a contribution to study physical aging of soil organic matter (SOM). Results are combined with  $^1\text{H}$  projections from  $^{13}\text{C}$  2D WISE experiments representing solely the broad Gaussian line. Furthermore,  $^1\text{H}$  structural information from soil samples is obtained from 2D PMLG measurements under magic angle spinning (MAS). Low water contents are improving the resolution of main functional groups.

## 6.6 Effects of Varying Water Adsorption on $\text{Cu}_3(\text{BTC})_2$ Metal-Organic Framework (MOF) as Studied by $^1\text{H}$ and $^{13}\text{C}$ Solid-State NMR Spectroscopy

F. Gul-E-Noor, M. Bertmer

The process of water adsorption on dehydrated  $\text{Cu}_3(\text{BTC})_2$  (copper (II) benzene 1,3,5-tricarboxylate) metal-organic framework (MOF) was studied with  $^1\text{H}$  and  $^{13}\text{C}$  solid-state NMR. Different relative amounts of water (0.5, 0.75, 1, 1.5, 2, and 5 mole equivalents

with respect to copper) were adsorbed via the gas phase.  $^1\text{H}$  and  $^{13}\text{C}$  MAS NMR spectra of dehydrated and water-loaded  $\text{Cu}_3(\text{BTC})_2$  samples gave evidence on the structural changes due to water adsorption within the MOF material as well as information on water dynamics. The analysis of  $^1\text{H}$  spinning sideband intensities reveals differences in the  $^1\text{H}$ - $^{63/65}\text{Cu}$  hyperfine coupling between dehydrated and water-loaded samples. The investigation was continued for 60 days to follow the stability of the  $\text{Cu}_3(\text{BTC})_2$  network under humid conditions. NMR data reveal that  $\text{Cu}_3(\text{BTC})_2$  decomposes quite fast with the decomposition being different for different water contents.

## 6.7 The Jahn-Teller effect in $\text{Cr}^{5+}$ -doped $\text{PbTiO}_3$ : a multi-frequency electron paramagnetic resonance study

R. Böttcher, A. Pöpl, J. Hoentsch, R.M. Rakhmatullin\*

\*MRS Laboratory, Kazan State University, Kremlevskaya 18, 420008 Kazan, Russia

Electron paramagnetic resonance (EPR) spectra of  $\text{Cr}^{5+}$  defects incorporated on  $\text{Ti}^{4+}$  sites in powdered ceramics of  $\text{PbTiO}_3$  were investigated in the temperature range 50-400 K at 9 GHz (X), 34 GHz (Q) and 94 GHz (W band). The Jahn-Teller effect stabilizes the vibronic ground state of the  $3d^1$  electron of the  $\text{Cr}^{5+}$  ion and leads to a tetragonally distorted defect- $\text{O}_6$  octahedron with the point symmetry  $D_{4h}$ . The spontaneous electrical polarization present in the ferroelectric phase of  $\text{PbTiO}_3$  appears as a further perturbation producing an additional  $g$ -tensor contribution by the quadratic field effect. Its symmetry is dependent on the orientation of the electrical polarization with respect to the Jahn-Teller distortion axis, the tetragonal axis of the defect- $\text{O}_6$  octahedron. If the polarization of a domain is anti- or parallel to this axis, the local tetragonal symmetry of the  $\text{Cr}^{5+}$  ion persists whereas it is reduced by a perpendicular orientation. Anisotropic EPR spectra of tetragonally and orthorhombic distorted  $\text{Cr}^{5+} \text{O}_{12}^{6-}$  are detected at low temperatures. Increasing the temperature, the peaks of the two spectra are broadened and a motionally averaged isotropic spectrum appears at 200 K.

## 6.8 Size Effects in Fine Barium Titanate Particles

P. Sedykh D. Michel E.V. Charnaya\*, J. Haase

\*St. Petersburg State University, Institute of Physics, Petrodvorets, Russia

$^{137}\text{Ba}$  NMR spectroscopy is very suitable to study size effects in very fine particles of barium titanate. The particle sizes varied between 155 and 15 nm. The NMR measurements were carried out within a temperature range of 295 to 420 K covering also the cubic to tetragonal phase transition at TC. Below TC the NMR line shape was explained by a superposition of two contributions the relative fractions of which were analyzed over a wider temperature range. Assuming the core-shell model the thickness of the outer shell was estimated. The shell thickness strongly decreased with decreasing particle size. The applicability of other structural models was also discussed.

## 6.9 Funding

### *Controlling Mesoscopic Phase Separation*

J. Haase

EU-FP6, CoMePhS, NMP4-CT-2005-517039.

### *Advanced Signal-Processing for Ultra-Fast Magnetic Resonance Spectroscopic Imaging, and Training*

J. Haase, H. Moeller

EU-CORDIS-FP6, MRTN-CT-2006-035801.

### *EuroMagNET, JRA NMR*

J. Haase

EU, RII3CT-2004-506239.

### *Magnetic Ground State and Dynamics in High-Temperature Superconductors*

J. Haase, O.P. Sushkov, B. Keimer

EU, DP0881336.

### *Quasi One-Dimensional Ferroelectrics*

R. Böttcher, E. Hartmann

DFG BO 1080/8-2 within DFG Forschergruppe FOR 522.

### *Funding for the Initiation and Enhancement of Bilateral Cooperation - Investigation of the local electronic structure of nitrogen donor in isolated and aggregated state in n-type $^4\text{H}$ and $^6\text{H}$ -SiC by pulsed EPR spectroscopy*

A. Pöpl

DFG PO 426/9-1.

### *Host-guest interactions and magnetic ordering in MOFs studied by electron and nuclear spin resonance spectroscopy*

A. Pöpl

DFG PO 426/6-1.

### *Charakterisierung der [2+2] Photodimerisierung von photoaktiven Substanzen auf der Basis von Zimtsäure eingebaut in Polymeren oder in supramolekularen Strukturen mit Festkörper-NMR-Spektroskopie*

M. Bertmer

DFG BE 2434/2-3.

### *Host-guest interactions and magnetic ordering in MOFs studied by electron and nuclear spin resonance spectroscopy*

M. Bertmer

DFG BE 2434/4-1 within SPP 1362.

### *SOM-AGING II. Hydration-dehydration mechanisms at Biogeochemical Interfaces*

M. Bertmer

within SPP 1315.

*Fabrication and physical properties of ferroelectrics confined in nanoporous materials*

D. Michel, E. V. Charnaya

DFG Mi 390/25-1.

*Hydrogen diffusion in Ti- V-Cr alloys*

D. Michel, V. I. Chizhik

DFG Mi 390/23-1.

## 6.10 Organizational Duties

J. Haase

- stellvertretender Direktor des Zentrums für magnetische Resonanz
- Referee: Physical Review, GIF

M. Bertmer

- Referee: Angewandte Chemie, Chemistry of Materials, Solid State Nuclear Magnetic Resonance

R. Böttcher

- Referee: Physical Review, Journal of Physics: Condensed Matter, Langmuir, Journal of Magnetic Resonance

A. Pöppel

- Referee: Journal of Magnetic Resonance, Journal of the American Chemical Society, Physical Chemistry Chemical Physics, Chemical Physics Letters
- Project Reviewer: German-Israel-Foundation for Scientific Research and Development-GIF

## 6.11 External Cooperations

### Academic

- Laboratoire National des Champs Magnétiques Pulsés Toulouse, France  
Prof. Dr. Geert Rikken
- University of Illinois at Urbana-Champaign, Department of Physics, USA  
Prof. Dr. Charles P. Slichter
- University of New South Wales Australia, School of Physics, Sydney, Australia  
Prof. Dr. Oleg P. Sushkov
- University of Illinois at Urbana-Champaign, Department of Electrical and Computer Engineering, USA  
Macro Prof. Dr. Andrew G. Webb
- The MacDiarmid Institute and Industrial Research Limited, New Zealand  
Dr. Grant V. M. Williams
- Dresden High Magnetic Field Laboratory, Forschungszentrum Dresden-Rossendorf  
Prof. Dr. Joachim Wosnitza

- Washington University, St. Louis, MO, USA, Department of Chemistry  
Prof. Dr. Sophia E. Hayes
- Universität Koblenz-Landau, Koblenz, Abteilung Chemie  
Prof. Dr. Gabriele E. Schaumann
- Martin-Luther-Universität Halle-Wittenberg, Physikalisches Institut  
Dr. H. T. Langhammer
- University of Vilnius, Faculty of Physics, Lithuania  
Prof. Dr. J. Banyš
- Universität Augsburg, Advanced Materials Science, Institut für Physik  
Prof. Dr. M. Hartmann
- Technische Universität München, Anorganisch-chemisches Institut  
Prof. Dr. K. Köhler
- NASU, Institute of Semiconductor Physics, Kiev, Ukraine  
Prof. Dr. E. N. Kalabukhovaa
- Université du Maine, Faculté des Sciences, Laboratoire de Physique de l'Etat Condensé, Le Mans, France  
Prof. Dr. A. Kassiba

### Industry

- NMR-Service, Erfurt  
M. Braun
- Bruker BioSpin, Rheinstetten  
F. Engelke

## 6.12 Publications

### Journals

- B. Jee, K. Eisinger, F. Gul-E-Noor, M. Bertmer, M. Hartmann, D. Himsl, A. Pöppl: *Continuous Wave and Pulsed Electron Spin Resonance Spectroscopy of Paramagnetic Framework Cupric Ions in the Zn(II) Doped Porous Coordination Polymer  $Cu_{3-x}Zn_x(btc)_2$* , J. Phys. Chem. C **114**, 16630-16639 (2010)
- M. Meilikhov, K. Yusenko, A. Torrisi, B. Jee, C. Mellot-Draznieks, A. Pöppl, R. A. Fischer: *Reduction of a Metal-Organic Framework by an Organometallic Complex: Magnetic Properties and Structure of the Inclusion Compound  $[(n_5-C_5H_5)_2Co]_{0.5} MIL-47(V)$* , Angew. Chem. Int. Ed. **49**, 6212-6215 (2010)
- P. Sedykh, D. Michel, E. V. Charnaya, J. Haase: *Size effects in fine barium titanate particles*, FERROELECTRICS **400**, 135-143 (2010)
- B. F. Borisov, E. V. Charnaya, S. V. Baryshnikov, A. L. Pirozerskii, A. S. Bugaev, C. Tien, M. K. Lee, D. Michel: *Ferroelastic phase transition in  $LiCsSO_4$  embedded into molecular sieves*, Physical Letters **375**, 183-186 (2010)

- S. V. Baryshnikov, E. V. Charnaya, A. Y. Milinskiy, Y. A. Shatskaya, C. Tien, D. Michel: *Stabilization of ferroelectricity in  $\text{KNO}_3$  embedded into MCM-41 molecular sieves*, *Physica* **405**, 3299-3302 (2010)
- D. V. Savchenko, A. Pöppl, E. N. Kalabukhova, E. F. Venger, M. P. Gadzira, G. G. Gnesin: *Intrinsic defects in nonstoichiometric  $\beta$ -SiC nanoparticles studied by pulsed magnetic resonance methods*, *Semiconductor Physics, Quantum Electronics and Optoelectronics*, **13**, 43-50 (2010)
- R. Böttcher, A. Pöppl, J. Hoentsch, R. M. Rakhmatullin: *The Jahn-Teller effect in  $\text{Cr}^{5+}$ -doped  $\text{PbTiO}_3$ : a multi-frequency electron paramagnetic resonance study*, *J. Phys. Condens. Matter* **22**, 065902 (2010)
- T. Meissner, S. K. Goh, J. Haase, B. Meier, D. Rybicki, P. L. Alireza: *New Approach to High-Pressure Nuclear Magnetic Resonance with Anvil Cells*, *Journal of Low Temperature Physics* **159**, 284 (2010)
- D. J. Awad, F. Conrad, A. Koch, U. Schilde, A. Pöppl, P. Strauch: *1,10-Phenanthroline-dithiolate mixed ligand transition metal complexes. Synthesis, characterization and EPR spectroscopy*, *Inorganica Chimica* **363**, 1488-1494 (2010)
- B. Jee, K. Eisinger, F. Gul-E-Noor, M. Bertmer, M. Hartmann, D. Himsl, A. Pöppl: *Continuous Wave and Pulsed Electron Spin Resonance Spectroscopy of Paramagnetic Framework Cupric Ions in the Zn(II) Doped Porous Coordination Polymer  $\text{Cu}_3\text{xZn}_x(\text{BTC})_2$* , *J. Phys. Chem.* **114**, 16630-16639 (2010)
- J. Barzola-Quiquia, P. Esquinazi, M. Villafuerte, S. P. Heluani, A. Pöppl, K. Eisinger: *Origin of the giant negative photoresistance of ZnO single crystals*, *Journal of applied Physics* **108**, 073530 (2010)
- M. Khalid, A. Setzer, M. Ziese, P. Esquinazi, D. Spemann, A. Pöppl, E. Goering: *Ubiquity of ferromagnetic signals in common diamagnetic oxide crystals*, *Physical Review*: **81**, 214414 (2010)
- M. Mendt, B. Jee, N. Stock, T. Ahnfeldt, M. Hartmann, D. Himsl, A. Pöppl: *Structural Phase Transitions and Thermal Hysteresis in the Metal-Organic Framework Compound MIL-53 As Studied by Electron Spin Resonance Spectroscopy*, *J. Phys. Chem.:* **114**, 19443-19451 (2010)
- B. Pattier, M. Henderson, A. Pöppl, A. Kassiba, A. Gibaud: *Multi-approach Electron Paramagnetic Resonance Investigations of UV-Photoinduced  $\text{Ti}^{3+}$  in Titanium Oxide-Based Gels*, *J. Phys. Chem.:* **114**, 4424-4431 (2010)
- B. Jee, D. Himsl, M. Icker, M. Hartmann, A. Pöppl: *Untersuchungen zur chemischen Stabilität von  $\text{Cu}_3(\text{BTC})_2$  (HKUST-1) durch  $\text{N}_2$ -Adsorption, Röntgenpulverdiffraktometrie und EPR-Spektroskopie*, *Chemie Ingenieur Technik*: **7**, 82 (2010)
- M. Burghoff, H.-H. Albrecht, S. Hartwig, I. Hilschenz, R. Körber, N. Höfner, H.-J. Scheer, J. Voigt, L. Trahms, G. Curio: *On the feasibility of neurocurrent imaging by low-field nuclear magnetic resonance*, *Appl. Phys. Lett.* **96**, 233701 (2010)

## Talks

G. Thörmer, N. Garnov, M. Moche, T. Kahn, H. Busse: *Dynamische Positionsbestimmung eines robotischen Manipulators für Interventionen in einem geschlossenen MRT: Methode und erste Ergebnisse*, 91. Deutscher Röntgenkongress, 12.–15. Mai 2010, Berlin

N. Garnov, G. Thörmer, W. Gründer, R. Trampel, R. Turner, T. Kahn, H. Busse: *In vivo MRT-Beurteilung der Kollagenstruktur des humanen Kniegelenkknorpels bei 7 T*, 91. Deutscher Röntgenkongress, 12.–15. Mai 2010, Berlin

H. Busse, N. Garnov, G. Thörmer, W. Gründer, T. Kahn, M. Moche: *Navigationslösung für MR-gestützte Interventionen in einem geschlossenen MRT*, 91. Deutscher Röntgenkongress, 12.–15. Mai 2010, Berlin

D. Seider, H. Busse, N. Garnov, G. Thörmer, S. Heinig, T. Riedel, T. Kahn, M. Moche: *Erste Erfahrungen mit navigierten Radiofrequenzablationen der Leber in einem geschlossenen 1.5 T-MRT*, 91. Deutscher Röntgenkongress, 12.–15. Mai 2010, Berlin

B. Jee: *Continuous wave (cw) and pulse EPR studies on Metal Organic Frameworks (MOF)*, DFG meeting: New Frontiers in Electron Spin Resonance Methodology; Hirschegg, 11.09.10

B. Jee: *Cw and pulse EPR spectroscopy of adsorbate interactions of small molecules ( $H_2/D_2$ , CO and  $CH_3OH$ ) with the metal organic framework compound copper(II)1,3,5-benzenetricarboxylate*, MPI für Polymerforschung, Mainz, 24.11.10

O. F. Erdem, D. Michel, J. Haase: *Molecular motion of molecules and glass transition embedded in confined geometry*, DPG Spring Meeting March 21st–26th 2010, Regensburg

D. Michel, P. Sedykh, E. V. Charnaya, J. Haase, R. Böttcher: *Size effects in  $BaTiO_3$  and  $PbTiO_3$  nanopowders*, NMR-Winterschule und Konferenz, St. Petersburg Staatliche Universität, 28.11.–3.12. 2010 (Prof. V. I. Chizhik)

D. Michel: *NMR studies of structural phase transitions in systems with incommensurately structurally modulated phases*, NMR-Winterschule und Konferenz, St. Petersburg Staatliche Universität, 28.11.–3.12. 2010 (Prof. V. I. Chizhik)

D. Michel: *Spin dynamics in solids. Fundamentals and recent developments of high-resolution solid-state NMR spectroscopy*, St. Petersburg Staatliche Universität, Lehrstuhl Festkörperphysik und Lehrstuhl Quanten-Magnetische Phänomene, Kolloquium, 7. Dezember 2010

P. Sedykh, D. Michel, E. V. Charnaya, J. Haase: *Size Effects in Fine Barium Titanate Particles*, DPG Spring Meeting March 21st–26th 2010, Regensburg

D. Michel, P. Sedykh, J. Haase, E. V. Charnaya: *Ferroelectricity in Confined Materials. Studied by Means of NMR spectroscopy*, AMPERE Conference, Masuria (Polen), 21–26 Juni 2010

D. Michel, O. F. Erdem: *Glass transition of molecules adsorbed in zeolites: Studies by means of MAS-NMR spectroscopy, nuclear spin relaxation and broad band dielectric measurements*, International Symposium and Summer School in St. Petersburg, Nuclear Magnetic Resonance in Condensed Matters, 7th Meeting "NMR in Heterogeneous Systems", 28.06.–02.07.2010

J. Haase: *Höchste Drücke und höchste Magnetfelder bei der Erforschung moderner Materialien (anorganische Festkörper, Supraleiter, Metalle) mittels magnetischer Kernresonanz (NMR)*, AC-Kolloquium an der LMU München, 22.04.2010

A. Pöpl: *Cw and Pulsed EPR Spectroscopy of Paramagnetic Transition Metal Ions in Metal-Organic Framework Compounds*, 32nd Discussion Meeting of the Magnetic Resonance Spectroscopy Division of the GDCH and Joint Benelux/German MR Conference, Münster, 2010

A. Pöpl: *Temperature-driven structural phase transition in chromium-doped MIL-53(Al)–An electron spin resonance*, 2nd International Conference on MOFs and open framework compounds, Marseille, 5.–8.9.2010

A. Jäger, M. Bertmer, G. E. Schaumann: *Dynamics and Structure of Soil investigated by solid state  $^1\text{H}$ -,  $^{13}\text{C}$ - and  $^{27}\text{Al}$ -NMR spectroscopy*, SPP 1315 annual colloquium, Dornburg, 04.–05.10.2010

## Posters

B. Jee, A. Pöpl, M. Hartmann, D. Hims: *Electron Spin Resonance (ESR) spectroscopy of isolated paramagnetic centers in HKUST-1 and MIL-53*, 2nd International Conference on Metal Organic Frameworks and Open Framework Compounds, 5.–8.9.2010, Marseille

G. V. M. Williams, J. Haase, M. Jurkutat, D. Rybicki: *Understanding High Temperature Superconducting Cuprates*, ISIS-18 Conference, 09.–11.02.2010, Wellington, NZ

H. Busse, G. Thörmer, N. Garnov, J. Haase, T. Kahn, M. Moche: *Technique for wireless position tracking of intravascular catheters: Performance evaluation in a vessel phantom*, ISMRM 2010, Stockholm, 01.–07.05.2010

N. Garnov, G. Thörmer, W. Gründer, R. Trampel, M. Moche, T. Kahn, H. Busse: *Systematic characterization of small inductively coupled radiofrequency coils as MR-visible markers at 1.5 T*, ISMRM 2010, Stockholm, 01.–07.05.2010

H. Busse, G. Thörmer, N. Garnov, J. Haase, T. Kahn, M. Moche: *On the heating of small inductively coupled RF coils mounted on an intravascular model catheter during MR imaging*, ISMRM 2010, Stockholm, 01.–07.05.2010

N. Garnov, G. Thörmer, Gründer, Trampel, Turner, T. Kahn, H. Busse: *In-vivo assessment of collagen fiber arrangement in articular cartilage with 7 T MRI*, ISMRM 2010, Stockholm, 01.–07.05.2010

G. Thörmer, N. Garnov, Fuchs, Heinig, Riedel, T. Kahn, H. Busse: *Navigated liver biopsies in a closed-bore MR scanner: first clinical experience*, ISMRM 2010, Stockholm, 01.–07.05.2010

Seider, H. Busse, N. Garnov, G. Thörmer, Heinig, Riedel, T. Kahn, M. Moche: *First clinical experience with navigated RF ablations of the liver in a closed-bore 1,5 T MRI*, ISMRM 2010, Stockholm, 01.–07.05.2010

G. Thörmer, N. Garnov, J. Haase, T. Kahn, M. Moche, H. Busse: *Automatic device tracking in a closed-bore MRI: principle and initial experimental results on a robotically driven needle*, ISMRM 2010, Stockholm, 01.–07.05.2010

G. Thörmer, N. Garnov, J. Haase, T. Kahn, M. Moche, H. Busse: *Performance and accuracy of a morphological MR marker localizatin at reduced spatial resolutions: results from simulated and real marker images*, ISMRM 2010, Stockholm, 01.–07.05.2010

N. Garnov, G. Thörmer, W. Gründer, M. Moche, T. Kahn, H. Busse: *Eignung von induktiv gekoppelten Miniaturspulen als MR-sichtbare Marker bei 1.5 T*, 91. Deutscher Röntgenkongress Berlin 12.–15.5.2010

G. Thörmer, N. Garnov, M. Moche, T. Kahn: *Eignung von drahtlosen MR-Markern für intravaskuläre Anwendungen: Erwärmung eines Modellkatheters in einem durchflossenen Gefäßphantom*, 91. Deutscher Röntgenkongress Berlin 12.–15.5.2010

T. Meissner, S. K. Goh, D. Rybicki, J. Haase: *A Novel Approach To Gigapascal NMR: First Applications*, DPG Spring Meeting March 21st–26th 2010, Regensburg

N. Georgieva, A. Pöpl, R. Böttcher, M. Bertmer, J. Haase, A. Sushkov: *EPR and NMR of Multiferroic  $\text{Eu}_x\text{Ba}_{1-x}\text{TiO}_3$* , DPG Spring Meeting March 21st–26th 2010, Regensburg

A. Jäger, J. Schwarz, M. Bertmer, G. E. Schaumann: *Soil Organic Matter Dynamics as Characterized with  $^1\text{H}$  and  $^{13}\text{C}$  Solid State NMR Techniques*, SPP 1315 annual colloquium, Dornburg, Oktober 2010

B. Meier, J. Haase, S. Greiser, F. Wolff-Fabris, T. Herrmannsdörfer, J. Wosnitza: *NMR in pulsed high magnetic fields*, DPG Spring Meeting March 21st–26th 2010, Regensburg

D. Rybicki, J. Haase, M. Lux, M. Greven, G. Yu: *Spatial Inhomogeneities in Single Crystal  $\text{HgBa}_2\text{CuO}_{4+d}$  from  $^{63}\text{Cu}$  NMR*, DPG Spring Meeting March 21st–26th 2010, Regensburg

M. Jurkutat, D. Rybicki, G. V. M. Williams, J. Haase:  *$^{17}\text{O}$  and  $^{63}\text{Cu}$  NMR of electron-doped High-Temperature Superconductor  $\text{Pr}_{1.85}\text{Ce}_{0.15}\text{CuO}_4$* , DPG Spring Meeting March 21st–26th 2010, Regensburg

S. Greiser, B. Meier, J. Haase, F. Wolff-Fabris, T. Herrmannsdörfer, J. Wosnitza: *Double resonance in pulsed magnetic fields*, EuroMagNET II User Meeting 2010, Dresden, 16.06.2010

A. V. Kuttatheyil: *Insights into the Structure of MOFs evidenced from Solid-State NMR Studies*, 2nd International Conference on MOFs and open framework compounds, Marseille, 5.–8.9.2010

F. Gul-E-Noor: *Solid State NMR on  $\text{Cu}_3(\text{BTC})_2$ : Adsorption Study and Resonance Assignment*, 2nd International Conference on MOFs and open framework compounds, Marseille, 5.–8.9.2010

A. Jäger, J. Schwarz, M. Bertmer, G. E. Schaumann: *Soil Organic Matter Dynamics as Characterized with  $^1\text{H}$  and  $^{13}\text{C}$  Solid State NMR Techniques*, EGU general assembly, Wien, 02.–07.05.2010

## 6.13 Graduations

### Diploma

- Juliane Bopst  
*The investigation of Iron Based Superconductors by Nuclear Magnetic Resonance*  
December 2010
- Marc Lux  
*Kernspinresonanz an Hochtemperatursupraleitern*  
September 2010

## 6.14 Guests

- Swee K. Goh, PhD  
Trinity College, Quantum Matter Group, Cavendish Laboratory, UK  
13.01.–15.01.2010
- Lina Klintberg, PhD  
Trinity College, Quantum Matter Group, Cavendish Laboratory, UK  
13.01.–15.01.2010
- Mikhail Andreevich Vovk  
St. Petersburg State University, Institute of Physics, Petrodvorets, Russia  
17.03.–16.04.2010
- Nicholas Curro, Prof.  
University of California, Department of Physics, Davis, CA  
24.03.–26.03.2010
- Swee K. Goh, PhD  
Trinity College, Quantum Matter Group, Cavendish Laboratory, UK  
28.03.–30.03.2010
- Anastasia Sokolova  
St. Petersburg State University, Institute of Physics, Petrodvorets, Russia  
18.04.–17.07.2010
- Henrik Bohr, Prof.  
Technische Universität Dänemark, DTU  
12.04.2010
- Sophia Hayes, Prof.  
Washington University, Department of Chemistry, St. Louis, USA  
23.06.–27.06.2010

- O. P. Sushkov, Prof.  
School of Physics, University of New South Wales, Sydney Australia  
30.07.2010
- Dariia Savchenko  
V.E. Lashkaryov Institute of Semiconductor Physics, National Academy of Sciences,  
Kyiv, Ukraine  
03.09.–29.11.2010
- Swee K. Goh, PhD  
Trinity College, Quantum Matter Group, Cavendish Laboratory, UK  
27.10.–29.10.2010
- A. Kassiba, Prof.  
Université du Maine, Faculté des Sciences, Laboratoire de Physique de l'Etat Condensé, Le Mans, France  
01.11.–04.11.2010
- Siegmund Greulich-Weber, Prof.  
Universität Paderborn, Fakultät für Naturwissenschaften, Department für Physik  
10.11.–12.11.2010
- Uwe Gerstmann, Dr.  
Universität Paderborn, Fakultät für Naturwissenschaften, Department für Physik  
10.11.–12.11.2010
- André Konopka, M. sc.  
Universität Paderborn, Fakultät für Naturwissenschaften, Department für Physik  
10.11.–12.11.2010
- A. Sushkov, Prof.  
Yale University, Department of Physics, Steve Lamoreaux Research Lab  
10.11.2010
- O. P. Sushkov, Prof.  
School of Physics, University of New South Wales, Sydney Australia  
10.11.2010
- Swee K. Goh, PhD  
Trinity College, Quantum Matter Group, Cavendish Laboratory, UK  
17.11.–19.11.2010



# 7

## Nuclear Solid State Physics

### 7.1 Introduction

The division of Nuclear Solid State Physics continued research in the field of material and life sciences. The working horse is the high-energy ion-nanoprobe LIPSION.

An important branch is ion beam analysis of solid objects, e.g. semiconductors or meteorites, as well as biomedical samples, e.g. *Drosophila* cross-sections, human brain cross-sections, and murine coronary arteries using standard techniques like Particle Induced X-Ray Emission (PIXE) and Rutherford Backscattering Spectrometry (RBS) with lateral resolutions down to about 300 nm, and Scanning Transmission Ion Microscopy (STIM) with lateral resolutions down to 100 nm. The RBS method, usually applied to the analysis of thin films, was extended to analyze micrometer-sized objects of arbitrary shape such as cylinders, also inhomogeneously coated, tubes, and needles with various cross-sections. In the field of tomography, STIM-T and PIXE-T were further developed. For PIXE-T of supported biological cells, a reconstruction algorithm for data of a limited angular range was developed. The method of Ion Beam Induced Charge (IBIC) was introduced at LIPSION. Of particular value was the substantial improvement of the energy resolution of photodiodes as particle detectors with a pre-amplifier box inside the target chamber. The installation of a turbomolecular pump with magnetic bearings helped to reduce vibrations.

The second important branch of research is Proton Beam Writing (PBW). With protons,  $H_2^+$ , and He-ions 3D-structures in a variety of photoresists and semiconductors can be created. The method of proton beam was invented here and various 3D-objects have been created and analyzed by STIM-T. An interesting application of PBW is the fabrication of structured Petri-dishes by irradiation of Agar films. Neurons, e.g. adhere in Agar-free areas and develop interconnections via axons and dendrites.

In the field of low dose radiobiology, programs were developed which allow a rapid cell recognition without stains and UV-light and a precise application of a counted number of ions in specific predetermined intra-cellular positions. Hit verification was accomplished by writing crosses with high current and comparing the destroyed cells with the fluorescence of the underlying Mylar foil.

Various  $TiO_2$  nanomaterials were studied via the nuclear quadrupole interaction of  $^{44}Ti(EC)^{44}Sc$  using the Time Differential Perturbed Angular Correlation (TDPAC) technique. A new fully digital TDPAC-spectrometer was developed and used. In-situ dissolution studies in a synthetic body fluid mimicking blood plasma showed no

measurable dissolution of 6 nm anatase nanoparticles at 37 °C within 4 weeks.

A highlight in 2010 was the International Conference on Nuclear Microprobe Technology and Applications (ICNMTA) which was hosted by our group in Leipzig, for the first time in Germany.

We gratefully acknowledge the financial support of our research by the European Commission, the Deutsche Forschungsgemeinschaft, and the Federal German Excellence Initiative and the cooperation with academic and industrial partners.

*Tilman Butz*

## 7.2 Spatially resolved quantification of elements in sense associated organs of *Drosophila melanogaster*

N. Barapatre, A. Reinert\*, S. Sachse\*, T. Reinert

\*Department of Evolutionary Neuroethology, MPI for Chemical Ecology, Jena

The vinegar fly (*Drosophila melanogaster*) is often used as model organism in biology. Its sequenced genome, fast replication cycle and easy handling makes it a preferred model for a variety of neurobiological experiments. The electrophysiological techniques generally used in such experiments disrupt the cellular barrier. Thus, a compensatory fluid called Ringer's solution needs to be applied to maintain physiological conditions. This solution contains mainly Na, Cl, K and Ca ions and is isotonic relative to the fly's body fluid, the lymph. For the recipe of Ringer's solution for studies on the olfactory and neurobiological system of *Drosophila melanogaster* we quantified the elements present in the brain, the antenna and its sensilla hairs, and in further sense-associated organs like the compound eye and mouthparts by micro-PIXE and RBS [1]. The wild type flies were cryofixed, cryosectioned in 14  $\mu\text{m}$  or 25  $\mu\text{m}$  slices and freeze-dried. Figure 7.1 shows the distribution of various elements in different compartments of the fly's head. The brain is particularly rich in P (162 mM) due to dense population of neurons and glia cells. A high concentration of K (57 mM) is observed in the olfactory organs, antenna and sensilla hairs. The ommatidia are the structural and functional units of vision. They show a strong localisation for Cl, K and Ca with concentrations as high as 56  $\mu\text{M}$ , 154  $\mu\text{M}$  and 26  $\mu\text{M}$ , respectively. This characterizes single compartments in the ommatidia.

[1] A. Reinert, et al., *Nucl. Inst. Meth.* (2011) In press.

## 7.3 Ion beam analysis of atherosclerotic lesions

A. Sickert, N. Barapatre, D. Teupser\*, T. Butz

\*Institut für Laboratoriumsmedizin

Atherosclerosis, a disease of the large arteries, is the primary cause of heart disease and stroke. It is a progressive disease characterized by the accumulation of lipids and

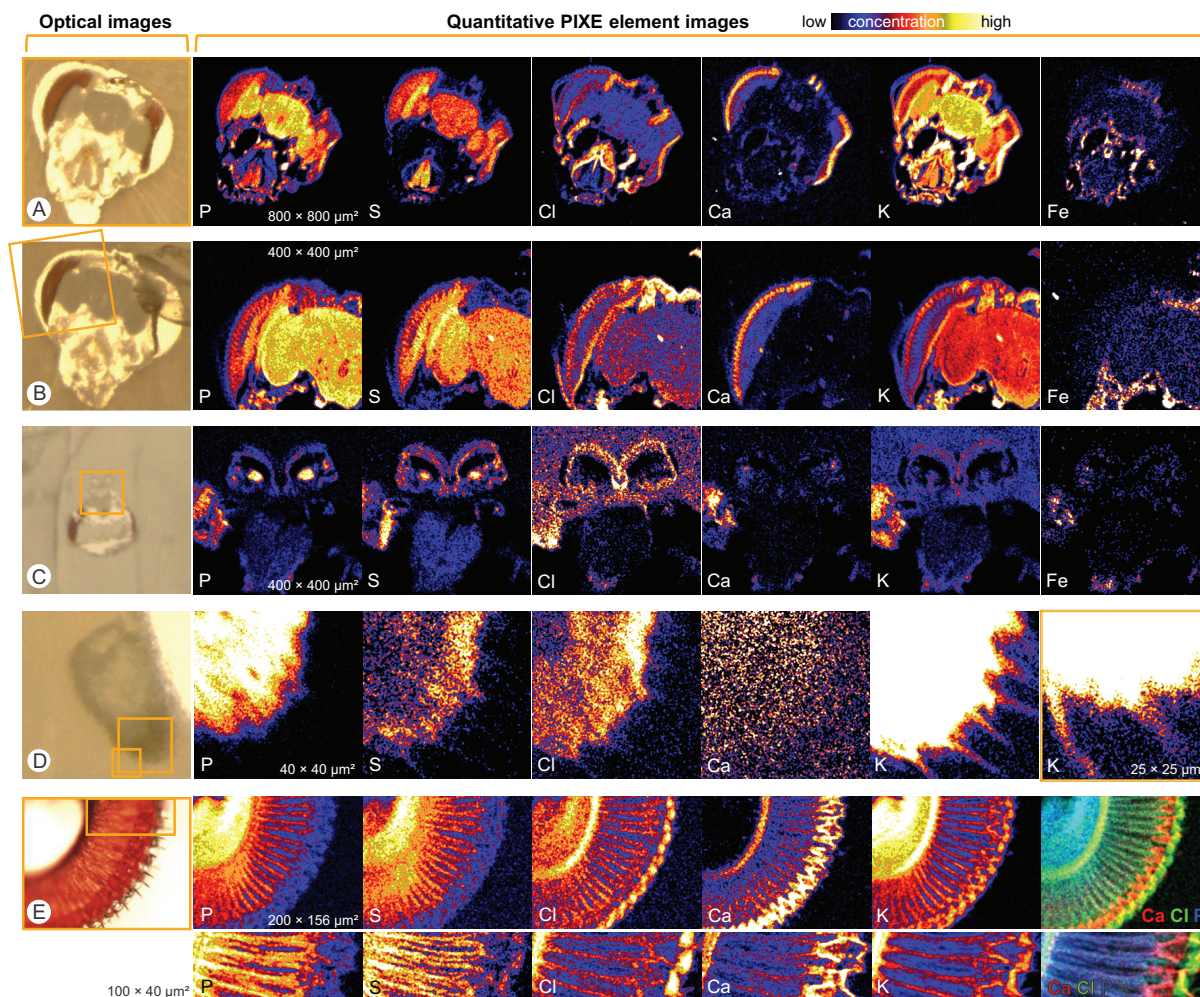


**Figure 7.1:** Quantitative element maps of: A) whole head section, B) brain/compound eye, C) proboscis/pharynx, D) antenna/sensilla, E) compound eye/ommatidia. The bottom row shows zoom-in versions of the maps in E).

fibrous elements inside the artery walls [1]. Trace elements like Fe and Cu are known to produce free radicals by the Fenton reaction [2]. To investigate the role of trace elements in the progression of atherosclerotic lesion an induced mutant mouse model [3] was used. The brachiocephalic artery (BCA) was removed and prepared further for ion beam analysis. Micro-PIXE and RBS measurements were performed simultaneously for spatially-resolved quantification of trace elements in the atherosclerotic lesions (fig. 7.2). Table 7.1 lists the mean concentration of various elements.

**Table 7.1:** Elemental content in the atherosclerotic lesions. Data are mean values ± mean error of 38 arteries.

P (mmol/l)	S (mmol/l)	Cl (mmol/l)	K (mmol/l)	Ca (mmol/l)	Fe (mmol/l)	Zn (mmol/l)
194 ± 97	197 ± 98	172 ± 95	33 ± 18	51 ± 28	2.7 ± 1.6	6.4 ± 4.0

Calcification of artery walls can already be seen in the lesion (fig. 7.2(c)). The magenta colour in the map is due to overlap of P (red) and Ca (blue). The measured Ca/P ratio

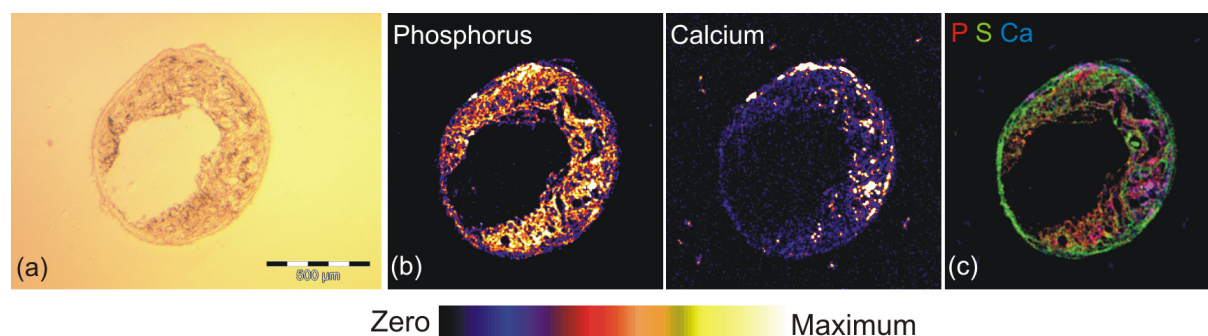


**Figure 7.2:** (a) Optical picture of a 10  $\mu\text{m}$  thin section of BCA showing an advanced atherosclerotic lesion. (b) Quantitative element maps of P and Ca, scan size  $1200 \times 1200 \mu\text{m}^2$ . (c) Three element map of P, S and Ca in false colours.

in this area is around 2.7. This suggests that these micro-calcifications are composed of calcium phosphate [4].

- [1] A.J. Lusis: *Nature* **407**, 233 (2000)
- [2] A. Jenner et al.: *Free Radical Biology & Medicine* **42**, 559 (2007)
- [3] D. Teupser et al.: *Arterioscler Thromb Vasc Biol.* **23**, 1907 (2003)
- [4] R.B. Roijers et al.: *Anal. Chem.* **80**, 55 (2008)

## 7.4 Microcarrier processing in cells using magnetite nanoparticles as reporters

U. Reibetanz\*<sup>†</sup>, St. Jankuhn

\*Institute for Medical Physics and Biophysics, Universität Leipzig

<sup>†</sup>Translational Centre for Regenerative Medicine Leipzig, Universität Leipzig

In recent years, layer-by-layer polyelectrolyte coated colloidal microcarriers have received increasing attention in the field of medical and pharmaceutical applications. Microcarrier-mediated drug delivery is hereby a main focus of the carrier application [1–4]. Based on the step-by-step coating of oppositely charged polyelectrolytes, biocompatible and biodegradable materials have to be used as basis-multilayers assembled onto a dissolvable core, eventually producing biopolymer capsules. The advantages of such a modular system can be clearly defined: Firstly, several active or reporter agents can be simultaneously integrated into the hollow shell or into the multilayer [5] to be transported and time-dependently released into the desired cell. Secondly, the amount of the agents can be adjusted to minimize or avoid side-effects in contrast to common systemic therapies (low dose application). And finally, additional surface modifications such as antibodies or cell penetrating peptides allow a specific targeting of the cell and an enhanced cell entry.

A specific part of the development of such a microcarrier system is the investigation of the adhesion, uptake and processing of the carriers within the cell. All steps from

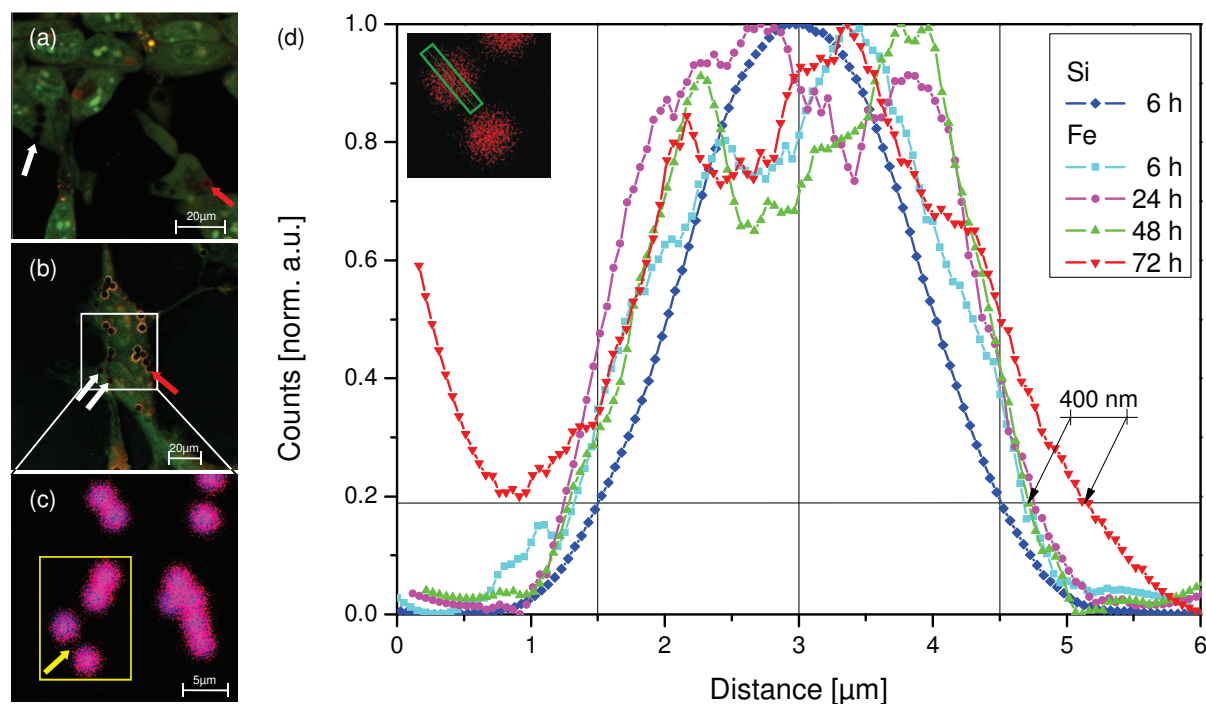


**Figure 7.3:** (a-c) Combined CLSM and PIXE analysis of MNP release from colloidal microcarriers exemplarily shown after a co-incubation time of 72 h. Microcarriers in endolysosomes are visualized by the red fluorescence of accumulated AO (red arrows), whereas microcarriers released into cytoplasm do not show any red fluorescence (white arrows): (a) CLSM image of AO-stained HEK293T/17 cells immediately after staining, (b) CLSM image after AO-staining followed by glutaraldehyde fixation and dehydration, (c) PIXE map of overlaid elemental distributions of Si (colloidal core, blue) and Fe (MNP, red) (specified in white marked regions according to the CLSM images in (b), yellow region marks carriers in cytoplasm showing a release of MNP). In (d), Fe line profiles of MNP-coated microcarrier elemental distributions after different co-incubation times are shown (■ 6 h, ● 24 h, ▲ 48 h, ▼ 72 h). Si profiles of the core remain constant over the entire investigation time frame (◆, exemplarily for 6 h; thin lines mark the size of the cores).

endocytotic uptake and storage, release of the carriers into the cytoplasm up to the cytoplasmatic decomposition of the multilayer are essential to develop a basis system for an efficient drug delivery. Reporter molecules (dye molecules, reporter DNA) or nanoparticles serve as a model for the active agents and allow to track the carrier in different steps of processing. In our project, the investigation of the time-dependent multilayer decomposition within the cytoplasm is focused. Here, magnetite nanoparticles ( $\text{Fe}_3\text{O}_4$  MNP) were used as reporter agents integrated into the protamine sulfate/dextran sulfate basis multilayer on colloidal  $\text{SiO}_2$  cores and the carriers were co-incubated with HEK 293T/17 cells. Staining of cell compartments and investigation with confocal laser scanning microscopy (CLSM) allows the identification of the carriers stored within endolysosomes and released into the cytoplasm. In correlation, the distributions of MNPs as multilayer constituents of cytoplasmatic released carriers as well as of MNPs already released into the cytoplasm were then visualized by means of proton-induced X-ray emission (PIXE) based on the elemental distribution of Si and Fe. After microcarrier/cell co-incubation of 6 h, 24 h, 48 h, and 72 h we could show that a MNP release and a slight

expansion into the cytoplasm occur (Fig. 7.3) but a longer co-incubation time frame of 72 h was needed to observe adequate results [6].

- [1] A.P.R. Johnston et al.: *Curr. Opin. Colloid Interface Sci.* **11**, 203 (2006), doi:10.1016/j.cocis.2006.05.001
- [2] G.B. Sukhorukov et al.: *Trends Biotechnol.* **25**, 93 (2007), doi:10.1016/j.tibtech.2006.12.007
- [3] B.G. De Geest et al.: *Soft Matter* **5**, 282 (2009), doi:10.1039/B808262F
- [4] U. Reibetanz et al.: *Macromol. Biosci.* **6**, 153 (2006), doi:10.1002/mabi.200500163
- [5] B.G. De Geest et al.: *Expert Opin. Drug Deliv.* **6**, 613 (2009), doi:10.1517/17425240902980162
- [6] U. Reibetanz et al.: *Nucl Instrum. and Meth. Phys. Res. B* (in press), doi:10.1016/j.nimb.2011.02.064

## 7.5 Quantification of nanoparticles uptake and distribution in culture cells (A549) at the single cell level

M. Dorn\*, St. Jankuhn, I. Estrela-Lopis\*, E. Donath\*

\*Institute of Medical Physics and Biophysics, Universität Leipzig

The degree and the mechanism of uptake, as well as localization and distribution of nanoparticles (NPs) in cells and organs are of major importance concerning toxicity studies and risk assessment of novel nanoproducts [1, 2]. Undesirable effects of nanomaterials on human health cannot be ruled out. Furthermore, the application of NPs as devices for diagnostic and therapeutic purposes requires novel means for monitoring their interaction with cells.

Ion Beam Microscopy (IBM) provides a unique and powerful tool for spatially resolved elemental analysis capable of detecting and characterizing nanomaterials within single cells. Proton Induced X-ray Emission (PIXE) and Rutherford Backscattering Spectrometry (RBS) were applied. We investigated the uptake, intracellular distribution and toxicity of ZnO, CeO<sub>2</sub>, FeO<sub>x</sub>, and TiO<sub>x</sub> as examples for metal oxide NPs in human lung adenocarcinoma epithelial cells (A549). Confocal Raman Microspectrometry (CRM) and Flow Cytometry complemented the IBM investigations.

Cells grown on polypropylene films were exposed to the various NPs. The cells were subsequently fixed with methanol and dried before IBM imaging.

Figure 7.4 shows images of cells exposed to different NPs at a concentration of 30 µg/ml during 48 h. Figure 7.4 displays maps of the NP constituting elements, Zn, Ce, and Ti. Their distributions overlay with the respective distributions of P being one of the main cellular elements. This demonstrates the uptake of metal oxide NPs into cells and their localization within or directly on cells.

In 70 % of the RBS spectra, backscattered protons from Ce atoms at the level of single cells incubated with CeO<sub>2</sub> NPs observed a significant energy loss. This proves the intracellular location of these NPs. The respective RBS spectra were fitted to various models of NPs distributions in or on the cells. This enabled us to distinguish between

internalization and extracellular attachment. The observed internalization of  $\text{CeO}_2$  NPs was supported also by CRM studies [3].

Data about cell composition, thickness, and accumulated charge were deduced from RBS spectra of single cells. These parameters were used as input for quantitative analysis in the PIXE data analysis program. The NP intracellular concentration was determined and statistically analysed. This provides the basis for intracellular dose dependent toxicity studies.

Post-modification of NPs in biological fluids were investigated. Co-localization of Ca and P elements with ZnO and  $\text{CeO}_2$  NPs were found.

This work was supported by the European Commission in the framework of FP7 Theme 4 – NMP - Nanosciences, Nanotechnologies, Materials and New Production Technologies, Proposal No: CP-FP 28825-2 HINAMOX.

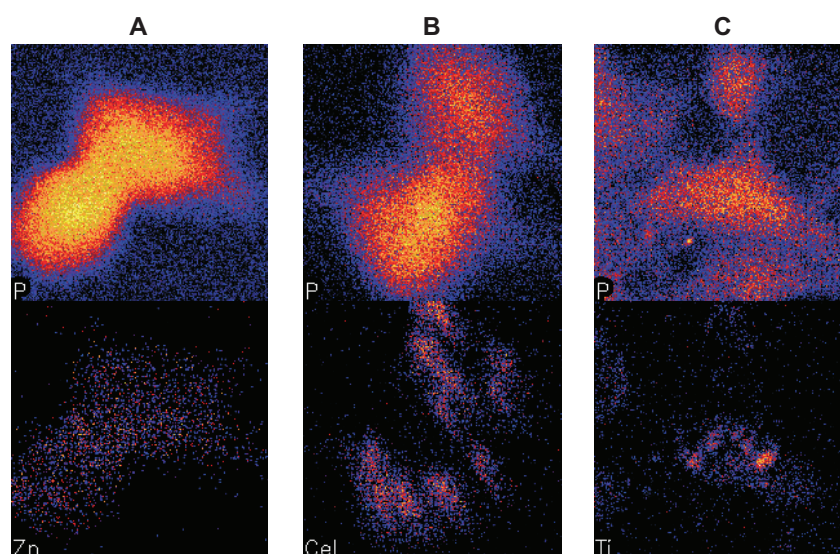


**Figure 7.4:** PIXE elemental maps of A549 cells exposed to ZnO (A),  $\text{CeO}_2$  (B), and  $\text{TiO}_x$  NPs at concentrations  $30 \mu\text{g/ml}$ , during 48 h. Top and respective bottom images demonstrate P and NP distributions (yellow is maximum, black is minimum). Area of all images is  $25 \times 25 \mu\text{m}^2$ .

- [1] J. Lee et al.: *Small* **5**, 1213 (2009), [doi:10.1002/sml.200801788](https://doi.org/10.1002/sml.200801788)
- [2] J.M. Hillegass et al.: *Wiley Interdiscip. Rev. Nanomed. Nanobiotechnol.* **2**, 219 (2010), [doi:10.1002/wnan.54](https://doi.org/10.1002/wnan.54)
- [3] I. Estrela-Lopis et al.: *JPCS A1-10* (2011, in press)

## 7.6 Trace element analysis of meteorites using particle induced X-ray emission

R. Wunderlich, J. Vogt, A. Bischoff\*, T. Butz

\*Institut für Planetologie (Universität Münster)

Extraterrestrial research is dominated by high tech, like spacecrafts or telescopes and therefore highly cost-intensive. On the other side meteorites provide a cheap source

of information about the creation and development of our and other solar systems. Of particular interest is the concentration of trace elements in the rock building crystals of meteorites. The knowledge of trace element concentrations in certain crystals enables to reconstruct the geological history of minerals, like temperature and pressure conditions during growth and alteration.

The investigated meteorite samples are classified as chondrites, which are characterized by millimeter-sized globular silicate grains, called chondrules, that are embedded in a small-grained matrix. These chondrules were molten and re-solidified independently of the meteorite mother body. Such kind of meteorites, like the analyzed Acfer094 meteorite (fig. 7.5) are the most unvaried and oldest rocks of our solar system. One of the main crystals of such chondrules is olivine  $(\text{Mg, Mn, Fe})_2[\text{SiO}_4]$  and compatible with the trace element nickel.

The method of particle induced X-ray emission (PIXE) has the advantage of significantly lower bremsstrahlung background compared to electron induced X-ray emission (EDX), which is a standard method in geoscience. Hence, PIXE provides a complementary technique especially for elements like nickel or calcium in an olivine crystal. Also important is the spatial distribution of certain trace elements. Depending on the conditions during melting of the chondrule forming material the concentration of diffusing trace elements in the chondrules and the uncrystallized surrounding melt differs. These differences lead to a characteristic fingerprint of the geological history and enables to reconstruct the processes of the formation of our solar system 4.5 billion years ago.

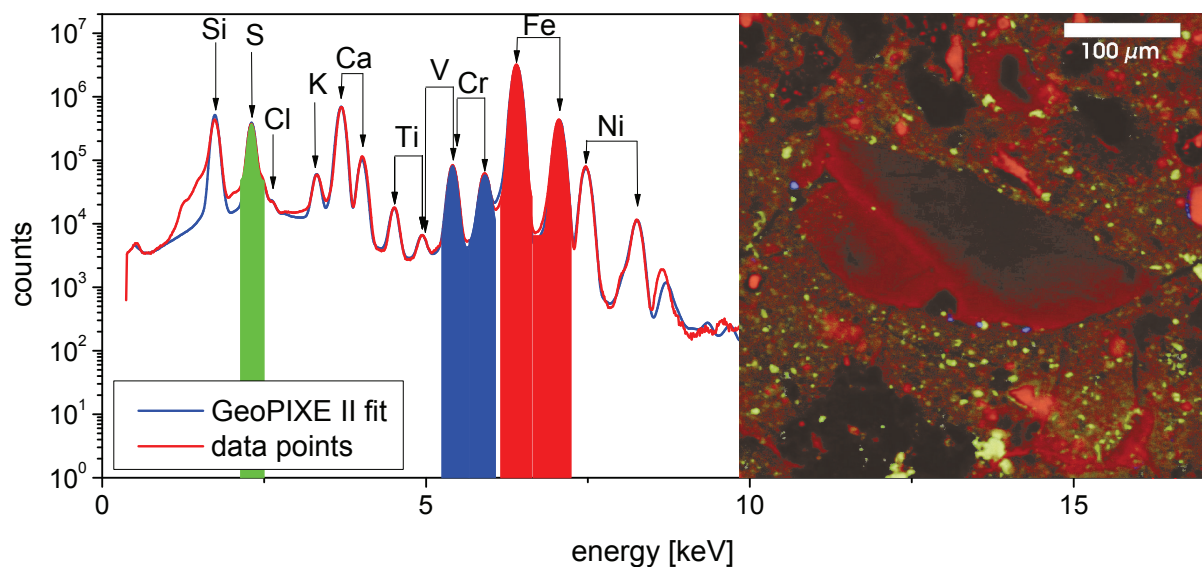


**Figure 7.5:** PIXE spectrum of a thin section of the meteorite Acfer094 and a false colour map of the analyzed region (red: iron, green: sulphur, blue: chromium).

## 7.7 High resolution STIM- and PIXE-Tomography

M. Rothmel, T. Andrea, T. Butz

Nowadays, there are many techniques for tomographic imaging. A unique possibility to determine the 3D density distribution and elemental composition in a simple

consecutive series of two experiments is the combination of scanning transmission ion microscopy tomography (STIM-T) and particle induced X-ray emission tomography (PIXE-T). An iterative algorithm (DISRA [1]) faces the complex probe-sample interactions (energy dependence of the proton stopping power and the X-ray production cross-sections) as well as the geometry of the experiment (attenuation of X-rays on their path to an extended X-ray detector solid angle, i.e. a cone-geometry). This algorithm uses a sketchy initial guess, ignoring the complexity of the problem. For the enhancement of the convergence of the algorithm a good first guess is desirable. Thus, we applied new filters in the backprojection step and implemented a GeoPIXE [2] batch analysis. The computation time which easily exceeded weeks/months on a 750 MHz Pentium III computer could be substantially reduced adapting the algorithm to modern computer architecture using a suitable software development environment (IDL - Interactive Data Language by ITT-VIS). This even allows for convenient tomogram examination (fig. 7.6).

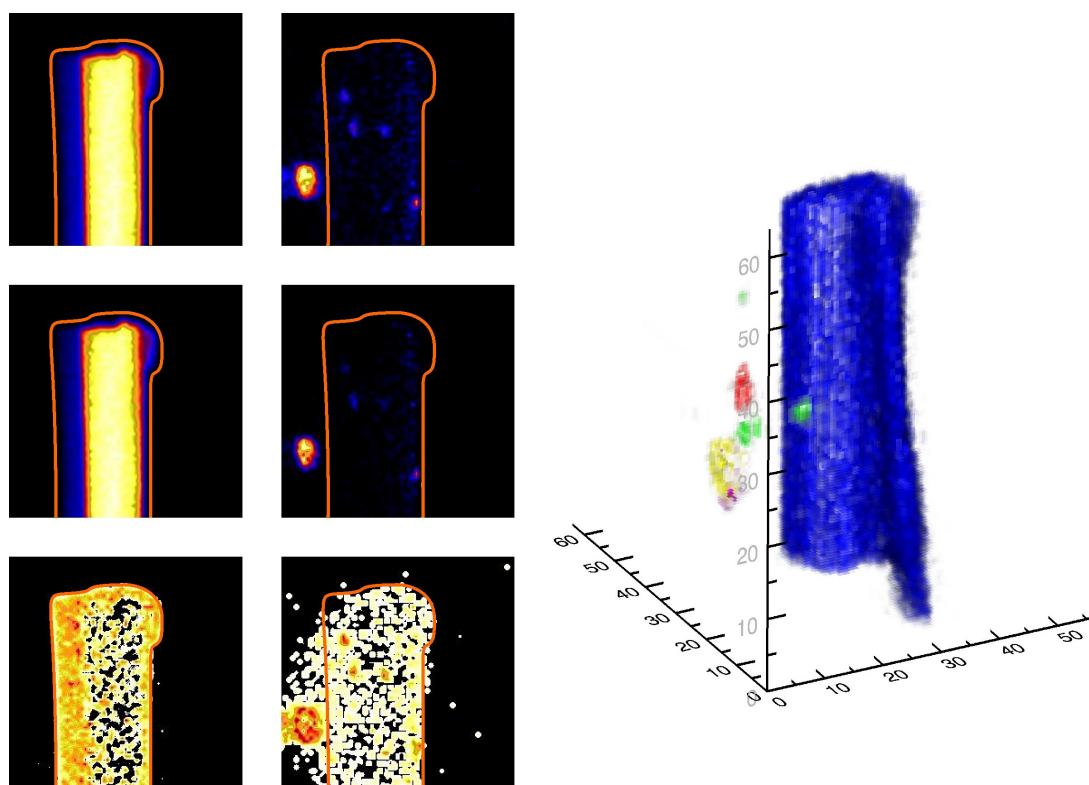


**Figure 7.6:** Left: Comparison of a single projection of the phantom analyzed by DISRA and GeoPIXE (top to bottom: GeoPIXE, DISRA, difference; left column: Zn, right column: Si). The orange line depicts the contour of the sample. Right: Tomogram of a phantom: Various oxide grains glued on a ZnO-wire (blue: Zn, yellow: Si, magenta: K, cyan: Mn, red: Fe, and green: Co). Compared to earlier PIXE-tomograms the shape of the phantom is reflected much better.

A first attempt in enhancing the beam resolution using an magnetic octupole correction lens in front of the third quadrupole of the ion beam focussing system did not lead to a satisfying performance. Thus, a new iron core and pole-tip design has been planned to optimize the homogeneity and strength of the magnetic field.

- [1] A. Sakellariou, M. Cholewa, A. Saint, G.J.F. Legge. *Meas. Sci. Technol.* **8**, 746-758 (1997)
- [2] C.G. Ryan, D.R. Cousens, S.H. Sie, W.L. Griffin, G.F. Suter, E. Clayton. *Nucl. Instr. and Meth. B* **47**, 55 (1990)

## 7.8 In-situ measurement of the resistivity of multi graphene under ion irradiation

R. Feder, J. Barzola-Quiquia\*, P. Esquinazi\*, T. Butz

\*Division of Superconductivity and Magnetism

In a cooperation between the groups of Nuclear Solid State Physics and Superconductivity and Magnetism the electric and magnetic properties of multi graphene layers during ion irradiation were studied. For this purpose, a setup is used that allows the in-situ measurement of the resistivity before, during and after the irradiation of the sample in vacuum, air and other atmospheric conditions with a focused beam of 2.25 MeV protons. Previous experiments with an external ion beam which irradiated the sample in air showed a decrease of the resistivity immediately after irradiation of the sample, followed by a relaxation to a slightly higher resistivity value. On the contrary, the irradiation under vacuum conditions leads to an increase of the resistivity during proton bombardment followed by a slow relaxation to a value slightly higher than that before irradiation. In order to exclude systematic errors, the same multi graphene flake was subsequently irradiated in air with an external proton beam as well and showed the same behavior as described in [1]. To clarify the differences in the measurements,

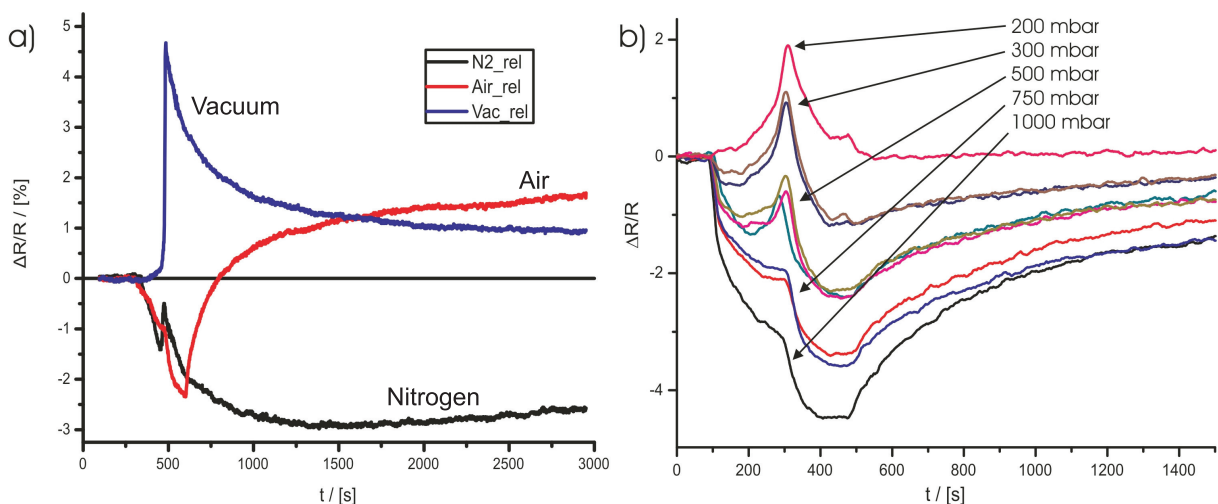


**Figure 7.7:** a) Comparison between three irradiation behaviors: Red:  $1.3 \times 10^{13} \text{ H}^+ \text{ cm}^{-2}$  in air; Blue:  $1.3 \times 10^{13} \text{ H}^+ \text{ cm}^{-2}$  in evacuated target chamber; Black:  $2.0 \times 10^{13} \text{ H}^+ \text{ cm}^{-2}$  under pure nitrogen atmosphere. b) Modification of the target chamber allows measurements with atmosphere at different pressures. Synthetic air was used to exclude the influence of air humidity. Start (150s) and Stop (480s) of the scans are visible. Sample is irradiated for approx. 300s. The transition in the behavior suggests an overlay of at least two competing effects.

several experiments with different pressures and compositions of the atmosphere were performed. Furthermore, the temperature dependence of the sample was studied to investigate the influence of sample heating during irradiation.

The project is part of the ESF-Nachwuchsforschergruppe "Funktionale multiskalige Strukturen" and is a part of the Graduate School Leipzig, School of Natural Sciences - Building with Molecules and Nano-objects (BuildMoNa).

[1] A. Arndt, Diploma Thesis. Universität Leipzig (2009)

## 7.9 Creation of 3D microsculptures in PMMA by proton irradiation from multiple angles

T. Andrea, M. Rothermel, T. Butz

An improvement has been achieved in the technique of proton beam sculpting, a method developed at the LIPSION accelerator facility. It combines proton beam writing with aspects of tomography. A variety of 3D microstructures could be produced by irradiating 90  $\mu\text{m}$  thin PMMA columns from multiple angles with 2.25 MeV protons. Up to now the columns were irradiated with patterns corresponding to the silhouettes of the desired structures with the fluence being either zero or  $1 \times 10^{14} \text{ cm}^{-2}$ . The microstructures produced with this method displayed sharp edges of 90 or 60 degrees depending on the number of irradiation angles. In order to permit the production of round structures, a new approach was chosen. By irradiating a target in one position with a sequence of different templates, rather than one only, the applied fluence could be varied within one scan. In this way a parabolic fluence profile could be generated. Two irradiations of a PMMA column at right angles with a parabolic fluence profile resulted in a deposited energy dose with circular symmetry. In a subsequent step of chemical development in a solution of methyl isobutyl ketone and isopropyl alcohol those portions that had accumulated a sufficient energy dose were dissolved, leaving

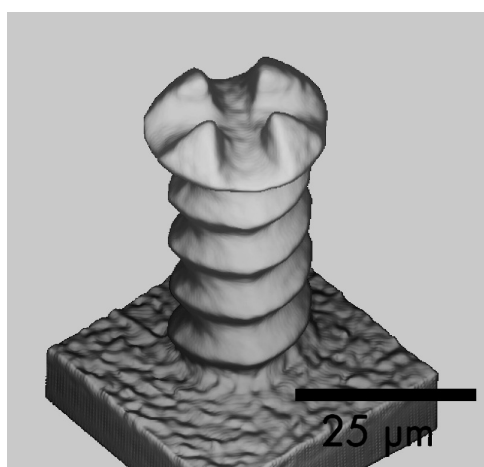


**Figure 7.8:** STIM tomogram of a PMMA microscrew produced by proton irradiation from two angles using a parabolic fluence profile.

behind the finished 3D sculpture, for example a screw with a diameter of 20  $\mu\text{m}$ . STIM (Scanning Transmission Ion Microscopy) tomography is the method of choice for the characterization of these microsculptures. It measures the energy loss of MeV ions traversing a microscopic sample and calculates the 3-dimensional density distribution from a set of scans covering an angular range of 180 degrees. The STIM tomogram of the structure (Fig. 7.8) shows that a microscrew with round edges could be created by irradiation from two angles only.

## 7.10 Structured Agar surfaces produced with PBW for developing neuronal networks with defined topology

W. Larisch, T. Butz

A necessary basis for many biological and biophysical studies, e.g. for cell-cell communication or neuronal networks, is confined cell growth on micro-structured surfaces. Especially the defined growth of small neuronal cultures forming stable networks is of great interest for the development of electrophysiological assays [1]. Agar gel is known as a medium for the growth of bacteria and fungi. However, other cell cultures avoid to grow on it [2, 3]. The technique of Proton Beam Writing is used to structure Agar gel layers directly [4]. First quadratic arrays for neuronal growth were successfully created and seeded with cells (see Fig. 7.9). These experiments show the possibility to fill a whole array with cells at defined positions. For further studies it will be necessary to mark the neurons with fluorescence dyes, especially for the monitoring of synapses and their readout with a fluorescence microscope. If this succeeds we will be able to monitor synaptic activity as well as the development of such networks under chemical and mechanical influences.

[1] P. Fromherz. *Physica E: Lowdimensional Systems and Nanostructures* **16**, 24-34 (2003)

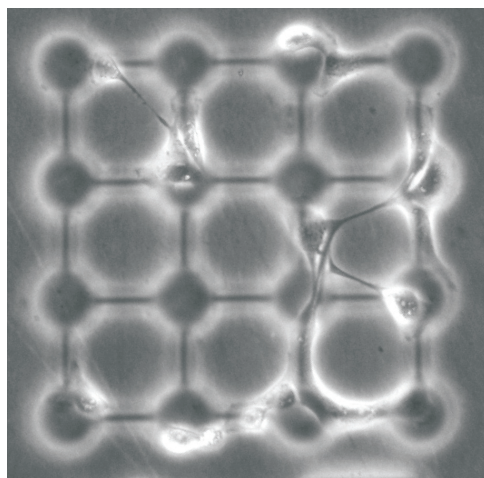


**Figure 7.9:** Microscopic picture of an quadratic array of  $4 \times 4$  compartments for neuronal growth. Nine Compartments are filled with cells and six of them developed links between each other.

- [2] S. Rohr, R. Flückiger-Labrada, J.P. Kucera. Pflügers Archiv European Journal of Physiology **446**, 125-132 (2003)
- [3] A. Rago, A. Napolitano, D. Dean, P. Chai, J. Morgan. Cytotechnology **56**, 81-90 (2008)
- [4] W. Larisch, T. Koal, R. Werner, M. Hohlweg, T. Reinert, T. Butz. Nuclear Inst. and Methods in Physics Research, B (in Press)

## 7.11 Creation of multilevel Ni-microstructures and sub-micrometer structures in InP by PBW

F. Menzel, D. Spemann, T. Butz

Proton beam writing (PBW) was already used for the creation of free-standing multilevel microstructures in negative resists [1] and of resist templates used for the production of Ni-microstructures by electrochemical metal plating [2]. These two methods were combined in order to fabricate multilevel Ni-microstructures (Fig. 7.10a). For this purpose, a several micrometer thick layer of the negative resist ma-N 490 applied on a Si substrate with a Cr/Cu conduction coating was structured by PBW using 2.25 MeV protons for the support structures as well as 1.125 MeV  $H_2^+$ -molecules and 1.5 MeV and 1.1 MeV  $He^+$ -ions for free-standing parts with different thicknesses. Subsequently, the obtained resist structures were used as templates for Ni-plating. The different heights of free space below the freestanding resist parts result in multilevel Ni-structures. After removing the resist and detaching the Ni-layer the Ni-microstructures can be used as

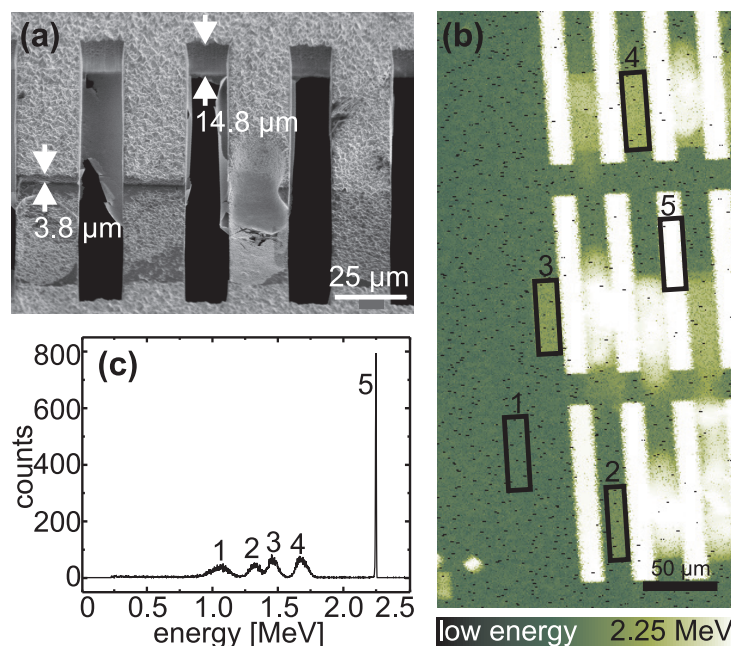


**Figure 7.10:** (a) REM image of part of a multilevel Ni-microstructure used for (b) STIM-imaging and (c) measurement of the energy of the transmitted ions. The energy spectrum is obtained from the signals of the marked regions in (b).

STIM (Scanning Transmission Ion Microscopy) standard sample for ion energy channel calibration (Fig. 7.10b,c). In addition, these structures, optionally combined with other standard shapes (e.g. grids), allow an easy and direct determination of the scan size as well as the ion beam focus.

In the field of microstructuring of semiconductor materials by PBW and subsequent electrochemical etching free-standing microstructures with the smallest structure dimension of  $0.6\ \mu\text{m}$  for a horizontal needle could be created in p-type InP by a combined irradiation with 2.25 MeV protons and 1.125 MeV  $\text{H}_2^+$ -molecules.

[1] F. Menzel et al.: Nucl. Instr. and Meth. B **231**, 372 (2005)

[2] J. A. van Kan et al.: Nucl. Instrum. Meth. B **231**, 170 (2005)

## 7.12 Improvement of the energy resolution of the STIM and RBS setup at the LIPSION nanoprobe

N. Klingner, J. Vogt, T. Butz

High energy resolution scanning transmission ion microscopy (STIM) and Rutherford backscattering spectrometry (RBS) analysis as a versatile tool for nondestructive morphological and elemental analysis are limited by the electronic signal processing. In order to improve the analytical capabilities of both techniques, the aim was to determine and improve the energy resolution for the STIM and RBS detector setups.

For this purpose, silicon nitride windows were coated on one half-side with an approximately 135 nm thick gold film and analyzed by STIM and RBS under different detector settings in the LIPSION nanoprobe. These measurements indicated that the energy resolution could be improved by removing certain sources of electronic noise. Furthermore, the optimization of the settings of the shaping amplifier, detector bias as well as the electronic circuit of the in-vacuum preamplifier resulted in an additional improvement of the energy resolution. For the STIM setup using 1.8 MeV  $\text{He}^+$  ions an improved energy resolution of 10.6 keV (previously 14 keV) was determined and for 2.25 MeV protons a minimum of 5.7 keV was achieved. Using the in-vacuum preamplifier and a small PIN-photo diode of  $4 \times 4\ \text{mm}^2$  area as RBS detector instead of the standard PIPS detector an energy resolution of 11.5 keV was obtained. The RBS PIPS-detector with  $50\ \text{mm}^2$  area yielded an energy resolution of 12 keV in combination with the in-vacuum preamplifier. Therefore, a new in-vacuum preamplifier module for the faceted RBS detector is currently under development in order to fully exploit the analytical capabilities possible with these standard particle detectors.

## 7.13 Investigation of $\text{TiO}_2$ nanomaterials by TDPAC

T. Butz

Commercial anatase nanoparticles from Ishihara Sangyo Co., Japan, (ST-01) and from Sachtleben Chemie, Germany, with primary particle sizes of 7 nm and 6 nm, respectively, and a BET surface area of  $320\ \text{m}^2/\text{g}$  were impregnated with  $^{44}\text{Ti}$  in 4 M HCl

and subsequently diffused at 180 °C for 2 hours. In addition, a spark generator aerosol (anatase) with primary particle size 4-5 nm and a BET surface area of 270.7 m<sup>2</sup>/g, produced at the Helmholtz-Zentrum München [1], and TiO<sub>2</sub> nanotubes (anatase) with approximately 20 nm diameter [2] were labelled with <sup>44</sup>Ti in the same way. The nuclear quadrupole interaction (NQI) at <sup>44</sup>Sc, the daughter of <sup>44</sup>Ti, was investigated by Time Differential Perturbed Angular Correlation (TDPAC) using the 68 keV - 78 keV cascade and a fully digital spectrometer [3]. Two inequivalent lattice sites were observed in all cases. The lower frequency was in the vicinity of the anatase bulk NQI and therefore ascribed to the "volume" fraction. The higher frequency was ascribed to Ti probes near the surface with OH-termination. The frequency distribution for both the volume and the surface fractions were rather broad. However, in all cases the symmetry of the electric field gradient was axial, like in anatase bulk. These observations are in agreement with previous studies of other TiO<sub>2</sub> nanomaterials [3].

The first two products exhibited distinctly different NQI's although they are nominally identical. The aerosol and the nanotubes exhibited the broadest distributions. It is concluded that the surface tension in such small particles is responsible for the distributions, i.e. the unit cells are no longer identical but compressed to various degrees while preserving the symmetry. The paradigm that a complete characterization of the nanomaterials allows the prediction of toxicity is questioned. It seems that a complete characterization of all relevant properties of such nanomaterials, probably on an atomic level, is impossible. The slow dissolution of ST-01 in a synthetic body fluid mimicking blood plasma was studied at 37 °C for 4 weeks. No dissolution was detected by TDPAC. The lack of enhanced activity in the supernatant after prolonged sedimentation gave an upper limit of 1 % dissolution. Thus these nanoparticles appear to be biopersistent. Surprisingly, both the surface and the volume fractions changed slightly when the nanoparticles were immersed into the synthetic body fluid.

[1] from Dr. W. Kreyling

[2] from Prof. Dr. P. Schmuki

[3] M. Jäger, K. Iwig, T. Butz. *Hyperfine Interactions* **198**, 167 (2011)

[4] T. Butz, S.-B. Ryu, St. Jankuhn, S.K. Das, S. Ghoshal. In: H. Jaeger and M.O. Zaccate (eds.) *Defects and Diffusion Studied Using Perturbed Angular Correlation Spectroscopy - Special Topic Volume of Defect and Diffusion Forum* **311**, 137-158 (2011)

## 7.14 Funding

*Leipzig School of Natural Sciences - Building with Molecules and Nano-objects (Build-Mona)*

Prof. Dr. T. Butz

GSC 185/1

*DFG Graduiertenkolleg Interdisciplinary Approaches in Cellular Neurosciences (InterNeuro)*

Prof. Dr. T. Butz

GRK 1097

*Non-Targeted Effects of ionising Radiation – NOTE*

Prof. Dr. T. Butz

EU Integrated Project FI6R-036465

## 7.15 Organizational Duties

T. Andrea

- Referee: Nucl. Instrum. Meth. B

N. Barapatre

- Referee: Nucl. Instrum. Meth. B

T. Butz

- Vertrauensdozent der Studienstiftung des deutschen Volkes
- Sprecher der Ortsgruppe Leipzig des deutschen Hochschulverbandes
- Co-tutor for students of Tautenburg (astrophysics), DESY/Zeuthen (particle physics)
- Reviewer: DFG, Studienstiftung des deutschen Volkes
- Referee: J. Phys.-Condens. Mat., Phys. Rev. B, Nucl. Instrum. Meth. B, Particle and Fibre Toxicology, Radiochimica Acta, Skin Pharmacology and Physiology, Computer Physics Communication, J. Investigative Dermatology, Defects and Diffusion Forum, Innovational Research Incentives Scheme Veni (Holland), Rev. Sci. Instrum., Rev. Mod. Physics

R. Feder

- Referee: Nucl. Instrum. Meth. B

St. Jankuhn

- Secretary: 12th ICNMTA, Leipzig
- Referee: Nucl. Instrum. Meth. B

F. Menzel

- Referee: Nucl. Instrum. Meth. B

M. Rothermel

- Referee: Nucl. Instrum. Meth. B
- Doktorandensprecher der Graduiertenschule "Leipzig School of Natural Sciences - Building with Molecules and Nano-objects" (BuildMoNa)
- Doktorandensprecher des Graduiertenzentrums Mathematik/Informatik und Naturwissenschaften der "Research Academy Leipzig"

D. Spemann

- Referee: Nucl. Instrum. Meth. B

J. Vogt

- Referee: Nucl. Instrum. Meth. B

## 7.16 External Cooperations

### Academic

- Université de Bordeaux I  
CENBG, Prof. Ph. Moretto
- CERN, Genf  
ISOLDE Collaboration
- Institute of Physics, Kraków  
Dr. Z. Stachura
- IOM Leipzig  
Dr. K. Zimmer, Dr. J. Gerlach, Ch. Meinecke
- KVL, Kopenhagen  
Dr. L. Hemmingsen
- MPI für Demografische Forschung, Rostock  
A. Fabig
- National University of Singapore  
Center for Ion Beam Applications, Prof. F. Watt, Dr. T. Osipowicz
- Universität Leipzig, Medizinische Fakultät  
Paul-Flechsig-Institut, Prof. T. Arendt, Dr. M. Morawski
- Universität Leipzig, Medizinische Fakultät  
Institut für Rechtsmedizin, Dr. M. Weber, S. Wernecke
- Universität Leipzig, Medizinische Fakultät  
Institut für Laboratoriumsmedizin, Kl. Chemie und Mol. Diagnostik, Prof. J. Thiery,  
Dr. D. Teupser
- Universität Leipzig, Medizinische Fakultät  
Institut für Medizinische Physik und Biophysik, Prof. E. Donath, Dr. U. Reibetanz,  
Dr. I. Estrela-Lopis, DBc. M. Dorn
- The University of Melbourne  
Microanalytical Research Centre, Prof. D. Jamieson
- TU Wien  
Prof. K. Schwarz, Prof. P. Blaha
- Universität Hannover  
Arbeitskreis Prof. P. Behrens
- Universität Hannover  
Arbeitskreis Prof. C. Vogt
- Universität Rostock  
Prof. Dr. G. Hildebrandt
- TU Bergakademie Freiberg, Freiberg  
Prof. J. Heitmann
- University of North Texas, Denton, TX, USA  
Assoc. Prof. T. Reinert

## Industry

- Solarion GmbH
- Dechema  
Dr. E. Zschau, Self-employed expert in materials research

## 7.17 Publications

### Journals

D. Hiller, R. Zierold, J. Bachmann, M. Alexe, Y. Yang, J. W. Gerlach, A. Stesmans, M. Jivanescu, U. Müller, J. Vogt, H. Hilmer, P. Löper, M. Künle, F. Munnik, K. Nielsch, M. Zacharias: *Low temperature silicon dioxide by thermal atomic layer deposition: Investigation of material properties*, J. Appl. Phys. **107** 064314 (2010)  
doi:10.1063/1.3327430

P. Esquinazi, J. Barzola-Quiquia, D. Spemann, M. Rothermel, H. Ohldag, N. Garcia, A. Setzer, T. Butz: *Magnetic order in Graphite: Experimental evidence, intrinsic and extrinsic difficulties*, J. Magn. Magn. Mater. **322** 1156-1161 (2010)  
doi:10.1016/j.jmmm.2009.06.038

M. Dubman, T. Shiroka, H. Luetkens, M. Rothermel, F.J. Litterst, E. Morenzoni, A. Suter, D. Spemann, P. Esquinazi, A. Setzer, T. Butz: *Low-energy  $\mu$ SR and SQUID evidence of magnetism in highly oriented pyrolytic graphite*, J. Magn. Magn. Mater. **322** 1228-1231 (2010)  
doi:10.1016/j.jmmm.2009.04.023

M. Lorenz, H. Hochmuth, Ch. Grüner, H. Hilmer, A. Lajn, D. Spemann, M. Brandt, J. Zippel, H. von Wenckstern, M. Grundmann: *Oxide thin film heterostructures with large-area, flexible doping, reduced dislocation density and smooth interfaces – grown by Pulsed Laser Deposition*, Laser Chemistry **2010** 140976 (2010)  
doi:10.1155/2010/140976

H. Ohldag, P. Esquinazi, E. Arenholz, D. Spemann, M. Rothermel, A. Setzer, T. Butz: *The role of hydrogen in room-temperature ferromagnetism at graphite surfaces*, New J. Phys. **12** 123012 (2010)  
doi:10.1088/1367-2630/12/12/123012

T. Andrea, M. Rothermel, R. Werner, T. Butz, T. Reinert: *Limited angle STIM and PIXE tomography of single cells*, Nucl. Instr. and Meth. in Phys. Res. B **268** 1884-1888 (2010)  
doi:10.1016/j.nimb.2010.02.049

M. Rothermel, T. Reinert, T. Andrea, T. Butz: *First results on ion micro-tomography at LIPSION*, Nucl. Instr. and Meth. in Phys. Res. B **268** 2001-2005 (2010)  
doi:10.1016/j.nimb.2010.02.117

D. Spemann, V. Gottschalch: *Boron lattice site location in (BGa)As and (BGa)P thin films studied using RBS and NRA with a channeled He<sup>+</sup> ion beam*, Nucl. Instr. and Meth. in Phys. Res. B **268** 2069-2073 (2010)  
doi:10.1016/j.nimb.2010.02.028

N. Barapatre, M. Morawski, T. Butz, T. Reinert: *Trace element mapping in Parkinsonian brain by quantitative ion beam microscopy*, Nucl. Instr. and Meth. in Phys. Res. B **268** 2156-2159 (2010)

doi:10.1016/j.nimb.2010.02.039

M. Khalid, A. Setzer, M. Ziese, P. Esquinazi, D. Spemann, A. Pöppel, E. Goering: *Ubiquity of ferromagnetic signals in common diamagnetic oxide crystals*, Phys. Rev. B **81** 214414 (2010)

doi:10.1103/PhysRevB.81.214414

D. Richard, E. L. Munoz, T. Butz, L. A. Errico, M. Rentería: *Electronic and structural properties, and hyperfine interactions at Sc sites in the semiconductor Sc<sub>2</sub>O<sub>3</sub>: TDPAC and ab initio study*, Phys. Rev. B **82** 035206 (2010)

doi:10.1103/PhysRevB.82.035206

D. Hiller, S. Goetze, F. Munnik, M. Jivanescu, J. W. Gerlach, J. Vogt, E. Pippel, N. Zakharov, A. Stesmans, M. Zacharias: *Nitrogen at the Si-nanocrystal/SiO<sub>2</sub> interface and its influence on luminescence and interface defects*, Phys. Rev. B **82** 195401 (2010)

doi:10.1103/PhysRevB.82.195401

T. Butz: *How to analyse powder nuclear quadrupole interaction data with non-axial symmetry for interdependent electric field gradient tensor components*, Phys. Scr. **82** 025702 (2010)

doi:10.1088/0031-8949/82/02/025702

M. Jäger, K. Iwig, T. Butz: *A user-friendly fully digital TDPAC-spectrometer*, Hyperfine Interactions **198**, 167 (2011)

doi:10.1007/s10751-010-0201-8

T. Butz, S.-b. Ryu, St. Jankuhn, S.K. Das, S. Ghoshal: *TiO<sub>2</sub> Nanomaterials Studies by <sup>44</sup>Ti(EC)<sup>44</sup>Sc Time Differential Perturbed Angular Correlations: Volume and Surface Properties*, Defect and Diffusion Forum **311**, 137 (2011)

doi:10.4028/www.scientific.net/DDF.311.137

K. Bechstein, J. Michels, J. Vogt, G. C. Schwartz, C. Vogt: *Position-resolved determination of trace elements in mandibular gnathobases of the Antarctic copepod Calanoides acutus using a multimethod approach*, Anal. Bioanal. Chem. **399**, 501-508 (2010)

doi:10.1007/s00216-010-4373-5

## Books

T. Butz: *Fouriertransformation für Fußgänger*, 6. Aufl. (Vieweg+Teubner, Wiesbaden 2009)

## in press

T. Andrea, M. Rothermel, T. Reinert, T. Koal, T. Butz: *Creation of 3D microsculptures in PMMA by multiple angle proton irradiation*, Nucl. Instr. and Meth. B (2011)

doi:10.1016/j.nimb.2011.02.038

W. Larisch, T. Koal, R. Werner, M. Hohlweg, T. Reinert, T. Butz: *Proton Beam Writing of microstructures in Agar gel for patterned cell growth*, Nucl. Instr. and Meth. B (2011)  
doi:10.1016/j.nimb.2011.02.041

R. Feder, F. Menzel, T. Butz: *Micro-fluidic target chamber machined by proton beam writing for the in-situ analysis of gas absorption in synthetic crystals*, Nucl. Instr. and Meth. B (2011)  
doi:10.1016/j.nimb.2011.02.048

D. Spemann, T. Reinert, J. Vogt, T. Andrea, N. Barapatre, R. Feder, A.M. Jakob, N. Liebing, Ch. Meinecke, F. Menzel, M. Rothermel, T. Butz: *Materials Analysis and Modification at LIPSION – Present State and Future Developments*, Nucl. Instr. and Meth. B (2011)  
doi:10.1016/j.nimb.2011.02.054

F. Menzel, D. Spemann, T. Koal, T. Butz: *3D-structures with Arbitrary Shapes Created in Negative Resists by Grayscale Proton Beam Writing*, Nucl. Instr. and Meth. B (2011)  
doi:10.1016/j.nimb.2011.02.060

F. Menzel, D. Spemann, T. Butz: *High-aspect Ratio Microstructures in p-type GaAs and InP Created by Proton Beam Writing*, Nucl. Instr. and Meth. B (2011)  
doi:10.1016/j.nimb.2011.02.061

A.M. Jakob, D. Spemann, R. Thies, J. Vogt, T. Butz: *A Characterisation of Electronic Properties of Alkaline-texturized Polycrystalline Silicon Solar Cells Using IBIC*, Nucl. Instr. and Meth. B (2011)  
doi:10.1016/j.nimb.2011.02.040

T. Reinert, N. Barapatre, A. Reinert, D. Spemann, T. Andrea, W. Larisch, Ch. Meinecke, T. Koal, R. Werner, M. Hohlweg, J. Vogt, T. Butz: *Biomedical Research at LIPSION – Present State and Future Developments*, Nucl. Instr. and Meth. B (2011)  
doi:10.1016/j.nimb.2011.02.071

U. Reibetanz, St. Jankuhn: *Magnetite nanoparticles as reporters for microcarrier processing in cytoplasm*, Nucl. Instr. and Meth. B (2011)  
doi:10.1016/j.nimb.2011.02.064

U. Scholz, F. Menzel, M. Pluta, W. Grill, T. Butz: *Acoustic mode converters micromachined in silicon by proton beam writing*, Nucl. Instr. and Meth. B (2011)  
doi:10.1016/j.nimb.2011.02.065

A. Reinert, N. Barapatre, S. Sachse, T. Reinert:  *$\mu$ PIXE for a  $\mu$ Brain: The Vinegar Fly's Brain, Antenna, Sensilla Hairs and Eye Ion Concentrations*, Nucl. Instr. and Meth. B (2011)  
doi:10.1016/j.nimb.2011.02.066

## Talks

T. Butz: *Hautpenetration von Nanopartikeln in Sonnenschutzmitteln*, Buchmesse Akademie Leipzig (March 30 2010)

M. Rothermel, T. Andrea, T. Reinert, T. Butz: *Ion micro-tomography*, Ion beam physics workshop 2010, Dresden-Rossendorf (March 29-31 2010)

R. Feder, F. Menzel: *Proton Beam Writing and Applications*, Ion beam physics workshop 2010, Dresden-Rossendorf (March 29-31 2010)

T. Butz: *What we Know about Dermal Penetration of Nanomaterials and What Should be Tackled Next*, Workshop: Innovations through Nanotechnology and Nanomaterials, Dresden (April 22 2010)

T. Andrea, M. Rothermel, T. Reinert, T. Koal, T. Butz: *Creation of 3D microsculptures in PMMA by multiple angle proton irradiation*, 12th Int. Conf. on Nuclear Microprobe Technology and Applications, Leipzig (July 26-30 2010)

T. Reinert, N. Barapatre, A. Reinert, D. Spemann, T. Andrea, W. Larisch, Ch. Meinecke, T. Koal, R. Werner, M. Hohlweg, J. Vogt, T. Butz: *Biomedical Research at LIPSION – Present State and Future Developments*, 12th Int. Conf. on Nuclear Microprobe Technology and Applications, Leipzig (July 26-30 2010)

U. Reibetanz, St. Jankuhn: *Colloidal microparticle-mediated transport and release of active agents in cells*, 12th Int. Conf. on Nuclear Microprobe Technology and Applications, Leipzig (July 26-30 2010)

A.M. Jakob, D. Spemann, R. Thies, J. Vogt, T. Butz: *A Characterisation of Electronic Properties of Alkaline-texturized Polycrystalline Silicon Solar Cells Using IBIC*, 12th Int. Conf. on Nuclear Microprobe Technology and Applications, Leipzig (July 26-30 2010)

F. Menzel, T. Butz: *Multilevel Ni-microstructures produced using particle beam written three-dimensional resist templates*, 12th Int. Conf. on Nuclear Microprobe Technology and Applications, Leipzig (July 26-30 2010)

T. Butz: *The Concept of Trajectories in the Data Analysis of Non-axially Symmetric Nuclear Quadrupole Interactions*, 3rd Joint International Conference on Hyperfine Interactions and International Symposium on Nuclear Quadrupole Interactions, CERN, Genf (August 16 2010)

C. Vogt, H. Drücker, F. Witte, J. Vogt: *Investigation of corrosion at biodegradable magnesium implants in vivo by solid state spectroscopy*, 2nd Symposium on Biodegradable Metals, Maratea, Italy, (August 31 - September 3 2010)

T. Butz: *Targeted high and low dose irradiation of single living cells*, NOTE final Meeting, Stockholm (September 5 2010)

R. Feder, J. Barzola-Quiquia, T. Butz, P. Esquinazi: *Defect Production by Ions Traversing Multi Graphene*, 1. Statusseminar der Nachwuchsforschergruppe Nano: Funktionale Multiskalige Strukturen, Leipzig, (September 27 2010)

T. Butz: *Surface and Volume Characterization of TiO<sub>2</sub> Nanomaterials by <sup>44</sup>Ti-TDPAC*, Second International Conference on Application of Radiotracers in Chemical, Environmental and Biological Sciences, Kolkata, India (November 10 2010)

D. Spemann: *The Role of Ion Beams in the Study of Defect Induced Magnetism*, Faculty Colloquium, University of North Texas, Denton, TX, USA (November 16 2010)

T. Butz: *Perkutane Absorption von Nanopartikeln und resultierende Sicherheitsbedenken*, ICADA-Fachtagung, Frankfurt/Main (November 17 2010)

### Posters

T. Andrea, M. Rothermel, T. Butz: *Limited-angle ion beam tomography of cells and 3D proton beam sculpting*, Third Scientific Symposium of the Graduate School BuildMoNa, Leipzig (March 29-30 2010)

M. Rothermel, T. Andrea, T. Butz: *Combined STIM- and PIXE-tomography at LIPSION*, Third Scientific Symposium of the Graduate School BuildMoNa, Leipzig (March 29-30 2010)

R. Feder, F. Menzel, T. Butz: *Micro-fluidic Target Chamber Machined by Proton Beam Writing for the in-situ Analysis of Gas Absorption in Synthetic Crystals*, Third Scientific Symposium of the Graduate School BuildMoNa, Leipzig (March 29-30 2010)

T. Andrea, M. Rothermel, T. Reinert, T. Koal, T. Butz: *3D microsculptures created in PMMA by focused proton beam irradiation from multiple angles*, 17th Int. Conf. on Ion Beam Modification of Materials, Montreal, Canada (August 22-27 2010)

N. Barapatre, M. Morawski, T. Reinert, T. Butz: *In situ quantification of trace elements in substantia nigra*, Int. Conf. on PIXE and its Applications, Guildford, UK, (June 27 - July 02 2010)

M. Rothermel, T. Andrea, T. Butz: *New Developments in Iterative Data Reconstruction in PIXE-tomography*, 12th Int. Conf. on Nuclear Microprobe Technology and Applications, Leipzig (July 26-30 2010)

D. Spemann, T. Reinert, J. Vogt, T. Andrea, N. Barapatre, R. Feder, A.M. Jakob, N. Liebing, Ch. Meinecke, F. Menzel, M. Rothermel, T. Butz: *Materials Analysis and Modification at LIPSION – Present State and Future Developments*, 12th Int. Conf. on Nuclear Microprobe Technology and Applications, Leipzig (July 26-30 2010)

T. Koal, W. Larisch, T. Reinert, T. Butz: *Low Dose Targeted Cell Bombardment with Counted Ions at LIPSION*, 12th Int. Conf. on Nuclear Microprobe Technology and Applications, Leipzig (July 26-30 2010)

N. Barapatre, M. Morawski, T. Reinert, T. Butz: *Trace Element Mapping in the Human Substantia Nigra by Quantitative Ion Beam Microscopy: Optimizing Measures for Statistical Studies*, 12th Int. Conf. on Nuclear Microprobe Technology and Applications, Leipzig (July 26-30 2010)

T. Reinert, S. Wernicke, N. Barapatre, A. Reinert, A. Weber: *High Sample Throughput in Quantitative Ion Beam Microscopy - A Study of Human Hippocampi of Opiate Abusers*, 12th Int. Conf. on Nuclear Microprobe Technology and Applications, Leipzig (July 26-30 2010)

A. Reinert, N. Barapatre, S. Sachse, T. Reinert:  *$\mu$ PIXE for a  $\mu$ Brain: The Vinegar Fly's Brain, Antenna, Sensilla Hairs Ion Concentrations*, 12th Int. Conf. on Nuclear Microprobe Technology and Applications, Leipzig (July 26-30 2010)

W. Larisch, T. Koal, R. Werner, M. Hohlweg, T. Reinert, T. Butz: *PBW of Microstructures in Agar Gel for Patterned Cell Growth*, 12th Int. Conf. on Nuclear Microprobe Technology and Applications, Leipzig (July 26-30 2010)

R. Feder, F. Menzel, T. Butz: *Micro-fluidic Target Chamber Machined by Proton Beam Writing for the in-situ Analysis of Gas Absorption in Synthetic Crystals*, 12th Int. Conf. on Nuclear Microprobe Technology and Applications, Leipzig (July 26-30 2010)

F. Menzel, D. Spemann, T. Koal, T. Butz: *3D-structures with Arbitrary Shapes Created in Negative Resists by Grayscale Proton Beam Writing*, 12th Int. Conf. on Nuclear Microprobe Technology and Applications, Leipzig (July 26-30 2010)

F. Menzel, D. Spemann, T. Butz: *High-aspect Ratio Microstructures in p-type GaAs and InP Created by Proton Beam Writing*, 12th Int. Conf. on Nuclear Microprobe Technology and Applications, Leipzig (July 26-30 2010)

U. Scholz, F. Menzel, M. Pluta, W. Grill, T. Butz: *Acoustic Mode Converters Micro-machined in Silicon by Proton Beam Writing*, 12th Int. Conf. on Nuclear Microprobe Technology and Applications, Leipzig (July 26-30 2010)

St. Jankuhn: *The World of Nuclear Microprobes*, 12th Int. Conf. on Nuclear Microprobe Technology and Applications, Leipzig (July 26-30 2010)

## 7.18 Graduations

### Diploma

- Alexander M. Jakob  
*Ortsaufgelöste Charakterisierung der elektronischen Eigenschaften von Solarzellen mittels hochenergetischen Ionen*  
February 2010
- Dirk Mehlhorn  
*Untersuchung von ZnO-Dünnschichtszintillatoren auf ihre Eignung als Ionentransmissionsdetektor*  
February 2010
- W. Larisch  
*Strukturierung von Petri-Schalen mittels Protonen-Strahl-Schreiben in Agar für neuronale Netze mit definierter Topologie*  
December 2010

### Bachelor

- Stefan Döge  
*Untersuchungen der mechanischen und neuronoptischen Eigenschaften von Si-Fe-Multischichtssystemen*  
June 2010
- Steffen Richter  
*Quantitative Na Detection in Cu(In,Ga)Se<sub>2</sub> Thin Film Solar Cells Using Ion Beam Analysis*  
December 2010

## 7.19 Guests

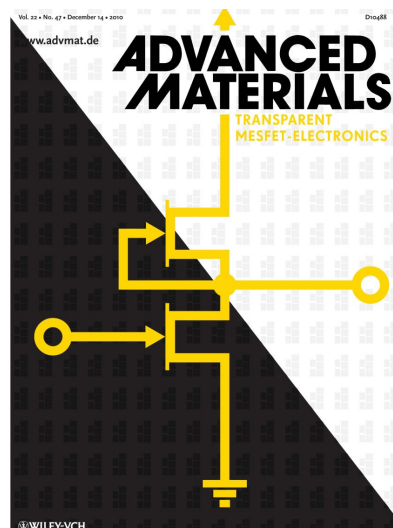
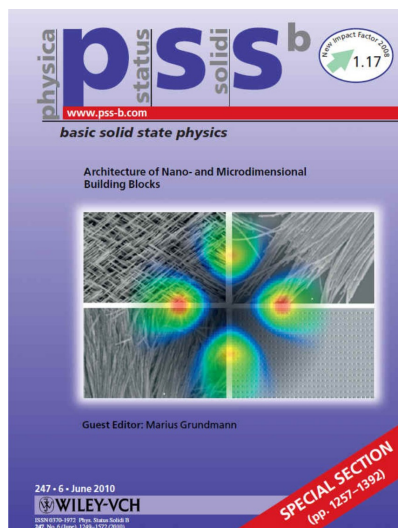
- Prof. Dr. Satyendra K. Das, Bhabha Atomic Research Centre, Kolkata, India  
August 15 – September 15 2010

## 8

# Semiconductor Physics

## 8.1 Introduction

This year we extended our work on transparent electronics to MESFET on amorphous GIZO (ZnO:Ga,In) layers. Channel and gate are deposited at room temperature and open the way for MESFET on flexible polymer substrates. Also high gain transparent inverters were demonstrated. The invention of transparent, rectifying contacts was awarded a patent early 2011 (DE 10 2009 030 045 B3). For work in this field Alexander Lajn has won a BuildMoNa award 2010 for distinguished research achievement, Dr. Heiko Frenzel the 2010 award of the Research Academy Leipzig for the best doctoral thesis in natural sciences, and Prof. Marius Grundmann the Leipziger Wissenschaftspreis 2011 of the Stadt Leipzig, Universität Leipzig and the Sächsische Akademie der Wissenschaften zu Leipzig.



The competing role of exciton localization in random compositional fluctuations and on impurities was clarified for alloys in the spectral and time domain. The interface abruptness of (Mg,Zn)O/ZnO quantum wells can be controlled in PLD (pulsed laser deposition) such that the QCSE (quantum confined Stark effect) can be turned on and off. The occurrence of rotation and mirror domains in heteroepitaxy was treated for all possible surface symmetries. Also the second edition of our textbook "The Physics

of Semiconductors" has appeared at Springer and the report of Forschergruppe 522 "Architecture of nano- and microdimensional building blocks" was published as a flight of papers in *physica status solidi (b)*.

In recognition of his outstanding research achievements and his commitment to teaching, PD Dr. Michael Lorenz has been appointed as apl. Prof., officially effective March 2011.

We are very grateful to our funding agencies in particular Deutsche Forschungsgemeinschaft (DFG) and European Social Fund (ESF). The work of our students and researchers together with our academic and industrial partners near and far was fruitful and enjoyable and thus it is with pleasure that the semiconductor physics group presents their progress report.

*Marius Grundmann*

## 8.2 Epitaxial Domains

M. Grundmann, T. Böntgen, M. Lorenz

Heteroepitaxy of material E (epilayer) on material S (substrate) is the growth of a bicrystal which is locally coherent at the interface. Heteroepitaxy is observed for combinations of quite dissimilar materials such as metals, semiconductors and dielectric materials. Depending on the 2D point symmetry of the substrate and epilayer at the interface, epitaxial domains with crystallographically equivalent interfaces arise.

The symmetry  $G$  of the E/S epitaxial system is given by the intersection of the symmetry groups  $G_S, G_E$  of the components, i.e.  $G = G_S \cap G_E$ . This goes back to Curie's principle of symmetry [1], which states that the group of symmetries of two or more objects regarded as an entity is the highest common subgroup of the symmetry groups of these objects. In terms of group orders, the number  $N$  of (orientation) variants is given by  $N = n(G_S)/n(G_S \cap G_E)$ . We have treated the problem for combinations of various rotational symmetry [2] and also including the mirror symmetries [3]. The result for all 2D point symmetries is given in Fig. 8.1.

As a practical example relevant to the field of transparent electronics we note the epitaxy of hexagonal, semiconducting ZnO and cubic (or tetragonal), ferroelectric BaTiO<sub>3</sub>. If ZnO is grown on BaTiO<sub>3</sub>, two rotation domains occur, for BaTiO<sub>3</sub>/ZnO, three rotation domains are observed as seen in X-ray  $\phi$ -scans (Fig. 8.2).

This work has been supported by Deutsche Forschungsgemeinschaft in the framework of SFB 762 "Functionality of Oxide Interfaces".

[1] P. Curie: *J. de Physique* **3**, 393 (1894)

[2] M. Grundmann, T. Böntgen, M. Lorenz: *Phys. Rev. Lett.* **105**, 146102 (2010)

[3] M. Grundmann: *phys. stat. sol. (b)* **248**, 805-824 (2011)

$G_S \backslash G_E$	1	$m$	2	$2mm$	3	$3m$	4	$4mm$	6	$6mm$
1	1	1	1	1	1	1	1	1	1	1
$m$	2	1 2	2	1 2	2	1 2	2	1 2	2	1 2
2	2	2	1	1	2	2	1	1	1	1
$2mm$	4	2 4	2	1 2	4	2 4	2	1 2	2	1 2
3	3	3	3	3	1	1	3	3	1	1
$3m$	6	3 6	6	3 6	2	1 2	6	3 6	2	1 2
4	4	4	2	2	4	4	1	1	2	2
$4mm$	8	4 8	4	2 4	8	4 8	2	1 2	4	2 4
6	6	6	3	3	2	2	3	3	1	1
$6mm$	12	6 12	6	3 6	4	2 4	6	3 6	2	1 2

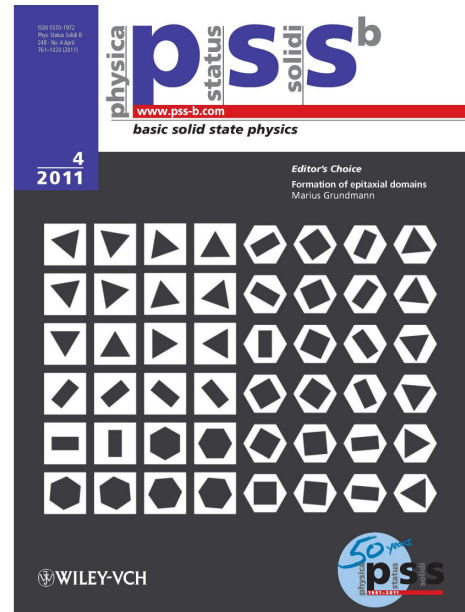


**Figure 8.1:** Number of rotational (or mirror) domains for all 2D point groups of substrate ( $G_S$ ) (rows) and epilayer ( $G_E$ ) (columns). When two numbers are given ( $x|y$ ), the first (second) number represents the number of domains if mirror symmetry planes of S and E align (misalign).

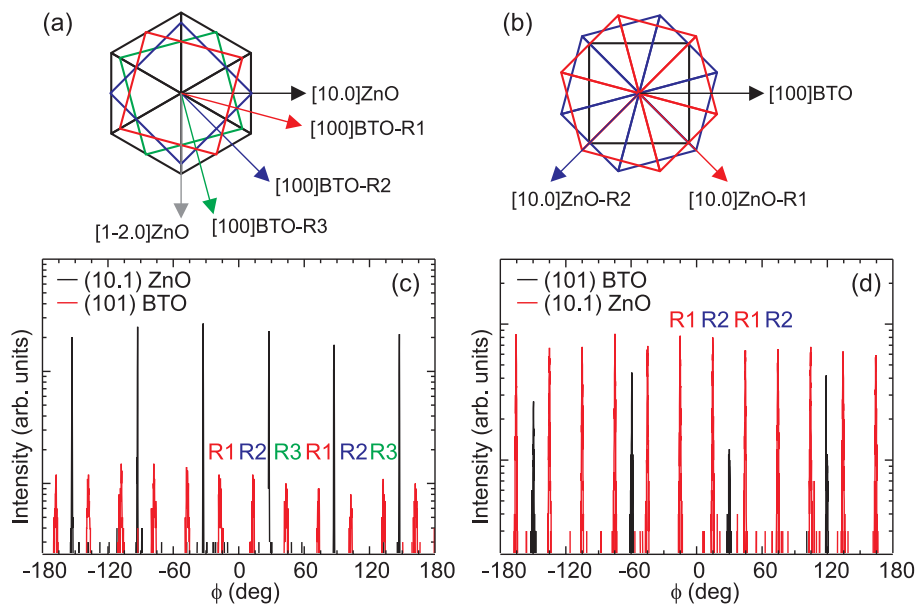


**Figure 8.2:** (c) High-resolution X-ray diffraction (HR-XRD)  $\phi$ -scan of 250 nm BaTiO<sub>3</sub>(001) thin film (BTO) on ZnO(00.1). The BaTiO<sub>3</sub> (101) exhibits twelve 30°-spaced peaks indicating, that the C<sub>4</sub>-symmetric (tetragonal) layer aligns in-plane within three rotational domains as shown schematically in panel (a). (d) HR-XRD  $\phi$ -scan of 800 nm ZnO(00.1) thin film on BTO(001). The ZnO (10.1) planes exhibit twelve 30°-spaced peaks indicating that the hexagonal layer aligns in-plane with two rotation domains as shown schematically in panel (b).

### 8.3 Low-temperature processed Schottky-gated field-effect transistors based on amorphous gallium-indium-zinc-oxide thin films

M. Lorenz, A. Lajn, H. Frenzel, H. von Wenckstern, M. Grundmann, P. Barquinha\*, R. Martins\*, E. Fortunato\*

\*CENIMAT/I3N, Departamento de Ciência dos Materiais, Faculdade de Ciências e Tecnologia, FCT, Universidade Nova de Lisboa and CEMOP-UNINOVA, 2829-516 Caparica, Portugal

Transparent amorphous oxide semiconductors (TAOS) and derivate devices are currently one of the most active research areas in semiconductor physics. Despite their amorphous structure these oxides can have Hall-effect mobilities up to several  $10 \text{ cm}^2/\text{Vs}$ . They can be deposited at low temperatures making them compatible to organic polymere substrates making cheap, flexible and transparent devices possible. Due to the homogeneity of the thin films large area electronics are cogitable. We have fabricated metal-semiconductor field-effect transistors (MESFET) based on gallium-indium-zinc-oxide (GIZO). The thin films were grown by radio frequency magnetron sputtering at room temperature (RT) on Corning 1737 glass substrates. All functional parts were fabricated at room temperature – in our case limited only by an annealing step of the thin films at  $150^\circ\text{C}$  for 60 min in ambient air.

GIZO thin films were grown with a thickness of 160 nm. The composition of the target material and the sputter deposition parameters were tuned such that the resulting net doping density and the related width of the space charge region below the Schottky contact (SC) permit low switching voltages. Figure 8.3(a) depicts a quasistatic capacitance-voltage measurement ( $1/C^2$  vs. the applied gate voltage  $V_G$ ) carried out on a MESFET based on an annealed GIZO channel and the derived net doping density ( $N_d$  vs. the width of the space charge region  $w$ ). For the bulk region of the channel a net doping density of  $N_d \approx 5 \times 10^{16} \text{ cm}^{-3}$  is obtained. For the as-grown GIZO channel a carrier concentration of about  $10^{16} \text{ cm}^{-3}$  is derived. This is consistent with the Hall-effect measurements (see Table 8.1). Annealed thin films have an increased Hall-effect mobility ( $\mu_{\text{Hall}} = 20.8 \text{ cm}^2/\text{Vs}$ ) of about one order of magnitude compared to their as-grown counterparts ( $\mu_{\text{Hall}} = 2.56 \text{ cm}^2/\text{Vs}$ ). This is caused by a reduction of the trap state density, local atomic rearrangement and improvement of the film compactness [1].

The MESFET were processed employing standard photolithography using lift-off technique [2]. The ohmic source and drain contacts were dc sputtered using a gold target in an argon atmosphere. The Ag-Schottky contacts were reactively sputtered in a mixed argon/oxygen atmosphere. Subsequently, a current spreading layer of Au was sputtered in argon atmosphere on top of the SC to form an equipotential surface. Figure 8.3(c) depicts the Schottky gate characteristics. The on/off-current ratio ( $I_{\text{SG}}(2\text{V})/I_{\text{SG}}(-2\text{V})$ ) for both as-grown and annealed thin film devices is about  $10^8$ . The forward direction of the diodes were fitted assuming thermionic emission only. The extracted effective Schottky barrier height  $\Phi_{\text{B,eff}}$  is about 0.95 eV for both devices. The ideality factor was determined for annealed devices to be  $\eta \approx 1.9$  and for as-grown devices  $\eta \approx 2$ . The values for  $\Phi_{\text{B,eff}}$  and  $\eta$  are well comparable with the parameters extracted from SC to ZnO on glass and sapphire substrates [2].

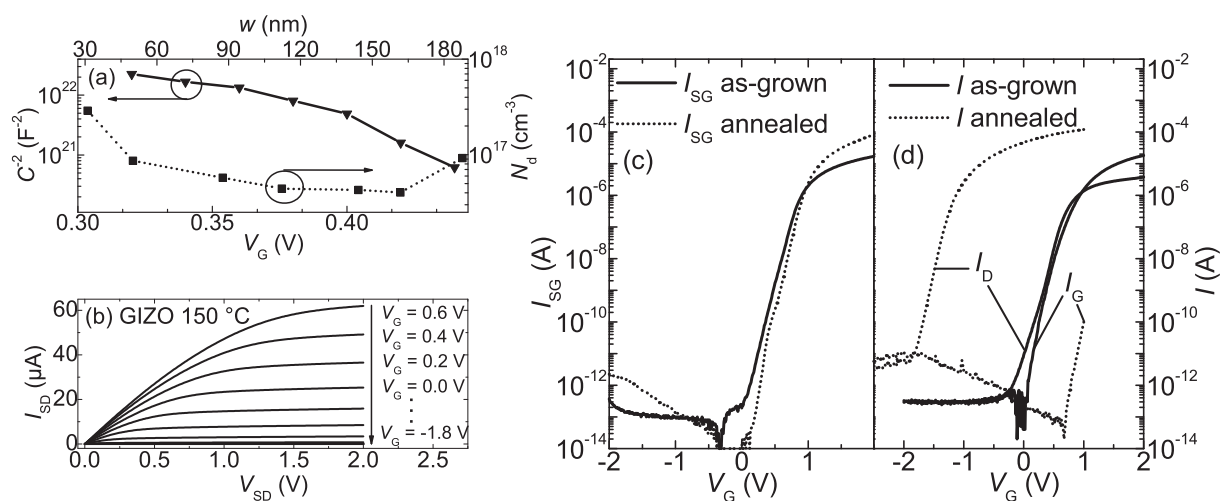


**Figure 8.3:** (a) QSCV measurement ( $1/C^2$  vs.  $V_G$ ) and the derived net doping density  $N_d$  vs. the width of the space charge region  $w$ . (b) Output characteristic of a MESFET with annealed GIZO channel. (c) Schottky  $IV$ -characteristics and (d) transfer characteristics  $I_D$  and the corresponding gate leakage currents  $I_G$  (dashed line).

In Figure 8.3(d) the transfer characteristic  $I_D$  together with the respective gate leakage current  $I_G$  is shown. The particular transistor based on as-grown GIZO channel depicted in the figure has a turn-on voltage of  $V_{on} = -0.5$  V. The on/off-current ratio is about  $10^6$ . The channel mobility of the transistor derived from the maximum of the transconductance is  $7.3$  cm<sup>2</sup>/Vs. Averaged over all 28 transistors on the sample chip the median value of the channel mobility  $\mu_{ch,med}$  is only  $0.01$  cm<sup>2</sup>/Vs indicating poor reproducibility. By annealing the thin films prior transistor fabrication the device characteristics were improved. Due to the increased carrier density the turn-on voltage shifts to  $V_{on} = -1.9$  V. The channel mobility increases to a value of  $14.1$  cm<sup>2</sup>/Vs for the particular transistor depicted in the figure 8.3(d). This value is almost identical to its median of  $\mu_{ch,med} = 14.7$  cm<sup>2</sup>/Vs (see Table 8.1). Thus the reproducibility and uniformity is largely improved. Apart from a higher on/off-current ratio of  $> 10^7$  and a reduced subthreshold swing (from  $123$  mV/decade for as-grown thin film transistors to  $112$  mV/decade for annealed devices), the transistors exhibit excellent switching behaviour with a gate sweep voltage of  $\Delta V_G = 2.4$  V as can be seen from figure 8.3(b). Clear and constant saturation is observed in the output characteristic for annealed MESFET devices.

This work has been supported by Deutsche Forschungsgemeinschaft in the framework of SFB 762 "Functionality of Oxide Interfaces".

- [1] P. Barquinha, L. Pereira, G. Gonçalves, R. Martins, E. Fortunato: J. Electrochem. Soc. **156**, H161-H168 (2009)
- [2] H. Frenzel, M. Lorenz, A. Lajn, H. von Wenckstern, G. Biehne, H. Hochmuth, M. Grundmann: Appl. Phys. Lett. **95**, 153503 (2009)
- [3] M. Lorenz, A. Lajn, H. Frenzel, H. von Wenckstern, M. Grundmann, P. Barquinha, R. Martins and E. Fortunato: Appl. Phys. Lett. **97**, 243506 (2010)

**Table 8.1:** Width-to-length ratio  $W/L$  of the Schottky gate contact, Hall-effect data (derived from 120 nm thick films) and measured electrical parameters of the MESFET with a channel thickness  $d = 160$  nm.

	$W/L$ ( $\mu\text{m}/\mu\text{m}$ )	$\mu_{\text{Hall}}$ ( $\text{cm}^2/\text{Vs}$ )	$N_{\text{Hall}}$ ( $10^{16}\text{cm}^{-3}$ )	$N_{\text{d}}$ ( $10^{16}\text{cm}^{-3}$ )	$\mu_{\text{ch}}$ ( $\text{cm}^2/\text{Vs}$ )	$\mu_{\text{ch,med}}$ ( $\text{cm}^2/\text{Vs}$ )	$S$ (mV/dec)
GIZO RT	430/20	2.56	1.3	1	7.3	0.01	123
GIZO 150 °C	430/10	20.8	4.5	5	14.1	14.7	112

## 8.4 Light and temperature stability of fully transparent ZnO-based inverter circuits

A. Lajn, T. Diez, F. Schein, H. Frenzel, H. von Wenckstern, M. Grundmann

Recently the concept of transparent rectifying contacts has been introduced[1], permitting the fabrication of fully transparent field-effect transistors and inverter circuits. In the following, the operational stability of fully transparent inverter circuits towards illumination with visible light and towards elevated temperatures is investigated.

Using pulsed-laser deposition (PLD), a 30 nm thick  $\text{Mg}_{0.003}\text{Zn}_{0.997}\text{O}$  film was deposited on an as-received a-plane sapphire substrate ( $p_{\text{O}_2} = 0.02$  mbar,  $T_{\text{growth}} = 670^\circ\text{C}$ ). First, channel mesas were wet chemically etched with phosphoric acid. Second, the 5 nm thick silver oxide gate contacts were fabricated by reactive dc-sputtering (room temperature,  $t = 30$  s,  $P = 5$  W,  $p = 0.02$  mbar 50:50 Ar/O<sub>2</sub>). Subsequently, the gate contact is capped in-situ with a 5 nm thin gold current-spreading layer, deposited by dc-sputtering (room temperature,  $t = 10$  s,  $P = 5$  W,  $p = 0.02$  mbar Ar). Third, the ohmic contacts of the inverter circuits are formed by dc-sputtering of a gold layer identically processed as the current spreading layer of the gate contacts. The mean device transmission in the visible spectral range exceeds 65 %.

The fully transparent inverter circuits consist of two transparent, normally-on MgZnO-based MESFETs (See left inset of Fig. 8.4a)). The gate of the load transistor ( $Q_L$ ) is short-circuited with its source and therefore a single output curve ( $V_G = 0$  V) is selected out of the set of output characteristics. The input voltage applied to the gate of the switching transistor ( $Q_S$ ) controls its channel conductivity.  $Q_L$  and  $Q_S$  form a voltage divider. In the switching regime the inverter's logical state is undefined; this voltage interval is characterized by the optimally small uncertainty level  $V_{\text{uc}} = \Delta V|_{|dV_{\text{out}}/dV_{\text{in}}|=1}$ . In the ideal case of two identical FETs, this interval is centered on 0 V input voltage. Aside from the logical inversion, the inverter can be used as voltage amplifier, characterized by the peak gain magnitude  $pgm = \max(dV_{\text{out}}/dV_{\text{in}})$ . Gain magnitudes up to 200 have been achieved using transparent ZnO-based MESFET inverter circuits [1]. The high and low output voltage levels generally deviate from the ideal values of  $V_{\text{DD}}$  and zero depending on the achievable channel resistivity ratios. Due to the usage of Schottky gate electrodes in MESFET-based inverter circuits, a further deviation for high input voltages from the ideal characteristics can be observed. The output voltage increases due to the increasing leakage current induced by thermionic emission over the Schottky barrier for positive gate-source voltages.

The samples were illuminated with red ( $\lambda = 628$  nm; FWHM = 20 nm), green ( $\lambda = 525$  nm; FWHM = 30 nm) and blue ( $\lambda = 435$  nm; FWHM = 25 nm) LEDs. The irradi-

ance was adjusted to about  $10 \text{ W/m}^2$  for all LEDs, which is comparable to typical indoor levels. The voltage transfer characteristics (VTC) of a transparent inverter circuit measured under dark conditions and illuminated by red, green and blue LEDs are depicted in Fig. 8.4a). Obviously, red and green light does not affect the VTC, whereas blue light slightly modulates the VTC. As the blue photon energy is lower than the fundamental band gap of MgZnO, it can be concluded that deep acceptor states in the channel provide the photo-generated carriers. Due to the fact that the load transistors' gate is short-circuited with the load transistors' source electrode, no photo voltage is generated there in contrast with the switching transistors' gate. At the latter gate electrode, a photo voltage, which is a reverse bias, is generated and increases the effective gate voltage due to the fixed input voltage. Consequently, the channel conductivity of the switching transistor is increased and the VTC is shifted to lower input voltages. Of course, the switching regime exhibits the most pronounced deviations, as it is most sensitive towards changes of the channel conductivity. Here, the blue light yields a 15 %-reduction of the pgm and the uncertainty level is increased by 15 %. The evolution of the VTC

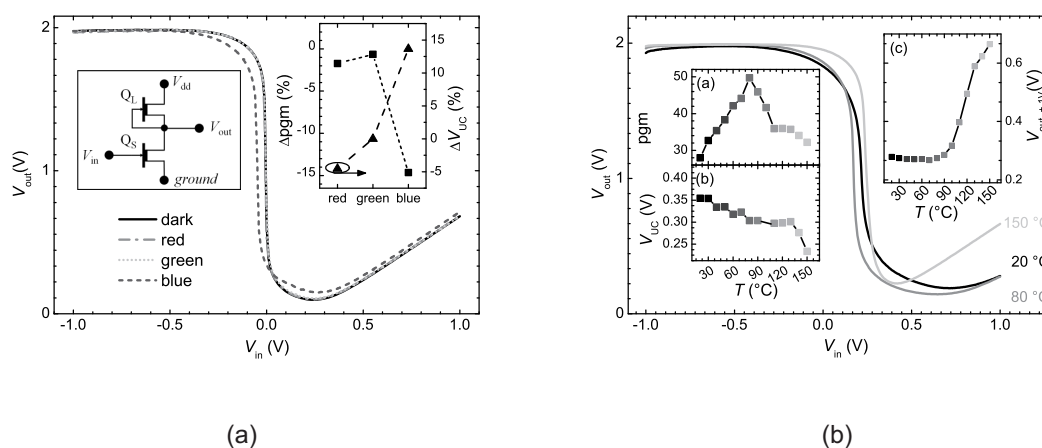


**Figure 8.4:** a) Influence of visible light on the VTC of transparent MgZnO-based Inverter. Left inset: Circuit diagram of an inverter. Right inset: Relative change of the pgm and the pgm-point. b) Influence of temperature on the VTC of transparent MgZnO-based Inverter. Insets: Change of a) pgm and b) uncertainty level with temperature. Inset c) Correlation of

with increasing temperature is depicted exemplarily for three temperatures in Fig. 8.4 b). Obviously, the inverting functionality is conserved even for operating temperatures as high as  $150^\circ\text{C}$ . The most obvious change occurs for positive input voltages. While a temperature increase up to about  $90^\circ\text{C}$  hardly affects the VTC, the output voltage increases considerably for higher temperatures (see inset c) of Fig. 8.4 b)). due to the irreversible degradation of the gate electrode. The gate degradation also affects the switching regime. For temperatures below the degradation threshold of about  $90^\circ\text{C}$ , the pgm increases, whereas with the onset of gate degradation the pgm also starts to decrease (see inset a) of Fig. 8.4 b)). In contrast, the gate degradation has no obvious effect on the uncertainty level; it decreases continuously with increasing temperature (See Inset b) of Fig. 8.4 b)).

Conclusively, the inverters are stable towards red and green light and elevated temperatures up to  $90^\circ\text{C}$ . For blue light minor changes of the inverter parameters are observed, for temperatures above  $90^\circ\text{C}$  the devices degrade. Nevertheless, they remain

operational up to 150°C.

This work has been supported by Deutsche Forschungsgemeinschaft in the framework of SFB 762 "Functionality of Oxide Interfaces" and the Graduate School "Leipzig School of Natural Sciences - Building with Molecules and Nano-objects (BuildMoNa, GS185), the Studienstiftung des Deutschen Volkes, the European Social Fund (ESF).

- [1] H. Frenzel, A. Lajn, H. von Wenckstern, M. Lorenz, F. Schein, Z. Zhang, M. Grundmann: *Advanced Materials* **22**, 5332 (2010)  
 [2] A. Lajn, T. Diez, F. Schein, H. Frenzel, H. von Wenckstern, M. Grundmann: *IEEE Electron Device Letters* **32**, 515 (2011)

## 8.5 Gate- and drain-Lag effects in (Mg,Zn)O-based metal-semiconductor field-effect Transistors

F.J. Klüpfel, A. Lajn, H. Frenzel, H. von Wenckstern, M. Grundmann

Recently the development of highly rectifying Schottky contacts on ZnO led to the fabrication of ZnO-based metal-semiconductor field-effect transistors (MESFETs) [1]. The usage of ultra thin gate contacts allows to fabricate these devices fully transparent [2]. As the operating frequency plays a crucial role in most applications, we investigated the dynamic properties of ZnO-based MESFETs in addition to the previously published static characteristics. With single devices this can be done either by current transient analysis, when a square wave voltage is applied, or by analyzing the frequency-dependent response of the source-drain current to a sinusoidal ac-voltage.

The channel material of our transistors was deposited by PLD using a ZnO target containing 0.25wt-% MgO. The source and drain contacts were fabricated by DC sputtering of Au in Ar ambient. For the gate contact the materials  $\text{Ag}_x\text{O}$ ,  $\text{PtO}_y$  and Au were compared, all deposited by DC sputtering in Ar/O<sub>2</sub> ambient. Spectroscopic ellipsometry determined a channel thickness of 25 nm. The net doping concentration of  $4 \times 10^{18} \text{ cm}^{-3}$  was determined by quasi-static C-V measurements.

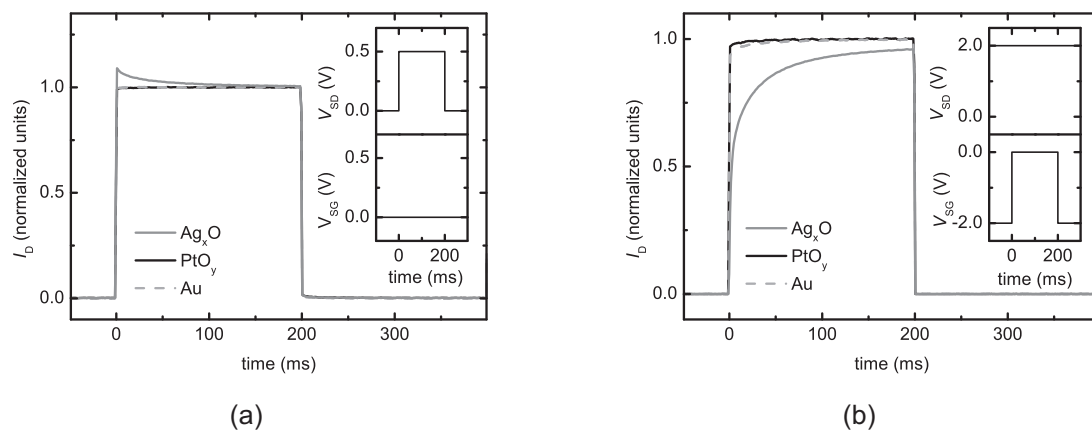


**Figure 8.5:** Measurement of a) drain lag and b) gate lag of MESFETs with different gate materials.

From other material systems like GaAs it is known that trap states in the device can significantly slow down the switching behavior of MESFETs (e.g. [3]). The responses of the source drain current to step-like changes of the drain or gate voltage are called drain lag and gate lag, respectively. After changing the drain voltage, usually a current overshoot is observed while the current response to a gate voltage change is delayed.

We observed this typical behavior for devices with  $\text{Ag}_x\text{O}$ -gates, as depicted in Fig. ??a (drain lag) and Fig. 8.5b (gate lag). For the gate materials  $\text{PtO}_y$  and Au no drain lag was observed within the time resolution of 1 ms. The gate lag transients for these materials amount to only 10% of the total current increase. The functional form of all measured transients is stretched exponential, which is in agreement to literature [4]. Fitting with this function gives the steady state current, which has been used to normalize the drain current in Fig. 8.5. It allows also to calculate average time constants for the delay mechanisms, which are between 10 ms and 50 ms, depending on the gate material as well as on the applied voltages.

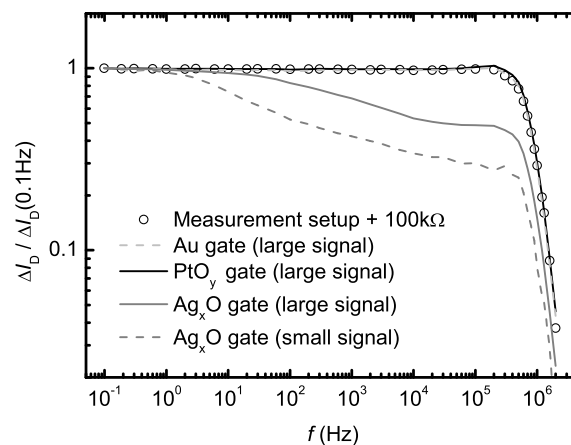


**Figure 8.6:** Measurement of the gate lag in the frequency domain. Large signal measurements were recorded using a sine shaped gate voltage around 0 V with an amplitude of 1.5 V. For the small signals the offset voltage was 1 V with an amplitude of 0.1 V.

The difference between the gate materials Au and  $\text{PtO}_y$  on the one hand and  $\text{Ag}_x\text{O}$  on the other hand was also observed in frequency-dependent measurements of the gate lag, as depicted in Fig. 8.6. The measured current amplitudes for the  $\text{Ag}_x\text{O}$ -FETs drop already significantly in the range of few Hertz, while the other devices show no restriction of the switching speed up to 1 MHz. For higher frequencies the measurement setup does not allow further investigations. We attribute the difference between the gate materials to the diffusion of Ag into the transistor channel during device fabrication, which has been reported to decrease the Schottky contact capacitance [5]. The clarification of this assumption will be the topic of further investigations.

This work has been supported by Deutsche Forschungsgemeinschaft within the Graduate School "Leipzig School of Natural Sciences - Building with Molecules and Nano-objects (BuildMoNa, GS185).

- [1] H. Frenzel, A. Lajn, M. Brandt, H. von Wenckstern, G. Biehne, H. Hochmuth, M. Lorenz, M. Grundmann: Applied Physics Letters **92**, 192108 (2008)

- [2] H. Frenzel, A. Lajn, H. von Wenckstern, M. Grundmann: Journal of Applied Physics **107**, 114515 (2010)
- [3] Y. Fujisaki and N. Matsunaga: Gallium Arsenide Integrated Circuit Symposium 235 (1988)
- [4] R. Vetry, N. Q. Q. Zhang, S. Keller, U. K. Mishra: IEEE Transactions on Electron Devices **48**, 560 (2001)
- [5] H. von Wenckstern, A. Lajn, A. Laufer, B. K. Meyer, H. Hochmuth, M. Lorenz, M. Grundmann: AIP Conf. Proc. **1199**, 122 (2009)

## 8.6 Transparent rectifying contacts for visible-blind ultraviolet photo-diodes based on ZnO

A. Lajn, M. Schmidt, H. von Wenckstern, M. Grundmann

Recently, the concept of transparent rectifying contacts (TRC) has been introduced, which permits to fabricate a variety of unipolar devices based on the wide-bandgap semiconductor such as ZnO including fully transparent diodes, transistors and logical circuits [1]. In the following, the applicability of TRC for the detection of ultraviolet light is presented.

Using pulsed-laser deposition (PLD), first an about 200 nm thick Al-doped ZnO film, serving as back side contact and subsequently a 1  $\mu\text{m}$  thick ZnO film were deposited on an a-plane sapphire substrate (Cf. inset of figure 8.7a) ( $p_{\text{O}_2} = 0.02$  mbar and  $T_{\text{growth}} = 670^\circ\text{C}$ ). Transparent rectifying contacts were fabricated by reactive dc-sputtering of an about 5 nm thick platinum oxide layer or silver oxide, which were subsequently capped by a metallic platinum or gold layer of 5 nm thickness. The transmission spectrum of both TRCs is depicted in figure 8.7 a). In order to exclude the zinc oxide absorption, the TRC layers were deposited directly on as-received fused quartz glass substrates with identical growth conditions as used for the photo-detectors. The  $\text{PtO}_y$  and the  $\text{Ag}_x\text{O}$  contacts achieve a mean transmission in the visible spectral range of 75% and 73%, respectively. From the  $IV$ -characteristic (not shown here), the rectification ratio ( $I(1\text{ V})/I(-1\text{ V})$ ), the barrier height  $\Phi_{\text{B}}$  and the ideality factor were extracted assuming thermionic emission to be the dominant current transport mechanism. For both TRC-materials, the barrier height is 0.73 V. The ideality factors of the contacts are as low as 1.6 (1.2) for the  $\text{PtO}_y$  ( $\text{Ag}_x\text{O}$ )-contacts. The rectification ratio is  $1 \times 10^4$  for  $\text{PtO}_y$  and  $1.5 \times 10^5$  for  $\text{Ag}_x\text{O}$ , respectively.

The external quantum efficiency

$$\eta_{\text{ext}} = \left( |I_{\text{ph}}| / qA_{\text{opt}} \right) / (P/h\nu) \quad (8.1)$$

and the responsivity  $R = \frac{\eta_{\text{ext}}}{h\nu}$  of the photo-detectors in photo-voltaic mode ( $V = 0$ ) are depicted in Fig. 8.7 b).  $A_{\text{opt}}$  is the contact area and  $P$  is the optical power at the considered wave length. For light with energy below the band gap of ZnO, photo-current generation is strongly suppressed, whereas for light above the band gap a large fraction of the incident light is converted to an electric current. For both  $\text{PtO}_y$  and  $\text{Ag}_x\text{O}$ , the UV-VIS rejection ratio is at least  $10^3$  for the blue, but exceeds  $10^4$  for the red and green

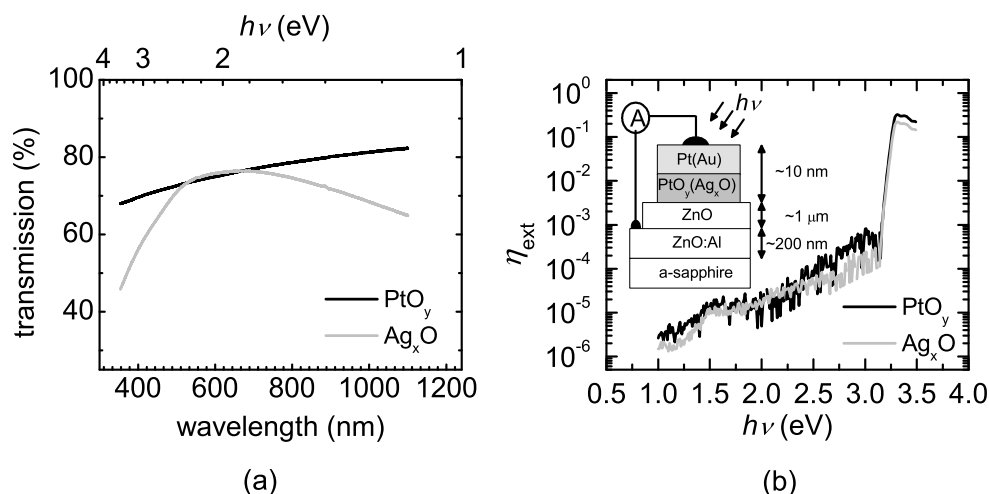


**Figure 8.7:** (a) Transmission of the TRC contact layers on a fused quartz glass substrate. (b) External quantum efficiency and responsivity of the transparent rectifying contact structures in dependence of the wave length of the incident light. For the  $\text{PtO}_y$  ( $\text{Ag}_x\text{O}$ )-contact the maximal external quantum efficiency and responsivity are 33% (22%) and 0.1 A/W (0.07 A/W). The inset depicts the device layout.

spectral range. The maximum external quantum efficiency and responsivity for the  $\text{PtO}_y$  ( $\text{Ag}_x\text{O}$ )-contact are 32% (22%) and 0.1(0.07) A/W, reached at an energy of 3.31 eV, which is about 60 meV below the fundamental band gap of ZnO [2]. Conclusively, the photo carriers are either generated by ionization of shallow donors or by generation and subsequent thermal dissociation of excitons, which have a binding energy in zinc oxide of about 60 meV. The normalized detectivity  $D^* = R ((\exp(\Phi_B/k_B T)) / (4qA^*T^2))^{1/2}$  for a Schottky photo-diode complying with the thermionic emission model was determined. The maximum values were  $D_{\text{max}}^* = 1.29 \times 10^{11} \text{ cmHz}^{1/2}\text{W}^{-1}$  for  $\text{PtO}_y$  as well as  $D_{\text{max}}^* = 0.9 \times 10^{11} \text{ cmHz}^{1/2}\text{W}^{-1}$  for  $\text{Ag}_x\text{O}$ , respectively. The data show, that the concept of fully transparent rectifying contacts is successfully transferred to two types of visible-blind UV-photodetectors. External quantum efficiencies up to 32 %, responsivities up to 0.1 A/W and UV/VIS rejection ratios of  $> 10^3$  were achieved.

This work has been supported by the Studienstiftung des Deutschen Volkes and the European Social Fund (ESF).

- [1] H. Frenzel, A. Lajn, H. von Wenckstern, M. Lorenz, F. Schein, Z. Zhang, M. Grundmann: *Advanced Materials* **22**, 5332 (2010)
- [2] A. Lajn, M. Schmidt, H. von Wenckstern, M. Grundmann: *J. Electron. Mater.* **40**, 473 (2011)
- [3] H. Frenzel, A. Lajn, H. von Wenckstern, M. Grundmann: German patent DE 10 2009 030 045 B3 (2011)

## 8.7 Wavelength-selective metal-semiconductor-metal photodetectors based on (MgZn)O-heterostructures

Z.P. Zhang, H. von Wenckstern, M. Schmidt, J. Lenzner, H. Hochmuth, M. Grundmann

For the ternary semiconductor (Mg,Zn)O, the band gap  $E_g$  increases with increasing Mg-content. Making use of this we utilized  $\text{Mg}_y\text{Zn}_{1-y}\text{O}/\text{Mg}_x\text{Zn}_{1-x}\text{O}$ -heterostructure having two different Mg-contents ( $0 \leq y < x \leq 0.5$ ) to construct wavelength-selective back-illuminated metal-semiconductor-metal photodetectors (MSM-PDs). The  $\text{Mg}_x\text{Zn}_{1-x}\text{O}$ -layer acts as an integrated, passive optical filter (see the schematic device layout in Fig. 8.8 (a)). Both layers were grown by pulsed-laser deposition on double-side polished a-plane sapphire substrate at a growth temperature of 720 °C. The Schottky contacts (SCs) of the interdigital MSM-structure were fabricated by photolithography and reactive dc-sputtering of palladium (Pd) and platinum (Pt), respectively [1]. The samples were investigated by current-voltage (IV) and photocurrent measurements.

Due to the utilization of layers with different Mg-content only light in a defined photon energy range ( $E_g^y < E_{ph} < E_g^x$ ) should contribute to the photo-response. The width of bandpass of the devices is given by the bandgap difference ( $\Delta E_g$ ) of the two MgZnO-layers, and the center of bandpass can be shifted by using different combination of  $x$  and  $y$ .

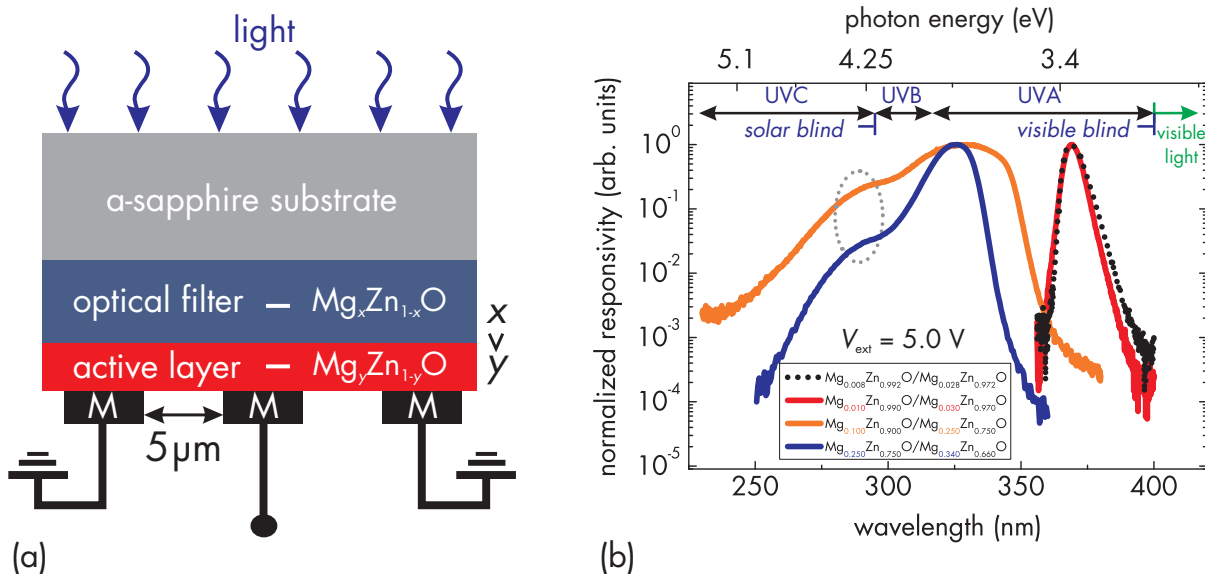


**Figure 8.8:** (a): Schematic layout of the  $\text{Mg}_y\text{Zn}_{1-y}\text{O}/\text{Mg}_x\text{Zn}_{1-x}\text{O}$ -heterostructure ( $y < x$ ) (b): normalized spectral responsivity of ultraviolet PDs under an external voltage of 5.0 V with different combinations of  $y$  and  $x$ . The gray circle indicate collection of charge carrier generated in the filter layer due to insufficient thickness of the active layer.

Fig. 8.8 (b) shows the generated normalized responsivity of MSM-PDs versus wavelength for varying combinations of  $x$  and  $y$ . The long-wavelength cutoff of the detectors responsivity is defined by the Mg-content  $y$  in the active layer, while the corresponding short-wavelength cutoff is due to the absorption within the passive optical filter layer. The signal-to-noise ratio of all PDs is more than 3 orders of magnitude.

The spectral response of  $\text{Mg}_{0.25}\text{Zn}_{0.75}\text{O}/\text{Mg}_{0.34}\text{Zn}_{0.66}\text{O}$  and  $\text{Mg}_{0.1}\text{Zn}_{0.9}\text{O}/\text{Mg}_{0.25}\text{Zn}_{0.75}\text{O}$  detectors are shown by the blue and orange line in fig. 8.8 (b), respectively. From the figure it is evident that a lower Mg-content  $y$  in the active layer red-shifts the long wavelength cutoff. The width of the absorption band depends on the difference of  $x$  and  $y$  which is larger for detector depicted by the orange line. The thickness of the active layer of these two detectors lower than optimal and , therefore, charge carriers, generated within the filter layer, contribute to the photocurrent (space-charge region below metal contacts extends into the filter layer) and is indicated by the gray-dotted circle.

For detectors with small bandwidth  $x$  must be only slightly smaller than  $y$  which we realized by two approaches: i) usage of PLD targets with only slightly different MgO admixtures, exemplarily shown by the red line in fig. 8.8 (b) ii) usage of only one PLD target but different oxygen partial pressures during deposition of the respective layers depicted by the black-dotted line. Note, the Mg-incorporation decreases with increasing different oxygen partial pressure. The FWHM of the absorption band is only 6.5 and 7.5 nm for case i) and ii), respectively.

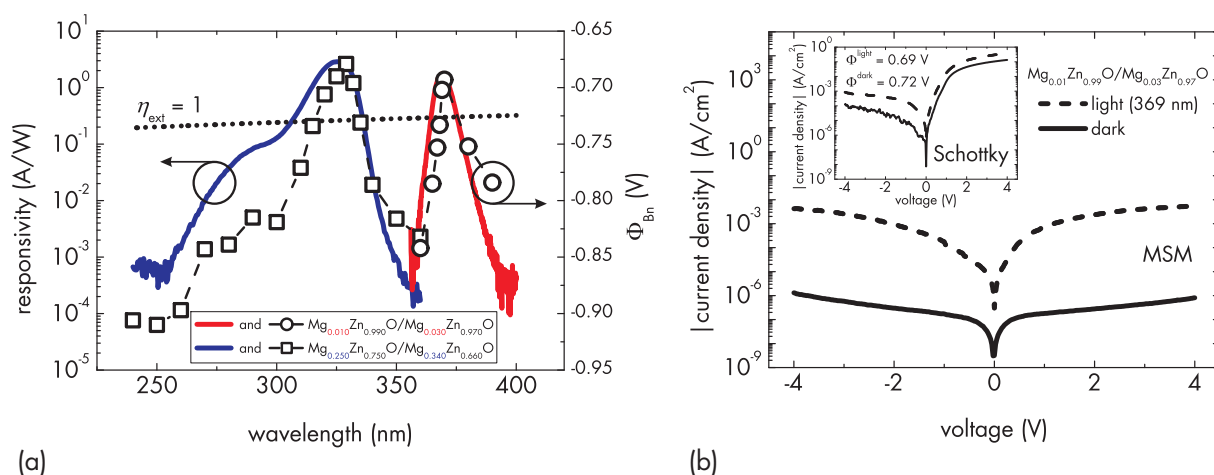


**Figure 8.9:** (a): Spectral responsivity of MSM-PDs based on MgZnO-heterostructure measured under  $V_{\text{ext}} = 5.0$  V with Schottky barrier heights; (b): current-voltage measurements for MSM-PD and adequate Schottky diode (inset) in dark and under backside illumination.

Fig. 8.9 (a) shows the spectral responsivity together with corresponding Schottky barrier heights of two MSM-PDs under backside illumination at  $V_{\text{ext}} = 5.0$  V. The maximum responsivity of both samples exceed well the external quantum efficiency  $\eta_{\text{ext}} = 1$ , indicating that an internal gain mechanism exists within the PDs. Because of the low doping level ( $10^{16} \text{ cm}^{-3}$ ), low ideality factor and temperature dependence of IV-measurements [2], the main transport mechanism is thermionic emission, not tunneling. Thus, a secondary photoresponse, caused by trapping of minority carrier (here holes) at metal/semiconductor interface [3] should be considered. Under illumination, photoexcited holes will be trapped by states at the  $\text{PdO}_z/\text{MgZnO}$  interface. This results in a lowering of the Schottky barrier height  $\Phi_{\text{Bn}}$  at the maximum of responsivity, which is also depicted in fig. 8.9 (a). The excellent agreement between the spectral photo response and  $\Phi_{\text{Bn}}$  calculated from IV-curves, which are measured under backside illumination in the whole spectral range, indicates that the model is valid and explains the internal gain mechanism in MSM-PDs based on MgZnO-heterostructures.

The IV-curves in dark and under UV-illumination at maximum photo response for MSM-PD and corresponding SC are shown in Fig. 8.9 (b). Upon 369 nm illumination, the current density of MSM and SC increases by three and one order(s) of magnitude compared with the dark current, respectively. The decreasing of barrier height of the SC demonstrates the model of photo carriers trapping at the metal/semiconductor interface.

- [1] H. Frenzel, A. Lajn, H. von Wenckstern, M. Lorenz, F. Schein, Z. Zhang and M. Grundmann: *Adv. Mat.* **22**, 5332 (2010), [doi:10.1002/adma.201001375](https://doi.org/10.1002/adma.201001375)
- [2] H. von Wenckstern, K. Brachwitz, M. Schmidt, C.P. Dietrich, M. Ellguth, M. Stölzel, M. Lorenz, M. Grundmann: *J. Electron. Mater.* **39**, 584 (2010), [doi:10.1007/s11664-009-0967-0](https://doi.org/10.1007/s11664-009-0967-0)
- [3] O. Katz, V. Graber, B. Meyler, G. Bahir, J. Salzman: *Appl. Phys. Lett.* **79**, 1417 (2001), [doi:10.1063/1.1394717](https://doi.org/10.1063/1.1394717)

## 8.8 Multi-barrier ZnO-Schottky contacts

S. Müller, H. von Wenckstern, J. Lenzner, O. Breitenstein\*, M. Grundmann

\*Experimental Department II, Max-Planck-Institut für Mikrostrukturphysik, Weinberg 2,  
06120 Halle, Germany

We report on investigations of Schottky contacts (SC) on ZnO thin films that exhibit discrete spatial variations of the barrier height. Current-voltage (IV)-characteristic of multi-barrier SCs on hydrothermal bulk ZnO and ZnO thin films were already published [1–3] and exhibit kinks in the forward direction, however, a discussion was not given. For this study we used nominally undoped ZnO thin films grown on a ZnO:Al buffer on 2 inch a-plane sapphire wafer by pulsed-laser deposition [4]. On the nominally undoped layer about 500 circular PdO<sub>y</sub>/ZnO-SCs were fabricated by reactive dc-sputtering. The areas of the SCs are in the range from  $1.8 \times 10^{-4}$  to  $4.4 \times 10^{-3}$  cm<sup>2</sup>. About 100 of the prepared SCs exhibit one or more kinks in the room temperature (RT) IV-characteristic being a clear indication for the existence of multiple barriers. The characteristics were modelled by assuming a parallel connection of two or more individual diodes [5]. From the model sets of the characteristic parameters (ideality factor and barrier height) for the low and high barrier region were deduced. Fig. 1 (a) shows the experimental and modelled characteristic of a SC with three barriers, the ideality factor and barrier heights at RT are, (1.33, 0.73 eV), (1.9, 0.81 eV) and (2.36, 0.88 eV), respectively.

Using dark lock-in thermography (DLIT) low-barrier patches were visualized for small forward currents. Current transport at low forward voltages for low temperatures occurs primarily through such patches. The overlay of DLIT amplitude and topography of the three barrier SC of Fig. 1 (a) is represented in Fig. 1 (b) and (c). For an applied voltage of about 1 V (Fig. 1 (b)), several low-barrier patches exhibit an increased amplitude of temperature modulation. The area of increased amplitude is enlarged for an voltage of 1.5 V (Fig. 1 (c)). If the forward voltage is increased such that the current density through the regions of different barrier heights becomes similar we observe a homogeneous DLIT signal (not shown). The origin for the local decrease of

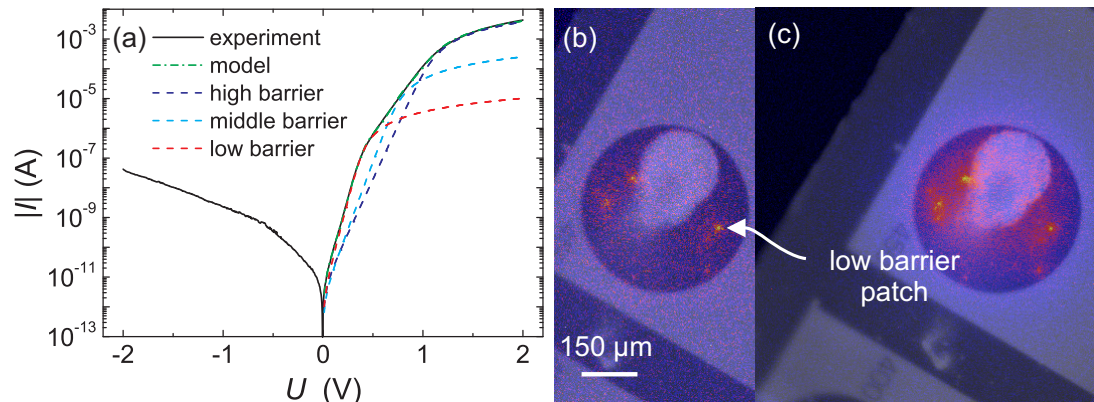


**Figure 8.10:** (a) *IV*-characteristic and corresponding three barrier fit of Pd/ZnO diode ( $T = 295$  K). (b) Overlay of DLIT amplitude and topography of the Pd/ZnO diode from (a). Applied voltage was (b) 1 V and (c) 1.5 V, respectively. Several low-barrier patches are visualized for both voltages. For 1.5 V the area around the patch exhibits an increased amplitude of temperature modulation.

barrier height was traced by energy dispersive X-ray spectroscopy on a cross section prepared by focused ion beam and is due to aluminium oxide particles in the buffer layer. However, this explanation cannot be extended to multi-barrier behavior SC on bulk ZnO [1, 2].

- [1] Martin W. Allen, M. M. Alkai, Steven M. Durbin: *Appl. Phys. Lett.* **89**, 103520 (2006), doi:10.1063/1.2346137
- [2] S.-H. Kim, H.-K. Kim, T.-Y. Seong: *Appl. Phys. Lett.* **86**, 112101 (2005), doi:10.1063/1.1862772
- [3] H. von Wenckstern, E. M. Kaidashev, M. Lorenz, H. Hochmuth, G. Biehne, J. Lenzner, V. Gottschalch, R. Pickenhain, M. Grundmann: *Appl. Phys. Lett.* **84**, 79 (2004), doi:10.1063/1.1638898
- [4] H. von Wenckstern, G. Biehne, R. Abdel Rahman, H. Hochmuth, M. Lorenz, M. Grundmann: *Appl. Phys. Lett.* **88**, 092102 (2006), doi:10.1063/1.1638898
- [5] D. Defives, O. Noblanc, C. Dua, C. Brylinski, M. Barthula, V. Aubry-Fortuna, F. Meyer: *IEEE Transaction on Electron Devices*, **449** (1999) doi:10.1109/16.748861

## 8.9 ZnO-based microresonators – design, photonic mode structure, and mode occupation

R. Schmidt-Grund, C. Sturm, H. Hilmer, T. Michalsky, B. Rheinländer, M. Grundmann

Microresonators are artificial, so-called "photonic" crystals for light where a photonic impurity mode, the so-called cavity-photon mode, is placed within a photonic band gap (Bragg stop-band) of, in the planar case, a 1D photonic band structure. Photons can massively occupy the cavity-photon mode, caused in their huge density of states, with a very high lifetime. If such a photonic system is in resonance with an electronic system, two regimes of coupling can occur, namely the weak and strong coupling regime. In the weak coupling regime, the mode structure of both systems does not alter each

other, but if these modes are occupied, the lifetime and density of states of the photonic system influence the decay rates of the electronic excitations (Purcell effect, Sec. 8.9.4). If the lifetimes of both, the photonic and the electronic (radiative lifetime) system, are higher than their decay rates, both systems couple strongly resulting in bosonic quasiparticles, the so-called cavity exciton-polaritons. The dispersion of these particles is characterized by, in the simplest case, two branches, the lower and the upper polariton branch (LPB and UPB, respectively), which show an anticrossing signature. This causes a varying curvature in dependence on the momentum, where the actual shape is strongly affected by the excitonic or photonic fraction of the polaritons, governed by the detuning between the non-interacting photonic and excitonic resonances. These light particles now can scatter in their ground state (Sec. 8.9.2) which can be massively occupied, leading to a coherent state, the so-called dynamic analogon to the equilibrium Bose-Einstein-Condensate, as predicted for ZnO, even at room temperature and above. Such a massive occupation is possible only, if electronic or photonic potential traps with an extent of the coherence length of such a condensate (in the order of some microns) are present (Sec. 8.9.3).

Our microresonators in general consist of a ZnO-based cavity and a ZnO-based active medium, sandwiched between two all-oxide Bragg reflectors (BR) which are considered as a 1D photonic crystal. Yttria stabilised zirconia and  $\text{Al}_2\text{O}_3$  are used as BR materials. The samples are grown by means of pulsed laser deposition (PLD) typically at temperatures of (150 – 650) °C and an oxygen background pressure of (0.02 – 0.002) mbar on *c*-sapphire substrates. The use of ZnO-based wurtzite structure cavity materials, which are optically uniaxial, causes some specialities in the PLD-growth properties and in the optical mode structure. For the growth, there is a competition between high-quality electronic properties and smooth layer interfaces (high-quality photonic system). One attempt for the realization of a well defined electronic system is to use quantum wells as active medium (Sec. 8.9.4). For the photonic system, the optical uniaxiality of ZnO-based materials requires a general approach for the description of the mode properties as the dispersion and the lifetime of the photons occupying the cavity-photon mode (Sec. 8.9.1). The mode properties as well as the occupation of these modes with photons, excitons, or exciton-polaritons and their corresponding lifetime was investigated by means of spectroscopic ellipsometry, reflection spectroscopy, and photoluminescence (PL) spectroscopy (time-integrated – cw and time-resolved). For the PL measurements, the microresonators were excited by a HeCd laser ( $\lambda = 325$  nm, cw) or a tripled Ti:Sapphire femtosecond-pulse laser ( $\lambda = 360$  nm or 264 nm).

### 8.9.1 Cavity-photon dispersion in anisotropic planar microresonators

For the description of the exciton-polariton dispersion the properties of the uncoupled cavity-photon modes have to be known. Therefore we developed a numerical approach in order to calculate the dispersion of the cavity-photon modes (in energy and lifetime) and to take into account the optical anisotropy of the cavity material as well as the finite size of the Bragg reflector (BR). The situation can be simplified in optically uniaxial cavity materials with the optical axis parallel to the surface normal as it is the case for the microresonators presented in the Secs. 8.9.2 - 8.9.4. Here, the microresonators possess a rotation symmetry so that the cavity-photons are degenerated at zero in-plane wave vector for the two linear polarizations (perpendicular (s) and parallel (p) polarized to the

plane of propagation). For the s-polarized cavity-photons the dispersion is exemplarily shown in Fig. 8.11a for a ZnO-based microresonator designed for the visible spectral range. Since the penetration depth of the electromagnetic wave into the BR differs for the two polarizations for non-zero in-plane wave vector, the energy of the cavity-photon splits up for the two polarizations, even for isotropic microresonators, which is known as TE-TM splitting. Due to the rotation symmetry, only the p-polarized cavity-photons are affected by the optical anisotropy. For a positive birefringent material, e.g. ZnO, the energy of the p-polarized cavity-photons is slightly reduced compared to that one of an isotropic cavity with  $n = \sqrt{\varepsilon_{\perp}}$ , whereas for such with a negative birefringence the energy is slightly enhanced. This causes also a change of the energy splitting (Fig. 8.11b). For the conventionally used wide bandgap cavity materials (ZnO and GaN), this change of the energy splitting is in the same order of magnitude as the splitting itself. Therefore the anisotropy has to be considered for a precise description of the energy splitting in these microresonators. For a general orientation of the optical axis, two cavity-photon modes appear in the s- and p-polarized spectrum, since the polarization of the two waves which propagate within the cavity is a linear combination of the s- and p-polarized one. Therefore the resonance condition of the microresonator can be fulfilled twice for each polarization. The impact of the anisotropy on the lifetime of the cavity-photons can be neglected, since it is mainly determined by the reflectivity of the BR. The change of the lifetime caused by the anisotropy was found to be less than 1%.

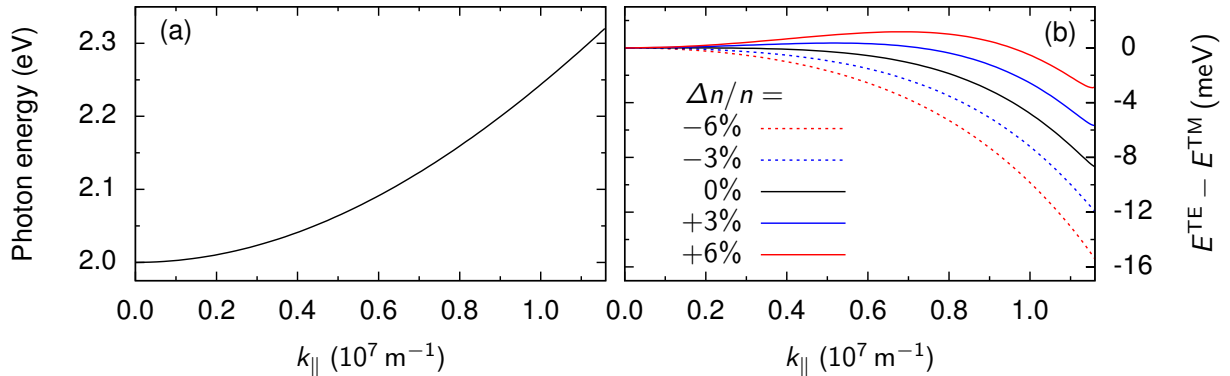


**Figure 8.11:** (a) The dispersion of the s-polarized cavity-photons for a ZnO-based microresonator ( $\Delta n/n = (n_{\parallel} - n_{\perp})/n_{\perp} = 3\%$ ). (b) The change of the TE-TM splitting for different values of the birefringence. (The optical axis is parallel to the surface normal).

### 8.9.2 Non-linear occupation of the lower polariton branch in a ZnO-based microresonator

For the realization of a massive occupation of the ground-state with exciton-polaritons the design of the microresonator is essential. For wide bandgap materials two opposed detuning ranges were reported to be the optimum one at room temperature: For ZnO-based microresonators numerical simulations by R. Johne *et al.* [1] yield a large positive detuning as the optimum one whereas Butté *et al.* [2] obtained experimentally that for GaN-based microresonators a large negative detuning is preferred. Therefore, excitation dependent measurements were performed. The microresonator has a wedge-shaped

cavity, allowing to change the detuning ( $\Delta = E_x - E_C$ ), i.e. the difference between uncoupled exciton ( $E_x$ ) and cavity-photon energy ( $E_C$ ), by the spot position on the microresonator.

For an intermediate detuning range ( $|\Delta| < 20$  meV) a superlinear enhancement of the lower polariton branch (LPB) occupation is obtained with increasing excitation density at  $T = 10$  K (Fig. 8.12). For large negative detunings ( $\Delta \approx -45$  meV) a superlinear enhancement of the ground-state is also observable. However the strongest enhancement is observed at the bottleneck region and not at the ground state. This we attribute to the fact, that the large negative detuning causes a large change of the curvature of the LPB in this region and therefore a large bottleneck effect. This hinders an efficient scattering of exciton-polaritons into the ground-state. For a large positive detuning ( $\Delta \approx 50$  meV), a tendency for a superlinear enhancement is observed for intermediate excitation densities. However, this enhancement is similar for all investigated in-plane wave vectors. Responsible for this finding is that the optical potential trap, formed by the bottleneck, at large positive detunings is too flat for capturing the exciton-polaritons at the ground-state. These results indicate that at  $T = 10$  K an intermediate detuning range ( $|\Delta| < 20$  meV) is preferred in order to reach a condensation of exciton-polaritons. By increasing the temperature, we obtained that this optimum detuning range shifts to negative values. These findings are in agreement with the experimental observation in GaN-based microresonators [2].

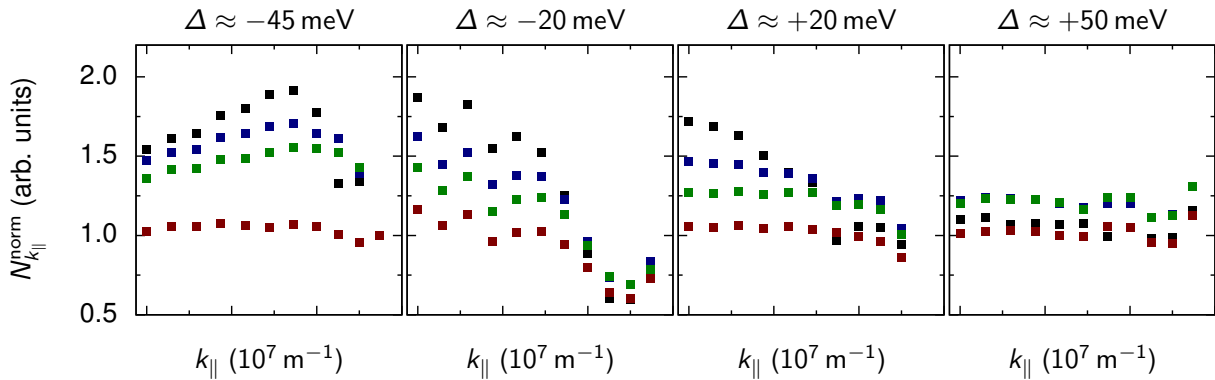


**Figure 8.12:** The normalized occupation number (normalized with respect to the excitation density) in dependence on the excitation density (black squares:  $P = 500$  W/cm<sup>2</sup>, blue squares:  $P = 130$  W/cm<sup>2</sup>, green squares:  $P = 40$  W/cm<sup>2</sup>, red squares:  $P = 2$  W/cm<sup>2</sup>).

### 8.9.3 ZnO mesa-structures in planar microcavities

For a ZnO-based microresonator with a wedge-shaped cavity a slightly superlinear behaviour of the LPB occupation was observed at low temperatures ( $T < 130$  K) (cf. Sec. 8.9.2). Unfortunately, a macroscopic occupation at the ground-state was not reached in these experiments. Responsible for this might be that the area of the photonic potential trap, induced by the exciting laser beam ( $\varnothing \approx 200$   $\mu$ m), is too large for an efficient capture of the exciton-polaritons in the ground state within an area corresponding to the coherence length of the condensate (typically some microns), and the potential well is too smooth. Therefore, the polaritons escape too fast from this area. The excitation density which would be needed to overcome this escape and so for the formation

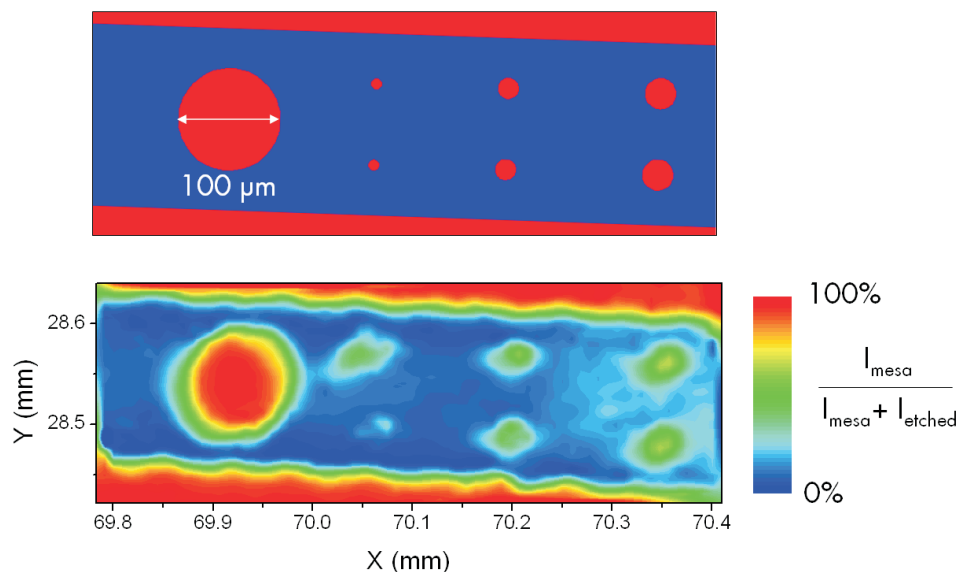


**Figure 8.13:** (a) Schematic of a photolithography mask for mesas and (b) normalized photoluminescence intensity ( $I_{\text{mesa}}/(I_{\text{mesa}} + I_{\text{etched}})$ ) of the lower polariton emission of a microresonator with mesas as photonic potential traps in dependence on the lateral position.  $I_{\text{mesa}}$  and  $I_{\text{etched}}$  denote the intensity of the lower polariton emission of the mesa and etched area, respectively.

of a condensate at the ground state is too large, so that the strong coupling regime breaks down before the critical density is reached. To overcome this disadvantage, a ZnO-based microresonator with an intentionally structured cavity was prepared.

So in contrast to samples mentioned above the ZnO-cavity was structured using a photolithography mask (Fig. 8.13a) with mesas with diameters ranging from 10 μm . . . 100 μm using a positive resist. The different diameters were chosen in order to investigate the impact of the size of the mesa on the cavity-photon dispersion. By a subsequent etching in highly diluted phosphoric acid the mesa structure is obtained. Here, the mesas have a slightly larger cavity thickness than the etched part of the cavity ( $\Delta d \approx 3$  nm). That means that the cavity-photon energy is lower for the cavity-photons in the mesa compared to the one in the etched surrounding area ( $\Delta E \approx 20$  meV). This leads to a lowering of the energy of the LPB within the mesa in the strongly coupled system. The normalized photoluminescence intensity of the LPB of the mesa (normalized to the summed LPB peak intensity from the mesa and the surrounded area) is shown in Fig. 8.13b. Thereby, the mesa structures are well observed. The edges of the mesas do not appear very sharp in the PL scan image due to the rather high spot diameter of about 50 μm.

#### 8.9.4 Planar microresonators with a MgZnO/ZnO-quantum well

Another attempt for the realization of a long-time stable coherent state is to improve the properties, especially the lifetime, of the electronic system, especially at elevated temperatures. Quantum well (QW) excitons are suitable, caused in the confined wavefunction and defined distribution within a small area compared to the widely distributed bulk excitons in a bulk microresonator as discussed above. Furthermore, in bulk microresonators the thickness of the cavity is in the same range as the penetration

depth of the light at the exciton energy and higher and therefore the higher branches (e.g. the upper polariton branch - UPB) are not observable. We investigated a planar microresonator with a MgZnO cavity material, acting as barrier for a 4 nm ZnO QW which is placed in the center of the cavity. The MgZnO barrier is transparent in the spectral range of the QW exciton emission and where the UPB is expected, at least for small emission angles. In order to correctly attribute the observed effects to be caused in the properties of the resonator, a so-called "half-resonator", which was a part of the resonator sample that was cleaved off before the top BR was deposited, was used for comparative investigations.

An anti-crossing between the excitonic mode and the photonic mode was not observed in angular-resolved photoluminescence (PL) and reflectivity measurements of the microresonator at  $T = 10$  K (c.f. Fig. 8.14), so that the strong coupling regime cannot be confirmed. For a detailed understanding of the interaction between the excitonic (QW) and the photonic (cavity-photons) system, e.g. the lifetime modification of the QW excitons within a resonator in the weak coupling regime (Purcell effect), time-dependent PL spectroscopy (t-PL) was performed. Thereby the dispersion relation of the microresonator has been specifically sampled for selected angles in order to understand the excitonic recombination processes as a function of the mode density within the Bragg stop band. Comparison of t-PL spectra of the resonator with spectra from the half-resonator showed a maximum decrease of the decay rate of 24 %, caused by the reduced mode density in the resonator, giving indications for the Purcell effect. This is a first step towards the possibility to precisely control the lifetime and associated emission rate of photons, which is of major significance in view of the realisation of low-threshold laser and manipulation of single atoms in the cavity.

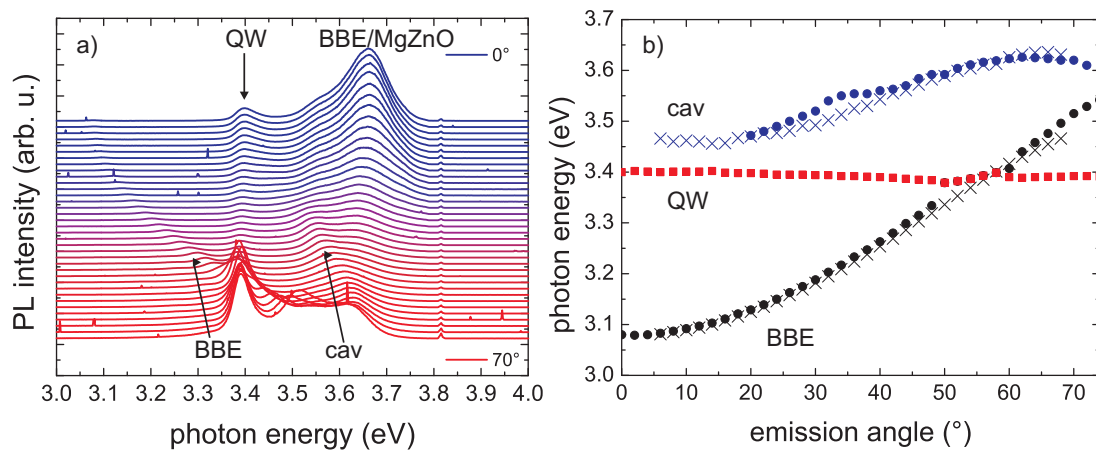


**Figure 8.14:** (a) Photoluminescence spectra of the QW-microresonator for p-polarisation as a function of the emission angle (b) Comparison of the dispersion of the cavity-photon mode (cav) and the lower Bragg band-edge mode (BBE) obtained from reflectivity (cross) and PL measurements (discs) (p-polarisation).

This work has been supported by Deutsche Forschungsgemeinschaft within the research project "Bose-Einstein-Kondensation von Exziton-Polaritonen bei Raumtemperatur" (GR1011/20-1) and the Graduate School "Leipzig School of Natural Sciences - Building with Molecules and Nano-objects (BuildMoNa, GS185) and by the European Social Fund (ESF).

- [1] R. Johne, D. D. Solnyshkov, G. Malpuech: Appl. Phys. Lett. **93**, 211105 (2008).  
 [2] R. Butté, J. Levrat, G. Christmann, E. Feltn, J.-F. Carlin, N. Grandjean: Phys. Rev. B **80**, 233301 (2009).  
 [3] C. Sturm, H. Hilmer, R. Schmidt-Grund, M. Grundmann: New. J. Phys. **11**, 073044

We acknowledge A. Müller and M. Stölzel for the time resolved PL measurements and discussions and M. Hahn for photolithography mask preparation.

## 8.10 Index matching in BaTiO<sub>3</sub> / SrTiO<sub>3</sub> heterostructures

T. Böntgen, J. Zippel, R. Schmidt-Grund, M. Lorenz, M. Grundmann

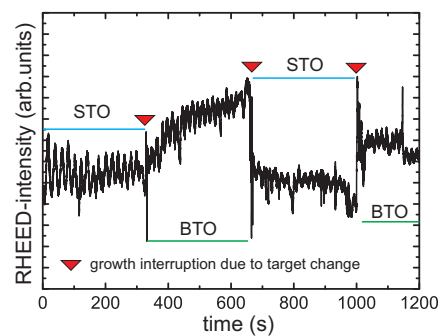


**Figure 8.15:** RHEED oscillations observed during growth of a BTO/STO heterostructure.

We have grown SrTiO<sub>3</sub> (STO) and BaTiO<sub>3</sub> (BTO) thin films and heterostructures under different oxygen partial pressures using pulsed laser deposition with in-situ monitoring of the growth by Reflection High Energy Electron Diffraction (RHEED). As shown in Fig.8.15 we are able to observe oscillations indicating the growth of several monolayers. Therefore the growth speed as well as the growth mode can be controlled for BTO/STO heterostructures. The optical properties have been determined using spectroscopic ellipsometry. As is known the band gap energy ( $E_G$ ) and therewith the refractive index below  $E_G$  is strongly affected by distortions in the crystal lattice. This can be caused in strain, poor crystallinity, or oxygen vacancies.[1][2] We have used this property to tune the refractive index of STO to match that of BTO for a specific wavelength  $\lambda_0$ , but keeping different electronic properties. The band structures of BTO and STO show allot of similarities. This is especially true for the low energy transitions. The lowest conduction band is constituted mainly by Ti 3d orbitals, as for most ATiO<sub>3</sub> perovskites. Admixture from the A atom (Ba,Sr) orbitals significantly influences the band-to-band transitions at higher energies only. The topmost valence band consists mainly of oxygen 2p orbitals, with only small admixtures from Sr or Ba.[3] These properties cause a similar low energy dielectric function or rather refractive index, especially for the spectral range near  $E_G$  and below (Fig. 8.16). Hence, distorting the crystal lattice, the below band gap optical properties can be tuned by altering the oxygen partial pressure and therewith the oxygen content in the film. The refractive index spectra for STO thin films grown at different oxygen partial pressures are shown in Fig.8.16 (right). The low energy refractive index increases with increasing oxygen partial pressure. We relate this to the incorporation of oxygen vacancies.[2] When comparing the refractive index to that of

a commercial STO substrate the dielectric function for the film with the highest partial pressure is close to that of the substrate.

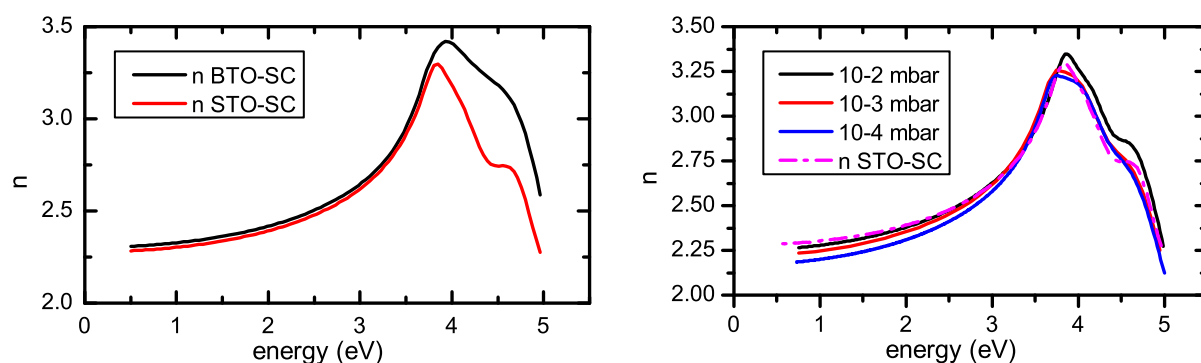


**Figure 8.16:** Refractive index spectra of BaTiO<sub>3</sub> and SrTiO<sub>3</sub> substrates (left) and SrTiO<sub>3</sub> thin films grown at different oxygen partial pressures (right).

The tunability of the refractive index can be used to match that of STO to that of BTO. This is particularly useful in multilayer structures to reduce (or enhance) the reflectivity of the system. To demonstrate this we have grown two samples with stacks of alternating BTO and STO layers with thickness (55 – 60 nm) and periodicity matching  $\lambda_0$ , corresponding to an energy of  $\approx 2.7$  eV. For such a system, the reflectivity at  $\lambda_0$  depends on the difference of the refractive indices. For the first sample the refractive index of STO was chosen to be different to that of BTO for  $\lambda_0$  and for the second one it was matched. As can be seen in Fig.8.17(left) the first sample shows a clear peak at 2.7 eV originating from the increased reflectivity due to the layered structure. In the second sample (Fig.8.17(right)) no clear peak is visible, indicating the index matching.

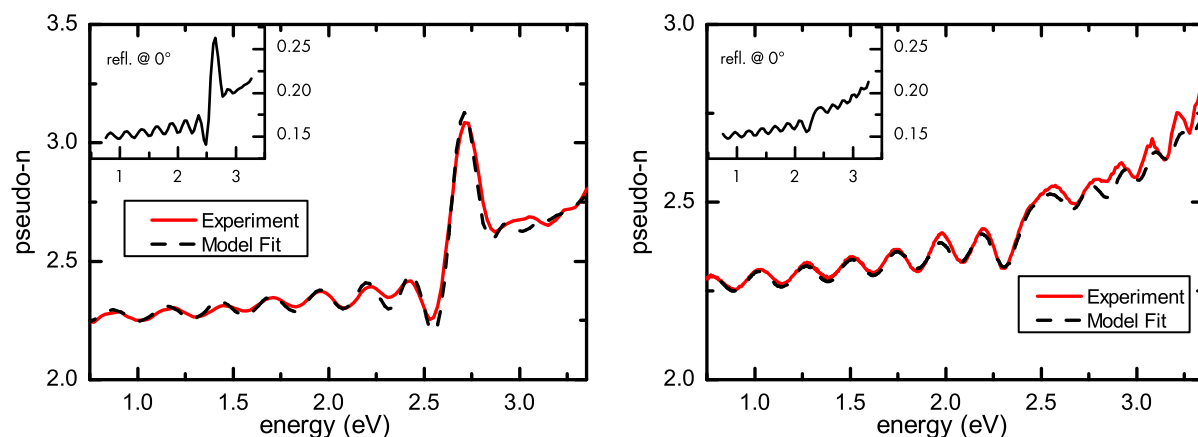


**Figure 8.17:** Experimental (red) and model calculated (black) pseudo-refractive index spectrum for a BTO/STO layer structure. left: No index matching, the peak in the curves is clear evidence for a strong reflectivity at  $\approx 2.7$  eV (c.f. inset). right: Index matching, the experimental curve do not show any prominent peak. Insets: model calculated reflectivity of the layer stack.

This work has been supported by Deutsche Forschungsgemeinschaft in the framework of SFB 762 "Functionality of Oxide Interfaces".

[2] A. Dejneka: *Fisika Twerdogo Tela*, 52, 1943 (2010)

[3] M. Cardona: *Phys. Rev.* 140 2A, A651 (1965) doi:10.1103/PhysRev.140.A651

## 8.11 Investigation of the temperature-dependent exciton localization in MgZnO

A. Müller, M. Stölzel, G. Benndorf, M. Grundmann

Time-resolved photoluminescence (PL) measurements have been performed on  $\text{Mg}_x\text{Zn}_{1-x}\text{O}$  thin films in dependence on temperature to investigate the exciton localization within the alloy. The samples, which have been grown on a-plane sapphire substrates, show the characteristic S-shaped shift of the luminescence maximum typically observed for alloys (not shown here).

For a thin film with  $x = 0.18$  measured transients are depicted in Fig. 8.18 (a) for selected temperatures. Up to 40 K, two decay processes can be clearly distinguished. The fast process is attributed to excitons bound at impurities, while the slow process results from the recombination of excitons localized within alloy-potential fluctuations [1]. With increasing temperature, a thermally activated transfer between states with different radiative decay times can be observed. For example, carriers are transferred from states with short lifetimes to states with slower decays, indicated by the slowdown of the decay at small times. Additionally, the nonradiative recombination gains importance, leading to a strong reduction of the observed mean luminescence decay times above 50 K. This correlates with the transfer of excitons into free states[2] above the mobility edge, where they can reach defects, enforcing the nonradiative decay. Above 120 K, most excitons have been transferred to free states, leading to the slight upward bending of the mean decay time visible in the Arrhenius plot in Fig. 8.18 (b).

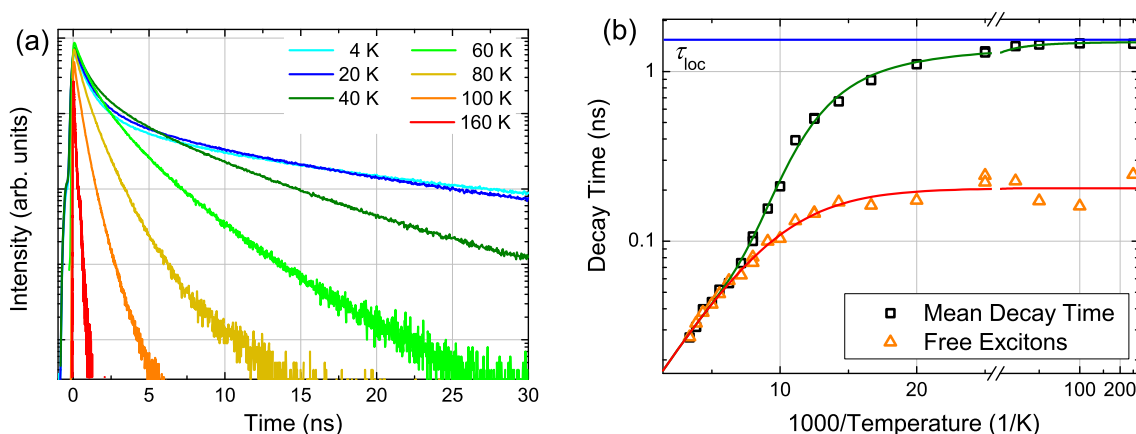


**Figure 8.18:** (a) PL transients measured at the spectral emission maxima of a  $\text{Mg}_{0.18}\text{Zn}_{0.82}\text{O}$  thin film for different temperatures. (b) The extracted decay times shown in an Arrhenius plot of this sample can be modeled by taking into account a superposition of bound/localized excitons with a temperature-independent mean decay time at low temperatures and the fast recombination of free excitons, dominating the emission above 150 K.

Time-delayed PL spectra have been calculated from transients measured at different spectral positions by summing intensity within selected time intervals. In Fig.

8.19 (a), the determined spectra are shown for  $T = 5$  K. The fast decay of the impurity-bound excitons is found on the low-energy side of the spectrum, the slowly redshifting emission from alloy-localized excitons can be observed on the high energy side of the spectrum. This shift of the emission energy takes place on the scale of 100 ns and can be attributed to temperature-independent tunneling processes of excitons from local potential minima into the deepest lying states.

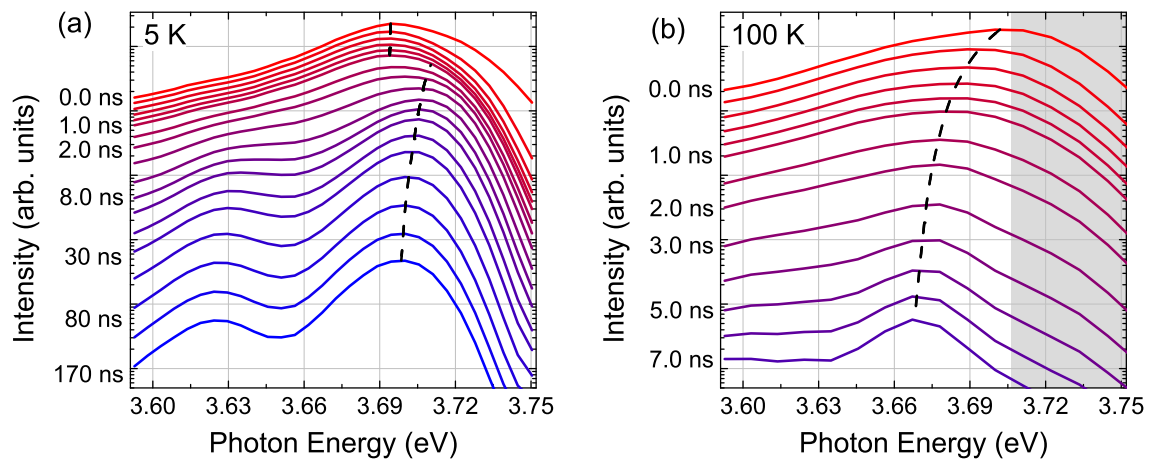


**Figure 8.19:** Time-delayed spectra of a  $\text{Mg}_{0.18}\text{Zn}_{0.82}\text{O}$  thin film measured for (a) 5 K and (b) 100 K. In (a), the fast decay of the bound excitons (on the low-energy side and the much slower decay of the localized excitons is marked. On the high energy side, the initial decay of the free excitons can be observed only in the first spectrum. For (b), the fast red-shift attributed to the thermal activation of the localized excitons is visible, while the fast decay of the free excitons can already be observed as a shoulder on the high-energy side of the spectrum (grey bar).

In contrast, the time-delayed spectra depicted in Fig. 8.19 (b), which were measured at 100 K, show a strong red-shift of the emission maximum on the scale of a few nanoseconds. This can be explained by the thermal activation of the excitons into free states observable on the high energy side of the spectra. While nearly all shallow localized states are activated at  $t = 1$  ns, deeper states partially resist the thermal activation, indicated by the stagnating redshift at longer times.

This work has been supported by Deutsche Forschungsgemeinschaft within the Graduate School "Leipzig School of Natural Sciences - Building with Molecules and Nano-objects (BuildMoNa, GS185).

- [1] A. Müller, M. Stölzel, C. Dietrich, G. Benndorf, M. Lorenz, M. Grundmann: *J. Appl. Phys.* **107**, 013704 (2010) doi:10.1063/1.3270431
- [2] C.P. Dietrich, M. Lange, G. Benndorf, J. Lenzner, M. Lorenz, M. Grundmann: *New J. Phys.* **12**, 033030 (2010) doi:10.1088/1367-2630/12/3/033030

## 8.12 Photoluminescence and transmission spectroscopy on ZnO/MgZnO quantum well structures

M. Stölzel, J. Kupper, A. Müller, G. Benndorf, M. Brandt, M. Lorenz and M. Grundmann

We performed photoluminescence (PL) and transmission (TM) measurements on ZnO/MgZnO quantum wells (QWs) grown by pulsed laser deposition in an oxygen ambient on a-sapphire substrates ( $T = 650\text{ }^{\circ}\text{C}$ ,  $p = 0.04\text{ mbar}$ , energy density =  $2.4\text{ J/cm}^2$ ).

For the deposition of the QW structure it is necessary to use a buffer layer on top of the substrate. In order to investigate the transmission properties of the QW, the buffer layer material has to be transparent in this spectral range. Therefore, we replaced the formerly used ZnO [1] by a MgZnO buffer layer with Mg contents up to 39%. This new buffer also enables the observation of the phonon replicas of the QW transition peak in PL experiments. The Mg content in the barrier layers was set to 16%.

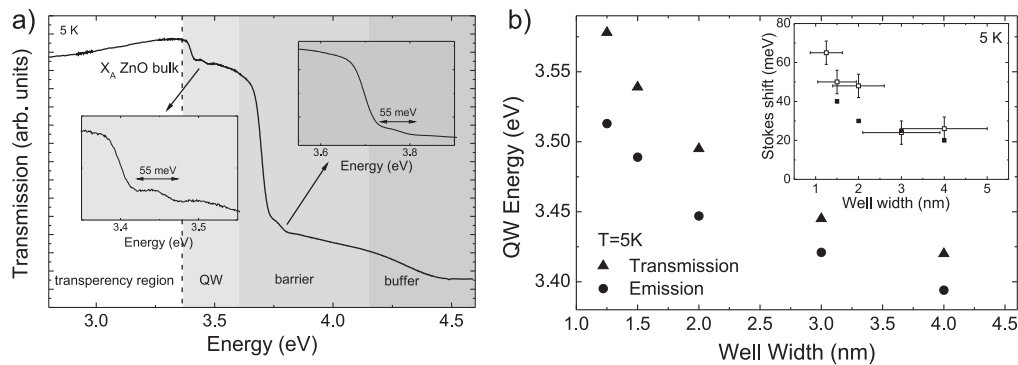


**Figure 8.20:** a) Transmission spectrum of a ZnO/MgZnO quantum well with a nominal thickness of 4 nm at 5 K. The insets show the transmission regions of the QW and the barrier layers. b) Energetic position of the transmission minimum and the photoluminescence maximum of QWs with different thickness. The inset shows the determined Stokes shift (open squares) in dependence on the well width compared to data obtained by Makino et al.[3] (full squares).

In Fig. 8.20 a) the TM spectrum of a QW with a nominal thickness of 4 nm is shown. The TM minima caused by the absorption of the QW, the barrier layers, and the buffer layer are clearly visible in the expected spectral regions. Both, the transmission in the spectral range of the QW and the barrier absorption show a double structure. The energy difference between the two minima is found to be 55 meV for both cases (see insets). For the barrier this effect can be explained with the absorption due to an exciton-phonon-complex [2]. For the QW, the double structure might originate from the absorption of the weakly allowed C-exciton, an excited excitonic state in the QW, or also from an exciton-phonon-complex.

The energetic position of the QW emission respective absorption in PL and TM as function of the well width is depicted in Fig. 8.20 b). One observes that with increasing well width the confinement energy decreases as the luminescence maximum shifts to lower energies. The energetic difference between the TM minimum and the PL maximum (the so-called Stokes shift) decreases with increasing well width (see inset). This tendency can be explained by the growing influence of thickness fluctuations and alloy broadening on the exciton wave function for decreasing well width. The obtained Stokes shifts are in good agreement with previously reported values.

This work has been supported by Deutsche Forschungsgemeinschaft within the Graduate School "Leipzig School of Natural Sciences - Building with Molecules and Nano-objects (BuildMoNa, GS185) and the European Social Fund (ESF).

- [1] S. Heitsch, G. Zimmermann, D. Fritsch, C. Sturm, R. Schmidt-Grund, C. Schulz, H. Hochmuth, D. Spemann, G. Benndorf, B. Rheinländer, Th. Nobis, M. Lorenz, and M. Grundmann: *J. Appl. Phys.* **101**, 083521 (2007), doi:10.1063/1.2719010
- [2] A. Müller, G. Benndorf, S. Heitsch, C. Sturm, and M. Grundmann: *Solid State Comm.* **148**, 570 (2008), doi:10.1016/j.ssc.2008.09.045
- [3] T. Makino, Y. Segawa, M. Kawasaki, and H. Koinuma: *Semiconductor Science and Technology* **20**, S78 (2005), doi:10.1088/0268-1242/20/4/010

## 8.13 Thermal stability of ZnO/ZnCdO/ZnO double heterostructures

M. Lange, C.P. Dietrich, G. Benndorf, J. Zúñiga-Pérez, M. Lorenz, M. Grundmann

$\text{Zn}_{1-x}\text{Cd}_x\text{O}$  is a semiconductor whose bandgap energy can be tuned between 1.75 eV and 3.4 eV. Therefore, it is applied in ZnO-based heterostructures that are necessary for the efficiency of optoelectronic devices such as light emitting or laser diodes. For device fabrication, the behavior of  $\text{Zn}_{1-x}\text{Cd}_x\text{O}$  thin-films and heterostructures during post-growth thermal processing is an important issue. Typically, for the dopant activation and metal-contact formation, thermal annealing temperatures above 600 °C are required that are far above the growth temperature of  $\text{Zn}_{1-x}\text{Cd}_x\text{O}$ .

In this regard, we studied the thermal stability of ZnO/ZnCdO/ZnO double heterostructures, grown by pulsed laser deposition [1]. Three samples grown at different temperatures, oxygen partial pressures and with different ZnCdO thicknesses were studied. They were annealed at seven different temperatures and photoluminescence spectra were recorded at  $T = 2$  K (see Fig. 8.21 a). The  $\text{Zn}_{1-x}\text{Cd}_x\text{O}$  related luminescence maximum shifts to higher energies with increasing annealing temperatures. For annealing temperatures up to 720 °C the shift is smaller than 10 meV, showing that the structures are relatively stable up to this temperature. The shift itself is explained by a diffusion process causing a reduction of the Cd-content of the  $\text{Zn}_{1-x}\text{Cd}_x\text{O}$  layer or rather a lowering of the Cd-profiles maximum along the growth direction of the structure.

Using growth-information (thickness of  $\text{Zn}_{1-x}\text{Cd}_x\text{O}$  and initial Cd-content) and luminescence information (maximum Cd-content of the profile) the diffusion coefficient was determined for each annealing temperature. It follows an Arrhenius equation from which the activation enthalpy of the diffusion process and the pre-exponential factor were extracted (see Fig. 8.21 b). For the activation enthalpy values between 2.1 eV and 3.5 eV are determined for the different samples. Non-stoichiometry and defect density that strongly depend on the growth conditions, should be the reason for the differences in the enthalpies of the samples that were grown at different temperatures/oxygen partial pressures.

This work has been supported by Deutsche Forschungsgemeinschaft within the Graduate School "Leipzig School of Natural Sciences - Building with Molecules and Nano-objects (BuildMoNa, GS185) and the European Social Fund (ESF).

- [1] M. Lange, J. Zippel, H. Hochmuth, G. Benndorf, M. Lorenz, M. Grundmann: *The Physics Institutes of Universität Leipzig, Report 2007*, M. Grundmann (Ed.), p.163

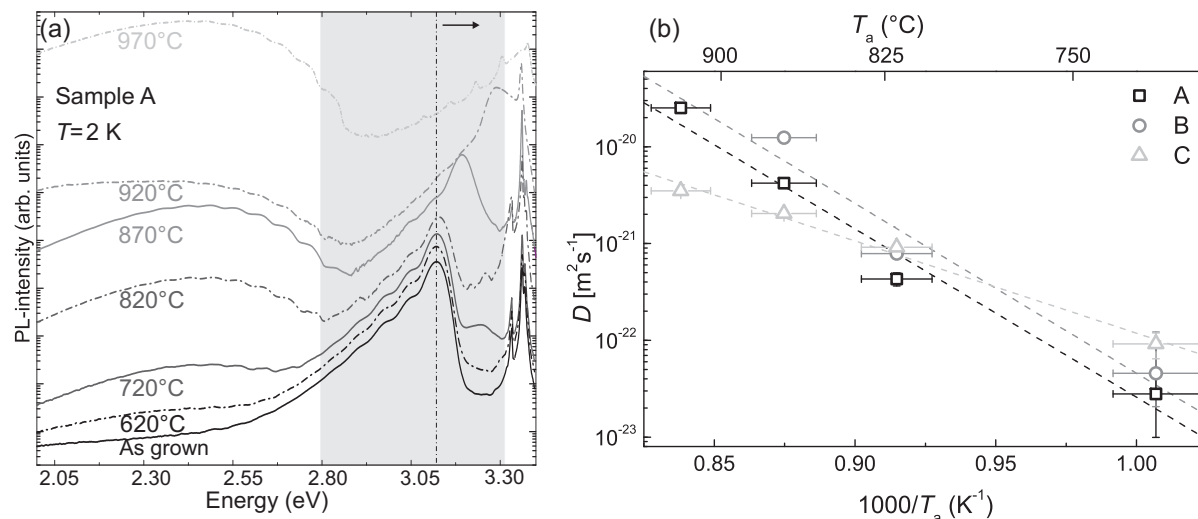


**Figure 8.21:** (a) PL-spectra of the ZnO Zn<sub>1-x</sub>Cd<sub>x</sub>O ZnO double heterostructures annealed at different temperatures measured at a temperature of 2 K (b) Arrhenius-plot of the diffusion coefficient for three samples.

## 8.14 MgZnO/ZnO quantum well nanowire heterostructures with large confinement energies

M. Lange, C.P. Dietrich, J. Zúñiga-Pérez, H. von Wenckstern, M. Lorenz, M. Grundmann

Nanostructures, particularly nanowires (NWs), experience a large interest due to their applicability as building blocks for optoelectronic devices on the nano-scale and their outstanding optical and electrical properties. However, the efficiency of modern devices is based on the usage of semiconductor heterostructures (HS). In this respect an approach to enhance the emission properties of NWs is the incorporation of quantum wells (QWs). They offer a tunable bandgap and allow a better performance in optical devices in comparison with bulk layers.

Due to a lack of Mg<sub>x</sub>Zn<sub>1-x</sub>O NWs in a low lateral density that exhibit a high Mg-content and high crystalline quality, an alternative approach is selected. ZnO NWs that are easily obtainable, are surrounded by Mg<sub>x</sub>Zn<sub>1-x</sub>O/ZnO/Mg<sub>x</sub>Zn<sub>1-x</sub>O QWs. Using a high pressure PLD chamber the ZnO NWs are first grown in a low lateral density. This secures a homogeneous QW-shell growth in the conventional PLD chamber. A barrier with high a Mg-content of 25 % and a large bandgap of 3.85 eV is applied as this energy restricts the emission energy of the QW energy as an upper limit.

Figure 8.22 shows an idealized growth scheme and room temperature cathodoluminescence (CL) spectra of the axial and radial QWs on the NW for different QW-thicknesses.

Besides the luminescence of the ZnO core and the Mg<sub>x</sub>Zn<sub>1-x</sub>O shell the luminescence of the QWs is observed. The QWs in axial and radial direction were clearly distinguished by their spatial luminescence distribution using scanning CL measurements. The QW emission energy was tuned in a large spectral range from 3.42 eV up to 3.68 eV.[1] Prior to that, the largest QW-emission energy was significantly lower with 3.52 eV.[2] Due to the directed growth process during shell growth the growth rates in axial and

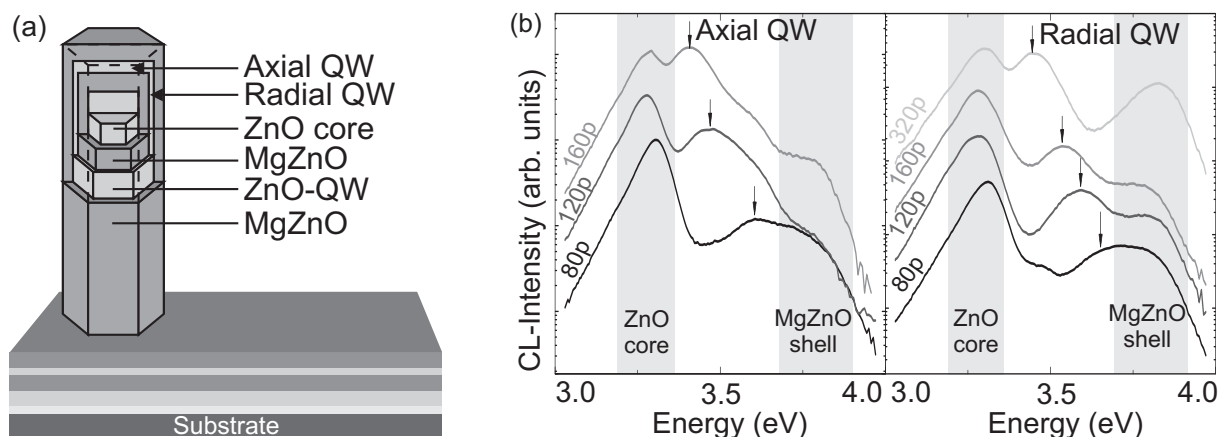


**Figure 8.22:** (a) growth scheme (idealized) of the  $\text{Mg}_x\text{Zn}_{1-x}\text{O}/\text{ZnO}$  QW NW-HS grown on freestanding ZnO NW. (b) Room temperature CL spectra of axial and radial QWs with different QW-thicknesses (number of ZnO pulses for QW). The baselines are shifted for clarity.

radial direction differ significantly, so that the respective QW emissions are observed at different spectral positions additionally to the different spatial origins. However, along the NWs' growth axis the luminescence energy of the radial QW is very homogeneous with a standard deviation of only 4 meV. Only in the upper 500 nm of the NW the luminescence energy increases which is explained by a locally reduced growth rate by up to 15%.

Finally, ZnO based quantum well nanowire heterostructures with large confinement energies up to 300 meV were obtained. A homogeneous emission of the radial quantum well was possible due to the low lateral density of the ZnO NWs, applied as core for the core/shell-structures.

This work has been supported by Deutsche Forschungsgemeinschaft within the Graduate School "Leipzig School of Natural Sciences - Building with Molecules and Nano-objects (BuildMoNa, GS185) and the European Social Fund (ESF).

- [1] M. Lange, C. P. Dietrich, J. Zúñiga-Pérez, H. von Wenckstern, M. Lorenz, M. Grundmann: *J. Vac. Sci. Technol. A*, 29, 03A104 (2011) doi:10.1116/1.3531709
- [2] W. I. Park, S. J. An, J. C. Yang, G.-C. Yi, S. Hong, Sangsu and T. Joo, M. Kim: *J. Phys. Chem. B*, 108, 15457 (2004) doi:10.1021/jp046559t

## 8.15 Strain distribution in bent ZnO microwires

C.P. Dietrich, M. Lange, F.J. Klüpfel, R. Schmidt-Grund, H. von Wenckstern, M. Grundmann

Nano- and microstructures are at the core of current semiconductor research on the pathway toward nanoscale and microscale technologies. Modern devices are complex and based on the usage of semiconductor heterostructures that underlie various strain effects due to lattice mismatch. As a consequence, device design is strongly correlated to strain engineering. Especially ZnO is a perfect material for the fabrication of strain generators and piezoelectric sensors. Therefore, the exact knowledge of strain-dependent

properties is even more of interest. We show that ZnO deformation parameters can easily be accessed in a precise manner by bending experiments of ZnO microwires[1].

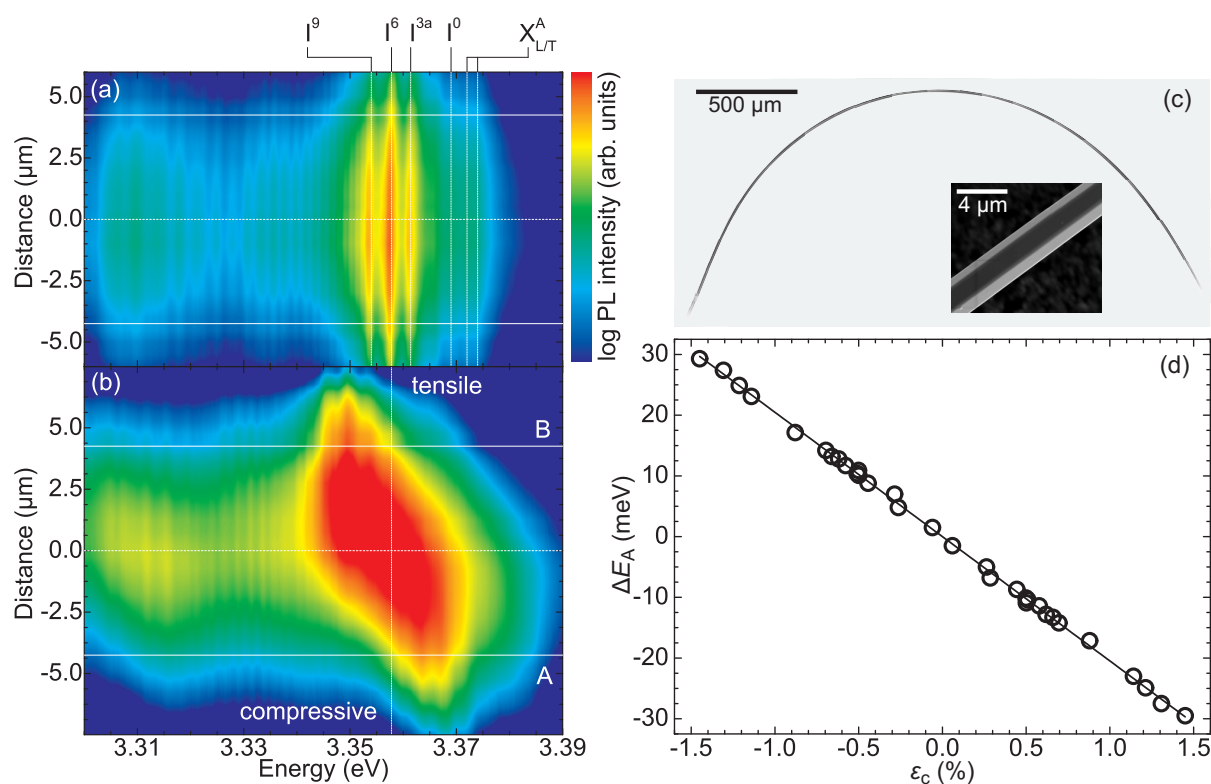


**Figure 8.23:** Low-temperature ( $T = 15$  K) PL linescan of a ZnO microwire with  $d = 8.5$  μm (a) before and (b) after bending, respectively. The center of the wire (neutral fiber) is set as zero for the position axis. The most prominent recombination peaks (indicated by vertical dotted lines) are labeled according to [2]. The edges of the microwire are highlighted by solid lines. (c) Composed optical microscopic and SEM image of a bent ZnO microwire. (d) Shift  $\Delta E_A$  of free A-exciton emission energy  $E_A$  vs. strain at low temperatures ( $T = 15$  K). The solid line represents a linear least-squares fit to the experimental data from six microwires with a slope of  $\partial E_A / \partial \epsilon_c = (-2.04 \pm 0.02)$  eV. Error bars are smaller than the symbol size.

The ZnO microwires are grown by carbothermal vapor phase transport [3]. We apply a uniaxial stress in ZnO microwires by bending. Therein, we are able to mechanically bend the wires to minimum radii of curvature of 400 μm and respective maximum  $c$ -axis strain of about  $\pm 1.5$  % (see Fig.8.23(c)). PL linescans perpendicular to the wire axis show maximum energetic shifts of the dominant excitonic recombination peaks of  $\pm 30$  meV. The compressive and tensile strain inside the wires is symmetrically distributed perpendicular to the wire axis (as can be seen in Fig.8.23(b)). For uniaxial stress, we determined the direct relation between energetic shift of the free A-exciton emission energy and strain to  $\partial E_A / \partial \epsilon_c = (-2.04 \pm 0.02)$  eV. We emphasize that within our experiments, it is possible to study large tensile stresses in materials which are not accessible by conventional pressure experiments.

This work has been supported by Deutsche Forschungsgemeinschaft within the Graduate School "Leipzig School of Natural Sciences - Building with Molecules and Nano-objects (BuildMoNa, GS185) and the European Social Fund (ESF).

- [1] C.P. Dietrich, M. Lange, F.J. Klüpfel, H. von Wenckstern, R. Schmidt-Grund, M. Grundmann: Appl. Phys. Lett. **98**, 031105 (2011). doi:10.1063/1.3544939
- [2] B.K. Meyer, H. Alves, D.M. Hofmann, W. Krügseis, D. Forster, F. Bertram, J. Christen, A. Hoffmann, M. Straßburg, M. Dworzak, U. Haboeck, A.V. Rodina: phys. stat. sol. **241**, 231 (2004). doi:10.1002/pssb.200301962
- [3] C.P. Dietrich, M. Brandt, M. Lange, J. Kupper, T. Böntgen, H. von Wenckstern, M. Grundmann: J. Appl. Phys. **109**, 013712 (2011). doi:10.1063/1.3530610

## 8.16 Characteristics of excitons in a 1D model alloy

A. Müller, M. Grundmann

In order to understand the carrier dynamics within  $A_xB_{1-x}$  alloys (e.g., considering  $Mg_xZn_{1-x}O$  as  $(MgO)_x(ZnO)_{1-x}$ ) model 1D electron-hole wave functions (WFs) have been calculated within the effective-mass approximation. In contrast to the classical approach where the exciton is considered as a hydrogen-like quasiparticle[1], here the discretized two-particle Schrödinger equation of electron and hole was solved. It was assumed that the single-particle potentials  $V_{e/h}(x_{e/h})$  of electron and hole, respectively, are determined by the random occupation of the corresponding crystal sites with the species A or B (where A shall be the constituent with the larger band gap). As the volume of the one-dimensional exciton is small compared to the 3D case, the band offsets between the two materials were scaled down in comparison to real alloys.

Using this ansatz, the partial differential eigenvalue equation

$$\left[ -\frac{\hbar^2}{2m_e}\Delta_{x_e} - \frac{\hbar^2}{2m_h}\Delta_{x_h} + V_e(x_e) + V_h(x_h) - \frac{C}{|x_e - x_h|} \right] \Psi(x_e, x_h) = E\Psi(x_e, x_h) \quad (8.2)$$

has been discretized and solved using the Arpack library [2]. In the equation,  $m_{e/h}$  are the effective masses of electron and hole, respectively, and  $C$  is an empirical constant to tune the exciton binding energy. Although this model still oversimplifies the situation within a real alloy, it can be applied to understand several properties of, e.g., absorption and emission processes.

2D plots of the probability amplitudes of selected two-particle WFs are shown in Fig. 8.24. Several cases can be distinguished. At lowest energies, the excitons are strongly localized as shown in Fig. 8.24 (a). Electron and hole can be found in a bound state only within a small band along the main diagonal where the two carriers are at the same position. Additionally, the exciton is confined along the main diagonal by the alloy potential fluctuations. As the energy of the exciton increases, the localization along the main diagonal decreases (see Fig. 8.24 (b)). The WF here spans several local potential minima. However, electron and hole can still be found near each other. This confinement is indicated by the small slope in Fig. 8.24 (e). For energies larger than the exciton binding energy, unbound states can be observed as shown in Fig. 8.24 (c). Electron and hole are spatially separated, there is only a small probability of presence along the main diagonal. A fourth case is shown in Fig. 8.24 (d), where electron and hole are not bound and their WF spans the whole 2D phase space volume. This leads to the large slope in Fig. 8.24 (e) for these states.

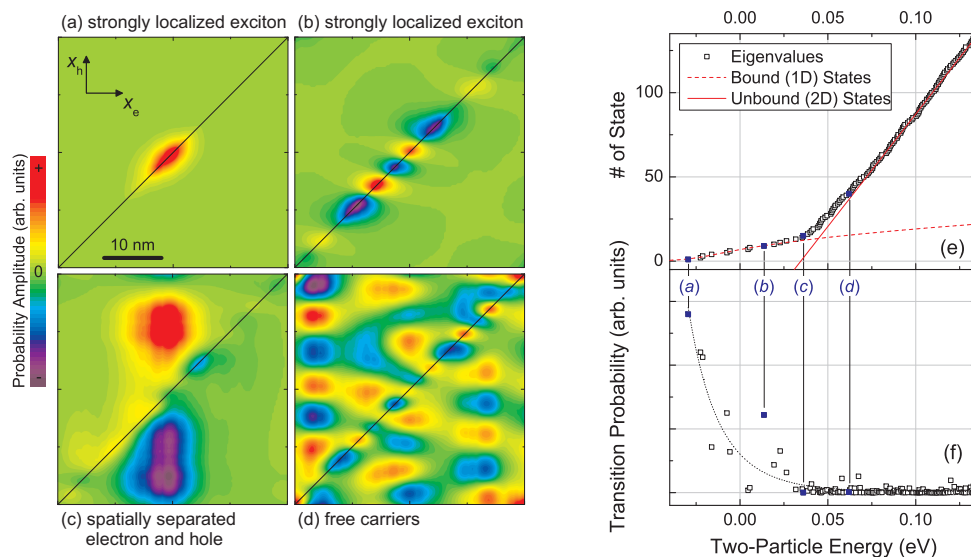


**Figure 8.24:** (a)-(d) Probability amplitudes of the electron-hole WFs within a 1D alloy semiconductor calculated on a  $128 \times 128$  grid. Electron and hole position are displayed in horizontal and vertical direction, respectively. The diagonal line marks the main diagonal where both carriers are at the same position. (e) Dispersion and (f) transition probabilities of the calculated two-particle states. Filled symbols correspond to the states shown left. While excitonic states can be found on the low-energy side, mainly unbound electron-hole states are visible on the high-energy side. For increasing energies, the transition probabilities decrease, indicated by the dotted line as guide to the eyes.

For the model WFs, the transition probabilities can be estimated by integrating  $\Psi(x_e, x_h)$  along the main diagonal. This can be applied to analyze the characteristic features of the absorption and emission spectra of alloys. As can be seen in Fig. 8.24 (f), the transition probabilities show a clear decreasing tendency for increasing energy. While for absorption processes many “dark” target states are available on the high-energy side of the spectrum, mostly the few “bright” states on the low-energy side take part in emission processes. This contributes to the large Stokes shift typically observed in alloys even for room temperature.

This work has been supported by Deutsche Forschungsgemeinschaft within the Graduate School "Leipzig School of Natural Sciences - Building with Molecules and Nano-objects (BuildMoNa, GS185).

- [1] E. Runge, in *Solid State Physics* 57, edited by H. Ehrenreich and F. Spaepen, Academic, San Diego (2003), pp. 149–305  
 [2] Arpack Software, <http://www.caam.rice.edu/software/ARPACK/>

## 8.17 Hexagonal phase of $\text{BaTiO}_3$ occurring in $\text{BaTiO}_3\text{-ZnO}$ -heterostructures at room temperature

C. Kranert, T. Böntgen, C. Sturm, R. Schmidt-Grund, M. Lorenz, M. Grundmann

The coupling between the switchable polarization of ferroelectric  $\text{BaTiO}_3$  (BTO) and the permanent polarization of pyroelectric ZnO leads to new physical phenomena [1]. The electric polarization is closely related to the structural properties of these materials. For the coupling effects the particular lattice structure near the interface has a great impact.

We investigated BTO-ZnO-heterostructures, where the BTO layers cover a wide range of thicknesses from below 10 nm to 2600 nm, by means of Raman spectroscopy. A ZnO:Al buffer layer, a nominally undoped ZnO layer and finally the BTO layer were deposited subsequently on an *a*-sapphire substrate using pulsed laser deposition. For the Raman measurements we use the 325 nm-line of a HeCd-laser for excitation. Light of this wavelength is strongly absorbed by both BTO and ZnO resulting in a high sensitivity to the topmost layer and suppression of Raman scattering in layers below.

The Raman spectra of all heterostructures exhibit a peak around  $640\text{ cm}^{-1}$  (vertical solid lines in Fig. 8.25) apart from the peaks typical for tetragonal BTO (t-BTO) crystals (dashed lines) and the LO peak originating from the ZnO layer. This additional peak does not occur in BTO layers grown on  $\text{SrTiO}_3$  substrates and can be assigned to the hexagonal high-temperature phase of BTO (h-BTO) [2]. As shown in Fig. 8.25a, its relative intensity compared to the peaks of t-BTO is stronger for the (111)-oriented films than for those with (001) orientation indicating a higher concentration of h-BTO. This can be understood by considering h-BTO as a variation of t-BTO with a stacking fault of the cubic perovskite lattice along the (111)-direction [3]. No change of the intensity relation could be observed throughout the thickness range. For the ultrathin BTO layer grown directly on ZnO:Al (see Fig. 8.25b) the h-BTO related peak is even more enhanced, emphasizing that the formation of the stacking fault strongly depends on the template the BTO layer is grown on.

This work has been supported by Deutsche Forschungsgemeinschaft in the framework of SFB 762 "Functionality of oxide interfaces".

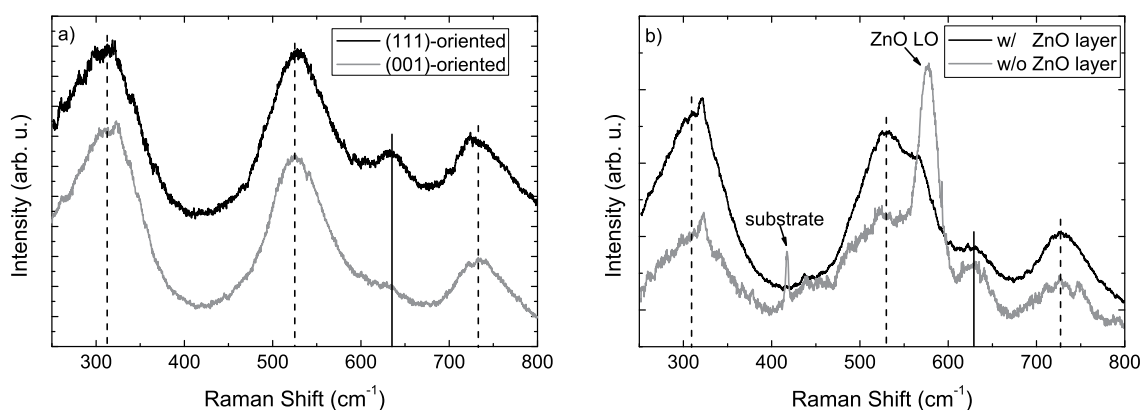


**Figure 8.25:** (a) The (111)-oriented BTO film shows a higher intensity of the h-BTO peak than the (001)-oriented one. (b) Ultrathin BTO layers grown directly on ZnO:Al show an enhanced h-BTO peak compared to those with an undoped ZnO layer in between (both (111)-oriented). Vertical dashed (solid) lines indicate Raman peaks from t-BTO (h-BTO).

[1] V. M. Voora, T. Hoffmann, M. Brandt, M. Lorenz, M. Grundmann: Appl. Phys. Lett. **94**, 142904 (2009) doi:10.1063/1.3116122

- [2] N. G. Eror, T. M. Loehr, B. c. Cornilsen: *Ferroelectrics* **28**, 321 (1980)  
doi:10.1080/00150198008227099
- [3] R. D. Burbank and H. T. Evans.: *Acta Cryst.* **1**, 330 (1948)  
doi:10.1107/S0365110X48000867

## 8.18 Strain in $\text{Mg}_x\text{Zn}_{1-x}\text{O}$ ( $x \leq 0.04$ ) thin films on ZnO:Al buffer

C. Kranert, M. Brandt, M. Stölzel, C. Sturm, R. Schmidt-Grund, M. Grundmann

The band gap of ZnO can be shifted to higher energies by alloying with Magnesium making the  $\text{Mg}_x\text{Zn}_{1-x}\text{O}$  compound an ideal barrier material for ZnO quantum wells. For the use in optoelectronic devices the introduction of a transparent back contact made from highly doped ZnO:Al is favourable.

We investigated the strain in  $\text{Mg}_x\text{Zn}_{1-x}\text{O}$  ( $0 \leq x \leq 0.04$ ) thin films (thickness of 500–1000 nm) grown by pulsed laser deposition on ZnO:Al buffer layers on *a*-sapphire substrates. For this purpose the Raman scattering from the  $E_2^{(2)}$  phonon mode was analyzed. This mode is strain sensitive but almost independent from the mass of the atom at the Zn place allowing to neglect the different mass of Mg in the compound crystals. Three phonon modes of the sapphire substrate were taken as reference to obtain an accuracy of the spectral position better than  $0.1 \text{ cm}^{-1}$ .

The effect of the strain caused by the pseudomorphic growth on the  $E_2^{(2)}$  mode of nominally pure ZnO thin films was examined by comparison to a relaxed film grown without ZnO:Al buffer layer. A red shift of the  $E_2^{(2)}$  mode of about  $0.55 \text{ cm}^{-1}$  was observed for the ZnO film grown on the buffer layer. According to [1] this corresponds to a biaxial tensile strain of about 0.1 % in this layer, which we relate to be caused by the increased *a* lattice constant in the Al-doped buffer layer [2].

The  $E_2^{(2)}$  mode of the  $\text{Mg}_x\text{Zn}_{1-x}\text{O}$  films exhibits an unusual behavior in dependence on *x* as shown in Fig. 8.26. A steep decrease of the phonon frequency is observed for  $x < 1\%$ . For higher Mg concentrations it increases again slightly. If only the phonon mode shifts by the change of the composition and the external strain are considered, a monotonic dependence would be expected. Therefore an additional internal, defect related strain must be present which is either induced or compensated by the introduction of Mg into the crystal. The minimum in Fig. 8.26b thereby indicates a saturation of this effect.

- [1] T. Gruber, G. M. Prinz, C. Kirchner, R. Reuss, W. Limmer, A. Waag: *J. Appl. Phys.* **96**, 289 (2004) doi:10.1063/1.1755433
- [2] M. N. Islam, T. B. Ghosh, K. L. Chopra, H. N. Acharya: *Thin Solid Films* **280**, 20 (1996) doi:10.1016/0040-6090(95)08239-5

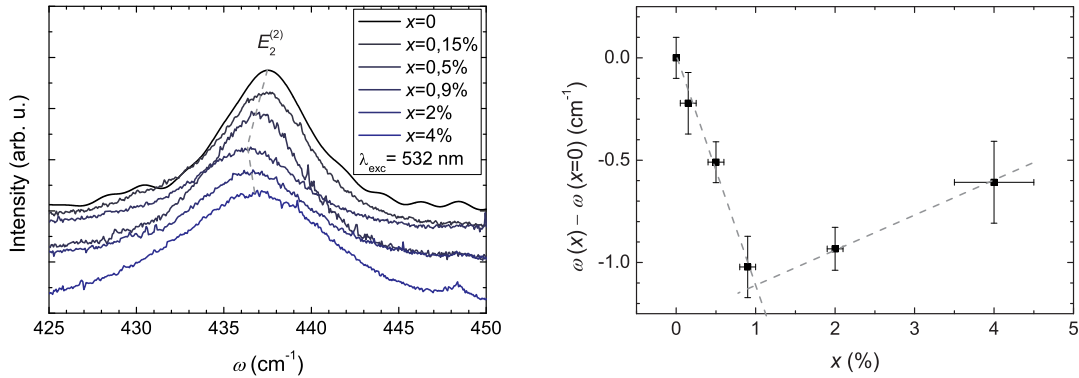


**Figure 8.26:** (a) Experimental spectra of the  $\text{Mg}_x\text{Zn}_{1-x}$  thin films after subtraction of the substrate peaks. The spectra are shifted vertically for clarity. (b) Peak position of the  $E_2^{(2)}$  phonon mode in dependence on the Mg concentration. Lines are guides to the eye.

## 8.19 Magnetic properties of manganese doped Zirconia thin films

J. Zippel, M. Lorenz, A. Setzer, C. Meinicke, H. Hochmuth, P. Esquinazi, M. Grundmann

The combination of both, charge and spin of the charge carriers offers a new field of devices with the potential to outperform conventional semiconductor devices [1].

As recently predicted, manganese doped, i.e. stabilized, zirconia ( $\text{ZrO}_2$ ) ( $\text{MnZO}$ ) could be a candidate for the realization of a ferromagnetic semiconductor with a Curie-temperature above room temperature [2].

Thin films of  $\text{MnZO}$  have been deposited on as received yttria stabilized zirconia (YSZ) (100) substrates by pulsed-laser deposition (PLD) technique using a focused KrF excimer laser LAMBDA PHYSIK LPX 305 operating at  $\lambda = 248$  nm. As target, we use pure  $\text{ZrO}_2$  ceramic targets as well as targets with 10 at. % or 20 at. %  $\text{MnO}_2$  made from  $\text{ZrO}_2$  powder (99 % Fluka Chemie) and  $\text{MnO}_2$  powder (99.999 % Alfa Aesar). The powders were pressed under 80 bar and subsequently sintered 6 hours at  $1500^\circ\text{C}$  in air. For deposition, the substrate temperature  $T_g$  and the oxygen partial pressure  $p(\text{O}_2)$  was varied between  $640^\circ\text{C}$  and  $790^\circ\text{C}$  and between 0.1 mbar and  $3.0 \times 10^{-4}$  mbar, respectively.

Figure 8.27 (a) shows the magnetic moment-field ( $m$ - $H$ ) plots at 300 K for films from source targets with  $x = 0$ ,  $x \approx 0.1$  and  $x \approx 0.2$ , whereas only for  $x \approx 0.2$  the cubic crystalline phase is visible. An open, i.e. ferromagnetic hysteresis loop becomes visible for all films at 300 K, in particular also for the undoped zirconia film. A dominating paramagnetism, in addition to the observed weak ferromagnetic signal is observed.

Figure 8.27 (b) shows the ferromagnetic saturation magnetization of all films as a function of the out-of-plane lattice strain. All cubic  $\text{MnZO}$  films show saturation magnetizations which are a factor of about 3 to 10 higher than that of the monoclinic films. This considerable enhancement of the saturation magnetization rules out that the ferromagnetic hysteresis is induced mainly by the chemical Mn content or possible trace impurities in the zirconia source target material. Instead, structural effects appear as possible origin of the differences of the magnetic performance.

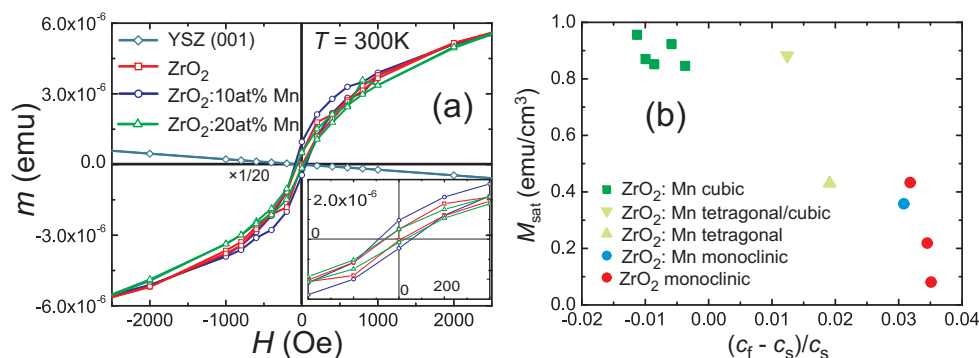


**Figure 8.27:** (a) Magnetic moment–field ( $m$ - $H$ ) plots at 300K for films from source targets with  $x = 0$ ,  $x \approx 0.1$  and  $x \approx 0.2$ . (b) Ferromagnetic saturation magnetization  $M_{\text{sat}}$  at 5 K of all films in relation to the out-of-plane lattice strain of film to substrate.  $M_{\text{sat}}$  is normalized to the film volume.

In summary, a direct connection between ferromagnetic ordering and the incorporation of Mn cannot be revealed. Instead, structural effects appear as possible origin of the observed ferromagnetic behavior.

This work has been supported by Deutsche Forschungsgemeinschaft within the Graduate School "Leipzig School of Natural Sciences - Building with Molecules and Nano-objects (BuildMoNa, GS185) and the European Social Fund (ESF).

- [1] S.A. Wolf, D.D. Awschalom, R.A. Buhrman, J.M. Daughton, R.S. von Molna, M.L. Roukes, A.Y. Chtchelkanova, D.M. Treger: *Science* **294**, 1488 (2008)
- [2] S. Ostanin, A. Ernst, L.M. Sandratskii, P. Bruno, M. Dane, I.D. Hughes, J.B. Staunton, W. Hergert, I. Mertig, J. Kudrnovsky: *Phys. Rev. Lett.* **98**, 016101 (2007)

## 8.20 Structural and electrical properties of zinc ferrite thin films grown by pulsed-laser deposition

K. Brachwitz, K. Mexner, M. Brandt, A. Setzer\*, M. Ziese\*, J. Lenzner, P. Esquinazi\*, M. Lorenz, M. Grundmann

\*Universitat Leipzig, Institut fur Experimentelle Physik II, Abteilung Supraleitung und Magnetismus

Zinc ferrite ( $\text{ZnFe}_2\text{O}_4$ , ZFO) is a spinel-type semi-transparent oxide, with various possible applications in magnetic devices due to its ferrimagnetic properties. We have investigated structural, electrical and magnetic properties of ZFO thin films grown by pulsed-laser deposition (PLD) with various conditions. Stoichiometric PLD targets were mixed, pressed and sintered from high-purity ZnO- and  $\text{Fe}_2\text{O}_3$ -powders. In order to optimize the thin film quality we grew ZFO thin films with oxygen partial pressures ( $p(\text{O}_2)$ ) in a range from 0.1 to  $5 \times 10^{-5}$  mbar. Furthermore, we have varied the substrate temperature ( $T_S$ ) by controlling the heater power ( $P_H$ ) in a range from room temperature ( $P_H = 0\text{W}$ ) to  $720^\circ\text{C}$  ( $P_H = 700\text{W}$ ). The ZFO thin films were grown on (100)-oriented strontium titanate (STO) single crystals. The preferential (111) out-of-plane orientation

of the films and the lattice constant  $a$  were obtained by X-ray diffraction (XRD) measurements. The Fe-content  $x = x_{Fe}^{mol} / (x_{Zn}^{mol} + x_{Fe}^{mol})$  was determined by energy dispersive X-ray spectroscopy. The composition and the out-of-plane lattice constant of the thin films depend on  $T_S$  and  $p(O_2)$  during growth, see Figure 8.28 (a). A nearly stoichiometric  $ZnFe_2O_4$  composition was obtained for high  $T_S$  and  $p(O_2) = 2 \times 10^{-3} - 3 \times 10^{-4}$  mbar. Consistently, XRD measurements reveal the smallest rocking curve FWHM of the ZFO films for these conditions.

The electrical properties were investigated in dependence on  $p(O_2)$  and  $T_S$ . The transport mechanism in zinc ferrite is attributed to electron hopping between  $Fe^{2+}$  and  $Fe^{3+}$  ions on octahedral B sites of the lattice [1]. For decreasing  $p(O_2)$  and  $T_S$  an increasing conductivity was obtained (Figure 8.28 (b)). Furthermore, broadening of the  $2\theta - \omega$  reflexes and of the rocking curve with decreasing  $T_S$  indicate a decreasing crystalline quality. This correlation is in good agreement with investigations of Marcu *et al.* [1], where not only electron hopping but also effects of structural disorders like grain boundaries and oxygen vacancies have great influence on the electrical conductivity. Magnetization measurements using a Superconducting Quantum Interference Device (SQUID) reveal ferrimagnetic behaviour of all investigated films. The magnetization is mainly in-plane and a decreasing coercive field  $H_C$  for decreasing  $T_S$  was observed. Typical values for saturation magnetization and coercive field at  $T = 300$  K are  $M_S = 300$  emu/cm<sup>3</sup> and  $H_C = 0.01$  T, respectively.

First field dependent Hall effect measurements up to high fields of  $B = 8$  T show the importance of the magnetization dependent anomalous Hall effect to extract carrier concentrations and mobilities in the ZFO films.

This work has been supported by Deutsche Forschungsgemeinschaft in the framework of SFB 762 "Functionality of oxide interfaces".

[1] A. Marcu, T. Yanagida, K. Nagashima, H. Tanaka, T. Kawai: J. Appl. Phys. **102**, 023713 (2007)

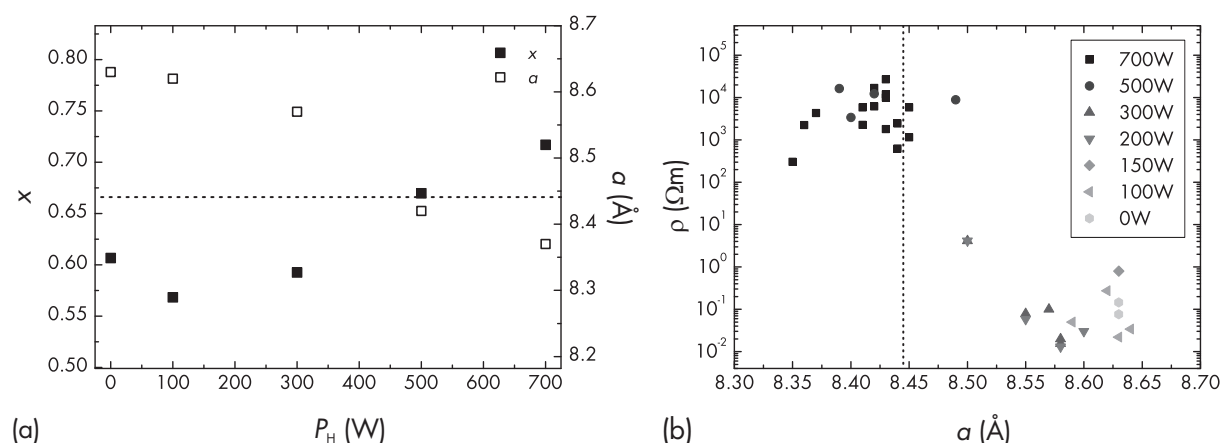


**Figure 8.28:** (a) Fe-content  $x$  and lattice constant  $a$  of ZFO thin films plotted as a function of the heater power for  $p(O_2) = 5 \times 10^{-5}$  mbar. The dotted line indicates bulk zinc ferrite  $x$  and  $a$ . (b) Resistivity correlated with the substrate temperature plotted as a function of  $a$ . The dotted line shows bulk zinc ferrite  $a$ .

## 8.21 Structural and magnetic properties of $\text{Zn}_{1-x}\text{Fe}_x\text{O}_z$ thin films grown on a-sapphire for $0.1 \leq x \leq 0.67$

K. Brachwitz, T. Böntgen, J. Lenzner, K. Ghosh\*, M. Lorenz, M. Grundmann

\*Department of Physics, Astronomy, and Materials Science, Missouri State University,  
901 South National Avenue, Springfield, MO 65897, USA

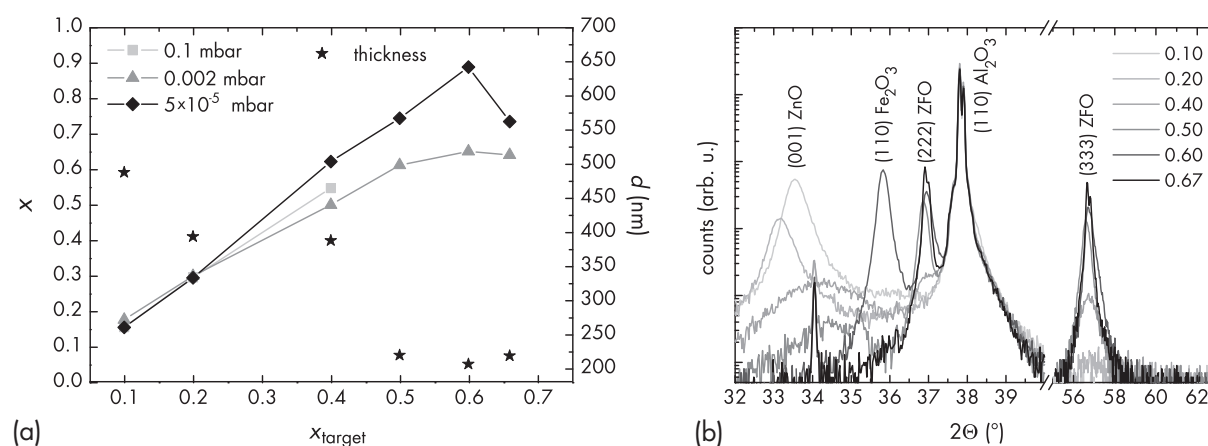


**Figure 8.29:** (a) Overview on the atomic Fe/(Zn+Fe) film composition ratio  $x$  (left scale) and film thickness  $d$  (right scale) in dependence on the target composition  $x_{\text{target}}$ . Film composition is shown for different  $p(\text{O}_2)$ , and thickness only for  $p(\text{O}_2) = 0.002$  mbar. (b) XRD  $2\theta - \omega$  scans (Cu  $K_\alpha$ ) of the  $\text{Zn}_{1-x}\text{Fe}_x\text{O}_z$  thin films for  $0.1 \leq x \leq 0.67$ , for  $p(\text{O}_2) = 0.002$  mbar.

Magnetically doped ZnO thin films attained considerable attention during the last decade. However, the search for diluted magnetic semiconductors based on ZnO reached up to now no clear and reproducible results. Instead, weak magnetic effects are reported due to clustering of the magnetic dopant oxide or due to structural defects, even in undoped oxide thin films. On the other hand, magnetite  $\text{Fe}_3\text{O}_4$  is a well known ferrimagnetic oxide in which the electrons are spin-polarized up to room temperature [1, 2]. Therefore, the interest in these spintronic materials increased recently, including the Zn-substituted, in relation to ZnO and  $\text{Fe}_3\text{O}_4$  intermediate compound zinc ferrite  $\text{ZnFe}_2\text{O}_4$ . For example, the group of R. Gross has investigated  $\text{Zn}_y\text{Fe}_{3-y}\text{O}_4$  thin films for  $0 \leq y \leq 0.9$ , which is the mixing range from pure  $\text{Fe}_3\text{O}_4$  up to  $\text{Zn}_{0.9}\text{Fe}_{2.1}\text{O}_4$  [3]. In this work, we focus on the mixing range from ZnO (corresponding to  $x = 0$ ) up to  $\text{ZnFe}_2\text{O}_4$  (corresponding to  $x = 0.67$ ). The oxygen content  $z$  in the  $\text{Zn}_{1-x}\text{Fe}_x\text{O}_z$  film samples varies from 1.0 for  $x = 0$  (corresponding to ZnO) up to 1.33 for  $x = 0.67$  (corresponding to  $\text{ZnFe}_2\text{O}_4$ ), confirmed by energy dispersive X-ray spectroscopy (EDX).

$\text{Zn}_{1-x}\text{Fe}_x\text{O}_z$  thin films were grown by pulsed-laser deposition (PLD) on (110)-oriented a-plane sapphire substrates. PLD targets were mixed, pressed and sintered from high-purity ZnO- and  $\text{Fe}_2\text{O}_3$ -powders according to the target compositions mentioned below. The thin films were grown at about  $720^\circ\text{C}$  substrate temperature and at oxygen partial pressures  $p_{\text{O}_2}$  from 0.1 to  $5 \times 10^{-5}$  mbar, with equal number of laser pulses. Figure 8.29(a) shows the atomic Fe composition ratio  $x = x_{\text{Fe}}^{\text{at}} / (x_{\text{Zn}}^{\text{at}} + x_{\text{Fe}}^{\text{at}})$  of the thin films as a function of the target composition  $x_{\text{target}}$  for different  $p_{\text{O}_2}$ .  $x$  was determined by EDX. The thickness values of the  $\text{Zn}_{1-x}\text{Fe}_x\text{O}_z$  thin films were obtained by spectroscopic ellipsometry. The

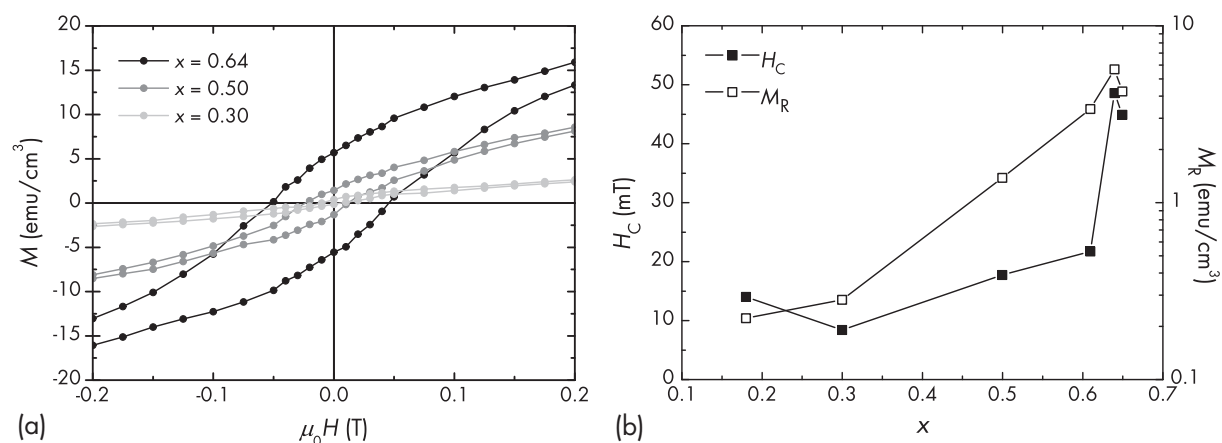


**Figure 8.30:** (a) Typical ferromagnetic hysteresis loops  $M(H)$  for three different  $\text{Zn}_{1-x}\text{Fe}_x\text{O}_z$  films, measured at  $T = 10$  K. The given  $x$ -values are the EDX values of the particular films. (b) Remanent magnetization  $M_R$  and coercive field  $H_C$  plotted as a function of  $x$ , at 10 K. All film samples were grown at  $p(\text{O}_2) = 0.002$  mbar.

decreasing film thickness with increasing  $x$  indicates the changing ablation dynamics of the PLD targets with increasing Fe target composition. Figure 8.29(a) also shows that the Fe content  $x$  mostly exceeds the corresponding target value. Due to the high growth temperature around  $700^\circ\text{C}$ , the more volatile Zn may be reevaporated from the film surface, thus explaining the typical Zn-deficiency in our samples. Of course, the reevaporation can be tuned by the oxygen partial pressure. This effect becomes visible in Fig 8.29(a) for  $x_{\text{target}} \geq 0.4$ . In particular, for  $p_{\text{O}_2} = 0.002$  mbar the film composition  $x$  nearly reaches the nominal zinc ferrite composition ( $x = 0.67$ ), while for lower pressure  $p_{\text{O}_2} = 5 \times 10^{-5}$  mbar the Zn reevaporation seems to be higher.

The X-ray diffraction (XRD)  $2\theta-\omega$  scans of the  $\text{Zn}_{1-x}\text{Fe}_x\text{O}_z$  thin films for  $p_{\text{O}_2} = 0.002$  mbar in Fig. 8.29(b) show the evolution of the crystalline phases. In particular, Fig. 8.29(b) shows the formation of a wurtzite ZnO phase and a spinel  $\text{ZnFe}_2\text{O}_4$  phase with varying peak intensities according to the varying  $x$ . With increasing  $x$ , the intensity of the ZnO (001) reflex decreases while that of  $\text{ZnFe}_2\text{O}_4$  (111) increases. Surprisingly, only for  $x = 0.6$  the phase segregated peak of  $\text{Fe}_2\text{O}_3$  (110) becomes visible in Fig. 8.29(b). However, this observation agrees with the maxima of the film Fe content from the EDX measurements for  $x = 0.6$  in Fig. 1(a), for both 0.002 and  $5 \times 10^{-5}$  mbar.

Figure 8.30(a) shows exemplary field dependent magnetization curves  $M(H)$  for three samples with different  $x$ , measured with a Superconducting Quantum Interference Device (SQUID). As expected, for increasing  $x$  the area of the hysteresis loops clearly increases. This trend is further demonstrated by the increasing remanent magnetization  $M_R$  and coercive field  $H_C$ , see Figure 8.30(b).  $M_R$  ranges from 0.2 to  $5.6 \text{ emu}/\text{cm}^3$ , and  $H_C$  from 8.3 to 48.5 mT, respectively. Magnetic force measurements using a scanning probe microscopy system Park XE-150 indicate a preferential in-plane magnetization of the investigated films.

This work has been supported by Deutsche Forschungsgemeinschaft in the framework of SFB 762 "Functionality of oxide interfaces".

[1] C.A. Kleint, H.C. Semmelhack, M. Lorenz, M.K. Krause: J. Magn. Magn. Mater. **140**, 725 (1995)

- [2] C.A. Kleint, M.K. Krause, R. Höhne, T. Walther, H.C. Semmelhack, M. Lorenz, P. Esquinazi: M. Lorenz, P. Esquinazi, J. Appl. Phys. **84**, 5097 (1998)
- [3] D. Venkateshvaran, M. Althammer, A. Nielsen, S. Geprägs, M.S. Ramachandra Rao, S.T.B. Goennenwein, M. Opel, R. Gross: Phys. Rev. B **79**, 134405 (2009)

## 8.22 Electrical and structural properties of Zn-Co-O thin films

F.-L. Schein, M. Lorenz, H. von Wenckstern, M. Grundmann

Considering that virtually all transparent oxide semiconductors (TOSs) are unipolar and most of them are  $n$ -type it is of great interest to investigate the few  $p$ -type TOSs due to enabling transparent bipolar devices or complementary circuits. A promising class of such materials are the zinc spinels  $\text{ZnM}_2\text{O}_4$  ( $M = \text{Co}, \text{Rh}, \text{Ir}$ ) [1]. They can be fabricated near and at room temperature; for  $\text{ZnRh}_2\text{O}_4$  [2] and  $\text{ZnCo}_2\text{O}_4$  [3] indications for stable  $p$ -type conductivity even in the amorphous state were reported.

We present the structural and electrical properties of  $\text{ZnCo}_2\text{O}_4$  thin films grown by pulsed-laser deposition (PLD). The PLD target was fabricated using commercial available powders (Alfa Aesar) of  $\text{CoO}$  and  $\text{ZnO}$ . They were mixed, pressed into a 25 mm diameter form and sintered at 1350 °C for 6 h in ambient air. For the investigations 200 nm thin films were grown on  $a$ -sapphire substrates using a KrF excimer laser ( $\lambda = 248$  nm). The substrates were mounted on a heatable holder and deposition of the films started with 300 pulses and a repetition rate of 1 Hz to form a nucleation layer and continued with 20000 pulses at 15 Hz. A variation of oxygen partial pressure  $p(\text{O}_2)$  from 0.001–0.25 mbar and heater power of the substrate holder from 0–700 W (i. e. deposition temperature) was carried out and found to be crucial for thin film properties. Beginning at 50 W corresponding to 220 °C one step in heater power (50 W, 100 W, 200 W, 300 W, 500 W and 700 W) corresponds to  $\approx 100$  °C temperature difference.

Structural properties have been investigated using X-ray diffraction (XRD). Samples deposited at room temperature show no XRD reflexes, thus they are in the amorphous state. For heater powers  $\geq 50$  W the  $\text{ZnCo}_2\text{O}_4$  grows along the {111} direction as XRD pattern (not shown) pointed out. However, these measurements also reveal  $\text{ZnO}$  (002) reflexes for samples grown at 500 W and 700 W. This indicates a separation of  $\text{ZnO}$  and  $\text{ZnCo}_2\text{O}_4$ . An explanation for this observation is given by Peiteado *et al.* [4] arguing that a reduction of  $\text{Co}^{3+}$  to  $\text{Co}^{2+}$  occurs for increasing temperature with an assumed starting temperature in the range of 400–600 °C. These divalent Co-ions occupy the tetrahedral positions in spinel structure by substituting  $\text{Zn}^{2+}$ . The result is a mixture of a cobalt-enriched spinel and  $\text{ZnO}$ , finally leading to a collapse of spinel structure for even higher temperatures. Atomic force microscopy measurements reveal root mean square (rms) roughnesses within a range of 0.42–0.65 nm for thin films fabricated at  $p(\text{O}_2) = 0.03$  mbar and heater powers up to 300 W. For 500 W rms roughness is 1.02 nm and even one order of magnitude larger for 700 W having rms roughness of 12.31 nm.

Figure 8.31a shows the electrical conductivity  $\sigma$  as a function of PLD heater power. The conductivity is  $\sigma = 9.1$  S/cm for the film deposited at room temperature, then increases to 15.1 S/cm for 50 W, decreases slightly until 300 W and drops down drastically

to 0.02 S/cm which is presumably due to ZnO/ZnCo<sub>2</sub>O<sub>4</sub> separation for higher temperatures. The conductivity is comparable to the highest value reported so far for ZnCo<sub>2</sub>O<sub>4</sub>  $\sigma = 21.8$  S/cm [3]. However, conductivities in the order of 10 S/cm are remarkable for *p*-type oxides usually having  $\sigma < 1$  S/cm with rare exceptions like CuCrO<sub>2</sub>:Mg (220 S/cm) or NiCo<sub>2</sub>O<sub>4</sub> (330 S/cm) [5]. Due to linear behavior shown in a  $\sigma$  vs.  $T^{-1/4}$  plot of a sample fabricated at  $p(\text{O}_2) = 0.016$  mbar and 300 W (inset of figure 8.31a) a percolation or hopping mechanism is present, therefore Hall-effect measurements have to be interpreted carefully [6].

For all samples presented here *p*-type nature has been ascertained by qualitative Seebeck measurements. In Addition, to prove the charge carrier type a heterostructure of *n*-ZnO and ZnCo<sub>2</sub>O<sub>4</sub> has been fabricated. First, a 200 nm ZnCo<sub>2</sub>O<sub>4</sub> layer was deposited on a-sapphire substrate ( $p(\text{O}_2) = 0.016$  mbar, 300 W). After in-situ change of PLD targets the growth continued with a 180 nm ZnO and a 90 nm ZnO:Al layer (both  $p(\text{O}_2) = 0.02$  mbar, 300 W). Utilising acid resistance of ZnCo<sub>2</sub>O<sub>4</sub>, standard photolithography enables selective removal of ZnO layers using diluted phosphoric acid. Finally, ohmic Au contacts were sputtered in an Ar atmosphere and ohmic behavior was verified. The current-voltage characteristic of the heterostructure demonstrates clear rectifying behavior (figure 8.31b), thus *p*-type nature of ZnCo<sub>2</sub>O<sub>4</sub> is obvious. The on/off current ratio is  $4 \times 10^3$  at  $\pm 2$  V exceeding the ratio of a *n*-InGaZnO/*p*-ZnCo<sub>2</sub>O<sub>4</sub> diode (on/off =  $1 \times 10^2$  at  $\pm 7$  V [3]) and is comparable to a *n*-InGaZnO/*p*-ZnRh<sub>2</sub>O<sub>4</sub> diode (on/off =  $1 \times 10^3$  at  $\pm 4$  V [2]).

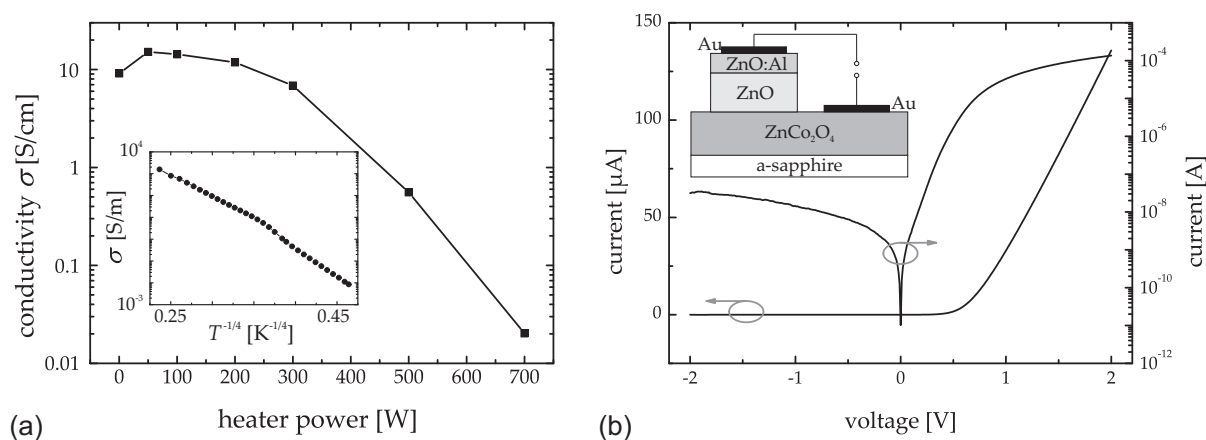


**Figure 8.31:** (a) Conductivity  $\sigma$  of ZnCo<sub>2</sub>O<sub>4</sub> thin films fabricated at oxygen partial pressure of  $p(\text{O}_2) = 0.03$  mbar and various heater powers. The inset shows temperature dependent behavior of  $\sigma$  following a  $\sigma = \sigma_0 \exp(-T_0/T)^{1/4}$  law (sample grown at  $p(\text{O}_2) = 0.016$  mbar and 300 W). (b) Current-voltage characteristic of the *n*-ZnO/*p*-ZnCo<sub>2</sub>O<sub>4</sub> heterostructure on linear and semi-logarithmic scale.

- [1] M. Dekkers, G. Rijnders, D. H. A. Blank: Appl. Phys. Lett. **90**, 021903 (2007)
- [2] T. Kamyia, S. Narushima, H. Mizoguchi, K. Shimizu, K. Ueda, H. Ohta, M. Hirano, H. Hosono: Adv. Funct. Mater. **15**, 968 (2005)
- [3] S. Kim, J. A. Cianfrone, P. Sadik, K.-W. Kim, M. Ivill, D. P. Norton: J. Appl. Phys. **107**, 103538 (2010)
- [4] M. Peiteado, A. Caballero, D. Makovec: J. Ceram. Soc. Jpn. **118**, 337 (2010)
- [5] A.N. Banerjee, K.K. Chattopadhyay: Prog. Cryst. Growth. Ch. **50**, 52 (2005)

[6] T. Kamiya, K. Nomura, H. Hosono: Appl. Phys. Lett. **96**, 122103 (2010)

## 8.23 Electrical conductivity of Mn-doped Zirconia thin films.

J. Zippel, M. Lorenz, A. Setzer, J. Lenzner, T. Hammer, H. Hochmuth, P. Esquinazi, M. Grundmann

Spintronics devices have attracted huge attention in the last years as fascinating alternatives to today's mainstream devices [1]. As proposed by density functional theory (DFT), manganese stabilized zirconia (MnZO) in its cubic crystalline phase could be a candidate for a half-metallic ferromagnetic semiconductor [2, 3]. Recently, we demonstrated experimentally weak defect induced magnetic effects in undoped and Mn doped zirconia thin films [4].

Here, we present the electrical conductivity of  $\text{Mn}_x\text{Zr}_{1-x}\text{O}_2$  thin films deposited on pre-treated yttria stabilized zirconia (YSZ) (100) and *a*-plane sapphire substrates. The films were synthesized by pulsed-laser deposition (PLD). The electronic properties were probed by DC-measurements in a wafer prober of SüssMicrotec and in addition by performing Seebeck-effect measurements at the Fraunhofer IPM.

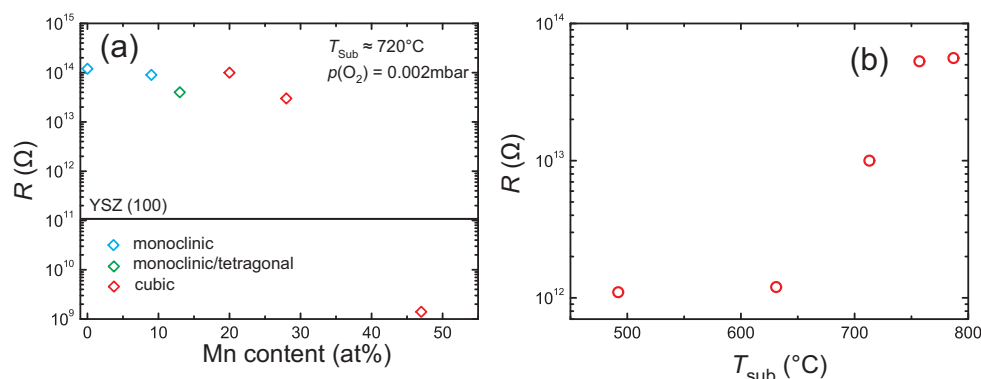


**Figure 8.32:** (a) Lateral resistance as a function of the Mn content for different MnZO thin films. The line represents the value of the YSZ (100) substrate. (b) Dependence of the electrical resistance on the growth temperature  $T_{\text{Sub}}$ .

Pure zirconia as well as stabilized zirconia are well known as ionic conductors at elevated temperatures [5]. Figure 8.32 (a) depicts the resistance of MnZO thin films as a function of the Mn content in lateral geometry. For  $x \leq 0.3$ , an insulating behavior with a resistance between  $10 \times 10^{13}$  Ω and  $10 \times 10^{14}$  Ω is observed. Either by further increasing the Mn content or by reducing the structural quality (see Fig. 8.32 (b)), i.e. reducing the growth temperature, the conductivity is enhanced leading to  $R \approx 10 \times 10^9$  Ω and  $R \approx 10 \times 10^{12}$  Ω, respectively. In addition, Seebeck effect measurements of a pure zirconia thin film and MnZO thin films with  $x = 0.2$  on *a*-plane sapphire substrates are presented in figure 8.33. As indicated by the plateau in the conductivity graph, a transition from p- to n-type conductivity at about  $T = 500$  K is present in both samples. This is supported by the change of the Seebeck coefficient from positive to negative values at the same

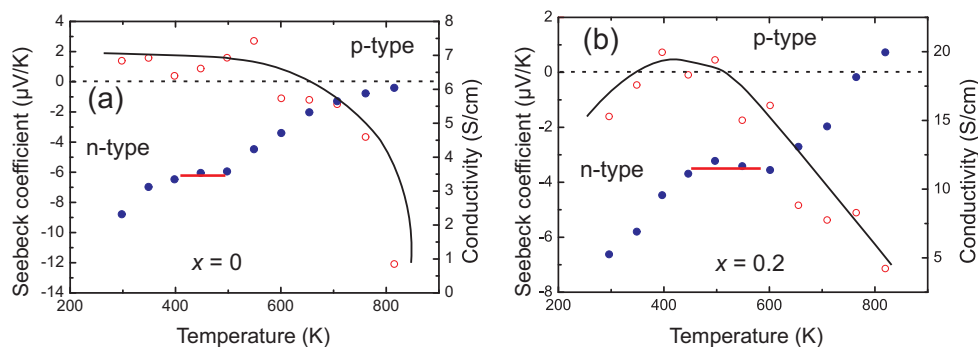


**Figure 8.33:** Seebeck-effect measurements of (a) an undoped ZrO<sub>2</sub> and a (b) MnZO thin film with  $x = 0.2$  grown on *a*-sapphire. The lines included are to guide the eye.

temperature. For  $T$  above 500 K the conduction mechanism dominated by the ionic conduction via oxygen vacancies leads to an electronic conduction of *n*-type charge carriers. In contrast, for pure ZrO<sub>2</sub> and  $T$  below 500 K a hole mediated conduction mechanism is dominant.

In summary, MnZO thin films are electrically insulating with  $R$  in the order of  $10 \times 10^{14} \Omega$  up to  $x = 0.3$ . By reducing the structural quality or by increasing the Mn content up to 50 at. %, the resistance is reduced down to  $10 \times 10^9 \Omega$ . Seebeck effect measurements clearly show a change from *p*-type to *n*-type conductivity at  $T \approx 500$  K maybe related to an increasing ionic conduction at elevated temperatures.

This work has been supported by Deutsche Forschungsgemeinschaft in the framework of SFB 762 "Functionality of oxide interfaces".

- [1] S.A. Wolf, D.D. Awschalom, R.A. Buhrman, J.M. Daughton, S. von Molnär, M.L. Roukes, A.Y. Chtchelkanova, D.M. Treger: *Science* **294**, 1488 (2001). doi:10.1126/science.1065389
- [2] S. Ostanin, A. Ernst, L.M. Sandratskii, P. Bruno, M. Dane, I.D. Hughes, J.B. Staunton, W. Hergert, I. Mertig, J. Kudrnovsky: *Phys. Rev. Lett.* **98**, 016101, (2007). doi:10.1103/PhysRevB.65.224109
- [3] X. Jia, W. Yang, M. Qin, J. Li: *JMMM*, **321**, 2354, (2009). doi:10.1016/j.jmmm.2009.02.132
- [4] J. Zippel, M. Lorenz, A. Setzer, G. Wagner, N. Sobolev, P. Esquinazi, M. Grundmann: *Phys. Rev. B.* **82**, 125209, (2010). doi:10.1103/PhysRevB.82.125209
- [5] X. Huang, W. Weppner: *Journal of the Chemical Society-Faraday Transaction*, **92**, 2173, (1996). doi:10.1039/FT9969202173

## 8.24 Electrical and optical properties of H plasma-doped ZnO single crystals

H. von Wenckstern, W. Anwand\*, G. Brauer\*, T.E. Cowan\*, H. Schmidt\*, V. Heera\*, W. Skorupa\*, M. Brandt<sup>†</sup>, G. Benndorf, M. Grundmann

\*Forschungszentrum Dresden-Rossendorf, PO Box 510 119,  
01314 Dresden, Germany

<sup>†</sup>now with Humboldt Universität zu Berlin, Mathematisch-Naturwissenschaftliche Fakultät I, Institut für Physik, Newtonstrasse 15, 12489 Berlin, Germany

Hydrogen is an ubiquitous contaminant in semiconducting materials and its role is manifold; it may passivate defects or may itself act as donor or acceptor species. In the transparent II-VI semiconductor ZnO hydrogen is one of the most abundant impurities and is at least partially responsible for the n-type conductivity of ZnO. Recent theoretical and experimental work indicates that hydrogen can form donor-like defect states if incorporated at the bond-centered interstitial position ( $H_i$ ) or by forming a multi-center bond by replacing oxygen ( $H_O$ ) [1, 2]. However, hydrogen must not be incorporated as donor, often a large amount of hydrogen is not electrically active in ZnO and is referred to as "hidden hydrogen" in the literature [3]. Within a cooperation with the Forschungszentrum Dresden-Rossendorf we investigated electronic and transport properties of ZnO single crystals grown by the hydrothermal method prior to and after a remote hydrogen plasma treatment at 350°C for one hour. Within the as-grown state the electrical properties of hydrothermal ZnO crystals vary strongly. This is due to the fact that the concentration of shallow donors  $N_{d,shallow}$  and compensating acceptors  $N_a$  is very similar and in the range of  $10^{17} \text{ cm}^{-3}$ . For one of the investigated crystals (denoted Sample A)  $N_{d,shallow} > N_a$ ; the room temperature free electron concentration  $n$  and Hall mobility  $\mu_H$  are  $7.8 \times 10^{15} \text{ cm}^{-3}$  and  $149 \text{ cm}^2/\text{Vs}$ , respectively [4]. For another (denoted Sample B)  $N_{d,shallow} < N_a$  resulting in a two orders of magnitude lower free electron concentration of  $7.5 \times 10^{13} \text{ cm}^{-3}$  at room temperature and a Hall mobility of  $130 \text{ cm}^2/\text{Vs}$ . Temperature-dependent Hall effect measurements showed that for Sample A both shallow donors and deep donors contribute to the free electron concentration at room temperature, the thermal activation energy is about 41 meV and 340 meV, respectively. For Sample B only the deeper donor level provides free electrons. The temperature dependence of the free electron concentration is depicted in fig. 8.34 for both samples.

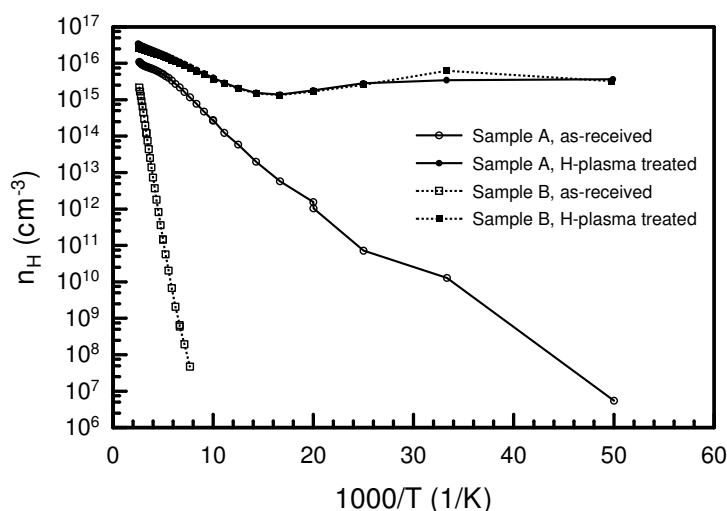


**Figure 8.34:** Temperature dependence of free electron concentration of samples A and B in the as-received state and after remote hydrogen plasma treatment.

The remote hydrogen plasma treatment produced significant changes of the samples electrical properties which are in principle the same after treatment (cf. fig. 8.34).

The free electron concentration first decreases with decreasing temperature but seemingly increases again for temperatures below 60 K (corresponding to  $16.7 \cdot 10^3/\text{K}$ ). The inhomogeneity of the samples after the H-plasma treatment causes this behavior. The plasma treatment creates degenerate doping levels in the vicinity of the surface; the conduction in this part of the samples is metal-like whereas it remains semiconducting in the bulk part not influenced by the plasma treatment. The electrical properties of the metal-like path can be determined from the low temperature data (20 K) and are the same for both treated samples: the electron concentrations are  $3.2 \times 10^{15} \text{ cm}^{-3}$  and the Hall mobilities are  $41 \text{ cm}^2/\text{Vs}$ . Due to the H-plasma treatment the density of compensating acceptors in the bulk part of the samples decreased to about  $8 \times 10^{16} \text{ cm}^{-3}$  resulting in much higher Hall mobility. Further, the density of free electrons in the bulk part of the samples increased to  $3.5 \times 10^{17} \text{ cm}^{-3}$ . Hence, the effect of the remote hydrogen plasma-doping is twofold: the incorporated hydrogen passivates acceptors and if H is incorporated at interstitial site or in an oxygen vacancy it acts as donor and increases the free electron density.

- [1] A. Janotti, C.G. Van de Walle: *Nature Mat.* **6**, 44 (2007).
- [2] E.V. Lavrov, F. Herklotz, J. Weber: *Phys. Rev. B* **79**, 165210 (2009).
- [3] G. Alvin Shi, Marjan Saboktakin, Michael Stavola, S. J. Pearton: *Appl. Phys. Lett.* **85**, 5601 (2004).
- [4] W. Anwand, G. Brauer, T.E. Cowan, V. Heera, H. Schmidt, W. Skorupa, H. von Wenckstern, M. Brandt, G. Benndorf, M. Grundmann: *phys. stat. sol. (a)* **207**, 2426 (2010).

## 8.25 Thermal admittance spectroscopy on non-polar a-plane homoepitaxial ZnO thin films

H. von Wenckstern, S. Lautenschläger\*, A. Lajn, F. Schmidt, B.K. Meyer\*, M. Grundmann

\*Justus Liebig Universität Giessen, I. Physikalisches Institut, Heinrich-Buff-Ring 16,  
D-35392 Giessen, Germany

Wide bandgap semiconductors like GaN and ZnO crystallize in the wurtzite structure exhibiting a spontaneous polarization directed antiparallel to the c-axis. If heterostructures like AlGaN/GaN or MgZnO/ZnO are grown along the c-axis there occurs a jump of the spontaneous polarization resulting in the formation of a sheet charge density at the interface. For a double heterostructure like a quantum well, the type of sheet charge carriers is different for the two opposite interfaces since the stacking sequence of layers along the growth direction is exchanged. With that an electric field exists between these two interfaces and in case of a quantum well it will cause quantum-confined Stark effect and reduced oscillator strength of excitonic transitions in the quantum well structure. This makes growth along non-polar crystallographic axis interesting, however, two-dimensional growth along non-polar axis' is especially for the case of ZnO still a challenge.

In collaboration with the Justus-Liebig Universität Giessen non-polar a-plane ZnO epilayers were grown by chemical vapor phase transport at 700°C on pre-annealed

a-plane ZnO single crystals grown by the hydrothermal method [1]. We realized Schottky contacts on the thin films by reactive sputtering of Pd. On the crystals back-side an ohmic Au contact was sputtered in pure Ar. The Schottky contacts were used to investigate the net doping density  $N_d - N_a$  and shallow defect levels by means of capacitance-voltage (CV) and thermal admittance spectroscopy (TAS), respectively. Prior to that the rectifying behavior of the Schottky diodes was evaluated by current-voltage measurements. Typical diodes show rectification of about 1000 which is limited by the comparatively low parallel resistance of 400 k $\Omega$ . Nevertheless, the rectification of these diodes is sufficient for CV measurements and TAS.

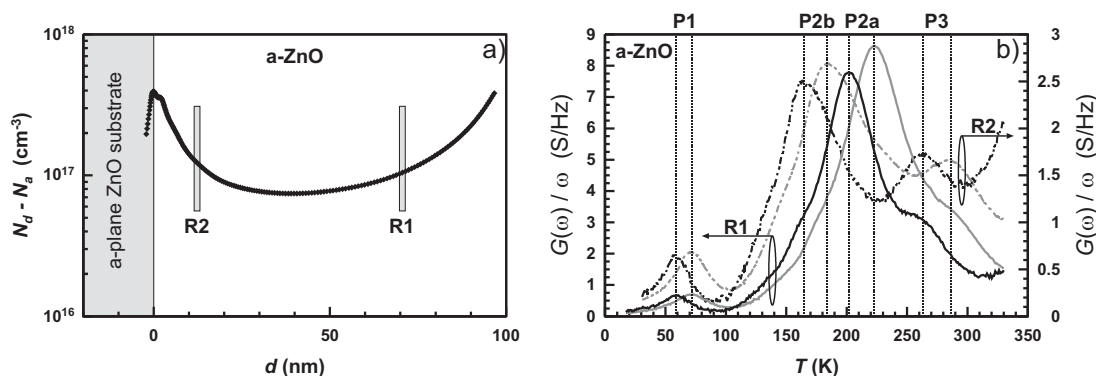


**Figure 8.35:** Net doping concentration vs. sample thickness a) and temperature dependence of the frequency normalized conductance measured for a zero bias (R1) and reverse voltage of 1 V (R2) b).

The net doping concentration calculated from the voltage dependence of the diodes capacitance depicted in fig. 8.35a) reveals an increase close to the substrate (this region is labelled R2 from now on) and towards the sample surface (labelled R1). The net doping profile is in close agreement to the concentration of group III elements, being shallow donors in ZnO, as secondary ion mass spectroscopy confirmed [1]. For TAS we chose reverse dc biases fixing the depletion layer width below the Schottky contact to R1 and R2, respectively. The normalized conductance of R1 and R2 is depicted in dependence on temperature for two different frequencies in fig. 8.35b). For both regions R1 and R2 three peaks are detected. The peaks, labelled P1 and P3, respectively, are observed at similar temperatures in R1 and R2 and have most likely the same origin. The thermal activation energy of P1 is 32 meV, a value commonly reported for ZnO thin films and bulk material [2, 3]. The defect P3 has within the error bars of the experiment the same thermal activation energy and apparent capture cross-section as the E3' defect reported by Auret et al. [3].

For intermediate temperatures thermal admittance spectroscopy revealed distinct differences for R1 and R2 (cf. fig. 8.35a). In R1 a peak labelled P2a, having a shoulder at the high temperature side being the superposition with P3, was observed. At the low temperature side of P2a another peak P2b is visible being the dominant signal in R2; P2a is with that preferentially incorporated in R1 while P2b is preferentially incorporated in R2. The defect parameters of P2a are similar to those of L1 attributed to an extrinsic defect [4]. P2b is similar to the T2 defect attributed to an intrinsic defect [5].

In summary, we investigated homoepitaxial a-plane ZnO thin films having a distinct increase of the net doping density towards the thin film/substrate interface and in the

vicinity of the sample surface. While the dominant shallow defect P1 and a deep level P3 are detected in both regions, the defects P2a and P2b are observed predominately close to the substrate and the surface, respectively.

- [1] S. Lautenschläger, S. Eisermann, M. N. Hofmann, U. Roemer, M. Pinnisch, A. Laufer, B. K. Meyer, H. von Wenckstern, A. Lajn, F. Schmidt, M. Grundmann, J. Blaesing, A. Krost: *J. Cryst. Growth* **312**, 2078 (2010).
- [2] U. Grossner, S. Gabrielsen, T. Moe Borseth, J. Grillenberger, A. Yu. Kuznetsov, B.G. Svensson: *Appl. Phys. Lett.* **85** 2259 (2004).
- [3] F.D. Auret, W.E. Meyer, P.J. Janse van Rensburg, M. Hayes, J.M. Nel, H. von Wenckstern, H. Schmidt, G. Biehne, H. Hochmuth, M. Lorenz, M. Grundmann: *Physica B* **401-402** 378 (2007).
- [4] A. Rohatgi, S.K. Pang, T.K. Gupta, W.D. Straub: *J. Appl. Phys.* **63** 5375 (1988).
- [5] M. Schmidt, M. Ellguth, C. Czekalla, H. von Wenckstern: R. Pickenhain, M. Grundmann, G. Brauer, W. Skorupa, M. Helm, Q. Gu, Ch. Ch. Ling: *J. Vac. Sci. Technol. B* **27** 1597 (2009).

## 8.26 Strain induced deep states in MgZnO

F. Schmidt, H. von Wenckstern, M. Schmidt, M. Stölzel, G. Benndorf, M. Grundmann

We investigated the influence of tensile and compressive strain on the incorporation of deep levels in  $\text{Mg}_x\text{Zn}_{1-x}\text{O}$  thin films using deep level transient spectroscopy (DLTS), Laplace-DLTS (LDLTS) and low-temperature photoluminescence (PL). The thin films with a Mg-content up to  $x = 0.02$  were grown by pulsed-laser deposition (PLD) on *a*-plane sapphire substrates. Prior to the growth of  $\text{Mg}_x\text{Zn}_{1-x}\text{O}$ , a 200 nm thick, highly conducting ZnO:Al layer was deposited to be used as ohmic back-contact resulting in Schottky diodes with low series resistance [1]. Schottky contacts were realized by reactive direct-current sputtering of palladium.

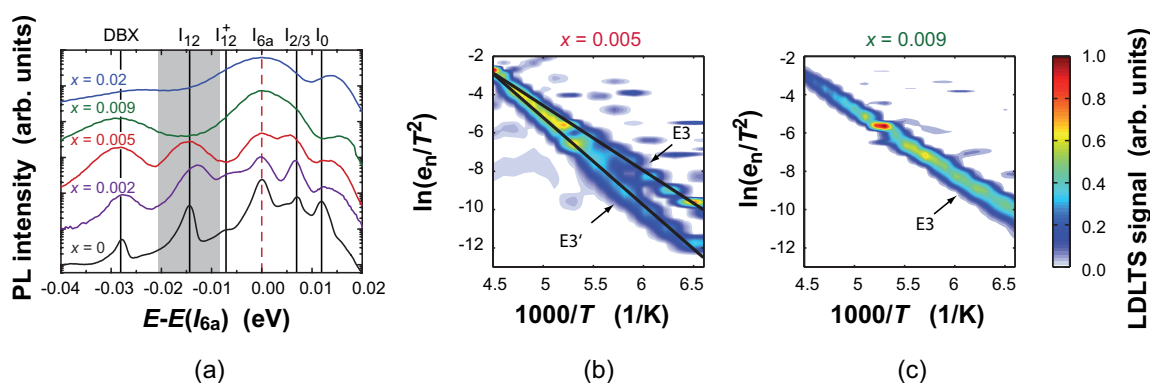


**Figure 8.36:** (a) Photoluminescence-spectra recorded at  $T = 2\text{K}$  for different Mg-contents in the  $\text{Mg}_x\text{Zn}_{1-x}\text{O}$  thin films. Arrhenius contour plots for the samples with (b)  $x = 0.005$  and (c)  $x = 0.009$ .

Fig. 8.36(a) shows the photoluminescence spectra of the  $\text{Mg}_x\text{Zn}_{1-x}\text{O}$  thin films. The lines have been shifted for clarity in vertical direction. In order to facilitate the

comparison of the samples with different Mg-content, the spectra were also shifted such that the transition energy of  $I_{6a}$  (indicated by the red-dashed line) is zero. For  $x \leq 0.005$  only the spectra contain a recombination line labeled  $I_{12}$  and the corresponding ( $D^+X$ ) transition  $I_{12}^+$ . Brandt *et al.* recently showed that the  $I_{12}$ -line is connected to tensile strain in ZnO layers [2]. The  $a$ -lattice constant of the ZnO:Al layer is higher than that of ZnO, further the  $a$ -lattice constant in  $Mg_xZn_{1-x}O$  increases with  $x$ . Hence there exists an  $x$ -value for which the  $Mg_xZn_{1-x}O$ -layer grows unstrained on ZnO:Al. The PL-measurements indicate, that this is the case for  $0.005 < x \leq 0.009$  since  $I_{12}$  is not observed for  $x \geq 0.009$ . For higher Mg-contents the  $Mg_xZn_{1-x}O$ -layer will be compressively strained.

Defects with electronic states in the upper third of the ZnO band gap were studied by DLTS and LDLTS in the temperature range from 20 K to 330 K and 150 K to 250 K, respectively. The DLTS measurements revealed the existence of the known defects E100 and E3 in all samples, regardless of the Mg-content. A defect labeled T2 [3] is only clearly observed in samples with  $x \leq 0.005$ . The LDLTS signals for samples with  $x = 0.005$  and  $x = 0.009$  are shown in form of Arrhenius contour plots in figure 8.36(b) and (c). Figure 8.36(b) shows two emission processes (indicated by the solid lines in this diagram) due to the electron emission of the defects E3 and E3'. In contrast to the sample with  $x = 0.005$  the LDLTS spectra of the sample with  $x = 0.009$  provide no evidence for the presence of two emission processes and therefore two defect levels. It is noteworthy that both  $I_{12}$  and E3' are visible for  $x \leq 0.005$  only, and this coincidence suggests that not only  $I_{12}$  but also E3' is connected to tensile strain.

- [1] H. von Wenckstern, G. Biehne, R. A. Rahman, H. Hochmuth, M. Lorenz, M. Grundmann: Applied Physics Letters 88, 092102 (2006).
- [2] M. Brandt, H. von Wenckstern, G. Benndorf, M. Lange, C. P. Dietrich, C. Kranert, C. Sturm, R. Schmidt-Grund, H. Hochmuth, M. Lorenz, M. Grundmann, M. R. Wagner, M. Alic, C. Nenstiel, A. Hoffmann: Phys. Rev. B 81, 073306 (2010).
- [3] M. Schmidt, M. Ellguth, F. Schmidt, T. Lüder, H. von Wenckstern, R. Pickenhain, M. Grundmann, G. Brauer, W. Skorupa: physica status solidi (b) 247, 1220 (2010).

## 8.27 Nickel-related defects in ZnO thin films

M. Schmidt\*, K. Brachwitz\*, F. Schmidt\*, M. Ellguth\*, H. von Wenckstern\*, R. Pickenhain\*, M. Grundmann\*, G. Brauer<sup>†</sup>, W. Skorupa<sup>†</sup>

\*Universität Leipzig, Institut für Experimentelle Physik II

<sup>†</sup>Helmholz-Zentrum Dresden-Rossendorf, Institut für Ionenstrahlphysik

Transition metal impurities can introduce multiple electronic defect states in the band gap of semiconductors. These often interact with both bands and hence are recombination centers. Therefore, regarding for example the efficiency of opto-electronic devices, it is necessary to characterise these defects, study their electronic properties, and learn how to keep their concentration in such devices low. In this study [1] we investigated nickel-related defects in nickel-doped zinc oxide (ZnO) thin films by space charge spectroscopy. With it we enhance the knowledge on this subject which was so

far mainly gained from optical spectroscopy at nickel doped ZnO single crystals [2, 3]. For Ni on Zn site,  $\text{Ni}_{\text{Zn}}$ , the charge states  $\text{Ni}_{\text{Zn}}^{2+}$  and  $\text{Ni}_{\text{Zn}}^{3+}$  are well known.  $\text{Ni}_{\text{Zn}}^{+}$  can be expected in the upper third of the band gap where it should be detectable by space charge spectroscopy.

Five pulsed laser deposited ZnO thin film samples were used in this study. Four (named “AG”, “AN”, “ZnIA”, “NiIA”) originate from a nominally undoped ZnO film grown onto a two inch sapphire wafer, the fifth, “NiT”, was a ZnO film intentionally doped with 20 ppm nickel oxide, see table 8.2.

**Table 8.2:** ZnO thin film samples used in this study.

sample	abbrev.	description
as-grown reference	AG	untreated
annealed reference	AN	700°C, 700 mbar oxygen at., 45 minutes
zinc implanted	ZnIA	$\text{Zn}^{+}$ implantation, 250 keV, $5 \times 10^{11} \text{ cm}^{-2}$ , annealing
nickel implanted	NiIA	$\text{Ni}^{+}$ implantation, 250 keV, $5 \times 10^{11} \text{ cm}^{-2}$ , annealing
nickel doped	NiT	ZnO target containing 20 ppm nickel oxide

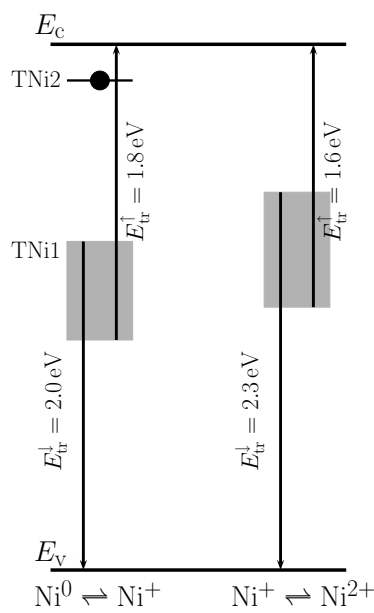
On the samples Pd/ZnO Schottky contacts were deposited by resistive evaporation [4]. This allowed the application of space charge spectroscopy to investigate electronic defect states.

In the samples containing nickel an electronic defect state – in the following labelled “TNi2” – was detected by deep level transient spectroscopy (DLTS). Since TNi2 was neither detectable in the AN sample nor in the ZnIA sample we excluded its generation to be due to implantation damage or annealing effects. Instead, there is evidence that TNi2 is related to nickel since it was detected in both nickel-containing samples although the doping methods applied were different<sup>1</sup>. The thermal activation energy of TNi2 amounts to  $\approx 540 \text{ meV}$  and the high temperature limit of the capture cross section for electrons is  $\approx 8 \times 10^{-16} \text{ cm}^2$ .

Photo-capacitance measurements (PCAP) proved the existence of a further defect state which we labelled “TNi1”. TNi1 is energetically located 1.4 eV to 1.8 eV below the conduction band edge. Therefore, the thermal emission of trapped electrons into the conduction band is too low to be measured by DLTS at temperatures below 400 K, which is the temperature where the Schottky contacts degenerate. TNi1 was – just like TNi2 – only present in the nickel containing samples. Since also the concentration of TNi1 was almost equal to the concentration of TNi2 we concluded that TNi1 and TNi2 are different states of the same defect TNi. From photo-capacitance transients the TNi1 photo-ionisation cross section spectra for the optical emission of trapped electrons into the conduction band and for trapped holes into the valence band, respectively, were calculated.

This work has been supported by Evangelisches Studienwerk Villigst e.V.

<sup>1</sup>From our study we do not obtain information whether TNi2 is an electronic state of  $\text{Ni}_{\text{Zn}}$  or some other defect involving nickel. This would require other experimental techniques.



The sketch, taken from [1], illustrates the picture of TNi we gained from our studies. If TNi is  $\text{Ni}_{\text{Zn}}$  the corresponding charge states are given in the bottom part of the figure. The arrows indicate the threshold energies  $E_{\text{tr}}$  for the optical emission of electrons and holes trapped in the TNi1 state. Due to the lattice distortion these energies differ when TNi2 is occupied by an electron (left) or empty (right). The optical threshold energies define the upper and lower limits for the energetical position (grey rectangles) of TNi1 in the band gap.

In summary, TNi is a positive  $U$  center with large Jahn-Teller lattice distortion. The TNi1 cross sections for optical emission of both, trapped electrons or holes into the corresponding bands are large so that the inverse process – radiative capture – is possible. Therefore, TNi is concluded to be a recombination center.

- [1] M. Schmidt, K. Brachwitz, F. Schmidt, M. Ellguth, H. von Wenckstern, R. Pickenhain, M. Grundmann, G. Brauer, W. Skorupa: *Phys. Stat. Sol.* (2011), doi:10.1002/pssb.201046634
- [2] P. Thurian, R. Heitz, A. Hoffmann, I. Broser: *Jour. Cryst. Growth* **117**, p. 727-731 (1992)
- [3] H. J. Schulz, M. Thiede: *Phys. Rev. B* **35**, p 18-34 (1987)
- [4] H. von Wenckstern, G. Biehne, R. A. Rahman, H. Hochmuth, M. Lorenz, M. Grundmann: *Appl. Phys. Lett.* **88**, p. 092102-092104 (2006)

## 8.28 Luminescence properties of fresnoite $\text{Ba}_2\text{TiSi}_2\text{O}_8$ thin films and bulk materials

A. Müller, M. Lorenz, K. Brachwitz, M. Grundmann, K. Mittwoch\*, T. Höche†

\*3D-Micromac AG, Technologie-Campus 8, 09126 Chemnitz (Germany)

†Leibniz-Institut für Oberflächenmodifizierung e.V., Permoserstr. 15, D-04318 Leipzig;

now: Fraunhofer-Institut für Werkstoffmechanik, Walter-Hülse-Str. 1, D-06120 Halle/Saale

Among many other oxide scintillator materials, fresnoite  $\text{Ba}_2\text{TiSi}_2\text{O}_8$  (BTSO) shows a very intense and broad emission band in the visible spectral range. Additional to its luminescence properties, BTSO exhibits pyro-, piezo-, ferroelectric as well as non-linear optical properties, making it a promising candidate for photonic applications.

BTSO thin films have been grown by pulsed laser deposition (PLD) on different substrates such as a-plane sapphire, fused silica, magnesium oxide (100) and silicon (100). Typical room temperature photoluminescence (PL) spectra of a thin film are shown in Fig. 8.37 (a) in comparison to the spectra of a BTSO single crystal, a BTSO pressed powder target and a  $\text{MgWO}_4$  pressed powder sample. While the BTSO single crystal and the BTSO pressed powder target show a very high luminescence efficiency similar to that of the established scintillator material  $\text{MgWO}_4$ , the luminescence intensities of

the thin films still is about two orders of magnitude weaker. On the one hand, this can be explained by the lower structural quality compared to the single crystal, on the other hand this results from the small absorption coefficient in the UV spectral range [1].

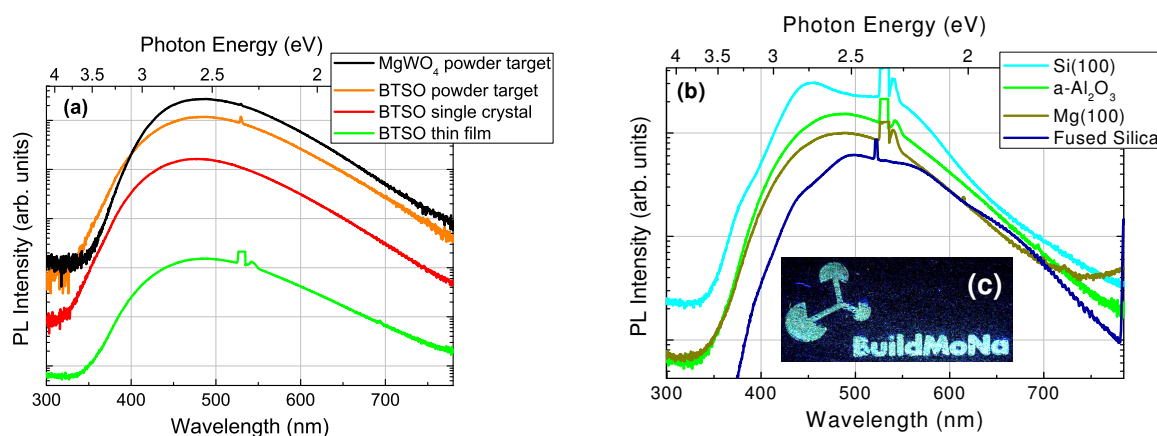


**Figure 8.37:** (a) PL comparison of different BTSO samples with a highly-efficient MgWO<sub>4</sub> phosphor. (b) PL comparison of PLD-grown BTSO thin films on different substrates. The intensities of all spectra are comparable up to a factor of 2. (c) Laser-written BuildMoNa logo on a BTSO thin film on a-sapphire, illuminated by UV light.

A comparison of the PL spectra of PLD-grown thin films on different substrates is shown in Fig. 8.37 (b). The intensities of thin films on the different substrates are quite similar. Although the film on a-sapphire exhibits the most pronounced (100) texture, the film on silicon (100) is brighter. We attribute this to the high light outcoupling efficiency due to the rough surface and the back-reflection of the film luminescence at the substrate.

One possible application for this material is the patterning of thin films by direct laser writing, e.g. as UV-sensitive security feature or as individualized branding. While the amorphous film shows a relative weak PL intensity, the luminosity can be selectively increased by local crystallization using a pulsed CO<sub>2</sub> laser with 10 W power. This is demonstrated in Fig. 8.37 (c) where the laser-written logo of the Graduate School BuildMoNa excited with a Hg lamp is shown.

- [1] A. Müller, M. Lorenz, K. Brachwitz, J. Lenzner, K. Mittwoch, W. Skorupa, M. Grundmann and Th. Höche: CrystEngComm, in press (2011), [doi:10.1039/C1CE05265A](https://doi.org/10.1039/C1CE05265A)

## 8.29 Identification of pre-breakdown mechanism of silicon solar cells at low reverse voltages

H. von Wenckstern, D. Lausch\*, R. Bakowskie<sup>†</sup>, J. Lenzner, C. Czekalla<sup>‡</sup>, K. Petter<sup>†</sup>, M. Grundmann

\*Mikrostrukturdiagnostik und Analytik, Fraunhofer-Center für Silizium-Photovoltaik (CSP), Walter-Hülse-Str. 1, D-06120 Halle (Saale), Germany

<sup>†</sup>R&D Silicon, Q-Cells SE, OT Thalheim, Sonnenallee 17-21, D-06766 Bitterfeld-Wolfen, Germany

‡now with AIXTRON SE, Kaiserstr. 98, 52134 Herzogenrath, Germany

Multi-crystalline silicon solar cells have much lower breakdown voltage than single-crystalline silicon  $pn$ -diodes. Recent publications showed that at least three different mechanisms are responsible for that early breakdown [1]. These can be identified by means of current-voltage measurements. The contribution to the total current of each of these mechanisms exhibits strong lateral variation. While this was facilitated to identify two out of three pre-breakdown mechanisms, occurring at higher reverse voltage  $U_r > 7\text{ V}$ , the third kind of pre-breakdown (labelled Type I from now on), occurring at lower  $U_r$ , remained puzzling.

We identified positions of Type I pre-breakdown sites on commercial multi-crystalline silicon solar cells using dark lock-in thermography and spatially-resolved, spectrally-integrated reverse-bias electroluminescence (ReBEL) [2]. We discuss one site showing Type I pre-breakdown which is representative for all sites investigated. A microscopic, optical image and a ReBEL image with spatial resolution on the  $\mu\text{m}$ -scale ( $\mu$ -ReBEL) of this representative site is depicted fig. 8.38. From the figure it is obvious that the position of light emission corresponds to the position of a stain. We note that the light is predominantly emitted at the borders of the stain. The spectrum of the emitted electroluminescence is a broad band ranging from 400 nm beyond 800 nm with a the maximum at about 715 nm. We performed chemical analysis of this pre-breakdown

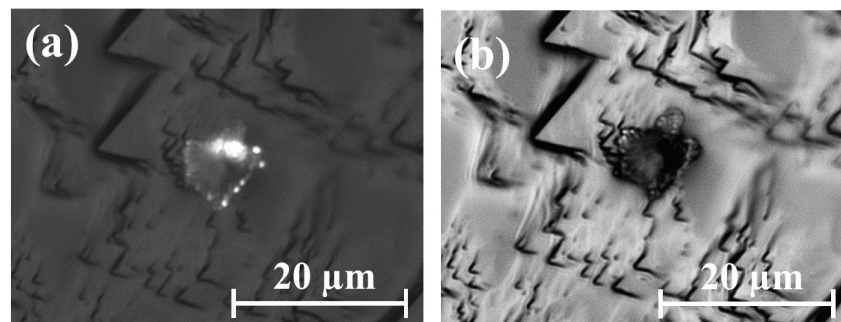


**Figure 8.38:**  $\mu$ -ReBEL image a) recorded for reverse bias of 3 V and reflected-light microscopy image b) of Type I pre-breakdown site.

site by energy dispersive X-ray spectroscopy (EDX). A secondary electron microscopy (SEM) image and EDX maps are depicted in fig. 8.39. Aluminum and oxygen are located at the position of the stain, only. Notably the borders of the stain, being the origin of light emission, are covered by silicon nitride; in other words, the oxidized Al stain must have been on the surface prior to deposition of the  $\text{SiN}_x$  anti-reflection layer.

On the basis of these findings we suggest the following process to explain light emission. The Al particle is already on the surface of the  $p$ -Si wafer prior to the processing of the solar cell. It will form a good ohmic contact to the  $p$ -Si. During realization of the  $n$ -type emitter at high temperatures an oxide layer forms between Al stain and  $n$ -Si emitter; locally a MIS-diode has formed. Under application of reverse bias this localized MIS-diode undergoes an avalanche breakdown. Now, electron and holes are generated by impact ionization and recombine via defect centers in the oxide layer which results in the broad EL band observed by  $\mu$ -ReBEL.

In summary, we have investigated Type I pre-breakdown sites of commercial mc-

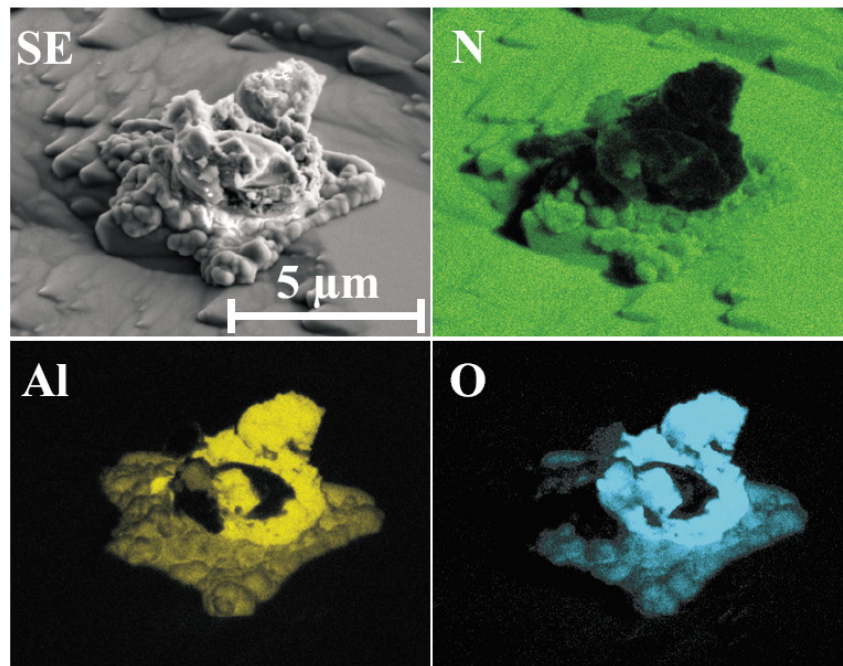


**Figure 8.39:** SE image and EDX mapping of the pre-breakdown site of fig. 8.38. The aluminum and the oxygen are clearly located at the pre-breakdown site and are partially covered by silicon nitride.

silicon solar cells and were able to trace their origin back to aluminum particles present on the *p*-Si wafers prior to the solar cell process.

- [1] W. Kwapil, M. Kasemann, P. Gundel, M. C. Schubert, W. Warta, P. Bronsveld, G. Coletti: *J. Appl. Phys.* **106**, 063530 (2009).
- [2] D. Lausch, K. Petter, R. Bakowskie, C. Czekalla, J. Lenzner, H. von Wenckstern, M. Grundmann: *Appl. Phys. Lett.* **97**, 073506 (2010).

## 8.30 Funding

*Leipzig School of Natural Sciences - Building with Molecules and Nano-objects (Build-MoNa)*

Prof. Dr. M. Grundmann  
DFG GS 185/1

*Polarisationswechselwirkung in Laser-MBE Wurtzit-Perowskit-Heterostrukturen*

Prof. Dr. M. Lorenz, Dipl.-Phys. M. Brandt, Dipl.-Phys. G. Zimmermann  
SFB 762/1-2008, TP A2 within SFB 762 *Funktionalität Oxidischer Grenzflächen*

*Optische Untersuchungen zur dielektrischen Funktion und Ihrer Dynamik an oxidischen Heterostrukturen*

Prof. Dr. M. Grundmann, Prof. Dr. H. Gräner (Martin-Luther-Universität Halle-Wittenberg), Dipl.-Phys. M. Brandt, Dipl.-Phys. T. Böntgen, Dipl.-Phys. F. Schein  
SFB 762/1-2008, TP B03 within SFB 762 *Funktionalität Oxidischer Grenzflächen*

*Lateraler Transport in oxidischen Feldeffekt-Strukturen*

Prof. Dr. M. Grundmann, Prof. Dr. J. Christen (Otto-von-Guericke-Universität Magdeburg), Dipl.-Phys. H. Frenzel

SFB 762/1-2008, TP B04 within SFB 762 *Funktionalität Oxidischer Grenzflächen*

*Spinabhängiges Tunneln in oxidischen Heterostrukturen*

Prof. Dr. M. Grundmann, Prof. Dr. I. Mertig (Matrin-Luther-Universität Halle-Wittenberg), Dipl.-Phys. M. Lorenz, Dipl.-Phys. F. Schmidt

SFB 762/1-2008, TP B06 within SFB 762 *Funktionalität Oxidischer Grenzflächen*

*Bose-Einstein-Kondensation von Exziton-Polaritonen bei Raumtemperatur*

Prof. Dr. M. Grundmann, Dr. R. Schmidt-Grund, Dipl.-Phys. C. Sturm, Dipl.-Phys. K. Brachwitz, Dipl.-Phys. F. Klüpfel

DFG GR 1011/20-1

*Herstellung und Charakterisierung von UV-Mikrokavitäten*

Dipl.-Phys. H. Hilmer

Landesinnovationsstipendium des Freistaates Sachsen im Rahmen des Europäischen Sozialfonds

*Herstellung und Charakterisierung von transparenten Feldeffekttransistoren*

Dipl.-Phys. A. Lajn

Landesinnovationsstipendium des Freistaates Sachsen im Rahmen des Europäischen Sozialfonds

*Herstellung und charakterisierung von Quantendraht-Heterostrukturen*

Dipl.-Phys. M. Lange

Landesinnovationsstipendium des Freistaates Sachsen im Rahmen des Europäischen Sozialfonds

*Magnetische Tunnelkontakte*

Dipl.-Phys. J. Zippel

Landesinnovationsstipendium des Freistaates Sachsen im Rahmen des Europäischen Sozialfonds

*Funktionalisierte Nanosäulen*

Prof. Dr. M. Grundmann, Dr. H. von Wenckstern, Dipl.-Phys. C.P. Dietrich, Dipl.-Phys. M. Stölzel

ESF-Nachwuchsforschergruppe *Funktionale multiskalige Strukturen* des Freistaates Sachsen im Rahmen des Europäischen Sozialfonds

*Internationale Zusammenarbeit in Bildung und Forschung mit Neuseeland: Grundlegende Eigenschaften und Anwendungen von MgZnO/ZnO Heterostrukturen*

Dr. H. von Wenckstern

NZL 10/010, Deutsches Zentrum für Luft- und Raumfahrt e. V., Internationales Büro des BMBF

*Internationale Zusammenarbeit in Bildung und Forschung mit Südafrika: Elektrische Charakterisierung von bei tiefen Temperaturen in ZnO Volumenmaterial und ZnO Nanostrukturen eingebrachten Defekten*

Dr. H. von Wenckstern, Dipl.-Phys. M. Schmidt, Dipl.-Phys. F. Schmidt  
 SUA 09/037, Deutsches Zentrum für Luft- und Raumfahrt e. V., Internationales Büro  
 des BMBF

## 8.31 Organizational Duties

M. Grundmann

- Direktor des Instituts für Experimentelle Physik II
- Coordinator of the European Network of Excellence on "Self-Assembled semiconductor Nanostructures for new Devices in photonics and Electronics" (SANDiE, <http://www.sandie.org>)
- Stellvertretender Sprecher der Graduiertenschule "Leipzig School of Natural Sciences - Building with Molecules and Nano-objects" (BuildMoNa), <http://www.buildmona.de>
- Stellvertretender Sprecher des Sonderforschungsbereiches zur "Funktionalität Oxidischer Grenzflächen" (SFB762), <http://www.physik.uni-halle.de/sfb762>
- Sprecher der Fächerübergreifenden Arbeitsgemeinschaft Halbleiterforschung Leipzig (FAHL), <http://www.uni-leipzig.de/~fahl>
- Mitglied des Beirats Ionenstrahlzentrum, FZR, Dresden-Rossendorf
- Project Reviewer: Deutsche Forschungsgemeinschaft (DFG), Alexander von Humboldt-Stiftung (AvH), Schweizerischer Nationalfonds zur Förderung der wissenschaftlichen Forschung (FNSNF), Fonds zur Förderung der Wissenschaften (FWF)
- Referee: Appl. Phys. Lett., Electr. Lett., J. Appl. Phys., Nature, Physica E, Phys. Rev. B., Phys. Rev. Lett., Phys. Stat. Sol. Science, Appl. Phys. A, and others

M. Lorenz

- Project Reviewer: Department of Energy, Office of Basic Energy Sciences (DOE-BES) U.S.A, Deutsche Forschungsgemeinschaft
- Referee: Advanced Materials, Applied Physics Letters, Applied Physics A, Applied Surface Science, diffusion Fundamentals, European Physics Journal, Journal of Alloys and Compounds, Journal of Physical Chemistry, Journal of Physics D, Journal of Applied Physics, Journal of Vacuum Sciences and Technology A and B, Nanoscale, Physica B, Physica Status Solidi (a) and RRL (He is listed as one of the 'Most active referees.), Small, Solid State Electronics, Semiconductor Science and Technology, Thin Solid Films

H. von Wenckstern

- Project Reviewer: Department of Energy, Basic Energy Sciences (U.S.A.), National Research Foundation (RSA)
- Referee: Adv. Mat., Appl. Surf. Sci., Electrochem. Solid St., J. Alloys Compd., J. Electrochem. Soc., Mater. Chem. Phys., Optics Express, Phys. Rev. B, Sensors, Appl. Phys. Lett., J. Appl. Phys., Thin Solid Films, Solid State Electron., Phys. Stat. Sol., Superlatt. Microstruct., J. Electron. Mater., Turk. J. Phys., J. Mater. Sci., Mater. Electron., J. Vac. Sci. Technol., Mater. Sci. Eng. B, J. Nanosci. Nanotechnol., Microelectron. Eng., J. Phys. D, J. Cryst. Growth, Surf. Sci.
- Editor: MRS Symposium Proceedings Vol. 1201: Zinc Oxide and Related Materials

R. Schmidt-Grund

- Referee: J. Appl. Phys, Phys. Stat. Sol. b, J. Alloy Comp.

## 8.32 External Cooperations

### Academic

- Leibniz-Institut für Oberflächenmodifizierung e. V., Leipzig, Germany  
Prof. Dr. B. Rauschenbach, Prof. Dr. S. Mayr, Dr. J. Gerlach
- Universität Leipzig, Fakultät für Biowissenschaften, Pharmazie und Psychologie  
Prof. Dr. A. Beck-Sickinger
- Universität Leipzig, Fakultät für Chemie und Mineralogie, Germany  
Prof. Dr. H. Krautscheid, Prof. Dr. R. Denecke
- Universität Halle-Wittenberg, Germany  
Prof. Dr. I. Mertig, Prof. Dr. W. Widdra
- Max-Planck-Institut für Mikrostrukturphysik, Halle/Saale, Germany  
Dr. O. Breitenstein, Dr. A. Ernst, Dr. P. Werner, Prof. Dr. D. Hesse
- Forschungszentrum Dresden-Rossendorf, Germany  
Prof. Dr. M. Helm, Dr. K. Potzger, Dr. H. Schmidt
- Technische Universität Berlin, Germany  
Prof. Dr. D. Bimberg, Prof. Dr. A. Hoffmann
- University of Aveiro, Portugal  
Prof. N. A. Sobolev
- Universität Gießen, Germany  
Prof. Dr. B. Meyer
- Universität Magdeburg, Germany  
Prof. Dr. A. Krost, Dr. J. Bläsing, Prof. Dr. J. Christen
- Universität Ulm, Germany  
Prof. Dr. F. Scholz, Prof. Dr. K. Thonke
- Göteborg University, Sweden  
Prof. Dr. M. Willander
- NCSR "Demokritos", Institute of Materials Science, Greece  
Prof. Dr. A. Travlos
- Université Joseph Fourier, Grenoble, France  
Prof. Dr. D. Le Si Dang
- University of Pretoria, South Africa  
Prof. F. D. Auret, Dr. Walter E. Meyer
- University at Buffalo, The State University of New York, USA  
Prof. Dr. S. Durbin
- University of Canterbury, Christchurch, New Zealand  
Prof. Dr. M. Allen

- University of Nebraska, Lincoln, USA  
Prof. Dr. M. Schubert
- Centre de Recherche sur l' Hétéro-Epitaxie et ses Applications (CNRS-CRHEA),  
Valbonne, France  
Dr. J. Zúñiga-Pérez

### Industry

- Solarion AG, Leipzig Germany  
Dr. Alexander Braun, Dr. Andreas Rahm
- OSRAM Opto-Semiconductors GmbH, Regensburg, Germany  
Dr. V. Härle, Dr. S. Lutgen
- Freiburger Compound Materials GmbH, Freiberg, Germany  
Dr. G. Leibiger
- Q-Cells SE, Thalheim, Germany  
Dr. K. Petter

## 8.33 Publications

### Journals

S. Acharya, S. Chuothe, C. Sturm, H. Graener, R. Schmidt-Grund, M. Grundmann, G. Seifert: *Charge carrier dynamics of ZnO and ZnO-BaTiO<sub>3</sub> thin films*, J. Phys. Conf. Ser. **210**, 012048 (4 pages) (2010)

A.O. Ankiewicz, J.S. Martins, M.C. Carmo, M. Grundmann, S. Zhou, H. Schmidt, N.A. Sobolev: *Ferromagnetic resonance on metal nanocrystals in Fe and Ni implanted ZnO*, J. Appl. Phys. **107**, 09B518 (3 pages) (2010)

O. Albrecht, R. Zierold, C. Patzig, J. Bachmann, C. Sturm, B. Rheinländer, M. Grundmann, D. Görlitz, B. Rauschenbach, K. Nielsch: *Magnetic tubular nanostructures based on glancing-angle deposited templates and atomic layer deposition*, phys. stat. sol. (b) **247**, 1365-1371 (2010)

W. Anwand, G. Brauer, T.E. Cowan, V. Heera, H. Schmidt, W. Skorupa, H. von Wenckstern, G. Benndorf, M. Grundmann: *Structural characterization of H plasma-doped ZnO single crystals by Hall measurements and photoluminescence studies*, phys. stat. sol. (a) **207**, 2426-2431 (2010)

M. Bachmann, K. Goede, A.G. Beck-Sickinger, M. Grundmann, A. Irbäck, W. Janke: *Mikroskopischer Mechanismus der spezifischen Adhäsion von Peptiden an Halbleitersubstraten*, Angew. Chemie **122**, 9721-9724 (2010)

M. Bachmann, K. Goede, A.G. Beck-Sickinger, M. Grundmann, A. Irbäck, W. Janke: *Microscopic Mechanism of Specific Peptide Adhesion to Semiconductor Substrates*, Angew. Chemie Int. Ed. **49**, 9530-9533 (2010)

- M. Brandt, M. Lange, M. Stölzel, A. Müller, G. Benndorf, J. Zippel, J. Lenzner, M. Lorenz, M. Grundmann: *Control of interface abruptness of polar MgZnO/ZnO quantum wells grown by pulsed laser deposition*, Appl. Phys. Lett. **97**, 052101 (3 pages) (2010)
- M. Brandt, H. von Wenckstern, G. Benndorf, M. Lange, C.P. Dietrich, C. Kranert, C. Sturm, R. Schmidt-Grund, H. Hochmuth, M. Lorenz, M. Grundmann, M.R. Wagner, M. Alic, C. Nenstiel, A. Hoffmann: *Identification of a donor-related recombination channel in ZnO thin films*, Phys. Rev. B **81**, 073306 (4 pages) (2010)
- B. Cao, J. Zúñiga-Pérez, C. Czekalla, H. Hilmer, J. Lenzner, N. Boukos, A. Travlos, M. Lorenz, M. Grundmann: *Tuning the lateral density of ZnO nanowire arrays and its application as physical templates for radial nanowire heterostructures*, J. Mat. Chem. **20**, 3848-3854 (2010)
- B.Q. Cao, M. Lorenz, G. Zimmermann, C. Czekalla, M. Brandt, H. von Wenckstern, M. Grundmann: *p-type Phosphorus Doped ZnO Wires for Optoelectronic Applications*, Nanowires, p. 117-132 (2010), P. Prete, ed., ISBN 978-953-7619-79-4
- J. Chai, R.J. Mendelsberg, R.J. Reeves, J. Kennedy, H. von Wenckstern, M. Grundmann, K. Doyle, T.H. Meyers, S.M. Durbin: *Identification of a deep acceptor level in ZnO due to silver doping*, J. Electr. Mat. **39**, 577-583 (2010)
- C. Czekalla, T. Nobis, A. Rahm, B. Cao, J. Zúñiga-Pérez, C. Sturm, R. Schmidt-Grund, M. Lorenz, M. Grundmann: *Whispering gallery modes in ZnO nano- and microwires*, phys. stat. sol. (b) **247**, 1282-1293 (2010)
- C.P. Dietrich, A. Müller, M. Stölzel, M. Lange, G. Benndorf, H. von Wenckstern, M. Grundmann: *Bound-exciton recombination in  $Mg_xZn_{1-x}O$  thin films*, Proc. Mat. Res. Soc. **1201**, 1201-H03-08 (6 pages) (2010)
- C.P. Dietrich, M. Lange, G. Benndorf, J. Lenzner, M. Lorenz, M. Grundmann: *Competing exciton localization effects due to disorder and shallow defects in semiconductor alloys*, New J. Phys. **12**, 033030 (10 pages) (2010)
- C.P. Dietrich, M. Lange, G. Benndorf, H. von Wenckstern, M. Grundmann: *Donor-acceptor pair recombination in non-stoichiometric ZnO thin films*, Sol. St. Comm. **150**, 379-382 (2010)
- H. Frenzel, A. Lajn, H. von Wenckstern, M. Lorenz, F. Schein, Zh. Zhang, M. Grundmann: *Recent Progress on ZnO-Based Metal-Semiconductor Field-Effect Transistors and their Application in Transparent Integrated Circuits*, Adv. Mater. **22**, 5332-5349 (2010)
- H. Frenzel, F. Schein, A. Lajn, H. von Wenckstern, M. Grundmann: *High-gain integrated inverters based on ZnO MESFET technology*, Appl. Phys. Lett. **96**, 113502 (3 pages) (2010)
- H. Frenzel, A. Lajn, H. von Wenckstern, M. Grundmann: *Ultrathin gate-contacts for MESFET devices: An alternative approach in transparent electronics*, J. Appl. Phys. **107**, 114515 (6 pages) (2010)
- H. Frenzel: *ZnO-based metal-semiconductor field-effect transistors*, Dissertation Universität Leipzig, Der Andere Verlag, Tönning, ISBN: 978-3-86247-099-0 (2010)

- M. Grundmann, H. Frenzel, A. Lajn, H. von Wenckstern, F. Schein, M. Lorenz: *ZnO-based MESFET Devices*, Proc. Mat. Res. Soc. **1201**, 1201-H01-01 (5 pages) (2010)
- M. Grundmann, T. Böntgen, M. Lorenz: *The Occurrence of Rotation Domains in Heteroepitaxy*, Phys. Rev. Lett. **105**, 146102 (4 pages) (2010)
- M. Grundmann, H. Frenzel, A. Lajn, M. Lorenz, F. Schein, H. von Wenckstern: *Transparent Semiconducting Oxides: Materials and Devices*, phys. stat. sol. (a) **207**, 1437-1449 (2010)
- M. Grundmann: *Architecture of nano- and microdimensional building blocks*, phys. stat. sol. (b) **247**, 1257-1264 (2010)
- D. Hiller, R. Zierold, J. Bachmann, M. Alexe, Y. Yang, J.W. Gerlach, A. Stesmans, M. Jivanescu, U. Müller, J. Vogt, H. Hilmer, P. Loper, M. Künle, F. Munnik, K. Nielsch, M. Zacharias: *Low temperature silicon dioxide by thermal atomic layer deposition: Investigation of material properties*, J. Appl. Phys. **6**, 064314 (2010)
- H. Hilmer, C. Sturm, R. Schmidt-Grund, B. Rheinländer, M. Grundmann: *Observation of strong light-matter coupling by spectroscopic ellipsometry*, Superlatt. Microstr. **47**, 19-23 (2010)
- R. Kaden, G. Wagner, C. Sturm, R. Schmidt-Grund, H. von Wenckstern, A. Prager, K. Bente, M. Grundmann: *Synthesis and physical properties of cylindrite micro tubes and lamellae*, phys. stat. sol. (b) **247**, 1335-1350 (2010)
- A. Lajn, H. von Wenckstern, G. Benndorf, C.P. Dietrich, M. Brandt, G. Biehne, H. Hochmuth, M. Lorenz, M. Grundmann: *Shallow Donors and Compensation in Homoepitaxial ZnO Thin Films*, J. Electr. Mat. **39**, 595-600 (2010)
- M. Lange, C. Dietrich, C. Czekalla, J. Zippel, G. Benndorf, M. Lorenz, J. Zúñiga-Pérez, M. Grundmann: *Luminescence Properties of ZnO/Zn<sub>1-x</sub>Cd<sub>x</sub>O/ZnO double heterostructures*, J. Appl. Phys. **107**, 093530 (8 pages) (2010)
- D. Lausch, K. Petter, R. Bakowskie, C. Czekalla, J. Lenzner, H. von Wenckstern, M. Grundmann: *Identification of Pre-Breakdown Mechanism of Silicon Solar Cells at Low Reverse Voltages*, Appl. Phys. Lett. **97**, 073506 (3 pages) (2010)
- S. Lautenschlaeger, S. Eisermann, M.N. Hofmann, U. Roemer, M. Pinnisch, A. Laufer, B.K. Meyer, H. von Wenckstern, A. Lajn, F. Schmidt, M. Grundmann, J. Blaesing, A. Krost: *Morphological, structural and electrical investigations on non-polar a-plane ZnO epilayers*, J. Cryst. Growth **312**, 2078-2082 (2010)
- M. Lorenz, A. Lajn, H. Frenzel, H. von Wenckstern, M. Grundmann, P. Barquinha, R. Martins, E. Fortunato: *Low-temperature processed Schottky-gated field-effect transistors based on amorphous gallium-indium-zinc-oxide thin films*, Appl. Phys. Lett. **97**, 243506 (3 pages) (2010)
- M. Lorenz, A. Rahm, B. Cao, J. Zúñiga-Pérez, E.M. Kaidashev, N. Zhakarov, G. Wagner, T. Nobis, C. Czekalla, G. Zimmermann, M. Grundmann: *Self-organized growth of ZnO-based nano- and microstructures*, phys. stat. sol. (b) **247**, 1265-1281 (2010)

M. Lorenz, M. Brandt, M. Lange, G. Benndorf, H. von Wenckstern, D. Klimm, M. Grundmann: *Homoepitaxial  $Mg_xZn_{1-x}O$  ( $0 \leq x \leq 0.22$ ) thin films grown by pulsed laser deposition*, *Thin Solid Films* **518**, 4623-4629 (2010)

M. Mäder, S. Perlt, T. Höche, H. Hilmer, M. Grundmann, B. Rauschenbach: *Gold nanostructure matrices by diffraction mask-projection laser ablation: extension to previously inaccessible substrates*, *Nanotechnology* **21**, 175304 (5 pages) (2010)

A. Müller, M. Stölzel, G. Benndorf, M. Lorenz, M. Grundmann: *Origin of the near-band-edge luminescence in  $Mg_xZn_{1-x}O$* , *J. Appl. Phys.* **107**, 013704 (6 pages) (2010)

St. Puttnins, H. Zachmann, A. Rahm, G. Benndorf, Marius Grundmann: *Quantum efficiency analysis of ion beam assisted deposition of  $Cu(In,Ga)Se_2$  solar cells on flexible substrates*, *Proceedings of the 25th European Photovoltaic Solar Energy Conference/5th World Conferenc on Photovoltaic Energy Conversion*, Valencia, Spain, pages 3369-3371 (2010)

C. Scarlat, K.M. Mok, S. Zhou, M. Vinnichenko, M. Lorenz, M. Grundmann, M. Helm, M. Schubert, H. Schmidt: *Voigt effect measurement on PLD grown NiO thin films*, *phys. stat. sol. (c)* **7**, 334-337 (2010)

M. Schmidt, M. Ellguth, F. Schmidt, Th. Lüder, H. von Wenckstern, R. Pickenhain, M. Grundmann, G. Brauer, W. Skorupa: *Defects in a nitrogen-implanted ZnO thin film*, *phys. stat. sol. (b)* **247**, 1220-1226 (2010)

R. Schmidt-Grund, H. Hilmer, A. Hinkel, C. Sturm, B. Rheinländer, V. Gottschalch, M. Lange, J. Zúñiga-Pérez, M. Grundmann: *Two-dimensional confined photonic wire resonators - strong light-matter coupling*, *phys. stat. sol. (b)* **247**, 1351-1364 (2010)

*Scientific report of the Forschergruppe 522*, *phys. stat. sol. (b)* **247**, p. 1257-1392 (2010), M. Grundmann, ed.

C. Sturm, H. Hilmer, R. Schmidt-Grund, M. Grundmann: *Polarization behavior of the exciton-polariton emission of ZnO-based microresonators*, *Proc. Mat. Res. Soc.* **1208E**, 1208-O18-08 (6 pages) (2010)

H. von Wenckstern, K. Brachwitz, M. Schmidt, C.P. Dietrich, M. Ellguth, M. Stölzel, M. Lorenz, M. Grundmann: *The E3 defect in  $Mg_xZn_{1-x}O$* , *J. Electr. Mat.* **39**, 584-588 (2010)

H. von Wenckstern, Z.P. Zhang, M. Lorenz, C. Czekalla, H. Frenzel, A. Lajn, M. Grundmann: *Light beam induced current measurements on ZnO Schottky diodes and MESFETs*, *Proc. Mat. Res. Soc.* **1201**, 1201-H04-02 (6 pages) (2010)

H. von Wenckstern, S. Müller, G. Biehne, H. Hochmuth, M. Lorenz, M. Grundmann: *Dielectric passivation of ZnO-based Schottky diodes*, *J. Electr. Mat.* **39**, 559-562 (2010)

Q.Y. Xu, S.Q. Zhou, D. Bürger, H. Hochmuth, M. Lorenz, M. Grundmann, H. Schmidt: *Electrical control of magnetoresistance in highly insulating Co-doped ZnO*, *Jpn. J. Appl. Phys.* **49**, 043002 (4 pages) (2010)

H. Zachmann, St. Puttnins, F. Daume, A. Rahm, K. Otte: *The impact of sodium on ion-beam induced defects in cigs absorber films*, Proceedings of the 25th European Photovoltaic Solar Energy Conference/5th World Conferenc on Photovoltaic Energy Conversion, Valencia, Spain, pages 3382-3385 (2010)

G. Zimmermann, M. Lange, B. Cao, M. Lorenz, M. Grundmann: *Resistivity control of ZnO nanowires by Al-doping*, phys. stat. sol. RRL **4**, 82-84 (2010)

J. Zippel, S. Heitsch, M. Stölzel, A. Müller, H. von Wenckstern, G. Benndorf, M. Lorenz, H. Hochmuth, M. Grundmann: *Optical properties of homo- and heteroepitaxial ZnO/Mg<sub>x</sub>Zn<sub>1-x</sub>O quantum wells grown by pulsed laser deposition*, J. Lumin. **130**, 520-526 (2010)

Jan Zippel, Michael Lorenz, Annette Setzer, Gerald Wagner, Nikolai Sobolev, Pablo Esquinazi, Marius Grundmann: *Defect induced ferromagnetism in undoped and Mn-doped zirconia thin films*, Phys. Rev. B **82**, 125209 (5 pages) (2010)

J. Zippel, M. Stölzel, A. Müller, G. Benndorf, M. Lorenz, H. Hochmuth, M. Grundmann: *Electronic coupling in ZnO/Mg<sub>x</sub>Zn<sub>1-x</sub>O double quantum wells grown by pulsed laser deposition*, phys. stat. sol. (b) **247**, 398-404 (2010)

## Books

M. Grundmann: *The Physics of Semiconductors, An Introduction including Nanophysics and Applications*, 2nd edition (Springer, Heidelberg, 2010) ISBN 978-3-642-13883-6

## Patents

H. Frenzel, A. Lajn, H. von Wenckstern, M. Grundmann: German patent DE 10 2009 030 045 B3 (2011)

M. Grundmann, H. Frenzel, A. Lajn, H. von Wenckstern: *TRANSPARENT RECTIFYING METAL/METAL OXIDE/SEMICONDUCTOR CONTACT STRUCTURE AND METHOD FOR THE PRODUCTION THEREOF AND USE*, PCT Application WO 2010/149616

## Talks

F. Daume, St. Puttnins, H. Zachmann, A. Rahm, Marius Grundmann: *Influence of sodium on the electrical properties of flexible CIGSe solar cells*, 74th DPG Spring Meeting, Regensburg, Germany, March 2010

M. Grundmann: *Transparente Elektronik*, plenary talk at 74th DPG Spring Meeting, Regensburg, Germany, March 2010, invited

M. Grundmann: *ZnO-Anwendungen in der Photonik*, 17. Dresdner Photonik-Kolloquium, IAAP, Dresden, Germany, June 2010

F. Klüpfel, S. Schmidt, A. Lajn, H. Frenzel, H. von Wenckstern, J. Käs, M. Grundmann: *ZnO-based On-Chip Devices for Cell Potential Measurements*, 74th DPG Spring Meeting, Regensburg, Germany, March 2010

P. Kühne, C. Czekalla, R. Schmidt-Grund, C. Sturm, M. Grundmann: *Determination of the refractive index of single crystal bulk samples and micro-structures*, 5th International Conference on Spectroscopic Ellipsometry (ICSE-V), Albany (NY), USA, May 2010

A. Lajn, H. Frenzel, F. Schein, H. von Wenckstern, M. Grundmann: *Transparent Rectifying Contacts*, 74th DPG Spring Meeting, Regensburg, Germany, March 2010

A. Lajn, H. Frenzel, T. Diez, F. Schein, H. von Wenckstern, M. Grundmann: *Transparent Rectifying Contacts*, Electronic materials conference, Notre Dame, Indiana, USA, 2010

A. Lajn, H. Frenzel, T. Diez, F. Schein, H. von Wenckstern, M. Grundmann: *Transparent Rectifying Contacts*, ZnO-Workshop, Changchun, China, 2010

A. Lajn, H. Frenzel, T. Diez, Fabian Klüpfel, F. Schein, H. von Wenckstern, M. Grundmann: *Transparent MgZnO-based Metal-semiconductor Field-Effect Transistors and Devices*, 2010 MRS Fall Meeting, Boston, USA, December 2010

M. Lange, C.P. Dietrich, J. Zúñiga-Pérez, M. Lorenz, M. Grundmann: *ZnO-based quantum well nanowire heterostructures with large confinement energies*, 6th International workshop on ZnO and related Materials, Changchun, China, August 2010

M. Lorenz, J. Zúñiga-Pérez, B. Cao, C. Czekalla, T. Nobis, G. Zimmermann, M. Lange, C.P. Dietrich, H. Hilmer, R. Schmidt-Grund, M. Grundmann: *ZnO-based nano- and microstructures for advanced optical and electronic applications*, 6th International workshop on ZnO and related Materials, Changchun, China, August 2010

A. Meissner, R. Schmidt-Grund, H. Hilmer, C. Sturm, J. Zúñiga-Pérez, M. Lange, M. Grundmann: *Strong light-matter coupling in ZnO nano-pillar resonators*, 74th DPG Spring Meeting, Regensburg, Germany, March 2010

A. Müller, M. Stölzel, G. Benndorf, M. Grundmann: *Temperature-Dependent Time-Resolved Photoluminescence on MgZnO*, 74th DPG Spring Meeting, Regensburg, Germany, March 2010

St. Müller, H. von Wenckstern, Zh. Zhang, H. Hochmuth, M. Lorenz, M. Grundmann: *Dielectric passivated ZnO-based Schottky diodes*, 74th DPG Spring Meeting, Regensburg, Germany, March 2010

St. Puttnins, F. Daume, H. Zachmann, A. Rahm, Marius Grundmann: *Current blocking and current collection in CIGSe solar cells depending on sodium content*, 74th DPG Spring Meeting, Regensburg, Germany, March 2010

R. Schmidt-Grund, M. Grundmann: *Conformal Coating of ZnO-based Nanostructures With Oxide Heterostructures*, 2010 MRS Spring Meeting, San Francisco, USA, April 2010 (invited)

R. Schmidt-Grund: *Optische Eigenschaften und Charakterisierung von TCOs*, EFDS workshop "Transparente leitfähige Oxide - Festkörperphysikalische Grundlagen und Technologie", Dresden, Germany, June 2010 (invited)

R. Schmidt-Grund, C. Czekalla, P. Kühne, C. Sturm, H. Hilmer, A. Hinkel, J. Zúñiga-Pérez, M. Lange, J. Lenzner, M. Lorenz, M. Grundmann: *Optical modes in ZnO nano- and micro-wire resonators - lasing and strong light-matter coupling*, 8th International Nanotechnology Symposium - New Ideas for Industry, Nanofair2010, Dresden, Germany, July 2010

R. Schmidt-Grund, H. Hilmer, B. Rheinländer, V. Gottschalch, A. Hinkel, C. Sturm, M. Lange, J. Zúñiga-Pérez, M. Lorenz, M. Grundmann: *Funktionalisierung der Oberflächen von Mikro- und Nanostrukturen mittels dielektrischer Mehrfachschichten*, ThGOT 2010, 2. Thüringer Kolloquium "Dünne Schichten in der Optik", Gera, Germany, September 2010

M. Stölzel, M. Brandt, A. Müller, G. Benndorf, M. Lorenz, M. Grundmann: *Quantum confined Stark effect in ZnO/MgZnO quantum wells fabricated with different PLD growth processes*, 74th DPG Spring Meeting, Regensburg, Germany, March 2010

C. Sturm, H. Hilmer, R. Schmidt-Grund, M. Grundmann: *Strong light matter coupling with free and localized donor bound excitons*, 74th DPG Spring Meeting, Regensburg, Germany, March 2010

H. von Wenckstern: *Electric and electronic properties of defects in semiconductors: Case studies of mc-Si and single-crystalline ZnO*, Friedrich-Schiller-Universität Jena, Jena, Germany, April 2010, invited

H. von Wenckstern: *Electrical properties of ZnO and its application in transparent electronics*, Leibniz-Institut für Kristallzüchtung, Berlin, Germany, April 2010, invited

H. von Wenckstern: *ZnO-based nanostructures and application of ZnO in transparent electronics*, Fraunhofer IWS Dresden, Dresden, Germany, May 2010, invited

H. von Wenckstern: *Elektrische Eigenschaften und Charakterisierung von transparenten leitfähigen Oxiden*, EFDS workshop "Transparente leitfähige Oxide - Festkörperphysikalische Grundlagen und Technologie", Dresden, Germany, June 2010, invited

H. von Wenckstern, A. Lajn, H. Frenzel, M. Grundmann: *Transparent Rectifying Contacts: An alternative Approach towards transparent Electronics*, Electronic Materials Conference 2010, Notre Dame, U.S.A., June 2010

H. von Wenckstern, St. Müller, M. Schmidt, F. Schmidt, M. Grundmann: *Optimization of dielectric passivation of ZnO-based Schottky diodes*, Electronic Materials Conference 2010, Notre Dame, U.S.A., June 2010

H. von Wenckstern, F. Schmidt, K. Brachwitz, M. Schmidt, C. Dietrich, M. Grundmann: *High-resolution Laplace DLTS on MgZnO PLD thin films*, Electronic Materials Conference 2010, Notre Dame, U.S.A., June 2010

J. Zippel, M. Lorenz, A. Setzer, J. Lenzner, H. Hochmuth, G. Wagner, P. Esquinazi, M. Grundmann: *Growth and Characterisation of Manganese stabilized Zirconia*, 74th DPG Spring Meeting, Regensburg, Germany, March 2010

**Posters**

K. Brachwitz, H. von Wenckstern, M. Schmidt, F. Schmidt, C.P. Dietrich, M. Stölzel, M. Lorenz, M. Grundmann: *Electrical characterization of electronic defects in MgZnO thin films grown by pulsed-laser deposition*, 74th DPG Spring Meeting, Regensburg, Germany, March 2010

C. Czekalla, P. Kühne, C. Sturm, R. Schmidt-Grund, M. Grundmann: *The refractive index of zinc oxide bulk and microwire single crystals*, 74th DPG Spring Meeting, Regensburg, Germany, March 2010

F. Daume, St. Puttnins, H. Zachmann, A. Rahm, M. Grundmann: *Influence of Damp and Heat on Roll-Over Effect in Cu(In,Ga)Se<sub>2</sub> Solar Cells*, E-MRS Spring Meeting, Strasbourg, France, June 2010

C.P. Dietrich, M. Lange, J. Zippel, J. Lenzner, M. Lorenz, M. Grundmann: *Growth and characterization of ZnO- and ZnO:P-microwires*, 74th DPG Spring Meeting, Regensburg, Germany, March 2010

H. Hilmer, C. Sturm, R. Schmidt-Grund, J. Zúñiga-Pérez, H. Hochmuth, M. Cornejo, F. Frost, M. Grundmann: *Fabrication of ZnO-cavities for planar microresonators*, 74th DPG Spring Meeting, Regensburg, Germany, March 2010

S. Jander, St. Puttnins, A. Rahm, Marius Grundmann: *Optimization of Cu(In,Ga)Se<sub>2</sub> solar cells under different irradiance*, 74th DPG Spring Meeting, Regensburg, Germany, March 2010

F. Klüpfel, A. Lajn, H. Frenzel, H. von Wenckstern, M. Grundmann: *Dynamic Properties of (Mg,Zn)O-based MESFETs*, 2010 MRS Fall Meeting, Boston, USA, December 2010

J. Kupper, A. Müller, G. Benndorf, M. Lange, M. Brandt, M. Lorenz, M. Grundmann: *Photolumineszenz- und Transmissionsmessungen an ZnO/MgZnO-Quantengrabenstrukturen*, 74th DPG Spring Meeting, Regensburg, Germany, March 2010

M. Lange, C.P. Dietrich, C. Czekalla, M. Lorenz, M. Grundmann: *ZnO-based Nanowire Structures and Heterostructures*, 74th DPG Spring Meeting, Regensburg, Germany, March 2010

St. Puttnins, St. Heinker, S. Jander, K. Sols, A. Rahm, M. Grundmann: *Influence of i-ZnO and ZnO:Al Properties on Low-Irradiance Efficiency of Flexible Cu(In,Ga)Se<sub>2</sub> Solar Cells*, E-MRS Spring Meeting, Strasbourg, France, June 2010

F. Schein, H. Frenzel, A. Lajn, M. Lorenz, H. von Wenckstern, M. Grundmann: *High-gain integrated inverters based on ZnO MESFET technology*, 74th DPG Spring Meeting, Regensburg, Germany, March 2010

R. Schmidt-Grund, D. Schumacher, P. Kühne, C. Czekalla, H. Hilmer, C. Sturm, H. Hochmuth, M. Lorenz, M. Grundmann: *Dielectric tensor of ZnO bulk and microwire single crystals and Mg<sub>x</sub>Zn<sub>1-x</sub>O thin films*, 30th International Conference on the Physics of Semiconductors, ICPS2010, Seoul, Korea, July 2010

R. Schmidt-Grund, H. Hilmer, A. Hinkel, J. Zúñiga-Pérez, C. Sturm, M. Lange, G. Zimmermann, J. Lenzner, M. Lorenz, M. Grundmann: *Two- and three-dimensional confined optical modes in nano-pillar resonators: strong light-matter coupling*, 30th International Conference on the Physics of Semiconductors, ICPS2010, Seoul, Korea, July 2010

S. Schöche, R. Schmidt-Grund, C. Sturm, M. Brandt, H. Hochmuth, M. Lorenz, M. Grundmann: *Crystal Structure and Dielectric Function of BaTiO<sub>3</sub> Single Crystals and Thin Films*, MRS Spring Meeting, San Francisco, USA, April 2010

D. Schumacher, R. Schmidt-Grund, P. Kühne, H. Hilmer, H. Hochmuth, M. Grundmann: *Low-temperature dielectric function of a-plane Mg<sub>x</sub>Zn<sub>1-x</sub>O*, 74th DPG Spring Meeting, Regensburg, Germany, March 2010

D. Schumacher, R. Schmidt-Grund, P. Kühne, H. Hilmer, C. Sturm, H. Hochmuth, M. Lorenz, M. Grundmann: *Low-Temperature Dielectric Tensor of a-plane Mg<sub>x</sub>Zn<sub>1-x</sub>O*, 5th International Conference on Spectroscopic Ellipsometry (ICSE-V), Albany (NY), USA, May 2010

C. Sturm, H. Hilmer, R. Schmidt-Grund, M. Grundmann: *Scattering behaviour of exciton-polaritons in a ZnO-based microresonator* Poster at the 30th International Conference on the Physics of Semiconductors, ICPS2010, Seoul, Korea, July 2010

C. Sturm, H. Hilmer, R. Schmidt-Grund, M. Grundmann: *Polarization behaviour of the exciton-polariton emission in ZnO microresonators*, 74th DPG Spring Meeting, Regensburg, Germany, March 2010

H. Zachmann, St. Puttnins, F. Daume, A. Rahm, K. Otte: *Generation of electrical defects in ion beam assisted deposition of Cu(In,Ga)Se<sub>2</sub> thin film solar cells*, E-MRS Spring Meeting, Strasbourg, France, June 2010

H. Zachmann, S. Puttnins, M.V. Yakushev, F. Luckert, R.W. Martin, A.V. Karotki, V.F. Gremenok, A.V. Mudryi: *Fabrication and characterisation of Cu(In,Ga)Se<sub>2</sub> solar cells on polyimide*, E-MRS Spring Meeting, Strasbourg, France, June 2010

## 8.34 Graduations

### Doctorate

- Amélia Olga Concalves Ankiewicz  
*Properties of self-assembled diluted magnetic semiconductor nanostructures*  
January 2010
- Matthias Brandt  
*Influence of the electric polarization on carrier transport and recombination dynamics in ZnO-based heterostructures*  
July 2010
- Heiko Frenzel  
*ZnO-based metal-semiconductor field-effect transistors*  
September 2010

- Gregor Zimmermann  
*Elektrische Charakterisierung PLD-gewachsener Zinkoxid-Nanodrähte*  
August 2010

## Diploma

- Robert Heinhold  
*Unterscheidung paralleler Leitungspfade in Halbleitern mittels magnetfeldabhängiger Transportuntersuchungen*  
April 2010
- Sebastian Jander  
*Schwachlichtverhalten und Sperrspannungscharakteristik von flexiblen CIGSe Solarzellen*  
September 2010
- Fabian Klüpfel  
*Design und Test einer On-Chip-Elektronik zur Messung von Zellpotentialänderungen*  
January 2010
- Christian Kranert  
*Aufbau eines UV-Raman-Messplatzes und Untersuchungen an  $Mg_xZn_{1-x}O$ - und  $BaTiO_3$ -Dünnschichten und  $ZnO$ - $BaTiO_3$ -Heterostrukturen*  
October 2010
- Johannes Kupper  
*Photolumineszenz- und Transmissions-Messungen an  $ZnO$ / $MgZnO$ -Quantengrabenstrukturen mit  $MgZnO$ -Puffer*  
August 2010
- Annekatrin Meißner  
*Optische Moden in  $ZnO$  Mikro- und Nanosäulenresonatoren*  
May 2010
- Stefan Müller  
*Dielektrische Passivierung von Zinkoxid-basierten Schottky-Kontakten*  
May 2010
- Florian Schmidt  
*Aufbau eines temperaturabhängigen Laplace-DLTS-Messplatzes zur Untersuchung eng benachbarter Energieniveaus*  
January 2010
- David Schumacher  
*Untersuchung zur  $ZnO$ -Valenzbandordnung mittels Tieftemperatur-Ellipsometrie*  
June 2010

## Master

- Florian Kumpfe  
*Investigation of String-Ribbon Solar Cells with a Numerical Computer Simulation*

*Program*  
July 2010

### **Bachelor**

- Robert Karsthof  
*Optische und kapazitätsspektroskopische Untersuchungen von Defekten in wärme-behandelten ZnO-Dünnschichten*, December 2010
- Katja Mexner  
*Struktur und elektrische Transporteigenschaften dünner Zinkferritfilme*  
September 2010
- Anna Reinhardt  
*Herstellung und Charakterisierung von Wolframoxid-basierten Schottky-Kontakten auf heteroepitaktischem Zinkoxid*  
September 2010
- Julia Tesch  
*Investigation of the phase composition of silicon carbide for water based slurry by XRD*  
August 2010

### **8.35 Guests**

- Prof. Dr. Kartik Ghosh  
Missouri State University, Physics, Astronomy and Materials Science, Springfield, USA  
2. July - 30. April 2010
- Prof. Dr. Anupam Madhukar  
University of Southern California, Los Angeles, USA  
2. September - 15. September 2010
- Dr. Jesús Zúñiga-Pérez  
Centre de Recherche sur L'Hétéro-Epitaxie et ses Applications (CNRS-CRHEA), Valbonne, France  
1. February - 30. April 2010

# 9

## Solid State Optics and Acoustics

### 9.1 Introduction

The research is concentrating on the study of transport properties of elementary excitations in condensed matter of the Bosonic type (Bosonic quasi particles). Concerning the conventional description this relates mainly to acoustical and optical excitation and detection of travelling waves and their interaction with matter. Special interest is given to the influence of anisotropy and inhomogeneity to the dynamics of mechanical excitations. Furthermore novel schemes and first principle modelling is developed for the study and in support of applications concerning nonlinear interaction of acoustic excitations.

Applications concentrate on the enhancement and application of high resolution monitoring in space and time. The respective technologies include scanning Bosonic confocal microscopy for which even a combined instrument for optical and acoustical excitations has been developed. Three dimensional microscopic imaging is further developed by novel technologies including microscopic holographic imaging and microscopic tomography. With relation to temporal resolution the developments pursued under the 7th European framework in the project Aircraft Integrated Structural Health Assessment (AISHA II) include the development of detection schemes capable of picosecond resolution. Scanning acoustic microscopy with vector contrast allows the resolution of the time needed for transport (time-of-flight, TOF) of the waves employed for imaging with a resolution down to 100 fs for signal collection times of only 5 ms.

Concerning microscopic applications fuel cell membranes are characterized in the project MultiPlat of the 7th European framework. For this purpose combined scanning acoustic and electric potential microscopy is under development. Bio-medical applications involve non-invasive high resolution acoustic imaging of living mesenchymal stem cells (MSCs) for substantial fractions of their life cycle, acoustic monitoring of cell constructs by optical and acoustic methods, and monitoring of the muscle dynamics of exercising athletes. The transport properties of transverse acoustic waves in fluids and soft matter are studied to determine rheological properties.

The development of monitoring technologies is supported in international co-operations including combined developments with institutions in Bangladesh, India and the USA, in European projects of the 7th Framework, and in international and national projects in cooperation with industry including also projects like MagnaCode in the project area (Vorhabensbereich) ForMat and NEMO Netzwerk "MONIFER") of

the Bundesministerium für Bildung und Forschung (BMBF).

Efforts in the area of education and teaching are concentrating on the International Physics Studies Program at our Faculty and efforts involving cooperative activities with international institutions on the level of Colleges, combined educational and research oriented State Institutes and Universities. Within this framework special emphasis is given to the exchange of students and support of experimental work of students from foreign countries including the participation in co-operative research with the supervisors of students from abroad.

*Wolfgang Grill*

## 9.2 Characterization of acoustic lenses with the Foucault test by confocal laser scanning microscopy

E.T. Ahmed Mohamed, A. Abdelrahman, M. Pluta, W. Grill

The geometrical and focusing properties of an acoustic lens operating in the range of 1.2 GHz were determined by confocal laser scanning microscope (CLSM) utilized as a tool for Foucault test [1]. The illumination pattern in CLSM which is restricted to an airy distribution in the focal region of the objective is a kind of pinhole. As a result, the detector (PMT) can only detect light that has illuminated a single point at a time and passed the detection pinhole [2] (figure 9.1, left). In this context, the projection of the

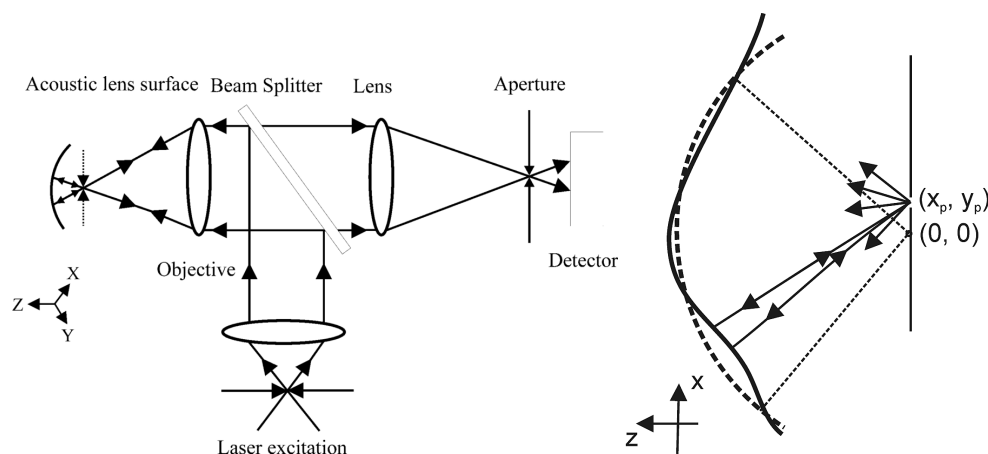


**Figure 9.1:** Left - schematic of the confocal imaging. Right - rays deflection by reflection at a deformed surface.

illumination pinhole replaces the knife edge, and the 2D scanning of the laser beam provides the transverse translation of the knife edge in analogy to that in the traditional Foucault test. In contrast to the Foucault test, the image of the laser focus is not scanned across the detection pinhole, but stays stationary. The image conjugated to both (source and detection) pinholes can be treated as a pinhole itself and for simplicity call it just "the point pinhole".

The wave aberration in the aperture of the lens under test  $W(x, y)$  is defined as the geometrical distance between ideal sphere centered in the focus and the real wave

front. By testing a reflecting surface, with the knife edge positioned at the focus, with the edge parallel to the Y axis, the bright area (figure 9.1, right) will be observed where the local slope of the wave aberration:

$$\frac{\partial W}{\partial x} > 0 \quad (9.1)$$

During scanning in the plane of the geometrical centre of curvature, light passes through the image of pinhole, travels towards the lens surface and then reflects back. A bright spot observed at  $(x_p, y_p)$  (figure 9.1, right) tells about the slope of the reflecting surface. In

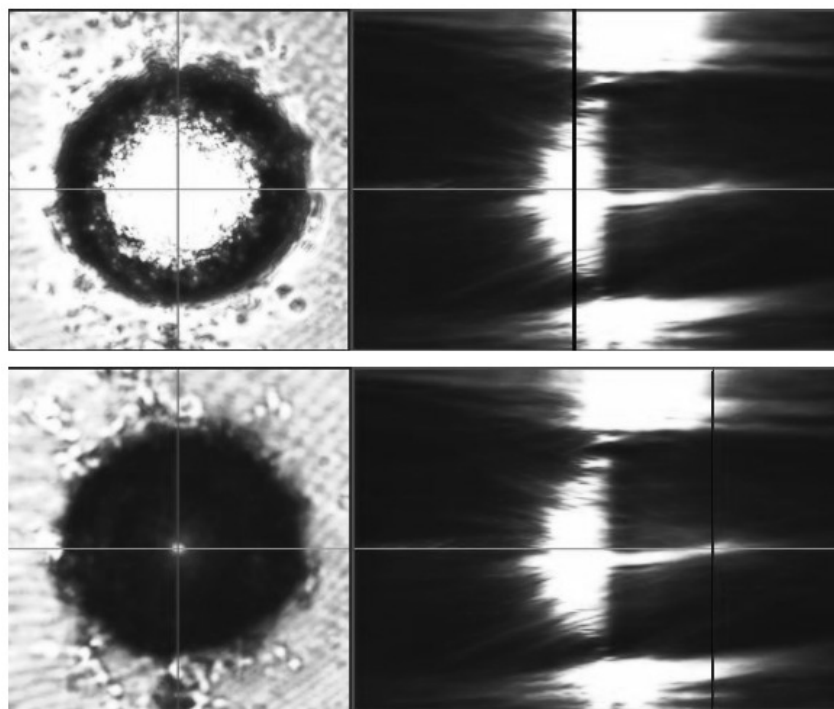


**Figure 9.2:** Image of the lens when focusing at the surface of the lens (upper, left) and when focusing at the focal point of the acoustic lens under test (bottom, left), with y-z distribution of the optical field for each case (upper right and bottom left, respectively).  $z = 128 \mu\text{m}$ , illumination laser  $\lambda = 543 \text{ nm}$ , objective  $20 \times / 0.5$  were used, area:  $89 \mu\text{m} \times 89 \mu\text{m}$

the approximation of the geometrical optics, the reflected ray comes back to the image of the pinhole, only in the case when the gradient of the local wave aberration fits to the position of the pinhole [3]. In the geometrical optics approximation the position of local intensity maximum  $(x_p, y_p)$  is related to the surface deformation  $W$

$$(x_p, y_p) \approx R \cdot \left( \frac{\partial W}{\partial x}, \frac{\partial W}{\partial y} \right). \quad (9.2)$$

Taking into account effects of diffraction, intensity of light observed in local maximum at  $(x_p, y_p, z_p)$  may be related not only to the gradient but also to the local Gaussian curvature of the surface. That value may be estimated with the help of the stationary phase arguments. Two sets of experiments were carried out. In the first one, the entire range of  $128 \mu\text{m}$  in the axial direction was optically sectioned in steps of  $1 \mu\text{m}$  with

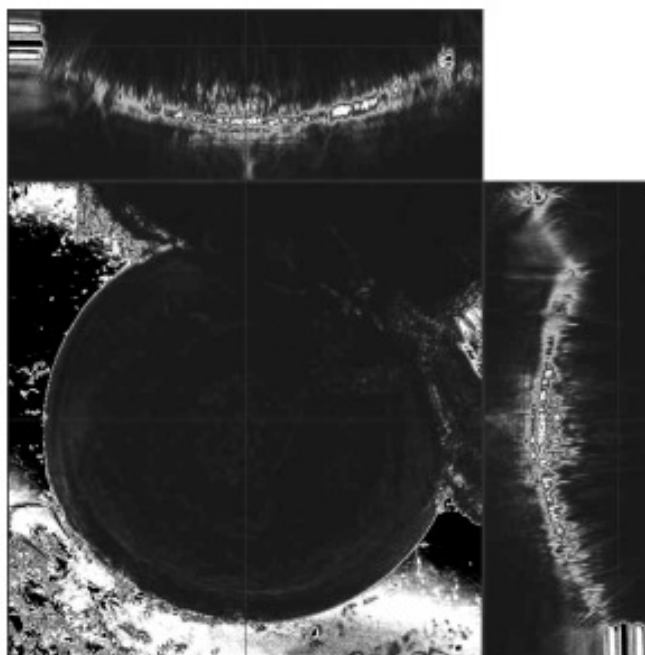


**Figure 9.3:** Cross-sections through the stack of high resolution 3D measurement

$20\times$  (NA= 0.63) lens which has a larger working distance (figure 9.2). In the second measurement, high resolution conditions were applied for optical sectioning at the region of interest. In the later case a stack of about 200 scans was collected, starting from the top of the lens towards the centre of curvature. The scan step size in  $z$  direction was  $0.11\ \mu\text{m}$ . High resolution objective (Plan-Neofluar  $40\times$  (NA= 1.3, oil immersion) was used for the illumination and collection of the back reflected light. Spectral line 488 nm of argon laser was applied. A cross-section through the stack is depicted in figure 9.3. High numerical aperture lens was necessary to gather the rays reflected from the peripheral areas of the lens surface.

The radius of the spherical part of the lens and the focal spot were determined from the stack of the high resolution CLSM images with the technique of 3D fitting to the sphere. Lens diameter  $D$  was estimated with the help of one picture from the stack taken for the CLSM focused at the planar part of the lens front. To identify the reasons for the observed optical and acoustic fields irregularities measured fields were compared with appropriate distributions calculated with the help of a custom designed program that calculates the propagation of angular spectrum of wave fields (figure 9.4). The program calculates, plane by plane, 3D wave field distributions behind the initial (source) plane. The assumed deformations of the lens surface were introduced as phase fluctuations at that plane. The amplitude in the source plane was windowed by a circle of the diameter  $D$ , equal to the diameter of focusing part of the lens. In case of the optical field simulation the deformations of the lens surface were doubled, because the light is reflected, while in case of acoustic field modeling the wave phase shift is related to the surface shape through the factor  $n - 1/n$ . That can easily be shown by considering figure 9.1. The time consumed by an acoustic ray in traversing the path length  $h$  is  $t = (n - 1/n)h/c$ , where  $c$  is the acoustic speed in the coupling fluid and  $n$  is the refractive index in going from the lens material to the coupling fluid.

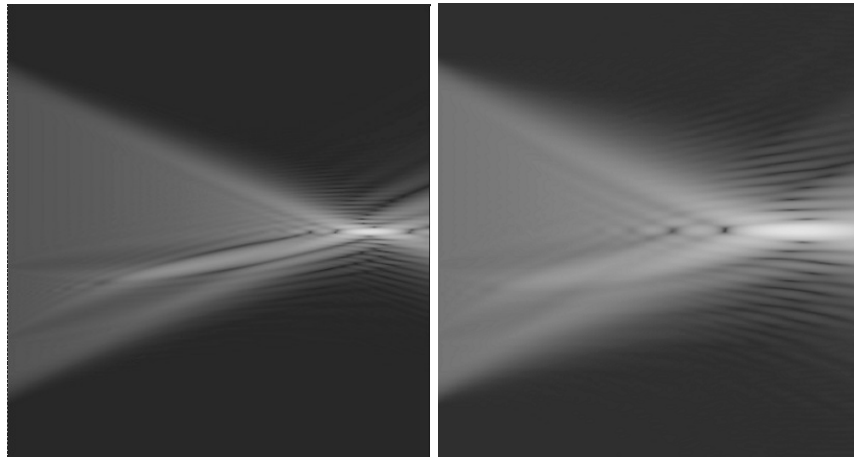


**Figure 9.4:** Simulated wave field intensity (in logarithmic scale) distributions in  $x-z$  plane. Left - for spherical wave of  $44 \mu\text{m}$  radius, with local ( $10 \mu\text{m}$  in diameter) inclusion of sphere of  $20 \mu\text{m}$  radius. The assumed wavelength was  $488 \text{ nm}$ . Right - simulation of acoustic field calculated for  $1.2 \text{ GHz}$  and initial wave aberration identical to that assumed in the case presented to the left.

- [1] T. Wilson: *The role of the pinhole in confocal imaging system*, in *Handbook of biological confocal microscopy*, Springer Science and Business media. Inc, New York, (1995).
- [2] L. M. Foucault: *Description des procédés employés pour reconnoitre la configuration des surfaces optiques*, C.R. Academic press. Paris **47**, 958 (1858), in *Handbook of biological confocal microscopy*, (Springer Science and Business media. Inc, New York, 1995).
- [3] E. V. Donald, D. H. William: *Quantitative evaluation of optical surface by means of an improved Foucault test approach*, *Optical engineering* **32**(8), 1951 (1993).

### 9.3 Determination of longitudinal sound velocity and acoustic impedance of thin chitosan films by phase-sensitive acoustic microscopy

A.E. Kamanyi, E.T. Ahmed Mohamed, W. Grill

The biomaterial chitosan is used in the paper manufacturing industry, as a wound healing agent and in filtration amongst others. It is a semi-crystalline natural polysaccharide which is generally considered as a biocompatible and biodegradable material. It is derived primarily from chitin by deacetylation. Chitin is one of the most abundant carbohydrates in nature, second only to cellulose and plays a critical role in the exoskeleton of invertebrates. For better control in its applications, the durability, stress resistance, flexibility and elasticity of the chitosan films should be known. We exploit the information from the phase and magnitude-contrast images obtained by vector-contrast acoustic microscopy to determine the sound velocity and acoustic impedance of thin films of chitosan of varying thicknesses. The results for three sample thickness

ranges are presented. The first two batches were thin films of the order of 200nm and 2  $\mu\text{m}$ , spin coated from a chitosan-acetate solution on glass substrates. The film thickness are controlled by the spin coating speeds. The third batch of the order of 40  $\mu\text{m}$  was obtained by increasing the concentration of the chitosan in the solution and casting on glass substrate.

### 9.3.1 $V(z)$ technique for materials characterization

Samples from each of the three batches were used for surface acoustic wave (SAW) velocity evaluation by means of the  $V(z)$  technique. The resulting amplitude contrast  $yz$  images for the thin films (thickness  $d \cong 200$  nm) and thicker films ( $d \cong 40$   $\mu\text{m}$ ) on glass substrates are presented in figures 9.5A and 9.5B respectively.

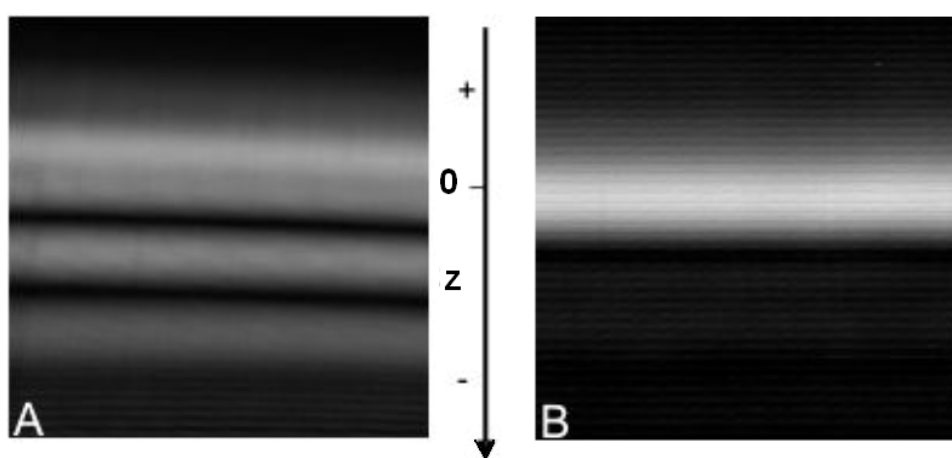


**Figure 9.5:**  $140 \times 31 \mu\text{m}^2$   $yz$  PSAM amplitude images of (A) 200 nm thick chitosan film on glass, (B) a half-space thick ( $>40 \mu\text{m}$ ) chitosan film on glass. Note the periodic bright bands in (A) suggesting the existence of surface acoustic waves. Main focus is at 0 and negative  $z$  implies shifting the focus into the film [1].

The existence of SAWs in the thin chitosan film-glass substrate sample is made evident as the resulting image (figure 9.5A) displays the expected defocus interference peaks (bright horizontal lines). As indicated in the  $z$  axis scale, the main maximum occurs at zero (which is with focus at the surface) while it is possible to observe some more oscillations in defocus. However the soft chitosan film itself does not generate surface waves and that which is seen is the influence of the thin film on the surface waves from the glass substrate. This is made evident in the thicker sample presented in figure 9.5B. Here are no indications of SAWs. This suggests that the thin film on the glass substrate acts dominantly as an extra attenuator for the acoustic interface waves. The values for the SAW velocity from fig. 9.5A are so close to that of plain glass substrate that at 200 nm thickness it was difficult to simulate the influence of the chitosan layer. The batch of intermediate thickness ( $d \cong 2 \mu\text{m}$ ) was then investigated. The  $yz$  image and the resulting  $V(z)$  curves along the line indicated are presented in figure 9.6. In this film thickness range, the effect of the chitosan on the  $V(z)$  curve and subsequently calculated surface acoustic wave velocity of the glass substrate could be simulated. We exploit the fact that for a known lens, the  $V(z)$  is mostly dependent on the reflectance function, which can be estimated for a three layered system (fluid-soft

layer-hard substrate). The resulting SAW velocities from the simulation are compared to the experimental value calculated from the  $V(z)$  curve. This leads to an estimation of the longitudinal velocity at  $1660 \pm 30 \text{ ms}^{-1}$ .

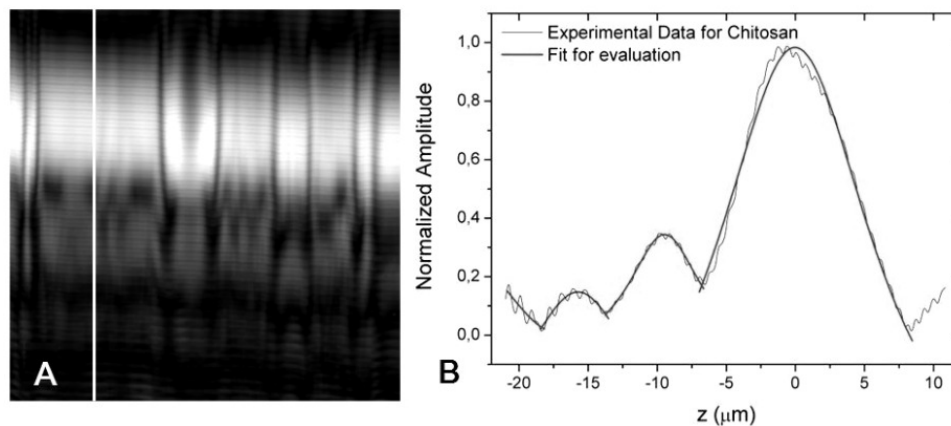


**Figure 9.6:** A):  $140 \times 31 \mu\text{m}^2$   $yz$  PSAM amplitude image of  $2 \mu\text{m}$  thick chitosan film ( $y$  - horizontal,  $z$  - vertical). B):  $V(z)$  curve extracted along the vertical line indicated in (A) [1].

### 9.3.2 PSAM acoustic reflectivity analysis

The acoustic reflectivity analysis technique is used for the thicker films which could not be evaluated with the  $V(z)$  analysis simulation technique. In order to extract acoustic properties from the PSAM magnitude contrast images of the chitosan by reflectivity analysis, it is necessary to eliminate any possible substrate influence in the image contrast. This is best done by imaging sufficiently thick films (thickness greater than working distance of the lens) such that all reflection is from the coupling fluid-sample interface only. If the sample does not generate surface waves, the acoustic reflectivity is mostly in reference to the primary reflection from the liquid couplant-sample surface. This approach determines the reflectivity in decibels relative to a defined value. To obtain the acoustic impedance we need to calibrate this with that of a known sample; in this case the glass substrate. A PSAM maximum amplitude image is used to determine the relative reflectivities. The maximum amplitude image extracts the maximum amplitude for each pixel  $(x, y)$  from a stack of images and displays the data in the image as at the focus. This typically takes care of slight tilt in the sample. In the PSAM, the tilt is evident in the phase image thus allowing for the correction of the brightness in the amplitude images from which the impedance (reflectivity) can be determined. Figures 9.7A and 9.7B show the maximum amplitude images for a plain glass sample and the thick chitosan film respectively. The intensity of the reflected signal from the chitosan film was estimated at 29% of the reflectivity from glass. This is a relative reflectivity of glass  $R_g$  which is  $3.45R_c$  (reflectivity of chitosan). The acoustic impedance of the glass substrated was calculated at  $Z_g = 13.2 \pm 0.2 \text{ MRayls}$  (acoustic impedance = density  $\times$  velocity). This is used to evaluate the reflectivity of the glass substrate by replacing  $Z_2$  with  $Z_g$  (see equation below).

$$R = \frac{Z_2 - Z_1}{Z_2 + Z_1}. \quad (9.3)$$

The relation between  $R_g$  and  $R_c$  is then used to evaluate the acoustic impedance of chitosan  $Z_c$  by replacing  $R$  and  $Z_2$  in equation (9.3) with  $R_c$  and  $Z_c$  respectively. These calculations yield an acoustic impedance of  $2.39 \pm 0.06$  MRayls for chitosan and a velocity of sound for perpendicular incidence at  $1838 \pm 46$  ms<sup>-1</sup>.

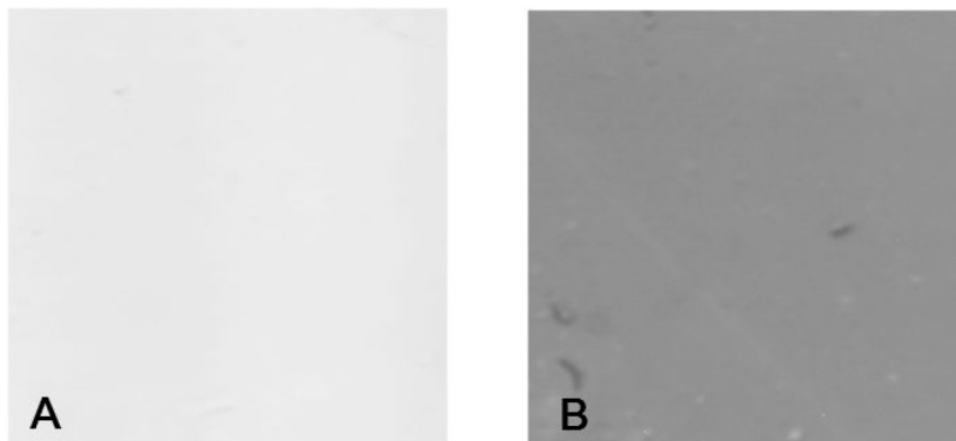


**Figure 9.7:** A):  $140 \times 140$   $\mu\text{m}^2$  PSAM maximum amplitude images of (A) glass slide and (B) thick chitosan film [1].

Generally, the results obtained by each of the models above, confirm that the velocity of sound in chitosan is indeed close to that of the coupling fluid (water). The values obtained for the thickness range of  $2$   $\mu\text{m}$  agree well with those from the previously reported acoustic interference analysis technique [2]. The discrepancies in the results for the different thicknesses can be attributed to the characteristics of the sample and the effects of sample preparation. These models could be further used in the investigation of other thin films or in the characterization of biological specimen such as gelatin, collagen, cellulose and even cells.

- [1] A. E. Kamanyi, E. T. Ahmed Mohamed, W. Ngwa, W. Grill, Proc. SPIE, **7650**, 76502A (2010)
- [2] E. T. Ahmed Mohamed, A. Kamanyi, M. von Buttlar, R. Wannemacher, K. Hillmann, W. Grill, Proc. SPIE **6935**, 69351Z (2008)

## 9.4 Advances in phase-sensitive acoustic microscopy studies of thin polymer blend films: annealing effects and micro-elastic characterization of PS/PMMA blends

A.E. Kamanyi, W. Grill

### 9.4.1 Structural Characterization

The effects of substrate, solvents, polymer concentrations, spin-coating speeds and temperature on film morphology were studied. The effects of solvent on morphology were

studied by using different solvents varying the vapour pressure of the solvents (from o-dichlorobenzene, toluene to chloroform; increasing vapour pressure). An immediate observation was the increase in roughness as the vapour pressure of the solvent increased, yielding much thicker and rougher films under otherwise same conditions for the more volatile solvents. The resulting phase-separation morphology also proved to be solvent-dependent [1, 2].

Immediately after spin coating the blend films are not in thermodynamic equilibrium. In order to bring them to a stable state, the films were annealed at temperatures at 190°C for over 24 hours in vacuum. The change in morphology upon annealing can be observed in figure 1 for a chloroform-based film.

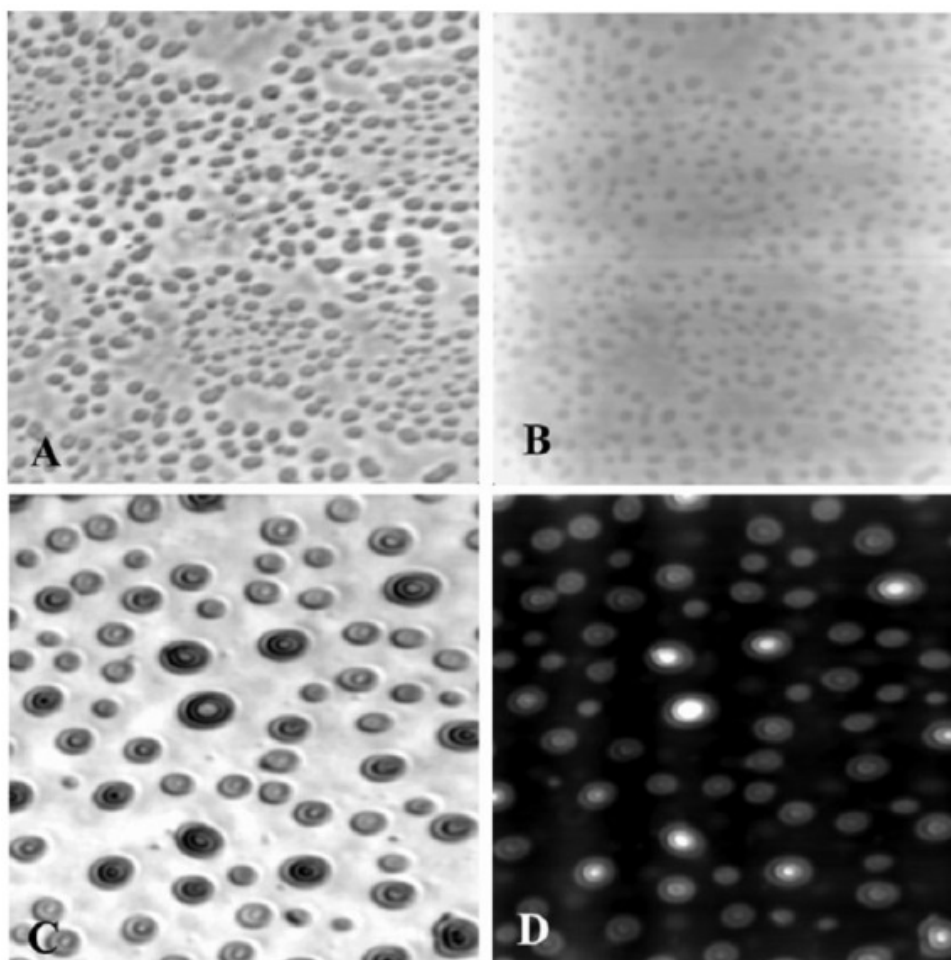


**Figure 9.8:** (A) and (C) are PSAM amplitude-contrast images of a chloroform-based PS/PMMA film on silicon substrate before and after annealing, respectively. (B) and (D) are the corresponding phase images of (A) and (C), respectively. Images are  $140 \times 140 \mu\text{m}^2$  [1]

After annealing, a system of spherical PS drops suspended in a PMMA film is observed. The contrast in the amplitude image allows the direct qualitative assignment of the domains to a particular component polymer. This ability of the PSAM represents one major advantage over AFM and could prove crucial especially when one does not want to destroy the polymer film system [1],[3]. Figure 2 summarizes the solvent and annealing effects in four steps (I - IV), with the solvent variation (chloroform, toluene and o-dichlorobenzene) from left to right [1]. The model in figure 6 starts after the

blend solution is dropped on the substrate (I); an initial vertical separation is formed due to the formation of wetting layers (II). Next, interfacial instabilities are introduced due to solvent concentration gradient throughout the film which results in lateral phase separation (III). The role of solvent vapour pressure is crucial in evaporation. In the case of chloroform film, one notes an incomplete phase separation process as evaporation set in quite early in the spin coating process, leaving thicker film with holey morphology. During annealing the PS coalesces to form droplets that wet the PMMA, leading to a thermodynamically equilibrated state with suspended droplets of PS in the PMMA matrix which is independent of solvent (IV).

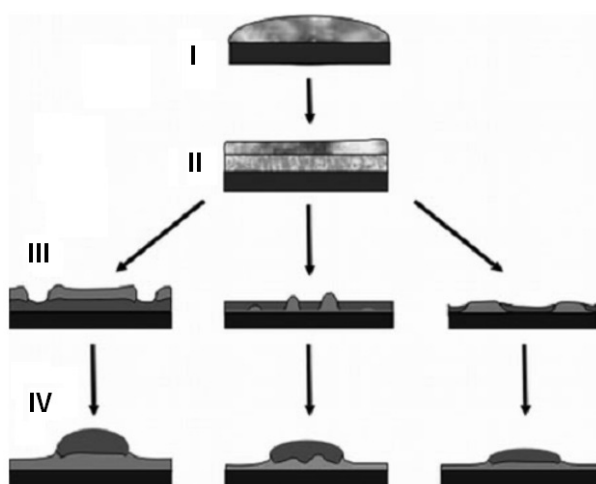


**Figure 9.9:** Representation of the possible steps in the structure formation process from spin coating before (I, II, III) and after annealing (IV) [1]. From left to right, solvents are chloroform, toluene, and o-dichlorobenzene, respectively. PS is represented in dark grey while PMMA is in a much lighter shade of grey.

In order to check the influence of thickness both before and after annealing, the solutions were spin coated at different speeds. A variation of the spin speed resulted in thinner films, reduced surface roughness as the speed increased and also smaller size of surface structures. However unlike suggested by some prior research, that the thickness influences the resulting morphology, this was not observed for thickness ranges from 60 nm right up to just under 1  $\mu\text{m}$ . As such it could be concluded that after annealing the PS/PMMA film has a morphology characterized by a system of PS droplets suspended in a thin PMMA matrix that is irrespective of solvent and thickness.

#### 9.4.2 Quantitative Characterization

It is difficult to use the well known  $V(z)$  technique for the thin film-substrate systems, since they only represent the surface acoustic wave velocity of the hard substrate with the influence of a thin soft film. This prompted the need for a model which would be able to evaluate film properties independent of substrate. Such a model was found by using the combined information from the PSAM phase contrast and the AFM topography. A step-like sample was obtained from an o-dichlorobenzene based PS/PMMA blend and an image of the same area was taken by both PSAM and AFM. A line profile along the same area in the PSAM phase contrast image and the AFM topography image was used

to obtain the information needed for the plot in figure 9.10. The PSAM phase variation was used to get the time-of-flight and the AFM image to obtain the height variation.

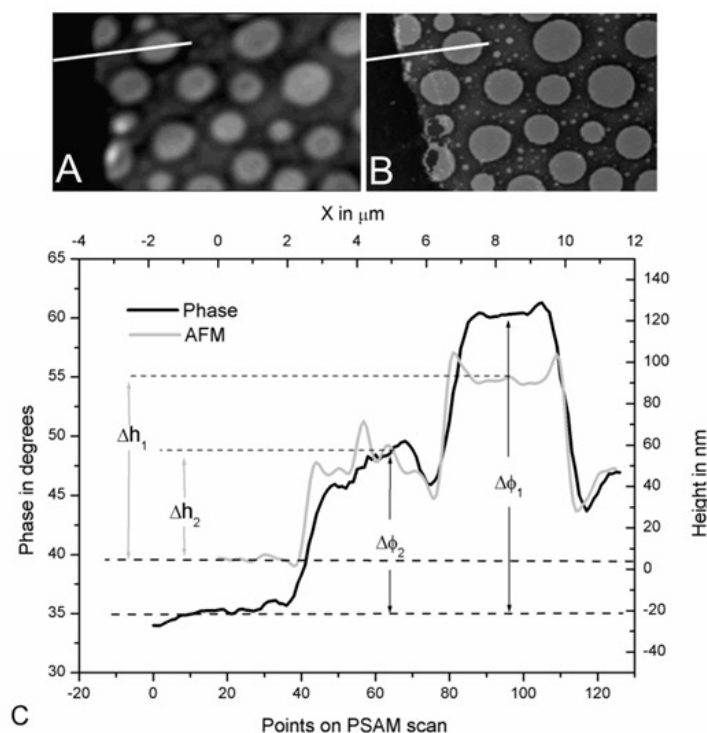


**Figure 9.10:** A)  $15 \mu\text{m} \times 30 \mu\text{m}$  PSAM phase contrast and B) AFM topography image of a PS/PMMA film after washing with cyclohexane [1]. C) Profiles of lines from PSAM phase image (black) and AFM topography image (grey), showing some points at which the height ( $\Delta h$ ) and phase ( $\Delta\phi$ ) variations were taken for the speed of sound calculation.

The variation in PSAM phase  $\Delta\phi$  is related to the variation in time-of-flight  $\Delta t$  in the film and the frequency  $f$  of the acoustic wave when the focus is set constant on the substrate by:

$$\Delta t = \frac{\Delta\phi}{2\pi f}. \quad (9.4)$$

The values from the graph in figure 3 were used to determine the speed of sound in the film using the relation of "distance  $\div$  time" for the speed of sound by inserting the time component  $\Delta t$  from equation (1) and the distance from the AFM topography information for film thickness ( $\Delta h$ ). Taking the Poisson's ratio  $\sigma$  and density  $\rho$  values from literature, the speed was then used to evaluate the modulus of elasticity  $E$  (Young's modulus) at these points with the help of the equation below [4]:

$$c_L = \sqrt{\frac{E(1 - \sigma)}{\rho(1 + \sigma)(1 - 2\sigma)}}. \quad (9.5)$$

In the annealed samples a layered model was used introducing the effects of change in speed as the sound travels from the water, through the PS droplet and PMMA before

getting reflected. The calculated speeds for PS and PMMA ( $c_{PS} = 2326 \pm 71$ )  $\text{ms}^{-1}$  and ( $c_{PMMA} = 2830 \pm 74$ )  $\text{ms}^{-1}$  yielding respective Young's moduli of  $E_{PS} = 3.4 \pm 0.3$  GPa and  $E_{PMMA} = 4.2 \pm 0.4$  GPa.

The use of PSAM in polymer blend thin film characterization has mostly been qualitative with difficulties in quantitative characterization due to substrate influence. This problem is solved in this work, with an appropriate model introduced and used to evaluate the elastic modulus at different points and over the entire area of the isotropic thin film.

- [1] A. Kamanyi, W. Ngwa, W. Luo and W. Grill, *J. Microsc.* **238** (2), 134 (2010)
- [2] A. Kamanyi, W. Ngwa, W. Luo and W. Grill, *Proc. SPIE* **6935**, 69351X.1 (2008)
- [3] W. Ngwa, W. Luo, A. Kamanyi, W. K. Fomba, W. Grill, *J. Microsc.* **218**, 208 (2005)
- [4] J. Krautkrämer and H. Krautkrämer: *Werkstoffprüfung mit Ultraschall*, (Springer, Heidelberg 1986)

## 9.5 Synchronous monitoring of muscle dynamics and muscle force for maximum isometric tetanus

M. Zakir Hossain, W. Grill

Skeletal muscle is a classic example of a biological soft matter. Soft matter in nature serves many essential functions, which also are needed in technical applications. New technology can potentially evolve from a design and use of materials according to nature. The combination of highly diverse functions (mechanical, optical, biological, diffusive, electrical) of soft-matter initiates and explores this research field with diverse expertise towards making of nature-inspired soft materials and their use in sophisticated mechanical and bio-medical applications. Examples are the high-strength nano gels of Haraguchi, in parallel to human knee meniscus and eye cornea, and porous gels as candidates for organ replacement (serving as functional matrix material) and the conducting gels of organic photovoltaic solar collectors [1]. Skeletal muscles are the multi scale biological intelligent soft matter, made mainly of water, and can possess characteristics of both a solid and a liquid. At the same time muscle is responds sensitive to any physical-chemical reactions initiated and controlled by brain (super computer). Muscle contraction in a tissue or organ produces motion and provides power and speed for mechanical activity. Skeletal muscle tissues are attached to the bone, allowing movement of the body parts with their contraction. The bio-chemical action of muscle fibers involve two stages, contraction and recovery. Get triggered from CNS and using the locally-stored fuel (ATP) the soft biological matter muscle oriented almost into a solid rigid matter till the optimum burn-out limit of the local energy supply. Leaving byproducts heat and lactated the muscle tend to get back to its initial stage. Produced bio-chemical end products were regulated by different autonomous subsections to re-fuel it for the next actions. To monitor and quantify these time dependent variables in muscle, an ultrasonic detection scheme employing chirp technology for high resolution and rapid monitoring of the change of the muscle extension with a temporal resolution down to 0.01 ms was developed by us [2]. The system has also been used to monitor

the sonic velocity variation under voluntarily activated muscle [3]. In this scheme a computer controlled arbitrary function generator produces a chirped ultrasonic wave that is observed with a similarly controlled synchronized transient recorder after passing through the observed muscle. Subsequently the time-of-flight (TOF) is determined with the implemented custom developed software.

Subsequent evaluation including mechanical modeling allows the determination of parameters relevant to characterize the behavior of intelligent soft matter (skeletal muscle). The psychological boosting-up influence the performance of an individual which ultimately enhance the muscle force and lateral expansion as well. The influence of boosting-up on muscle force and muscle dynamics have also been quantified from this study.

### 9.5.1 Method

To study the behavior of muscle we have monitored several trained sportsmen of same age group ( $32 \pm 1.5$ ). Persons are informed and habituated earlier with the defined isometric contraction of the monitored medial gastrocnemius (MG) muscle: quick isometric contraction, maintain all-out isometric tetanus up-to the maximum limit and then relax the muscle suddenly. The isometric (same-length) contraction of the monitored muscle was initiated by an audio beep to trigger the quick and all-out initiation of the intelligent and super regulated drive from the brain. Movement (planter flexion) of the joint was resist with a custom developed novel sonic force sensors to monitor the activated MG muscle force. To synchronously monitored the side ways expansion and dilatation of the activated muscle, two ultrasonic transducers were placed at opposite sides of the gastrocnemius muscle with an elastic band. The external trigger (boosting-up command) was given during holding time to further energies the drive or effort. To test the functional capacity of the transmitting circuit (auditory system), the functionality of the other transmitting circuit (ophthalmic system) is stopped by pre-trigger value (early information).

Data accusation and audio signal were triggered at zero time. Boosting-up command was given to observe and quantify the psychological effect. Following is the schematic for data accusation process and derived performance curves for the psychological effect. Following is the schematic for data accusation process and derived performance curves for initiated muscle activity (figure 9.11)

First order polynomial fit is used to determine the slopes of different stages of the biological soft-matter dynamics and force. The different phases have named as: activation phase, sustained activation phase, deactivation phase and restoration phase respectively. The soft-matter restoration curve has been fitted with an exponential decay curve to quantify. The activation (state alteration phase) on-set time of the monitored soft matter is termed as the movement reaction time for the integrated super-system (athlete).

The graphs below(9.12) are showing different quantitative parameters of the muscle performance for two different athlete.

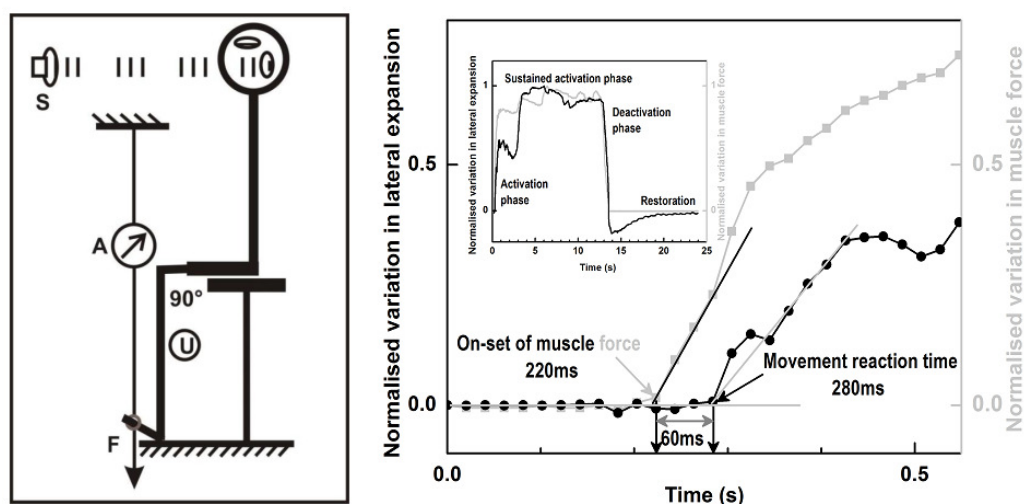


**Figure 9.11:** Left - data acquisition procedure for synchronised monitoring of the muscle dynamics and the muscle force. S: audio signal, U: ultrasonic monitoring, F: applied force, and A: ultrasonic force sensor. Right - the analysed transients that demonstrate the determined results: the movement reaction time, on-set of muscle activation and muscle force and time lag between them. Inset is the graph which represent monitored muscle performance data: black - muscle movement; gray - the muscle force with different phases of muscle dynamics.

## 9.5.2 Discussion

The provided cheer-up command was observed from the enhanced step of the muscle movement and muscle force curves. The applied enhanced effort increases the lateral expansion further up till 3.57 s and force till 3.35 s. So, the average TL for all the three steps is about 60 ms. Holding slope for muscle movement  $-0.16$  mm/s and muscle force  $0.15$  kN/s. Under-shoot of 19% and 2.76 s recovery time constant was observed. Stiffening and reformation speed  $1.28$  mm/s and  $1.62$  mm/s. Impulse for contraction  $4.99$  kN/s and for reformation  $-2.96$  kN/s are observed.

Recovery time constant is a quantitative measure for refueling time from the disturbance of applied isometric tetanus. Synchronous monitoring scheme allow us to identify that muscle force generation is preceded by any state-alteration phase of muscle dynamics with a value of 40 to 60 ms. Quantification of impulse and movement speed opens the door to derive further important parameters like, muscle power and efficiency. Psychological boosting-up effect has probably been attempted to quantified for the first time. The quantitative results after boosting-up command clarifies the fact that when stretched or shortened beyond optimum length of the muscle (whether due to the action of the muscle itself or by an outside force), the maximum active force generated decreases. This decrease is minimal for small deviations, but the force drops off rapidly as the length deviates further from the ideal. This total recovery process involves infinitesimal period. With our differential monitoring scheme we have determined that recovery time accurately. Length-tension or force-length and force-velocity relationship can also be derived quantitatively by employing this scheme to monitor the isotonic contraction of muscle. The focus of this part of our study was to investigate the applied force and mechanical behavior of the MG muscle. Analysis of other individual or group of muscle are also admissible with our simple economic detection scheme.

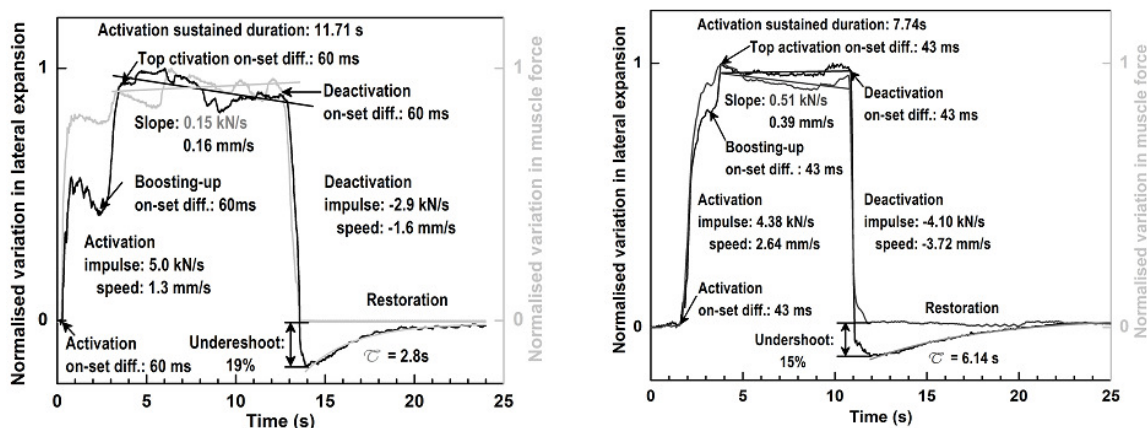


**Figure 9.12:** The graphs of the obtained data for synchronised monitoring of the muscle force (grey) and the muscle dynamics (black) for two different person. The analysed transients graph demonstrating the determination of the activation and deactivation on-set difference between muscle dynamics and muscle force. Activation and deactivation impulse and speed, boosting-up on-set difference, boosting-up effect, sustained activation phase, undershoot; and restoration time constant  $\tau$  for the monitored soft-matter deactivation dynamics.

### 9.5.3 Conclusion

This non-invasive, light-weight, compact and portable economic detection scheme provides solutions to push the limits in sporting success. The scheme has effectively been used for on-field monitoring of athletes to quantify parameters like movement reaction time, muscle contraction and relaxation speed, holding time and slope, muscular endurance, recovery time, muscle fiber recruitment and de-recruitment rate, muscle force, muscle power, rate of energy expenditure and other parameters of use for the optimization of designing and developing the performance or to quantify the behavior of this multidimensional soft matter. Researchers, coaches and trainers could get quantitative information to assess each individual or to reach a better method to intensify the performance of selective muscle. Similarly this novel monitoring scheme is allowed us to investigate the underlying biophysical mechanisms responsible for active and passive behavior of biological soft matter and quantify a number of functions, such as softness and toughness, extensibility and rigidity, expansion and recovery etcetera. These values could also be compared with similar soft-matter findings to strengthen the doors in various soft matter studies and advanced research field of bio-technology.

### 9.5.4 Acknowledgement

The support of the European Union under the 7th Framework Program within AISHA II (Aircraft Integrated Structural Health Assessment) is gratefully acknowledged.

- [1] K. Haraguchi, T. Takehisa: *Nanocomposite hydrogels: a unique organic-inorganic network structure with extraordinary mechanical, optical, and swelling/de-swelling properties*, *Adv. Mater.*, **14**, 1120 (2002)
- [2] M. Zakir Hossain, E. Twerdowski, W. Grill: *High speed ultrasound monitoring in the field of sports biomechanics*, In Tribikram Kundu (Ed.), *Health Monitoring of Structural and Biological Systems*, SPIE, **6935**, 6935-70 (2008)

- [3] M. Zakir Hossain, H. Voigt, W. Grill: *High speed ultrasonic detection scheme for sports performance monitoring*, In Tribikram Kundu (Ed.), *Health Monitoring of Structural and Biological Systems*, SPIE, 7295, 7295-16 (2009)

## 9.6 Focused GHz ultrasound as a tool for micro-displacement and cell manipulation

M. von Buttlar, E. von der Burg, W. Grill

Ultrasound causes acoustic streaming in fluids and radiation forces which act on insonified matter. These effects can aggregate particles, remotely move atomic force microscope (AFM) cantilevers, and deform biological cells. A recently developed combined optical and acoustic microscope was modified and used in experiments demonstrating these phenomena on a small scale. The combined microscope includes a confocal laser scanning microscope (CLSM) and a phase-sensitive scanning acoustic microscope positioned on opposite sides of the sample with the acoustic lens coaxially aligned with the optical objective. The acoustic lens is used to emit the focused ultrasound beam with frequencies up to 1.2 GHz.

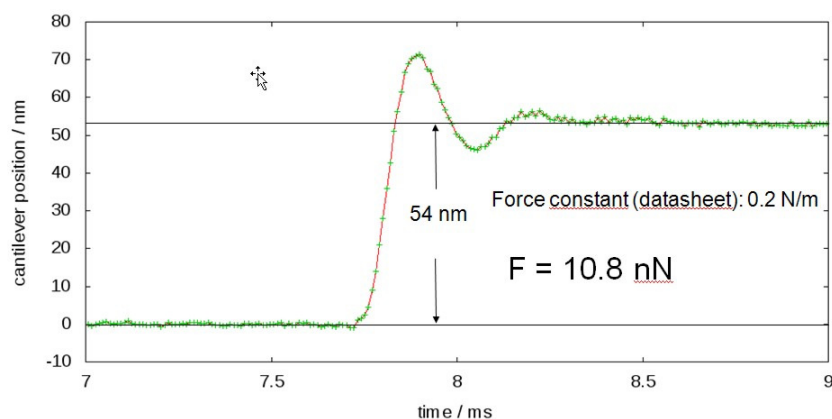


**Figure 9.13:** Measurement of the cantilever position with push-pulses and without. With the given force constant of the cantilever of 0.2 N/m the exerted forces amount to 10.8 nN

In a new operation mode the acoustic microscope combines actor and sensor functions. The average acoustic intensity is modulated by ultrasound pulses which are additionally introduced in the pulse-echo sequence. This changes the duty cycle for ultrasound emission from 1% to 23% and thereby modulates the radiation force. Figure 9.13 shows the displacement of an AFM cantilever due to ultrasound modulation. The cantilever is moved by the additional push-pulses. In Figure 9.13 the cantilever position is shown with the applied push-pulses and without. The cantilever position itself is measured by phase detection of the ultrasound signal. Total displacement is 54 nm and the exerted forces amount to 10.8 nN.

Figure 9.14 shows the magnitude image of a living ovine mesenchymal stem cell which was recorded with the acoustic microscope. The push-pulses were switched on and off after 5 lines creating the stripe-pattern. The acoustic radiation force and the

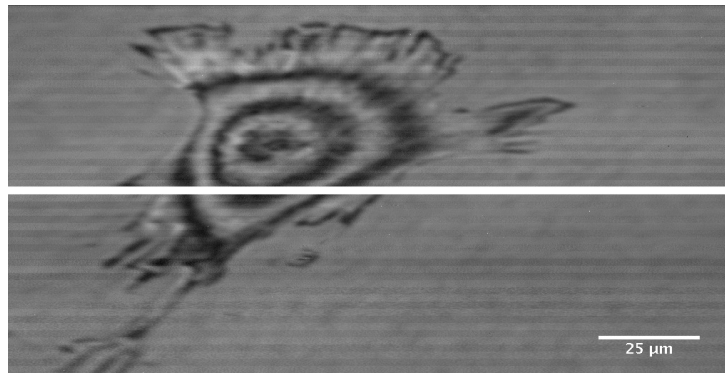


**Figure 9.14:** Magnitude image of a living ovine mesenchymal stem cell which was recorded with the acoustic microscope. The modulation of the acoustic intensity (alternating every 5 lines) creates the stripes. The white bar indicates the linescan position of figure 9.15.

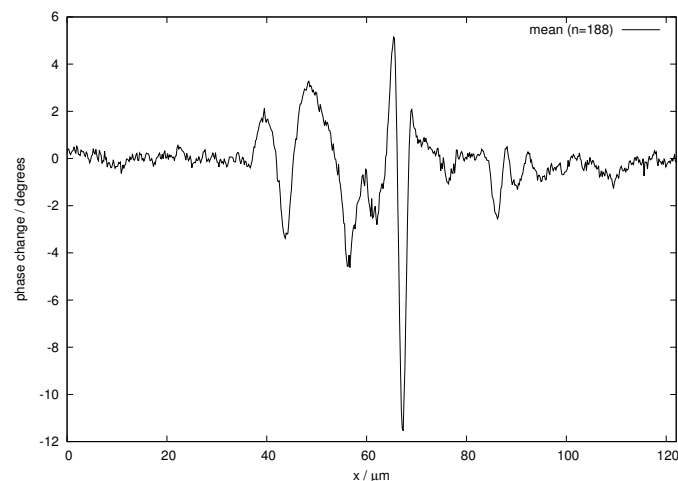


**Figure 9.15:** For the linescan position indicated in figure 9.14 the phase changes due to the compression of the cell by acoustical means are displayed.

streaming of the coupling media deform the cell (during push-pulses). In addition there are visible interference effects between the echo signal from the surface of the cell and from the substrate. Therefore, additional modeling is required to deduce the exact deformation of the cell. Figure 9.15 shows the phase change due to the acoustic compression of the cell in a linescan. The linescan position is indicated in figure 9.14 (white bar).

### 9.6.1 Conclusion

The system can remotely apply radiation forces in the nN range while simultaneously measuring deformations with sub nm axial resolution. This extends the capabilities of the phase-sensitive acoustic microscope and allows invasive probing of the sample with high spatial and temporal resolution. The method expands the possibilities of measuring the mechanical properties of tissue and single cells e.g. [1–3].

[1] J. Guck, R. Ananthakrishnan, H. Mahmood, T.J. Moon, C.C. Cunningham, J. Kas:

- The optical stretcher: A novel laser tool to micromanipulate cells*, Biophysical Journal **81**(2), 767 (2001).
- [2] U. Hamhaber, V. A. Grieshaber, J. H. Nagel, U. Klose: *Comparison of quantitative shear wave MR-elastography with mechanical compression tests*, Magnetic Resonance in Medicine **49**(1), 71 (2003).
- [3] X. J. Ren, C. W. Smith, K. E. Evans, P. J. Dooling, A. Burgess, J. Wiechers, N. Zahlan: *Experimental and numerical investigations of the deformation of soft materials under tangential loading*, International Journal of Solids and Structures, **43**(7-8), 2364 (2006).

## 9.7 Lumped circuit mechanical models and lattice dynamics approach to the dependence of the time-of-flight of bulk and guided acoustical modes on elongation

K.S. Tarar, U. Amjad, W. Grill

Lattice dynamics extends the concept of crystal lattice to an array of atoms with finite masses that are capable of motion. This motion is not random but is a superposition of vibrations of atoms around their equilibrium positions due to the interaction with neighboring atoms. The problem of lattice dynamics is to find the normal modes of vibration of a crystal which in the simplest approach is represented by a linear chain. This is achieved by calculating the energies (or frequencies) of the phonons as a function of their wave vector  $k$ . The relationship between  $\omega$  and  $k$  is called phonon dispersion relation. Dispersion relations describe the ways that wave propagation varies with the wavelength or frequency of a wave.

### 9.7.1 Harmonic vibrations

Continuum mechanics cannot provide a microscopic approach that allows to identify the origin of effects related to the transport of acoustic waves under applied stress. Therefore the lattice dynamics approach is employed here to illustrate the dependencies of velocity and time-of-flight (TOF) on external forces causing anharmonicity as well. The given model is applied to investigate longitudinal modes under two conditions: harmonic conditions relating to Hooke's law, and a generalized condition in which harmonic and anharmonic effects are included. Derived is the velocity and especially the time-of-flight needed to pass a finite sample elongated under stress.

To emphasize the linear spring we denote the spring constant now as  $C_1$  since the linear relation will later be replaced by more complicated functions, where a linear approximation would at best be a first order term. A stress induced externally by two opposing pulling forces, with  $F$  as the amount of each, acting at the far ends of the chain (along its extension) leads to a lattice parameter  $a_F$  that will establish under static equilibrium and is given by

$$a_F = F/C_1 + a_0, \tag{9.6}$$

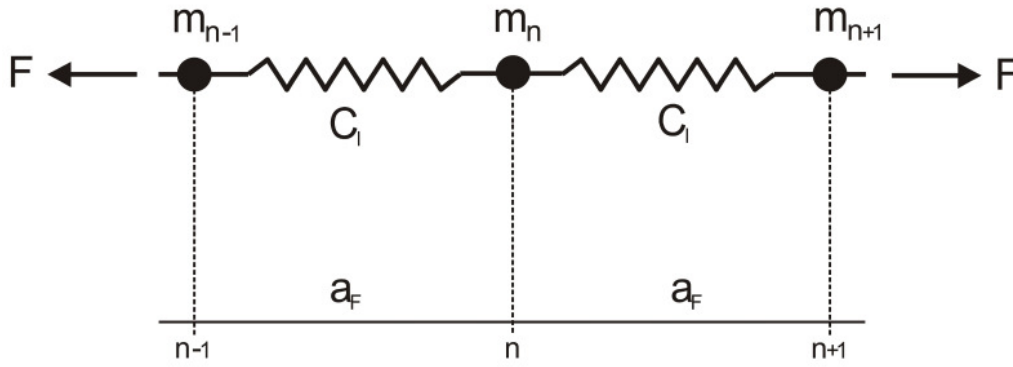


**Figure 9.16:** Linear chain of masses and mass free springs as under externally applied stress in (static) equilibrium condition

with the lattice distance  $a_0$  for no pull or push applied (zero stress). The dispersion relation (equation 2) for harmonic vibrations in a linear chain is modified under extensional stress to:

$$\omega_F = 2(C_1/m)^{1/2} \sin(kaF/2), \quad (9.7)$$

The time-of-flight (TOF) needed to pass a single unit cell of the chain calculated from equation 9.7  $TOF = (m/C_1)^{1/2}$  in case of linear springs does not depend on the pulling force.

### 9.7.2 Generalized vibrations including harmonic and anharmonic effects

Anharmonicity in materials as modeled here is represented by a non-linear mass-spring system. For a non-linear spring the conventional Hooke's law can be amended to 2nd, 3rd, and nth order corrections with respect to the displacement. This is visualized here by splitting the acting spring into two parts, one linear (harmonic) and the other non-linear as exemplified in figure 9.19. For simplicity only the second order correction is employed here in the Taylor expansion describing anharmonic springs by a modification of Hooke's law. Higher order terms can be used to describe the Lennard-Jones potential, usually employed to model inter-atomic forces.

The anharmonic spring as displayed concerning the dependence of force on elongation can locally be represented by a spring constant derived from the actual slope. For zero elongation and oscillations with negligible small amplitudes the spring constant is given by the linear term  $C_l$  only (same as for the harmonic case). For elongated springs as caused by extensional stress the effective (local) spring constant  $C_g$  will be reduced for the spring assumed here which turns soft on elongation. Under the given assumptions the linear spring-mass chain can be treated for small deviations as caused by oscillations with diminishing amplitude by

$$a_F = F_g/C_g + a_0. \quad (9.8)$$

The dispersion relation can be amended to:

$$\omega_F = 2(C_g/m)^{1/2} \sin(kaF/2), \quad (9.9)$$

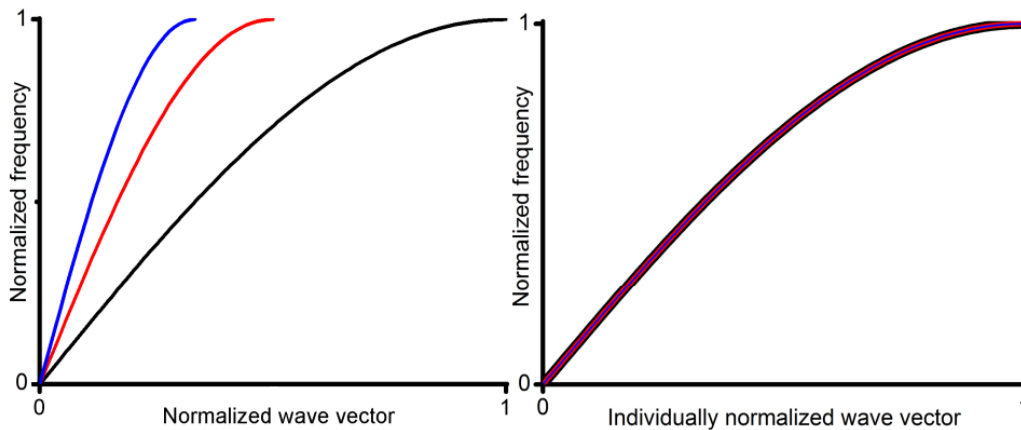


**Figure 9.17:** Graphical representation of the dispersion relation (equation 9.7) for springs following Hooke's law. In the left graph the wave vector is normalized to the dispersion relation valid in the absence of tension for the range to the zone boundary resulting from the periodicity of the structure. Extension by external forces leads to steeper dispersion relations and an increase of the unit length resulting in a decrease of the periodicity of the dispersion relation. Respective results are given for forces leading to a doubling and tripling of the distances between point masses. The result of interest here is the slope of the dispersion relation in the low frequency limit representing the phase and group velocity of respective acoustic waves. This velocity increases under stress. In the right graph the dispersion relations are normalized individually to the wave vector at the zone boundary. The different dispersion relations under stress coincide in that representation, demonstrating that TOF per unit cell is constant under stress in the harmonic approximation.

In the left graph in the figure 9.19 the wave vector is normalized to the dispersion relation valid in the absence of tension for the range to the zone boundary. Extension by external forces leads to steeper dispersion relations and an increase of the distance between neighboring point masses resulting in a decrease of the periodicity of the dispersion relation. Respective results are given for forces leading to a doubling and tripling of the distance between point masses. The rise of velocity present for doubling is reduced in the next step to tripling of the distance due to progressive softening. The anharmonicity affects the curves such that the velocity does not increase linearly with pulling forces. In the right graph in the figure 9.19, the wave numbers are individually normalized, to show the variation in the time-of-flight needed to pass a single unit cell (velocity is so to speak if derived from that representation from the slope not normalized to meters but to unit cell length) with length  $a_F$  which doubles and triples with respect to the length for the unstressed chain. TOF decreases under extension.

The time-of-flight in the case of anharmonic spring is

$$TOF = (m/C_g)^{1/2}. \quad (9.10)$$

The anharmonic model treated here in the lowest order approximation can already provide a valuable picture of the discussed problem. The dependence of the TOF of longitudinal polarized acoustic waves in the limit of large wavelengths if treated even on a simple theoretical approach can explain the TOF variation due to external pull. Variations can only be present if anharmonic effects are included.

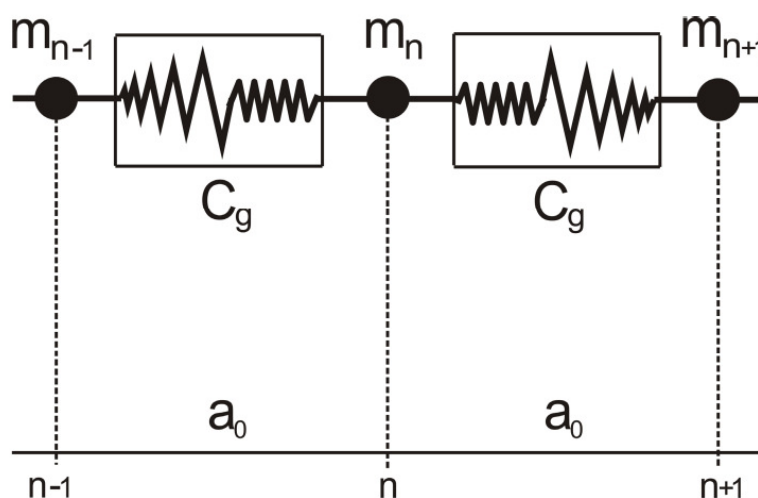


**Figure 9.18:** A combined mass spring system including both harmonic and anharmonic effects in the equilibrium state.

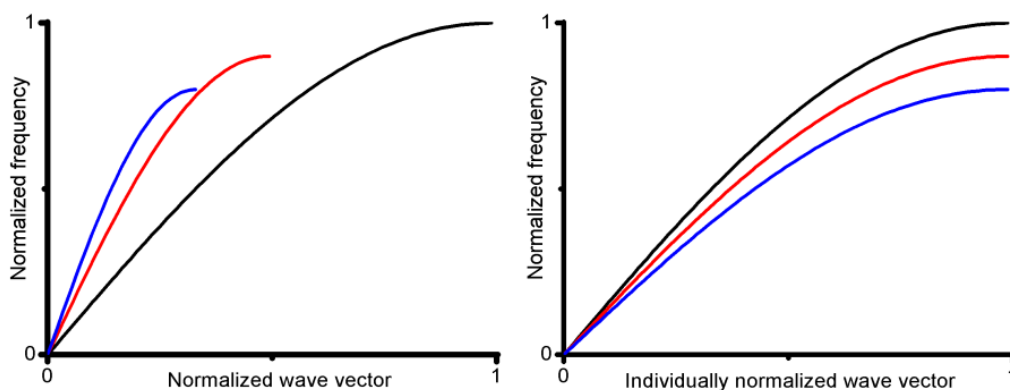


**Figure 9.19:** Graphical representation of the dispersion relation 9.9 for anharmonic springs under variable stress. Description of wave number normalization in text.

### 9.7.3 Conclusion

The mass-spring linear chain model has been employed to demonstrate in a simple manner that the velocity of longitudinal polarized waves traveling on a linear chain depends on the pulling force. Even though this holds also for harmonic springs, the TOF needed to pass any fixed number of chain elements remains even under extended length constant. This situation changes if anharmonic effects are included. The repetitive modeling presented here can be taken as an extension of the previously used traditional one-dimensional model<sup>4</sup>. These effects are exemplified here since it is often stated that under extension the transit time will increase since after all the sample will increase in length. It is demonstrated here, that such arguments are invalid. Similar as for thermal extension such variations are only present if the springs modeling interatomic forces are anharmonic. As already demonstrated in an earlier publication<sup>3</sup>, geometrical stiffening can overcome anharmonic softening and even lead to a reduction of the time-of-flight under extensional stress. Even though as demonstrated here such effects cannot be present for longitudinal polarized acoustic waves on point mass chains, they can arise

for transversal polarizations and may be enhanced by suitable boundary conditions. The oscillating piano wire or any string on a string instrument is a well known example for geometrical stiffening. Here the tune obtained for a string of fixed length will increase under tension. Geometrical stiffening can in this case reduce or overcome anharmonic effects. Depending on the definitions to determine anharmonicities from static experiments the geometrical stiffening may or may not be included in the derived anharmonic elastic constants.

### 9.7.4 Acknowledgement

The support of the European Union under the 7th Framework Program within AISHA II (Aircraft Integrated Structural Health Assessment) is gratefully acknowledged.

## 9.8 Funding

*Multiparametric Monitoring and Steering of Mesenchymal Stem Cell derived Cartilage Formation in 3D Production Systems (MS CartPro)*

*Development of a 2D bioreactor with integrated phase-sensitive acoustic microscopy combined with confocal laser microscopy (AP2.2)*

*Integration of a multi-parameter online monitoring system in a 3D bioreactor (AP2.3)*

W. Grill, E. von der Burg, M. von Buttlar

BMBF FKZ 0313836

*Aircraft Integrated Structural Health Assessment II (AISHA II)*

W. Grill, U. Amjad, M. Pluta, M. Zakir Hossain,

EU Seventh Framework Programme (FP7) Grant Agreement No. 212912

*Biomimetic Ultrathin Structures as Multipurpose Platform for Nanotechnology-Based Products (MultiPlat)*

W. Grill, A. Kamnyi, A. Abdelrahman,

EU Seventh Framework Programme (FP7) Grant Agreement No. 228943

*MagnaCode in the project area (Vorhabensbereich) ForMat*

W. Grill, A. Abdelrahman,

Bundesministerium für Bildung und Forschung (BMBF)

*NEMO Network "MONIFER"*

W. Grill,

Bundesministerium für Bildung und Forschung (BMBF)

## 9.9 Organizational Duties

Wolfgang Grill

- Adjunct Professor and Member of the Graduate School, Department of Physics and Astronomy, The University of Georgia, Athens, Georgia, USA
- Conference Co-Chair, SPIE yearly conference on Health Monitoring of Structural and Biological Systems

## 9.10 External Cooperations

### Academic

- University of the Witwatersrand, Johannesburg, South Africa  
Prof. Dr. A. Every
- Wrocław Institute of Technology, Wrocław, Poland  
Prof. hab. T. Gudra
- University of Arizona, Tucson, Arizona, USA  
Prof. Dr. T. Kundu
- University of Central Florida, Orlando, Florida, USA  
Prof. Dr. W. Luo  
Dr. W. Ngwa
- Stanford University, Stanford, California, USA  
Dr. K. Vodopyanov
- Johann Wolfgang Goethe-Universität, Frankfurt  
Prof. Dr. J. Bereiter-Hahn
- Bernard Nocht Institute for Tropical Medicine, Hamburg  
Dr. T. W. Gilberger

### International Organizations

- European Space Organization ESA/ESTEC

### Industry

- Schott GLAS Mainz
- EPCOS AG, Surface Acoustic Wave Components

## 9.11 Publications

### Journals

M. von Buttlar, E. T. Ahmed Mohamed, W. Grill: *Signal Processing for time-lapsed cell imaging with vector-contrast scanning acoustic microscopy*, in J. Jones & H. Lee (Eds.), *Acoustical Imaging*, **30**, (Springer 2010)

E. T. Ahmed Mohamed, A. Kamanyi, M. von Buttlar, R. Wannemacher, K. Hillmann, W. Ngwa, W. Grill: *Ultra-high resolution thin film thickness delineation using reflection phase-sensitive acoustic microscopy*, In J. P. Jones & H. Lee (Eds.), *Acoustical Imaging*, **30**, Springer, (2010)

E. T. Ahmed Mohamed, A. Abdelrahman, M. Pluta, W. Grill: *Characterization of acoustic lenses with the Foucault test by confocal laser scanning microscopy*, In Tribikram Kundu (Ed.), *Health Monitoring of Structural and Biological Systems*, SPIE **7650**, 76501W (2010), doi: 10.1117/12.847412

U. Amjad, E. T. Ahmed Mohamed, A. Abdelrahman, W. Grill: *Determination of the speed of ultrasound in thin materials by observation in reflection or transmission*, In Tribikram Kundu (Ed.), *Health Monitoring of Structural and Biological Systems*, SPIE **7650**, 765028 (2010), doi: 10.1117/12.847702

U. Amjad, K. S. Tarar, A. Shelke, T. Kundu, M. Pluta, W. Grill: *Generalized representations and universal aspects of Lamb wave dispersion relations*, In Tribikram Kundu (Ed.), *Health Monitoring of Structural and Biological Systems*, SPIE, **7650**, 76502F (2010), doi: 10.1117/12.847673

E. von der Burg, W. Grill: *Characterization of elastomers with transverse sonic waves*, *Polymer Testing*, **29**,(2), 281 (2010), <http://dx.doi.org/10.1016/j.polymertesting.2009.12.001>

J. Galle, A. Bader, P. Hepp, W. Grill, B. Fuchs, J. A. Kaes, B. Marquass, K. Mueller, J. Schiller, R.M. Schulz, M. von Buttler, E. von der Burg, M. Zscharnack, M. Loeffler: *Mesenchymal Stem Cells in Cartilage Repair: State of the Art and Methods to monitor Cell Growth, Differentiation and Cartilage Regeneration*, *Current Medicinal Chemistry*, **17**, (21), 2274 (2010)

A. Habib, U. Amjad, M. Pluta, U. Pietsch, W. Grill: *Surface acoustic wave generation and detection by Coulomb excitation*, In Tribikram Kundu (Ed.), *Health Monitoring of Structural and Biological Systems*, SPIE **7650**, 76501T (2010), doi: 10.1117/12.847685

K. Hahn, U. Amjad, K. S. Tarar, D. Jha, W. Grill: *Mode selective excitation and detection of Lamb waves*, In Tribikram Kundu (Ed.), *Health Monitoring of Structural and Biological Systems*, SPIE **7650**, 76500D (2010), doi: 10.1117/12.847740

M. Z. Hossain, W. Grill: *Synchronous monitoring of muscle dynamics and muscle force for maximum isometric tetanus*, In Tribikram Kundu (Ed.), *Health Monitoring of Structural and Biological Systems*, SPIE **7650**, 76502V (2010), doi: 10.1117/12.847670

A. E. Kamanyi, W. Grill, W. Ngwa, W. Luo: *Advances in phase-sensitive acoustic microscopy studies of polymer blend films: annealing effects and micro-elastic characterization of PS/PMMA blends*, *JOURNAL OF MICROSCOPY-OXFORD*, **238** (2), 134 (2010), doi: 10.1111/j.1365-2818.2009.03344.x

A. E. Kamanyi, E. T. Ahmed Mohamed, W. Ngwa, W. Grill: *Determination of sound velocity and acoustic impedance of thin chitosan films by phase-sensitive acoustic microscopy*, In Tribikram Kundu (Ed.), *Health Monitoring of Structural and Biological Systems*, SPIE **7650**, 76502A (2010), doi: 10.1117/12.847745

K.S. Tarar, U. Amjad, W. Grill: *Lumped circuit mechanical models and lattice dynamics approach to the dependence of the time-of-flight of bulk and guided acoustical modes on elongation*, In Tribikram Kundu (Ed.), *Health Monitoring of Structural and Biological Systems*, SPIE **7650**, 76500I (2010), doi: 10.1117/12.847723

## 9.12 Graduations

### Doctorate

- Albert Kamanyi  
*Mesoscale characterizatrion of soft matter systems by phase-sensitive acoustic microscopy*  
December 2010

## 9.13 Guests

- Humboldt Research Award Laureate Prof. Dr. Tribikram Kundu,  
Department of Civil Engineering and Engineering Mechanics  
University of Arizona, Tucson, USA  
6. 7. 2010 - 31. 7. 2010
- Humboldt Research Fellow Dr. Amit Shelke  
Department of Civil Engineering and Engineering Mechanics,  
University of Arizona, Tucson, USA  
25. 1. 2010 - 24. 7. 2010
- Anowarul Habib, M.Sc.  
Universität Siegen, Siegen, Germany  
15. 11. 2010 - 30. 11. 2010
- Prof. Dr. Rajendra Kumar Singh  
Banaras Hindu University, Varanasi, India  
27. 5. 2010 - 29. 5. 2010



# 10

## Superconductivity and Magnetism

### 10.1 Introduction

The research of the Division of Superconductivity and Magnetism is focused on the study of magnetic ordering and superconductivity in a range of materials, especially carbon-based systems and magnetic oxides. Highlight of 2010 were the study of interlayer exchange coupling in  $\text{La}_{0.7}\text{Sr}_{0.3}\text{MnO}_3/\text{SrRuO}_3$  superlattices with the discovery of many interesting features ranging from structural transitions of the  $\text{SrRuO}_3$  layers to inverted magnetization hysteresis loops, and the x-ray magnetic dichroism results on graphite surfaces with the discovery of the hydrogen influence on the magnetic order.

*Pablo Esquinazi*

### 10.2 Tailoring Magnetic Interlayer Coupling in $\text{La}_{0.7}\text{Sr}_{0.3}\text{MnO}_3/\text{SrRuO}_3$ Superlattices

M. Ziese, I. Vrejoiu<sup>\*</sup>, E. Pippel<sup>\*</sup>, P. Esquinazi, D. Hesse<sup>\*</sup>, C. Etz<sup>\*</sup>, J. Henk<sup>\*</sup>, A. Ernst<sup>\*</sup>, V. Maznichenko<sup>†</sup>, W. Hergert<sup>†</sup>, I. Mertig<sup>\*†</sup>

<sup>\*</sup>Max Planck Institute of Microstructure Physics, 06120 Halle, Germany

<sup>†</sup>Institute of Physics, Martin Luther University Halle-Wittenberg, 06120 Halle, Germany

The magnetic interlayer coupling in  $\text{La}_{0.7}\text{Sr}_{0.3}\text{MnO}_3/\text{SrRuO}_3$  superlattices was investigated. High quality superlattices with ultrathin  $\text{La}_{0.7}\text{Sr}_{0.3}\text{MnO}_3$  and  $\text{SrRuO}_3$  layers were fabricated by pulsed laser deposition. The superlattices grew coherently with Mn/Ru intermixing restricted to about one interfacial monolayer. Strong antiferromagnetic interlayer coupling depended delicately on magnetocrystalline anisotropy and intermixing at interfaces. Ab initio calculations elucidated that the antiferromagnetic coupling is mediated by the Mn–O–Ru bond. The theoretical calculations allowed for a quantitative correlation between the total magnetic moment of the superlattice and the degree of Mn/Ru intermixing. For illustration the magnetization of three superlattices with varying  $\text{SrRuO}_3$  layer thickness (3, 5 and 8 nm) is shown in Fig. 10.1.

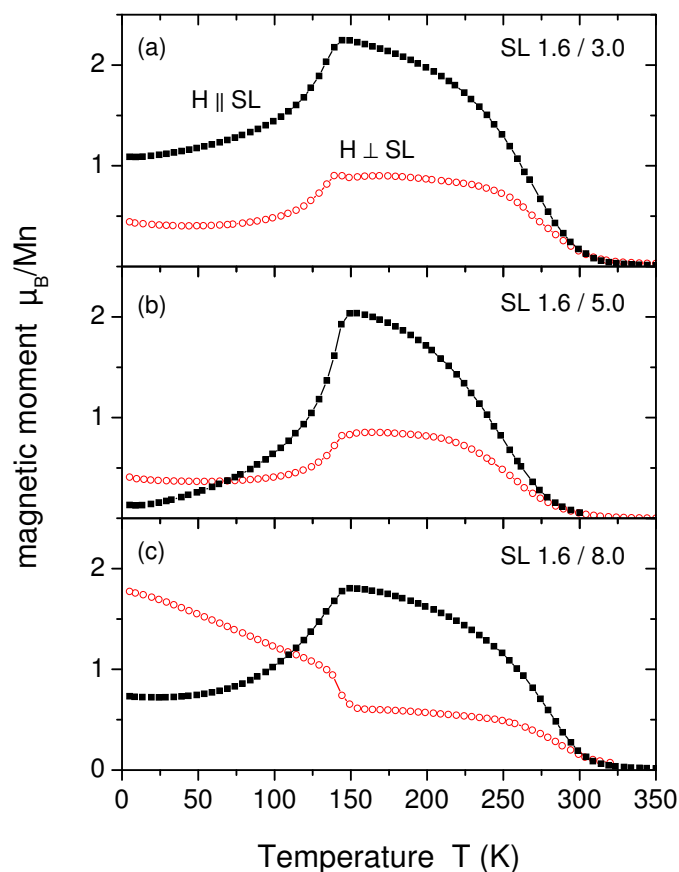


**Figure 10.1:** Field cooled in-plane (squares) and perpendicular-to-plane (circles) magnetic moment of three superlattices measured in a magnetic field of 0.1 T.  $\text{La}_{0.7}\text{Sr}_{0.3}\text{MnO}_3$  layer thickness was 1.6 nm and  $\text{SrRuO}_3$  layer thickness varied from 3.0 to 8.0 nm. The decrease of the magnetic moment below 145 K shows the presence of antiferromagnetic interlayer coupling.

### 10.3 Inverted hysteresis and giant exchange bias in $\text{La}_{0.7}\text{Sr}_{0.3}\text{MnO}_3/\text{SrRuO}_3$ superlattices

M. Ziese, I. Vrejoiu\*, D. Hesse\*

\*Max Planck Institute of Microstructure Physics, 06120 Halle, Germany

The magnetization reversal mechanisms in a  $\text{La}_{0.7}\text{Sr}_{0.3}\text{MnO}_3/\text{SrRuO}_3$  superlattice with ultrathin individual layers were studied. Due to the strong exchange bias between  $\text{La}_{0.7}\text{Sr}_{0.3}\text{MnO}_3$  and  $\text{SrRuO}_3$  layers inverted hysteresis loops were observed at temperatures below 62 K; at higher temperatures the superlattice showed an unconventional reversal mechanism with the magnetically hard  $\text{SrRuO}_3$  layers switching first on reducing the magnetic field from saturation. These observations were corroborated by micromagnetic simulations and were interpreted as arising from interfacial Bloch walls. The magnetization of the superlattice in both temperature regimes is shown in Fig. 10.2.

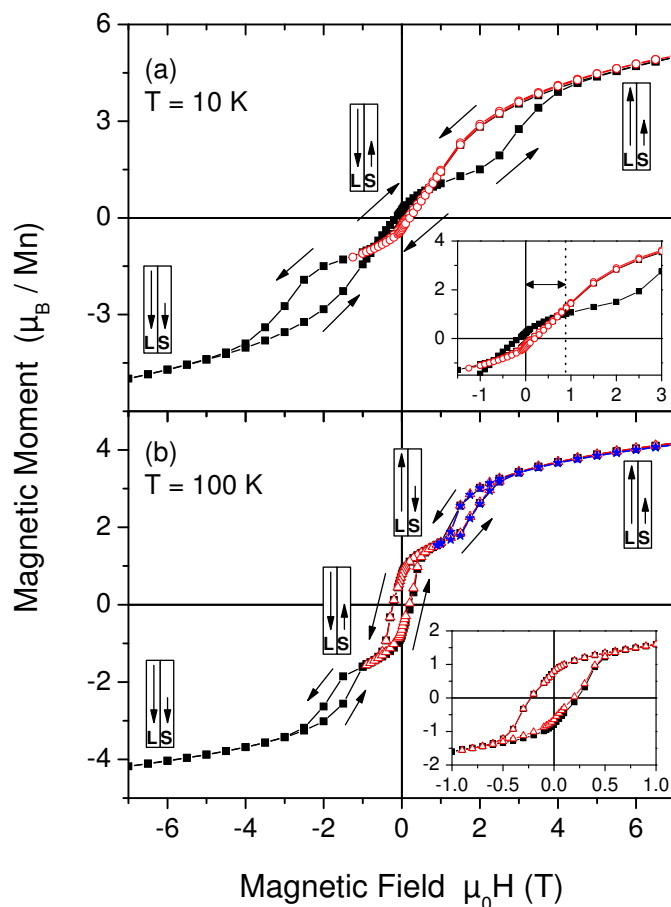


**Figure 10.2:** Full (solid symbols) and minor hysteresis loops at (a) 10 K and (b) 100 K. At 10 K one reversible minor loop is cycled between +7 T and  $-1.25$  T, at 100 K two minor loops were measured, one (triangles) between +7 and  $-0.9$  T and a second (stars) between +7 and +0.9 T. The arrows indicate the sweep direction. The relative layer magnetization orientation is illustrated in the diagrams showing schematically a superlattice unit cell with a LSMO (L) and a SRO (S) layer. The insets show zooms of the central sections of the loops. At 10 K a clear rightshift of the minor loop is seen with a large exchange bias field of about +0.9 T, at 100 K exchange biasing cannot be determined from the magnetization measurements.

## 10.4 Structural symmetry and magnetocrystalline anisotropy of $\text{SrRuO}_3$ films on $\text{SrTiO}_3$ (001)

M. Ziese, I. Vrejoiu\*, D. Hesse\*

\*Max Planck Institute of Microstructure Physics, 06120 Halle, Germany

The structural, magnetic, and magnetotransport properties of  $\text{SrRuO}_3$  films grown on  $\text{SrTiO}_3$  (001) substrates were investigated with the aim to determine the crystalline symmetry, crystalline orientation, and magnetocrystalline anisotropy of an ultrathin (5 nm)  $\text{SrRuO}_3$  film. 60- and 40-nm-thick  $\text{SrRuO}_3$  films were extensively studied by transmission electron microscopy as well as magnetic and magnetotransport techniques, respectively. These studies showed orthorhombic symmetry with a slight monoclinic distortion and a well-defined long-range order of crystallographic domains with the  $[001]_0$  axis parallel to terraces on the slightly vicinal  $\text{SrTiO}_3$  substrate. The magne-

to crystalline anisotropy is very strong. The easy axis lies in the  $[001]_o$  plane under a temperature-dependent angle of about  $35^\circ$  with respect to the  $[110]_o$  direction that is along the film normal. The angular-dependent anisotropic magnetoresistance shows distinctive characteristics of the monoclinic symmetry that can be used as a fingerprint. Transmission electron microscopy images of the 5 nm thin  $\text{SrRuO}_3$  film show a coherently strained state. Using the fingerprints from the angular magnetoresistance it could be clearly shown that this ultrathin  $\text{SrRuO}_3$  film, although grown in step-flow growth mode as well, has still monoclinic symmetry, but lacks long-range order of the crystallographic domains. A fraction of 30-40% of misaligned domains (rotated in plane by  $90^\circ$ ) was estimated from the magnetoresistance curves. Fig. 10.3 shows the typical magnetoresistance symmetry of  $\text{SrRuO}_3$  for magnetic field rotation in the  $[001]_o$  and  $[1\bar{1}0]_o$  planes, respectively.

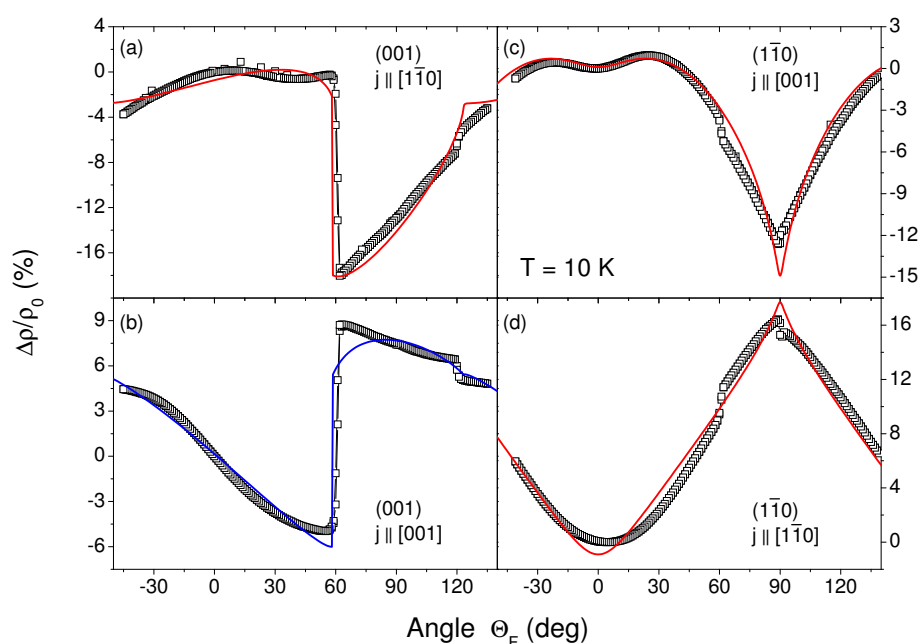


**Figure 10.3:** Angular dependent magnetoresistance of a 40 nm thick  $\text{SrRuO}_3$  at 10 K in an applied field of 8 T. Rotation planes and current density directions are indicated in the figure. The solid lines were obtained by an iterative procedure using both the expressions for the magnetoresistance and magnetocrystalline anisotropy energy in monoclinic symmetry.

## 10.5 Detection of ferromagnetic signals in common diamagnetic oxide crystals

M. Khalid, A. Setzer, M. Ziese, P. Esquinazi, D. Spemann, A. Pöpl, E. Goering\*

\*Max-Planck-Institut für Metallforschung, D-70569 Stuttgart, Germany

The magnetic properties of  $\text{MgO}$ ,  $\text{MgAl}_2\text{O}_4$ ,  $\text{SrTiO}_3$ ,  $\text{LaAlO}_3$ , LSAT, and  $\text{ZnO}$  single crystals were investigated. These crystals show three contributions to the magnetization, namely, an intrinsic diamagnetic contribution, a paramagnetic contribution, due to various transition-metal impurities, as well as a ferromagnetic contribution. The latter

shows coercive field values that are rather independent of the actual crystal material. The saturation magnetization, however, was found to vary strongly from batch to batch. The origin of the ferromagnetic contribution as arising from either defect-induced ferromagnetism or ferromagnetic impurities is discussed. Fig. 10.4 shows typical magnetization curves for a variety of oxide crystals.

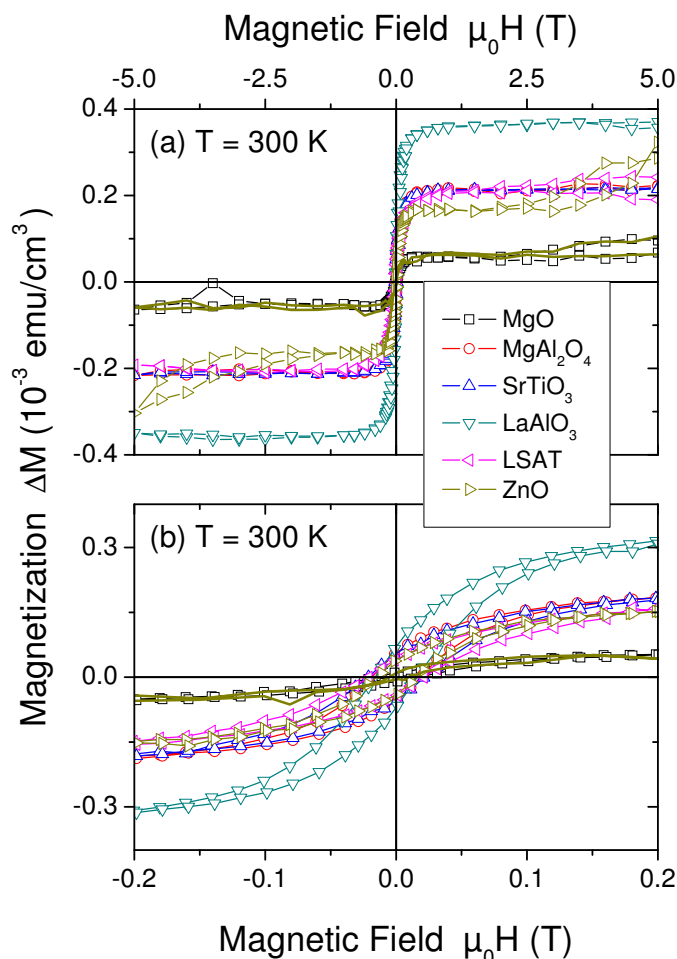


**Figure 10.4:** Volume magnetization of the ferromagnetic-like contribution of the crystals at 300 K in (a) a wide and (b) a narrow field range.

## 10.6 Disordered electrical potential observed on the surface of SiO<sub>2</sub> by electric field microscopy

N. García\*, Z. Yan\*, A. Ballestar, J. Barzola-Quiquia, F. Bern, P. Esquinazi

\*Laboratorio de Física de Sistemas Pequeños y Nanotecnología, Consejo Superior de Investigaciones Científicas, E-28006 Madrid, Spain

The electrical potential on the surface of about 300 nm thick SiO<sub>2</sub> layers grown on single-crystalline Si substrates was characterized at ambient conditions using electric field microscopy. The results show an inhomogeneous potential distribution with fluctuations up to 0.4 V within regions of 1  $\mu\text{m}$ . The potential fluctuations observed at the

surface of these common dielectric templates of graphene sheets should induce strong variations in the graphene charge densities and provide a simple explanation for some of the anomalous behaviors of the transport properties of graphene. Fig. 10.5 shows the experimental arrangement and typical results.

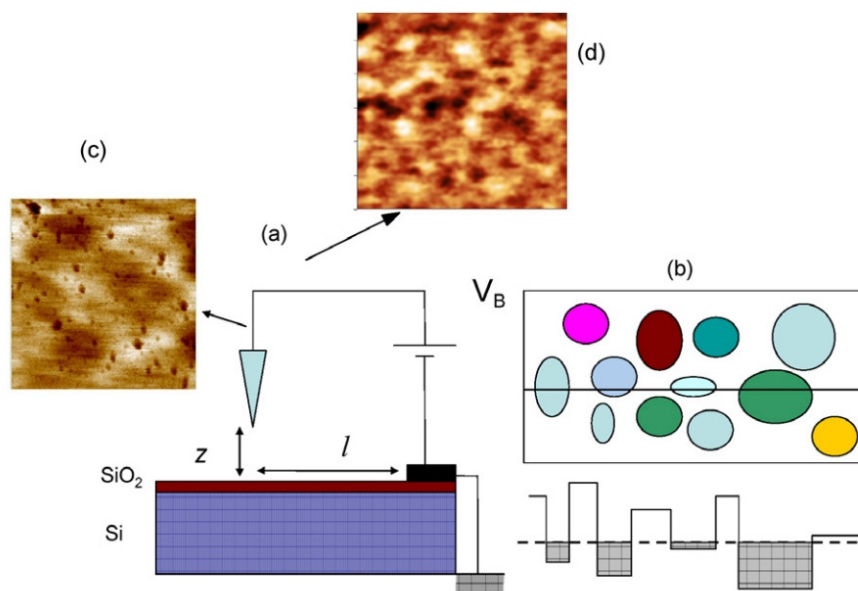


**Figure 10.5:** (a) Sketch of the experimental arrangement. The distance  $z$  between tip and surface can be varied as well as the distance  $l$  to the mass contact. (b) Sketch of the potential distribution that potentially might affect a graphene layer. The scan line below represents a one-dimensional potential with differently filled wells of graphene carriers. The dashed line represents the Fermi energy of the graphene layer on top of the disordered potential surface. (c) EFM image ( $4 \times 4 \mu\text{m}^2$ ) of a  $\text{SiO}_2$  surface in a sample in which a resin rest (dark spots) was left. (d) EFM picture ( $6 \times 6 \mu\text{m}^2$ ) of a resin-free sample. These results were obtained with two different microscopes and different EFM tips. For both EFM pictures the potential gradients between light and dark broad areas (not spots) are  $\leq 0.4 \text{ V}$ .

## 10.7 The influence of $\text{Ga}^+$ irradiation on the transport properties of mesoscopic conducting thin films

J. Barzola-Quiquia, S. Dusari, G. Bridoux, F. Bern, A. Molle, P. Esquinazi

The influence of 30 keV  $\text{Ga}^+$ -ion irradiation – commonly used in focused-ion-beam (FIB) devices – on the transport properties of thin crystalline graphite flakes,  $\text{La}_{0.7}\text{Ca}_{0.3}\text{MnO}_3$  and Co thin films was studied. Changes in electrical resistance were measured in situ during irradiation; the temperature and magnetic field dependence was measured ex situ before and after irradiation. The results show that the transport properties of these materials strongly change already at  $\text{Ga}^+$  fluences much below those used for patterning and ion-beam-induced deposition (IBID), seriously limiting the use of FIB when the intrinsic properties of the materials of interest are of importance. A method to protect the samples as well as to produce selective irradiation-induced modifications was devised.

Fig. 10.6 shows the nanostructures as well as the influence of  $\text{Ga}^+$  irradiation on the resistance of the devices.

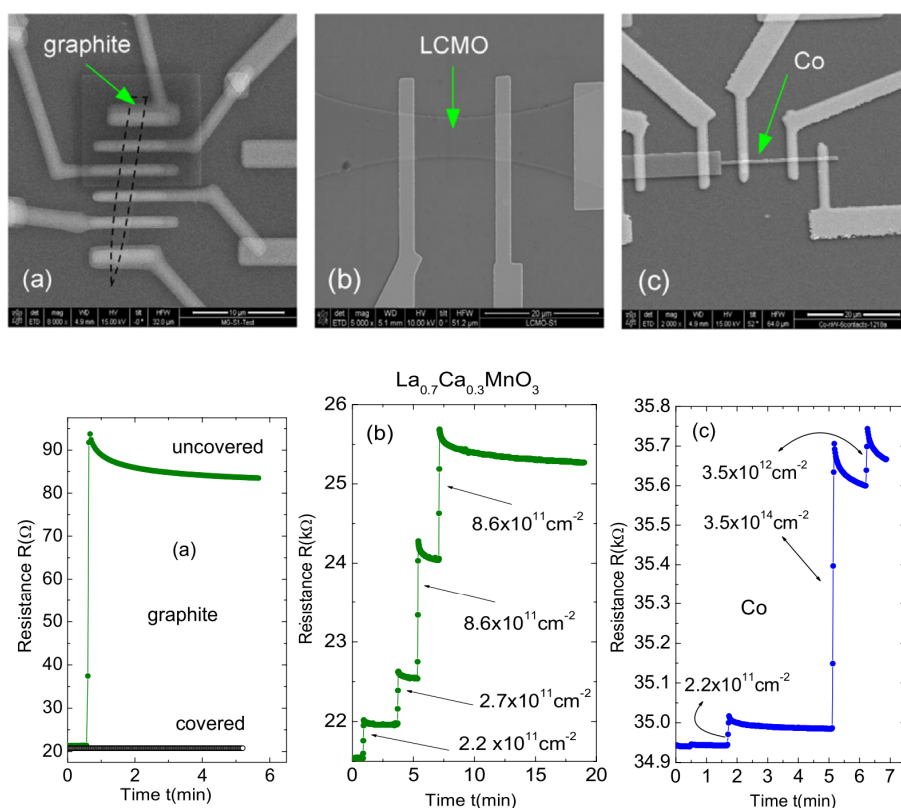


**Figure 10.6:** Upper panel: scanning electron microscope images of: (a) a graphite flake; (b) a  $\text{La}_{0.7}\text{Ca}_{0.3}\text{MnO}_3$  film and (c) a Co microwire. The irradiation was done on the whole region and the electrical resistance was measured. Lower panel: resistance as a function of time before, during and after  $\text{Ga}^+$  irradiation inside the FIB chamber for the samples from the upper panel. All these measurements were done in situ and at room temperature.

## 10.8 Giant negative photoresistance of ZnO single crystals

J. Barzola-Quiquia, P. Esquinazi, M. Villafuerte\*, S.P. Heluani\*, A. Pöppl, K. Eisinger

\*Dpto. de Física, Universidad Nacional de Tucumán, Argentina

The temperature dependence of the electrical resistance of ZnO single crystals prepared by a hydrothermal method was measured in the temperature range between 30 and 300 K in darkness and under ultraviolet light illumination. After illumination the resistance decreases several orders of magnitude at temperatures  $T < 200$  K. Electron paramagnetic resonance studies under illumination reveal that the excitation of Li acceptor impurities is the origin for the giant negative photoresistance effect. Permanent photoconductivity is also observed, which remains many hours after leaving the crystal in darkness.

## 10.9 Funding

*Study of intrinsic and extrinsic phenomena in the electrical transport properties of multi-graphene*

Prof. P. Esquinazi

DFG ES 86/16-1

*Defect-induced Magnetism in Oxides*

Prof. P. Esquinazi and Dr. M. Ziese

DFG SFB762 B1

*Spin-dependent Transport and Exchange-Biasing in multiferroic Heterostructures*

Dr. M. Ziese and Prof. P. Esquinazi

DFG SFB 762 B5

*Defect induced magnetic order in ZnO and TiO<sub>2</sub> thin films*

Prof. P. Esquinazi

DAAD

*Study of the anisotropy ratio of the conductivities of graphite*

Prof. P. Esquinazi

DAAD

*Measurements of the mean free path and of the transport anisotropy in multigraphene*

Prof. P. Esquinazi

Buildmona

*Transport properties of oxide nanostructures*

Prof. P. Esquinazi

Buildmona

## 10.10 Organizational Duties

P. Esquinazi

- Dean of Studies
- Project Reviewer: Deutsche Forschungsgemeinschaft (DFG), National Science Foundation (USA), German-Israeli Foundation (GIF), Israel Science Foundation, Department of Energy (Washington), DAAD
- Referee: Phys. Rev. Lett, Phys. Rev. B., Appl. Phys. Lett., Chem. Phys. Lett., Physica C, Phys. Lett. A, phys. stat. sol., J. Low Temp. Phys., Carbon, J. Chem. Phys., Eur. J. Phys. B, J. Magn. Magn. Mater.

M. Ziese

- Head of the Undergraduate Physics Laboratory
- Member of the study commission
- Referee: Phys. Rev. Lett., Phys. Rev. B., J. Phys.: Condens. Matter, J. Phys. D: Appl. Phys., phys. stat. sol., J. Magn. Magn. Mater., Eur. J. Phys. B, Thin Solid Films

W. Böhlmann

- Referee: J. Physical Chemistry, J. of American Chemical Society, Microporous and Mesoporous Materials

## 10.11 External Cooperations

### Academic

- State University of Campinas, Campinas, Brazil  
Prof. Dr. Yakov Kopelevich
- Universidad Autónoma de Madrid, Spain  
Prof. Dr. Miguel Angel Ramos
- University of Ioannina, Greece, Ioannina, Greece  
Prof. I. Panagiotopoulos,
- University of Sheffield, UK  
Prof. G. Gehring
- University of the Negev, Beer Sheva, Israel  
Dr. Alex Shames
- Max-Plank Institute of Microstructure Physics, Halle, Germany  
Dr. Ionela Vrejoiu
- Max-Plank Institute of Microstructure Physics, Halle, Germany  
Prof. Dietrich Hesse
- Max-Plank Institute of Microstructure Physics, Halle, Germany  
Dr. Marin Alexe
- Max-Plank Institute of Microstructure Physics, Halle, Germany  
Dr. Arthur Ernst
- Martin-Kuther Universität Halle-Wittenberg, Halle, Germany  
Prof. Ingrid Mertig
- Martin-Kuther Universität Halle-Wittenberg, Halle, Germany  
Prof. Wolfram Hergert
- Martin-Kuther Universität Halle-Wittenberg, Halle, Germany  
Dr. Angelika Chassé
- Martin-Kuther Universität Halle-Wittenberg, Halle, Germany  
Dr. Manfred Dubiel
- Stanford Synchrotron Radiation Laboratory, USA  
Dr. Hendrik Ohldag
- Max-Planck-Institut für Metallforschung, Stuttgart, Germany  
Dr. Eberhard Goering
- Laboratorio de Física de Sistemas Pequeños y Nanotecnología, Consejo Superior de Investigaciones Científicas, Madrid, Spain  
Prof. N. García (Madrid)

- Forschungszentrum Dresden-Rossendorf e.V., Institut für Ionenstrahlphysik und Materialforschung, Germany  
Dr. W. Anwand
- Forschungszentrum Dresden-Rossendorf e.V., Institut für Ionenstrahlphysik und Materialforschung, Germany  
Dr. G. Brauer
- Tucuman University, Argentina  
Prof. S. P. de Heluani
- University of La Plata, Argentina  
Dr. C. E. Rodriguez Torres

## 10.12 Publications

### Journals

- X. Gao, B. J. Rodriguez, L. Liu, B. Birajdar, D. Pantel, M. Ziese, M. Alexe and D. Hesse: Microstructure and Properties of Well-Ordered Multiferroic  $\text{Pb}(\text{Zr,Ti})\text{O}_3/\text{CoFe}_2\text{O}_4$  Nanocomposites  
*ACS Nano* **4**, 1099 (2010)
- M. Ziese, I. Vrejoiu, E. Pippel, P. Esquinazi, D. Hesse, C. Etz, J. Henk, A. Ernst, I. V. Maznichenko, W. Hergert and I. Mertig: Tailoring Magnetic Interlayer Coupling in  $\text{La}_{0.7}\text{Sr}_{0.3}\text{MnO}_3/\text{SrRuO}_3$  Superlattices  
*Phys. Rev. Lett.* **104**, 167203 (2010)
- N. García, Z. Yan, A. Ballestar, J. Barzola-Quiquia, F. Bern and P. Esquinazi: Disordered electrical potential observed on the surface of  $\text{SiO}_2$  by electric field microscopy  
*J. Phys.: Condens. Matter* **22**, 045002 (2010)
- S. Dusari, J. Barzola-Quiquia, P. Esquinazi and S. P. Heluani: Changes in the electrical transport of ZnO under visible light  
*Solid State Commun.* **150**, 22 (2010)
- J. Barzola-Quiquia and P. Esquinazi: Ferromagnetic- and Superconducting-Like Behavior of the Electrical Resistance of an Inhomogeneous Graphite Flake  
*J. Supercond. Nov. Magn.* **23**, 451 (2010)
- J. Barzola-Quiquia, S. Dusari, G. Bridoux, F. Bern, A. Molle and P. Esquinazi: The influence of  $\text{Ga}^+$  irradiation on the transport properties of mesoscopic conducting thin films  
*Nanotechnology* **21**, 145306 (2010)
- M. A. Ramos, J. Barzola-Quiquia, P. Esquinazi, A. Muñoz-Martin, A. Climent-Font and M. García-Hernández: Magnetic properties of graphite irradiated with MeV ions  
*Phys. Rev. B* **81**, 214404 (2010)

M. Dubman, T. Shiroka, H. Luetkens, M. Rothermel, F. J. Litterst, E. Morenzoni, A. Suter, D. Spemann, P. Esquinazi, A. Setzer and T. Butz:

Low-energy  $\mu$ SR and SQUID evidence of magnetism in highly oriented pyrolytic graphite

J. Magn. Magn. Mater. **322**, 1228 (2010)

M. Khalid, A. Setzer, M. Ziese and P. Esquinazi:

Ubiquity of ferromagnetic signals in common diamagnetic oxide crystals

Phys. Rev. B **81**, 214414 (2010)

J. Zippel, M. Lorenz, A. Setzer, G. Wagner, N. Sobolev, P. Esquinazi and M. Grundmann:

Defect-induced ferromagnetism in undoped and Mn-doped zirconia thin films

Phys. Rev. B **82**, 125209 (2010)

J. Barzola-Quiquia, P. Esquinazi, M. Villafuerte, S. P. Heluani, A. Pöppl and K. Eisinger:  
Origin of the giant negative photoresistance of ZnO single crystals

J. Appl. Phys. **108**, 073530 (2010)

P. Esquinazi, J. Barzola-Quiquia, D. Spemann, M. Rothermel, H. Ohldag, N. García, A. Setzer and T. Butz:

Magnetic order in graphite: Experimental evidence, intrinsic and extrinsic difficulties

J. Magn. Magn. Mater. **322**, 1156 (2010)

F. Golmar, M. Villafuerte, A. Mudarra Navarro, C. E. Rodríguez Torres, J. Barzola-Quiquia, P. Esquinazi and S. P. Heluani:

ZnO:Co diluted magnetic semiconductor or hybrid nanostructure for spintronics?

J. Mater. Sci. **45**, 6174 (2010)

M. Ziese, I. Vrejoiu and D. Hesse:

Inverted hysteresis and giant exchange bias in  $\text{La}_{0.7}\text{Sr}_{0.3}\text{MnO}_3/\text{SrRuO}_3$  superlattices

Appl. Phys. Lett. **97**, 052504 (2010)

M. Ziese, I. Vrejoiu and D. Hesse:

Structural symmetry and magnetocrystalline anisotropy of  $\text{SrRuO}_3$  films on  $\text{SrTiO}_3$

Phys. Rev. B **81**, 184418 (2010)

H. Ohldag, P. Esquinazi, E. Arenholz, D. Spemann, M. Rothermel, A. Setzer and T. Butz:

The role of hydrogen in room-temperature ferromagnetism at graphite surfaces

New J. Phys. **12**, 123012 (2010)

J. Fritsch, M. Rose, P. Wollmann, W. Böhlmann and Stefan Kaskel:

New Element Organic Frameworks Based on Sn, Sb, and Bi, with Permanent Porosity and High Catalytic Activity

Materials **3** 2447 (2010)

M. Rose, N. Klein, W. Böhlmann, B. Böhringer, S. Fichtner and Stefan Kaskel:

New element organic frameworks via Suzuki coupling with high adsorption capacity for hydrophobic molecules

Soft Matter **6** 3918 (2010)

J. Weber, J. Schmidt, A. Thomas and W. Böhlmann:  
Micropore Analysis of Polymer Networks by Gas Sorption and  $^{129}\text{Xe}$  NMR Spectroscopy: Toward a Better Understanding of Intrinsic Microporosity  
*Langmuir* **26** 15650 (2010)

## 10.13 Graduations

### Master

- Francis Bern  
*Magnetization reversal and exchange bias effect studied in Cobalt nanowires by means of transport measurements*  
October 2010

### Bachelor

- Justus Krüger  
*Magnetotransportmessungen an Carbon Nanotubes*  
September 2010
- Alexander Lessig  
*Patterning of Exchange Bias Bilayers*  
September 2010
- Thomas Megel  
*Magnetic properties of Strontium Ruthenate*  
September 2010
- Andreas Schadewitz  
*Angle and field dependence of the magnetoresistance of a multigraphene sample*  
September 2010

## 10.14 Guests

- Özgün Kocabiyik  
Sabancı University, Istanbul, Turkey  
28.06.2010 - 02.10.2010
- Shaivya Joshi  
Exchange student, India  
15.05.2010 - 26.07.2010
- Eunice Kuotsoo Amon  
DAAD student, Ghana  
01.07.2010 - 31.08.2010
- Guangyu Ding  
DAAD student, China  
15.07.2010 - 14.09.2010

- Dr. Robson Ricardo de Silva  
State University of Campinas, Campinas, Brazil  
05.10.2010 - 03.12.2010
- Dr. Gabriela Simonelli  
Universidad Nacional de Tucumán, Argentina  
11.10.2010 - 23.10.2010
- Maria Cecilia Zapata  
Universidad Nacional de Tucumán, Argentina  
10.10.2010 - 03.12.2010
- Prof. Yakov Kopelevich  
State University of Campinas, Campinas, Brazil  
18.12.2010 - 31.12.2010



**III**

**Institute for Theoretical Physics**



# 11

## Computational Quantum Field Theory

### 11.1 Introduction

The Computational Physics Group performs basic research into classical and quantum statistical physics with special emphasis on phase transitions and critical phenomena. In the centre of interest are the physics of spin glasses, diluted magnets and other materials with quenched, random disorder, soft condensed matter physics with focus on fluctuating paths and interfaces, biologically motivated problems such as protein folding, aggregation and adsorption as well as related properties of homopolymers, and the intriguing physics of low-dimensional quantum spin systems. Our investigations of a geometrical approach to the statistical physics of topological defects with applications to superconductors and superfluids and research into fluctuating geometries with applications to quantum gravity, e.g., dynamical triangulations, build on the recently concluded European Research Training Network (RTN) "ENRAGE": *Random Geometry and Random Matrices: From Quantum Gravity to Econophysics*, a collaboration of 13 teams throughout Europe. Moreover, within a bi-national Institute Partnership of the Humboldt Foundation the statistical mechanics of complex networks is studied in collaboration with our partner university in Krakow, Poland.

The methodology is a combination of analytical and numerical techniques. The numerical tools are currently mainly Monte Carlo computer simulations and high-temperature series expansions. The computational approach to theoretical physics is expected to gain more and more importance with the future advances of computer technology, and is likely to become the third cornerstone of physics besides experiment and analytical theory. Already now it can help to bridge the gap between experiments and the often necessarily approximate calculations of analytical work. To achieve the desired high efficiency of the numerical studies we develop new algorithms, and to guarantee the flexibility required by basic research all computer codes are implemented by ourselves. The technical tools are Fortran, C, and C++ programs running under Unix or Linux operating systems and computer algebra using Maple or Mathematica. The software is developed and tested at the Institute on a cluster of PCs and workstations, where also most of the numerical analyses are performed. Currently we are also exploring the possibilities of the rapidly developing graphics card computing, that is computer simulations on graphics processing units (GPUs) with many cores.

Large-scale simulations requiring vast amounts of computer time are carried out at the Institute on quite powerful compute servers, at the parallel computers of the University computing centre, and, upon successful grant application at the national supercomputing centres in Jülich and München on IBM and Hitachi parallel supercomputers. This hierarchy of various platforms gives good training opportunities for the students and offers promising job perspectives in many different fields for their future career.

Within the University, our research activities are closely integrated into the Graduate School “BuildMoNa”: Leipzig School of Natural Sciences – *Building with Molecules and Nano-objects* funded by the German Research Foundation (DFG) within the German Excellence Initiative and the international DFH-UFA Graduate School *Statistical Physics of Complex Systems* with Nancy Université, France, supported by the Deutsch-Französische Hochschule. For the latter we submitted in 2010 a successful extension proposal, securing enhanced funding for the period 2011–2014. The two Graduate Schools are both “Classes” of the Research Academy Leipzig (RALeipzig), providing the organizational frame for hosting visiting students, offering language courses, organizing childcare and for many other practical matters. At the post-graduate level our research projects are embedded into the “Sächsische DFG-Forschergruppe” FOR877 *From Local Constraints to Macroscopic Transport*, which also has been successfully extended in 2010 for the period 2011–2014, the International Max Planck Research School (IMPRS) *Mathematics in the Sciences* and into two of the top level research areas (“Profilbildende Forschungsbereiche (PbF)”) and the Centre for Theoretical Sciences (NTZ) of the University. Beside “BuildMoNa” the latter structures are instrumental for our cooperations with research groups in experimental physics and biochemistry.

On an international scale, our research projects are carried out in a wide net of collaborations funded by the German Academic Exchange Service (DAAD) and the Alexander von Humboldt Foundation through the Institute Partnership with the Jagiellonian University in Krakow, Poland, as well as their Fellowship Programmes, and in part initiated by the European Research Training Network “ENRAGE”. Since 2008 our group is annually hosting the Humboldt Research Prize Winner Professor Bernd A. Berg from Florida State University, Tallahassee, USA, for a few months. Further close contacts and collaborations are established with research groups in Armenia, Austria, China, France, Great Britain, Israel, Italy, Japan, Poland, Russia, Spain, Sweden, Taiwan, Turkey, Ukraine, and the United States. These contacts are refreshed and furthered through topical Workshops and Tutorials and our International Workshop series *CompPhys: New Developments in Computational Physics*, taking annually place at the end of November just before the first advent weekend.

Wolfhard Janke

## 11.2 Large-Scale Computer Simulations of Spin Glasses

A. Nußbaumer, E. Bittner\*, W. Janke

\*Present address: Institut für Theoretische Physik, Universität Heidelberg, Germany

One of the most challenging problems in the statistical physics of disordered systems is the nature of the low-temperature phase of spin-glass systems such as the short-ranged

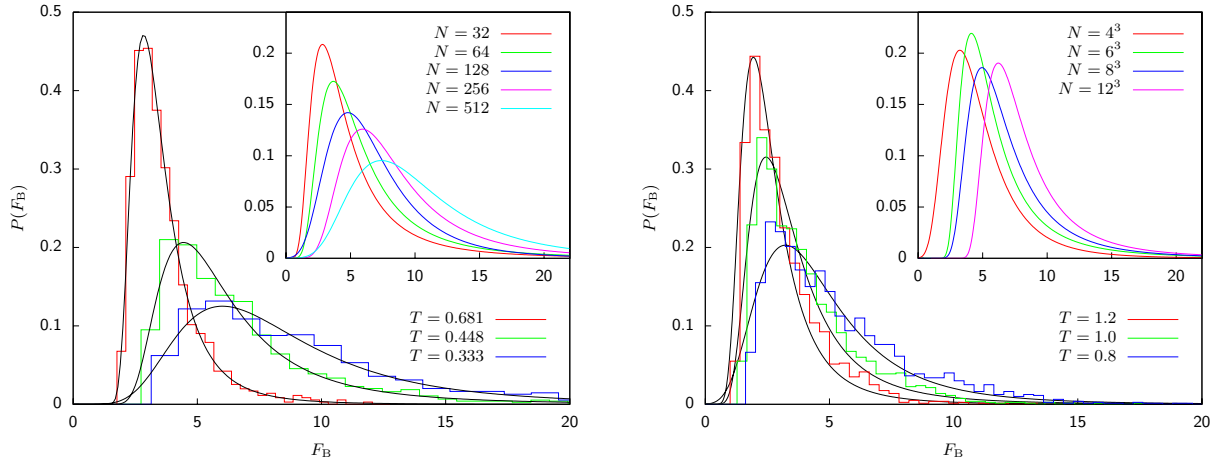


**Figure 11.1:** Left: Distribution of free-energy barriers  $F_B$  for the SK model with  $N = 256$  spins at different temperatures. The inset shows the distribution for  $T = 1/3$  for different numbers of spins. Right: The same type of graph for the EA model with  $N = 4^3$  spins. The inset shows the distribution for  $T = 0.8$  for different lattice sizes.

Edwards-Anderson (EA) and mean field Sherrington-Kirkpatrick (SK) models [1–3]. The origin of the numerical problems can be traced back to the combination of disorder and frustration which leads in the spin-glass phase for  $T < T_c$  to a rugged free-energy landscape with probable regions separated by rare-event states [4]. Consequently, conventional Monte Carlo simulations tend to get stuck in local free-energy valleys. In this project we try to overcome this kind of problem by using a novel update algorithm which combines the parallel tempering method [5] with the multi-overlap Monte Carlo algorithm [6].

From large-scale computer simulations we obtained the free-energy barriers  $F_B$  characterizing these rare-event states. Their distribution becomes broader for lower temperatures and is expected to be represented by a Fréchet extreme-value distribution for fat-tailed distributions [7]. In general, extreme-value statistics can be classified into different universality classes, depending on whether the tails of the original distribution are fat tailed (algebraic), exponential, or thin tailed (decaying faster than exponential). Fitting our data with a generalized extreme-value distribution (GEV),

$$F_{\xi;\mu;\sigma}(x) = \exp \left[ - \left( 1 + \xi \frac{x - \mu}{\sigma} \right)^{-1/\xi} \right]$$

with  $1 + \xi(x - \mu)/\sigma > 0$ , we find a shape parameter  $\xi > 0$ , i.e., a Fréchet distribution. The distributions and fits are shown in Fig. 11.1. The histograms of the SK model for low temperatures show deviations from the Fréchet distribution for small values of  $F_B$ , so a much larger number of disorder realizations would be needed to determine both tails of the distribution properly. We determined the parameters  $\sigma$ ,  $\mu$  and  $\xi$  for different temperatures and found that  $\sigma$  grows linearly and  $\mu$  logarithmically with inverse temperature  $1/T$ , whereas  $\xi$  stays more or less constant at  $\xi \approx 0.33$ . If we keep the temperature fixed and look at the size dependence of the distribution, we find that for a larger number of spins the distribution becomes broader, c.f. the inset of Fig. 11.1 (left). To quantify this behaviour we use the scaling relations  $\sigma \propto N^{\alpha(\sigma)}$  and  $\mu \propto N^{\alpha(\mu)}$ , which lead to  $\alpha(\sigma) \approx 0.25$  and  $\alpha(\mu) \approx 0.31$  for our lowest temperatures.

We find a temperature dependence of the exponents  $\alpha(\sigma)$  and  $\alpha(\mu)$  with negative and positive slope for increasing  $T$ , respectively. For the EA model we also find fat-tailed distributions, but the broadening of the distribution with increasing number of spins is much weaker than for the SK model, see Fig. 11.1 (right).

- [1] K. Binder, A.P. Young: *Rev. Mod. Phys.* **58**, 801 (1986)
- [2] K.H. Fischer, J.A. Hertz: *Spin Glasses* (Cambridge University Press, Cambridge (England) 1991)
- [3] A.P. Young (ed.): *Spin Glasses and Random Fields* (World Scientific, Singapore 1997)
- [4] W. Janke (ed.): *Rugged Free Energy Landscapes: Common Computational Approaches to Spin Glasses, Structural Glasses and Biological Macromolecules*, *Lect. Notes Phys.* **736** (Springer, Berlin 2008)
- [5] K. Hukushima, K. Nemoto: *J. Phys. Soc. Jpn.* **65**, 1604 (1996)
- [6] B.A. Berg, W. Janke: *Phys. Rev. Lett.* **80**, 4771 (1998)
- [7] E. Bittner et al.: in *NIC Symposium 2008*, ed. by G. Münster et al., *NIC Series Vol. 39* (John von Neumann Institute for Computing, Jülich 2008) p 229

### 11.3 Shape Anisotropy of Polymers in Disordered Environment

V. Blavatska\*, W. Janke

\*Institute for Condensed Matter Physics, National Academy of Sciences of Ukraine, Lviv, Ukraine

Topological properties of macromolecules, such as their shape and size, are of interest in various respects. The shape of proteins affects their folding dynamics and motion in a cell and is relevant in comprehending complex cellular phenomena, such as catalytic activity. The hydrodynamics of polymer fluids is essentially affected by the size and shape of individual macromolecules, and polymer shapes also play an important role in determining the molecular weight in gel filtration chromatography.

An obvious shape measure of macromolecules is provided by the normalized average eigenvalues  $\lambda_i$  of the gyration tensor. Their computation is, however, difficult because one must explicitly diagonalize the gyration tensor for each realization in an ensemble of polymers. It was therefore proposed to characterize the asymmetry of polymer conformations by rotationally invariant universal quantities, such as the averaged asphericity  $\langle A_d \rangle$  and prolateness  $\langle S \rangle$  [1, 2].  $\langle A_d \rangle$  takes on a maximum value of one for a completely stretched, rodlike conformation, and equals zero for spherical form, thus obeying the inequality:  $0 \leq \langle A_d \rangle \leq 1$ . The quantity  $\langle S \rangle$ , defined in  $d = 3$  dimensions, takes on a positive value for prolate ellipsoidlike conformation, and is negative for oblate shapes, being bounded to the interval  $-1/4 \leq \langle S \rangle \leq 2$ , cf. Fig. 11.2.

In real physical processes, one is often interested in the behaviour of macromolecules in the presence of structural disorder, e.g., in colloidal solutions or microporous membranes. In particular, a related problem is relevant when studying protein folding dynamics in cellular environments which are highly disordered due to the presence

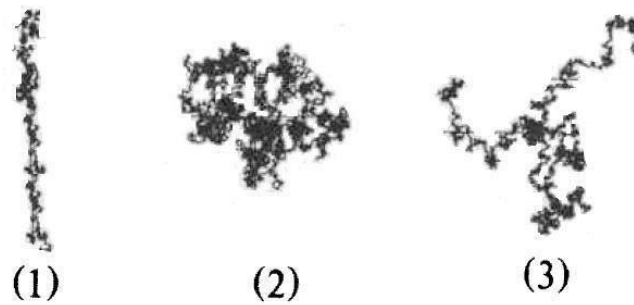


**Figure 11.2:** Schematic representation of a polymer chain conformation which is (1) rod-like, (2) almost spherical, and (3) oblate.

of a large amount of soluble and insoluble biochemical species occupying up to 40% of the total aquabased volume [3]. It is known that structural obstacles strongly effect protein folding and aggregation as well as their shape characteristics.

In this project we study a minimalistic lattice model [4] in which the allowed sites are restricted to the fractal structure of a percolation cluster and the polymers are modeled by self-avoiding walks [5, 6]. Applying the pruned-enriched Rosenbluth method (PERM) [7], we performed chain-growth computer simulations in  $d = 2$  and  $d = 3$  and obtained numerical estimates for the averaged asphericity, prolateness, and size ratio [8, 9]. All the shape characteristics increase gradually with increasing polymer chain length – the structure of a fractal percolation cluster drives the longer polymer chain conformations to become more and more prolate. Our results quantitatively indicate that the shape parameters of typical polymer conformations change significantly relative to the obstacle-free case: The shape tends to be more anisotropic and elongated due to the fractal structure of the disordered environment.

- [1] J.A. Aronovitz, D.R. Nelson: *J. Phys. (Paris)* **47**, 1445 (1986)
- [2] J. Rudnick, G. Gaspari: *J. Phys. A* **19**, L191 (1986); G. Gaspari et al.: *J. Phys. A* **20**, 3393 (1987)
- [3] S. Kumar, M.S. Li: *Phys. Rep.* **486**, 1 (2010)
- [4] C. Vanderzande: *Lattice Models of Polymers* (Cambridge University Press, Cambridge (England) 1998)
- [5] V. Blavatska, W. Janke: *Europhys. Lett.* **82**, 66006 (2008); *Phys. Rev. Lett.* **101**, 125701 (2008); *J. Phys. A* **42**, 015001 (2009)
- [6] V. Blavatska, W. Janke: *Phys. Rev. E* **80**, 051805 (2009); in *Computer Simulations in Condensed Matter Physics XXII*, ed. by D.P. Landau et al., *Physics Procedia* **3**, 1431 (2010)
- [7] P. Grassberger: *Phys. Rev. E* **56**, 3682 (1997)
- [8] V. Blavatska, W. Janke: *J. Chem. Phys.* **133**, 184903 (2010)
- [9] V. Blavatska, W. Janke: *Θ-polymers in crowded media under stretching force*, to appear in *Comput. Phys. Commun.*, in print (2011)

## 11.4 Scaling Behaviour of Self-Avoiding Walks on Critical Ising Clusters

N. Fricke, W. Janke

The discrete self-avoiding walk (SAW) is one of the most fundamental systems in the realm of statistical physics: It is the simplest non-trivial model for a polymer, and features universal asymptotic scaling behaviour, which is intimately related to the critical behaviour of spin systems. In particular, the exponent  $\nu$  describing the scaling of the mean end-to-end distance  $\langle R \rangle$  with the number of steps  $N$  ( $\langle R \rangle \sim N^\nu$ ) is a universal quantity, depending only on fundamental properties of the system such as its dimensionality. Its value is non-integer, in general even non-rational, reflecting the SAW's fractal nature.

The case where the substrate itself has a non-Euclidean, fractal dimension is of particular interest and has attracted a considerable amount of attention in recent decades. Exact mathematical fractals have been investigated [1] as well as percolation clusters [2–4], which are an example of disordered, statistical fractals. However, the understanding of such systems is still far from being exhaustive. We therefore investigated SAWs on clusters occurring for the 2D Ising model at the critical temperature. These represent another type of statistical fractal whose properties have been extensively studied, see [5, 6]. Contrary to the percolation case, the disorder for this system is correlated, which may also effect the scaling behaviour.

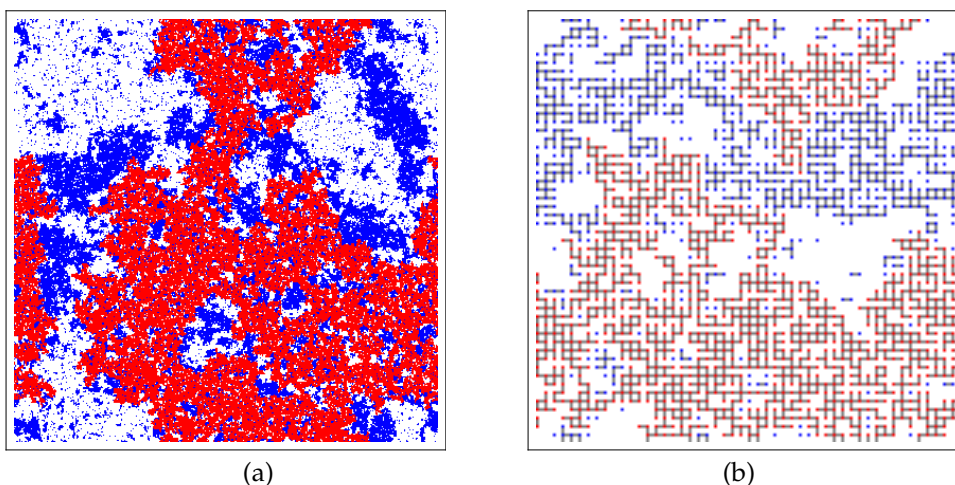


**Figure 11.3:** Ising model at criticality. In (a), the percolating Fortuin-Kasteleyn cluster is marked in red. Spins on the blue sites have the same alignment, but no connecting bonds to the percolating Fortuin-Kasteleyn cluster. In (b), active bonds between spins are displayed.

Monte Carlo methods were applied to both, creating the Ising clusters and simulating the SAWs. For the creation of the clusters a Swendsen-Wang type algorithm [7] has been used. The SAWs have been sampled using a chain-growth method, the so-called “pruned enriched Rosenbluth method” (PERM) [8]. Three slightly different situations have been studied: In the first cases, the walker was only allowed to move between sites belonging to the lattice-spanning Fortuin-Kasteleyn cluster [9] (red sites in Fig. 11.3(a)), which at criticality is a fractal object. In the second case, the walker

was allowed to visit all connected sites having the same spin direction (blue and red sites in Fig. 11.3(a)). Finally, the walker was only permitted to step between sites which are connected by a bond in the Fortuin-Kasteleyn representation [9] (Fig. 11.3(b)). All three structures have different fractal dimensions, and indeed, three distinct values for the exponent  $\nu$  have been found. However, a systematic monotonous dependence on the Hausdorff dimension could not be established, indicating that other factors do also play a significant role.

- [1] Y. Shussman, A. Aharony: J. Stat. Phys. **77**, 545 (1994)
- [2] V. Blavatska, W. Janke: Europhys. Lett. **82**, 66006 (2008)
- [3] C. v. Ferber et al.: Phys. Rev. E **70**, 035104(R) (2004)
- [4] Y. Meir, A.B. Harris: Phys. Rev. Lett. **63**, 26 (1989)
- [5] A.L. Stella, C. Vanderzande: Phys. Rev. Lett. **10**, 62 (1989)
- [6] W. Janke, A.M.J. Schakel: Nucl. Phys. B [FS] **700**, 385 (2004) [cond-mat/0311624]; Phys. Rev. E **71**, 036703 (2005) [cond-mat/0410364]
- [7] R.H. Swendsen, J.-S. Wang: Phys. Rev. Lett. **58**, 86 (1987)
- [8] P. Grassberger: Phys. Rev. E **56**, 3682 (1997)
- [9] C.M. Fortuin, P.W. Kasteleyn: Physica **57**, 536 (1972)

## 11.5 Mass Transport by Thermal Ratchets

M. Aust, R. Valiullin\*, J. Kärger\*, W. Janke

\*Abteilung Grenzflächenphysik, Institut für Experimentelle Physik I

Non-equilibrium mass transport on nanoscopic scales through ratchet effects or Brownian motors has attracted much attention in the recent literature [1]. The basic ingredients for a ratchet are (i) a periodic but asymmetric potential and (ii) a mechanism to disturb thermal equilibrium, since the second law of thermodynamics forbids a net flux of particles otherwise. The disturbance can be a periodic variation of the potential (pulsating ratchet), a periodic driving force with vanishing average (tilting ratchet) or temperature variations in time (temperature ratchet) or space (Seebeck ratchet). Most ratchets and Brownian motors discussed in the literature consider single (independent) particles, but there are also a few examples using collective effects. Being out-of-equilibrium, Curie's principle predicts a non-zero effect due to the broken symmetry. But in general there is no direct way to predict the strength or even the direction of the effect. On variation of some parameters one even can create a current inversion. So one has to consult computer simulations or do experiments for specific informations.

We proposed a new thermal ratchet setup to model periodic but asymmetric pores filled with a binary liquid mixture with a liquid-liquid phase transition at temperature  $T_c$ . The three-dimensional pore geometry sketched in Fig. 11.4 depends on the two dimensionless length ratios  $R_{\max}/R_{\min}$  and  $L/R_{\max}$ . For temperatures periodically switched between two temperatures above and below  $T_c$ , one expects asymmetric mass transport, moving the two types of liquids in different directions. The considered system can be classified as a collective temperature ratchet with an entropic potential. The role of the potential is played by the varying diameter of the pores effectively producing entropic barriers. The phase transition is then used to trigger the ratchet effect

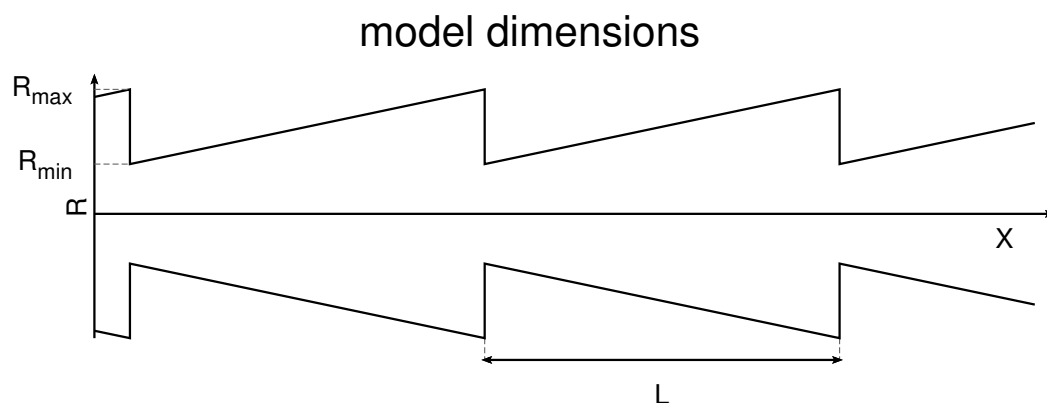


**Figure 11.4:** Geometry parameters of the proposed ratchet model, characterized by the pore radii  $R_{\min}$  and  $R_{\max}$  and the segment length  $L$  of long three-dimensional channels. In the computer simulations, we set  $R_{\max}/R_{\min} = 5$  and  $L/R_{\max} = 4$ .

by switching between droplet formation and dissolution. This phase transition is the crucial ingredient making the proposed system an example for a generally new class of ratchets.

Computer simulations were performed to provide at least qualitative answers to the problem of how to optimize the profile and the diameter of the pores and the temperature schedule, in order to obtain a maximal ratchet effect. The simulations were kept as simple as possible. This is partly due to the fact that most of the advanced simulation techniques rely on thermal equilibrium to hold [2], whereas for the ratchet effect to occur, this must be broken. In effect, simple random walk simulations (dynamical Monte Carlo) were performed to investigate the driven diffusive behaviour. In a first step, we studied independent “pointlike” random walkers confined to the three-dimensional periodic pores modeled by hard walls forming cells. The geometry parameters were chosen as  $R_{\max}/R_{\min} = 5$  and  $L/R_{\max} = 4$ . Starting all walks from a given fixed position  $x_0$  on the central axis of the pore ( $R = 0$ ), during the first steps a net drift could be observed, before the system reached equilibrium. This simulation would model the part of the ratchet, when one of the two liquids has formed droplets which sit on average at a given position inside each cell, and the temperature is raised above  $T_c$  so that now free diffusion is possible. The observed net drift depends in strength and direction on the chosen starting position, also including a neutral position from where no drift would result. In a second step, the average position of the droplets was determined again by independent random walks in the same geometry, but this time the particles had a non-zero extent, making the entropic barriers much more severe. The average position deviated slightly from the neutral position mentioned above, thus leading to a ratchet effect. However, the drift and thus the resulting ratchet effect turned out to be always so small that up to now no reliable predictions for the optimal pore geometry of this model system could be obtained.

[1] P. Reimann: Phys. Rep. **361**, 57 (2002)

[2] W. Janke: Lect. Notes Phys. **716**, 207 (2007); Lect. Notes Phys. **739**, 79 (2008)

## 11.6 Stochastic Transport Models

B. Waclaw<sup>\*</sup>, J. Sopik<sup>†</sup>, H. Nagel, W. Janke, H. Meyer-Ortmanns<sup>\*</sup>

<sup>\*</sup>SUPA, School of Physics and Astronomy, University of Edinburgh, United Kingdom

<sup>†</sup>School of Engineering and Science, Jacobs University, Bremen, Germany

Stochastic transport processes out-of-equilibrium are of importance in many different fields of physics. Examples are traffic flow, ranging from macroscopic applications to pedestrian or car traffic down to the intracellular level, force propagation in granular media, aggregation and fragmentation of clusters, and many others [1]. The transport is classically modeled by probabilities for hopping events from one site to another. Since such processes are in general out-of-equilibrium and specified in terms of dynamical rules without any energy concept, it is difficult to predict and classify the possible stationary states and to identify transitions between phases like a liquid phase or a phase with a condensate (“traffic jam”) that are associated with the different stationary states. In particular one observes the phenomenon of spontaneous symmetry breaking already in one-dimensional systems, in which the symmetry breaking manifests itself in the spontaneous formation of a condensate: A finite fraction  $M'$  of constituent particles condenses onto a finite extension  $W$  in space (sometimes even on a single site) in the thermodynamic limit, in which the number of particles  $M$  along with the volume  $N$  is sent to infinity, with the density  $\rho = M/N$  fixed.

In this joint DFG project with the Jacobs University Bremen and in collaboration with the University of Edinburgh we concentrate on a class of models which lead to steady states that factorize over the links of arbitrary connected graphs, so-called pair-factorized steady states (PFSS) [2–4]. This enables at least partially an analytic treatment of the transport properties. For systems in one and two dimensions we derive the phase structure from these states, in particular the transition from a liquid phase to a phase with a condensate. In one dimension we predict the critical mass density at the transition, the shape of the condensate, and its scaling with the system size. The shape of the condensate is not universal, but can be tuned from an extended to a localized one via the competition of local ( $K$ ) and ultralocal ( $p$ ) interactions that are implemented in the hopping rates. In the equivalent language of solid-on-solid (SOS) models in the context of surface roughening [5] this corresponds to the energy  $E = -\ln K(|m - n|) - (1/2) [\ln p(m) + \ln p(n)]$  of an interface within a 1+1-dimensional space (where the interface refers to the envelope of occupation numbers  $m$  and  $n$  at neighboring sites) [6]. The resulting phase diagram for the choice  $K(x) \propto \exp(-x^\beta)$  and  $p(m) \propto \exp(-m^\gamma)$  and the exponent  $\alpha$  in the predicted scaling behaviour of the condensate extension,  $W \sim M'^\alpha$ , are shown in Fig. 11.5.

Many of these usually approximate analytic predictions for pair-factorized steady states have been confirmed by computer simulations of the hopping events. This also allowed us to study dynamic properties of the condensation process which is governed by a time scale  $\tau \propto M'^\delta$ , where the dynamical exponent  $\delta$  depends on symmetry properties of the hopping dynamics: For a spatially *asymmetric* hopping rule we find  $\delta \approx 2$ , whereas for *symmetric* hopping  $\delta \approx 3$ , similar to the previously observed behaviour of simpler, ultralocal zero-range processes (ZRP).

[1] M.R. Evans et al.: Phys. Rev. Lett. **97**, 010602 (2006)

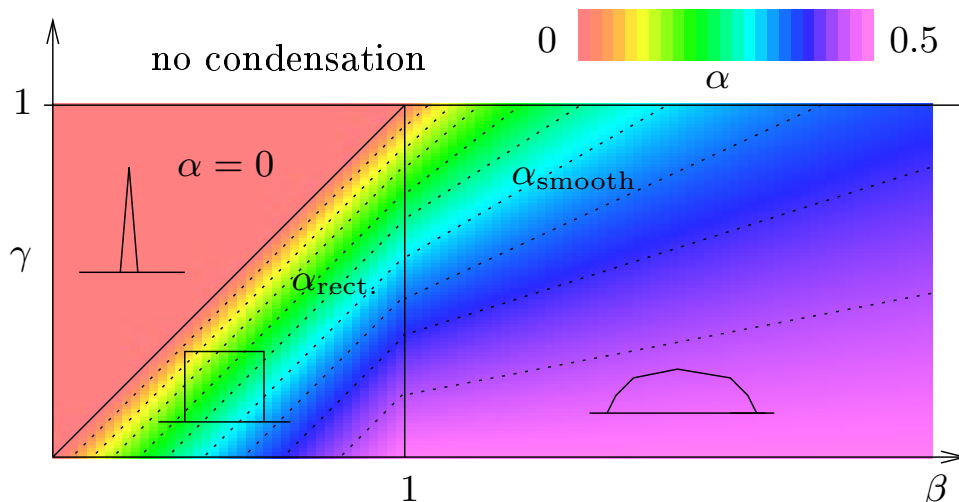


**Figure 11.5:** Phase diagram for  $K(x) \sim e^{-x^\beta}$  and  $p(m) \sim e^{-m^\gamma}$ . Values of the exponent  $\alpha$  in the scaling law for the extension  $W$  of the condensate with the number  $M'$  of condensed particles,  $W \simeq M'^\alpha$ ,  $\alpha_{\text{rect}} = (\beta - \gamma)/(\beta - \gamma + 1)$  for a rectangular and  $\alpha_{\text{smooth}} = (\beta - \gamma)/(2\beta - \gamma)$  for a smooth condensate, are represented by the color (gray) code. The dotted lines show  $\alpha = 0.05, 0.1, \dots, 0.45$  (from left to right).

- [2] B. Waław et al.: J. Phys. A: Math. Theor. **42**, 315003 (2009)
- [3] B. Waław et al.: Phys. Rev. Lett. **103**, 080602 (2009)
- [4] B. Waław et al.: J. Stat. Mech. P10021 (2009)
- [5] S.T. Chui, J.D. Weeks: Phys. Rev. B **23**, 2438 (1981); T.W. Burkhardt: J. Phys. A: Math. Gen. **14**, L63 (1981); J.M.J. van Leeuwen, H.J. Hilhorst: Physica A **107**, 319 (1981)
- [6] B. Waław et al.: J. Phys.: Conf. Ser. **246**, 012011 (2010)

## 11.7 Birth of the First Large Condensation Droplet

A. Nußbaumer, E. Bittner\*, M. Wiedenmann, W. Janke

\*Present address: Institut für Theoretische Physik, Universität Heidelberg, Germany

The “birth” of the first large droplet in condensation phenomena is an important problem in many physical systems, ranging from atoms to colloids to macromolecules. With early theoretical work dating back to the 1960s, this problem has been taken up many times and further advanced both analytically and numerically. Yet, there are still many open questions we try to answer in this project. One goal is to evaluate by how much asymptotic theoretical predictions are affected by finite-size effects. A second goal is to test the degree of universality suggested by the analytical treatment. Finally, we also study the free-energy barrier associated with the “birth” of the first large droplet.

The results of our extensive Monte Carlo simulations of the two-dimensional Ising lattice-gas model [1–3] clearly confirm the asymptotic predictions of Biskup et al. [4, 5] and extend them to practically accessible system sizes. The observed finite-size scaling behaviour matches perfectly with the predicted infinite-volume limit. By comparing

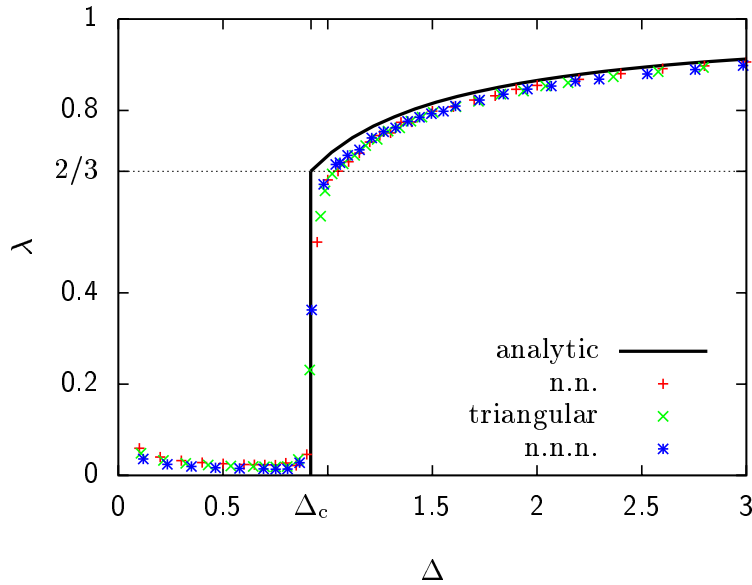


**Figure 11.6:** Comparison of the fraction  $\lambda$  of particles in the largest droplet for the three considered Ising models: NN square, NN triangular, and NNN square lattice. In all three cases the lattice size is  $L = 640$  and the simulation temperature was chosen as  $T \approx 0.66 T_c$ .

square and triangular lattices with next-neighbour (NN) interactions and a square lattice with next-nearest-neighbour (NNN) interactions, we obtained recently compelling evidence for the insensitivity of the droplet condensation mechanism to microscopic details provided the reduced temperature  $T/T_c$  is kept fixed [6], see Fig. 11.6. For technical reasons, the mathematical work of Biskup et al. only applies to *square* lattices with *NN* couplings. Our results thus show that the theoretical arguments can indeed be carried over to other lattice types and interactions as well, as expected on physical grounds. All simulations were performed in thermal equilibrium and the suppression of droplets of intermediate size could be unambiguously verified.

We also measured the distribution of the fraction  $\lambda$  of particles in the largest droplet [6]. The observed double-peak structure at the evaporation/condensation transition point implies a free-energy barrier, similar to a first-order phase transition. By analyzing the ratio of peak maximum to minimum in simulations with fixed magnetisation (adjusted such that the two maxima agree) for different lattice sizes  $L$ , we clearly observe an exponential scaling  $\approx \exp(c L^{2/3})$  compatible with the theoretical expectation. Alternatively, by measuring (integrated) autocorrelation times  $\tau_{\text{int}}$  in simulations with the magnetisation fixed directly at the evaporation/condensation point, we also find a compatible asymptotic scaling behaviour  $\tau_{\text{int}} \approx \exp(c L^{2/3})$ . In both cases, however, the parameter  $c$  is difficult to determine reliably with the present data sets. Presumably much larger lattices are needed to arrive at a firm estimate.

Currently we are performing simulations and analyses for the three-dimensional case, where a similar behaviour is expected in the thermodynamic limit. In three dimensions it appears, however, numerically much harder to reach the scaling region. Once the relevant length scales are fully understood, off-lattice simulation studies with Lennard-Jones particles in a similar vein would be a very interesting future project with many applications of practical relevance.

- [1] A. Nußbaumer et al.: *Europhys. Lett.* **75**, 716 (2006)
- [2] A. Nußbaumer et al.: *Phys. Rev. E* **77**, 041109 (2008)
- [3] A. Nußbaumer et al.: in *Computer Simulations in Condensed Matter Physics XX*, ed. by D.P. Landau et al., *Physics Procedia* **7**, 52 (2010)
- [4] M. Biskup et al.: *Europhys. Lett.* **60**, 21 (2002)
- [5] M. Biskup et al.: *Comm. Math. Phys.* **242**, 137 (2003)
- [6] A. Nußbaumer et al.: *Prog. Theor. Phys. Suppl.* **184**, 400 (2010)

## 11.8 Hierarchies in Peptide Nucleation Transitions

C. Junghans\*, M. Bachmann†, W. Janke

\*Max-Planck-Institut für Polymerforschung, Mainz, Germany

†IFF-2 and IAS-2, Forschungszentrum Jülich, Germany

Understanding cooperative effects leading to structure formation of polymers is a challenging problem of statistical mechanics and thermodynamics. An important example is the aggregation of macromolecules which can be considered as a special case of nucleation processes. In biosystems, the aggregation of peptides can lead to plaque formation, often with disastrous consequences. A prominent example is the aggregation of  $A\beta$  peptides in the human brain which is associated to the neurodegenerative Alzheimer's disease.

Structural properties of interacting polymers can be well described by means of simple, coarse-grained "bead-stick" models with typically Lennard-Jones interactions among the monomers [1–3]. In this work [4] we considered the aggregation of up to four peptide chains with 13 monomers each, modeled by the minimalistic hydrophobic-polar AB model [5, 6] where only two types of residues, hydrophobic (A) and hydrophilic (B) ones, line up in a linear heteropolymer sequence. All four chains have the same Fibonacci sequence  $AB_2AB_2ABAB_2AB$  [4]. Employing multicanonical computer simulations we determined the density of states  $g(E)$ , giving immediately the microcanonical entropy  $S(E) = k_B \ln g(E)$  and temperature  $T(E) = [\partial S(E)/\partial E]^{-1}$  [1–3]. The entropy turned out to be a convex curve in the aggregation transition region as is characteristic for a first-order-like nucleation transition of a finite system [7, 8]. The details of the transition regime are highlighted in Fig. 11.7 where the (microcanonical) temperature  $T(E)$  is shown. In this plot the various stages or subphases of the nucleation process are clearly reflected by the oscillations in the transition region. Representative conformations in the different structural phases are depicted in the right panel.

For high energies  $e > e_{\text{frag}} \approx 0.05$  all chains can form individual conformations, almost independently of each other, and are hence fragmented. If two chains aggregate (subphase 1 in Fig. 11.7), the translational entropy of the individual chains is reduced by  $k_B \ln V$ , where  $V$  is the volume (corresponding to the simulation box size), but this is overcompensated by the more favorable (= lower) energy of the aggregate compared to the fragmented chains. Here, the energy associated with the interaction between different chains, i.e., the cooperative formation of *inter*-chain contacts between residues of different peptides, is highly relevant. In a subsequent step an additional peptide joins the two-peptide cluster and the system enters subphase 2. This procedure continues

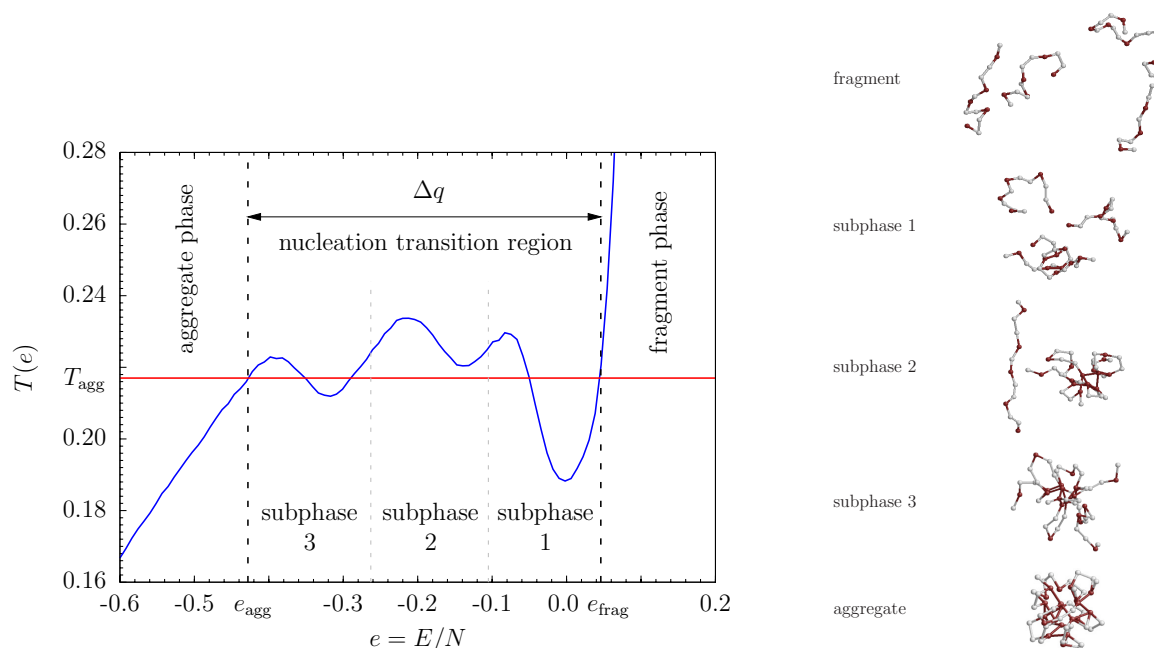


**Figure 11.7:** Left: Microcanonical temperature in the nucleation transition regime. The horizontal so-called Maxwell line marks the aggregation temperature  $T_{\text{agg}}$ , obtained by a Gibbs construction [7]. Right: Representative conformations in the different structural subphases of the peptide aggregation process.

until for  $e < e_{\text{agg}} \approx -0.43$ , conformations of a single, entangled aggregate, composed of all four peptide chains forming a hydrophobic core, dominate.

Our data thus show that heteropolymer aggregation can be understood as a composite nucleation processes consisting of hierarchical subphase transitions, each of which exhibits features of first-order-like transitions. A closer look into the data reveals that with an increasing number of chains the strength of the subphase transitions becomes weaker and weaker. This suggests that in the thermodynamic limit of infinitely many chains the first-order nucleation process is composed of an infinite number of infinitesimally “weak” first-order-like subphase transitions.

- [1] C. Junghans et al.: Phys. Rev. Lett. **97**, 218103 (2006)
- [2] C. Junghans et al.: J. Chem. Phys. **128**, 085103 (2008)
- [3] C. Junghans et al.: Europhys. Lett. **87**, 40002 (2009)
- [4] C. Junghans et al.: *Hierarchies in nucleation transitions*, Mainz/Jülich/Leipzig preprint, to appear in Comput. Phys. Commun., in print (2011)
- [5] F.H. Stillinger et al.: Phys. Rev. E **48**, 1469 (1993); F.H. Stillinger, T. Head-Gordon: Phys. Rev. E **52**, 2872 (1995)
- [6] M. Bachmann et al.: Phys. Rev. E **71**, 031906 (2005)
- [7] W. Janke: Nucl. Phys. B (Proc. Suppl.) **63A-C**, 631 (1998)
- [8] D.H.E. Gross: *Microcanonical Thermodynamics* (World Scientific, Singapore 2001)

## 11.9 Polymer Crystallization with Advanced Multicanonical Monte Carlo Methods

S. Schnabel\*, M. Bachmann<sup>†</sup>, W. Janke

\*Center for Simulation Physics, University of Georgia, Athens, USA

<sup>†</sup>IFF-2 and IAS-2, Forschungszentrum Jülich, Germany

This project is devoted to numerical investigations of the freezing or crystallization transition of a single elastic polymer [1, 2]. In the model that we employ the bond length is adaptive in a way that highly symmetric conformations can form in the crystalline phase. By means of multicanonical Monte Carlo computer simulations we identified a nontrivial systematic chain-length dependence that is associated with the type of growth of the nucleus. However, a conventional scaling behaviour has not been found – it simply does not exist. This is also known from atomic clusters [3]. A particularly sharp transition signal from fluctuating quantities, such as the specific heat, is obtained for “magic” chain lengths  $N = 13, 55, 147, 309, \dots$ . In these cases almost perfect icosahedra can form which are particularly stable and typically represent the core cells in the structure formation of longer chains [1, 2].

To arrive at these results a couple of algorithmic improvements were necessary which we developed along the way [4]. First, we introduced energy-dependent step lengths of the proposed Monte Carlo moves that enable a novel general optimization scheme for systems with continuous degrees of freedom. Key to this idea is a bias correction in the acceptance criterium. Applying this procedure to multicanonical sampling with a flat energy distribution one obtains constantly high acceptance rates everywhere in energy space and hence reliable estimates of the density of states over several *thousands* of orders of magnitudes.

The second methodological improvement concerns the types of proposed update moves. We proposed two bond-exchange moves which allow the reordering of polymer bonds without alteration of monomer positions, cf. Fig. 11.8(a) and (b). Moreover, with the monomer cut-and-paste update sketched in Fig. 11.8(c) we introduced a novel Monte Carlo move which increased the efficiency of the simulation further in two ways. First, the update allows the tunneling of energy barriers in the solid phase and second, it performs larger changes in the unstructured globular and random-coil phases.

The third class of improvements deals directly with the multicanonical method. By enabling variations in system size at runtime we extended the multicanonical ensemble to treat also the monomer number in a “dynamical” way. This led to an additional gain in efficiency since the thus modified algorithm was able to circumvent certain energy barriers or to penetrate them where they are low, i.e., at their “weak” points. As a result we obtained information about the entire state space over a large polymer-size interval from a single simulation. Finally, confronted with the problem of broken ergodicity and low-temperature solid-solid transitions, we developed a second extension to the standard multicanonical technique. Due to the application of additional weight functions it is possible to retain ergodicity and to reach “hidden” ground states by circumventing the “blocking” states at intermediate temperatures. Although we yet have demonstrated the potential of this method for homopolymers only, it is a general approach and, in combination with suitable order parameters, it might lead to substantial

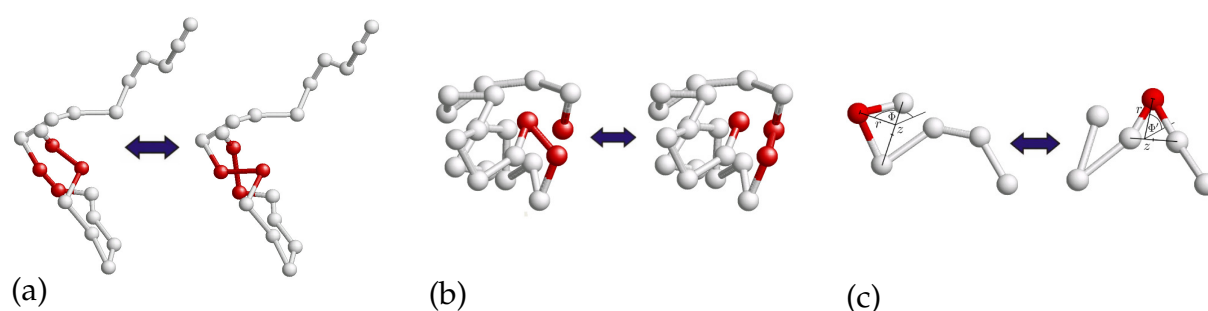


**Figure 11.8:** (a) Bond-exchange, (b) end-bond-exchange, and (c) monomer cut-and-paste update moves.

progress in the investigation of many other systems as well.

- [1] S. Schnabel et al.: Chem. Phys. Lett. **476**, 201 (2009)
- [2] S. Schnabel et al.: J. Chem. Phys. **131**, 124904 (2009)
- [3] J.P.K. Doye, F. Calvo: J. Chem. Phys. **116**, 8307 (2002)
- [4] S. Schnabel et al.: J. Comput. Phys. **230**, 4454 (2011)

## 11.10 The Influence of Grafting onto Freezing, Collapse and Adsorption of a Single Polymer in Solution

M. Möddel, M. Bachmann\*, W. Janke

\*IFF-2 and IAS-2, Forschungszentrum Jülich, Germany

In our previous studies of macromolecular adsorption transitions [1, 2] it turned out that a combined canonical and microcanonical analysis is able to reveal some properties that are hidden in a purely canonical approach [3]. We therefore extended this method to all other transitions a polymer of finite length close to an attractive substrate undergoes [4]. We studied a simple bead-stick model with 12–6 Lennard-Jones (LJ) interaction between nonbonded monomers, a weak bending stiffness and an attractive interaction with a flat substrate at  $z = 0$  that is proportional to a parameter  $\epsilon_s$ . This surface attraction is a 9–3 LJ potential obtained by integrating the 12–6 LJ potential over a half space and, e.g.,  $\epsilon_s = 5$  roughly gives a surface attraction that exceeds the monomer-monomer attraction by a factor of five. To evaluate the influence of the translational entropy and the restrictions of the commonly studied grafted case, the polymer is once considered in a box within which it can move freely and once with one end grafted to the substrate.

The goal was to rediscover all transitions in the microcanonical entropy, which is proportional to the logarithm of the density of states. To this end we analyzed its slope and curvature as well as other observables as a function of energy. For an example, see Fig. 11.9. This provides additional information, e.g., about the nature of the transition. Due to the finite size of the polymer the two ensembles are not equivalent and also the nature of the transition can still differ from the limiting infinite-size behaviour as was

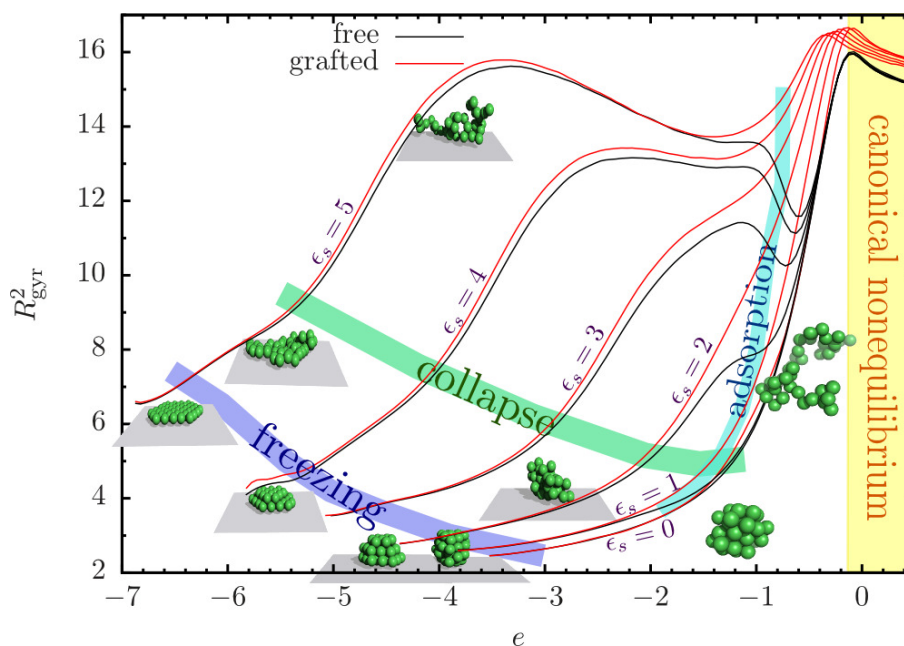


**Figure 11.9:** The radius of gyration squared  $R_{\text{gyr}}^2$  versus energy per monomer  $e$  for several surface attraction strengths  $\epsilon_s$ . The energy regimes of the main transitions are indicated and the pseudophases are illustrated by exemplified conformations. Depending on  $\epsilon_s$  the collapse occurs at higher or lower  $e$  than the adsorption.

indeed found for the freezing and adsorption transitions. The former is not strongly affected by the grafting, since the fraction of forbidden conformations due to the constraint is comparable above and below the freezing. But the first-order-like nature of this transition only arises if the chain exceeds a certain length, whereas short chains exhibit a continuous freezing transition. The adsorption transition, however, is strongly affected by the grafting. Here, both, the translational and conformational entropy of desorbed polymers are much stronger restricted by the grafting than of adsorbed polymers. One consequence is a first-order-like adsorption for short free chains and strong surface attraction, while grafted polymers always adsorb continuously.

All simulations were performed with the parallel tempering Monte Carlo method that allowed to highly parallelize the simulation and obtain good statistics over the whole energy range [4].

- [1] M. Möddel et al.: *Phys. Chem. Chem. Phys.* **12**, 11548 (2010)
- [2] M. Möddel et al.: *Adsorption of finite polymers in different thermodynamic ensembles*, Leipzig/Jülich preprint, to appear in *Comput. Phys. Commun.*, in print (2011)
- [3] M. Möddel et al.: *J. Phys. Chem. B* **113**, 3314 (2009)
- [4] M. Möddel et al.: *Comparison of the adsorption transition for grafted and non-grafted polymers*, Leipzig/Jülich preprint, in preparation

## 11.11 Thermodynamics of Polymer Adsorption to a Flexible Membrane

S. Karalus, M. Bachmann\*, W. Janke

\*IFF-2 and IAS-2, Forschungszentrum Jülich, Germany

The interaction of macromolecules with cell membranes is essential for almost all biological processes. Membrane proteins like glycoproteins and transmembrane proteins govern the exchange of signals, small molecules, and ions between the intra- and extra-cellular solvent. Membrane embedded receptors are specific for the binding of ligands. The conformational changes caused by the binding process can, e.g., trigger cellular motion, drug delivery, or enzymatic catalysis.

It is therefore an important problem to investigate the conformational behaviour of a polymer interacting with a *flexible, fluctuating* substrate such as a membrane under thermal conditions. So far much work has been dedicated to the identification of structural transitions polymers and peptides experience when adsorbing to *solid* substrates [1–3]. In this project we extend these studies by considering a simple coarse-grained off-lattice model system consisting of a polymer grafted to a fluctuating substrate and performing extensive generalized-ensemble Monte Carlo computer simulations [4]. Adjacent monomers of the polymer are tied together by a finitely extensible nonlinear elastic (FENE) potential and all monomers interact pairwise via a standard 12–6 Lennard-Jones (LJ) potential. The fluctuating substrate is modeled by a tethered membrane with the individual building segments (nodes) again tied together by a FENE potential according to a square lattice structure with  $L_x \times L_y$  nodes in total. Finally, the interaction between the polymer, which is anchored at the membrane center, and the membrane is modeled by another LJ potential between all pairs of monomers and membrane nodes.

By means of extensive parallel tempering Monte Carlo simulations we have shown that the system exhibits a rich phase behaviour ranging from highly ordered, compact to extended random coil structures and from desorbed to completely adsorbed or even partially incorporated conformations, cf. Fig. 11.10. These findings are summarized in a pseudophase diagram indicating the predominant class of conformations as a function of the external parameters temperature and polymer-membrane interaction strength. By comparison with adsorption to a stiff membrane surface it is shown that the flexibility of the membrane gives rise to qualitatively new behaviour. At low temperatures, we found the membrane adapting its structure such that it partially incorporates the polymer. This leads to the “embedded compact” (MC), oblate shaped and the “embedded expanded” (ME), almost linearly stretched conformations shown in Fig. 11.10, which both most clearly reflect the influence of the back-reaction between polymer and membrane fluctuations.

- [1] M. Bachmann, W. Janke: Phys. Rev. Lett. **95**, 058102 (2005); Phys. Rev. E **73**, 041802 (2006); Phys. Rev. E **73**, 020901(R) (2006); Phys. Part. Nucl. Lett. **5**, 243 (2008)
- [2] M. Möddel et al.: J. Phys. Chem. B **113**, 3314 (2009)
- [3] M. Möddel et al.: Phys. Chem. Chem. Phys. **12**, 11548 (2010); and *Adsorption of finite polymers in different thermodynamic ensembles*, to appear in Comp. Phys. Commun., in print (2011)

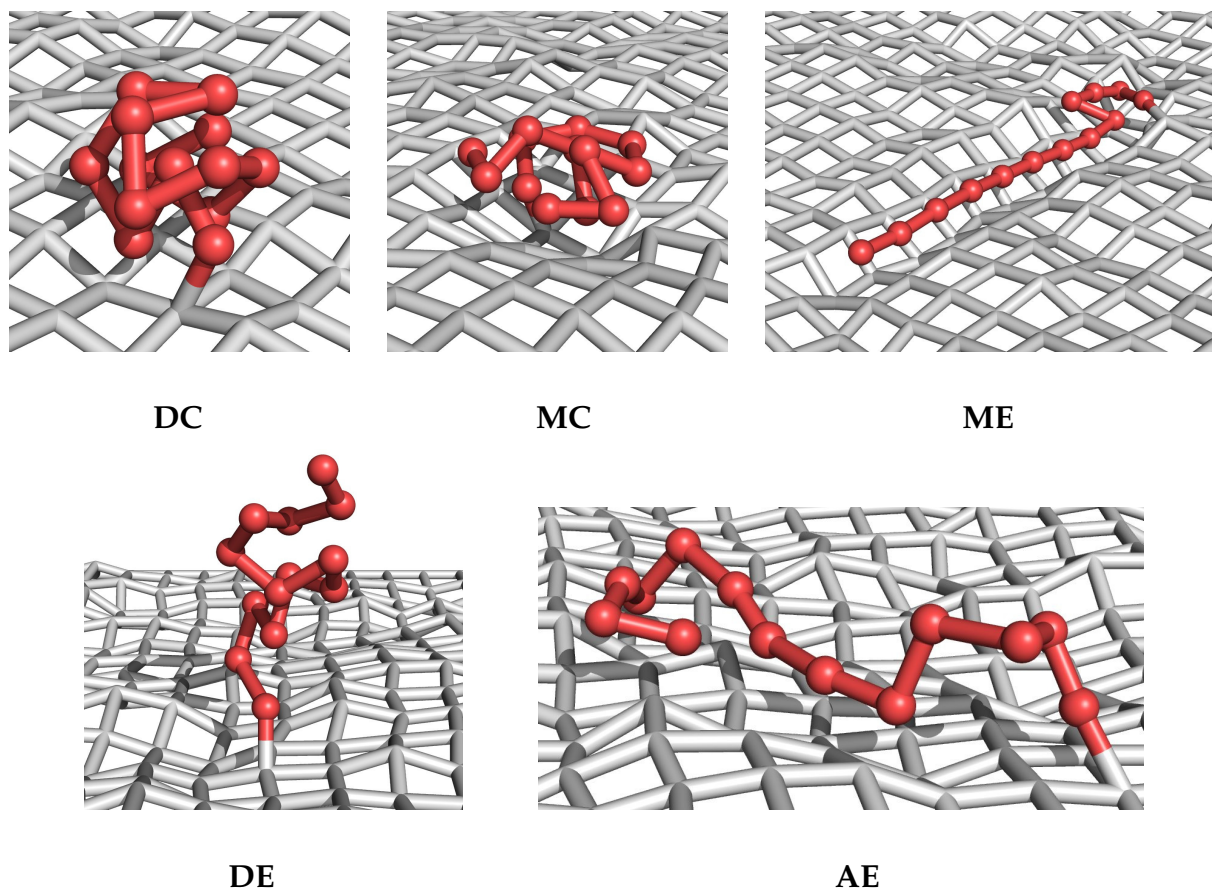


**Figure 11.10:** Typical conformations of a polymer grafted to a flexible membrane. The letter code classifies the polymer shapes (DC: desorbed compact; MC and ME: embedded compact and expanded; DE and AE: desorbed and adsorbed expanded).

[4] S. Karalus et al.: *Thermodynamics of polymer adsorption to a flexible membrane*, Leipzig/Jülich preprint, submitted to Phys. Rev. E

## 11.12 Microscopic Mechanism of Peptide Adhesion to Semiconductor Substrates: Simulations and Experiments

M. Bachmann<sup>\*</sup>, K. Goede<sup>†</sup>, A.G. Beck-Sickinger<sup>‡</sup>, M. Grundmann<sup>†</sup>, A. Irbäck<sup>§</sup>, W. Janke

<sup>\*</sup>IFF-2 and IAS-2, Forschungszentrum Jülich, Germany

<sup>†</sup>Semiconductor Physics Group, Institut für Experimentelle Physik II

<sup>‡</sup>Institut für Biochemie

<sup>§</sup>Computational Biology & Biological Physics Division, Lunds Universitet, Lund, Sweden

In the past few years, the interest in hybrid systems consisting of “soft” molecular matter and “hard” material substrates has rapidly grown as these are relatively easily accessible candidates for novel biosensors or electronic devices [1]. One important

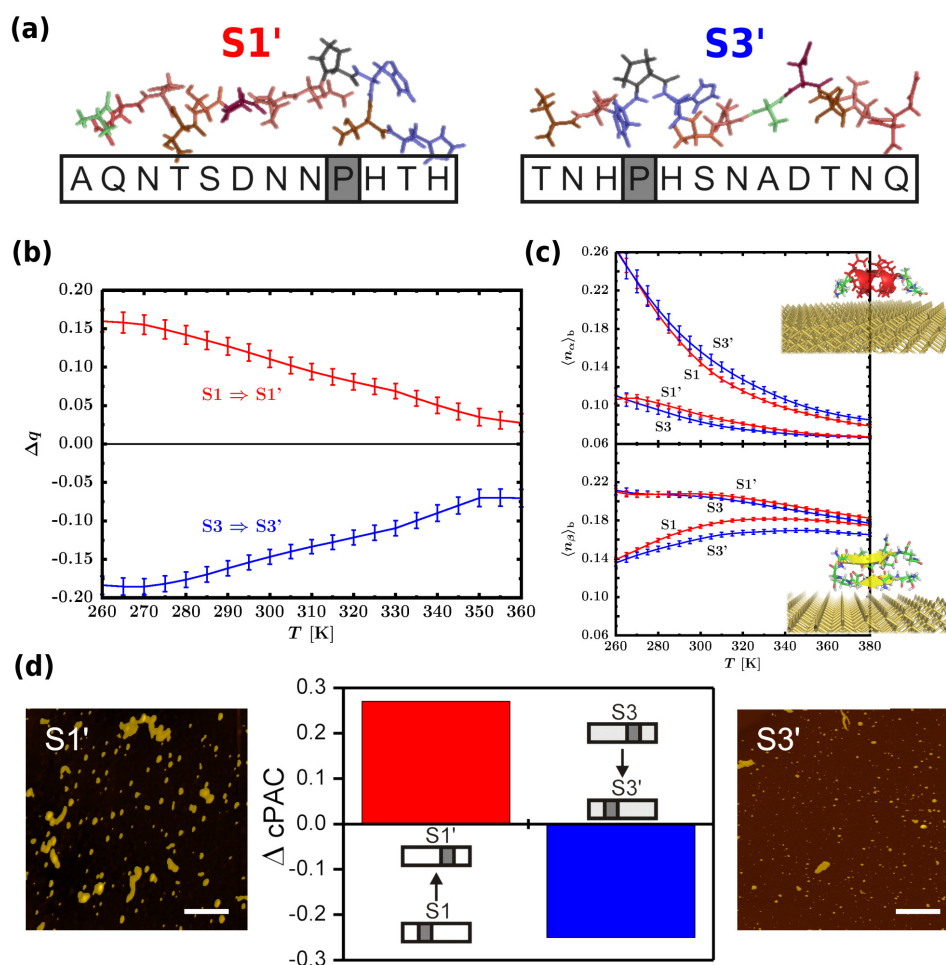


**Figure 11.11:** Reversed adsorption propensity of (a) the proline-mutated peptides S1' and S3'. (b) Adsorption parameter  $\Delta q$  and (c)  $\alpha$ -helix content  $\langle n_\alpha \rangle_b$  and  $\beta$ -strand content  $\langle n_\beta \rangle_b$  of bound peptides versus temperature as obtained in our computer simulations. The peptide conformations depicted in the insets are the identified (but at room temperature rather weakly occupied) lowest-energy structures representing the preferred trends in secondary-structure formation. (d) Confirmation by AFM experiments (scale bar = 1  $\mu$ m) at room temperature.

property is the adhesion propensity of polymers, proteins, or protein-like synthetic peptides to solid materials such as, e.g., metals [2] and semiconductors [3–5]. Basic theoretical considerations of simplified polymer-substrate [6, 7] and protein-substrate [8] models have predicted complex pseudophase diagrams.

In bacteriophage display experiments, only a few peptides out of a library of  $10^9$  investigated sequences with 12 amino acid residues were found to possess a particularly strong propensity to adhere to (100) gallium-arsenide (GaAs) surfaces [3]. The sequence-specificity of adsorption strength is a remarkable property, but it is not yet understood how this is related to the individual molecular structure of the peptides. In this joint project with experimentalists and biochemists within the BuildMoNa collaborative project we show by means of computer simulations and experiments that the adsorption properties of synthetic peptides at semiconductor surfaces exhibit a clear sequence-dependent adhesion specificity [9]. Our Monte Carlo simulations of a novel hybrid peptide-substrate model reveal “in silico” in particular the strong correlation between

proline mutation and binding affinity to a clean (100) silicon substrate. Subsequently, in atomic force microscopy (AFM) experiments with the mutated amino-acid sequences synthesized according to our theoretical predictions, we could confirm “in vitro” the relevance of the selective mutations upon adhesion, cf. Fig. 11.11.

- [1] M. Sarikaya et al.: *Nature Mat.* **2**, 577 (2003)
- [2] S. Brown: *Nature Biotechnol.* **15**, 269 (1997)
- [3] S.R. Whaley et al.: *Nature* **405**, 665 (2000)
- [4] K. Goede et al.: *Nano Lett.* **4**, 2115 (2004)
- [5] K. Goede et al.: *Langmuir* **22**, 8104 (2006)
- [6] M. Bachmann, W. Janke: *Phys. Rev. Lett.* **95**, 058102 (2005); *Phys. Rev. E* **73**, 041802 (2006)
- [7] M. Möddel et al.: *J. Phys. Chem. B* **113**, 3314 (2009); *Phys. Chem. Chem. Phys.* **12**, 11548 (2010)
- [8] M. Bachmann, W. Janke: *Phys. Rev. E* **73**, 020901(R) (2006)
- [9] M. Bachmann et al.: *Angew. Chem. Int. Ed.* **49**, 9530 (2010) [*Angew. Chem.* **122**, 9721 (2010), in German]

## 11.13 Replica-Exchange Simulations of Polymers on GPUs

J. Gross, M. Bachmann\*, W. Janke

\*IFF-2 and IAS-2, Forschungszentrum Jülich, Germany

Computer simulations have become a fundamental pillar in physics. This is particularly apparent in structural biophysics and polymer physics, where many-body interactions and disorder effects cannot be tackled by means of analytical approaches alone. However, despite large advances in the design of central processing unit (CPU) architectures, the computation time for simulations on single CPU systems can become interminable. One way around this problem is parallel computing using a message passing interface (MPI) on clusters or multithreaded programming on multicore CPUs. A currently rapidly emerging third approach are computations on graphics processing units (GPUs) with their massively parallel architecture (see Fig. 11.12), whose power has been driven originally mainly by the professional computer gaming industry. With the latest release of NVIDIA’s convenient programming language CUDA, GPUs have also become quite popular in scientific applications [1, 2].

The purpose of this project was to evaluate whether GPU simulations can also quite efficiently be performed for off-lattice polymer models without the need of highly sophisticated tricks of implementation. By employing straightforward parallel tempering (replica-exchange) Monte Carlo simulations, we investigated the possible speed-up provided by the massive parallelization on GPUs. We tested the two GT200-based GPUs Tesla C1060 and GTX285 with 240 cores and NVIDIA’s new generation Fermi-based GTX480 card with 480 cores. As reference CPU system one core of a quadcore Xeon E5620 processor was considered [3, 4].

With the most naive implementation of distributing the replica of the parallel tempering algorithm over the cores, only moderate speed-up factors of about 6 to 9 could

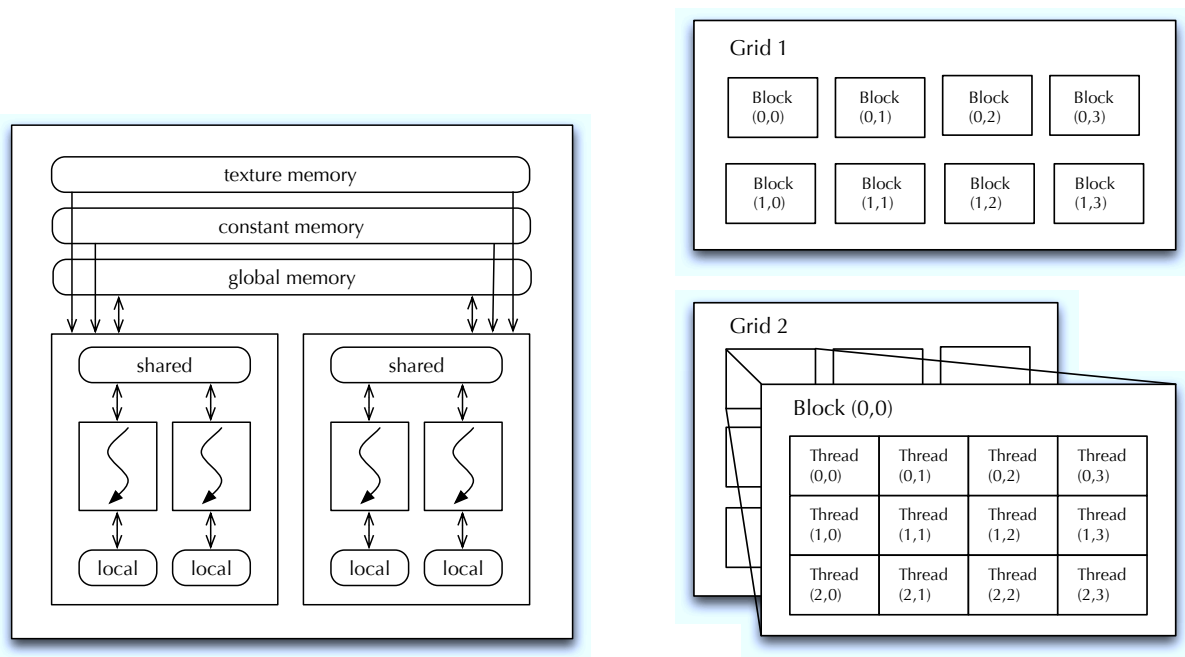


**Figure 11.12:** Memory layout on a GPU device (left) and grids with thread blocks (right).

be achieved. Having observed that, an improved version was implemented with a parallel calculation of the energy function. This implementation is much faster than the CPU version, when more than 2 replica are simulated. The maximum speed-up factor for the Tesla C1060 card is 68, for the GTX285 card it is 78 and for the Fermi-based GTX480 card even 130. Furthermore it is possible to access multiple graphics cards in a single workstation from one and the same program with no extra effort. Also nodes of established cluster computers can be equipped with GPUs, a combination of the traditional message passing interface (MPI) and CUDA is used in such a scenario. Thus GPUs promise great gains in productivity as well as energy efficiency and are already now on their way to enter the architecture of the next-generation supercomputers [5, 6].

- [1] T. Preis et al.: *J. Comput. Phys.* **228**, 4468 (2009)
- [2] M. Weigel: *Performance potential for simulating spin models on GPU*, preprint arXiv:1101.1427; *Simulating spin models on GPU*, preprint arXiv:1006.3865, to appear in *Comput. Phys. Commun.*, in print (2011)
- [3] J. Gross et al.: *Massively parallelized replica-exchange simulations of polymers on GPUs*, Leipzig/Jülich preprint, to appear in *Comput. Phys. Commun.*, in print (2011)
- [4] J. Gross et al.: *A GPU approach to parallel replica-exchange polymer simulations*, Leipzig/Jülich preprint, to appear in *Computer Simulations in Condensed Matter Physics XXIV*, ed. by D.P. Landau et al., *Physics Procedia*, in print (2011)
- [5] The Top500 List: The 500 most powerful commercially available computer systems, <http://www.top500.org>
- [6] The Green500 List: Environmentally responsible supercomputing, <http://www.green500.org>

## 11.14 Ground-State Analysis of Tip4p Water Parameterizations in the Ice $I_h$ Phase

J. Zierenberg, B.A. Berg\*, W. Janke

\*Dept. of Physics, Florida State University, Tallahassee, USA

Today, many computer simulations are performed in order to investigate processes on a biological or chemical scale, often involving water molecules. Simulating over large temperature ranges, it has to be ensured that the water model behaves correctly over the whole range. Because of its frequent use, we investigated the Tip4p (*4-point-transferable-intermolecular-potential*) water model [1], with four points of interaction (see Fig. 11.13). It describes rigid molecules with 12–6 Lennard-Jones (LJ) interaction between oxygen atoms ( $r_{OO}$ ) and Coulomb interaction between charges  $q_i, q_j$  from different molecules. The interaction Hamiltonian between two molecules (a, b) is given by

$$\mathcal{H}^{ab} = k_C \sum_i^{\text{in a}} \sum_j^{\text{in b}} \left( \frac{q_i q_j}{r_{ij}} \right) + \frac{\text{TipA}}{r_{OO}^{12}} - \frac{\text{TipC}}{r_{OO}^6}, \quad (11.1)$$

where  $k_C$  is the Coulomb constant and  $\text{TipA}, \text{TipC}$  are specified by the parameterization [1–3].

In our study, we analyzed the ground states of water molecules in the ordinary ice phase (ice  $I_h$ ) known from day-to-day life. In this phase, the oxygen atoms are arranged in a hexagonal lattice (see Fig. 11.13), forming tetrahedra with their four nearest neighbors. A valid ground-state configuration requires that exactly one hydrogen atom lies between two neighboring oxygen atoms. Thus, there exist multiple (in principle degenerate) ground states [4, 5].

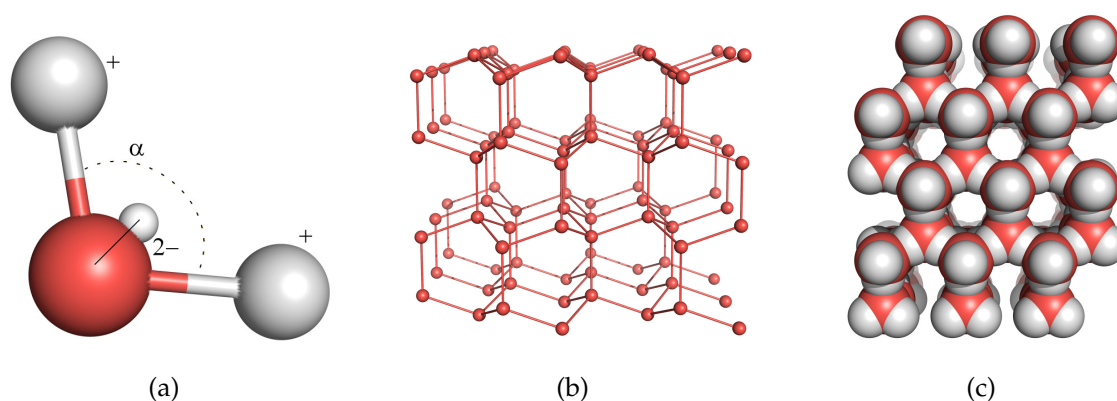


**Figure 11.13:** (a) Tip4p water model with a rigid angle  $\alpha$  and 4 points of interaction, namely the two hydrogen atoms (white), the oxygen atom (red) and the oxygen charge (small white) shifted along the dipole out of the oxygen, (b) hexagonal lattice formed by the oxygen positions in the ordinary ice phase, and (c) spherical occupation of the water molecules in the hexagonal layer, showing vacant shafts.

It was possible to show that the Tip4p water model provides stable hexagonal ice  $I_h$  ground states, with the lattice constant depending on the parameterization and the ground-state energy degeneration being slightly lifted [6].

- [1] W.L. Jorgensen et al.: J. Chem. Phys. **79**, 926 (1983)
- [2] J.L.F. Abascal et al.: J. Chem. Phys. **122**, 234511 (2005)
- [3] J.L.F. Abascal, C. Vega: J. Chem. Phys. **123**, 234505 (2005)
- [4] L. Pauling: J. Am. Chem. Soc. **57**, 2680 (1935)
- [5] B.A. Berg et al.: Phys. Rev. B **75**, 092202 (2007)
- [6] J. Zierenberg et al.: *Tip4p water model in the ice  $I_h$  configuration*, Leipzig/Tallahassee preprint, in preparation

## 11.15 Quantum Critical Phenomena in Uniform and Mixed Heisenberg Spin Chains

R. Bischof, W. Janke

The quantum Heisenberg model (which, here, stands synonymously for all its generalizations) is one of the most fundamental models of quantum magnetism. High-temperature superconducting cuprates can be successfully described as 1D and 2D quantum antiferromagnets at low doping. Above that, it exhibits a rich variety of zero-temperature quantum critical phenomena, depending on the specific choice of spins and different types of coupling mechanisms. The low-temperature properties of quantum spin chains depend significantly on the size of spins involved. Uniform chains of half-odd integer spins have no energy gap between the ground state and first excited states (i.e., they are quantum critical), whereas chains with integer spins do show an excitation gap [1]. Above that, spin chains can be driven to and away from criticality by tuning appropriate parameters (such as bond alternation, exchange anisotropy, next-nearest-neighbour interaction, spin-phonon coupling, etc.). While there exists wide literature about quantum critical phenomena in uniform chains, mixed spin chains have yet rarely been considered.

In order to investigate quantum critical phenomena of mixed anisotropic Heisenberg (XXZ) spin chains with bond alternation we use self-implemented versions of the continuous time loop algorithm [2] and Lanczos exact diagonalization. Specifically, we consider two different mixed 1D quantum XXZ models consisting of two different kinds of spins,  $S_a = 1/2$  and  $S_b = 1$  or  $3/2$ , that appear alternatingly in pairs [3]. By successful generalization of recently proposed quantum reweighting methods [4] to improved estimators of the loop algorithm, we have been able to determine the phase diagram in the XY-like region to high precision. In the following analysis we could establish a line of continuously varying critical exponents which strongly suggests that mixed spin chains are in the Gaussian universality class characterized by a central charge of  $c = 1$ . Furthermore, we could show the presence of logarithmic corrections in our mixed spin models at the SU(2) symmetric isotropic point. These logarithmic corrections influence the scaling and finite-size scaling behaviour on all length scales, which makes the extraction of critical exponents particularly difficult. It is well known that the homogeneous spin chains of  $S = 1$  do exhibit such types of corrections [5].

We have identified several scaling dimensions that can all be parametrized in terms of one fundamental parameter, a typical sign of the Gaussian universality class. To this end we proposed novel string-like order parameters as a generalization of the

disorder parameters of the quantum Ashkin–Teller model. For the  $S = 1$  chain our generalization corresponds to the order parameter of the dimerized phase in contrast to the usual string order parameter of the Haldane phase. These new order parameters offer access to scaling dimensions that differ from those of spin operators, and thus the validity of scaling relations can be tested with higher accuracy.

Another exotic order parameter is called twist order parameter, as introduced in [6]. It is particularly well suited to signal quantum phase transitions between different valence bond configurations in various 1D quantum spin systems. Despite its potential to accurately give pseudo-critical points in quantum Monte Carlo simulations, the scaling behaviour of the twist order parameter has not yet been studied. Our attempts to identify scaling behaviour seem to fail due to the inherently non-local nature of the twist order parameter, even though according to [6] a scaling dimension can be assigned.

- [1] F.D.M. Haldane: Phys. Rev. Lett. **50**, 1153 (1983)
- [2] B.B. Beard, U.J. Wiese: Phys. Rev. Lett. **77**, 5130 (1996); H.G. Evertz: Adv. Phys. **52**, 1 (2003)
- [3] K. Takano: Phys. Rev. Lett. **82**, 5124 (1999); Phys. Rev. B **61**, 8863 (2000); Z. Xu et al.: Phys. Rev. B **67**, 214426 (2003)
- [4] M. Troyer et al.: Braz. J. Phys. **34**, 377 (2004)
- [5] C.J. Hamer et al.: Phys. Rev. Lett. **68**, 214408 (2003); T. Papenbrock et al.: Phys. Rev. B **68**, 024416 (2003)
- [6] M. Nakamura, S. Todo: Phys. Rev. Lett. **89**, 077204 (2002)

## 11.16 Re-Examining the Quantum Compass Model with Screw-Periodic Boundary Conditions

S. Wenzel\*, W. Janke, A. Läuchli†

\*Institute of Theoretical Physics, École Polytechnique Fédérale de Lausanne, Switzerland

†Max Planck Institute for the Physics of Complex Systems (MPI PKS), Dresden, Germany

Due to its connection to interesting quantum phenomena ranging from orbital order in transition metal compounds to topologically protected qubits [1–3] the so-called compass model has recently attracted much interest in the literature. In two dimensions the model is defined by the Hamiltonian

$$\mathcal{H} = (1/4) \sum_i \left( J_x \sigma_i^x \sigma_{i+e_x}^x + J_z \sigma_i^z \sigma_{i+e_z}^z \right), \quad (11.2)$$

where  $\sigma$  are the usual Pauli operators,  $J_x, J_y$  coupling constants and  $e_x, e_z$  unit vectors in  $x$  and  $z$  direction. Although simple looking at first sight, this Hamiltonian is rather hard to study. It was shown to possess rich physics ranging from highly degenerate ground states to quantum phase transitions to an exciting thermal phase transition. In a recent Letter [4] it was proposed that directional order in the quantum compass model is rather stable against dilution, which is not the case for the classical model.

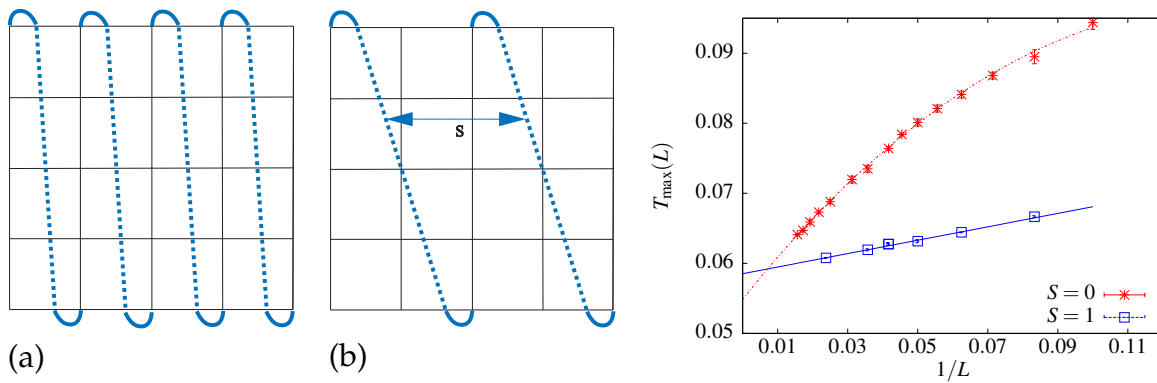


**Figure 11.14:** Left: Illustration of screw-periodic boundary conditions along the  $y$ -axis with pitch parameter (a)  $S = 1$  and (b)  $S = 2$ . Right: Finite-size scaling plot of the pseudocritical temperatures for the quantum compass model from the susceptibility maxima comparing periodic ( $S = 0$ ) and screw-periodic boundary conditions ( $S = 1$ ). The latter clearly lead to a considerable improvement of the finite-size scaling behaviour.

To investigate these questions in more detail, we have performed a comprehensive study of the two-dimensional (2D) compass model on square lattices for classical and quantum spin degrees of freedom using Monte Carlo computer simulations [5]. We employed state-of-the-art implementations using Metropolis, stochastic series expansion (SSE) and parallel tempering (PT) techniques to obtain the critical ordering temperatures and critical exponents. In the classical case we compared the finite-size scaling (FSS) behaviour of ordinary periodic boundary conditions with so-called annealed boundary conditions. We found that periodic boundary conditions suffer from extreme finite-size effects, which might be caused by closed loop excitations on the torus, so that one needs to go to very large lattice sizes to see the true asymptotic scaling behaviour. Our numerical results are at odds with recent literature on the subject which we can trace back to neglecting these strong finite-size effects on periodic lattices. Our analysis showed, however, that one arrives at quite different conclusions when these effects are properly taken into account [5]. This observation may also have an impact on previous conclusions for the quantum model concerning dilution effects because a precise estimate of the critical temperature  $T_c$  enters crucially into this analysis [4].

The precision of our results for the quantum model, however, was still rather low compared to the classical case. It was therefore a challenging goal to devise and analyze special boundary conditions for the quantum model with improved FSS behaviour compared to periodic boundary conditions. To this end, we recently re-examined the model and, in fact, obtained several significant improvements [6]. First, for the classical case, we proposed an improved update scheme which builds on the Wolff cluster algorithm in one-dimensional subspaces of the configuration space. This allowed us to study much larger classical systems up to  $L = 512$  and to provide compelling evidence for the presence of strongly anomalous scaling for periodic boundary conditions which is much worse than anticipated before. Second, for both the classical and the quantum case, we proposed to work with screw-periodic boundary conditions [7] sketched in Fig. 11.14, which do not make use of extended configuration spaces of the annealed boundary schemes and demonstrated that they completely remove the problem with

finite-size scaling. In particular for the quantum problem the use of screw-periodic boundary conditions gives a considerably improved estimate for the critical temperature (cf. Fig. 11.14) which should be of interest for future studies on the compass model. The origin of the anomalous scaling for periodic boundary conditions is also discussed.

- [1] K.I. Kugel, D.I. Khomskii: Sov. Phys. Usp. **25**, 231 (1982)
- [2] B. Douçot et al.: Phys. Rev. B **71**, 024505 (2005)
- [3] A. Kitaev: Ann. Phys. **321**, 2 (2006)
- [4] T. Tanaka, S. Ishihara: Phys. Rev. Lett. **98**, 256402 (2007)
- [5] S. Wenzel, W. Janke: Phys. Rev. B **78**, 064402 (2008); see also “Publisher’s Note” in Phys. Rev. B **78**, 099902(E) (2008) [Fig. 1 selected for Phys. Rev. B “Kaleidoscope” August 2008]
- [6] S. Wenzel et al.: Phys. Rev. E **81**, 066702 (2010) [arXiv:1002.3508]
- [7] E. Bittner et al.: Nucl. Phys. B **820**, 694 (2009)

## 11.17 Monte Carlo Simulations with the Worm Algorithm

W. Janke, M. Marenz, T. Neuhaus\*, A.M.J. Schakel†

\*Jülich Supercomputing Centre, Forschungszentrum Jülich, Germany

†Laboratório de Física Teórica e Computacional, Departamento de Física, Universidade Federal de Pernambuco, Recife, Brazil

About a decade ago, Prokof’ev and Svistunov [1] have introduced a novel Monte Carlo update scheme for spin models and lattice field theories that, although based on local updates, does away with critical slowing down almost completely. Their algorithm is based on the high-temperature series expansion of the partition function  $Z$ , leading to closed lines or loops of non-zero bond variables, and of the spin-spin correlation function  $\langle s_{i_0} s_{j_0} \rangle$ , containing an open line or chain of non-zero bonds connecting the lattice sites  $i_0$  and  $j_0$  [2]. This so-called *worm algorithm* generates loop configurations through the motion of the end points of the *open* line – the “head” and “tail” of a “worm”. A loop is generated in this scheme when the head bites the tail, or through a “back bite” where the head erases a piece (bond) of its own body and thereby leaves behind a detached loop and a (possibly drastically) shortened open chain. Typical conformations of the chain immersed into the background of loops are depicted in Fig. 11.15.

Recently we have evaluated the performance of the worm algorithm for the two-dimensional Ising model where two equivalent high-temperature representations are possible: one with unrestricted bond occupation numbers  $N_b = 0, 1, 2, \dots$  and another with restricted bond occupation numbers  $N_b = 0, 1$ . There is, however, no reason to believe that also the quantitative dynamical behaviour of the worm update algorithm is the same for the two formulations. Our numerical tests on square lattices show that the restricted representation with  $N_b = 0, 1$  is slightly favorable.

The worm algorithm is perfectly suited for pursuing the loop-gas approach to lattice spin systems providing an alternative description in terms of fluctuating geometrical

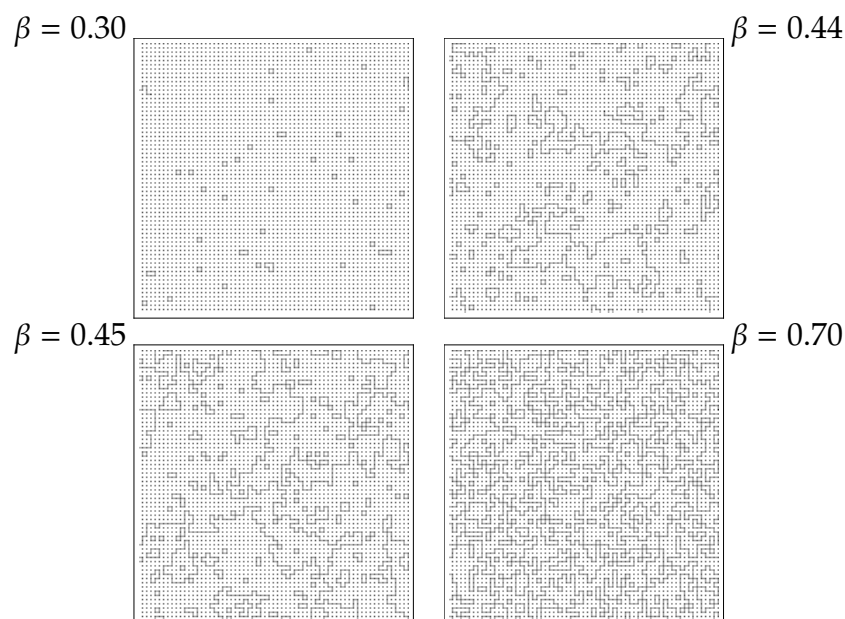


**Figure 11.15:** Typical high-temperature graph configurations on a  $64 \times 64$  square lattice (where  $\beta_c = 1/k_B T_c = 0.440686\dots$ ) with periodic boundary conditions.

objects, the loops. Physical observables are no longer estimated by sampling an ensemble of spin configurations, but by sampling a grand canonical ensemble of (mostly closed) lines, known as a *loop gas*, instead. The weight of a given high-temperature graph is typically determined by its total size, the number of intersections, and the number of loops contained in the tangle. In relativistic quantum field theories formulated on a space-time lattice, the high-temperature expansion is replaced by the strong-coupling expansion, representing the hopping of particles from one lattice site to the next, which is closely connected to Feynman's space-time approach to quantum theory [3].

As a first application we performed Monte Carlo "worm" simulations for the two-dimensional Ising or  $O(1)$  loop model on a honeycomb lattice [4] and used concepts from percolation theory – the paradigm of a geometrical phase transition – and the theory of self-avoiding random walks to analyze the critical behaviour of the model in terms of observables that naturally arise in a loop-gas approach, e.g., the radius of gyration of loops and chains or the end-to-end distance of chains [5, 6]. The honeycomb lattice serves as a prototype because here ambiguities in the loop interpretation can be avoided due to its coordination number  $z = 3$  (on a square lattice with  $z = 4$ , for example, "knots" are possible). Furthermore, for the Ising model on this lattice various exact results are known, which provide a yardstick for our numerical results and also for the feasibility of our approach in general.

- [1] N. Prokof'ev, B. Svistunov: Phys. Rev. Lett. **87**, 160601 (2001)
- [2] H.E. Stanley: *Introduction to Phase Transitions and Critical Phenomena* (Oxford University Press, New York 1971)
- [3] R.P. Feynman: Rev. Mod. Phys. **20**, 367 (1948)
- [4] W. Janke et al.: Nucl. Phys. B **829**, 573 (2010)
- [5] W. Janke, A.M.J. Schakel: Nucl. Phys. B [FS] **700**, 385 (2004)
- [6] W. Janke, A.M.J. Schakel: Phys. Rev. Lett. **95**, 135702 (2005)

## 11.18 Self-Adaptive Simulations of Critical Phenomena

E. Bittner\*, W. Janke

\*Present address: Institut für Theoretische Physik, Universität Heidelberg, Germany

In the past few years much attention has been paid to improved simulations of first-order phase transitions and systems with rugged free-energy landscapes where generalized ensembles techniques (umbrella, multicanonical, Wang-Landau, parallel/simulated tempering sampling) [1] proved to be very successful. For critical phenomena, on the other hand, the merits of this non-Boltzmann sampling approach have been fully appreciated only quite recently [2]. Here one often needs an extended temperature range around the critical point when analyzing second-order phase transitions by means of finite-size scaling analyses. To cover the complete “desired” temperature range in a single simulation for each lattice size, we combined in Ref. [2] multibondic sampling [3] with the Wang-Landau recursion [4], where the precise meaning of “desired” follows from a careful finite-size scaling (FSS) analysis of all relevant observables [5].

In this project we developed an alternative method based on the parallel-tempering algorithm [6] combined with cluster updates [7] and an improved adaptive routine [8] to determine the “desired” temperature range. The performance of our method is assessed by monitoring the integrated autocorrelation time  $\tau_{\text{int}}(T_i, L)$  for each replica at temperature  $T_i$  and system size  $L$ . If the requested overlap of the energy histograms for the different replica is chosen appropriately, the needed number of replica  $N_{\text{rep}}$  of the parallel tempering algorithm stays constant as a function of  $L$ . In this case the maximum of  $\tau_{\text{int}}(T_i, L)$  over all replica, that is the relevant time scale of the full self-adaptive algorithm, scales only weakly  $\propto L^z$ . For the energy we obtain  $z = 0.27$  in 2D and  $z = 0.62$  in 3D, cf. Fig. 11.16, which is asymptotically a great improvement over the multibondic Wang-Landau method with  $z \approx 1.05$  in both dimensions [9]. But also for moderate system sizes we gain one to two further orders of magnitude in the performance compared to our earlier method in Ref. [2], which is, however, already a great improvement over the standard multicanonical variant.

- [1] W. Janke (ed.): *Rugged Free Energy Landscapes: Common Computational Approaches to Spin Glasses, Structural Glasses and Biological Macromolecules*, Lect. Notes Phys. **736** (Springer, Berlin 2008)
- [2] B.A. Berg, W. Janke: Phys. Rev. Lett. **98**, 040602 (2007)
- [3] W. Janke, S. Kappler: Phys. Rev. Lett. **74**, 212 (1995)
- [4] F. Wang, D.P. Landau: Phys. Rev. Lett. **86**, 2050 (2001)
- [5] B.A. Berg, W. Janke: in *Computer Simulation Studies in Condensed-Matter Physics XX*, ed. by D.P. Landau et al., Physics Procedia **7**, 19 (2010)
- [6] K. Hukushima, K. Nemoto: J. Phys. Soc. Jpn. **65**, 1604 (1996)
- [7] R.H. Swendsen, J.-S. Wang: Phys. Rev. Lett. **58**, 86 (1987)
- [8] E. Bittner et al.: Phys. Rev. Lett. **101**, 130603 (2008)
- [9] E. Bittner, W. Janke: PoS (LAT2009) 042; and *Parallel tempering cluster algorithm for computer simulations of critical phenomena*, Leipzig preprint, submitted

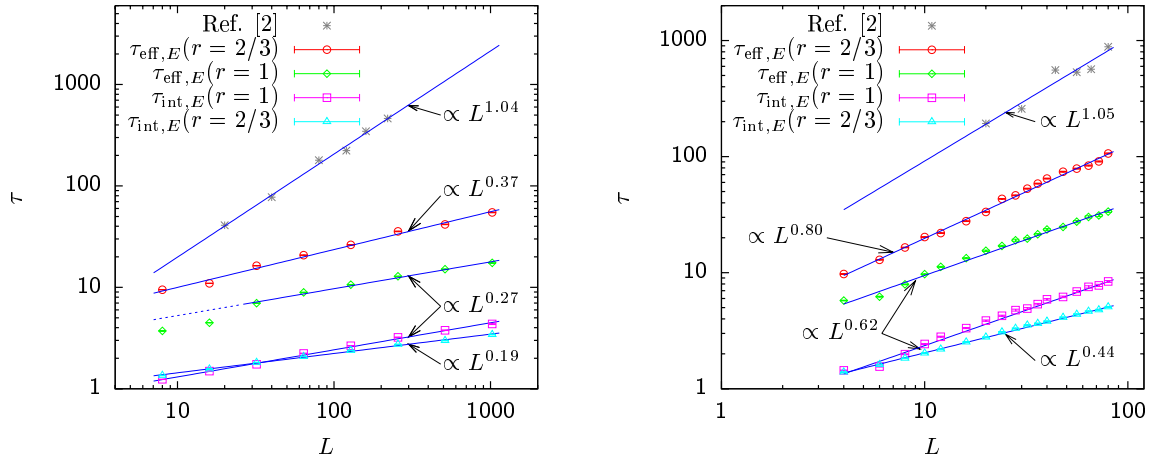


**Figure 11.16:** Autocorrelation times  $\tau_{\text{int}}$  and  $\tau_{\text{eff}}$  for the energy of the Ising model in 2D (left) and 3D (right). Here  $\tau_{\text{eff}} = N_{\text{rep}} \tau_{\text{int}}$  with  $N_{\text{rep}}$  being the number of replica of the parallel tempering algorithm. The parameter  $r$  determines the size of the “desired” temperature range [2, 9].

## 11.19 Critical Amplitude Ratios of the Baxter-Wu Model

L.N. Shchur\*, W. Janke

\*Landau Institute for Theoretical Physics, Chernogolovka, Russia

One of the central results of the theory of phase transitions and critical phenomena is the formulation of the universality hypothesis [1, 2]. According to the theory, all systems with the same dimensionality, the same symmetry of the ordered phase and the same number of order parameters are described by the same set of critical exponents at the critical point [2]. Additionally, thermodynamic functions vary with temperature in such a way that some combinations of their critical amplitudes take the same values for all systems within a universality class [3]. A typical example is provided by the scaling relation for the magnetic susceptibility  $\chi$  which in the vicinity of the critical temperature  $T_c$  behaves according to  $\chi \sim \Gamma_{\pm} |T/T_c - 1|^{-\gamma}$ , where  $\gamma$  is the critical exponent and  $\Gamma_+$  and  $\Gamma_-$  denote the critical amplitudes in the high- and low-temperature phase, respectively. The ratio  $R_{\chi} = \Gamma_+/\Gamma_-$  is then such a universal amplitude ratio.

Special interest in the properties of universality classes derives from cases in which for some representative models the singular behaviour is complicated by logarithmic corrections [4]. This is for instance the case for the two-dimensional 4-state Potts model which gives the name to this specific universality class. Another two-dimensional model which belongs to the same universality class, but *without* logarithmic corrections to its singular behaviour, is the Baxter-Wu model on a triangular lattice [5].

The objective of this project was to investigate the influence of the logarithmic corrections by estimating the critical amplitudes of the Baxter-Wu model numerically and comparing them with the universal amplitude ratios available for the 4-state Potts model (e.g.,  $R_{\chi} = 6.5 \pm 0.4$  [6]). To this end we simulated the model with the traditional Metropolis Monte Carlo algorithm and analyzed the magnetization and polarization in the ordered phase, and the energy, specific heat and magnetic susceptibility in both phases. One of our central findings for the Baxter-Wu model is the result  $R_{\chi} = 3.9 \pm 0.1$  [7], which is in very good agreement with approximate analytical estimates [8, 9] for this

ratio predicting  $R_\chi = 4.013$  and  $R_\chi = 4.02$ , but clearly deviates from the estimate [6] for the 4-state Potts model. This clearly indicates that the numerical estimate for the 4-state Potts model is strongly affected by logarithmic corrections, despite all the care exercised in the analysis [6]. Also for other universal combinations involving the specific-heat and magnetization amplitudes we obtained for the Baxter-Wu model perfect agreement with analytical approximations [7].

- [1] M.E. Fisher: Phys. Rev. Lett. **16**, 11 (1966)
- [2] R.B. Griffiths: Phys. Rev. Lett. **24**, 1479 (1970)
- [3] V. Privman et al.: in *Phase Transitions and Critical Phenomena*, ed. by C. Domb, J.L. Lebowitz, vol. 14 (Academic Press, New York 1991) pp. 1–134, 364–367
- [4] R. Kenna et al.: Phys. Rev. Lett. **96**, 115701 (2006); Phys. Rev. Lett. **97**, 155702 (2006)
- [5] R.J. Baxter, F.Y. Wu: Phys. Rev. Lett. **31**, 1294 (1973); Aust. J. Phys. **27**, 357 (1974)
- [6] L.N. Shchur et al.: Nucl. Phys. B **811**, 491 (2009); B. Berche et al.: Comput. Phys. Commun. **180**, 493 (2009)
- [7] L.N. Shchur, W. Janke: Nucl. Phys. B **840**, 491 (2010)
- [8] G. Delfino, J.L. Cardy: Nucl. Phys. B [FS] **519**, 551 (1998)
- [9] G. Delfino, P. Grinza: Nucl. Phys. B **682**, 521 (2004)

## 11.20 Geometrothermodynamics Applied to Black Holes

W. Janke, D.A. Johnston<sup>\*</sup>, R. Kenna<sup>†</sup>

<sup>\*</sup>Department of Mathematics and the Maxwell Institute for Mathematical Sciences,  
Heriot-Watt University, Edinburgh, United Kingdom

<sup>†</sup>Applied Mathematics Research Centre, Coventry University, United Kingdom

The application of information geometric ideas to statistical mechanics using a metric on the space of states, as pioneered by Ruppeiner [1] and Weinhold [2], has proved to be a useful alternative approach to characterizing phase transitions [3, 4]. The results obtained by using either the Ruppeiner or Weinhold metric (which are conformally related to each other) were found to be consistent in these applications. Some puzzling anomalies become apparent, however, when these methods are applied to the study of black hole thermodynamics. A possible resolution was suggested by Quevedo et al. [5] who emphasized the importance of Legendre invariance in thermodynamic metrics. They found physically consistent results for various black holes when using a Legendre invariant metric, which agreed with a direct determination of the properties of phase transitions from the specific heat. Recently, information geometric methods have been employed by Wei et al. [6] to study the Kehagias-Sfetsos (KS) black hole in Hořava-Lifshitz gravity [7, 8]. The formalism suggests that a coupling parameter in this theory plays a role analogous to the charge in Reissner-Nordström black holes or angular momentum in the Kerr black hole and the calculation of the specific heat shows a singularity which may be interpreted as a phase transition. When the curvature of the Ruppeiner metric is calculated for such a theory, it does not, however, show a singularity at the phase transition point. We show in this project that the curvature of a particular Legendre invariant (“Quevedo”) metric for the KS black hole is singular at

the phase transition point [9]. We contrast the results for the Ruppeiner, Weinhold and Quevedo metrics and in the latter case investigate the consistency of taking either the entropy or mass as the thermodynamic potential [9].

- [1] G. Ruppeiner: Phys. Rev. A **20**, 1608 (1979); Rev. Mod. Phys. **67**, 605 (1995); **68**, 313(E) (1996); Phys. Rev. D **75**, 024037 (2007); Phys. Rev. D **78**, 024016 (2007)
- [2] F. Weinhold: J. Chem. Phys. **63**, 2479 (1975)
- [3] W. Janke et al.: Phys. Rev. E **66**, 056119 (2002)
- [4] W. Janke et al.: Phys. Rev. E **67**, 046106 (2003)
- [5] H. Quevedo: Gen. Rel. Grav. **40**, 971 (2008); J.L. Alvarez et al.: Phys. Rev. D **77**, 084004 (2008); H. Quevedo, A. Sanchez: JHEP **0809**, 034 (2008); Phys. Rev. D **79**, 024012 (2009); Phys. Rev. D **79**, 087504 (2009)
- [6] S.-W. Wei et al.: *Thermodynamic geometry of black hole in the deformed Hořava-Lifshitz gravity*, preprint arXiv:1002.1550
- [7] P. Hořava: Phys. Rev. D **79**, 084008 (2009); JHEP **0903**, 020 (2009); Phys. Rev. Lett. **102**, 161301 (2009)
- [8] E.M. Lifshitz: Zh. Eksp. Toer. Fiz. **11**, 255, 269 (1941)
- [9] W. Janke et al.: J. Phys. A: Math. Theor. **43**, 425206 (2010)

## 11.21 Cross Correlations in Statistical Error Estimation

M. Weigel\*, W. Janke

\*Institut für Physik, Johannes Gutenberg-Universität Mainz, Germany

The success of Monte Carlo computer simulations, in particular Markov chain based methods, is largely due to the development and refinement of a number of advanced simulation techniques such as cluster algorithms and generalized-ensemble methods. Equally important to the efficient generation of simulation data, however, is their correct and optimal analysis. This includes finite-size scaling (FSS) approaches [1], turning the limitation to finite system sizes into a systematic tool for accessing the thermodynamic limit, reweighting techniques [2], yielding continuous functions of estimates from a single simulation, and statistical tools for error estimation such as the jackknife and other resampling schemes [3].

Of these techniques, the statistical error analysis appears to have received the least attention. In particular the effects of cross correlations have been mostly neglected to date (see, however, Refs. [4–6]), but are only systematically being discussed following our recent suggestion [7, 8]. In this project, we investigate how such cross correlations lead to systematically wrong estimates of statistical errors of averaged or otherwise combined quantities when a naive analysis is employed, and how a statistically correct analysis can be easily achieved within the framework of the jackknife resampling method. Furthermore, one can even take benefit from the presence of such correlation effects for significantly reducing the variance of estimates without substantial additional effort. We demonstrate the practical relevance of these considerations for a finite-size scaling study of the Ising model in two and three dimensions and report in some cases improvement factors of up to 10 in simulation time [9]. A typical example for averaging correlated data is shown in Fig. 11.17.

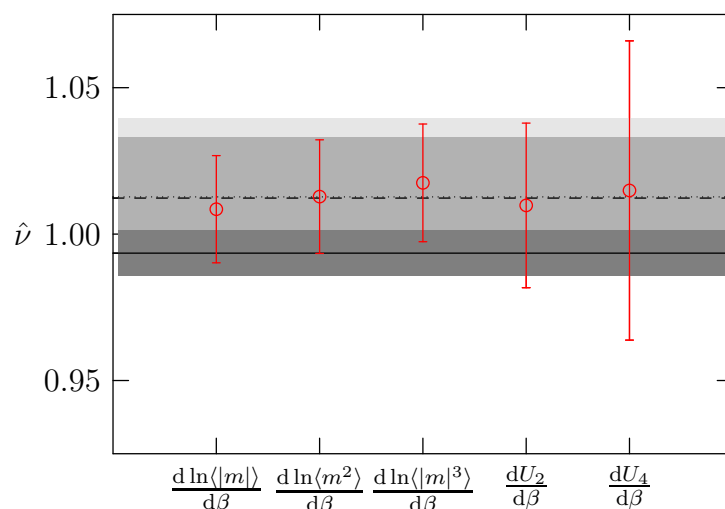


**Figure 11.17:** Mutually correlated estimates of the critical exponent  $\nu$  of the 2D Ising model from finite-size scaling fits of the indicated observables (circles). The (almost identical) dotted and dashed lines indicate the plain average and the error-weighted mean, respectively. The covariance-weighted mean corresponds to the solid line. While counterintuitive at first sight, this is the statistically correct averaging procedure for correlated data. The shaded areas indicate the corresponding one-sigma error intervals of the mean values.

- [1] W. Janke: Lect. Notes Phys. **739**, 79 (2008)
- [2] W. Janke: Lect. Notes Phys. **716**, 207 (2007)
- [3] B. Efron, R.J. Tibshirani: *An Introduction to the Bootstrap* (Chapman and Hall, Boca Raton 1998)
- [4] H.G. Ballesteros et al.: Phys. Lett. B **387**, 125 (1996)
- [5] W. Janke, T. Sauer: J. Chem. Phys. **107**, 5821 (1997)
- [6] M. Weigel, W. Janke: Phys. Rev. B **62**, 6343 (2000)
- [7] M. Weigel, W. Janke: Phys. Rev. Lett. **102**, 100601 (2009)
- [8] L.A. Fernández, V. Martín-Mayor: Phys. Rev. E **79**, 051109 (2009)
- [9] M. Weigel, W. Janke: Phys. Rev. E **81**, 066701 (2010)

## 11.22 Funding

Graduate School “BuildMoNa”: Leipzig School of Natural Sciences – Building with Molecules and Nano-objects

W. Janke (Principal Investigator)

Deutsche Forschungsgemeinschaft (DFG), Excellence Initiative

Graduate School *Statistical Physics of Complex Systems*

W. Janke (with B. Berche, Nancy)

Deutsch-Französische Hochschule, “Deutsch-Französisches Doktorandenkollegium (DFDK)” with “Co-tutelle de Thèse”, jointly with Nancy Université, France, Grant No. CDFA-02-07

International Max Planck Research School (IMPRS) *Mathematics in the Sciences*

W. Janke (Scientific Member)  
Max Planck Society and Klaus Tschira Foundation

Forschergruppe 877 *From Local Constraints to Macroscopic Transport*  
W. Janke (Principal Investigator)  
Deutsche Forschungsgemeinschaft (DFG)

Institute Partnership *Statistical Mechanics of Complex Networks*  
W. Janke (with Z. Burda, Krakow)  
Alexander von Humboldt Foundation, "Institutspartnerschaft" with the Jagiellonian University, Krakow, Poland, Grant No. 3.4-Fokoop-DEU/1117877

Host of *Alexander von Humboldt Research Prize Winner* Bernd A. Berg (Florida State University, Tallahassee, USA)  
W. Janke  
Alexander von Humboldt Foundation

*Dynamik und Statik von Spingläsern*  
W. Janke  
Deutsche Forschungsgemeinschaft (DFG), Grant No. JA483/22-2

*Phasenübergänge in Systemen mit einschränkender Geometrie*  
W. Janke  
Deutsche Forschungsgemeinschaft (DFG), Grant Nos. JA483/23-1 and 2

*Investigation of Thermodynamic Properties of Lattice and Off-Lattice Models for Proteins and Polymers*  
M. Bachmann and W. Janke  
Deutsche Forschungsgemeinschaft (DFG), Grant Nos. JA483/24-1 and 2

*Molecular Conformation Mechanics of Proteins and Polymers*  
W. Janke  
Deutsche Forschungsgemeinschaft (DFG), Grant No. JA483/24-3

*Mass Transport Models on Networks*  
W. Janke (twin project with H. Meyer-Ortmanns, Jacobs University Bremen)  
Deutsche Forschungsgemeinschaft (DFG), Grant No. JA483/27-1

*Monte Carlo Simulationen der Statik und Dynamik von Spingläsern*  
E. Bittner and W. Janke  
NIC Jülich (computer time grant for "JUROPA"), Grant No. hlz10

*Statistical Mechanics of Protein and Polymer Structure Formation Processes*  
M. Bachmann and W. Janke  
NIC Jülich (computer time grant for "JUROPA"), Grant No. hlz11

*Quantum Monte Carlo Simulations of Quantum Spin Models*  
W. Janke  
NIC Jülich (computer time grant for "JUROPA"), Grant No. hlz12

*Grafted and Non-Grafted Polymer Adsorption to (Patterned) Substrates*

W. Janke and M. Möddel

NIC Jülich (computer time grant for "JUROPA"), Grant No. hlz17

*Quanten Monte Carlo Simulationen von (ungeordneten) Quantenspinsystemen*

R. Bischof

Landesgraduiertenstipendium

## 11.23 Organizational Duties

Elmar Bittner

- Co-organizer of the contribution *Fußball-Fieber statistisch betrachtet*, 11. Leipziger Buchmesse-Akademie, Book Fair Leipzig (with W. Janke, A. Nußbaumer), Neue Messe, Leipzig, 20. March 2010
- Co-organizer of the contribution *Fußball-Fieber wissenschaftlich betrachtet*, Studieninformationstag der Universität Leipzig, Campus Augustusplatz (with W. Janke, A. Nußbaumer), Leipzig, 8. May 2010
- Referee for Physical Review Letters, Physical Review E, Journal of Physics A, European Journal of Physics B, Computer Physics Communications

Wolfhard Janke

- Director, Naturwissenschaftlich-Theoretisches Zentrum (NTZ), Universität Leipzig
- Member of the Board of the Faculty of Physics and Earth Sciences, Universität Leipzig
- Chairperson of the Programme Committee "Scientific Computing" of Forschungszentrum Jülich
- Member of the Scientific-Technical-Council of the Supervisory Board ("Aufsichtsrat") of the Forschungszentrum Jülich GmbH
- External Member of the Jagiellonian University Graduate School *International Ph.D. Studies in Physics of Complex Systems*, Krakow, Poland
- Specialist Editor, Computer Physics Communications (CPC), Elsevier, Amsterdam, The Netherlands
- Editor "Computational Sciences", Lecture Notes of Physics, Springer, Berlin, Heidelberg, Germany
- Editor "Computational Physics", Central European Journal of Physics, Krakow, Poland
- Member of Editorial Board, *Condens. Matter Phys.*, Lviv, Ukraine
- Permanent Member of the "International Advisory Board", *Conference of the Middle European Cooperation in Statistical Physics (MECO)*
- Member of International Organization Committee of the 10th International Conference *Path Integrals* (with L.S. Schulman (USA), M. Gutzwiller (USA), A. Inomata (USA), J.R. Klauder (USA), D. Fujikawa (Japan) und Chookyu Lee (South Korea)), Washington DC, USA, 11.–16. July 2010
- Member of the Programme Committee for the *European Conference on Complex Systems 2011 (ECCS'11)*, Vienna, Austria, 12.–16. September 2011
- Co-organizer of the contribution *Fußball-Fieber statistisch betrachtet*, 11. Leipziger Buchmesse-Akademie, Book Fair Leipzig (with E. Bittner, A. Nußbaumer), Neue Messe, Leipzig, 20. March 2010

- Co-organizer of the contribution *Fußball-Fieber wissenschaftlich betrachtet*, Studieninformationstag der Universität Leipzig, Campus Augustusplatz (with E. Bittner, A. Nußbaumer), Leipzig, 8. May 2010
- Co-organizer of the contribution *Fußballfieber wissenschaftlich betrachtet, Lange Nacht der Wissenschaft* (with A. Nußbaumer), Universität Leipzig, 24. September 2010
- Organizer of the “BuildMoNa” Theory Module *Probability in Physics* (with K. Kroy), Universität Leipzig, 10.–11. November 2010
- Organizer of the Workshop *CompPhys10 – 11th International NTZ Workshop on New Developments in Computational Physics*, ITP, Universität Leipzig, 25.–27. November 2010
- Organizer of the Workshop *CompPhys11 – 12th International NTZ Workshop on New Developments in Computational Physics*, ITP, Universität Leipzig, 24.–26. November 2011
- External Reviewer for Humboldt-Stiftung (AvH); Deutsche Forschungsgemeinschaft (DFG); Studienstiftung des deutschen Volkes; the Jeffress Memorial Trust, Bank of America, Virginia, USA; “Fond zur Förderung der wissenschaftlichen Forschung (FWF)”, Österreich; “The Royal Society”, Great Britain; The “Engineering and Physical Sciences Research Council (EPSRC)”, Great Britain; The University of Warwick, England, Great Britain; Coventry University, England, Great Britain; CECAM, Lausanne, Switzerland; National Science Foundation (NSF), USA; Natural Sciences and Engineering Research Council of Canada (NSERC), Canada; Israel Science Foundation, Israel
- Referee for Physical Review Letters, Physical Review B, Physical Review E, Journal of Chemical Physics, Europhysics Letters, Physics Letters A, Physics Letters B, The European Physical Journal B, Physica A, Proceedings of the Royal Physical Society, Journal of Physics A, Computer Physics Communications, JSTAT, Journal of Statistical Physics, New Journal of Physics, International Journal of Modern Physics C

Andreas Nußbaumer

- Co-organizer of the contribution *Fußball-Fieber statistisch betrachtet*, 11. Leipziger Buchmesse-Akademie, Book Fair Leipzig (with E. Bittner, W. Janke), Neue Messe, Leipzig, 20. March 2010
- Co-organizer of the contribution *Fußball-Fieber wissenschaftlich betrachtet*, Studieninformationstag der Universität Leipzig, Campus Augustusplatz (with E. Bittner, W. Janke), Leipzig, 8. May 2010
- Co-organizer of the contribution *Fußballfieber wissenschaftlich betrachtet, Lange Nacht der Wissenschaft* (with W. Janke), Universität Leipzig, 24. September 2010

## 11.24 External Cooperations

### Academic

- Institut für Festkörperforschung (IFF-2) and Institute for Advanced Simulation (IAS-2), Forschungszentrum Jülich  
PD Dr. Michael Bachmann, Dr. Thomas Vogel

- Institute of Physics, Jagiellonian University, Kraków, Poland  
Prof. Dr. Piotr Białas, Dr. Leszek Bogacz, Prof. Dr. Zdzisław Burda
- CEA/Saclay, Service de Physique Théorique, France  
Dr. Alain Billoire
- Institut für Physik, Universität Mainz  
Prof. Dr. Kurt Binder, Dr. Hsiao-Ping Hsu, Prof. Dr. Friderike Schmid, Dr. Martin Weigel
- Laboratoire de Physique des Matériaux (UMR CNRS No 7556), Nancy Université, France  
Prof. Dr. Bertrand Berche, Dr. Christophe Chatelain, Dr. Olivier Collet, Prof. Dr. Malte Henkel, Dr. Dragi Karevski
- Groupe de Physique des Matériaux (UMR CNRS No 6634), Université de Rouen, France  
Dr. Pierre-Emmanuel Berche
- SUPA, School of Physics and Astronomy, University of Edinburgh, Scotland, UK  
Dr. Richard A. Blythe, Prof. Dr. Martin Evans, Dr. Bartłomiej Waclaw
- Istituto Nazionale di Fisica Nucleare, Sezione di Milano-Bicocca, Milano, Italy  
Prof. Dr. Pablo Butera
- Jülich Supercomputing Centre (JSC), Forschungszentrum Jülich  
Prof. Dr. Peter Grassberger, PD Dr. Thomas Neuhaus
- IAC-1, Universität Stuttgart  
Prof. Dr. Rudolf Hilfer, Anjan Prasad Gantapara
- Complex Systems Division, Department of Theoretical Physics, Lunds Universitet, Lund, Sweden  
Prof. Dr. Anders Irbäck, Simon Mitternacht
- Department of Mathematics and the Maxwell Institute for Mathematical Sciences, Heriot-Watt University, Edinburgh, Scotland, UK  
Prof. Dr. Desmond A. Johnston
- Applied Mathematics Research Centre, Coventry University, England, UK  
Dr. Ralph Kenna, PD Dr. Christian von Ferber
- Inst. für Theoretische Physik, FU Berlin  
Prof. Dr. Hagen Kleinert
- Max-Planck Institut für Physik komplexer Systeme, Dresden  
Dr. Andreas Läuchli
- Atominstytut, TU Wien, Austria  
Prof. Dr. Harald Markum, Dr. Rainer Pullirsch
- Jacobs Universität Bremen  
Prof. Dr. Hildegard Meyer-Ortmanns
- Applied Mathematics, Universitat Pompeu Fabra, Barcelona, Spain  
Dr. Ramon Villanova
- EPF Lausanne, Switzerland  
Dr. Sandro Wenzel

- Engineering of Physics, Ankara University, Turkey  
Prof. Dr. Handan Arkın (Olgar)
- Dept. of Physics, Hacettepe University, Ankara, Turkey  
Prof. Dr. Tarik Çelik, Gökhan Gökoğlu
- Institute for Condensed Matter Physics, National Academy of Sciences, Lviv, Ukraine  
Dr. Viktoria Blavatska, Prof. Dr. Yuriy Holovatch
- Yerevan Physics Institute, Yerevan, Armenia  
Prof. Dr. David B. Saakian
- Landau Institute for Theoretical Physics, Chernogolovka, Russia  
Prof. Dr. Lev N. Shchur
- Banaras Hindu University, Varanasi, India  
Prof. Dr. Sanjay Kumar
- Dept. of Physics, Florida State University, Tallahassee, USA  
Prof. Dr. Bernd A. Berg
- Dept. of Physics, Michigan Technological University, Houghton, USA  
Prof. Dr. Ulrich H.E. Hansmann
- Center for Simulational Physics, The University of Georgia, Athens, USA  
Prof. Dr. David P. Landau, Dr. Stefan Schnabel
- The University of Tokyo, Japan  
Prof. Dr. Nobuyasu Ito
- Nagoya University, Japan  
Prof. Dr. Yuko Okamoto
- Laboratory of Statistical and Computational Physics, Institute of Physics, Academia Sinica, Nankang, Taipei, Taiwan  
Prof. Dr. Chin-Kun Hu
- Zhejiang Institute of Modern Physics, Zhejiang University, Hangzhou, P.R. China  
Prof. Dr. He-Ping Ying, Prof. Dr. Bo Zheng

## 11.25 Publications

### Journals

M. Bachmann, K. Goede, A. Beck-Sickinger, M. Grundmann, A. Irbäck, W. Janke: *Microscopic Mechanism of Specific Peptide Adhesion to Semiconductor Substrates*, *Angew. Chem. Int. Ed.* **49**, 9530–9533 (2010)

M. Bachmann, K. Goede, A. Beck-Sickinger, M. Grundmann, A. Irbäck, W. Janke: *Mikroskopischer Mechanismus der spezifischen Adhäsion von Peptiden an Halbleitersubstraten*, *Angew. Chem.* **122**, 9721–9724 (2010)

B.A. Berg, W. Janke: *Wang-Landau Multibondic Cluster Approach to Simulations of Second-Order Transitions*, in *Computer Simulations in Condensed Matter Physics XX*, ed. by D.P. Landau, S.P. Lewis, H.-B. Schüttler, *Physics Procedia* **7**, 19–28 (2010)

V. Blavatska, W. Janke: *Fractals Meet Fractals: Self-Avoiding Random Walks on Percolation Clusters*, in *Computer Simulations in Condensed Matter Physics XXII*, ed. by D.P. Landau, S.P. Lewis, H.-B. Schüttler, *Physics Procedia* **3**, 1431–1435 (2010)

V. Blavatska, W. Janke: *Shape Anisotropy of Polymers in Disordered Environment*, *J. Chem. Phys.* **133**, 184903-1–7 (2010)

W. Janke, D.A. Johnston, R. Kenna: *Geometrothermodynamics of the Kehagias-Sfetsos Black Hole*, *J. Phys. A: Math. Theor.* **43**, 425206-1–11 (2010)

W. Janke, T. Neuhaus, A.M.J. Schakel: *Critical Loop Gases and the Worm Algorithm*, *Nucl. Phys. B* **829**, 573–599 (2010)

M. Möddel, W. Janke, M. Bachmann: *Systematic Microcanonical Analyses of Polymer Adsorption Transitions*, *Phys. Chem. Chem. Phys.* **12**, 11548–11554 (2010)

A. Nußbaumer, E. Bittner, W. Janke: *Free-Energy Barrier at Droplet Condensation*, *Prog. Theor. Phys. Suppl.* **184**, 400–414 (2010)

A. Nußbaumer, E. Bittner, T. Neuhaus, W. Janke: *Universality of the Evaporation/Condensation Transition*, in *Computer Simulations in Condensed Matter Physics XX*, ed. by D.P. Landau, S.P. Lewis, H.-B. Schüttler, *Physics Procedia* **7**, 52–62 (2010)

L.N. Shchur, W. Janke: *Critical Amplitude Ratios of the Baxter-Wu Model*, *Nucl. Phys. B* **840**, 491–512 (2010)

B. Waćław, J. Sopik, W. Janke, H. Meyer-Ortmanns: *Mass Condensation on Networks*, *J. Phys.: Conf. Ser.* **246**, 012011-1–11 (2010)

M. Weigel, W. Janke: *Error Estimation and Reduction with Cross Correlations*, *Phys. Rev. E* **81**, 066701-1–15 (2010)

S. Wenzel, W. Janke, A. Läuchli: *Re-examining the Directional-Ordering Transition in the Compass Model with Screw-Periodic Boundary Conditions*, *Phys. Rev. E* **81**, 066702-1–9 (2010)

**in press**

V. Blavatska, W. Janke:  *$\Theta$ -Polymers in Crowded Media under Stretching Force*, to appear in *Comput. Phys. Commun.*, in print (2011)

J. Gross, W. Janke, M. Bachmann: *Massively Parallelized Replica-Exchange Simulations of Polymers on GPUs*, to appear in *Comput. Phys. Commun.*, in print (2011)

J. Gross, W. Janke, M. Bachmann: *A GPU Approach to Parallel Replica-Exchange Polymer Simulations*, to appear in *Computer Simulations in Condensed Matter Physics XXIV*, ed. by D.P. Landau, S.P. Lewis, H.-B. Schüttler, *Physics Procedia*, in print (2011)

W. Janke, T. Neuhaus, A.M.J. Schakel: *Worms Exploring Geometrical Features of Phase Transitions*, to appear in *Computer Simulations in Condensed Matter Physics XXIV*, ed. by D.P. Landau, S.P. Lewis, H.-B. Schüttler, *Physics Procedia*, in print (2011)

C. Junghans, W. Janke, M. Bachmann: *Hierarchies in Nucleation Transitions*, to appear in *Comput. Phys. Commun.*, in print (2011)

M. Möddel, W. Janke, M. Bachmann: *Adsorption of Finite Polymers in Different Thermodynamical Ensembles*, to appear in *Comput. Phys. Commun.*, in print (2011)

S. Schnabel, W. Janke, M. Bachmann: *Advanced Multicanonical Monte Carlo Methods for Efficient Simulations of Nucleation Processes of Polymers*, to appear in *J. Comput. Phys.*, in print (2011)

**Talks**

E. Bittner: *Free-Energy Barrier of the Evaporation/Condensation Transition*, Spring Meeting of the German Physical Society, Universität Regensburg, 21.–26. March 2010

E. Bittner: *Free-Energy Barriers of the 3D Edwards-Anderson-Ising Spin Glass Model*, Spring Meeting of the German Physical Society, Universität Regensburg, 21.–26. March 2010

E. Bittner: *Parallel Tempering Cluster Algorithm for Computer Simulations of Critical Phenomena*, StatPhys24 Conference, Cairns, Australia, 18.–23. July 2010

E. Bittner: *Replica-Exchange Cluster Algorithm*, MASCOS Workshop on Monte Carlo Algorithms in Statistical Physics, University of Melbourne, Australia, 27.–29. July 2010

W. Janke: *Formation/Dissolution of Equilibrium Droplets*, PbF2 Workshop, Universität Leipzig, 13. January 2010

W. Janke: *Computer Simulation Studies of Macromolecules*, Global Challenges for Sustainable Development: GSSD'2010 – Sustainable Chemistry & Related Areas, Université européenne de Bretagne (UEB), Rennes, France, 25.–26. February 2010

W. Janke: *Generalized Ensemble Simulations of Molecular Systems*, invited talk, 239th American Chemical Society National Meeting, San Francisco, USA, 21.–25. March 2010

W. Janke: *Computer Simulations of Macromolecular Systems in Generalized Ensembles*, SFG FOR877 Meeting, MPI-CBG, Dresden, 28. April 2010

W. Janke: *Exploring Critical Loop Gases with Worms*, Lattice Seminar, Humboldt Universität zu Berlin, 21. June 2010

W. Janke: *Polymers in Crowded Environment under Stretching Force: Globule-Coil Transitions*, Conference on Computational Physics (CCP 2010), NTNU Trondheim, Norway, 23.–26. June 2010

W. Janke: *Unconventional Quantum Phase Transition of Coupled Spin Dimers*, StatPhys24 Conference, Cairns, Australia, 18.–23. July 2010

W. Janke: *Error Estimation and Reduction with Cross Correlations*, invited talk, MAS-COS Workshop on Monte Carlo Algorithms in Statistical Physics, University of Melbourne, Australia, 27.–29. July 2010

W. Janke: *Exploring Random-Graph Ensembles with Worms*, invited talk, NORDITA Workshop *Random Graphs and Networks*, Stockholm, Sweden, 01.–03. November 2010

W. Janke: *Monte Carlo Simulations and Critical Phenomena*, Physikalisches Kolloquium, Bergische Universität Wuppertal, 29. November 2010

W. Janke: *Computer Simulations of Macromolecular Systems*, invited talk, NORDITA Workshop *Random Geometry and Applications*, Stockholm, Sweden, 03. December 2010

W. Janke: *The Ising Model in Statistical Physics I*, IMPRS Ringvorlesung *Discrete Structures in Physics*, International Max Planck Research School, Max-Planck-Institut für Mathematik in den Naturwissenschaften, Leipzig, 14. December 2010

M. Möddel: *Systematic Microcanonical Analyses of Polymer Adsorption Transitions*, Global Challenges for Sustainable Development: GSSD'2010 – Sustainable Chemistry & Related Areas, Université européenne de Bretagne (UEB), Rennes, France, 25.–26. February 2010

M. Möddel: *First-Order-Like Behavior at the Adsorption Transition of Short Polymers in the Microcanonical Ensemble*, Spring Meeting of the German Physical Society, Regensburg, 21.–26. March 2010

M. Möddel: *Thermodynamics of a Finite Homopolymer Near an Attractive Substrate*, Computational Biology Cluster Seminar, Forschungszentrum Jülich, Germany, 16. June 2010

M. Möddel: *Systematic Microcanonical Analyses of Polymer Adsorption Transitions*, Conference on Computational Physics (CCP 2010), NTNU Trondheim, Norway, 23.–26. June 2010

M. Möddel: *Grafted and Non-Grafted Polymer Adsorption in Different Thermodynamical Ensembles*, Seminar of the CDFA-DFDK, Nancy, France, 6. July 2010

**Posters**

M. Aust, M. Dvoyashkin, J. Kärger, R. Valiullin, W. Janke: *Particle Dynamics in Nano-Structured Channels*, SFG-FOR877–Defense Symposium, Universität Leipzig, 1.–2. July 2010

R. Bischof, W. Janke: *Critical Exponents and Phase Diagram of Mixed Spin Chains with Bond Alternation and Exchange Anisotropy*, 35th Conference of the Middle European Cooperation in Statistical Physics MECO35, Pont-à-Mousson, France, 15.–19. March 2010

R. Bischof, W. Janke: *Universality Class of Mixed Quantum Spin Chains*, Conference on Computational Physics (CCP 2010), NTNU Trondheim, Norway, 23.–26. June 2010

E. Bittner, W. Janke: *Replica-Exchange Cluster Algorithm*, NIC Symposium 2010, Forschungszentrum Jülich, 24.–25. February 2010

E. Bittner, W. Janke: *Free-Energy Barrier of the Evaporation/Condensation of Ising Droplets*, 35th Conference of the Middle European Cooperation in Statistical Physics MECO35, Abbaye des Prémontrés, Pont-à-Mousson, 15.–19. March 2010

M.H. Gerlach, W. Janke: *Monte Carlo Study of the Droplet-Strip Transition in the Two-Dimensional Ising Model*, 11th International NTZ-Workshop on New Developments in Computational Physics – CompPhys10, Universität Leipzig, 25.–27. November 2010

A.P. Gantapara, W. Janke, R. Hilfer: *Flat Histogram Monte Carlo Study of the Order Parameter Distribution*, Spring Meeting of the German Physical Society, Regensburg, 21.–26. March 2010

J. Gross, W. Janke, M. Bachmann: *Multithreading Monte Carlo Simulations of Polymer Models*, Spring Meeting of the German Physical Society, Regensburg, 21.–26. March 2010

J. Gross, W. Janke, M. Bachmann: *Massively Parallelized Replica-Exchange Simulations of Polymers on GPUs*, Workshop BioScience 2010, Forschungszentrum Jülich, 15.–19. November 2010

W. Janke, V. Blavatska: *Polymers in Crowded Environment Under Stretching Force: Globule-Coil Transitions*, Spring Meeting of the German Physical Society, Regensburg, 21.–26. March 2010

W. Janke, K. Kroy: *Polymer Conformations and Diffusive Transport in Disordered Environments*, SFG-FOR877–Defense Symposium, Universität Leipzig, 1.–2. July 2010

S. Karalus, W. Janke, M. Bachmann: *Cutting the Energy Range in Multicanonical Monte Carlo Simulations*, Spring Meeting of the German Physical Society, Regensburg, 21.–26. March 2010

M. Marenz, A. Nußbaumer, W. Janke: *Worm Algorithm in Ordered and Disordered Media*, 11th International NTZ-Workshop on New Developments in Computational Physics – CompPhys10, Universität Leipzig, 25.–27. November 2010

M. Möddel, W. Janke, M. Bachmann: *Microcanonical Analyses of Polymer Adsorption*, 35th Conference of the Middle European Cooperation in Statistical Physics *MECO35*, Pont-à-Mousson, France, 15.–19. March 2010

M. Möddel, W. Janke, M. Bachmann: *Systematic Microcanonical Analyses of Polymer Adsorption*, Spring Meeting of the German Physical Society, Regensburg, 21.–26. March 2010

M. Möddel, W. Janke, M. Bachmann: *Systematic Microcanonical Analyses of Polymer Adsorption*, 3rd Scientific Symposium of the Graduate School *BuildMoNa*, Universität Leipzig, 29.–30. March 2010

M. Möddel, W. Janke, M. Bachmann: *Microcanonical Analyses of Polymer Adsorption*, Workshop *BioScience 2010*, Forschungszentrum Jülich, 15.–19. November 2010

M. Müller, M. Bachmann, T. Neuhaus: *Towards Optimized Parallel Tempering*, 11th International NTZ-Workshop on *New Developments in Computational Physics – CompPhys10*, Universität Leipzig, 24.–27. November 2010

H. Nagel, B. Waclaw, W. Janke: *Time Scale of Mass Condensation in Stochastic Transport with Pair Factorized Steady States*, 11th International NTZ-Workshop on *New Developments in Computational Physics – CompPhys10*, Universität Leipzig, 24.–27. November 2010

A. Nußbaumer, E. Bittner, W. Janke: *Gibbs-Thomson Effect in the Ising Model*, 11th International NTZ-Workshop on *New Developments in Computational Physics – CompPhys10*, Universität Leipzig, 24.–27. November 2010

S. Schöbl, K. Kroy, W. Janke: *Effect of Disorder on Equilibrium Conformations of Semiflexible Polymers*, 35th Conference of the Middle European Cooperation in Statistical Physics *MECO35*, Pont-à-Mousson, France, 15.–19. March 2010

S. Schöbl, K. Kroy, W. Janke: *Effect of Disorder on Equilibrium Conformations of Semiflexible Polymers*, 3rd Scientific Symposium of the Graduate School *BuildMoNa*, Universität Leipzig, 29.–30. March 2010

M. Wiedenmann, A. Nußbaumer, E. Bittner, W. Janke: *Evaporation/Condensation Transition of 3D Ising Droplets*, 35th Conference of the Middle European Cooperation in Statistical Physics *MECO35*, Pont-à-Mousson, France, 15.–19. March 2010

M. Wiedenmann, A. Nußbaumer, E. Bittner, W. Janke: *Monte Carlo Study of the Evaporation/Condensation Transition of Ising Droplets*, 3rd Scientific Symposium of the Graduate School *BuildMoNa*, Universität Leipzig, 29.–30. March 2010

J. Zierenberg, B.A. Berg, W. Janke: *Structure of the Tip4p Water Model in the Ice  $I_h$  Phase*, 11th International NTZ-Workshop on *New Developments in Computational Physics – CompPhys10*, Universität Leipzig, 25.–27. November 2010

## 11.26 Graduations

### Diploma

- Hannes Nagel  
*Mass Condensation in Stochastic Transport Processes and Complex Networks*  
19. February 2010
- Jonathan Groß  
*Multithreading Monte Carlo Simulationen eines minimalistischen Polymermodells*  
26. February 2010
- Niklas Fricke  
*Self-Avoiding Walks on Disordered Lattices*  
01. July 2010
- Steffen Karalus  
*Thermodynamics of Polymer Adsorption to a Flexible Membrane*  
20. September 2010
- Martin Marenz  
*Worm Algorithm in Ordered and Disordered Media*  
25. November 2010

### Master

- Johannes Zierenberg  
*Tip4p Water Model in the Ice  $I_h$  Configuration*  
21. December 2010

### Bachelor

- Benjamin Winkler  
*Nichtgleichgewichtsrelationen vom Jarzynski-Typ zur Bestimmung von Grenzflächen-  
spannungen*  
23. August 2010
- Kieran Austin  
*Exakte Enumeration von Polymeren an Oberflächen*  
29. October 2010

## 11.27 Guests

- Mario Collura  
Nancy Université, France  
01. January – 30. June 2010
- Prof. Dr. Nihat Berker  
Sabanci University, Istanbul, Turkey, and MIT, Boston, USA  
*Anisotropy Effects and Impurity Induced Antiferromagnetism: Renormalization-  
Group Theory of  $d=3$  Electronic Models*  
29.–30. January 2010

- Dr. Thomas Vogel  
IFF-2 and IAS-2, Forschungszentrum Jülich, Germany  
08.-12. March 2010
- Prof. Dr. Bernd A. Berg  
Florida State University, Tallahassee, USA  
Research Prize Winner of the Alexander von Humboldt Foundation  
*Search for Non-Perturbative Mechanisms to Generate a W Boson Mass*  
11. May – 31. July 2010
- Dr. Viktoria Blavatska  
Institute for Condensed Matter Physics, Lviv, Ukraine  
Humboldt Fellow/FOR877 guest  
*Shape Anisotropy of Polymers in Disordered Environment*  
07. April – 18. June 2010
- Jeremi Ochab  
Jagiellonian University, Krakow, Poland  
*Epidemics on Networks*  
01. October – 31. December 2010
- Marcin Zagorski  
Jagiellonian University, Krakow, Poland  
02.-06. October 2010
- Prof. Dr. Herbert Wagner  
LMU Munich, Germany  
BuildMoNa Tutorial *Probability in Physics*  
09.-12. November 2010
- Dr. Richard Blythe  
University of Edinburgh, UK  
BuildMoNa Tutorial *Probability in Physics*  
09.-12. November 2010
- Dr. Martin Weigel  
Universität Mainz, Germany  
*Performance Potential for Simulating Spin Models on GPU*  
23.-28. November 2010
- Dr. Ralph Kenna  
Coventry Univ., UK  
*Size Matters, Except Perhaps for Pure Mathematicians*  
24.-27. November 2010
- Dr. Sandro Wenzel  
EPF Lausanne, Switzerland  
*Critical Properties of the 120 Degree Model for Orbital Ordering*  
24.-27. November 2010
- Prof. Dr. Antun Balaz  
Scientific Computing Laboratory, Institute of Physics, University of Belgrade, Serbia  
*Fast Converging Path Integrals for Time-Dependent Potentials*  
24.-28. November 2010

- Prof. Dr. Ferenc Iglói  
Institute of Theoretical Physics, Research Institute for Solid State Physics and Optics,  
Budapest, Hungary  
*Infinite Disorder Scaling of Random Quantum Magnets in Three and Higher Dimensions*  
24.–28. November 2010
- PD Dr. Thomas Neuhaus  
Jülich Supercomputing Centre, Forschungszentrum Jülich, Germany  
*More on Quantum Adiabatic Computations*  
24.–28. November 2010
- Prof. Dr. J.J. Ruiz-Lorenzo  
Univ. Extremadura, Badajoz, Spain  
*Ising Spin-Glass Transition in Magnetic Field out of Mean-Field: Numerical Simulations and Experiments*  
24.–28. November 2010
- Marcin Zagorski  
Jagiellonian University, Krakow, Poland  
*Model Gene Regulatory Networks under Mutation-Selection Balance*  
24.–28. November
- Dr. Stefan Schnabel  
University of Georgia, Athens, USA  
*On the Low-Temperature Behavior of a Geometrically Frustrated Heisenberg Antiferromagnet*  
24. November – 31. December 2010
- Prof. Dr. Harald Markum  
TU Wien, Austria  
*Formulation of Time from Aristotle to Monte Carlo Simulations and to Noncommutative Geometry*  
25.–26. November 2010
- Prof. Dr. A. Hartmann  
Universität Oldenburg, Germany  
*Large-Deviation Properties of Largest Component for Random Graphs*  
26.–27. November 2010
- Prof. Dr. Bernd A. Berg  
Florida State University, Tallahassee, USA  
*From Data to Probability Densities without Histograms*  
16.–17. December 2010



# 12

## Molecular Dynamics / Computer Simulation

### 12.1 Introduction

In our research group methods of statistical physics and computer simulations are used to investigate classical many-particle systems interacting with interfaces. One basic motivation of our work has always been to build up a bridge between theoretical and experimental physics exchanging challenges and stimuli in both directions.

By means of analytical theories of statistical physics and computer simulations (Molecular dynamics, Monte Carlo procedures, percolation theories) using modern workstations and supercomputers we examine subjects for which high interest exists in basic research and industry as well. The examinations involve transport properties (diffusion of guest molecules) in zeolites and the new exciting class of porous Metal-Organic-Frameworks (so called MOF's) and the structural and phase behaviour of complex fluids on bulk conditions and in molecular confinements.

Especially we are interested to understand

- the diffusion behaviour of guest molecules in porous crystals in dependence on thermodynamic parameters, steric conditions, intermolecular potentials and the concentration of the guest molecules,
- structure and phase equilibria of complex (aqueous) fluids in interfacial systems (e.g. pores, thin films, model membranes) in dependence on geometric and thermodynamic conditions,
- and the migration of molecules in (random) porous media by the use of percolation theories.

in microscopic detail and to compare the results with experimental data.

The use of a network of PC's and workstations (Unix, Linux, Windows), the preparation and application of programs (Fortran, C, C<sup>++</sup>), and the interesting objects (zeolites, MOF's, membranes) give excellent possibilities for future careers of undergraduates, graduate students and postdocs. Our research is part of several national and international programs (DFG - Schwerpunktprogramm SPP1362, including a joint research project DFG/TRF-Thailand, and, an International Research Graduate Training program (IRTG 1056), a joint research project DAAD/TRF-Thailand and joint research projects

with UOIT Oshawa and SHARCNET, Canada) and includes a close collaboration with the Institute of Experimental Physics I (Physics of Interfaces and Biomembranes) of Leipzig University and many institutions in Germany and other countries. Details are given in the list of external cooperations.

*H.L.Vörtler and S. Fritzsche*

## 12.2 Analytical Treatment and Computer Simulations of the influence of the crystal surface on the exchange of guest molecules between zeolite nanocrystals and the surrounding gas phase

S. Fritzsche\*, O. Saengsawang\*, M. Knauth\*, S. Vasenkov<sup>†</sup>

\*Abteilung MDC

<sup>†</sup>University of Florida, Gainesville, USA

The research within the framework of the DFG priority program SPP 1155 in which we investigated the surface effects influencing the dynamics of adsorption of guest molecules into porous crystals was successfully finished with the end of this SPP. The results of our work during all periods of the SPP1155 are summarized in [1]. During the final period we investigated the transport through a crystallite and the surrounding mesopore under nonequilibrium conditions using special technics as e.g. dual control volume MD [2] and [3].

- [1] O. Saengsawang, T. Nanok, S. Vasenkov, S. Fritzsche, *Relationship between Sorbate Transport Inside and at the Margins of Zeolite Crystal*, Soft Materials (accepted 2010).
- [2] S. Fritzsche, M. Knauth, S. Vasenkov, *Transport of guest molecules through a membrane containing microporous crystals and mesopores*, Talk at the International Workshop Molecular Modelling, "Molecular Modelling and Simulation for Industrial Applications: Physico-Chemical Properties and Processes", March 22, 2010, Würzburg, Germany
- [3] S. Fritzsche, M. Knauth, S. Vasenkov, *Interplay between Microcrystal and Gas Phase*, Talk February 17th 2010 at the Chulalongkorn University, Bangkok, Thailand

## 12.3 Diffusion and Rotation of Water in the Zeolite Chabazite

S. Fritzsche\*, R. Channajaree\*, P. A. Bopp<sup>†</sup> J. Kärger<sup>‡</sup>,

\*Abteilung MDC

<sup>†</sup>University Bordeaux, France

<sup>‡</sup>Institut für Experimentelle Physik I, Abteilung GFP

The investigations of diffusion of water in the zeolite chabazite basing on own earlier work [1] and new methods in a project in the framework of the International

Research Training Group (IRTG) "Diffusion in Porous Materials" was continued. The nonmonotonic dependence of the self diffusion coefficient upon the concentration of water molecules could be explained and the rotational diffusion of the water molecules was now also included into this research and could be treated successfully [2].

The small diffusion coefficients have been investigated by so called boost potential MD a highly efficient method for the treatment of rare events that is based on analytical Transition State Theory.

A PhD thesis [3] could be submitted. A paper was submitted and meanwhile accepted by Microporous and Mesoporous Materials [4].

- [1] S. Jost, P. Biswas, A. Schüring, J. Kärger, P. A. Bopp, R. Haberlandt, Siegfried Fritzsche, *J. Phys. Chem. C*, **111**, 14707 (2007)
- [2] R. Channajaree, S. Fritzsche, J. Kärger, Ph. A. Bopp, *On the Motions of Water in Chabazite, a Molecular Dynamics Study*, talk (given by Ph. A. Bopp) at the NACCPC Humboldt - Kolleg, 2nd North African Conference on Computational Physics and Chemistry 2010, 12-14 December 2010 in Algeria
- [3] R. Channajaree, *The Motions of Guest Water Molecules and Cations in Chabazite*, PhD thesis submitted to the university of Leipzig 2010
- [4] R. Chanajaree, P. A. Bopp, J. Kärger, S. Fritzsche, *The Motions of Guest Water Molecules in Chabazite*, accepted by Microporous and Mesoporous Materials

## 12.4 Investigation of the rotation and diffusion of pentane in the zeolite ZK5

S. Fritzsche\*, O. Saengsawang\* A. Schüring\*, P. Magusin† M.-O. Coppens‡ A. Dammers‡  
D. Newsome‡

\*Abteilung MDC

†Eindhoven University, The Netherlands

‡Delft University, The Netherlands

Earlier investigations [1] for the system pentane/ZK5 have been continued. The very slow diffusion of pentane molecules in the zeolite ZK5 has now been studied using a new method, called HTCE, that was a recently developed in our group [2]

This method is based on Transition State Theory. It could be successfully applied to the present problem [3].

- [1] O. Saengsawang, A. Schüring, T. Remsungnen, A. Loisuangsinn, S. Hannongbua, P. C. M. M. Magusin and S. Fritzsche, *J. Phys. Chem. C* **112**, 5922 (2008)
- [2] A. Schüring, S. M. Auerbach and S. Fritzsche, *A simple method for sampling partition function ratios*, *Chem. Phys. Lett.* **450** (2007) 164–169
- [3] O. Saengsawang, A. Schüring, T. Remsungnen, S. Hannongbua, D. A. Newsome, A. J. Dammers, M. O. Coppens, S. Fritzsche, *Diffusion of n-Pentane in the Zeolite ZK5 Studied by High-Temperature Configuration-Space Exploration*, *Chem. Phys.* **368** (2010) 121–125

## 12.5 Diffusion of Guest Molecules in Metal Organic Frameworks

S. Fritzsche\*, K. Seehamart\* S. Hannongbua<sup>†</sup>, T. Remsungnen<sup>‡</sup>, J. Kärger<sup>§</sup>, C. Chmelik<sup>§</sup>

\*Abteilung MDC

<sup>†</sup>Chulalongkorn University, Bangkok, Thailand

<sup>‡</sup>Khon Khaen University, Khon Khaen, Thailand

<sup>§</sup>Institut für Experimentelle Physik I, Abteilung GFP

The promising new nanoporous materials called Metal Organic Frameworks (MOF's) are investigated within the framework of the SPP1362 in a common DFG project with experimental groups (Prof. Kärger, Leipzig, Prof. Caro, Hannover, Dr. Wiebcke, Hannover) and NRCT (Thailand, Prof. Hannongbua and other groups).

A breakthrough could be reached when our common examinations with Prof. Krishna (Amsterdam), published in [1] could show, that the lattice flexibility of the MOF Zntbip did not only influence the size of the self diffusion coefficient of ethane in Zntbip but, lead to a qualitatively different concentration dependence of this self diffusion coefficient. The effect is cause mainly by the change of the lattice structure of the highly flexible MOF and could be explained in [2].

This is particularly important because most simulations about MOF are still being done by simplifying the system by use of a rigid framework.

- [1] K. Seehamart and T. Nanok and R. Krishna and J. M. van Baten and T. Remsungnen and S. Fritzsche, *A Molecular Dynamics investigation of the influence of structural flexibility on self-diffusion of ethane in Zn(tbip)*, Microporous and Mesoporous Materials **125**(2009)97–100
- [2] K. Seehamart, T. Nanok, J. Kärger, C. Chmelik, R. Krishna, S. Fritzsche, *Investigating the Reasons for the Significant Influence of Lattice Flexibility on Self-Diffusivity of Ethane in Zn(tbip)*, Microporous and Mesoporous Materials **130** (2010) 92

## 12.6 Funding

*Analytical Treatment and Computer Simulations of the influence of the crystal surface on the exchange of guest molecules between zeolite nanocrystals and the surrounding gas phase*

S. Fritzsche, S. Vasenkov, T. Nanok, O. Saengsawang,  
SPP1155, DFG-code FR1486/2-3

*Diffusion of Water in the Zeolite Chabazite*

S. Fritzsche, R. Channajaree,  
DFG: IRTG 1056

*Investigation of the rotation and diffusion of pentane in the zeolite ZK5*

S. Fritzsche, O. Saengsawang,  
DFG: IRTG 1056

*Diffusion of Guest Molecules in Metal Organic Frameworks*

K. Seehamart

funded by a stipend of the University of Technology Isan (RMUTI), Kon Khaen, Thailand,

S. Fritzsche,

SPP1362, DFG-code FR1486/5-1

## 12.7 Organizational Duties

H.L. Vörtler

- Speaker of the MDC group
- Reviewer for projects (Czech Science Foundation)
- Referee for journals (J.Chem. Phys, Physica A, Chem. Phys. Lett, J. Molec. Liquids, Chem. Phys)

S. Fritzsche

- Project leader of one project in the International Research Training Group, IRTG 1056
- Project leader of one project in the SPP1155, DFG-code FR1486/2-2
- Project leader of one project in the SPP1362, DFG-code FR1486/5-1
- Referee for journals (Chem. Phys. Lett., Microporous and Mesoporous Materials, Journal of Molecular Graphics and Modelling)

## 12.8 External Cooperations

### Academic

- Chulalongkorn University, Bangkok, Thailand  
Prof. Dr. S. Hannongbua
- Khon Khaen University, Khon Khaen, Thailand  
Prof. Dr. T. Remsungnen, Dr. P. Puphasuk
- University Bordeaux, France  
Prof. Dr. P. A. Bopp
- Eindhoven University, Eindhoven, The Netherlands  
Prof. Dr. P. Magusin
- Technical University, Delft, The Netherlands  
Prof. Dr. M.-O. Coppens, Dr. A. Dammers, Dr. D. Newsome
- Leibniz University Hannover  
Prof. Dr. J. Caro, Dr. M. Wiebcke
- Van't Hoff Institute for Molecular Sciences, University of Amsterdam, The Netherlands  
Prof. R. Krishna

## 12.9 Publications

### Journals

O. Saengsawang, A. Schüring, T. Remsungnen, S. Hannongbua, D. A. Newsome, A. J. Dammers, M. O. Coppens, S. Fritzsche, *Diffusion of n-Pentane in the Zeolite ZK5 Studied by High-Temperature Configuration-Space Exploration*, Chem. Phys. **368** (2010) 121–125

K. Seehamart, T. Nanok, J. Kärger, C. Chmelik, R. Krishna, S. Fritzsche, *Investigating the Reasons for the Significant Influence of Lattice Flexibility on Self-Diffusivity of Ethane in Zn(tbip)*, Microporous and Mesoporous Materials **130** (2010) 92

O. Saengsawang, T. Nanok, S. Vasenkov, S. Fritzsche, *Relationship between Sorbate Transport Inside and at the Margins of Zeolite Crystal*, Soft Materials (accepted 2010).

S. Fritzsche, *Influence of the lattice flexibility on self-diffusion of ethane in the metal - organic framework Zn(tbip)*, in Scientific Research in Saxony, ZIH Dresden, 2010

### Talks

R. Channajaree, S. Fritzsche, J. Kärger, Ph. A. Bopp, *On the Motions of Water in Chabazite, a Molecular Dynamics Study*, Talk (given by Ph. A. Bopp) at the NACCPC Humboldt - Kolleg, 2nd North African Conference on Computational Physics and Chemistry 2010, 12-14 December 2010 in Algeria

S. Fritzsche, M. Knauth, S. Vasenkov, *Interplay between Microcrystal and Gas Phase*, Talk February 17th 2010 at the Chulalongkorn University, Bangkok, Thailand

S. Fritzsche, *Basic Spirit of MD Computer Simulations*, Talk August 18th 2010 at the Chulalongkorn University, Bangkok, Thailand

S. Fritzsche, M. Knauth, S. Vasenkov, *Transport of guest molecules through a membrane containing microporous crystals and mesopores*, Talk at the International Workshop Molecular Modelling, 'Molecular Modelling and Simulation for Industrial Applications: Physico-Chemical Properties and Processes', March 22, 2010, Würzburg, Germany

H. Bux, F.-Y. Liang, Y.-S. Li, J. Cravillon, M. Wiebcke, C. Chmelik, J. Kärger, S. Fritzsche, J. Caro, *Transport through zeolitic imidazolate frameworks: from molecular diffusion to membrane permeation*, Talk by H. Bux at the 22. Deutsche Zeolith-Tagung, 03.03.2010 - 05.03.2010, Universität München

### Posters

M. Knauth, K. Kirchner, S. Fritzsche, C. Chmelik, J. Kärger, T. Remsungnen, K. Seehamart, J. Caro, H. Bux, *Molecular dynamics investigation of the Influence of lattice flexibility and partial charges on the migration of guest molecules in the metal-organic framework ZIF-8*, Poster, MOF 2010 '2nd International Conference on Metal-Organic Frameworks and Open Framework Compounds', 5 to 8 September 2010 in Marseille/France.

O. Saengsawang, M. Knauth, A. Pianwanit, C. Kritayakornupong, M. Wiebcke, S. Fritzsche, S. Hannongbua,  
*Structural Prediction of Dinuclear Layer Pillar Metal Organic Frameworks: Studied by Quantum Calculations*, Poster, MOF 2010 '2nd International Conference on Metal-Organic Frameworks and Open Framework Compounds', 5 to 8 September 2010 in Marseille/France.

K. Seehamart, M. Knauth, S. Fritzsche, T. Remsungnen, R. Krishna, C. Chmelik, J. Kärger,  
*Molecular Dynamics Investigation of the Self-Diffusion of Guest Molecules in the Metal - Organic Framework Zn(tbip) With Rigid and Flexible Framework*, Poster, MOF 2010 '2nd International Conference on Metal-Organic Frameworks and Open Framework Compounds', 5 to 8 September 2010 in Marseille/France.

## 12.10 Graduations

### Diploma

- Loreen Hertäg  
*Untersuchung der Effekte bei der Diffusion von Methan und Wasserstoff in ZIF-8 mittels Molekulardynamischer Computersimulation.*  
May 2010
- Silvio Kalisch  
*MC Simulation und theorie von geometrisch beschränkten Hard-core Fluiden im Übergangsbereich von drei zu zwei Dimensionen*  
January 2010
- Kathlen Kirchner  
*Diffusion of Methanol in ZIF-8*  
August 2010

## 12.11 Guests

- Prof. Dr. T. Remsungnen  
Khon Khaen University, Thailand  
22.09.-19.10.2010
- Dr. P. Puphasuk,  
Khon Khaen University, Thailand  
22.09.-19.10.2010



# 13

## Quantum Field Theory and Gravity

### 13.1 Temperature Dependence of the Casimir Force

M. Bordag

The vacuum of quantum fields shows a response to changes in external conditions with measurable consequences. The most prominent manifestation is the Casimir effect. It belongs to the few number of macroscopic quantum effects and it is of big importance in nanometer sizes systems. At present, the problem of the dependence of the Casimir forces on temperature is in the focus of actual interest. There are two reasons for, the possibility to measure these forces due to improved experimental techniques and the more theoretical question on the violation of the third law of thermodynamics observed in a certain model.

Actual research was on the temperature dependent Casimir force between a sphere and a plane and on media with temporal dispersion, [1, 2].

[1] M. Bordag and I.G. Pirozhenko, Phys. Rev. D **82** (2010) 125016

[2] M. Bordag, B. Geyer, G.L. Klimchitskaya, V.M. Mostepanenko, J. Phys. A **43** (2010) 015402

### 13.2 Higher order correlation corrections to color ferromagnetic vacuum state at finite temperature

M. Bordag, V. Skalozub\*

\*U Dnepropetrovsk

Topic of the investigation is the stability of the ground state of QCD with temperature and color magnetic background field by means of the calculation of the polarization tensor of the gluon field. Special attention was devoted to the investigation of the polarization tensor for the color charged gluons at finite temperature. A new technique for a parametric representation was found which allowed for an explicit separation of the Debye and the magnetic masses and, for instance, for an easy calculation of the Debye mass's field and temperature dependence [1].

Another line of research in this collaboration was on long range magnetic fields.

- [1] M. Bordag, V. Demchik, and V. Skalozub, in: K.A. Milton and M. Bordag (Eds.), *Proceedings of the 9th Conference on Quantum Field Theory Under the Influence of External Conditions (QFEXT09)*, World Scientific, Singapore, 2010

### 13.3 Structure of the gauge orbit space and study of gauge theoretical models

G. Rudolph, Sz. Charzynski\*, H. Grundling<sup>†</sup>, J. Huebschmann<sup>‡</sup>, P. Jarvis<sup>§</sup>, J. Kijowski\*, M. Schmidt

\*U Warsaw

<sup>†</sup>U Sydney

<sup>‡</sup>U Lille

<sup>§</sup>U Hobart

The investigation of gauge theories in the Hamiltonian approach on finite lattices with emphasis on the role of nongeneric strata was continued. Based on [1], the work on the stratified Kähler quantization for gauge groups SU(2) and SU(3) was continued [2, 3] and extended to arbitrary compact gauge groups [4]. Aspects of the classical dynamics of these models were investigated [5].

Based on [6] and in collaboration with H. Grundling, the investigations of specific models of quantum lattice gauge theory in terms of gauge invariant quantities concerning the structure of the algebra of observables and its representations were continued.

The work on the classification of the orbit types of the action of the group of local gauge transformations on the space of connections for arbitrary compact gauge group was continued [7].

- [1] J. Huebschmann, G. Rudolph, M. Schmidt, *Commun. Math. Phys.* **286**, Nr. 2 (2009) 459–494
- [2] M. Schellenberger-Costa: Konstruktion des kostratifizierten Hilbertraums für die SU(3), diploma thesis, University of Leipzig, 2010
- [3] F. Fürstenberg: Charakterisierung der Strata eines SU(2)-Gitterreichmodells durch geometrische Invariantentheorie, diploma thesis, University of Leipzig, 2011
- [4] M. Hofmann: On the costratified Hilbert space structure of a lattice gauge model with semisimple gauge group, diploma thesis, University of Leipzig, 2011
- [5] A. Jäschke: Gauge field theory, singular Marsden-Weinstein reduction and applications to lattice gauge theory, diploma thesis, University of Leipzig, 2010
- [6] J. Kijowski, G. Rudolph, C. Śliwa, *Annales H. Poincaré* **4** (2003) 1137  
J. Kijowski, G. Rudolph, *J. Math. Phys.* **46** (2005) 032303; *Rep. Math. Phys.* **55** (2005) 199  
P. Jarvis, J. Kijowski, G. Rudolph, *J. Phys. A* **38** (2005) 5359
- [7] A. Hertsch, G. Rudolph, M. Schmidt, *Rep. Math. Phys.* **66** (2010) 331  
*Ann. H. Poincaré* **12**, nr. 2 (2011) 351

## 13.4 Quantum field theory on non-commutative geometries, quantum field theory and cosmology, generally covariant quantum field theory

R. Verch, M. Borris, T. Ludwig, M. Gransee F. Lindner, A. Knospe, B. Eltzner, J. Zschoche

One of the questions of recent interest is if there is a general framework for quantum field theory on non-commutative spacetimes. This question is analysed in collaboration with M. Borris. On one hand, an approach to Lorentzian non-commutative geometry in the spirit of spectral geometry is being established. On the other hand, the quantization of such structures is shown to lead to simple examples of quantum field theories on non-commutative spacetimes for concrete non-commutative spacetime models. The research on these topics is in progress. The relation between the Euclidean and Lorentzian approach to non-commutative quantum field theory is investigated with T. Ludwig, in collaboration with H. Grosse and G. Lechner.

In collaboration with C.J. Fewster it is investigated how to specify that quantum field theories are the same on all spacetimes, which is an extension of the framework of generally covariant quantum field theory.

The definition and analysis of states which can be viewed as local thermal equilibrium states in quantum field theory will be extended to quantum fields in curved spacetime, with a view on application in cosmological situations. Current research work with J. Schlemmer analyzes the question of existence of thermal equilibrium states. Further work with F. Lindner investigates the stability of local thermal equilibrium with respect to variations of the spacetime metric. Solutions to the semiclassical Friedman equations in local thermal equilibrium states are studied with M. Gransee and A. Knospe, the results indicate that quantum corrections lead to an increase in temperature in scenarios of early cosmology compared to the classical results. The role of the renormalization ambiguity in cosmic temperature evolution is investigated in collaboration with K. Fredenhagen and T.-P. Hack.

## 13.5 Funding

*Spectral Zeta Functions and Heat Kernel Technique in Quantum Field Theory with Nonstandard Boundary Condition*

M. Bordag

Heisenberg-Landau programme

*New Trends and Applications of the Casimir Effect (CASIMIR)*

Research Networking Program of the ESF (European Research Foundation)

M. Bordag – Member of the Steering Committee

*Non-commutative quantum field theory*

M. Borris, T. Ludwig

IMPRS fellowship

*Local thermodynamic equilibrium in cosmological spacetimes*

B. Eltzner, M. Gransee, J. Zschoche  
IMPRS fellowship

*Workshop "Mathematics and Quantum Theory", ITP, University of Leipzig, April 13, 2010*

RALeipzig, PbF2

*27th LQP Workshop "Foundations and Constructive Aspects of QFT", ITP, University of Leipzig, Nov. 19-20, 2010*

Ev. Studienwerk Villigst, RALeipzig, PbF2

ESI Program "Quantum field theory on curved space-times and curved target-spaces" Vienna, March 1 - July 30, 2010 ESI; participant March/April 2010

University of York, research visit, June 2010

R. Verch

## 13.6 Organizational Duties

Priv.-Doz. Dr. Michael Bordag

- Referee: J. Phys. A, Phys. Rev. D, J. Math. Phys.
- Chair of the International Organizing Committee of the Conference on Quantum Field Theory under the Influence of External Conditions (QFEXT11), Benasque (Spain), 18-24.9.2011
- Member of the Steering Committee of the ESF Research Networking Program *New Trends and Applications of the Casimir Effect (CASIMIR)*

Prof. Dr. G. Rudolph

- Referee: Class. Quant. Grav., J. Math. Phys., J. Geom. Phys., J. Phys. A, Rep. Math. Phys., Commun. Math. Phys.
- Referee for the German Research Council (DFG) and the Alexander von Humboldt Foundation

Dr. Matthias Schmidt

- Referee: J. Phys. A, Int. J. Mod. Phys. A, Class. Quant. Grav., Gen. Relativity Gravitation

Prof. Dr. Rainer Verch

- Speaker, Profilbildender Forschungsbereich 2 (since Nov. 2010)
- Director of the Institute for Theoretical Physics, University of Leipzig
- Quality Assurance Officer, Faculty of Physics and Earth Sciences
- Chairman of Examining Board, Physics and Meteorology
- Head of Quality Assurance Committee, Faculty of Physics and Earth Sciences
- Associate Editor, Journal of General Relativity and Gravitation
- Book Series Editor, Fundamental Theories of Physics (Springer)
- IMPRS Board Member
- Referee for the Alexander von Humboldt Foundation
- Referee for Studienstiftung des Deutschen Volkes

- Referee: Commun. Math. Phys., J. Math. Phys., JHEP, Rev. Math. Phys., Class. Quantum Grav., Gen. Rel. Grav.
- Organizer, Workshop “Mathematics and Quantum Theory”, ITP, University of Leipzig, April 13, 2010
- Organizer, 27th LQP Workshop “Foundations and Constructive Aspects of QFT”, ITP, University of Leipzig, Nov. 19-20, 2010

## 13.7 External Cooperations

### Academic

- II. Inst. f. Theoretische Physik, Universität Hamburg  
Prof. Dr. K. Fredenhagen
- Mathematisches Institut, Universität Göttingen  
Prof. Dr. D. Bahns
- Mathematisches Institut, Universität Münster  
Prof. Dr. R. Wolkenhaar
- Institut für Mathematik, Universität Paderborn  
Dr. Ch. Fleischhack
- Department of Mathematics, University of York, England  
Dr. C.J. Fewster
- School of Mathematics, Cardiff University, Wales  
Prof. Dr. S. Hollands
- Dipartimento di Science, Università di Trento, Italy  
Prof. Dr. V. Moretti
- Dipartimento di Matematica, Università di Genova, Italy  
Prof. Dr. N. Pinamonti
- Université des Sciences et Technologies de Lille  
Prof. Dr. J. Huebschmann
- Polish Academy of Sciences, Center for Theoretical Physics, Warsaw  
Prof. Dr. J. Kijowski  
Dr. Sz. Charzynski
- National University, Dnepropetrovsk  
Prof. V. Skalozub
- St. Petersburg University  
Prof. Yu.V. Novozhilov
- VIK Dubna  
Dr. V. Nesterenko, Dr. I. Pirozhenko
- University of Tasmania, Hobart  
Prof. Dr. P. Jarvis
- University of New South Wales, Sydney  
Prof. H. Grundling

## 13.8 Publications

### Journals

M. Bordag, V. Demchik, V. Skalozub

Characteristics of gluon plasma in chromomagnetic field at high temperature

In K.A. Milton and M. Bordag, editors, *Proceedings of the 9th Conference on Quantum Field Theory Under the Influence of External Conditions (QFEXT09)*. World Scientific, Singapore, 2010.

M. Bordag, B. Geyer, G.L. Klimchitskaya, V.M. Mostepanenko

On the definition of dielectric permittivity for media with temporal dispersion in the presence of free charge carriers

J. Phys. A **43** (2010) 015402

M. Bordag and V. Nikolaev

First analytic correction beyond the proximity force approximation in the Casimir effect for the electromagnetic field in sphere-plane geometry

Phys. Rev. D **81** 2010 (065011)

M. Bordag, I.G. Pirozhenko

On the Casimir entropy for a ball in front of a plane

Phys. Rev. D **82** (2010) 125016

M. Borris, R. Verch

Dirac field on Moyal-Minkowski spacetime and non-commutative potential scattering.

Commun.Math.Phys. **293** (2010) 399-448

A. Degner, R. Verch

Cosmological particle creation in states of low energy.

J.Math.Phys. **51** (2010) 022302

A. Hertsch, G. Rudolph, M. Schmidt

On the gauge orbit types for theories with classical compact gauge group

Rep. Math. Phys. **66** (2010) 331–353

### Talks

M. Bordag

Vacuum energy between a sphere and a plane at finite temperature (inv. T)

Plenary talk at the workshop *Cosmology, the Quantum Vacuum, and Zeta Functions*, Barcelona (Spain), March 8–10, 2010

M. Bordag

Vacuum energy between a sphere and a plane at finite temperature (inv. T)

NPQFT workshop, University of Oklahoma in Norman, USA, April 9–10, 2010

M. Bordag

On the magnetic mass of gluons in Abelian magnetic background field

Talk at the workshop (T)

6th International Workshop on Critical Point and Onset of Deconfinement, Dubna (RF), August 23–29, 2010

M. Bordag

On the Casimir entropy for a ball in front of a plane (inv. T)

Plenary talk at the *III International Conference "Models in Quantum Field Theory" (MQFT-2010)*, St.Petersburg (RF), October 18–22, 2010

M. Bordag

On the Casimir entropy for a ball in front of a plane (inv. T)

Plenary talk at the *Petrov 2010 Anniversary Symposium on General Relativity and Gravitation*, Kazan (RF), November 1–6, 2010

R. Verch

Dirac Field on Lorentzian Non-Commutative Spacetime (T)

Mathematisches Forschungsinstitut Oberwolfach, Workshop Noncommutative Geometry and Loop Quantum Gravity: Loops, Algebras and Spectral Triples, February 07–13, 2010

R. Verch

Local Thermal Equilibrium and Gravity (inv. T)

74. Jahrestagung der DPG und DPG Frühjahrstagung Bonn, March 15–19, 2010

R. Verch

Dirac field on NC Moyal Minkowski spacetime, NC potential scattering (T)

Bayrischzell Workshop 2010, Noncommutativity and Physics: Spacetime Quantum Geometry Bayrischzell, May 14–17, 2010

R. Verch

Dirac field on Moyal-Minkowski spacetime and noncommutative potential scattering (T)

Geometry and Physics in Cracow, Jagiellonian University, Cracow, September 21–25, 2010

R. Verch

Quantum fields and cosmology: Particle production and local thermal equilibrium (T)

Conference Quantum Field Theory and Gravity, Regensburg, September 28–October 1, 2010

## 13.9 Graduations

### Diploma

- Michael Schellenberger-Costa  
*Konstruktion des kostratifizierten Hilbertraums für die SU(3)*  
July 21, 2010
- Sören Graupner  
*Ashtekar-Variablen: Bündeltheorie und Schwarze Löcher*  
July 26, 2010

- André Jäschke  
*Gauge field theory, singular Marsden-Weinstein reduction and applications to lattice gauge theory*  
August 24, 2010

### **Bachelor**

- Stephan Preiß  
*Raumzeit mit geschlossenen zeitartigen Kurven und das "No-Cloning Theorem"*  
October 2010
- Adam Reichold  
*Geometrisch-modulare Wirkung und geometrische Thermalisierung*  
October 2010

## **13.10 Guests**

- Prof. Dr. Peter Jarvis (Humboldt fellow)  
January 10–February 6, 2010
- Prof. Dr. H. Grundling  
University of New South Wales, Sydney  
July 1–11, 2010  
November 26–December 3, 2010
- I. Pirozhenko  
JINR Dubna  
November 28–December 11, 2011

# 14

## Statistical Physics

### 14.1 Introduction

The focus of research in the STP group is on low-dimensional and mesoscopic interacting systems. These systems are fascinating because on the one hand they allow to study fundamental questions of quantum statistical mechanics, and on the other hand they have a great potential for technological applications. The interplay of a reduced dimensionality with enhanced interaction effects, non-equilibrium physics, and possibly disorder allows the observation of many interesting phenomena, which pose a stimulating challenge for theoretical analysis. The mathematical language used for the description of these systems is quantum field theory, including techniques like functional integrals, renormalization group, instanton calculus, the Keldysh technique for non-equilibrium situations, and the replica method for disordered systems. These analytical tools are supplemented by the use of computer algebra (Mathematica) and numerical calculations (Matlab, Perl, C++). We try to combine the analysis of theoretically interesting problem with relevance to experiments on nanostructures.

Fractional quantum Hall (QH) systems display perhaps the richest and most beautiful physics of all condensed matter systems. They are a prime example for the idea that the whole is more than the sum of its parts, as low lying excitations of a fractional QH fluid carry only a fraction of the electron charge and are thus qualitatively different from the system constituents. Recently, interest in fractional QH physics has been reinvigorated by the prospect that quasiparticles (QPs) of the fractional QH state at filling fraction  $5/2$  may be non-abelian anyons, i.e. their braiding may not only gives rise to a multiplication of the wave function with a complex phase, but in addition corresponds to a unitary transformation of the highly degenerate ground state. Due to the topological nature of braiding, these unitary transformations are robust against local perturbations and guarantee a high degree of stability of the quantum weave of braids, lending it to the construction of topological quantum bits. Future research in this field will concentrate on both the analysis of qualitative properties of topologically ordered systems and the description of experimentally relevant consequences in nanostructured systems.

Similarly to the edge states of QH systems, in single channel nanowires interactions strongly modify the dynamics of electrons. In the presence of strong spin-orbit coupling and in proximity to a superconductor, nanowires can support a topologically ordered state suitable for the formation of topological quantum bits. In multimode nanowires,

a quantum phase transition between superconductor and diffusive metal can occur, which is tuned by an external magnetic field and is experimentally realized in niobium and molybdenum-germanium systems. Comparatively small changes in the external magnetic field can give rise to a large change in conductivity. In the quantum critical region, there are interesting signatures in thermoelectric transport. In the presence of disorder, this quantum phase transition is controlled by a strong disorder fixed point in the universality class of the random transverse field Ising model.

*B. Rosenow*

## 14.2 Dynamical Conductivity at the Dirty Superconductor-Metal Quantum Phase Transition

A. Del Maestro<sup>\*</sup>, B. Rosenow, J.A. Hoyos<sup>†</sup>, T. Vojta<sup>‡</sup>

<sup>\*</sup>UBC Vancouver

<sup>†</sup>Universidade de Sao Paulo

<sup>‡</sup>Missouri University

Recent advances in experimental techniques have allowed for the fabrication of ultrathin metallic nanowires having diameters smaller than the bulk superconducting coherence length, but large enough to include many transverse channels for electronic conduction. Resistance measurements have shown that the thicker among these wires exhibit a well-defined phase transition from a resistive to a superconducting state with decreasing temperature, while thinner wires appear to remain resistive down to the lowest temperatures measured [1]. It has been proposed [2] that these experiments may be understood in terms of a superconductor-metal quantum phase transition (SMT) driven by pair-breaking interactions, possibly due to random magnetic moments trapped on the wire surface.

As the nanowires are prone to random variations in diameter and because of the random positions of the pair-breaking moments, quenched disorder plays an important role. The thermodynamics of the disordered SMT has been analyzed [3] in the relevant case of one space dimension. It is governed, for any nonzero disorder strength, by a non-perturbative infinite-randomness critical point (IRCP). This IRCP is in the same universality class as the magnetic quantum critical point of the random transverse-field Ising chain despite the fact that the two systems have different symmetries: The clean transverse-field Ising chain can be described by relativistic free fermions (and, therefore, dynamical exponent  $z = 1$ ) whereas the clean SMT is described by overdamped O(2) fluctuations with  $z = 2$ . The homology lies in the marginal dynamics of finite size clusters in both models which are the famous *rare regions* of Griffiths-McCoy physics.

Because of universality, many asymptotically exact results for the random transverse-field Ising chain apply directly to the SMT. The IRCP is characterized by activated dynamical scaling:  $L_\Omega \sim [\ln(\Omega_0/\Omega)]^{1/\psi}$ . Here,  $\Omega$  is the characteristic energy of the order-parameter fluctuations on length scale  $L_\Omega$ ,  $\Omega_0$  is a high-energy reference scale, and  $\psi = 1/2$  is known as the tunneling exponent. The exponential length-energy relation implies that the dynamical exponent  $z$  is formally infinite. Moreover, the magnitude of the order parameter fluctuations  $\mu$  also scales logarithmically with energy,

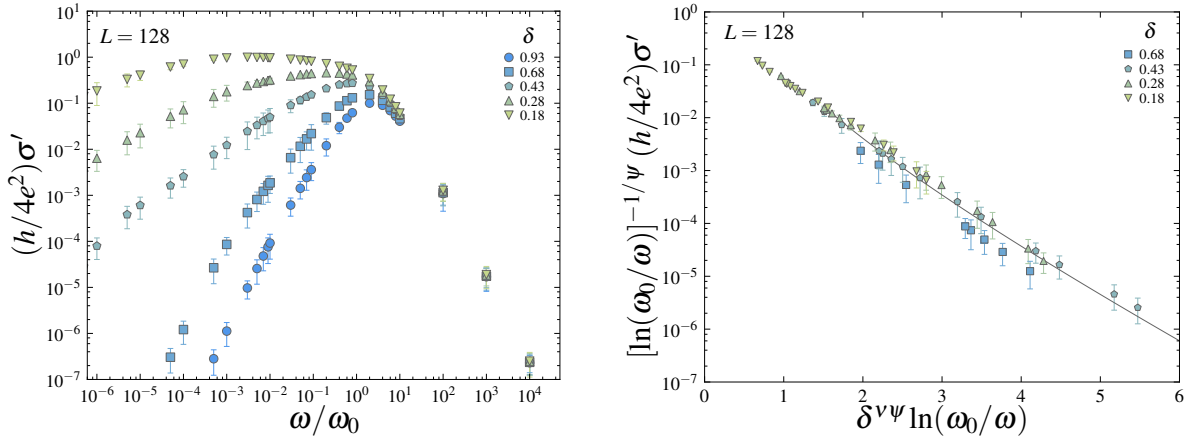


**Figure 14.1:** Left panel: the disorder averaged real conductivity for chains of 128 sites as a function of frequency measured in terms of a UV cutoff  $\omega_0$  for different values of the distance from the critical point,  $\delta$ . Right panel: scaling plot of the same data as a function of the dimensionless scaling variable  $x = \delta^{\nu\psi} \ln(\omega_0/\omega)$  as criticality is approached from above. The line is a guide to the eye showing the probable functional form of the scaling function.

$\mu_\Omega \sim [\ln(\Omega_0/\Omega)]^\phi$ , where the cluster exponent  $\phi = (1 + \sqrt{5})/2$  is the golden ratio. Approaching criticality, the correlation length diverges as  $\xi \sim |\delta|^{-\nu}$  where  $\nu = 2$  and  $\delta$  measures the relative distance to the critical point.

We study the experimentally important transport properties at the pair-breaking SMT of disordered nanowires. Specifically, we report both analytical and numerical calculations of the zero-temperature finite-frequency fluctuation corrections to the conductivity  $\sigma(\omega)$ . At criticality, the real part of the conductivity diverges as  $\sigma'(\omega) \sim [\ln(\omega_0/\omega)]^{1/\psi}$  with vanishing frequency  $\omega$  ( $\omega_0$  is a reference frequency). Off criticality, it satisfies the unconventional activated scaling form [4]

$$\sigma'(\delta, \omega) = \frac{4e^2}{h} \left( \ln \frac{\omega_0}{\omega} \right)^{1/\psi} \Phi_\sigma \left( \delta^{\nu\psi} \ln \frac{\omega_0}{\omega} \right), \quad (14.1)$$

where  $\Phi_\sigma(x)$  is a universal scaling function. This scaling form leads to data collaps of conductivity values obtained from numerically solving self-consistency equations in the large-N limit [4].

- [1] A. Rogachev, A. T. Bollinger and A. Bezryadin, *Phys. Rev. Lett.* **94**, 017004 (2005).
- [2] A. Del Maestro, B. Rosenow, N. Shah, and S. Sachdev, *Phys. Rev. B* **77**, 180501(R) (2008).
- [3] A. Del Maestro, B. Rosenow, M. Muller, and S. Sachdev, *Phys. Rev. Lett.* **101**, 035701 (2008).
- [4] A. Del Maestro, B. Rosenow, J.A. Hoyos, T. Vojta, *Dynamical conductivity at the dirty superconductor-metal quantum phase transition*, *Phys. Rev. Lett.* **105**, 145702 (2010).

## 14.3 Quantitative description of Josephson-like tunneling in quantum Hall exciton condensates

T. Hyart, B. Rosenow

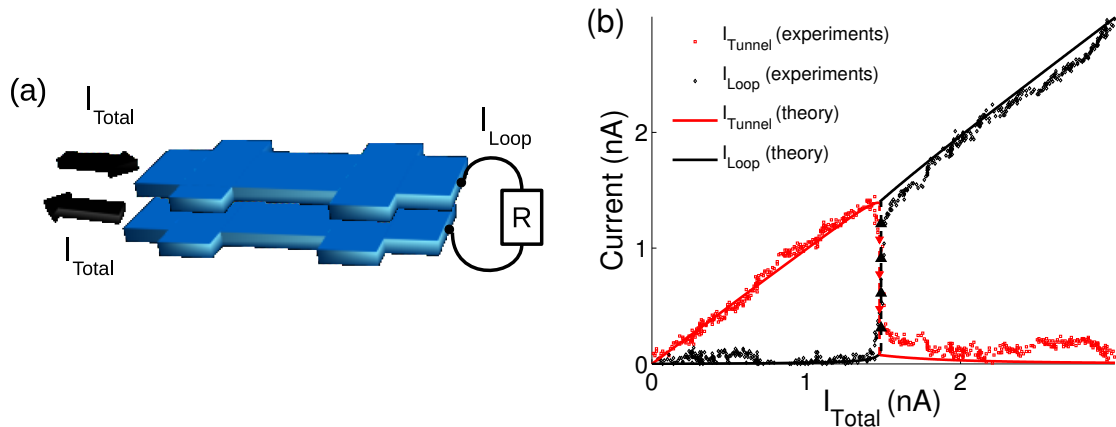


**Figure 14.2:** (a) Counterflow geometry. A dc input current is applied to the top layer and the current which passes through the top layer is redirected via a loop resistor into the bottom layer. The difference between the total current and the loop current describes the current which tunnels between the layers. (b) Tunneling and loop currents as a function of total current. The theoretical model used in Ref. [4] captures well the experimentally observed [3] sharp transition in the tunneling and loop currents occurring at the critical current  $I_{\text{Total}} \approx 1.5$  nA.

The different quantum Hall states display a rich diversity of exotic effects induced by Coulomb interactions. One state of particular interest is the bilayer quantum Hall state at total filling factor  $\nu_T = 1$ , which is theoretically expected to realize a Bose-Einstein condensate of excitons [1]. The condensation in this system occurs essentially because each layer has a half-filled Landau level corresponding to equal number of electrons and holes inside the layer, and the Coulomb interactions favor a state with a spontaneous interlayer phase-coherence similar to the BCS state in superconductors.

Theoretically, the  $\nu_T = 1$  bilayer quantum Hall state is characterized by remarkable electronic properties such as counterflow superconductivity and a tunneling supercurrent similar to the Josephson current between two superconductors. Experimentally, a strong enhancement of the tunneling conductance at small interlayer bias voltage was observed [2], but many of the main features of the experimental observation has remained unexplained. In particular, a consistent picture explaining the magnitudes of the tunneling currents and their dependencies on experimental control parameters has been missing so far. More recently, intriguing observations were made in bilayer samples with larger tunneling amplitude. In particular, jumps of the tunnel current were observed and described in terms of critical tunnel currents about two orders of magnitude larger than in previous experiments [3].

In our recent manuscript [4], we analyzed a theory of interlayer tunneling in the presence of disorder-induced topological defects, so-called merons. We were able to show that within this approach, a large number of experimental observations can be theoretically explained, including the parametric dependencies on sample area,

tunneling amplitude, applied parallel magnetic field and temperature. In addition, we are able to explain the recent experiments in the regime of stronger interlayer coupling, especially the intriguing observations made in the tunneling experiments in counterflow geometry in Ref. [3] [see Fig. 14.2 (a)]. There, it was found that the tunneling current was large as long as the injected drive current was smaller than a certain critical current at which point a transition into a new regime with negligible tunneling current was observed. Fig. 14.2 (b) shows the comparison of the theoretical and experimental results for the tunneling and loop currents and demonstrates that the model which takes the disorder induced merons into account can capture the experimentally observed sharp transition in tunneling and loop currents remarkably well.

- [1] J.P. Eisenstein and A.H. MacDonald, *Nature* **432**, 691 (2994).
- [2] I. B. Spielman *et al.*, *Phys. Rev. Lett.* **84**, 5808 (2000).
- [3] Y. Yoon *et al.*, *Phys. Rev. Lett.* **104**, 116802 (2010).
- [4] T. Hyart and B. Rosenow, *Physical Review B*, in press; arXiv:1011.5684 (2010).

## 14.4 Funding

*Untersuchungen zum topologischen Quanten-Computing*

B. Rosenow together with J. Smet (MPI FKF) and W. Dietsche (MPI FKF)  
BMBF 01BM0900

## 14.5 Organizational Duties

B. Rosenow

- Member of the Studienkommission of the Faculty of Physics and Earth Science
- Referee for *Phys. Rev. Lett.*, *Phys. Rev. B*, *Europhys. Lett.*, *Adv. Cond. Matter*, *JSTAT*, *Physica A*, *Studienstiftung des Deutschen Volkes*

## 14.6 External Cooperations

**Academic**

- MPI für Festkörperforschung Stuttgart  
Prof. W. Dietsche, Dr. J. Smet, Prof. K. von Klitzing
- Harvard University  
Prof. B.I. Halperin, Prof. C.M. Marcus, Prof. S. Sachdev
- Weizmann Institute for Science  
Prof. Y. Gefen, Prof. A. Stern, Prof. Y. Oreg
- Oxford University  
Prof. S. Simon
- California Institute of Technology  
Prof. G. Refael

- Universität zu Köln  
Prof. A. Altland
- Missouri University of Science and Technology  
Prof. T. Vojta
- Universidade de Sao Paulo  
Prof. J.A. Hoyos
- UBC Vancouver  
Dr. A. Del Maestro
- The University of Maryland College Park  
Dr. S. Takei
- FU Berlin  
Dr. D. Meidan

## 14.7 Publications

### Journals

A. Del Maestro, B. Rosenow, J.A. Hoyos, T. Vojta, *Dynamical conductivity at the dirty superconductor-metal quantum phase transition*, Phys. Rev. Lett. 105, 145702 (2010).

### in press

R. Ilan, B. Rosenow, and A. Stern, *Signatures of non-Abelian statistics in non-linear coulomb blockaded transport*, to appear in Phys. Rev. Lett.; arXiv:1005.4772 (2010).

B.I. Halperin, A. Stern, I. Neder, and B. Rosenow, *Theory of the Fabry-Perot Quantum Hall Interferometer*, to appear in Phys. Rev. B; arXiv:1010.4598 (2010).

T. Hyart and B. Rosenow, *Quantitative description of Josephson-like tunneling in  $\nu_T = 1$  quantum Hall bilayers*, to appear in Phys. Rev. B; arXiv:1011.5684 (2010).

### under review

J. Larson and M. Horsdal, *Photonic Josephson effect, phase transitions, and chaos in optomechanical systems*, submitted to Rapid Communication, Phys. Rev. A; arXiv:1009.2945 (2010)

### Talks

Conference *Market Microstructure - Confronting many viewpoints*, Ecole Centrale and Capital Fund Management Paris, December 2010.

Solid State Physics Seminar, ETH Zürich, December 2010.

Workshop on *Low Dimensional Topological Matter*, Aspen Center for Physics, July 2010.

Conference *Correlated Phenomena in Low-Dimensional Systems*, Max-Planck Institute for Complex Systems Dresden, July 2010.

Physics Colloquium, Universität Würzburg, Mai 2010.

Theoretical Physics Seminar, LMU München, Mai 2010.

Theoretical Physics Colloquium, Universität zu Köln, February 2010.

## 14.8 Guests

- Dr. Tony Wright  
MPI FKF Stuttgart  
May 30 to June 4
- Dr. So Takei  
MPI FKF Stuttgart  
September 6-7
- Dr. Dganit Meidan  
FU Berlin  
September 9
- Prof. Gil Refael  
California Institute of Technology  
September 20-23
- Dr. Dgnait Meidan  
FU Berlin  
September 23
- Prof. Yuval Gefen  
Weizmann Institute of Science  
October 9-13
- Prof. Werner Dietsche  
MPI FKF Stuttgart  
October 18-20
- Dr. Stefan Kirchner  
MPI PKS Dresden  
October 29
- Dr. Giniyat Khaliullin  
MPI FKS Stuttgart  
December 16-17



# 15

## Theory of Condensed Matter

### 15.1 Introduction

Major research topics in our group include nonequilibrium phenomena and pattern formation in systems of various nature, e.g. in soft condensed matter and in biological systems. Modern analytic methods of statistical physics and computer simulations complement and stimulate each other. Cooperations with mathematicians, theoretical and experimental physicists, biologists and medical researchers in Germany, Europe and around the world are well established. Specifically we are interested in the following problems.

**Noise induced phenomena** (Behn). Noise induced non-equilibrium phase transitions are studied in coupled arrays of stochastically driven nonlinear systems. Furthermore, stability and statistical characteristics of stochastic nonlinear systems with time delay are investigated.

**Mathematical modeling of the immune system** (Behn). Using methods of nonlinear dynamics and statistical physics, we study the architecture and the random evolution of the idiotypic network of the B-cell subsystem and describe the regulation of balance of the Th1/Th2-cell subsystem including regulatory T-cells, its relation to allergy and the hyposensitization therapy (cooperation with G. Metzner, Clinical Immunology).

**Non-equilibrium dynamics in soft-condensed-matter systems** (Kroy). The systems under investigation range from desert dunes spontaneously developing as a generic consequence of aeolian sand transport, through non-equilibrium gels of adhesive colloids and proteins, the viscoelastic mechanics of the cytoskeleton, to the non-equilibrium dynamics of single DNA molecules under strong external fields. (Related experimental work is currently in progress at EXP1: PWM, PAF.) A common feature is the presence of strong fluctuations and stochastic dynamics on the micro-scale. The emergence of macroscopic structure and (non-linear) deterministic macroscopic dynamics is to be understood. The applied methods range from analytical studies of stochastic integro-differential equations through liquid-state theories, mode-coupling theory, effective hydrodynamic equations, phenomenological modeling, to numerical simulations.

## 15.2 First-passage and First-exit Times of a Bessel-like Stochastic Process

E. Martin\*, U. Behn, G. Germano\*

\*Fachbereich Chemie und WZMW, Philipps-Universität Marburg

We study a stochastic process  $X_t$  related to the Bessel and the Rayleigh processes defined by the stochastic differential equation  $dX_t = (nD/X_t)dt + \sqrt{2D}dW_t$  where  $W_t$  denotes the Wiener process.

The process has various applications in physics, chemistry, biology, economics, finance, and other fields. For example, with  $n = d - 1 - U/D$  the process describes the dynamics of the radial component of a  $d$ -dimensional random walk in a logarithmic potential  $U \log X_t$ .

We analyze the nature of the singular point at the origin, which depends on the value of  $n$ . First we adopt a heuristic approach by Bray [1], then we present a more sophisticated analysis following a scheme proposed by Feller [2]. Different natures of the boundary at the origin arise depending on the real parameter  $n$ : entrance, exit, and regular. To calculate the probability density of the first-passage time or of the first-exit time we derive the backward Kolmogorov equation, formulate the boundary value problem which is of Sturm-Liouville type, and give the general solutions for different ranges of  $n$ . The analytical results are corroborated by numerical simulations [3].

Nontrivial behaviour is observed in the case of a regular boundary: Despite the singularity of the drift at the origin zero-crossings can occur.

[1] A.J. Bray, Phys. Rev. E **62**, 103–112 (2000)

[2] W. Feller, *An Introduction to Probability Theory and Its Applications*, 3rd edition, Wiley, New York 1971

[3] E. Martin, U. Behn, G. Germano: *First-passage and first-exit times of a Bessel-like stochastic process*, Phys. Rev. E **83**, 051115 (2011), 16 pp

## 15.3 Stochastic Phenomena in Systems with Many Degrees of Freedom

U. Behn, F. Anselmi, M. Handrek, M. Höll, N. Kühn, R. Kürsten

Arrays of spatially coupled nonlinear dynamical systems subject to multiplicative or additive noise show close analogies to phase transitions in equilibrium [1]. Concepts such as symmetry (or ergodicity) breaking, order parameter, critical behaviour, critical exponents etc. developed to describe equilibrium phase transitions can be transferred to noise induced nonequilibrium phase transitions.

In the limit of strong coupling there is a clear separation of time scales: The fast degrees of freedom of the relative coordinates  $r_i$  are enslaved by the slow center of mass coordinate  $R$  which exhibits a critical behaviour.

For multiplicative noise, essential characteristics of phase transitions can be found already in finite arrays. Analytical results for probability distribution and expectation value are confirmed by simulations [2].

We developed self-consistent mean field theories to determine the probability distributions of both center of mass and relative coordinates, where the mean value  $\langle R \rangle$  and the variance  $\langle r_i^2 \rangle$  serve as order parameters. Applications include systems with additive and multiplicative noise where the inverse coupling strength and/or inverse system size are considered as small parameters (Anselmi [3], Kürsten, Höll).

For arrays of coupled Stratonovich models where the control parameter is changed according to different protocols we investigate, using both analytical and numerical methods, the validity of various fluctuation theorems (N. Kühn).

For a simple linear system with delayed time argument we have elaborated on the equivalence, at the threshold of stability, of the fundamental solution and a solution exploiting the Lambert  $W$  function [4]. The result is of interest in the context of our research on stochastic systems with temporal delay.

[1] F. Sagués, J. García-Ojalvo, J.M. Sancho, *Rev. Mod. Phys.* **79**, 829 (2007)

[2] F. Senf et al.: *New J. Phys.* **11**, 063010 (2009), 18 pp

[3] F. Anselmi: Diplomarbeit, Universität Leipzig, 2010

[4] M. Handrek: Bachelor Thesis, Universität Leipzig, 2010

## 15.4 Randomly Evolving Idiotypic Networks

U. Behn, A. Kühn, H. Schmidtchen, H. Sachsenweger, B. Werner, S. Willner

The paradigm of idiotypic networks developed about three decades ago by Jerne [1] finds today a renewed interest mainly from the side of system biology and from clinical research. A review with focus on modeling is given in [2], biological concepts and clinical applications are discussed in [3].

B-cells express receptors (antibodies) of a given idiootype. Crosslinking these receptors by complementary structures (antigen or antibodies) stimulates the lymphocyte to proliferate; unstimulated B-cells die. Thus a macroscopically large, though finite, functional network of lymphocytes, the idiotypic network emerges. The dynamics is driven by the influx of new idiotypes randomly produced in the bone marrow and by the population dynamics of the lymphocytes themself.

In our minimalistic model [4] idiotypes are represented by bitstrings. The model network evolves to a highly organized dynamical architecture where groups of nodes which share statistical characteristics can be identified. We can analytically compute size and connectivity of these groups and calculate in a modular mean field theory mean occupation and mean life time of the nodes [5].

We extended the mean field theory considering correlations within and between the different groups of the 12-group architecture. The approach is based on a detailed structural analysis and on the notion of conditional independence. The agreement with simulations is improved by an order of magnitude [6].

To describe biological features we allowed for weighted links and included antigens. For a range of parameters a bistable situation was found where the antigen induces an

internal image which persists after the antigen is defeated. In a second exposition to the antigen the network responds faster and more efficient [7, 8]. Further, in the presence of a long lasting self-antigen the architecture of the network organizes in such a way that the idiotypes complementary to self are only weakly occupied. This is a first hint that our model can describe self-tolerance [7].

A new method to describe a broad class of patterns in the network based on the algebraic properties of Cayley graphs was proposed in [8]. Furthermore, the Shannon entropy associated with the mean occupation of nodes was shown to distinguish different patterns.

- [1] N.K. Jerne: *Ann. Inst. Pasteur Immunol.* **125C**, 373 (1974)
- [2] U. Behn: *Immunol. Rev.* **216** 142 (2007)
- [3] U. Behn: *Idiotype Network*, in: *Encyclopedia of Life Sciences*, John Wiley & Sons, Ltd, Chichester, DOI: 10.1002/9780470015902.a0000954.pub2 (Online posting date: 15th April 2011)
- [4] M. Brede, U. Behn: *Phys. Rev. E* **67**, 031920 (2003)
- [5] H. Schmidtchen, U. Behn: in *Mathematical Modeling of Biological Systems*, Volume II. ed. by A. Deutsch et al. (Birkhäuser, Boston 2008) p157; H. Schmidtchen et al., in preparation
- [6] A. Kühn: Diplomarbeit, Universität Leipzig, 2011.
- [7] B. Werner: Diplomarbeit, Universität Leipzig, 2010.
- [8] S. Willner: Diplomarbeit, Universität Leipzig, 2011.

## 15.5 T Cell Regulation and Allergy

U. Behn, F. Groß\*, D. Kröber, G. Metzner†

\*European School of Molecular Medicine, Milan

†Institute of Clinical Immunology, University Leipzig

T-helper lymphocytes have subtypes which differ in their spectrum of secreted cytokines. These cytokines have autocrine effects on the own subtype and cross-suppressive effects on the other subtype and regulate the type of immunoglobulines secreted by B-lymphocytes. In allergy, the balance of Th1- and Th2-cells is perturbed: the response to allergen is Th2-dominated.

Recent clinical studies show that during specific immunotherapy the concentration of Tregs is increasing [3, 4]. We extended our previous model [1] to include these regulatory T-cells [5]. If successful, the periodic injections of allergen in the maintenance phase of the therapy drive the system towards a stable fixed point where a high population of Tregs dominates both Th2- and Th1-cells, similar to experimental findings. We used the stable manifold of the unstable fixed point of a stroboscopic map to determine the boundary between the basins of attraction of the stable fixed points [5].

We further aim at refining our model to include the novel Th-subtype Th17 which plays a role, e.g., in allergic asthma. In this context we are interested to develop a minimalistic model of the differentiation of peripheral CD4<sup>+</sup> T cells by the networks of cytokines and transcription factors [6] (Kröber).

- [1] J. Richter et al.: *J. Theor. Med.* **4**, 119 (2002)
- [2] R. Vogel, U. Behn: in *Mathematical Modeling of Biological Systems*, Volume II. ed. by A. Deutsch et al. (Birkhäuser, Boston 2008) p145
- [3] M. Larché et al.: *Nature Reviews Immunology* **6**, 761 (2006)
- [4] E. Mamessier et al.: *Clin. Exp. Allergy* **36**, 704 (2006)
- [5] F. Groß et al.: *J. Theor. Biol.* **269**, 70-78 (2011), doi:10.1016/j.jtbi.2010.10.013
- [6] J. Zhu, W.E. Paul, *Immunol. Rev.* **238**, 247-262 (2010)

## 15.6 Tube width Fluctuations in F-Actin Solutions

J. Glaser, K. Kroy

We develop a microscopic liquid state theory of entangled solutions of stiff polymers in terms of a “segment fluid”, with the aim to further establish the tube model of entangled solutions microscopically and to explain experimental observations of tube heterogeneities. This systematic approach to the complicated many-body problem generalizes the prevailing mean-field tube theory by introducing a local version of the binary collision approximation. In this theory, the polymer solution is mapped onto a fluid of entanglement segments interacting via an effective topological pair potential. The local packing structure of this segment fluid is found to provide a faithful representation of the spatial microstructure of the polymer solution, and renders it accessible to an analytical description [1]. In particular, the predicted tube radius distribution is shown to be in good quantitative agreement with experimental data for F-actin solutions [2]. The latter have been measured in a collaboration with the research group of R. Merkel (FZ Jülich).

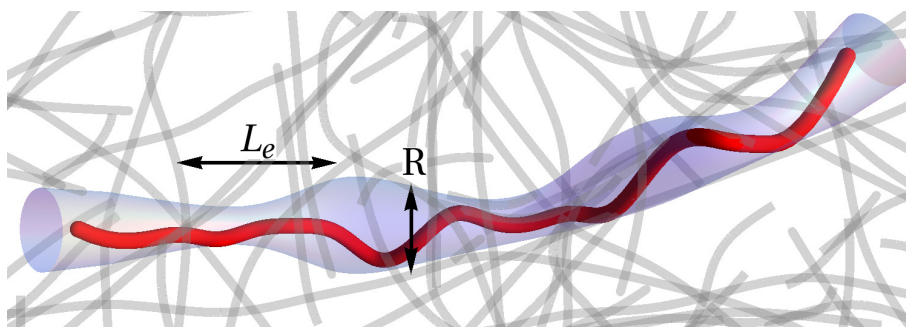


**Figure 15.1:** Test polymer in a background solution, confined into a tube of spatially varying radius  $R(s)$ . The chemical distance  $L_e$  indicates the characteristic scale of the tube heterogeneities.

- [1] J. Glaser, K. Kroy: submitted to *Phys. Rev. E* (2010)
- [2] J. Glaser et al.: *Phys. Rev. Lett.* **105**, 037801 (2010), doi:10.1103/PhysRevLett.105.037801

## 15.7 Dynamical stretching and relaxation response of a biopolymer held by an optical trap

O. Otto\*, S. Sturm, K. Kroy, U.F. Keyser\*

\*Cavendish Laboratory, University of Cambridge

During the last few years, the non-equilibrium dynamics of stiff and strongly stretched biopolymers has been put on a firm theoretical foundation by a rigorous multiple-scale analysis that encompasses several isolated asymptotic scenarios treated in earlier works and also covers the crossover regimes inbetween [1]. Although this yields a rich phenomenology with a variety of intermediate scaling laws depending strongly on boundary conditions and observation timescales, only few dynamical regimes are sufficiently long-lived to be accessible by typical rupture experiments probing biopolymer dynamics on a timescale of seconds [2]. By measuring the relaxation of bead-attached prestretched DNA in a harmonic laser trap using high-speed optical tracking [3], it is however possible to monitor the longitudinal dynamics on a ms timescale. Extending the above formalism to the scenario of an external harmonic potential, we can thus put the short-time predictions of tension propagation theory to the test. Experimental data is provided by Oliver Otto and Ulrich Keyser in Cambridge.

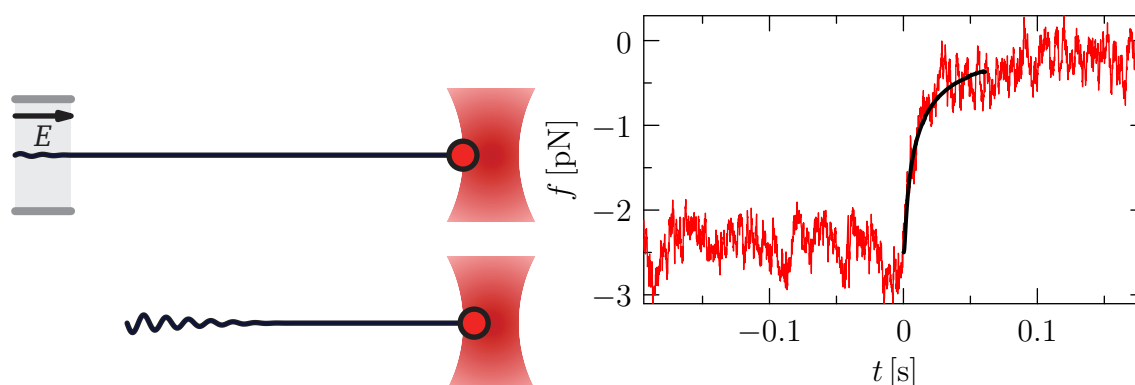


**Figure 15.2:** (Left) Sketch of the experimental setup: DNA is stretched electrophoretically; after turning off the electric field, the ensuing relaxation of the bead is monitored, yielding the force transmission time and the time-resolved backbone tension at the right end of the polymer. (Right) Example trace showing the measured bead relaxation (red) vs. the corresponding theoretical prediction (numerical solution of the relevant crossover regime). The relaxation process takes 25 ms.

- [1] O. Hallatschek et al.: Phys. Rev. Lett. **94**, 077804 (2005),  
doi:10.1103/PhysRevLett.94.077804
- [2] J. K. Fisher et al.: Proc. Nat. Acad. Sci. (2009), doi:10.1073/pnas.0812723106
- [3] L. Steinbock et al.: J. Phys.: Condens. Matter **22** (2010),  
doi:10.1088/0953-8984/22/45/454113

## 15.8 Inelastic mechanics of biopolymer networks

L. Wolff, P. Fernandez\*, K. Kroy

\*Department of Physics, TU München, James Franck Straße 1, 85748 Garching, Germany

The mechanical properties of tissue cells are to a large degree determined by the *cytoskeleton*, a network of semiflexible and stiff polymers which are interconnected by cross-linking molecules. In experiments on tissue cells, many striking and universal observations have been made, for example that cells soften in response to a transient stretch (e. g. lung cells during a deep breath) or that for oscillatory stimulus, the stiffness of the cell increases with a weak power law with driving frequency (a feature called power-law rheology). In contrast to the highly sophisticated experimental methods available to probe cell mechanics, theorists are just starting to understand the reasons and interconnections of the plethora of universal findings.

We develop a minimal model for a network of crosslinked stiff polymers. The main assumption is that the (possibly crosslinker- or molecular-motor-mediated) polymer-polymer interactions can be summarized in a mean effective interaction potential. We find that upon nonlinear deformation, a competition between single-polymer stiffening and inelastic (bond-breaking) softening sets in. Due to inelastic bond-breaking, the system undergoes a “physical”, “passive” remodelling (as opposed to the well-known active biological remodelling). We demonstrate that already at small driving amplitudes, passive remodelling significantly affects the linear and weakly nonlinear response of a material.

In spite of its conceptual simplicity, our model provides an intuitive physical explanation for many astonishing mechanical properties of biopolymer networks and cells. In particular, it identifies a link between seemingly unrelated features such as power-law rheology, non-Maxwellian absorption patterns, and inelastic softening. Starting from this simple model, one can add new features (e. g. allowing for permanent deformations to describe plastic phenomena) and one can start to gradually increase the complexity to turn from a qualitative to a quantitative understanding.

[1] L. Wolff et al.: *New J. Phys.* **12**, 5 (2010), doi:10.1088/1367-2630/12/5/053024

## 15.9 Hot Brownian Motion—Effective Theory and Molecular Simulation

D. Chakraborty, D. Rings, M. Selmke\*, F. Cichos\*, K. Kroy

\*Molekulare Nanophotonik, Institut für Experimentalphysik I

Even a century after its first theoretical explanation, Brownian motion remains an active area of research among theoreticians as well as experimentalists. It is not only a versatile paradigm in theoretical modeling of complex systems, but is extensively exploited in experiments to probe nano-structured environments. In our present research project we both develop an effective Markovian description based on the theory of

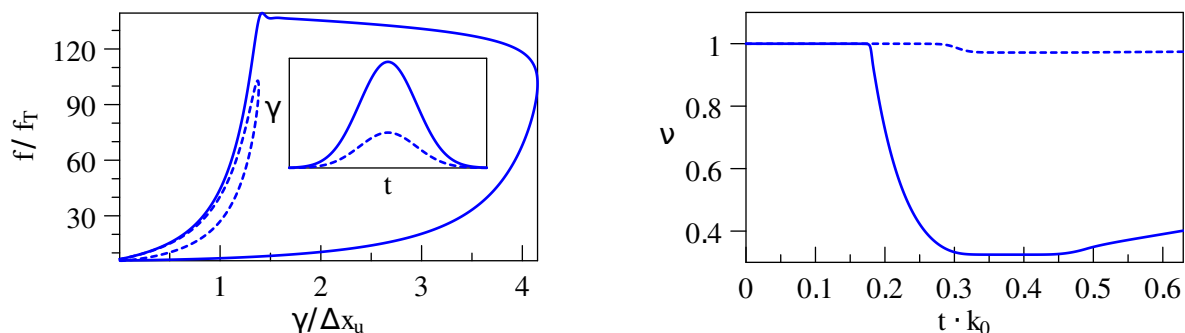


**Figure 15.3:** Exemplary force displacement curve (left panel) for the response of the inelastic bond-breaking material to an displacement pulse of Gaussian shape (see inset) with large (solid line) and small (dashed line) amplitude. For the large pulse, a sudden decrease in the fraction of closed bonds (passive remodeling, right panel) causes the formation of a pronounced force peak at a rate-dependent yield force.

fluctuating hydrodynamics, and employ molecular dynamics simulations in order to investigate “hot Brownian motion” [1]. This scientifically and technologically important non-equilibrium generalization of Brownian motion arises whenever a Brownian particle is kept at an elevated temperature with respect to the ambient conditions. It is, for instance, easily realized when a colloid diffuses in the focus of laser beam. The change in the refractive index of the surrounding fluid is easily detected using a second laser. This provides the basis for dynamical photo-thermal particle tracking techniques with a high potential of complementing conventional fluorescence techniques [2]. Besides validating our theoretical findings, we use our simulations to investigate the various microscopic phenomena and hydrodynamic boundary conditions associated with “hot Brownian motion”, which are neither directly accessible to theory nor to experiment.

[1] D. Rings et al.: Phys. Rev. Lett. **105**, 090604 (2010),

[doi:10.1103/PhysRevLett.105.090604](https://doi.org/10.1103/PhysRevLett.105.090604)

[2] R. Radünz et al.: J. Phys. Chem. A **113**(9), 1674-1677 (2009), [doi:10.1021/jp810466y](https://doi.org/10.1021/jp810466y)

[3] D. Rings et al.: Soft Matter (2011), [doi:10.1039/C0SM00854K](https://doi.org/10.1039/C0SM00854K)

## 15.10 Aeolian sand transport

M. Lämmel, L. Kimme, D. Rings, K. Kroy

Wind driven sand transport is an extensively studied phenomenon in geophysics. A wealth of different aspects have been studied starting at ripple and dune formation, over dust production induced by sand grain bombardment, up to meteorological effects in particular those related to dust, e. g. the influence of dust transport and cover on the climate.

The main mechanism for wind driven sand transport is so-called saltation (lat. *saltare* – jump, leap). Grains are lifted and accelerated by the wind, and they may eject other

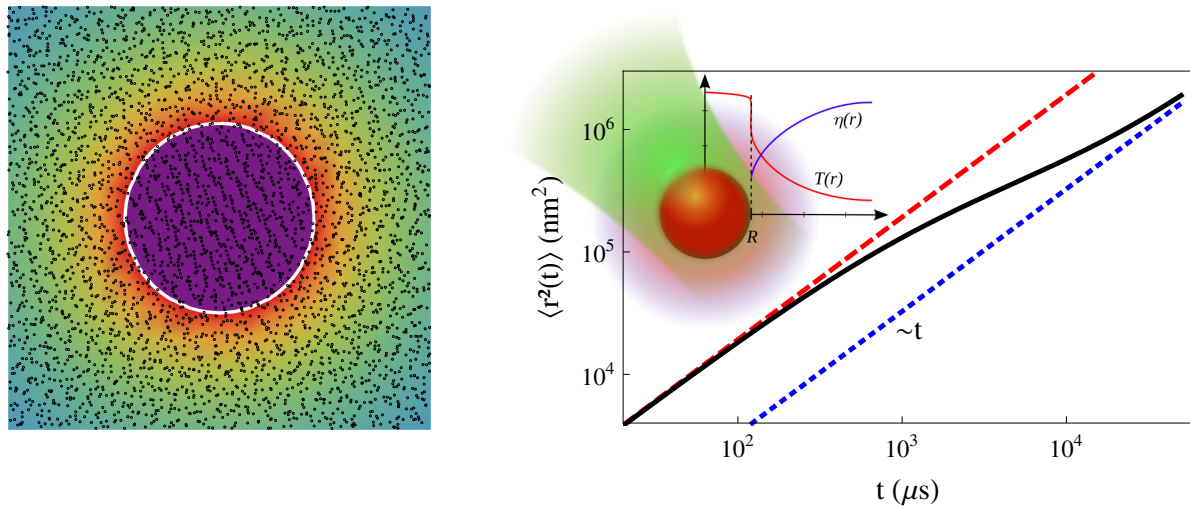


**Figure 15.4:** **Left:** A cross-section through a simulation snapshot of “hot Brownian motion”. The Brownian particle is depicted at the center while the black points represent the fluid atoms. The color coding represents the steady state temperature profile  $T(r)$ . **Right:** The theoretically predicted mean square displacement of a Brownian particle in the inhomogeneous focus of a heating laser beam. The asymptotes correspond to a homogeneous system kept at the lowest resp. highest temperature the particle reaches in the focus. **Inset:** The schematic abstraction of the system, on which our theory is based—both temperature and viscosity vary radially around the Brownian particle and attain their ambient values at infinity.

soil grains upon rebounding. In this way, momentum is transferred from the wind to the grain and further into the ground where a certain fraction of the grains’ momentum is lost, thus impeding the wind’s capability to bear mobile grains. Under favorable conditions a steady state is attained where the sand mass flux reaches its saturated value.

In this project, an aeolian sand transport model has been developed which is based on the continuum saltation model introduced by Sauermann et al. [1], but adds major extensions to it widening the range of the model’s applicability. The main conceptual progress has been achieved by dividing the sand flux into two fractions referring to high-energy saltating and low-energy reptating grains. This two species model results in a transport law which is in remarkable agreement with several wind tunnel observations [2], cf. Fig. 15.5.

[1] G. Sauermann et al.: Phys. Rev. E **64**(2), 031305 (2001),  
doi:10.1103/PhysRevE.64.031305

[2] J. D. Iversen, K. R. Rasmussen: Sedimentology **46**(4), 723-731 (1999),  
doi:10.1103/PhysRevE.64.031305

## 15.11 Funding

*Humboldt fellowship*

D. Chakraborty (together with F. Cichos)

*Sächsische Forschergruppe*

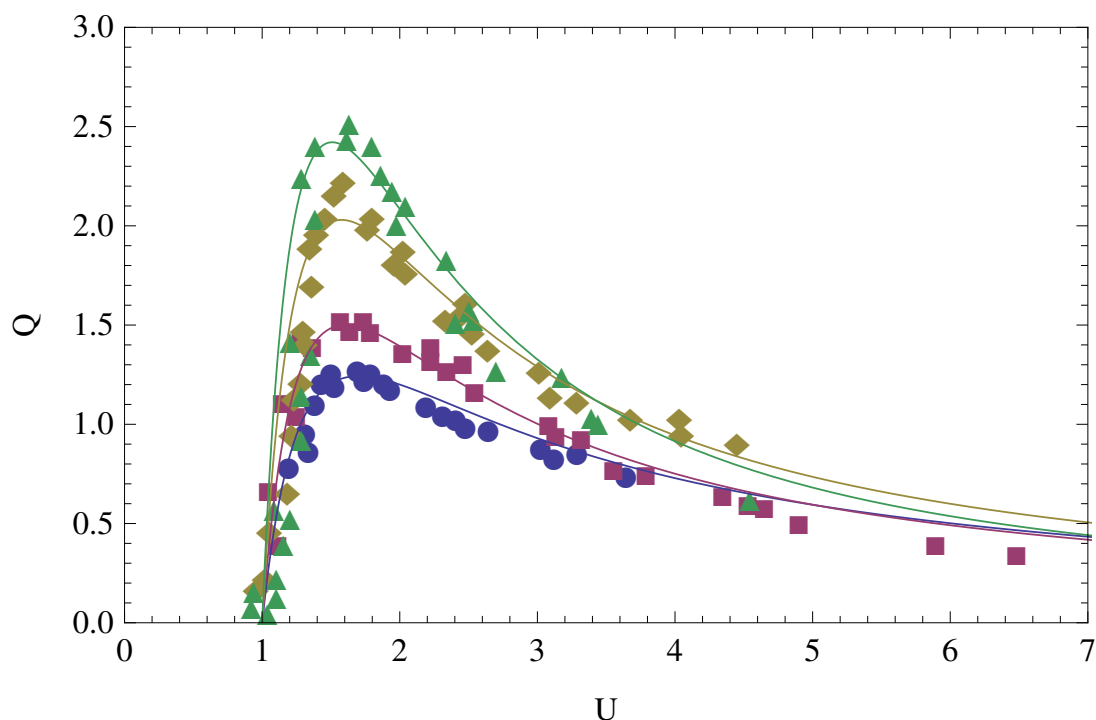


**Figure 15.5:** The dimensionless saturated flux  $Q$  as a function of the rescaled friction velocity  $U = u_*/u_{*t}$  for several grain sizes (the diameters are  $125 \mu\text{m}$ ,  $170 \mu\text{m}$ ,  $242 \mu\text{m}$ ,  $320 \mu\text{m}$  from the lower to the upper curve). The symbols represent wind tunnel measurements [2].

DFG FOR 877 (P3)  
J. Glaser, D. Rings

*The Leipzig Graduate School "Building with Molecules and Nano-objects"*  
S. Sturm, L. Wolff

## 15.12 Organizational Duties

U. Behn

- Speaker of the Condensed Matter Theory Group
- Vertrauensdozent für die Nobelpreisträgertagungen in Lindau
- Bibliotheksbeauftragter of the Faculty
- Member of PbF2
- Scientific Member of the International Max Planck Research School "Mathematics in the Sciences"
- Referee: Phys. Rev. E
- Reviewer: University of Georgia, Athens; University of Illinois at Chicago; Brown University Graduate School, Providence

K. Kroy

- Vice Director of the Institute for Theoretical Physics
- Organization of faculty- & physics colloquia
- Organization of "Die mitteldeutsche Physikcombo"

- Member of the graduation committee
- Member of the committee for information & communication technology
- Study counselor for physics
- Member of PbF1 and PbF2
- PI in FG877 and The Leipzig Graduate School "Building with Molecules and Nano-objects"
- Scientific Member of the International Max Planck Research School "Mathematics in the Sciences"
- Referee: Nature, Phys. Rev. E
- Reviewer: DFG, NSF

## 15.13 External Cooperations

### Academic

- FZ Jülich  
Prof. R. Merkel, Dr. M. Degawa
- University of Cambridge  
Dr. U. Keyser
- Molekulare Nanophotonik, Institut für Experimentalphysik I  
Prof. F. Cichos
- Otto-von-Guericke-Universität Magdeburg  
Prof. Dr. J. Richter
- Joint Institute for Nuclear Research, Dubna, Russia  
Prof. Dr. N.M. Plakida
- Ernst-Moritz-Arndt-Universität Greifswald  
Prof. Dr. H. Fehske
- Institut für Klinische Immunologie  
Prof. Dr. G. Metzner
- European School of Molecular Medicine, Milan, Italy  
Dipl.-Phys. F. Groß
- Philipps-Universität Marburg  
Prof. Dr. G. Germano, Dr. E. Martin
- Max-Planck-Institut für Physik komplexer Systeme, Dresden  
Dipl.-Phys. L. Wetzel
- Physik Weicher Materie, Institut für Experimentalphysik I  
Prof. Dr. A. Käs, Dipl.-Math. M. Knorr

## 15.14 Publications

### Journals

J. Glaser, D. Chakraborty, K. Kroy, I. Lauter, M. Degawa, N. Kirchgeßner, B. Hoffmann, R. Merkel, M. Giesen: *Tube Width Fluctuations in F-Actin Solutions*, Phys. Rev. Lett. **105**, 037801 (2010)

M. Härtel, J. Richter, D. Ihle, S.-L. Drechsler: *Thermodynamics of a two - dimensional frustrated spin - 1/2 Heisenberg ferromagnet*, Phys. Rev. B **81**, 174421 (2010)

D. Rings, R. Schachoff, M. Selmke, F. Cichos, K. Kroy: *Hot Brownian Motion*, Phys. Rev. Lett. **105**, 090604 (2010), doi:[10.1103/PhysRevLett.105.090604](https://doi.org/10.1103/PhysRevLett.105.090604)

L. Wolff, P. Fernandez, K. Kroy: *Inelastic mechanics of sticky biopolymer networks*, New J. Phys **12**, 5 (2010)

B. Zenker, D. Ihle, F.X. Bronold, H. Fehske: *Existence of excitonic insulator phase in the extended Falicov - Kimball model: SO(2) - invariant slave - boson approach*, Phys. Rev. B **81**, 115122 (2010)

### Books

J. Glaser, K. Kroy: *Fluctuations of Stiff Polymers and Cell Mechanics*, in: Biopolymers, Ed. M. Elnashar. Sciyo, 2010

### in press

U. Behn, *Idiotypic Networks*, in: Encyclopedia of Life Sciences, John Wiley & Sons, Ltd, Chichester, doi:[10.1002/9780470015902.a0000954.pub2](https://doi.org/10.1002/9780470015902.a0000954.pub2) (Online posting date: 15th April 2011)

F. Gross, G. Metzner, U. Behn: *Mathematical Modelling of Allergy and Specific Immunotherapy: Th1-Th2-Treg Interactions*, J. Theor. Biol. **269**, 70-78 (2011), (available online since 14 October 2010) doi:[10.1016/j.jtbi.2010.10.013](https://doi.org/10.1016/j.jtbi.2010.10.013)

M. Knorr, D. Koch, T. Fuhs, U. Behn, J.A. Käs, *Stochastic Actin Dynamics in Lamellipodia Reveal Parameter Space for Cell Type Classification*, Soft Matter **7**, 3192-3203 (2011), DOI: [10.1039/C0SM01028F](https://doi.org/10.1039/C0SM01028F)

E. Martin, U. Behn, G. Germano: *First-passage and first-exit times of a Bessel-like stochastic process*, Phys. Rev. E **83**, 051115 (2011), 16 pp

D. Rings, M. Selmke, F. Cichos, K. Kroy: *Theory of Hot Brownian Motion*, Soft Matter (2011), doi:[10.1039/C0SM00854K](https://doi.org/10.1039/C0SM00854K)

### under review

J. Glaser, K. Kroy: *Segment fluid representation of entangled stiff polymers*, submitted to Phys. Rev. E

## Talks

U. Behn: *Evolution von Netzwerken*, Buchmesse-Akademie, Leipzig, March 3, 2010

U. Behn, F. Gross, G. Metzner: *Mathematical Modeling of T Cell Regulation in Allergy and Specific Immunotherapy*, World Immune Regulation Meeting 2010, Davos, March 29-April 1, 2010.

J. Glaser: *Tube Width Fluctuations in F-Actin Solutions*, Seminar talk, University of Bonn, Research group Prof. Alt, January 14, 2010

J. Glaser: *GPU accelerated Brownian Dynamics of effective stiff polymer solutions*, Seminar talk, Technical University Chemnitz, February 11, 2010

J. Glaser: *Tube Width Fluctuations in F-Actin Solutions*, Contributed talk, Spring meeting of the German Physical Society, Regensburg, March 21-26, 2010

J. Glaser: *From Stiff Polymers to Cell Mechanics*, Contributed talk & poster, YES 2010 - fourth Workshop of Young European Scientists Krakow, Poland, September 5-10, 2010

J. Glaser: *From Stiff Polymers to Cell Mechanics*, Contributed talk, Symposium of the Saxonian Research Group FOR 877, Leipzig, October 10, 2010

K. Kroy: *Hot Brownian Motion*, Kolloquium Theoretische Physik, University of Konstanz, May 3, 2010

K. Kroy: *Brownian Motion - a paradigm of soft matter and biological physics & Hot Brownian Motion & Dynamics of Stiff Polymer*, Invited talk and 2 lectures, Taipei International Workshop for Soft Matter and Biophysics, May 25-28, 2010

K. Kroy: *Hot Brownian Motion*, Oberseminar Theorie komplexer Systeme, University of Heidelberg, November 11, 2010

K. Kroy: *From Polymers to living cells. A bottom-up approach to cell mechanics.*, Workshop "Innovative Packaging Technologies for Optical Biosensors", Dresdner DFG-Graduiertenkolleg, November 29, 2010

K. Kroy: *Hot Brownian Motion*, Condensed Matter Theory Colloquium, University of Oxford, December 3, 2010

## Posters

D. Chakraborty, J. Glaser, F. Cichos, K. Kroy: *Simulating hot nano beads*, International Soft Matter Conference, Granada, Spain, July 5-8, 2010

J. Glaser: *Tube Width Fluctuations in F-Actin Solutions*, International Soft Matter Conference, Granada, Spain, July 5-8, 2010

M. Hennes, K. Kroy: *The conformations of a stiff polymer in random media*, 74. Annual Meeting of the German Physical Society, Regensburg, March 21-26, 2010

M. Lämmel, K. Kroy: *Turbulent fluctuations in the saltation process. Dust emission.*, 74. Annual Meeting of the German Physical Society, Regensburg, March 21-26, 2010

G. Metzner, F. Gross, U. Behn: *Mathematical Modeling of T Cell Regulation in Allergy and Specific Immunotherapy*, 14th International Congress of Immunology, Kobe, August 22-27, 2010

D. Rings, D. Chakraborty, M. Selmke, R. Radünz, F. Cichos, K. Kroy: *Brownian motion of heated particles*, 74. Annual Meeting of the German Physical Society, Regensburg, March 21-26, 2010

D. Rings, A. Parmeggiani, M. Selmke, R. Schachoff, F. Cichos, K. Kroy: *Diffusivity with reverse size-dependence for heated nano-particles*, International Soft Matter Conference, Granada, Spain, July 5-8, 2010

S. Sturm, K. Kroy: *Dynamical stretching response of a biopolymer held by an optical trap*, Third BuildMoNa Symposium, Leipzig, March 29-30, 2010

S. Sturm, J. Glaser, K. Kroy: *Force propagation through the cytoskeleton*, International Soft Matter Conference, Granada, Spain, July 5-8, 2010

L. Wolff, A. Kramer, K. Kroy: *Nonlinear cell mechanics is plastic mechanics*, 74. Annual Meeting of the German Physical Society, Regensburg, March 21-26, 2010

L. Wolff, K. Kroy: *Inelastic mechanics of sticky biopolymer networks*, Third BuildMoNa Symposium, Leipzig, March 29-30, 2010

## 15.15 Graduations

### Diploma

- Benjamin Werner  
*Idiotypische Netzwerke mit Allergenen: Gedächtnis und Selbsttoleranz*  
January 2010
- Frank Anselmi  
*Stark global gekoppelte nichtlineare Systeme mit additivem Rauschen*  
February 2010

### Bachelor

- Matti Gralka  
*Dynamics of semi-flexible polymers in entangled solutions*  
August 2010
- Michael Handrek  
*Comparing Solutions of a Simple Differential-Difference Equation*  
September 2010
- Lukas Kimme  
*Simulation von Dünenbildung und -entwicklung mittels Mathematica*  
September 2010

## 15.16 Awards

BuildMoNa Award for outstanding scientific results (2010), 1st prize,

Lars Wolff

Leipzig School of Natural Sciences “Building with molecules and nano-objects”

Participation in the workshop YES 2010 - fourth Workshop of Young European Scientists, Krakow, Poland

Jens Glaser

selected by the section CPP of the German Physical Society



# Author Index

## A

Abdelrahman, A. ....	232
Agte, S. ....	112
Ahmed Mohamed, E.T. ....	232, 235
Alireza, P.L. ....	127
Alonso, S. ....	114
Amecke, N. ....	42
Amirjalayer, S. ....	81
Amjad, U. ....	248
Andrea, T. ....	148, 151
Anwand, W. ....	206
Arnrich, S. ....	88
Aust, M. ....	279

## B

Bachmann, M. 284, 286, 287, 289, 290, 292	
Bakowskie, R. ....	214
Ballestar, A. ....	261
Bandari, R. ....	78
Barapatre, N. ....	142
Barquinha, P. ....	168
Barzola-Quiquia, J. ....	150, 261–263
Beck-Sickinger, A.G. ....	290
Beckert, S. ....	78
Behn, U. ....	344–346
Benndorf, G. ....	187, 188, 190, 206, 210
Berg, B.A. ....	294
Bern, F. ....	261, 262
Bertmer, M. ....	129
Binder, T. ....	84
Bischof, R. ....	295
Bischoff, A. ....	147

Bittner, E. ....	274, 282, 300
Blaschke, D. ....	129
Blavatska, V. ....	276
Brachwitz, K. ....	199, 201, 211, 213
Brandt, M. ....	188, 197, 199, 206
Brauer, G. ....	206, 211
Braun, M. ....	36, 38
Breitenstein, O. ....	178
Bridoux, G. ....	262
Brugella, A. ....	37
Brunner, C. ....	110
Bräuer, P. ....	88, 89
Buchmeiser, M.R. ....	78
Butz, T. ....	142, 147, 148, 150–154
Bux, H. ....	84, 85
Bär, M. ....	114
Böntgen, T. ....	166, 185, 195, 201
Böttcher, R. ....	130

## C

Caro, J. ....	84, 85
Chakraborty, D. ....	349
Charnaya, E.V. ....	130
Chmelik, C. ....	84–87
Cichos, F. ....	36–38, 40–42, 349
Cowan, T.E. ....	206
Czekalla, C. ....	214

## D

Dietrich, C.P. ....	190–192
Dietrich, U. ....	114
Diez, T. ....	170
Donath, E. ....	146

- Dorn, M. .... 146  
 Dubbeldam, D. .... 79  
 Dusari, S. .... 262  
 Dvoyashkin, M. .... 77
- E**
- 
- Ebert, S. .... 106  
 Ehrlicher, A. .... 110  
 Eisinger, K. .... 263  
 Ellguth, M. .... 211  
 Elmahdy, M.M. .... 63, 64, 67  
 Ene, R. .... 62  
 Enke, D. .... 89  
 Ernst, A. .... 257  
 Esquinazi, P. .... 150, 198, 199, 205, 257,  
 260–263  
 Estrela-Lopis, I. .... 146  
 Etz, C. .... 257
- F**
- 
- Feder, R. .... 150  
 Feist, A. .... 40  
 Fernandez, P. .... 349  
 Fortunato, E. .... 168  
 Frenzel, H. .... 168, 170, 172  
 Fricke, N. .... 278  
 Fritsch, A. .... 106  
 Fritzsche, S. .... 85  
 Fuhs, T. .... 110
- G**
- 
- Galvosas, P. .... 82  
 García, N. .... 261  
 Gascon, J. .... 79  
 Germano, G. .... 344  
 Ghosh, K. .... 201  
 Glaser, J. .... 347  
 Goede, K. .... 290  
 Goering, E. .... 260  
 Goh, S.K. .... 127  
 Gratz, M. .... 81, 82  
 Grill, W. .... 232, 235, 238, 242, 246, 248  
 Groß, F. .... 346  
 Gross, J. .... 292
- Grundmann, M. .... 166,  
 168, 170, 172, 174, 176, 178, 179,  
 185, 187, 188, 190–192, 194, 195,  
 197–199, 201, 203, 205, 206, 208,  
 210, 211, 213, 214, 290
- Gul-E-Noor, F. .... 129  
 Gutsche, C. .... 63, 64, 67  
 Gyger, M. .... 106  
 Gögler, M. .... 110
- H**
- 
- Haase, J. .... 127, 130  
 Hammer, T. .... 205  
 Heera, V. .... 206  
 Heluani, S.P. .... 263  
 Henk, J. .... 257  
 Hergert, W. .... 257  
 Hertel, S. .... 81, 82  
 Hertäg, L. .... 85  
 Hesse, D. .... 257–259  
 Hibbe, F. .... 84, 86  
 Hilmer, H. .... 179  
 Hochmuth, H. .... 176, 198, 205  
 Hoentsch, J. .... 130  
 Hoffmann, R. .... 63  
 Horch, C. .... 82  
 Hoyos, J.A. .... 336  
 Huber, F. .... 109  
 Hyart, T. .... 338  
 Händel, C. .... 114  
 Höche, T. .... 213
- I**
- 
- Iacob, C. .... 53, 55, 57–60  
 Irbäck, A. .... 290
- J**
- 
- Janke, W. .... 274, 276, 278, 279, 281,  
 282, 284, 286, 287, 289, 290, 292,  
 294–296, 298, 300–303  
 Jankuhn, St. .... 144, 146  
 Jaroniec, M. .... 89  
 Jasiurkowska, M. .... 60  
 Jee, B. .... 128  
 Johnston, D.A. .... 302

Junghans, C. .... 284  
 Jäger, A. .... 129

## K

Kalies, G. .... 88–90  
 Kamanyi, A.E. .... 235, 238  
 Kapteijn, F. .... 79  
 Karalus, S. .... 289  
 Kenna, R. .... 302  
 Keyser, U.F. .... 348  
 Khalid, M. .... 260  
 Kiessling, T. .... 106  
 Kimme, L. .... 350  
 Kipnusu, W.K. .... 53  
 Klingner, N. .... 154  
 Klüpfel, F.J. .... 172, 192  
 Knauth, M. .... 85  
 Koch, D. .... 110  
 Kondrashova, D. .... 76  
 Kossack, W. .... 61  
 Kranert, C. .... 195, 197  
 Krautscheid, H. .... 81, 90  
 Kremer, F. .... 50, 51, 53, 55–64, 67, 69  
 Krishna, R. .... 85  
 Kroy, K. .... 38, 347–350  
 Kröber, D. .... 346  
 Kupper, J. .... 188  
 Kärger, J. .... 85, 86, 279  
 Käs, J.A. .... 106, 109, 110, 112, 114  
 Kühn, A. .... 345

## L

Lajn, A. .... 168, 170, 172, 174, 208  
 Lange, M. .... 190–192  
 Larisch, W. .... 152  
 Lausch, D. .... 214  
 Lautenschläger, S. .... 208  
 Lenzner, J. .... 176, 178, 199, 201, 205, 214  
 Lincke, J. .... 81, 90  
 Lorenz, M. .... 166, 168, 185, 188, 190, 191,  
 195, 198, 199, 201, 203, 205, 213  
 Lämmel, M. .... 350  
 Lässig, D. .... 90  
 Läuchli, A. .... 296

## M

Mapesa, E.U. .... 50, 51, 53  
 Marenz, M. .... 298  
 Marthala, V.R.R. .... 86  
 Martin, E. .... 344  
 Martins, R. .... 168  
 Massalska-Arodz, M. .... 60  
 Maznichenko, V. .... 257  
 Meier, B. .... 127  
 Meinicke, C. .... 198  
 Meissner, Th. .... 127  
 Menzel, F. .... 153  
 Mertig, I. .... 257  
 Metzner, G. .... 346  
 Mexner, K. .... 199  
 Meyer, B.K. .... 208  
 Meyer-Ortmanns, H. .... 281  
 Michalsky, T. .... 179  
 Michel, D. .... 130  
 Mittwoch, K. .... 213  
 Moellmer, J. .... 90  
 Molle, A. .... 262  
 Möddel, M. .... 287  
 Müller, A. .... 187, 188, 194, 213  
 Müller, S. .... 178

## N

Nagel, H. .... 281  
 Neuhaus, T. .... 298  
 Nnetu, D. .... 106  
 Nußbaumer, A. .... 274, 282

## O

Otto, O. .... 348

## P

Papadopoulos, P. .... 60–62, 69  
 Pawlizak, S. .... 106  
 Petter, K. .... 214  
 Pickenhain, R. .... 211  
 Pippel, E. .... 257  
 Pluta, M. .... 232  
 Pumpa, M. .... 41  
 Pusch, A.-K. .... 80, 82

Pöpl, A. .... 128, 130, 260, 263

## R

Rakhmatullin, R.M. .... 130  
 Rauch, P. .... 110  
 Reibetanz, U. .... 144  
 Reichenbach, A. .... 112  
 Reichenbach, C. .... 76, 89, 90  
 Reinert, A. .... 142  
 Reinert, T. .... 142  
 Rheinländer, B. .... 179  
 Rings, D. .... 38, 349, 350  
 Rockmann, R. .... 89  
 Rosenow, B. .... 336, 338  
 Rothermel, M. .... 148, 151  
 Rybicki, D. .... 127

## S

Sachse, S. .... 142  
 Sachsenweger, H. .... 345  
 Sangoro, J.R. .... 53, 55–59  
 Schakel, A.M.J. .... 298  
 Schein, F. .... 170  
 Schein, F.-L. .... 203  
 Schlayer, S. .... 80, 82  
 Schmid, R. .... 81  
 Schmidt, F. .... 208, 210, 211  
 Schmidt, H. .... 206  
 Schmidt, M. .... 174, 176, 210, 211  
 Schmidt-Grund, R. .... 179, 185, 192, 195, 197  
 Schmidtchen, H. .... 345  
 Schnabel, S. .... 286  
 Schnauß, J. .... 109  
 Schubert, T. .... 55  
 Sedykh, P. .... 130  
 Selmke, M. .... 36, 38, 349  
 Semenov, I. .... 69  
 Serghei, A. .... 50, 51  
 Setzer, A. .... 198, 199, 205, 260  
 Shchur, L.N. .... 301  
 Sickert, A. .... 142  
 Singer, D. .... 63  
 Skorupa, W. .... 206, 211  
 Snurr, R.Q. .... 79  
 Sopik, J. .... 281

Spemann, D. .... 153, 260  
 Stallmach, F. .... 78–82  
 Stangner, T. .... 64, 67  
 Strehle, D. .... 109  
 Sturm, C. .... 179, 195, 197  
 Sturm, S. .... 348  
 Stölzel, M. .... 187, 188, 197, 210

## T

Tarar, K.S. .... 248  
 Teupser, D. .... 142  
 Thommes, M. .... 90  
 Titze, T. .... 84, 87  
 Treß, M. .... 50, 51

## U

Ueberschär, O. .... 67

## V

Valiullin, R. .... 76, 77, 279  
 Villafuerte, M. .... 263  
 Vogt, J. .... 147, 154  
 Vojta, T. .... 336  
 von Buttlar, M. .... 246  
 von der Burg, E. .... 246  
 von Wenckstern, H. .... 168, 170, 172, 174, 176,  
 178, 191, 192, 203, 206, 208, 210  
 Vrejoiu, I. .... 257–259

## W

Waclaw, B. .... 281  
 Wagner, C. .... 63, 67  
 Wagner, R. .... 40  
 Wehring, M. .... 79, 82  
 Weigel, M. .... 303  
 Weitkamp, J. .... 86  
 Wenzel, S. .... 296  
 Werner, B. .... 345  
 Wetzel, F. .... 106  
 Wiedenmann, M. .... 282  
 Willner, S. .... 345  
 Wolff, L. .... 349  
 Wunderlich, R. .... 147

**Y**

---

Yan, Z. ....261

**Z**

---

Zakir Hossain, M. ....242

Zeigermann, P. ....77

Zhang, Z.P. ....176

Zierenberg, J. ....294

Ziese, M. ....199, 257–260

Zink, M. ....106

Zippel, J. ....185, 198, 205

Zúñiga-Pérez, J. ....190, 191



Wolfgang Schenk | Friedrich Kremer (Hrsg.)

# Physikalisches Praktikum

13. Auflage

**STUDIUM**



**VIEWEG+  
TEUBNER**

Graduate Texts in Physics

Marius Grundmann

## The Physics of Semiconductors

An Introduction Including Devices and Nanophysics  
Second Edition

*The Physics of Semiconductors* provides ample material for a comprehensive upper-level undergraduate or beginning graduate course, guiding readers to the point where they can choose a special topic and begin supervised research. The textbook provides a balance between essential aspects of solid-state and semiconductor physics, on the one hand, and the principles of various semiconductor devices and their applications in electronic and photonic devices, on the other. It highlights many practical aspects of semiconductors such as alloys, strain, heterostructures, nanostructures, that are necessary in modern semiconductor research but typically omitted in textbooks. Coverage also includes additional advanced topics, such as Bragg mirrors, resonators, polarized and magnetic semiconductors. The text derives explicit formulas for many results to support better understanding of the topics. The Physics of Semiconductors requires little or no prior knowledge of solid-state physics and evolved from a highly regarded two-semester course. In the second edition many topics are extended and treated in more depth, e.g. dopant diffusion, nanowires, recombination in organic semiconductors, multi-junction solar cells, quantum dot and organic LEDs, thin film transistors, carbon-based nanostructures and transparent conductive oxides.

Physics



► [springer.com](http://springer.com)

Graduate Texts in Physics

Marius Grundmann

# The Physics of Semiconductors

An Introduction Including Devices and Nanophysics

Second Edition

 Springer

Grundmann



The Physics of Semiconductors

2nd Ed.